DEEP FOUNDATIONS INSTITUTE

DFI®

PFSF

PILING AND FOUNDATION SPECIALISTS FEDERATION



PROCEEDINGS

2026 DFI-PFSF Piling & Ground Improvement

May 18-20, 2026 | Sydney, Australia

DOI: 10.37308/PFSF26.2026

Welcome to the third joint conference between the Piling and Foundation Specialists Federation and the Deep Foundations Institute! It is pleasing to see industry recognizing the value of this conference series - with growth in delegate numbers and exhibitors in each successive conference from the first in 2017 and the second COVID-delayed conference in 2022.

2026 is a historic year for both DFI, which has just celebrated it's 50th year, and the Piling Federation which marks its 25th anniversary this year.

Engineering the ground is both a science and an art. It is a field where engineers must live daily with risk and which is rich with opportunities for innovation. It is a field where we can all learn from the experience of others – both for projects which were a success, and importantly from projects where engineers had to rise to the challenge of the unexpected. Conferences such as this provide an important opportunity for delegates to share in these experiences both in formal sessions and informal discussions, and to familiarize themselves with the state-of-the-art technologies available.

This year's conference will highlight panel discussions on the Melbourne's North East Link project – collectively Australia's largest foundation works; a session on a key safety initiative being progressed by PFSF in regard to CFA piling; a panel on the critical and contentious issue of working platforms; and a forum on Artificial Intelligence and its application and implications to the foundation and ground improvement industry. Other plenary sessions will cover Case Studies, Innovation, Design, and Smart Practice. The speakers are all thanked for sharing their experiences, and for the time and effort in submitting abstracts, writing their papers, and putting together their presentations. But behind each paper which has been submitted is an army of reviewers – 2 to 3 for every paper – who have selflessly given of their time to ensure that the papers meet the high standards required by DFI of submitted papers. These reviewers are a critical ingredient without which this conference would not be possible.

DFI have a well-honed conference roll-out process which is administered by a very professional team under the direction of Executive Director, Theresa Engler. We would like to particularly thank Angie Gibble, Jaime Cettina, Angelina Servin, Lisa Rayment and Matthew Glisson for their tireless efforts and support. DFI has grown enormously under the leadership of Theresa since I first had contact with DFI and Theresa – in the very early 2000s – becoming an organization with truly international reach, and encompassing all manner of geotechnical works, and inclusive of professionals in all sectors of the industry – true to its tagline "Finding Common Ground".

On this side of the Pacific, Mark Johnson, the Executive Director of the Australian Piling Federation has been a strong advocate for the foundation industry, and a driving force for change and improvements especially in the area of safety, to steer through initiatives such as the new High Risk Licence (HRL) for the operation of Piling Rigs with SafeWork Australia– an 11 year journey, and a new journey to legislate changes relating to cleaning of CFA concrete pump lines. Amongst many other achievements, Mark has also coordinated with State and National Roads organizations to assist with the development of informed and practical foundation specifications.

Together, Mark and Theresa have been the driving force behind this series of DFI-PFSF Conferences, and we thank them for their vision, energy and drive in the service of the foundation industry.

Finally, we gratefully acknowledge all the exhibitors and all our sponsors without whose generous support this conference would not be possible.

Case Studies of Successes or Failures With Lessons Learned

Assessment of Impact Rolling for Ground Improvement on A Site With Variable Soil Condition
A. Akoochakian & P. Band *1*

Pile Foundation Optimisation for Rail Bridge: A Case Study From Dodson Road, Bunbury, Western Australia
Y. Arumugam, M.Old, & J. Thomas *11*

Early Specialist Contractor Involvement Enabling Alternative Design for Sustainable Dam Stabilisation
B. Brown, G. Webley, A. Hubaut, A. Vencer, & J. Rola *21*

Jet Grout Retention and Deep Tension Piles in Very Soft, Normally Consolidated Clay: Challenges From the Melbourne Arts Centre Redevelopment
J. Fetherston & C. Taylor *31*

Challenges in Construction of HS2 Diaphragm Wall Shafts and Portal (UK)
S. Kavanagh & N. Taylor *41*

Two-Tiered Sheet Pile Wall Systems: Design, Execution, and Field Performance
S.K. Paluri & S.K. Tan *56*

Pile Driving in Soft Ground and Mitigation Measures to Minimise Impact on Existing Infrastructure
G. Quigg, J. Zeerak, & D. Ungureanu *66*

Construction Installation Data: Using Measurement While Drilling (MWD) or Pile Driving Monitoring for Design and Quality Control/Assurance, Data Management, Data Presentation, AI, etc.

Challenges in Pile Foundation Design in Northland Allochthon
K. Lontzetidis, C. Ritchie, & K. Lentfer *74*

Smart Execution: Digital Integration and Quality Control for Diaphragm Wall and Barrette Delivery
J. Paouros & Z. Khan *83*

Designing and Constructing Safely and Effectively in Urban Environments, Including Working Platforms

A Critical Look at Working Platform Design
S. Buttling, D. Corke, M. Larisch, & S. Jacobs *94*

Developments, Innovations and Trends in: Research; Construction Equipment, Methods and Materials; Code Requirements; Foundations for Solar Farms; Safety

Sheet Pile Seal: A Locally Engineered Sheet Pile Sealant Solution
D. Cantali *106*

Helical Anchor Pullout Capacity in Sand Overlain By Clay: Experimental and Numerical Insights
S. Goodall, R. Merifield, C. Lloyd, J. Murphy, & Olivier Buzzi *108*

Geotechnical Design Challenges for Solar Farm Tracker Piles in Reactive Clays
S. Goodall *119*

Understanding the Influence of Tremie Embedment on Concrete Flow Mechanisms During Deep Foundation Construction
T. Mitchell, C. Barker, & C. Li *138*

Development of Regulatory Framework for the Design of Deep Foundations and Ground Improvement in New Zealand
A. Murashev, K. Saligame, N. Wharmby, & N. Lloyd *148*

Micropiled Precast Foundations for Energy Transmission Lines: A Practical Innovation Journey
B. Okumusoglu & M. Sentry *159*

Hybrid Grouting for Remediation of Taupo Control Gate, Waikato River
N. Townsend & R. Denny *168*

Installation of Large Diameter Steel Piles in Very High Strength Rock
M.Wilkinson & M. Johnson *178*

A Consolidated Earth Pressure Model for Geotechnical Stability Design of Embedded Cantilever Walls
C. Yuen, M. Cai, W. Liew, & C. Tan *184*

Ground improvement solutions for structural support and retention works

Design and Optimization of Olivier Inclusions for Residential Towers on Soft Ground in Auckland: 3D Finite Element Analysis and Field Validation
F. Yarmohammadi, K. Lontzetidis, & T. Donnelly *194*

Instrumentation, Load Testing, Non-Destructive Testing and Short-and Long-Term Monitoring

Design of Geogrid Reinforced Temporary Working Platforms for Tracked Plant - Insights From A Large-Scale Field Trial on Soft Lacustrine Clay
J. Klompmaker, L. Vollmert, C. Füger, & S. Vogt *205*

Pragmatic Use of Pile Testing Methods to Verify Driven Pile Capacity on Linear Infrastructure Projects
E. Smith & J. Slatter *215*

Downhole Magnetic Gradiometry for Estimating the Length of Existing Piles
J. Valencic & B. Mcpherson *231*

Seismic Design Considerations

Research Progress on Modular Construction Technology and Seismic Performance Evaluation for Generation III Nuclear Power Plant
W. Gong & D. Feng *242*

Structural and Geotechnical Design and Construction Solutions to Foundation Problems

Estimation of Installation Torque and Axial Ultimate Capacity of Screw Piles in Tropical Soils Using SPT Data
D.G.Yanez & D. Renosto *252*

Selecting Design Parameters From In-Situ Tests to Design Passive Piles
W.D. Guo *264*

Rate Aware Pile Design in Glaciogenic Silts: From Fabric to Serviceability
R.H. Kee, S. Terzaghi, & A. O'Sullivan *276*

A Systematic Approach to Foundation Selection for Remote Transmission Line Projects: The Investigative Drilling Method
M. Manafi, B. Juett, B. Evans, & M. Turner *287*

Fast-Track Pile Design and Construction for the Fitzroy River Bridge Replacement, Western Australia
H. Moore *300*

Automation in Geotechnical Engineering: AI-Enabled Foundation Design Workflow
W. Ng & H. Chow *314*

Converting Uncontrolled Fill Sites Into Controlled Engineered Fills Through Rapid, Cost-Effective, and Quantifiable Impact Rolling
R. Power, R. King, M. Clenton, & D. Avalle *324*

Mandurah Estuary Bridge Duplication – Sustainable Geotechnical Design
S.K. Tan, J. Mcilquham, & K. Chen *336*

Foundation and Retention Solutions in Geology Susceptible to Lateral Soil Movements Impacting Sensitive Wharf Structures
C. Taylor, E. Chong, & J. Fetherston *346*

Assessing the Impacts of Embankment Construction Over Soft Soil on an Adjacent Bridge
J. Thayalan & I. Tse *357*

Sustainability in Planning, Designing, Contracting and Construction

Risk Management Through Sustainable Temporary Working Platforms
J. Buckley, J. Kawalec, J. Cook, M. Bhawanin, & K.R. Zamara *367*

Sensitivity Analysis of Thermo-Mechanical Energy Pile Response Based on Dimensionless Form of Analytical Solutions
D. Perić & C.B. Acharige *375*

ASSESSMENT OF IMPACT ROLLING FOR GROUND IMPROVEMENT ON A SITE WITH VARIABLE SOIL CONDITIONS

Alireza Akoochakian, Senior Geotechnical Engineer, Kleinfelder Australia Pty Ltd, Adelaide, SA, Australia, +61 422 765 422, aakoochakian@kleinfelder.com
Phil Band, Principal Geotechnical Engineer, Kleinfelder Australia Pty Ltd, Newcastle, NSW, Australia, +61 452 392 692, pband@kleinfelder.com

ABSTRACT

Impact rolling is a ground improvement technique used to enhance the density and bearing capacity of soils, particularly for shallow foundation applications. This paper presents a case study of an impact rolling project carried out at a commercial development site in Marion, South Australia, where impact rolling was employed to improve the soil conditions for shallow footings. The site was underlain by a combination of fill material, soft to firm sandy/silty clay, with granular lenses. The objective was to provide a building pad capable of supporting shallow footings. This paper described the methodology used to assess the effectiveness of impact rolling, particularly on cohesive materials, and to determine the improvement in subgrade stiffness and settlement control. Pre- and post-treatment testing, including Cone Penetration Testing (CPT) and Dynamic Cone Penetrometer (DCP), was conducted to evaluate soil conditions before and after treatment. The results demonstrated that impact rolling improved the soil in granular zones, reducing settlement by up to 200 mm; however, in cohesive materials, such as clay and silt, the treatment showed limited effectiveness. The study concludes that while impact rolling is a viable method for improving ground conditions in certain soil types, its effectiveness is less reliable in fine-grained soils and may require supplementary measures for areas with poor responsiveness.

Keywords: impact rolling, ground improvement, shallow foundations, geotechnical investigation, cohesive materials

INTRODUCTION

Urban developments on previously filled land without Level 1 or 2 certification often face geotechnical challenges due to the variability and compressibility of existing subsurface materials. These issues are particularly critical when shallow footings are proposed, as they can lead to differential settlement and compromise structural integrity. In such cases, ground improvement becomes a key consideration in design and construction planning. Impact rolling has emerged as a practical and cost-effective technique to improve ground conditions for shallow foundation systems. It works by applying high-energy dynamic loads to densify loose or compressible soils, primarily targeting the upper few metres of the subsurface profile; however, its effectiveness varies significantly with soil type and conditions, and requires thorough assessment to ensure adequate performance.

This paper presents a case study from a proposed commercial development in Marion, South Australia, where impact rolling was adopted as the primary ground improvement technique. The goal was to assess its suitability in mitigating the risk of settlement under shallow footings. A combination of Cone Penetration Testing (CPT) and Dynamic Cone Penetrometer (DCP) testing was used to evaluate the subgrade conditions before and after treatment. This study aims to provide practical insight into the effectiveness of impact rolling across variable ground conditions, and to highlight lessons learned for future applications.

SITE DESCRIPTION AND GROUND CONDITIONS

Based on the Geological Survey of South Australia, published by the Department for Energy and Mining (map.sarig.sa.gov.au), the site is underlain by the Pooraka Formation and Holocene alluvial and fluvial sediments. A geotechnical investigation comprising 8 boreholes was undertaken to assess

 © Deep Foundations Institute 2026

the geology of the site and this revealed a variable subsurface profile. The upper 1 m comprised fill material, underlain by soft to firm sandy/silty clay with some granular lenses extending to depths of approximately 5 m. In most locations, this transitioned into stiff to very stiff sandy clay below 6 m depth.

In a few boreholes, loose to medium dense granular material was encountered between 1 and 6 m depth, suggesting heterogeneity in the depositional environment. Groundwater was encountered at around 5 m below ground level in four of the boreholes, further contributing to variability in ground conditions and influencing the selection and performance of ground improvement methods.

The client wished to avoid using deep foundations to keep costs down, so various ground improvement methods were considered. The selected treatment method—impact rolling—was proposed as a way to densify the fill and upper natural soils, aiming to achieve a minimum bearing capacity of 100 kPa to support the proposed shallow foundation.

GROUND IMPROVEMENT METHODOLOGY AND RESULTS

The site was divided into five distinct areas that has been identified as needing improvement based upon the building layouts and existing ground conditions. Impact rolling was implemented using a non-circular, four-sided roller capable of delivering dynamic loads through successive passes over the exposed subgrade. The process was monitored in real time, with induced surface settlements recorded after each pass.

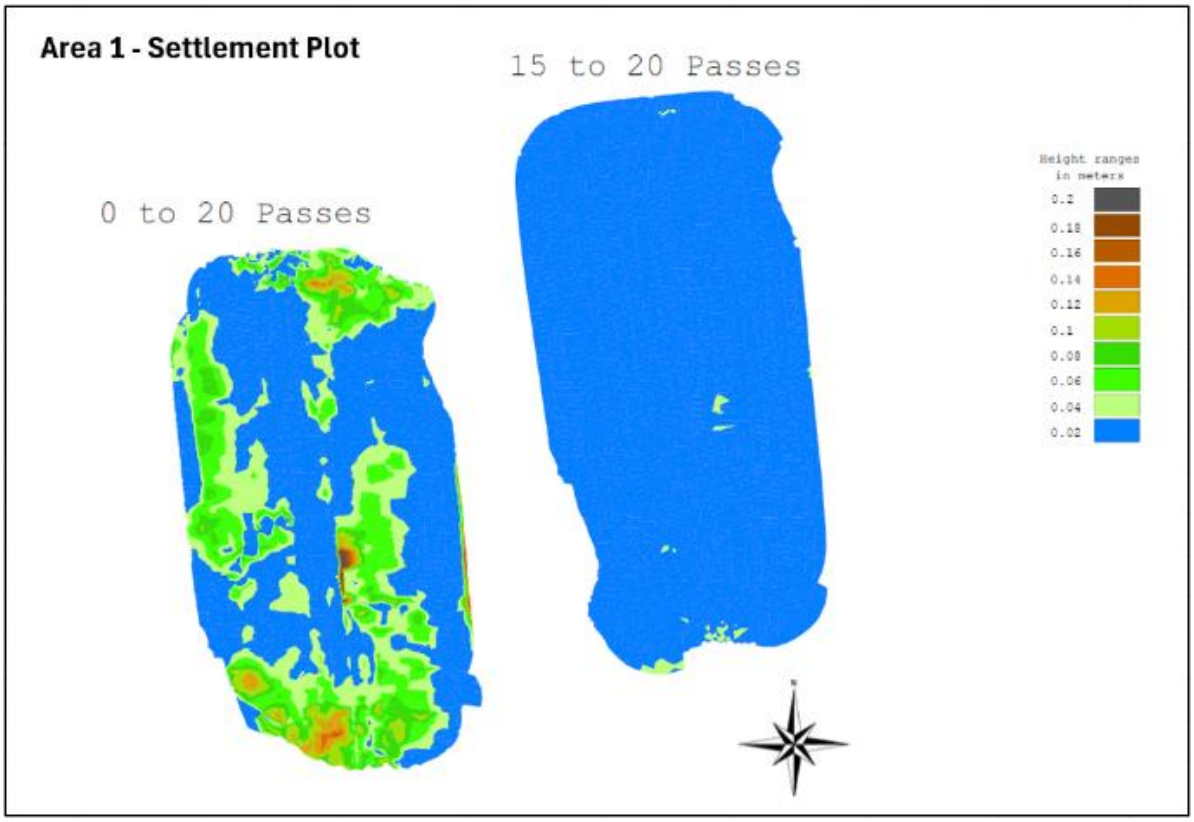
Rolling continued until the induced settlements reduced to negligible values (typically less than 5 mm) over five consecutive passes, which was taken as an indicator of soil stiffness improvement and completion of the rolling process in each area. Figure 1 illustrates the induced settlement profiles during and at completion of the impact rolling.

Ground improvement works were carried out across five treatment areas using impact rolling. The process was implemented in increments of five passes and continued until surveyed settlement measurements indicated negligible incremental movement. The number of passes and corresponding settlement measurements for each treatment area are summarised in Table 1.

Table 1. Summary of Impact Rolling Results

Area	Number of Passes	Maximum Settlement (mm)	Minimum settlement (mm)	Average settlement before the last 5 passes (mm)	Average settlement in the last 5 passes (mm)
Area 1	20	200	20	14	<5
Area 2	30	200	20	91	<5
Area 3	20	200	20	73	<5
Area 4	20	200	20	47	<5
Area 5	20	200	20	90	<5

 © Deep Foundations Institute 2026



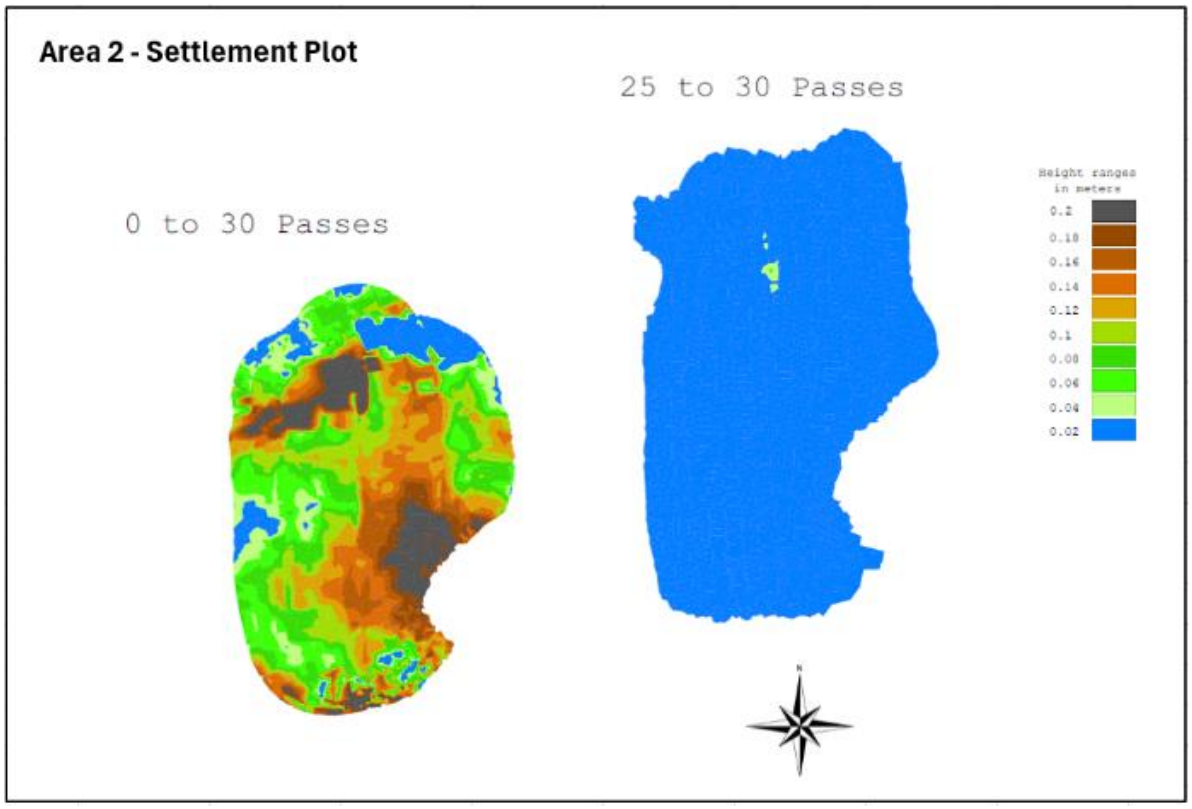
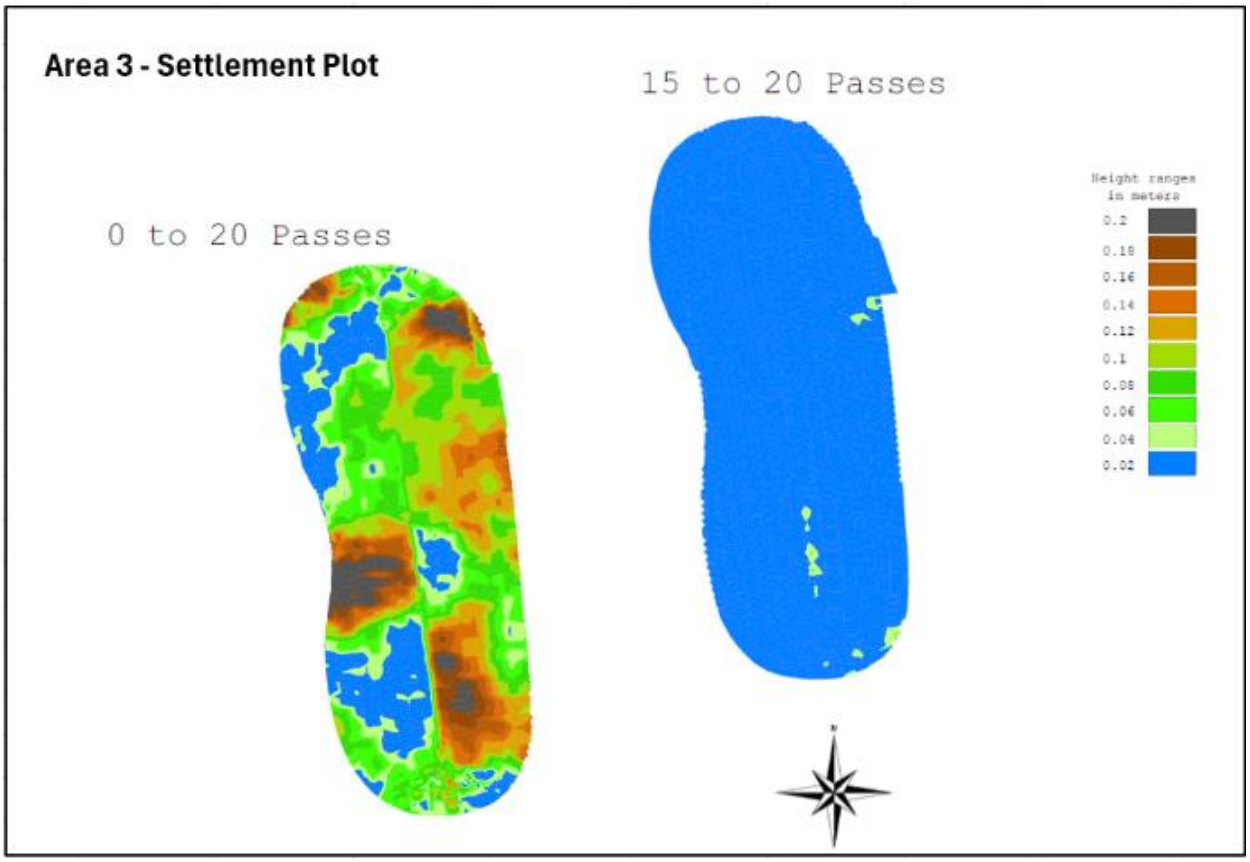


Fig. 1. (cont.)

 © Deep Foundations Institute 2026



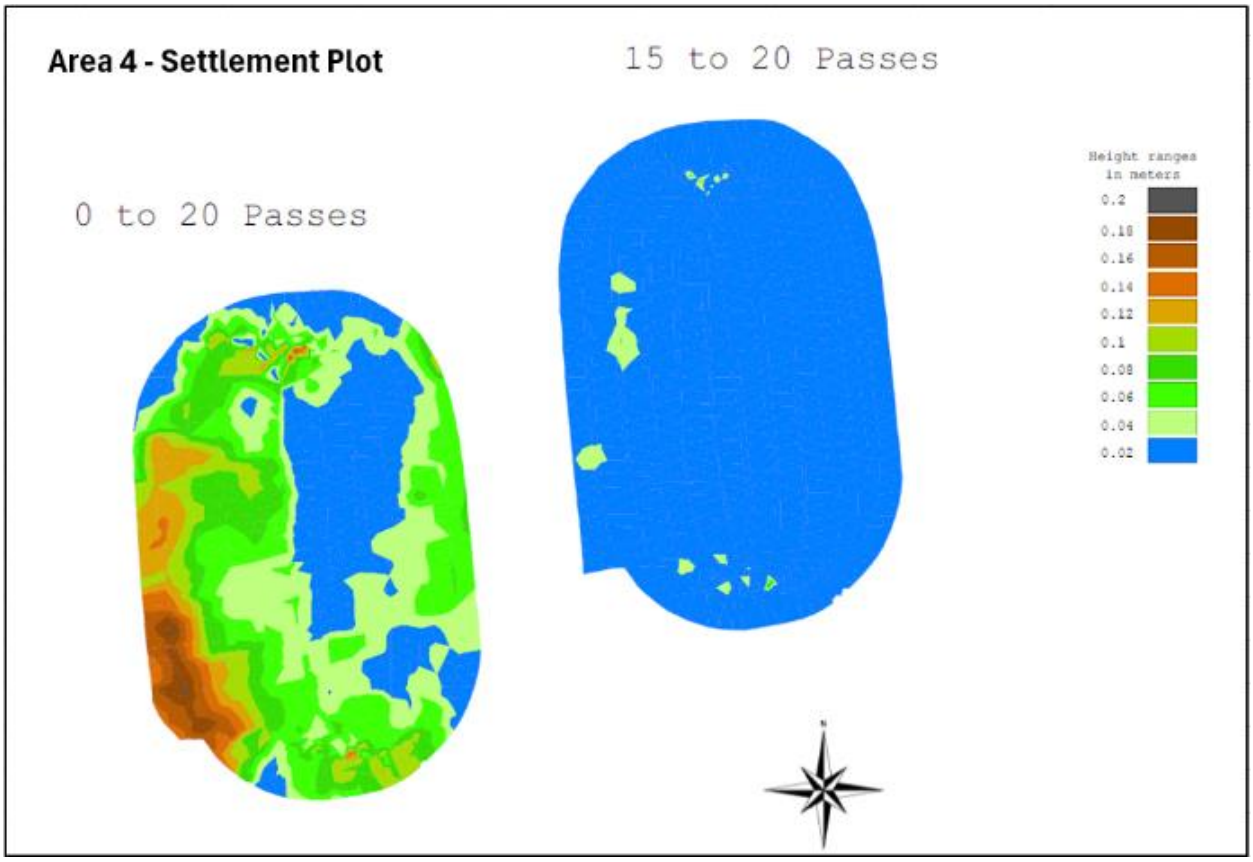


Fig. 1. (cont.)

 © Deep Foundations Institute 2026

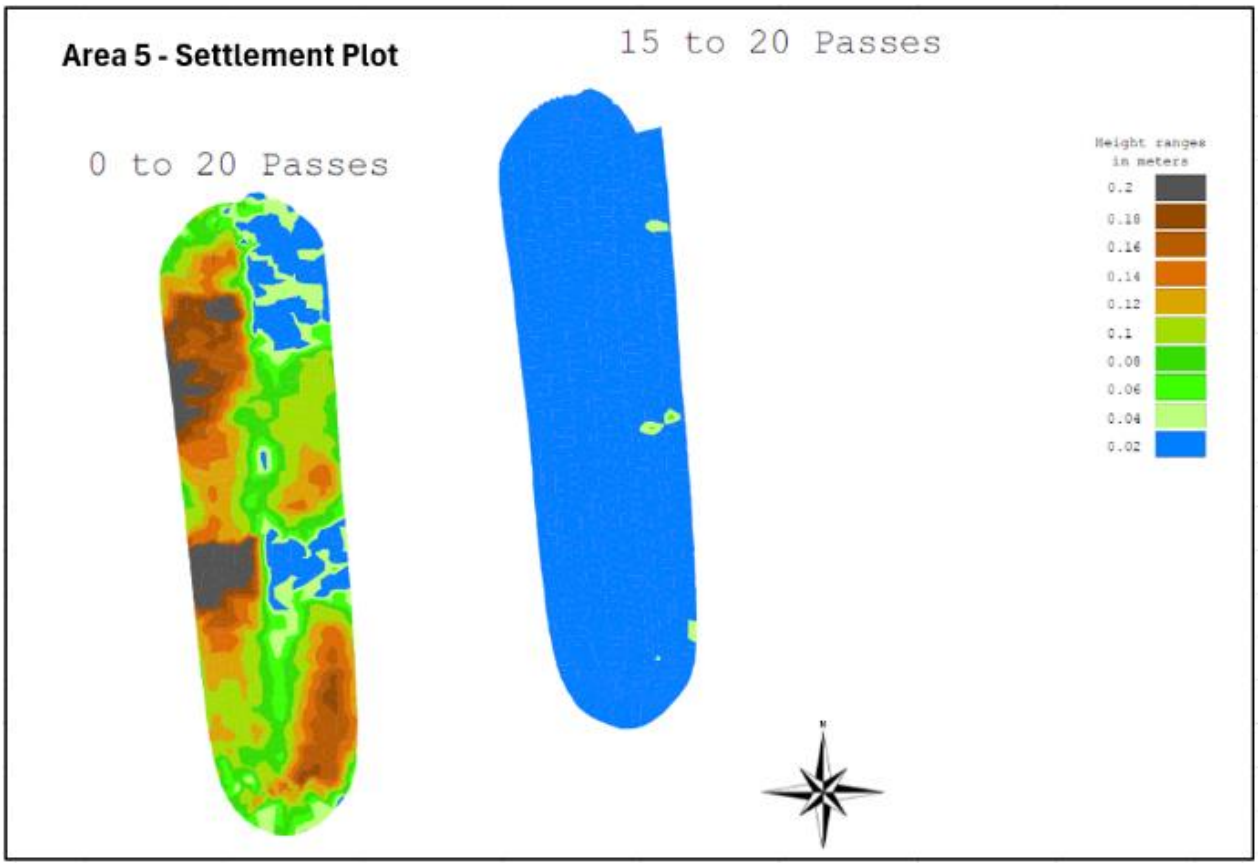


Fig. 1. Settlement Plot - Impact Rolling

PRE AND POST TREATMENT TESTING RESULTS AND ANALYSIS

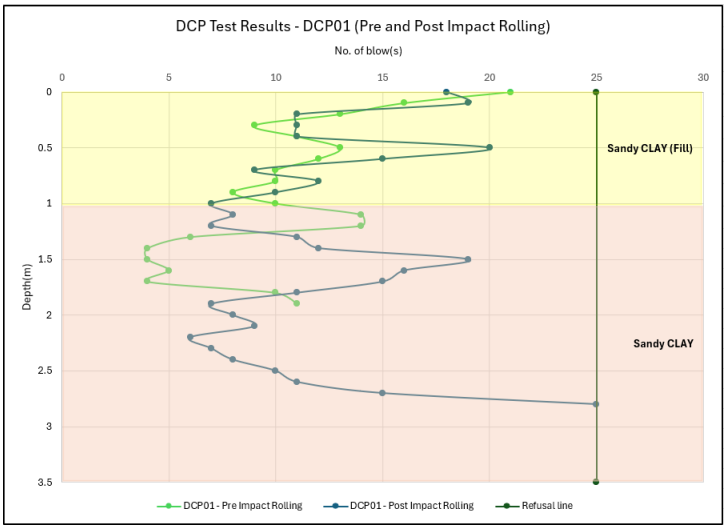
Pre- and post-treatment CPT and DCP tests were conducted at identical locations to assess the changes in soil resistance and verify the effectiveness of the treatment.

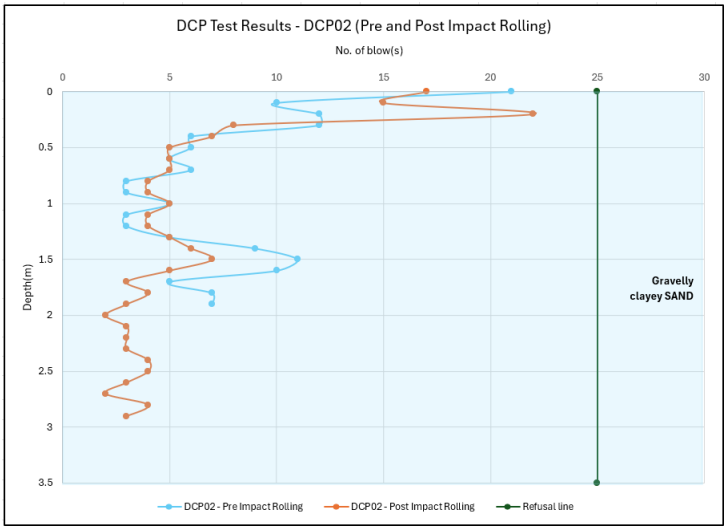
A total of 11 Dynamic Cone Penetrometer (DCP) tests and seven Cone Penetration Tests (CPTs) were conducted both before and after the impact rolling activities. Each DCP test was carried out to a depth of 3 m to assess the extent and depth of ground improvement.

The DCP results indicated increases in penetration resistance, particularly within the upper 1.5 to 2.0 m of the soil profile. Similarly, the CPT data showed increases in cone resistance values at shallow depths (approximately 0.6 to 1.4 m), confirming that the influence of the impact rolling was largely confined to the near-surface layers.

Field observations and data from the heatmap settlement survey revealed surface settlements ranging from 20 mm to 200 mm across the site, with an average settlement in the range of 60–70 mm during the rolling process. Areas underlain by greater thicknesses of granular soils exhibited greater settlement and more pronounced improvement in response to impact energy, while zones consisting primarily of fine-grained soils (clays and silts) showed minimal response.

 © Deep Foundations Institute 2026





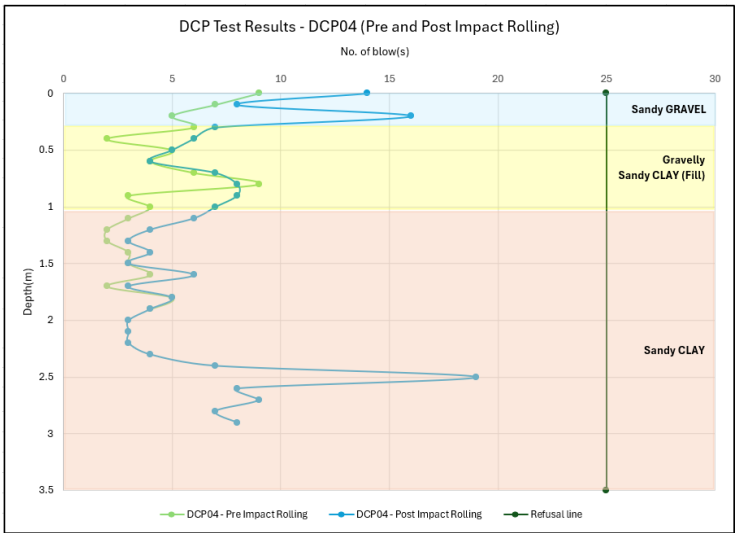
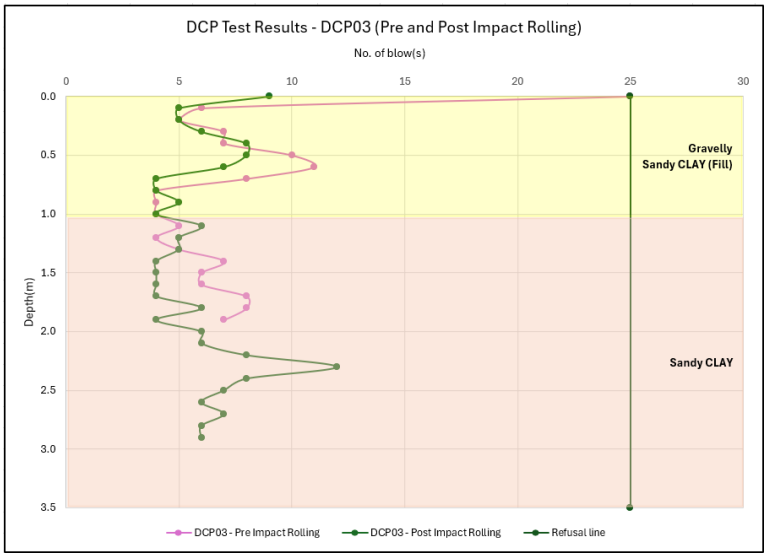
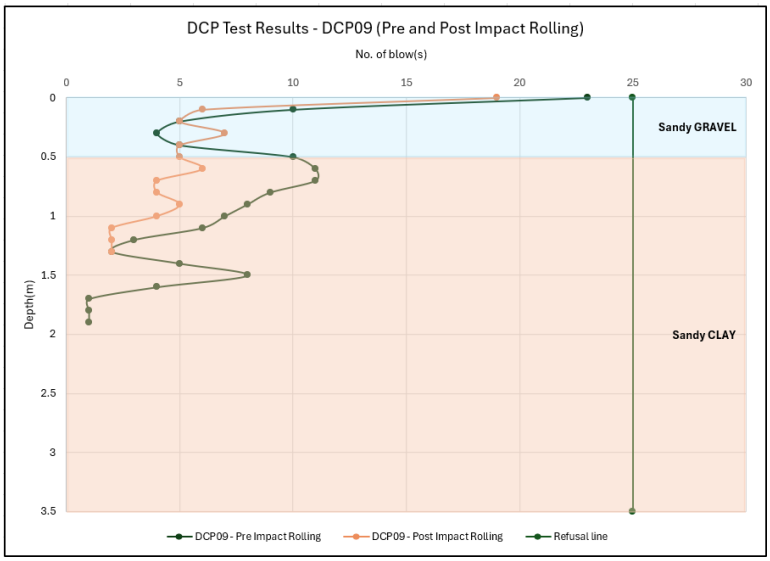


Fig. *2.* (cont.)

 © Deep Foundations Institute 2026





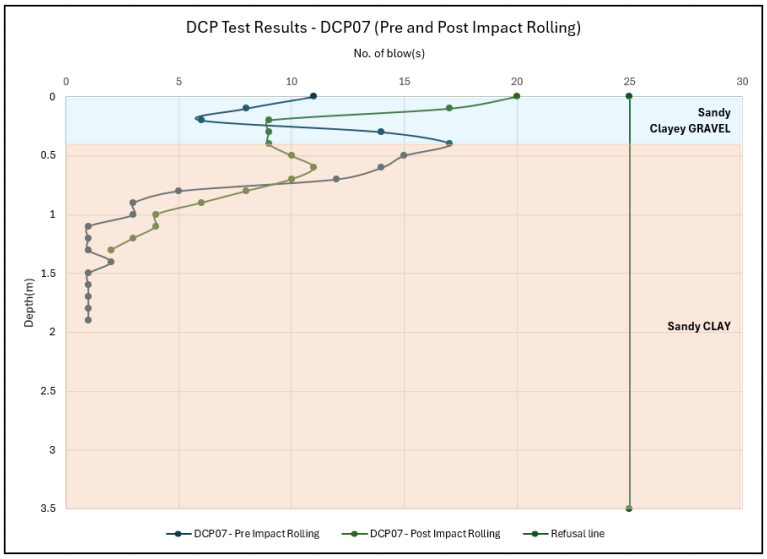


Fig. 2. Summary of DCP results Pre and Post Impact Rolling

 © Deep Foundations Institute 2026

Soil profiles at all CPT locations were interpreted using the Robertson chart and analysed with CPeT-IT software. The CPT results are summarised in Table 2.

Table 2: Interpreted Soil Profile Post Impact Rolling

Material	Depth of the base of strata (m)						
	CPT01	CPT02	CPT03	CPT04	CPT05	CPT06	CPT07
Loose to Medium Dense SAND/ Clayey SAND/ Silty SAND	0.1	0.3	4.4	0.3	0.6	0.2	0.3
Firm to Stiff Sandy SILT/SANDY CLAY	0.4	1.0	-	1.2	1.4	1.2	0.6
Soft to Firm Sandy SILT/SANDY CLAY	4.05	6.27	4.97	7.08	5.88	4.86	-
Loose to Medium Dense SILT/SANDY CLAY	-	-	-	-	-	-	2.9
Soft to Firm Sandy SILT/SANDY CLAY	-	-	-	-	-	-	5.27
Total Depth	4.05	6.27	4.97	7.08	5.88	4.89	5.27

The post-treatment data confirmed that impact rolling was most effective in zones containing granular soils, where compaction could increase density and stiffness. Conversely, in clayey or silty areas with lower permeability and higher plasticity, the improvement was limited. This was attributed to the inability of fine-grained soils to dissipate pore pressure and rearrange particles effectively under dynamic loading.

The depth of influence was generally limited to the upper 2 m, with diminishing effects observed below this level. As such, impact rolling proved useful as a shallow ground improvement method but was not sufficient in addressing deeper compressible layers or highly plastic materials.

DISCUSSION

A comparison was undertaken between the post-impact rolling CPT interpreted logs and the pre-treatment geotechnical investigation data (including bore logs and CPT logs) to assess changes in soil consistency and density. The following observations were identified:

- Pre-Treatment Bore Logs: The bore logs indicated the presence of soft to firm cohesive materials within the upper 3 m, supported by low Standard Penetration Test (SPT) blow counts and Pocket Penetrometer (PP) readings.
- Pre-Treatment CPT Data: CPT data collected before treatment supported the observed post-treatment improvements, with noticeable increases in cone resistance (qc) and friction ratio (Fr%) following impact rolling.
- Post-Treatment CPT Logs: The interpreted CPT logs showed a slight improvement in soil consistency at shallow depths, evidenced by increased qc and Fr% values. In most locations, soil conditions improved from soft to firm to firm to stiff consistency within the top 0.6–1.4 m.

Overall, the comparison indicates a modest improvement in shallow subgrade conditions following impact rolling; however, due to the continued presence of localised soft cohesive zones, further treatment such as local excavation and replacement with engineered fill or stabilised sand was recommended in those areas.

 © Deep Foundations Institute 2026

The findings highlight the variable effectiveness of impact rolling, driven primarily by soil type. For sites with heterogeneous fill profiles, a uniform ground improvement outcome is difficult to achieve without supplemental treatment. Additional measures such as excavation and replacement were recommended in softer zones where impact rolling alone was inadequate.

Routine DCP testing at each footing location was also advised post excavation to confirm the bearing capacity of the improved subgrade, ensuring consistency in foundation performance across the site.

Proof rolling was carried out following the completion of impact rolling to evaluate subgrade stability. The subgrade was prepared by excavating the existing surface to the design level, followed by impact rolling. Proof rolling was conducted using a fully loaded truck with a total weight exceeding 15 tonnes to identify signs of rutting, cracking, or uneven surface deformation. The following observations were made:

- The proof roll revealed vertical deflections greater than 5 mm, with rutting observed in the western footprint of the site. These locations were marked for further remedial action. Additional DCP testing was then undertaken at these locations to profile the depth of soft spots and unsuitable material.
- Remedial measures included excavating the soft spots to the profiled depth and replacing the material with suitable engineered fill (e.g., PM2/20), backfilling in layers not exceeding 300 mm of loose thickness, and compacting to the specified dry density.

It was further recommended that subgrade conditions be monitored both before and during the construction of the upper pavement layers. Should any signs of softening, erosion, or instability be observed—particularly after periods of heavy or prolonged rainfall—additional assessment and remedial action would be required.

DCP testing at each footing location was also advised after excavation to confirm the bearing capacity of the soil at each specific location.

CONCLUSION

Impact rolling provided measurable improvement in shallow ground conditions, particularly in granular zones, enabling the use of shallow footings in most areas of the site. However, its limited effectiveness in fine-grained soils necessitated additional treatment in specific locations.

This case study underscores the importance of detailed pre- and post-treatment testing and highlights the need for adaptive design strategies when dealing with heterogeneous fill conditions. Impact rolling can be a valuable part of a ground improvement strategy, but its application must be tailored to site-specific subsurface conditions and validated after completion with additional remedial works specified where required.

The close collaboration between the managing contractor and the geotechnical and structural engineers ensured that project objectives were achieved in that a building platform suitable for the proposed construction was established without the additional cost and time required for the construction of deep foundations.

REFERENCES

South Australian Resource Information Gateway (SARIG) - https://map.sarig.sa.gov.au – 04/03/2024
Nature Maps - NatureMaps (environment.sa.gov.au) - 04/03/2024
Standards Australia (2007), AS1170.4-2007, Structural Design Actions, Part 4: Earthquake Actions in Australia
Standards Australia (2017), AS1726-2017, Geotechnical Site Investigations
Standards Australia (2007), AS3798-2007, Guidelines on Earthworks for Commercial and Residential Developments

 © Deep Foundations Institute 2026

Standards Australia (2009), AS2159-2009, Piling Design and Installation
Standards Australia (2017), AS1289-2017, Methods of Testing Soils for Engineering Purposes
Terzaghi, K., Peck, R.B., & Mesri, G. (1996). Soil Mechanics in Engineering Practice (3rd ed.). John Wiley and Sons, New York.
Meyerhof, G.G. (1965). “Shallow Foundations.” Journal of the Soil Mechanics and Foundations Division, ASCE, 91(SM2)

 © Deep Foundations Institute 2026

PILE FOUNDATION OPTIMISATION FOR RAIL BRIDGE: A CASE STUDY

Yogeshwaran Arumugam, Lead Geotechnical Engineer, Worley Consulting, Australia, yogeshwaran.arumugam@worley.com
Matthew Old, Principal Structural Engineer, Worley Consulting, Australia, matthew.old@worley.com
Joyis Thomas, Principal Geotechnical Engineer, Worley Consulting, Australia, joyis.thomas@worley.com

ABSTRACT

This paper presents a case study on the design of a replacement rail bridge along the South West Mainline at Dodson Road crossing, Bunbury, Western Australia. The site posed geotechnical challenges, including underlying acid sulphate soils and a ~3 m thick, very dense sand layer at the East Abutment, requiring a tailored foundation solution. A comprehensive geotechnical investigation guided the evaluation of suitable piling options under the site's geotechnical and environmental constraints. Initially, steel tubular piles were proposed to mitigate acid sulphate soil handling issues associated with CFA/bored piling. Considering the commercial and technical aspects, a comparative analysis was undertaken between 762 mm steel tubular piles and 400 mm square precast concrete piles, assessing axial and lateral load capacities as well as pile drivability. The very dense sand layer overlying a clay layer presented significant risks for driving concrete piles, prompting a trial piling program to evaluate performance in situ. The trial pile results confirmed that concrete displacement piles could effectively penetrate the very dense sand layer without compromising structural integrity, offering a viable, cost-effective and constructible solution. The project ultimately adopted less expensive driven concrete displacement piles, supported by performance monitoring and load testing to ensure compliance with design criteria. This case illustrates how early-stage investigation, comparative design evaluation, additional geotechnical investigation and trial implementation can inform optimal pile selection, mitigate drivability risks, and support cost-effective infrastructure outcomes. The findings contribute to best practices in geotechnical engineering for transport projects, particularly where environmental considerations and challenging soil conditions exist.

Keywords: displacement piles, geotechnical investigation, acid sulphate soils, pile drivability

INTRODUCTION

The Dodson Road Bridge Line 2 is a non-electrified, single-track narrow-gauge section of the South West Mainline, currently serving the Australind train operated by Transwa between Perth and Bunbury. The existing structure is a four-span timber bridge featuring a ballasted timber deck supported by timber piers and abutments. Due to the aging condition of the foundation, the bridge has been identified for replacement as part of ongoing maintenance efforts. An initial geotechnical investigation was undertaken to assess the subsurface conditions and inform the foundation design for the replacement structure. The investigation provided critical insights into the ground profile and geotechnical parameters necessary for foundation selection and design development. This paper outlines the design evaluation process, including the selection of pile types and the implementation of pile testing to validate the design assumptions. The study highlights the integration of geotechnical data into structural design and the importance of field testing in ensuring the reliability, constructability and performance of the proposed foundation system.

SOIL CONDITION

The subsurface at the project site comprises rail embankment fill overlying alluvial deposits, underlain by the Guildford Formation. Initially, two CPTs were conducted at both the East and West Abutments, followed by a borehole investigation at the East Abutment to calibrate the CPT profiles. However, the borehole data from the East Abutment did not correlate well with the CPT traces obtained at the West Abutment.

 © Deep Foundations Institute 2026

Due to the high cost of mobilising a borehole drill rig, the project team decided to carry out additional CPT investigations prior to installing the production piles, aiming to reduce the risk of early refusal or encountering adverse ground conditions. Consequently, eight additional CPTs were completed at the West Abutment and three at the East Abutment before piling commenced. Although these additional CPT results were not plotted in the ground model as shown in Fig. 3, they were considered in the interpretation of the ground profile.

CPT results from the West Abutment show alternating layers of clay and sand, mostly medium dense sandy layers with cone resistance around 10 MPa. In contrast, CPT traces from the East Abutment reveal very dense sandy layers only about 20 m away, especially between 2 mRL and -5 mRL, with cone resistance around 30 MPa. The CPT profiles for both abutment areas are shown in Fig. 1 and Fig. 2 below. The interpretated ground model shown in Fig. 3.

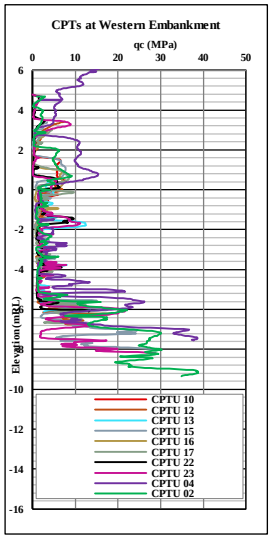


Fig. 1. CPT testing at West Abutment

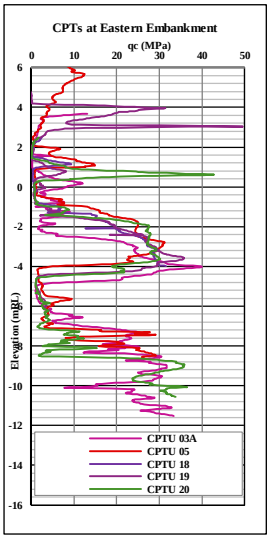


Fig. 2. CPT testing at East Abutment

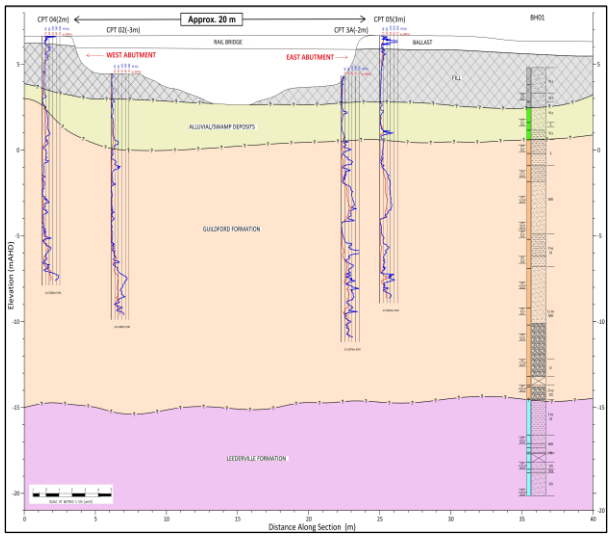


Fig. 3. Inferred ground model, based on initial geotechnical investigation

ACID SULPHATE SOILS

The Guildford Formation soils range from fine grained clays and silts near riverbanks to coarse grained sands and gravels in higher-energy channels, with some organic-rich sediments present in low-energy environments. To assess the potential for Acid sulfate soils (ASS), a combination of rapid field tests and detailed Chromium Reducible Sulfur (CRS) laboratory analyses were undertaken and are shown in Fig. 4 and Fig. 5. Field results showed extreme reaction rates and significant pH drops, indicating strong Potential Acid Sulfate Soil (PASS). CRS testing confirmed the presence of ASS in nearly all selected samples, with sulfide levels exceeding the DWER (2015a) action threshold of 0.03% S. Given the confirmed presence of ASS, careful management during construction is essential to mitigate environmental risks. As bored and CFA piling could disturb ASS layers and trigger acid generation, displacement or driven piles are recommended as more suitable foundation options.

DESIGN OPTIMISATION

The original design proposed five 762 mm diameter steel open ended driven tubular piles (≈16 m long, 2050 kN ultimate capacity, shaft-resistance-driven), but field ΔpH values and CRS results indicate a strongly acidic, highly corrosive soil environment with both immediate and long-term durability risks for steel, and pre-augering spoil would also require regulated disposal or treatment; therefore, the contractor's proposal to adopt concrete piles is a more suitable and lower-risk solution for these ground conditions.

 © Deep Foundations Institute 2026

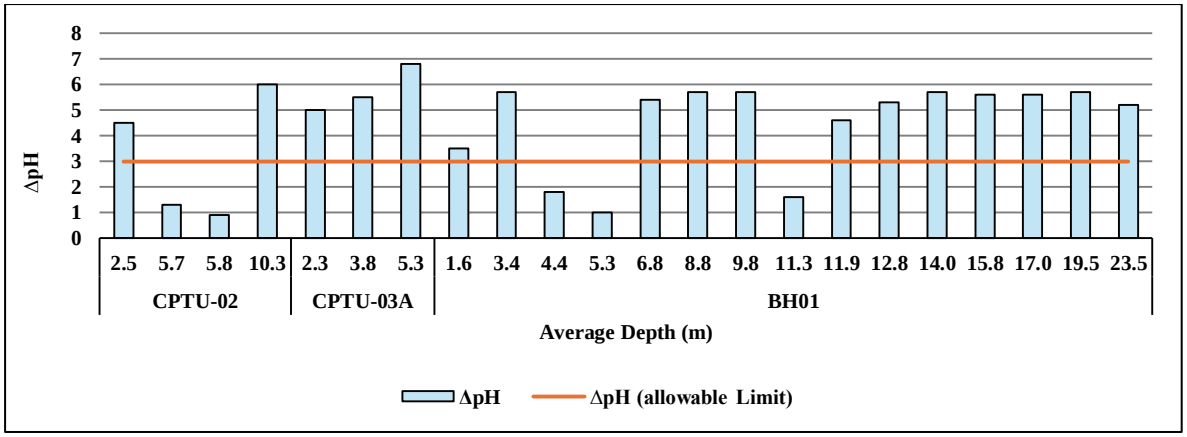


Fig. 4. Soil field pH test results

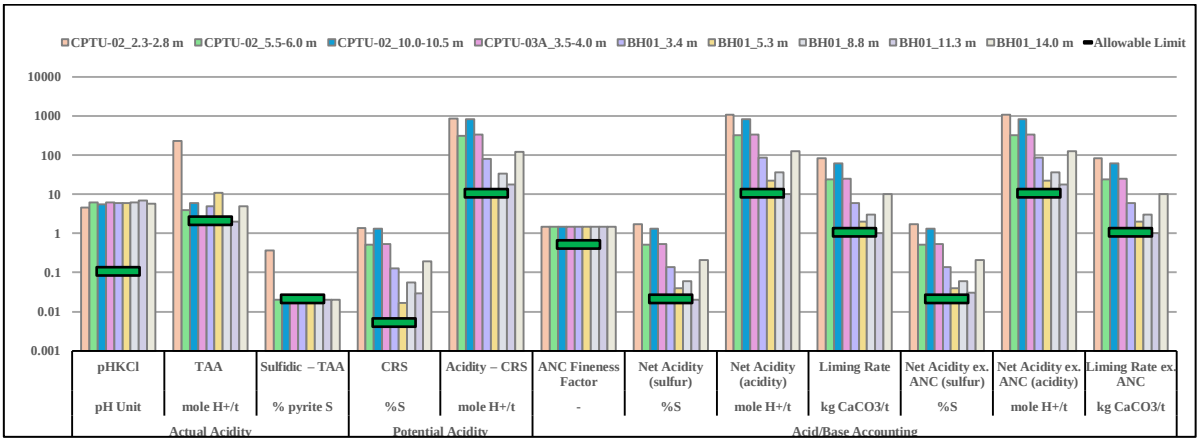


Fig. 5. Acid sulfate soil CRS suite analyses results

The contractor proposed using 400 mm square precast concrete driven displacement piles as a practical and cost-effective alternative, and the client accepted this option. The design team confirmed the structural adequacy of the change, and a third-party durability consultant verified that concrete piles are suitable for acid sulfate soil conditions. In these environments sulfate-resistant cement is preferred because increased cover alone is not enough, and standard reinforcing steel is generally acceptable when placed in durable low-permeability concrete.

The revised design replaced the five steel piles at each abutment with fourteen 400 mm square precast concrete piles, each approximately 13 m in length and designed for a factored load of 870 kN, mobilising both shaft friction and end-bearing resistance. The final pile arrangement is shown in Fig. 6 below.

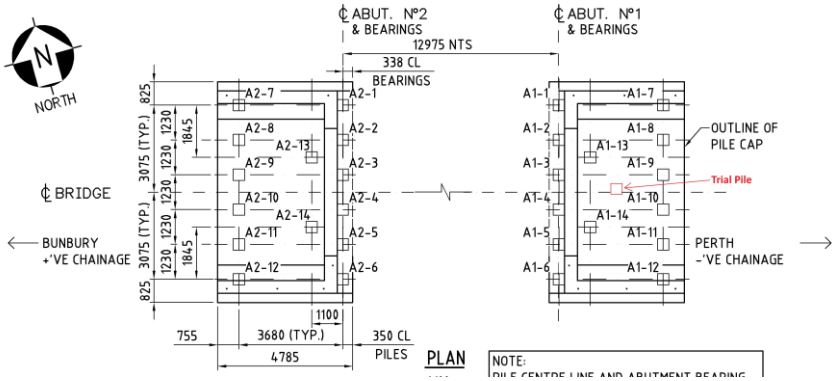


Fig. 6. Pile arrangement of precast concrete piles

 © Deep Foundations Institute 2026

AXIAL PILE CAPACITY BASED ON FHWA METHOD

The ultimate axial capacity of the concrete piles was calculated using the FHWA method using A-Pile 2023 version 10.5. For tension loading, the ultimate capacity was conservatively taken as 80% of the calculated compression shaft capacity. A geotechnical strength reduction factor (ϕ_g) of 0.75 was applied to the ultimate axial compression and tension capacity values to derive the design capacity values to satisfy limit state design as per Australian Standard AS 2159-2009 Piling - Design and Installation.

Pile capacities for the East and West Abutments were assessed separately because the West Abutment is underlain by weaker soil strata compared to the East. At the East Abutment, pile driving was more difficult due to a very dense sand layer overlying clay. For the West Abutment, a minimum toe level of RL –9.3 m was adopted to meet the 1160 kN design load, and this toe depth has considered the project's scour requirements. A comparison of measured capacities from CAPWAP analyses with predicted values and the required design capacities is presented in Fig. 7.

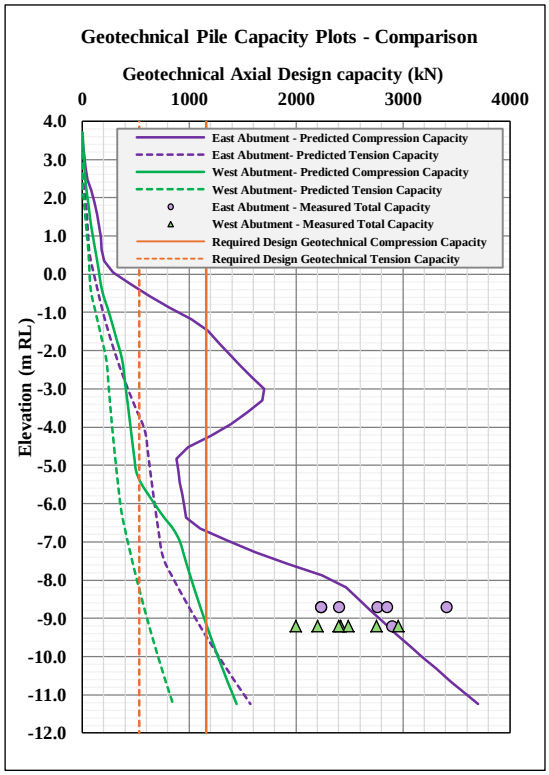


Fig. 7. Geotechnical pile capacity plots

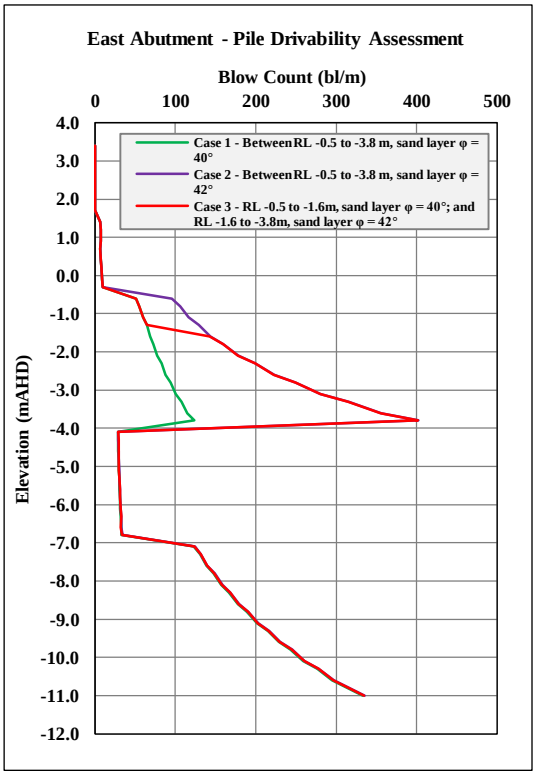


Fig. 8. Comparison of SRD profiles for varying soil layer cases

PILE DRIVABILITY ASSESSMENT

A pile drivability assessment was undertaken for the East Abutment piles to verify that the proposed concrete piles could be installed using the selected hammer without overstressing the piles or causing structural damage. The analysis was performed in GRLWEAP (2014), based on the contractor-proposed Junttan HHK7S hydraulic hammer. For this project, the Soil Resistance to Driving (SRD) was estimated using the standard setup approach incorporated in the GRLWEAP program. A preliminary hammer drop height of 700 mm was adopted for the drivability assessment, although it is noted that delivered energy may vary for production piles.

For the East Abutment, three scenarios were evaluated in the drivability assessment to account for potential variations in the strength of the very dense sand layer between RL -0.5 m and RL -3.8 m, with each case defined by distinct geotechnical parameters as below.

- Case 1: Sand layer from RL -0.5 to -3.8 m with an internal friction angle φ = 40°.
- Case 2: Sand layer from RL -0.5 to -3.8 m with φ = 42°.
- Case 3: Sand layer from RL -0.5 to -1.6 m with φ = 40° and from RL -1.6 to -3.8 m with φ = 42°.

The sensitivity analysis shown in Fig. 8 indicates that the piles are drivable in the East Abutment under Case 1 conditions. However, for Cases 2 and 3, driving through the very dense sand layer may be challenging and could potentially require predrilling. Given that even minor variations in soil strength could affect driveability, it was decided to install a trial pile. Continuous monitoring of driving parameters was recommended to ensure both pile integrity and successful installation to the required depth.

TRIAL PILE

A 400 mm square precast concrete trial pile was installed at the East Abutment using a Junttan piling rig with an HHK7S hammer. Dynamic testing was carried out with Pile Dynamics' Pile Driving Analyzer (PDA) in accordance with the Australian Piling Code AS 2159-2009, at both End of Drive (EOD) and during a restrike (RST) conducted the following day.

The trial pile comprised a 12 m bottom segment and a 6 m top segment, joined with a mechanical splice cast into each segment. Driving continued until the target toe level was achieved at a penetration depth of 14.5 m below the platform level RL 5.0 m, corresponding to a pile toe level of RL -9.5 m.

During driving, the drop height was generally 800 mm, higher than that adopted for the production piles. For the RST, the drop height was increased to 1500 mm to assess maximum stresses in the pile. It is noted that although the trial pile was located within the East Abutment footprint, it does not form part of the design production piles. The PDA data was analyzed using the Case Pile Wave Analysis Program (CAPWAP) to estimate mobilised shaft and end bearing resistances. The CAPWAP results are summarised in Table 1 and the stress levels induced during testing are presented in Table 2.

Table 1. Summary of trial pile results

Pile tested at	Driven Depth (m)	Design Load (kN)	Geotechnical Strength Reduction Factor (ϕ_g)	Required Ultimate Capacity (kN)	Mobilised Total Resistance (kN)	Mobilised Shaft Resistance (kN)	Mobilised Base Resistance (kN)	Mobilised End Bearing (MPa)
EOD	13.25	870	0.75	1160	2701	470	2231	13.9
RST	14.5	870	0.75	1160	4500	1539	2962	18.5

Table 2. Summary of stresses induced in the pile during testing

Pile tested at	Pile Size (mm)	Age of Pile at Test (days)	Design Concrete Strength (MPa)	Estimated Strength at Test (MPa)	Max. Allow. Comp. Stress (MPa)	Max. Allow. Tens. Stress (MPa)	Measured Max Comp. Stress (MPa)	Measured Max Tens. Stress (MPa)
EOD	400	100+	65	80	64	7.9	40.5	5.6
RST	400	100+	65	80	64	7.9	31.9	7.9

The trial pile test results at the East Abutment indicate that unfactored mobilised total resistances of 2701 kN (EOD) and 4500 kN (RST) were achieved at toe levels RL -8.25 m and RL -9.5 m, respectively. These values exceed the required geotechnical ultimate capacity of 1160 kN. Additionally, the induced pile stresses during driving remained within allowable limits, ensuring structural integrity throughout installation. The test also confirmed that no pre-drilling was required for production piles at the East Abutment, simplifying the construction process and improving efficiency.

Based on the test results, the production piles were selected as 15 m long, constructed and transported to the site as a single continuous length.

DYNAMIC TEST ASSESSMENT

A total of fourteen piles were installed at each abutment, with blow counts recorded during installation for all piles. PDA testing was performed on seven piles at each abutment, and the results are summarised in Table 3. The RST associated with the PDA testing was conducted the day after installation for most piles, except for A1-P2 and A1-P12, which were tested two days after installation.

Table 3. Summary of production pile test results

CAPWAP Results	Unit	East Abutment							West Abutment						
		A1-P1	A1-P2	A1-P3	A1-P4	A1-P5	A1-P6	A1-P12	A2-P1	A2-P2	A2-P3	A2-P4	A2-P5	A2-P6	A2-P12
Pile Embedment	m	13.5	13.5	13.5	13.5	13.5	13.8	13.8	14.2	14.2	14.1	14.1	14.1	14	14
Avg. Shaft quake	mm	1.8	5	3	4	5	4	3	3.5	4	5	4	5	5	1.5
Toe Quake	mm	4.9	7.4	8.8	8.3	6.5	6.4	3.5	6.9	7.1	8.6	6.5	8.6	6.1	5.3
Avg. shaft smith damping	s/m	1	1.2	0.64	0.59	0.6	0.83	0.8	0.17	0.62	0.64	0.63	0.39	0.95	1
Top smith damping	s/m	0.48	0.3	0.42	0.63	0.7	0.4	0.78	0.66	0.55	0.77	0.77	1	1.1	0.6
CAPWAP match quality	-	2.69	2.02	2.07	2.16	2.18	2.37	2.13	3.12	2.5	2.58	2.75	3.25	2.8	2.62
Max. Transferred Energy	kJ	30.7	32.2	44.7	34.7	27.5	30.5	29.1	30.9	29.4	32.1	31.4	34.1	21.4	28.4
Top Compressive Stress	MPa	22.1	22	28.7	24.3	20.9	20.5	22.1	22.6	21.8	22.8	23.9	22.8	17.2	22
Max. Compressive Stress	MPa	24.9	24.4	31.2	27.2	22.9	23.6	26	23.1	24.2	22.8	23.9	24.7	19.5	24.5
Max. Tensile Stress	MPa	-2.22	-1.11	-1.88	-2.5	-2.47	-3.04	-3.52	-2.23	-2.28	-2	-2.52	-2.57	-1.74	-2.22
Ultimate Capacity	kN	2235	2235	2760	2403	2852	2900	3408	2957	2420	2200	2489	2400	2000	2757
Shaft Capacity	kN	1189	1093	1523	1363	1563	1105	1427	1395	1464	1320	1351	1263	1138	1252
Toe Capacity	kN	1046	1143	1237	1040	1289	1795	1980	1563	956	880	1138	1137	862	1505
Observed Final Set	mm	6.0	2.0	2.0	2.0	1.0	1.0	0.5	1.0	2.0	4.0	2.0	2.0	2.0	0.1

Comparison Between Predicted and Measured Blow Counts

The predicted blow counts for all three cases at the East Abutment are shown in Fig. 8, with measured blow counts presented in Fig. 10. All fourteen piles exhibit a broadly consistent trend, highlighting a distinct very dense sand layer between RL -0.5 m and -3.8 m. The trial pile records relatively lower blow counts due to higher hammer drop heights, approximately 800 mm for EOD and 1500 mm for RST when compared with 500 to 600 mm for the production piles.

Densification of the sand layers within this interval varies across the East Abutment, likely caused by sand layers being squeezed through softer strata, although no definitive explanation has been established.

Overall, Case 1 of the predicted model aligns well with measured blow counts from the production piles. CAPWAP analysis shows match quality values between 2.0 and 3.3 for all piles, indicating the test results are typically considered reliable.

Compressive and Tensile Stresses

During design, GRLWEAP predicted compressive stresses of about 28 MPa and tensile stresses between 1.7 MPa and 10.8 MPa for a 700 mm drop height. To reduce the risk of tension-induced damage, it was recommended to lower the drop height after trial driving, and a pile cushion was provided to further control driving stresses.

Table 2 indicates that the maximum tensile stress recorded during both EOD and RST testing was 5.6 and 7.9 MPa, which aligns well with the initial predictions. The maximum compressive and tensile stresses observed during PDA testing for the East and West Abutments, along with the corresponding CAPWAP-calculated stresses, are presented in Fig. 9 and Fig. 11. These results confirm that the stress levels remained well within the allowable limits specified in AS 2159-2009.

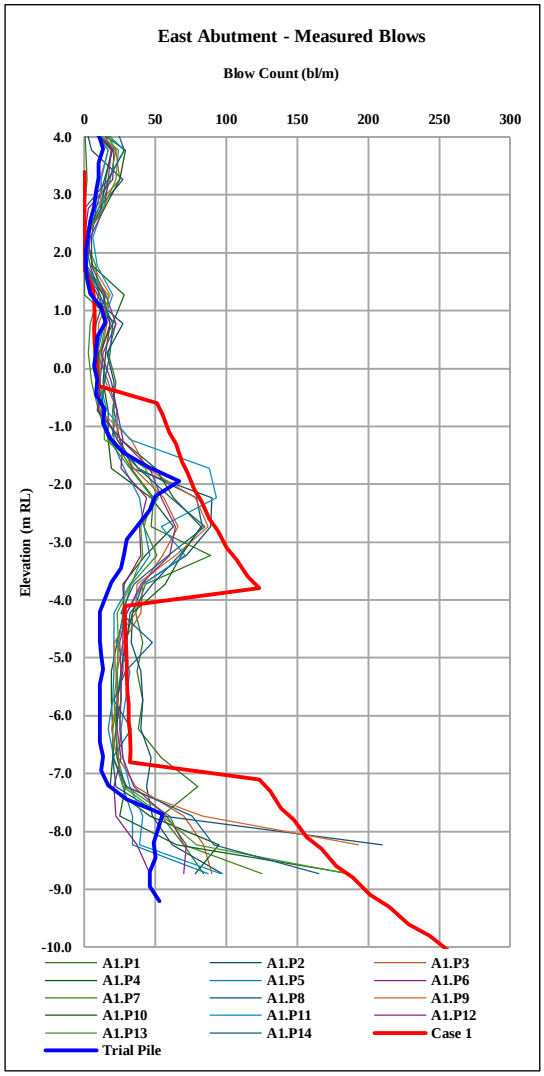


Fig. 10. Measured blow counts at East Abutment

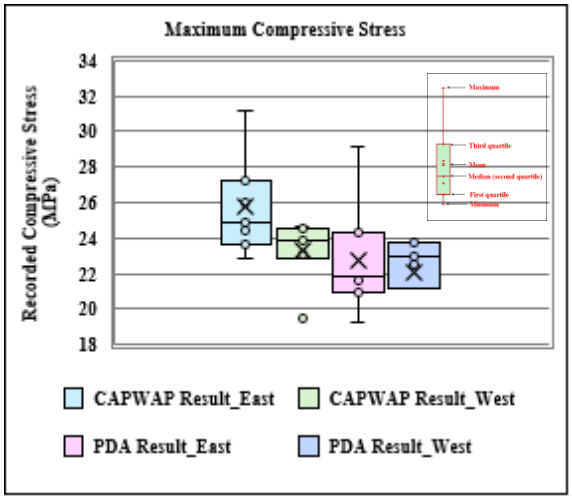


Fig. 9 Maximum compressive stresses

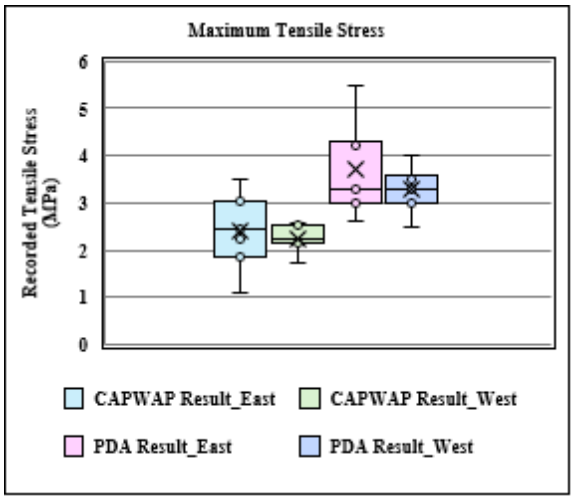


Fig. 11. Maximum tensile stresses

 © Deep Foundations Institute 2026

Energy Transfer

The hammer and soil-pile interaction during installation governs the energy transferred from the hammer to the pile, which in turn controls penetration, driving stresses, and installation performance, making transfer efficiency a critical factor in assessing drivability. Excessive energy loss or overstressing can cause refusal, pile damage, or inadequate embedment. In this study, transferred energy at the East Abutment ranged from 27.5 to 44.7 kJ, with pile A1-P3 recording the highest value, likely reflecting stiffer ground conditions or greater resistance to penetration, while at the West Abutment values were lower (21.4 to 34.1 kJ), with A2-P6 experiencing the lowest transfer, suggesting comparatively softer soils or more efficient dissipation of energy. Notably, higher ultimate pile capacities did not always align with higher transferred energies; for example, A1-P12 achieved the greatest estimated capacity (3408 kN) but only 29.1 kJ of transferred energy. This indicates that transferred energy is governed more by real-time driving resistance and soil–pile interaction than by ultimate capacity and should therefore be regarded primarily as an indicator of installation performance and drivability rather than a direct measure of geotechnical capacity. Refer to Fig. 12 for maximum transferred energy per pile.

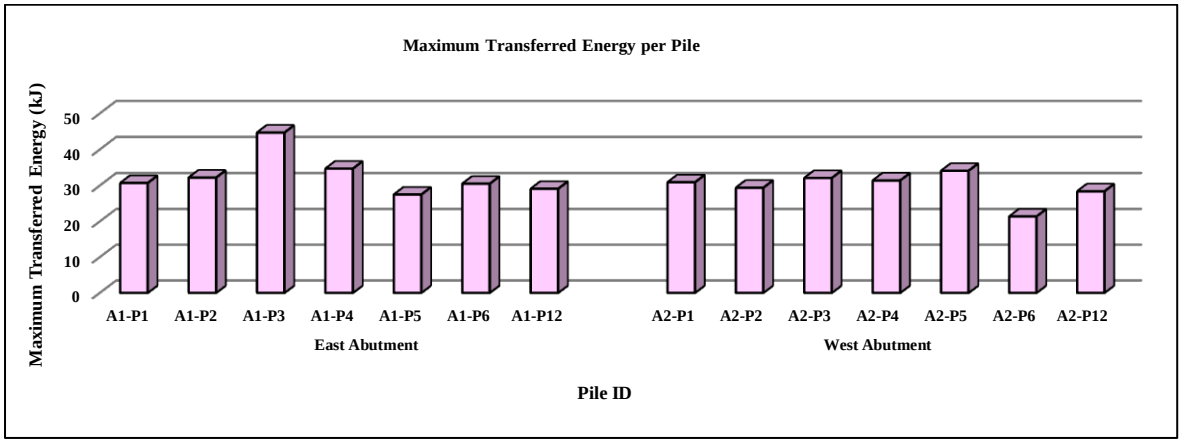


Fig. 12. Maximum transferred energy per pile

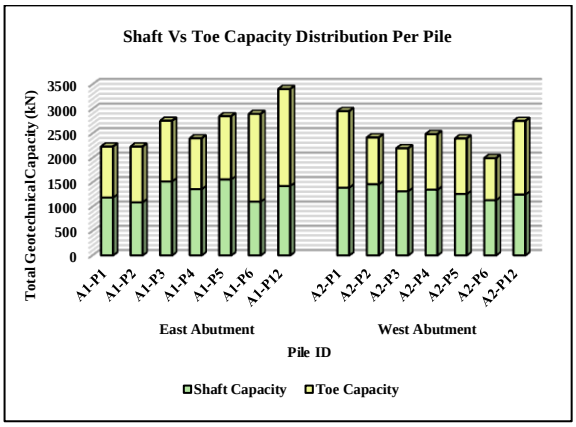


Fig. 13. Shaft vs. toe capacity distribution

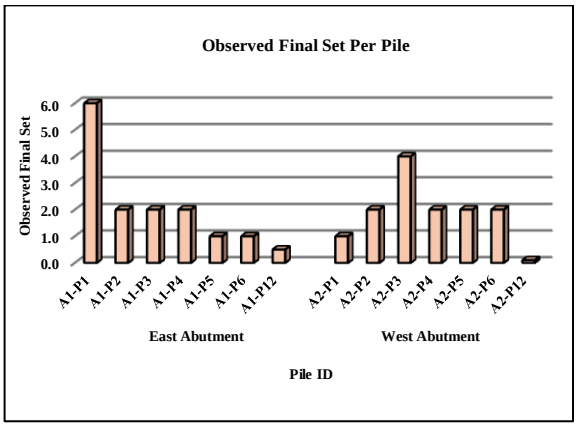


Fig. 14. Observed final set

Geotechnical Capacity

The total capacity transfer between shaft and toe varies notably among both abutment piles. These differences highlight localized heterogeneity in the subsurface at short distance. A majority of the East Abutment piles derive a significant share of their capacity from end-bearing and West Abutment piles rely more heavily on shaft friction due to relatively less competent toe strata. The shaft and toe capacity distributions are shown in Fig. 13.

The predicted shaft and toe capacities were compared against the measured values at both the East and West Abutments. At the East Abutment, the measured shaft capacities generally aligned with the predicted values at pile toe level, although some were slightly lower than expected. In contrast, the West Abutment measured shaft capacities consistently exceeded the predictions. For toe resistance, most measured values at the East Abutment were slightly lower than predicted, with only two piles exceeding the estimates, whereas at the West Abutment the measured toe capacities were higher than the predictions. These outcomes suggest that the East Abutment is influenced by variable subsurface conditions, with alternating dense sand and clay layers causing more variation in load transfer than anticipated. Conversely, the West Abutment is underlain by relatively uniform soil strata, leading to measured capacities that consistently exceeded predictions. Figures 15 to 18 present the predicted and measured shaft and toe capacities.

Similar to the shaft and toe comparison, the achieved total capacities at both abutments were compared with the predicted geotechnical capacities. At the East Abutment, two piles recorded measured capacities slightly lower than the predictions, while at the West Abutment the measured capacities consistently exceeded the predicted values. Importantly, all piles at both abutments achieved capacities greater than the required design values for this project. The comparison is presented in Fig. 7.

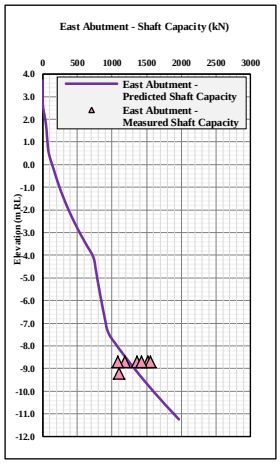


Fig. 15. East Abutment: Predicted vs. measured shaft capacity

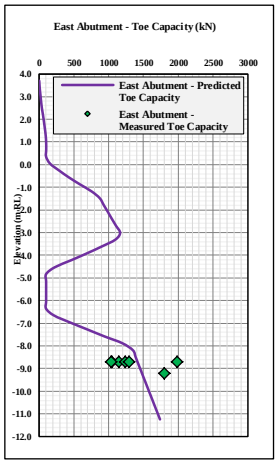


Fig. 16. East Abutment: Predicted vs. measured toe capacity

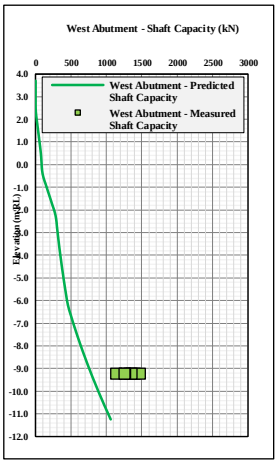


Fig. 17. West Abutment: Predicted vs. measured shaft capacity

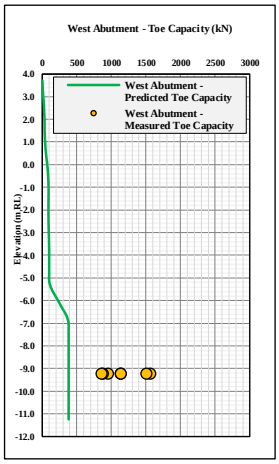


Fig. 18. West Abutment: Predicted vs. measured toe capacity

Observed Final Set

The observed set values provide a direct indication of driving resistance of the piles. Refer to Fig. 12: A majority of the East Abutment piles, including A1-P1 (6 mm) and A2-P3 (4 mm), correspond to piles with comparatively weaker toe response. The majority of piles exhibit final sets between 1 to 2 mm, reflecting the presence of relatively stiff strata at the toe level. Notably, exceptionally minimal sets were recorded for A1-P12 (0.5 mm) and A2-P12 (0.1 mm), confirming termination in very dense or hard strata, which is consistent with their relatively high toe capacities. The observed final set is graphically shown in Fig. 14.

SUMMARY AND CONCLUSIONS

Based on the pile design, drivability assessments, and interpretation of field and testing data, the following conclusions are drawn:

- Subsurface conditions at the Dodson Road project site vary significantly across the ~20 m span, with notable differences between the East and West Abutments. In particular, a dense sand layer is present at the East Abutment.

 © Deep Foundations Institute 2026

- The pile design was revised from steel driven piles to concrete displacement piles based on the contractor's recommendation for a more cost-effective solution.
- Drivability analysis indicated a potential risk of pile refusal within the dense sand layer at the East Abutment, necessitating a trial pile program.
- The trial pile successfully penetrated the dense sand layer without compromising structural integrity, confirming that the production piles can be driven safely.
- High-strain dynamic load testing (PDA) was performed on 50% of the installed piles, providing reliable datasets to validate predicted capacities and confirm concrete pile integrity.
- Comparisons of predicted and measured capacities show that the lower-bound design predictions generally align well with field results, although some capacities, particularly at the East Abutment are slightly lower than predicted. However, all measured capacities meet the design requirements.
- Due to differing subsurface conditions, load transfer mechanisms varied between abutments, with East Abutment piles mobilizing relatively larger end-bearing resistance than the West Abutment piles.
- The project achieved an estimated savings of approximately $800,000 to $1 million by switching from steel driven piles to precast concrete square piles. This savings reflect reduced material and installation costs, avoidance of acid sulfate soil removal and treatment, and lower overall field-related expenses. Although 50% of PDA testing was undertaken at the East Abutment due to limited geotechnical information, the project still realised substantial net savings.

ACKNOWLEDGEMENTS

The authors gratefully acknowledge Arc Infrastructure, particularly Mr. Darshak Panya and Ms. Zia Rice, for their approval, continuous support, and encouragement in publishing the data presented in this paper.

REFERENCES

A-Pile Technical Manual, 2023. A program for the study of driven piles under axial loads, Ensoft Inc.

Australian Standard AS 2159 – 2009. Piling - Design and Installation.

Design and Construction of Driven Pile Foundations – Volume I, 2016. Publication No. FHWA-NHI-16-009 FHWA GEC 012 for US Department of Transportation Federal Highway Administration.

Identification and investigation of acid sulfate soils and acidic landscapes, Guideline, 2015. Government of Western Australia, Department of Environment Regulation.

Tan. S. K and Chapman. G. A, 2019. Design, driveability, driving and dynamic testing of large diameter close ended steel tube piles for a pedestrian bridge. Proceedings of 13th Australia New Zealand Conference on Geomechanics.

 © Deep Foundations Institute 2026

EARLY SPECIALIST CONTRACTOR INVOLVEMENT ENABLING ALTERNATIVE DESIGN FOR SUSTAINABLE DAM STABILISATION

Benjamin Brown, Menard Oceania, Sydney, NSW, AUS, +61 419 987 614, bbrown@menard.com.au
Gary Webley, Menard Oceania, Sydney, NSW, AUS, +61 417 658 172, gwebley@menard.com.au
Andrew Vencer, Menard Oceania, Sydney, NSW, AUS, +61 473 610 894, avencer@menard.com.au
Alexandre Hubaut, Menard Oceania, Sydney, NSW, AUS, +61 400 852 620, ahubaut@menard.com.au
Joe Rola, SRK Consulting, Perth, WA, AUS, +61 403 860 547, jrola@srk.com.au

ABSTRACT

A review of a tailings storage facility embankment in New South Wales identified that historic tailings deposits and organic material in the foundation beneath the embankment were potentially liquefiable, resulting in an undrained factor of safety (FoS) below the recommendations in the Australian National Committee on Large Dams guidelines. Stability analyses indicated a relatively high probability of failure due to seismically induced liquefaction of the foundation soils. Through an early contractor involvement process, the dam owner engaged Menard Oceania to develop the conforming design of deep soil mixed columns. In partnership with SRK Consulting, Menard/SRK conducted a comprehensive review of nine ground improvement solutions and developed a detailed three-dimensional ground model to inform an optimised alternative design utilising stone columns as the driving ground improvement technique. A comprehensive construction field trial was performed to assess the performance of stone columns under site-specific conditions. Various replacement ratios were assessed, both with and without wick drains, to evaluate their effect on drainage and soil consolidation. An extensive instrumentation array comprising vibrating wire piezometers and settlement plates was installed to monitor pore pressure and soil deformation. Post-installation in-situ testing was performed to quantify soil strength improvements. The trial results enabled further optimisation of the stone column solution and provided critical insight into the impact stone column installation has on pore pressure generation and dissipation in the foundation layers. The alternative solution enhanced constructability and reduced foundation seepage risks by avoiding the creation of low-permeability cementitious barriers inherent to the deep soil mixing method. The final stone column solution achieved an 84% reduction in carbon footprint (equivalent to 44,962 tCO_2e), quantified via a life cycle assessment compared to the initial design. Overall, the final solution presented considerable program and cost savings for the dam owner.

Keywords: ground improvement, stone columns, seismic design, tailings dam, early contractor involvement, sustainability, construction trial, life cycle assessment.

INTRODUCTION

In 2019, a revision to Australia's National Committee on Large Dams' (ANCOLD) guidelines for design of dams and appurtenant structures for earthquakes was completed, following significant advancements made in seismic hazard assessments, analysis, and design. A review of the tailings storage facility in New South Wales by the engineer of record found that the tailings dam had an existing undrained factor of safety (FoS) below the guideline's recommendations and a relatively high probability of failure due to seismically induced liquefaction of the foundation. As a 'declared dam' in NSW with risks above the safety threshold, the owner needed to develop an action plan to reduce risk and to get the dam below the safety threshold. A ground improvement (GI) based solution for the strengthening of existing dam and tailings embankments can often be one of the most economical solutions. Engagement of a specialist GI company in an early contractor involvement (ECI) model provides an owner and its consultants with specialist insights that can optimise project designs and lead to best-practise implementation of GI techniques. This paper presents how the ECI model benefited the project through a comprehensive full-scale construction trial to provide confidence in stone columns as an alternative GI methodology for the project. As a result of the alternative

 © Deep Foundations Institute 2026

approach, the project's sustainability is explored and compared with the conforming base case solution. A carbon impact assessment based on a life cycle assessment (LCA) method is used to compare the carbon reduction impact of the alternative solution.

PROJECT BACKGROUND

The dam is part of a tailings storage facility located on the New South Wales east coast. The site came into operation in the 1960s, and over the period of 1960-1980, four stages of tailings containment structures were built. The final stage consisted of a 25 m high; 2 km long embankment completed in 1982. The embankment (presented in Fig. 1) is a zoned earth fill embankment built with a clay core and a central vertical aggregate chimney filter connected to a horizontal aggregate blanket for drainage, and a downstream toe berm. The dam was designed as a water retention structure, with the decant pond located at the upstream slope of the main embankment. A trial embankment was constructed in the central area, which was later incorporated into the upstream portion of the embankment earthworks.

Legacy drawings detailed the main section of the dam incorporated a former retaining structure constructed across what once was a shallow valley. The tailings deposits retained by this historic embankment are understood to have been hydraulically placed with two clear layers defined as coarse and fine ash. At the deepest point the tailings deposit is 8 m thick. Underlying the historic tailings and coinciding with the natural ground surface from the 1960s is a continuous very soft organic clay layer.

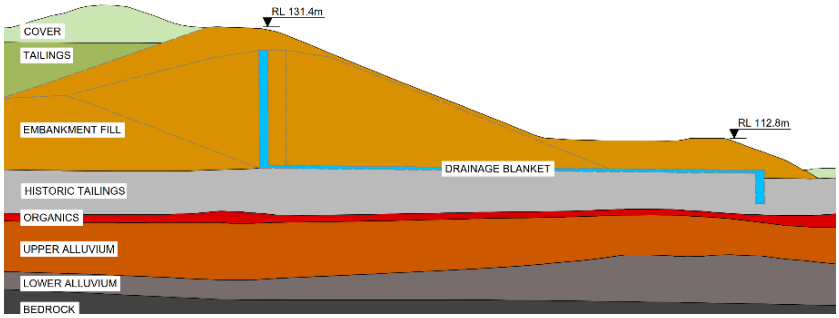


Fig. 1. Typical cross section of the tailings storage dam located at the site

A review of the dam found that the earlier tailings deposits and natural materials in the foundation beneath the dam were weak and potentially liquefiable in the event of seismic loading. A stability analysis indicated a high probability of failure of the dam due to seismically induced liquefaction of the dam foundations. The embankment did not satisfy the FoS recommendations set out in the ANCOLD guidelines. During reviews, it was determined further investigations and remedial works were required to address the risks that had been identified.

Given the embankment's condition at the time of assessment, the need to stabilise the foundation was clear. The project scope was established to improve the FoS to achieve ANCOLD compliance, whilst maintaining the performance of the underlying drainage system. The key project requirements for the design were to:

- Prior to commencing GI works, achieve the safety threshold, being an undrained FoS $\geq$ 1.3 under short-term loading conditions (assessed using peak strength parameters).
- Upon completion of the stabilisation works:
  - achieve a drained and undrained FoS $\geq$ 1.5.
  - achieve a post seismic FoS $\geq$ 1.1. This requirement included failures relating to long term safety evaluation for earthquake events and post liquefaction stability for causes other than seismic.

During the early tender phase of the project, the existing organic layer was not given significance in the site investigation modelling by the engineer of record (Rola et.al. 2024). Design specifications

 © Deep Foundations Institute 2026

sought to provide stabilisation for the post-seismic loading condition. This oversight pushed the initial design and solutions towards a pre-conceived solution that improves the in-situ soil properties by mechanically mixing a cement grout with the in-situ soil profile using Deep Soil Mixing (DSM) methods. The conforming design presented a series of DSM shear walls installed through the downstream berm of the dam. DSM columns would be overlapped to create a nominally 1.32 m-thick, 46 m-long transverse shear walls-oriented perpendicular to the axis of the dam. The shear walls would be spaced at centres of 5.28 m producing a minimum replacement ratio of 25%. The shear walls provide the major reinforcement of the downstream slope to resist both seismic deformation of the foundation soils and a downstream slope failure during and following a seismic event. The transverse walls would be embedded into the underlying residual soils at specified depths across the embankment's span of 800 m. The design would have seen an approximate 6,000 DSM columns installed totalling 28,880 square metres of GI area. The pre-conceived option of GI for the works was based on an excellent proven performance record for liquefaction mitigation, slope stability and well-established design procedures from reference stabilisation projects completed internationally.

EARLY CONTRACTOR INVOLVEMENT (ECI) PROCESS

The project was initiated as an ECI model to integrate construction expertise into the preliminary design. The framework facilitated direct collaboration between the asset owner, the specialist ground improvement contractor (Menard Oceania), and Menard's chosen subject matter expert (SME) design consultant (SRK Consulting). Whilst the ECI model is not a technical breakthrough, the inclusion of specialist contractors in an ECI phase is rare. Specialist contractors are not commonly provided the opportunity to collaborate in this process and are typically engaged when designs are reaching a mature stage, preventing specialists from influencing project design outcomes. The use of this framework for the project enabled the specialist GI contractor and SME to promote integration of different technical disciplines collaboratively within the design as it progressed, to best optimise the project.

DESIGN DEVELOPMENT AND ALTERNATIVE GI REVIEW

With the expanse of the project site compounded by a complex heterogenous layering of material through historic staged uses and development of the land, it was vital to develop a comprehensive ground model. A three-dimensional (3D) ground model was developed as part of the early design work, utilising data from 5 separate site investigation campaigns. In total, information gathered included: 206 cone penetration tests (CPTs), 37 boreholes, 36 test pits, and a variety of in-situ testing. This data was combined with digitised and georeferenced historical drawings and plans from archival records along with a site topographical survey. To utilise the CPT data effectively, it was processed to derive distinct material behaviours based on parameters such as corrected tip resistance, sleeve friction resistance, pore water pressure ratio, and soil behaviour type index. Sottile et al. (2024) presents the process of how each CPT interpretation was compared with information from the nearest borehole using a predictive modelling approach, followed by manual review and iterative refinement to delineate the different geotechnical units based on CPT response and physical logs. Rola et al. (2024) presents the process of building the model using Seequent Leapfrog Geo software using the available data and the CPT interpretations. From the development of the 3D ground model, the underlying geological units were able to be broken down into nine separate layers (shown in Fig. 2). The construction of this model led to the discovery of the continuous organic layer. During the detailed 30%, 75%, 100%, issued for construction and optimisation design phases, the model allowed for rapid development of additional analyses of sections cut at any chainage of the embankment. The model developed for design input parameters subsequently evolved into an important method of cross-checking the embankment's condition during construction when unexpected readings or alarms were triggered within the live-monitoring instrumentation. This research is presented in Dellamea et al. (2025). The model developed by the SME during the early phase of the project allowed a relatively small design team to manage schedule and cost constraints and was a valuable benefit of the ECI process.

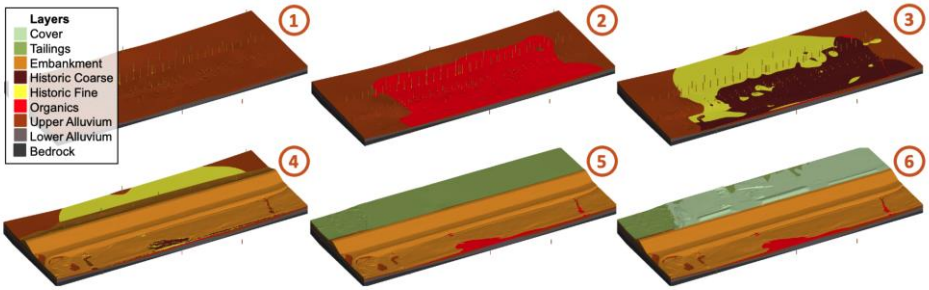


Fig. 2. Output layers developed from comprehensive 3D ground model

In parallel to the design development and model generation, an extensive historical review of previous similar projects was undertaken to determine the industry best practise for embankment dam seismic upgrades. Figure 3 presents the latest case studies where ground improvement has been adopted for downstream stabilisation of seismically deficient dams globally.

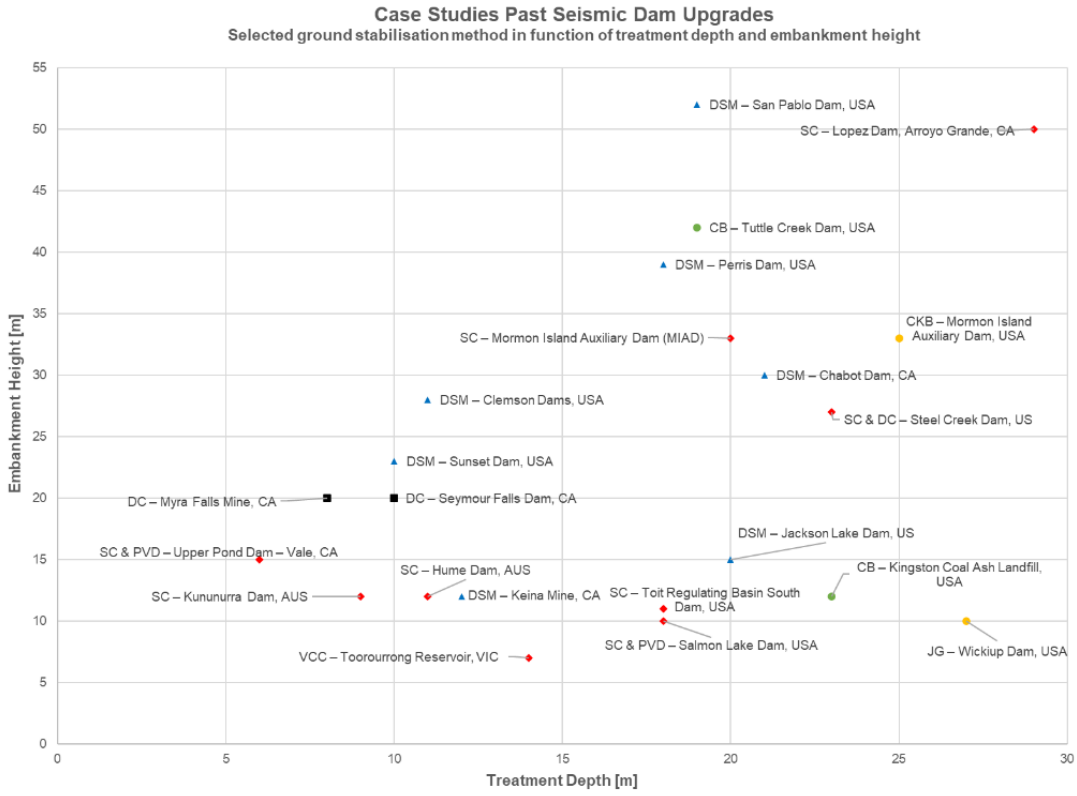


Fig. 3. Historical review of completed dam stability projects displaying embankment height vs treatment depth

Seven ground stabilisation construction methods were compared and evaluated for the proposed remediation works, these were: excavate and replace, dynamic compaction, stone columns (SC), rigid inclusions, jet grouting, deep soil mixing and self-hardening cement bentonite (CB) slurry panels. Further, vibro-compaction, blasting densification, compaction grouting and plastic concrete shear wall methods were considered but were deemed impractical or of limited benefit. Following evaluation of the ground improvement alternatives for the project, Menard / SRK shortlisted the following three options:

- Deep soil mixing
- Cement bentonite slurry panels
- Stone columns

Transverse shear panels formed of overlapping DSM columns or CB self-hardening slurry panels are considered more effective than semi-rigid inclusions (i.e., SC) to resist both deformation and downstream slope failure in both static and seismic condition. However, it was collaboratively decided to further explore a SC solution as the preferred ground improvement option during the early design phase based on drainage considerations, increased productivity and the sustainability benefit from reduced material consumption. Cement-based methods (DSM and CB) create impermeable zones in the foundation. On the downstream side of an embankment, this formed a risk of increasing the pore-water pressure in the embankment and foundation with potential adverse effects on the stability of the embankment under static and dynamic loading conditions. Whilst these effects can be managed by providing additional drainage, a risk mitigation option for the foundation's seepage control was preferred by all project stakeholders.

In the case of the embankment's ground conditions, the use of SCs presented an opportunity to further validate and demonstrate their effectiveness while addressing stakeholder concerns. A full-scale construction field trial with test results and live monitoring data feeding back into the design development was planned. The targets of the trial were to:

- Understand vibration induced by the construction process, which may propagate in the surrounding foundation material, inducing undrained conditions.
- Determine if the presence of fines (historic tailings and alluvium) prevents the densification and stiffening of the surrounding soil.
- Determine the required replacement ratios to achieve suitable GI block strength (i.e., SC size and spacing).
- Determine if there is a benefit from installation of prefabricated vertical drains (PVDs).
- Determine the drainage effect of stone columns.
- Determine an optimal construction sequence.

FIELD TRIAL AND INSTRUMENTATION

The trial program involved four pads, A1, A2, A3, and B, each configured to investigate specific design objectives and verify the performance of the proposed ground improvement measures. The layout of trial pad B is presented in Fig. 4.

Trial pad A1 served as a control, constructed with embankment material only, to a height of 5 m on virgin ground without any GI treatment. The trial pad was heavily instrumented, to benchmark the behaviour of untreated soils under embankment loading conditions. Trial pad A1 along with the process of CPT collecting is presented in Fig. 5.

Trial pad A2 included a 5 m constructed embankment overlaying SCs installed at a 25.1% replacement ratio. This pad was divided into sections with and without PVD, allowing comparison of drainage-assisted and unassisted consolidation.

Trial pads A3 and B were used exclusively for in-situ testing and did not include embankment loading. These pads featured SCs installed with five replacement ratios (14.5%, 22.7%, 25.1%, 30.4%, and 35.8%, with and without PVDs). The goal was to assess strength and stiffness improvements through a range of geotechnical tests without the influence of surface loading. In total, 183 SCs and 165 PVDs were installed during the trials.

 © Deep Foundations Institute 2026

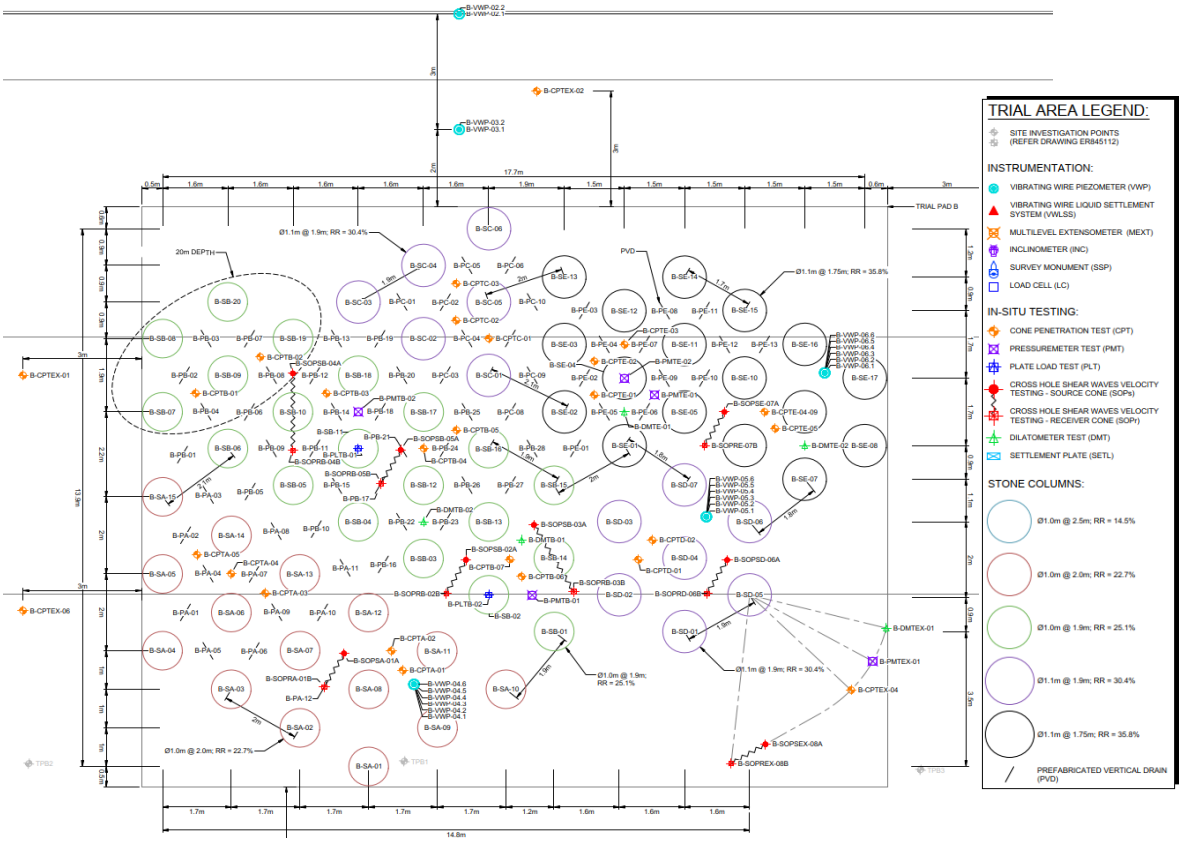


Fig. 4. Layout of trial pad B highlighting 5 replacement ratios, PVDs, live monitoring and testing locations

To enable the installation of SC for the trial, a 120T crawler crane was used to suspend a 22 m free hanging penetration unit fitted with a V23 Vibroflot from Vibroservices GmbH. The Vibroflot was powered by a 330 kVA generator mounted on the crane. SCs were installed using the dry-bottom feed method of installation with auxiliary skid steers and loaders for stone placement into the winch operated skip bin. Figure 5 presents the setup of the SC installation rig conducting the trial works.



Fig. 5. Left-SC being installed on trial pad B, Right-SCPTu being conducted next to trial pad A1

A range of geotechnical instruments were installed across the trial pads to monitor and gather data. These included 42 vibrating wire piezometers to monitor pore pressure response, 10 vibrating wire

 © Deep Foundations Institute 2026

liquid settlement systems (VWLSS) for vertical deformation tracking, and vertical and horizontal inclinometers, totalling 5, to observe lateral displacements. Additionally, 2 settlement plates and 27 survey monuments were installed to monitor surface displacement over time. A suite of post-installation testing was conducted as part of the trial campaign, including a total of 45 seismic cone penetration tests (SCPTu), 8 vane shear tests, and 8 ball penetrometer tests, 13 seismic dilatometer tests (DMT), 5 pressuremeter tests, 5 cross hole shear wave velocity tests and 2 plate load tests (PLT).

The data collected from pad A1 allowed calibration of soil stiffness and permeability for virgin conditions, which were incorporated into numerical models developed using Plaxis. For pad A2, the settlement and pore pressure behaviour was compared against numerical predictions, with SC stiffness validated using both PLT and VWLSS results. Pads A3 and B provided data on strength and stiffness gains between SCs through pre- and post-improvement testing. Roldan et al. (2024) presents a performance study on the various soil types using the SCPTu data collected as part of the trial. DMT and cross-hole shear wave velocity test results were considered inconclusive. The field trial's results were evaluated with the key findings summarised below:

- The upper alluvium, organic and historic tailings develop a high pore water pressure response within close proximity to the SC installation location. This response becomes negligible at distances greater than 10 m. The built-up pore water pressure was observed to dissipate within hours in the coarse layers of historic tailings and within several days in the organics and upper alluvium due to their fine nature.
- As identified in Roldan et al. (2024), there was significant improvement observed in coarse materials between the SCs and minimal to negligible increase of strength in soil between the SC in the finer materials. The measured strength increase supports the use of an improved undrained shear strength ratio for design in coarse-grained soils between the columns.
- The trial confirmed SCs of design diameter 1.1 m were able to be installed with the construction equipment used for the trial.
- PVDs installed in tandem with SCs did not conclusively improve the GI areas, so were not put forward into the design of the project.

The trial verified stone columns were a viable solution for the project, without negatively impacting the current condition of the embankment, thus maintaining the dam's existing FoS. Further, the trial validated design assumptions, allowed for optimisation of material input parameters and generated critical performance data under site-specific conditions, enabling refinement of the ground model calibration. This iterative process of field testing and design refinement served as a primary risk mitigation strategy, directly addressing uncertainties associated with the site's heterogeneous and liquefiable foundation soils.

ALTERNATIVE SOLUTION LIFE CYCLE ASSESSEMENT

A carbon impact assessment was undertaken, comparing the initial DSM reference design with the completed final alternative SC solution. The analysis was structured as a comparative LCA, adhering to ISO 14044 (2006) recommendations and utilising the Australian Life Cycle Assessment Society (ALCAS) AusLCI database. A functional unit was defined as "Improving a 100 m² section of the project's total area using ground improvement techniques to a depth of 30 metres" to ensure a direct, like-for-like comparison between the two project solutions. The study's boundaries encompassed the key life cycle phases, including the production and transport of raw materials, equipment mobilisation, on-site fuel consumption and personnel transportation. The input assumptions of the study used the base case solution of 6,000 DSM columns treating an area of 28,880 square metres, compared with the optimised alternative solution of 6,400 SC treating an area of 21,400 square metres. The reduction in area between the DSM and SC is a result of the SC's ability to be installed further downstream of the embankment. This change to the location of treatment does attribute to an increased quantity of earthworks required for the solution. The LCA data sources used in this study comprised of a combination of the below sources:

- Verified AusLCI unit processes, available on the AusLCI website and serving as the primary dataset.
- Unit processes from the "shadow database," which is a modified version of the Ecoinvent v2.2 database incorporating Australian data for crucial background processes, creating a self-sufficient regionalised database.
- A few datasets were sourced from the EFFC/DFI Carbon Calculator v5.0, along with specific environmental product declaration sheets from local companies.

Table 1 compares the contribution each life cycle stage has on the final carbon impact across both GI solutions. The assessment revealed a profound difference in the carbon profiles of the two solutions. The reference DSM design, heavily reliant on high-embodied-energy materials, was projected to emit approximately 53,372 tonnes of carbon dioxide equivalent (tCO2e) over its planned treatment area of 28,880 square metres. In contrast, the optimised SC solution was calculated to emit only 8,566 tCO_2e over its revised treatment area of 21,400 square metres. This design optimisation resulted in a total carbon saving of 44,962 tCO_2e, representing an 84% reduction in the project's overall carbon footprint. This substantial decrease is primarily attributed to the elimination of approximately 34,900 tonnes of cement and 2,700 tonnes of structural steel, which were central to the DSM methodology.

Table 1. Contribution of each life cycle stage for DSM and SC design

Distribution by life cycle stage	DSM Reference Case (tCO2e)	SC Alternative Solution (tCO2e)
Raw Materials Production for the Design	43,065.4	1,782.1
Raw Materials Production for the Earthworks	298.5	856.3
Transport of Raw Materials and People	614.2	1,843.0
Transport of Equipment	39.2	5.6
Fuel Consumption Related to Work Execution	9,354.8	4,078.7
Total	53,372.0	8,565.7

A detailed contribution analysis highlights the fundamental shift in the project's environmental impact sources; these are displayed in Fig. 6 below. For the reference DSM scenario, raw material production was the dominant contributor, accounting for over 80% of total emissions. Specifically, the manufacturing of cement and steel were the most carbon-intensive processes, responsible for 77% and 22% of the total potential impact reduction, respectively.

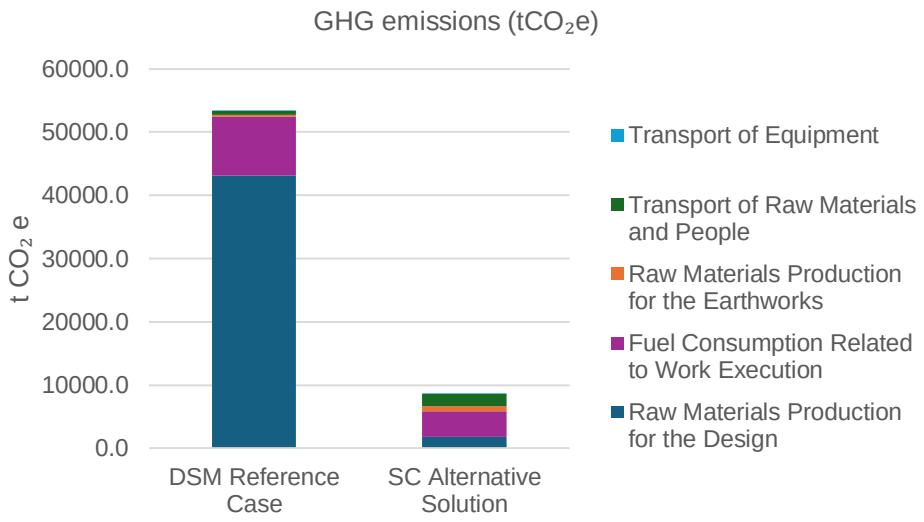


Fig. 6. GHG emissions (tCO2e) for the reference case vs alternative solution

 © Deep Foundations Institute 2026

For the optimised SC solution, the emissions profile shifted significantly. The impact of raw material production dropped to just 21% of the total, while fuel consumption (48%) and material transport (22%) became the primary contributors due to the large quantities of stone aggregate required. However, the absolute emissions from these sources were far lower than those from the cement and steel in the initial design. Further, the alternative SC solution presented an opportunity for increased production rates compared to a DSM approach, resulting in significant program reductions and an estimated saving of 1,550,000 litres of diesel.

CONCLUSION

The successful stabilisation of the tailings dam presented in this paper outlines the benefits of engaging a specialist contractor in an ECI model. The ECI model and involvement of specialist subcontractors is not a breakthrough in the industry; however, specialist subcontractors are typically engaged later in the project life cycle phase or act as an advisor to the main contractor for a small portion of works. This layering and late engagement inhibits design alternatives and adaptability if engaged too late in the project life cycle. The ECI process allowed for a re-evaluation of the initial design, moving beyond a conventional, carbon-intensive DSM solution that was accepted due to an excellent proven performance record for liquefaction mitigation, slope stability and well-established design procedures. The result was a more innovative and sustainable solution.

By deploying a comprehensive full-scale field trial campaign, uncertainties on the effectiveness of the alternative SC solution were able to be satisfied. The trial campaign utilised 4 separate trial pads with varying designs, replacement ratios and column diameters across 183 SCs. The trial used a combination of pre- and post-installation instrumentations and in-situ testing methods to determine key outcomes for the design feedback loop. It established that the chosen alternative did not have a compromising impact on the liquifiable soils of the foundation, improved soil strength between the SCs, and that the chosen diameters of 1.1 m were achievable. This data-driven approach not only gave all stakeholders the confidence to proceed with the alternative design but also enabled significant optimisation and confirmed that the SC solution could meet stringent seismic safety requirements without the adverse drainage impacts associated with cement-based methods.

The outcome of the project has proven that challenging pre-conceived design options can lead to alternative solutions that are more productive and environmentally beneficial. The installed SC solution achieved a remarkable 84% reduction in its carbon footprint, saving approximately 44,962 tCO_2e compared to the initial DSM design.

ACKNOWLEDGEMENTS

The authors gratefully acknowledge Menard and SRK for generously providing the data and technical information that made this paper possible. Their support and collaboration were instrumental in completing this work. As well as the asset owners for their setup of the project environment, ensuring collaboration between all stakeholders was used to its full potential.

REFERENCES

Australian Life Cycle Assessment Society (ALCAS), n.d. *AusLCI Database*, developed by ALCAS, https://www.alcas.asn.au/auslci

Dellamea, R., Rola, J., Sottile, M., and Eldridge, J., 2025. Evaluating unexpected piezometer trends in a tailing dam: insights from dissipation testing, Life of Mine | Mine Waste and Tailings Conference 2025

European Federation of Foundation Contractors (EFFC) and Deep Foundations Institute (DFI), n.d. EFFC-DFI Carbon Calculator Tool v5.0, EFFC & DFI, https://www.effc.org/how-we-operate/eco2-foundations/

International Organization for Standardization (ISO), 2006. ISO 14044: Environmental management — Life cycle assessment — Requirements and guidelines, ISO, Geneva.

 © Deep Foundations Institute 2026

Rola, J., Sottile, M., Rivas, N., Roldan, L. and Sfriso, A., 2024. Development of a 3D ground model to design the stabilisation of a dam founded on weak liquefiable ground, Proceedings of the 7th International Conference on Geotechnical and Geophysical Site Characterization (ISC) June 18-21, 2024, Barcelona, Spain

Roldan, L., Sottile, M., Sfriso, A. and Rola, J., 2024, Ground improvement between stone columns: a performance study on various soil types using in-situ testing, Proceedings of the XVIII ECSMGE 2024.

Sottile, M., Crocker, J. Roldan, L., 2024. Interpretation of CPTu data using machine learning techniques to develop the ground model of a dam, Proceedings of the 7th International Conference on Geotechnical and Geophysical Site Characterization (ISC) June 18-21, 2024, Barcelona, Spain

 © Deep Foundations Institute 2026

JET GROUT RETENTION AND DEEP TENSION PILES IN VERY SOFT, NORMALLY CONSOLIDATED CLAY: CHALLENGES FROM THE MELBOURNE ARTS CENTRE REDEVELOPMENT

Jared Fetherston, Keller, jared.fetherston@keller.com.au
Clifford Taylor, Keller, Cliff.Taylor@keller.com.au

ABSTRACT

The Melbourne Arts Centre redevelopment involved excavation of a 10 to 15 m deep basement within Coode Island Silt, a very soft, normally consolidated clay, with a high groundwater table and significant heritage and access constraints. Legacy ground anchors from the original Arts Centre structure imposed physical limitations on retention options, making secant piles and diaphragm walls impractical. The adopted solution comprised soldier piles with jet grout infill columns and a jet grout base block, restrained by Continuous Flight Auger (CFA) and polymer-supported bored tension piles extending to depths of up to 32 m to resist uplift forces.

Managing groundwater inflow and wall performance in soft soils was a key geotechnical challenge. Jet grout columns were used to limit seepage and provide local retention between soldier piles, while the jet grout base block contributed to base heave resistance and overall system stability in combination with the tension piles. The presence of existing anchors required careful coordination and modification of pile layouts and grout block geometry.

Access limitations beneath the heritage-listed spire further constrained construction, necessitating low-headroom piling in restricted zones alongside conventional CFA tension piles requiring full-length reinforcement cages.

This paper presents a case history of the geotechnical design approach, construction methodology, verification, and key lessons learned in delivering a combined foundation and retention system in very soft ground under tight urban and heritage constraints.

INTRODUCTION

Construction in Melbourne's Southbank is complicated by Coode Island Silt (CIS), a very soft, normally consolidated clay up to 25 m deep with a high water table. The Reimagining Arts Centre Melbourne (RACM) required a 10 m to 15 m deep basement immediately adjacent to a heritage spire and within a footprint congested by legacy anchors and piles, where conventional secant or diaphragm walls were impractical. An integrated system of CFA soldier piles with jet grout infill and a jet grout base block, restrained by CFA and low-headroom polymer-supported bored tension piles, was adopted to control movements, uplift and seepage. This was one of the first recent deep basements in Melbourne constructed entirely in CIS, and inclinometer monitoring confirmed performance was within acceptance criteria. This paper presents the geotechnical design, construction methodology and verification, and draws out lessons for future projects in similar ground.

SITE CONDITIONS AND CONSTRAINTS

The RACM project site is located within Melbourne's Southbank precinct, an area with a long history of ground engineering challenges. The existing Arts Centre basement was originally constructed in the 1970s and imposes direct constraints on the new development.

Two rows of redundant permanent ground anchors comprising 120 mm diameter solid steel bars installed at approximately 45°, were present across the footprint of the proposed excavation installed in the existing basement wall at RL0mAHD and RL-6.1mAHD respectively (RL – Reduced Level, AHD – Australian Height Datum). These anchors were unable to be accurately identified in the

 © Deep Foundations Institute 2026

ground, and accordingly the installation tolerance of the anchors from original documentation of +/- 4° had to be considered. In addition, a series of redundant raked H-piles, driven to support the former concourse structure, remained in place. Figure 1 shows the location and number of anchors and H-piles. Both anchor and pile obstructions intersected the alignment of the new retention wall and had to be systematically addressed to allow installation of new piles and jet grout columns.

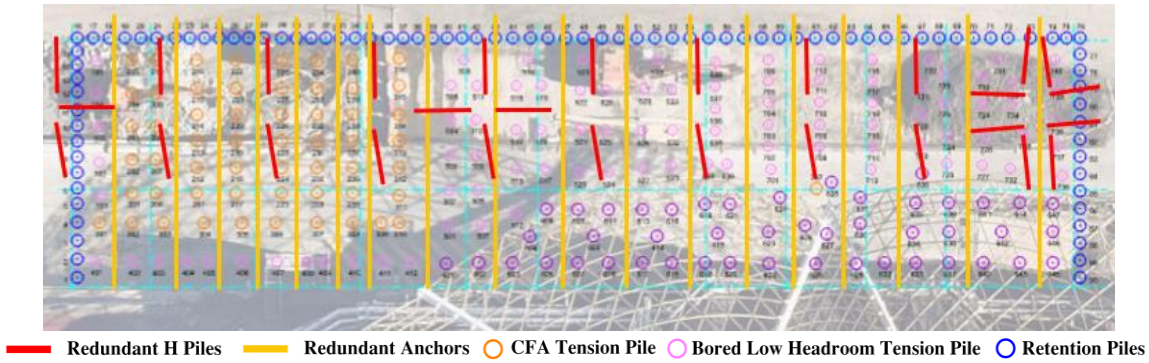


Fig. 1. Site basement layout showing tension and retention piles, redundant anchors, H pile obstructions and existing heritage spire overhang.

The Arts Centre's heritage-listed wire spire presented a further complication. The lowest point of the spire extended across roughly one-third of the basement footprint, restricting headroom to between 14 m and 23 m. This required the use of modified low-headroom piling and jet grouting rigs, along with careful sequencing of works and detailed crane lift studies to ensure exclusion zones were maintained around the spire at all times. Stakeholder concerns about piling masts operating within 1 m of the spire demanded safety control, risk assessments, daily monitoring and physical barriers placed on site to ensure full height equipment did not clash with the spire.

Groundwater conditions also influenced the approach. While the general design groundwater level was taken at RL0.5m, due to settlement of the CIS beneath the existing basement there was a localised zone of pressurised groundwater which had been confirmed by inspection of valves for existing cathodic protection wells. This presented risks for base stability and inflow during excavation particularly, considering the new basement would undermine the existing basement in zones creating a direct path to this pressurised water zone.

Access to the site was limited to a single entry point shared with ongoing Arts Centre operations. This required that emergency and service vehicle access be maintained throughout the project, constraining both site logistics and construction sequencing. The Arts Centre function spaces were to remain fully operational during the project, which meant major deliveries had to be timed around events and additional controls were required to monitor noise and vibration from the works.

In combination, these legacy works, heritage constraints, and operational access requirements created a uniquely constrained environment in which the design and construction of the retention system had to be developed.

GEOTECHNICAL CONDITIONS

The site lies within the Yarra Delta geology, which is highly variable, with soft compressible Coode Island Silt (CIS) overlying denser founding strata. A typical profile comprised fill to about 6m depth, followed by CIS. The CIS was encountered as very soft to soft, normally consolidated silty clay with sandy lenses and organic inclusions. At the southern end it extended to RL-21.8m, whereas at the northern end it was truncated at about RL-4.5m by a basalt flow. CIS is well known in Melbourne for creep settlement and large deformations during excavation and was the controlling stratum for the basement and retention design. In-situ testing confirmed that despite local drainage during the original 1970s basement excavation, the CIS remained very soft to soft.

 © Deep Foundations Institute 2026

The subsurface profile varied markedly between the north and south due to the basalt. At the northern end, basalt was encountered from RL-4 m with thickness up to 8 m, slightly weathered to fresh, with Unconfined Compressive Strength (UCS) values of 20MPa to 80MPa. It thinned toward the south of the site to 0.2m and presented as basaltic gravel. This variability presented major challenges for piling and jet grouting, and the basement footprint was shifted south to avoid the thickest basalt zones. The main founding layer, Melbourne Formation siltstone was encountered between RL-22m to RL-23m across the site as moderately to highly weathered, UCS 2MPa to 10MPa.

Groundwater was typically at about RL0.5m, creating risks of inflow, heave and buoyancy within the very soft CIS. These conditions drove the adoption of a jet grout base block and jet grout curtain wall to supplement the CFA soldier piles.

Table 1 summarises the stratigraphy at the site, and Fig. 2 shows the interpreted cross section.

Table 1. Site geotechnical profile

Geological Unit	Soil/Rock Description	Southern Zone Approx. RL (m AHD)		Northern Zone Approx. RL (m AHD)	
		From	To	From	To
Uncontrolled fill	Variable.	3.5	-3.3	3.5	0.5
Coode Island Silt	Very Soft to Soft clay. Controlling layer.	-3.3	-21.8	0.5	-4.5
Holocene Sands	Medium dense to dense.	-21.8	-23.0	-	-
Basalt	Slightly weathered high strength to residual gravel. Thins to a gravel in the southern zone.	-23.0	-23.3	-4.5	-11
Fishermen's Bend Silt	Firm to Stiff clay.	-	-	-11.0	-18
Moray Street Gravels	Medium dense to dense sands.	-	-	-18.0	-23.3
Melbourne Formation	HW-MW siltstone. UCS = 2MPa to 10MPa.	-23.3	-26.8	-23.3	-26.8

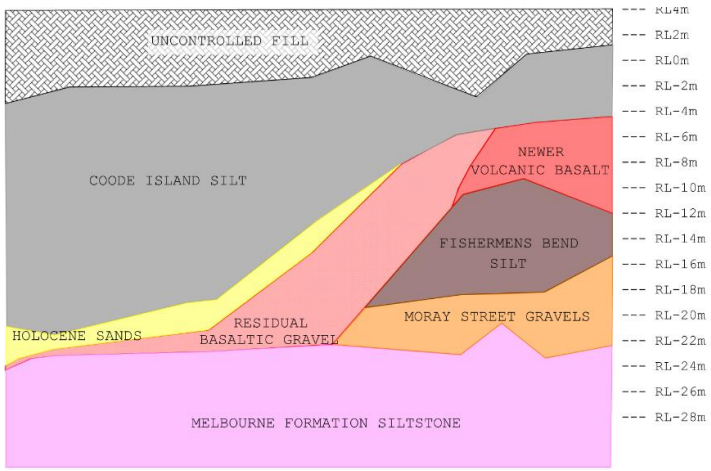


Fig. 2. Site geotechnical profile

RETENTION, BASEBLOCK AND TENSION PILE DESIGN

The retention system was made up of 900 mm CFA soldier piles at about 1.2 m to 1.4 m centres with a jet grout infill curtain and a jet grout base block below. Soldier piles in lieu of a secant pile system,

 © Deep Foundations Institute 2026

allowed flexibility in sequencing and positioning in the event of clashes with existing anchors. The excavation needed multiple rows of restraint, the first was formed by sections of top-down slabs and band beams at ground level where the geometry worked, and the second row of propping was near RL-2m. The jet grout base block also propped the wall immediately below the Bulk Excavation Levels (BEL), which were RL-9.7 m for the truck lift zone and RL-6.3 m for the scenery dock. The overall aim was to keep the wall stiff enough to limit movement in the soft CIS but still be buildable under the tight access.

Finite element modelling of the excavation, the base block and the pile loads was done by a specialist FEM subcontractor in both 2D and 3D. Keller provided the soil and grout parameters and used the outputs to finalise the pile design. The analyses indicated that substantial sustained shear forces and bending moments would occur within about 2 m of the tension pile toes, and these had to be considered for both ultimate and service conditions. This precluded the use of central reinforcement bars, as the largest available sections did not have sufficient capacity, so the design required full-length reinforcement cages down to 30 m. In practice, the governing case for reinforcement design was serviceability crack control rather than ultimate strength, because of the long spans in the cages and the need to limit crack widths.

The design acceptance criteria for the retention system were set to limit retaining wall deflections at ground level to less than 74 mm and 38 mm for the truck lift and scenery dock locations respectively and to maintain inflows within pumping capacity.

The uplift design was based on contributory area to each tension pile. The uplift pressure was taken as the theoretical full overburden stress at the underside of the jet grout block, accounting for both swell and water pressures. In the truck lift zones the design uplift pressure was 275 kPa, and in the scenery dock zones it was 230 kPa, which showed good agreement with values from the 3D analysis. The site was divided into seven uplift zones (100 to 700 series) depending on BEL, pile diameters and maximum contributory area for groups of piles. There was a small no-go area around the lowest point of the spire, with increased spans of jet grout, which needed sensitivity checks to block stresses. These checks were undertaken by modelling a representative three-dimensional area incorporating the anticipated pile layout dictated by site access constraints. The model was then assessed using varying jet grout block thicknesses to evaluate stress and strain behaviour.

The jet grout block and infill columns were designed to provide both structural restraint and water cut-off, with target parameters of UCS about 1,000 kPa, modulus about 150 MPa, and permeability 1×10^{-7}m/s or less. The block was typically 2.5 m thick but was increased to 5.0 m in the truck lift areas. These were minimum target values, and sensitivity checks were carried out using 2D FEM, by varying the jet grout modulus, block thickness and shear strength across anticipated upper and lower bound ranges. Stress and strain responses were assessed for each case, with total strains required to remain below 0.3%. Although this limit was exceeded in some localised areas under conservative assumptions, these were judged to be minor and not to compromise the overall stability or performance of the jet grout block.

The bond between the CFA piles and the jet grout block was also a critical design parameter. An ultimate shear stress of 500 kPa was adopted, based on a minimum grout block UCS of 1 MPa. With a reduction factor of 0.6 this gave a design friction value of 300 kPa. When combined with the ultimate load factors required by AS 1170 and AS 2159, this equated to an overall factor of safety of about 2.0 and implied a required mean UCS of 1.5 MPa (Topolnicki, 2017). Figure 3 summarises the resulting uplift capacities of the tension pile components for both pile diameters and highlights the governing role of the pile to jet grout bond when compared with socket capacity. These bond values governed the pile numbers and layouts in each zone once compared with the uplift demands.

As the majority of the tension resistance was developed by sockets in the Melbourne Formation siltstone, creep behaviour was not considered a significant mechanism for the sustained tension loads. However, as the rock strength varied between 2 MPa and 10 MPa, the piles were also checked under

long-term sustained loads. A sustained load limit of 80% of short-term socket capacity was adopted, consistent with published work for soft soils (Yanni, 2016) but considered conservative for low-strength rock.

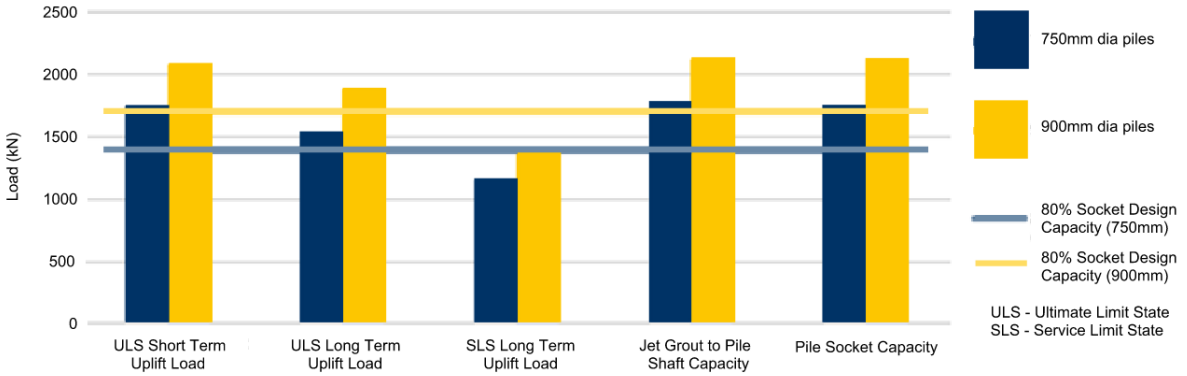


Fig. 3. Tension pile components uplift capacities

Negative skin friction within the CIS due to long-term creep settlement was another design driver. Drag forces (q_n) were estimated using a β coefficient of 0.3 applied to effective vertical stress ($q_n = \beta\sigma'_v$), consistent with Fellenius (1984). To resist these effects, at least every fourth pile was extended as a king pile socketed into the siltstone at about RL-23 m, while the three intermediate floating piles were assumed to attract drag loads which were then transferred back into the king piles.

These assumptions were to be verified by inclinometer monitoring, pile testing and a jet grout pull-out trial during construction.

PILE METHODOLOGY AND PERFORMANCE

The design pile diameter, founding criteria and geological profile necessitated the use of highly specialised equipment. For the deep CFA retention and tension piles a 140 T piling rig was used, capable of piles up to 35 m in depth in a single pass with 100 T pull out force. The torque and height of this rig combined with specialised drill heads assisted to ensure founding depth and sufficient rock sockets were achieved in a single pass without the need for auger extensions. Particularly critical in the tension piles, the rock socket in the Melbourne formation siltstone can be problematic for undersized rigs or incorrect cutting heads whilst using the CFA method.

For the low headroom zone bored tension piles, a 78 T piling rig with 300 kNm of torque was selected, primarily for its low headroom capability, corresponding kelly bar and sufficient torque and crowd force to ensure founding criteria was met. Polymer drilling fluids and viscosity modifying additives were used to maintain bore stability within the CIS and underlying sands, together with silicate-based agents to assist with annulus control.

Another key consideration when CFA piling in CIS is the tendency for fresh pile to fresh pile interaction due to installation effects. This communication between piles is due to the lateral displacement and compression of the soft soils as a result of the concrete pumping and head pressure. Overconsumption of concrete in piles within the CIS can typically be in the order of 40-60% and often approach values over 100%. Pile sequencing was planned in minute detail to ensure adequate space between any piles of 10 m installed in one day.

The biggest challenge for the CFA piles was installing reinforcement cages down to the full 30 m depth. Given the average workability time of self-compacting concrete, plunging a cage into the last portion of the pile, often the first concrete placed, at the toe was difficult. This was non-negotiable in the design, as even an early refusal of 0.5 m would have been unacceptable and required reinstallation. The contractor worked closely with the concrete supplier to ensure the workability life

of the mix allowed sufficient slump retention for cages to be plunged to 30 m. At the same time, the site team streamlined the cage lifting and handling procedure to minimise delays and ensured operators avoided over-pressurising the concrete during pouring or applying excessive force while drilling sockets, which could generate heat and cause premature curing in the socket.

The pile positions were set out to avoid the known redundant anchors, allowing a 4° tolerance for the anchors that fanned out from the Arts Centre. This worked in most cases but 16 piles still refused on anchors that had strayed beyond the tolerance fan. These clashes were all more than 15 m from the Arts Centre wall reinforcing that the clashes were likely due to anchors deviating more than 4°. Each time the contractor had to revise the pile position, which needed careful planning because of the adjustment and the increase in contributory area for the tension piles, or for the increased load span for retaining wall king piles that were affected.

JET GROUTING METHODOLOGY AND PERFORMANCE

A site-specific jetting trial was carried out to establish achievable column diameters and improved soil parameters. The trial parameters were based on prior experience in CIS and refined using observed data. Two forms of verification methods were used to confirm the column diameters: both methods mentioned below are based on bars installed within boreholes at varying radii from the centre of the jetted column.

1) An Acoustic Column Inspector (ACI) tool was used to confirm constructed radius of the columns. This involves recording of the acoustic resonance in feeler pipes, caused by the jetting stream impacting the radius feeler pipes which is then assessed against tell tales; and
2) Observation of Radius bars (tell tales) where scouring of the painted surface is evidence of column contact by the grout jet and therefore diameter.

Figure 4 shows output of the ACI. The trial also established dosage rates, rotation speeds and lift rates for different diameters. Columns of 2.5 m, 1.5 m and 0.6 m were ultimately used to form the base block.

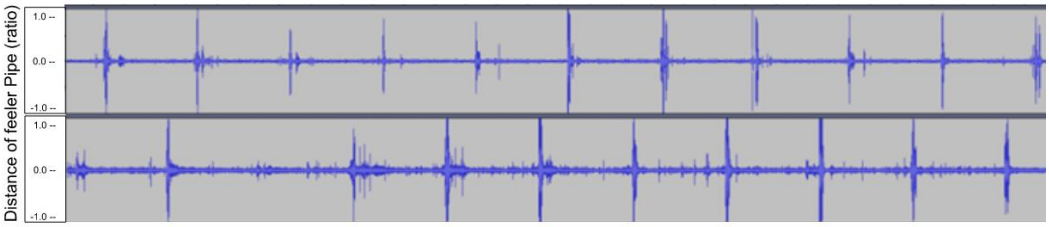


Fig. 4. Acoustic column inspector output

For the verification of target strength, jet grout material was sampled at surface during the jetting process. These samples were formed into cylinders, cured in water baths and tested for UCS and Young's modulus.

For the jet grout block, the decision was made to carry out the jet grouting after installation of the piling had been completed. The reasoning for this was to maximise the bond strength between the jet grout and the pile as it was such a critical part of the basement stability. Shadowing is a common effect in jet grouting when obstructions or inclusions are encountered within soil being treated, Arcos et al (2024) clearly shows the shadowing effect. Given the existing legacy obstructions within the basement footprint the decision to grout post piling further added to shadowing effects by jet grouting after the installation of 200 tension piles. This resulted in significantly more jet grout columns being required during pre-construction planning.

The construction team approached this issue with a targeted quality assurance plan. By monitoring/measuring deviation of each jet grout column through the drill stem using a vertical

 © Deep Foundations Institute 2026

inclinometer with roll guides, they were able to accurately plot the location of each column across the entire treatment depth. This allowed real time relocation or adjustment of column dimension to ensure complete coverage of the treatment. This method resulted in significant optimisation of the number of columns required for the project due to being able to maximise the effective area of each column and minimise shadowing.

Due to the nature of the CIS, a significant risk exists due to lack of consistent spoil returns during jetting. This can result in significant ground heave and lateral displacement. This is the result of collapse within the drilling annulus. To limit this impact, a combination of pre-cutting over the full bore and use of borehole liners was planned to manage the risk of hole collapse, specifically adjacent to the existing structures. Despite these controls, spoil returns were still inconsistent. To combat this the site team trialled polymers and stable chemical admixtures. While it was difficult to conclusively demonstrate improvement, field observations indicated that these additives assisted progress.

VERIFICATION AND OBSERVED PERFORMANCE

Piling

Three per cent of CFA and Bored piles were tested with Pile Dynamic Analysis. Across 11 tests, Case Pile Wave Analysis Program (CAPWAP) analysis indicated a mean shaft friction of 520 kPa in the siltstone sockets, verifying the design value of 400 kPa. CAPWAP also predicted end bearing stiffness approximately twice the design assumption, although full base capacity could not be mobilised within the applied test loads. For early piles constructed adjacent to boring locations, the pile drilling parameters (torque, crowd, penetration) were checked against expected socket conditions. The construction team recorded and plotted top-of-socket levels for each pile throughout the project to confirm alignment with surrounding piles. Selected piles were sampled for moisture content and Is_{50} (50 mm corrected point load index). The measured values were consistent with expected siltstone strengths, noting that UCS values for low strength, extremely to moderately weathered rock are commonly inferred to be of the order of 10 times Is_{50}. The results were used as a verification check to confirm the adopted socket design assumptions. Detailed calculations were undertaken prior to testing to establish allowable pile stress limits. This ensured that stresses induced during dynamic testing remained within acceptable limits and that no damage to the piles occurred.

In addition, a static load pull-out test on a micropile was carried out on a jet grout block trial to confirm the critical design parameter of pile to jet grout bond strength. Whilst this did not exactly replicate the installation method for the bored and CFA piles, it was considered acceptable and preferable given the cost effectiveness compared with a full-scale test on a bored or CFA pile within a jet grout block. The micropile was installed prior to jet grouting to replicate the construction sequence adopted for the permanent tension piles and base block.

Inclinometers were installed by the Contractor at six locations along the retaining wall, with in-place sensors used to continuously monitor movements. Alarms were configured in line with trigger levels defined by the design team, using a traffic-light system with green, amber and red representing limits of 60%, 80% and 110% of the predicted deflections.

Figure 5 shows the 2D and 3D FEM deflection predictions by Foundation Specialists Group (FSG) together with the inclinometer results. The inclinometer monitoring recorded a maximum deflection of about 15 mm, compared with 3D predictions ranging from 10 mm to 33 mm and 2D predictions up to 34 mm. The measured deflection profile peaked at RL4mAHD, whereas the FEM predictions placed the maximum deflection at approximately RL-3mAHD.

Keller requested that FSG carry out a back-analysis to investigate these differences. FSG's sensitivity checks concluded that the discrepancy was largely due to the use of a conservative lower-bound modulus for the jet grout base block and an assumption of poor connectivity with the existing Arts Centre basement in both the 2D and 3D analyses. Varying the CIS parameters did not improve the match between prediction and measurement. When mean or upper-bound values were adopted for the

 © Deep Foundations Institute 2026

jet grout modulus and hard contact was assumed with the existing basement, the predicted deflection profiles correlated closely with the inclinometer measurements.

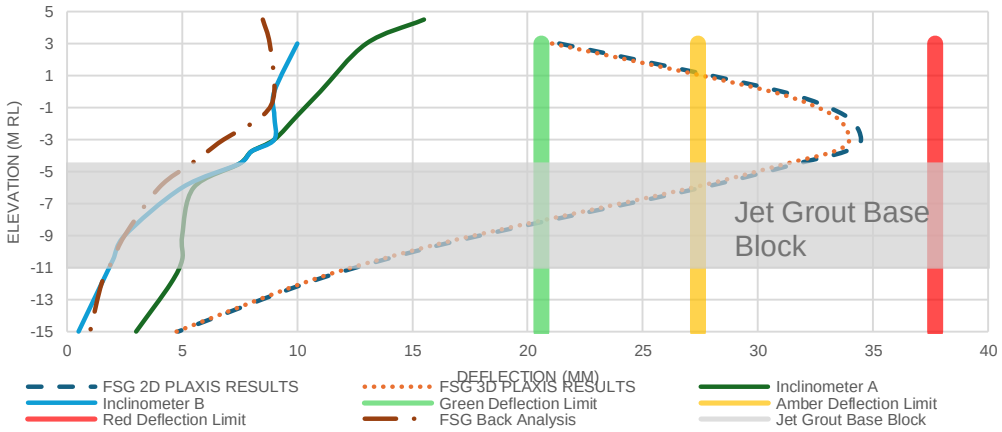


Fig. 5. FEM wall deflection predictions and actual inclinometer results

Jet grout

Following the determination of achievable jet grout diameters, a trial was undertaken to determine the tensile bond between the improved soil and a pile element, with the intent to verify the design assumptions. In this case a smaller diameter micropile was selected to represent the permanent tension piles. This proved to be a more economical and practical solution compared to a full scale (900 mm dia. pile), with limited space on site available. Critical to the test was ensuring the overburden material was completely de-bonded and any vertical movement of the jetted block during loading was identified. A simplified sketch of the test set-ups is shown below in Fig. 6.

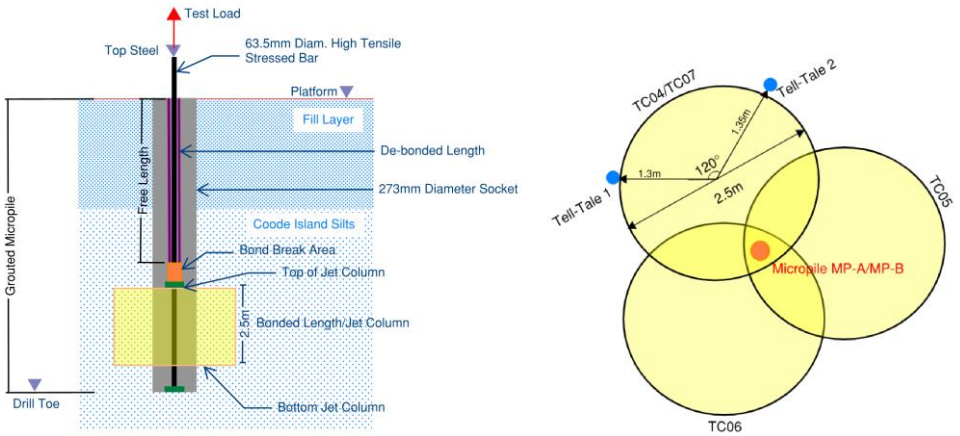


Fig. 6. Jet grout pull out test sketch

Two no. pull out tests were completed, with both tests exceeding the target design results. Ultimately the lower value of the two tests was used to verify the design. The lower of the two pull-out tests achieved a maximum bond stress of 657 kPa (average along the pile length), giving a factor of safety of 2.2 against the 300 kPa design value. No creep was observed and the displacement of the jet grout block was less than 1 mm when the test was stopped at the apparatus capacity. This indicates that additional capacity could likely have been mobilised with a larger test set-up. The results confirm that the adopted design bond value was conservative and appropriate.

Figure 7a and 7b show the test results from jet grout sampling for UCS and permeability. Jet grouting UCS testing was carried out on 217 samples returning a mean value of 4.2 MPa with a standard deviation of 2.5 MPa at 28-day strengths. Sampling of jet grout material was as per the site trials where material was collected at surface during the jetting process. Samples were formed into

cylinders (2:1 Height to Width ratio) and cured in temperature-controlled water baths. UCS testing was conducted in accordance with AS5101.4 and permeability testing to AS1289.6.7.3.

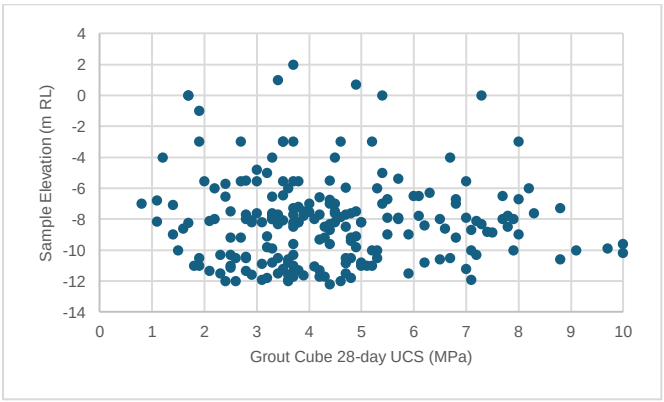


Fig. 7a. Jet grout UCS testing results

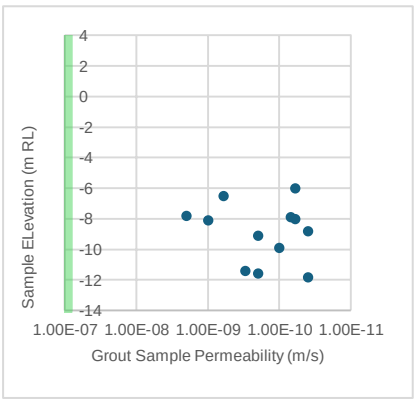


Fig. 7b. Jet grout permeability test results

LESSONS LEARNED AND INNOVATIONS

Deep pile cages in concrete CFA piles: One of the main lessons from the project was that full-length reinforcement cages to 30 m in CFA piles can be achieved under the right circumstances. Typically cages of this depth have only been constructed in CFA piles using grout. The authors are not aware of another project where cages of this depth have been installed reliably on such a large scale. Careful planning of the concrete mix design and cage handling on site was essential, with the workability window for self-compacting concrete being critical. Any early refusal, even by 0.5 m, was not acceptable. Close coordination with the concrete supplier and the site crews allowed consistent cage placement, but this remains a high-risk activity that must be managed from the outset.

Low headroom piling: Working under the spire highlighted the importance of having the right equipment for low headroom piling. The use of the low headroom piling rig with polymer slurry allowed bored piles to be constructed in restricted areas. Handling long cages in these zones was slower and required extra care, particularly with splicing and spacer selection. Attention must also be given to verticality and positional tolerance due to the greater number of kelly bar stages required in low headroom conditions.

Redundant Legacy Anchor Obstructions: Successfully working around the redundant anchors was achieved through careful planning by all stakeholders. Rectification strategies for different clash scenarios were prepared ahead of time, which helped minimise delays. It became evident that the legacy anchors were not all installed within the tolerances indicated in the QA records for the original structure. Information on as-built structures, as always, should be treated with caution and verified where possible.

Jet Grouting: The main innovation for the jet grout was being able to reduce the number of columns from the original layout substantially. This was achieved by using survey information from the vertical inclinometer to optimise effective jet grouting area by minimising overlap. This benefited the programme without reducing performance of the block in strength or permeability. The use of a micropile pull out test in a jet grout block to confirm pile to grout bond was also a useful approach, being cost-effective and giving confidence in the critical design parameter without needing to attempt a full scale CFA pile pull out in grout. The use of superplasticiser admixtures was trialled to improve spoil return fluidity. Field observations suggested this was beneficial, with increased UCS strength and reduced permeability, although further work is needed to confirm the extent of improvement.

FEM modelling vs measured deflections: The 2D and 3D finite element predictions demonstrated the benefit of three dimensional analysis for this project. The 2D models were generally more conservative, particularly in the truck lift pit where the 2D FEM predicted a maximum deflection of 67 mm compared to 50 mm from the 3D model, which showed closer agreement with the

inclinometer results. Outside the truck lift pit, the 2D and 3D FEM predictions were more closely aligned, as shown in Figure 5.

Back-analysis indicated that conservative assumptions for jet grout modulus and connectivity were the likely cause of the stiffer wall performance. For future projects, adopting mean values of jet grout strength where data are available may yield better correlation between predicted and actual deflections. Inclinometer monitoring remains essential, both to confirm performance and to refine modelling assumptions for subsequent designs.

CONCLUSIONS

The RACM project represented one of the first recent basements of 10 m to 15 m depth constructed in Coode Island Silt. The project highlighted a number of lessons for both designers and contractors, some of which reflected challenges not encountered previously in this area due to the advancement of construction technology and design methods since the last comparable basements in these conditions. The case history offers insights for future projects of a similar nature. Whilst the design analyses were shown to overpredict deflections and pile forces, the conservatism adopted was appropriate given the relative rarity of this type of excavation and the consequences of potential failures.

Early engagement and coordination between stakeholders, to agree on design methodology and parameters, was critical in progressing the project. Collaborative design input allowed challenges to be addressed as they arose and ensured that the retention and foundation system was developed with appropriate care and detail. This process also enables substantial planning to be undertaken prior to commencement, which facilitated clarity on sequencing and programme. Verification testing was prioritised across all elements of the design intent to ensure quality control requirements were consistently achieved.

This case demonstrates that deep basements in CIS can be successfully delivered with integrated structural geotechnical solutions, provided design conservatism, collaborative planning, and comprehensive verification are adopted

ACKNOWLEDGEMENTS

The authors acknowledge the contributions of Louis King and Parisa Oskooei of FSG for their support with finite element modelling, and Tom Ross, Project Manager, for his vital input throughout the works. The design engineers Alicja Kisielak and former colleague Richard Flynn are also recognised for their significant roles in developing the design and assisting with delivery of the project.

REFERENCES

Arcos, J.L., Fernández, R., and Gómez, P. 2024. Design and execution of retaining walls using the reinforced jet grouting technique. Proceedings of the XVIII ECSMGE, 2024, pp. 2071 - 2075

Fellenius, B.H. 1984. Negative skin friction and dragload on piles. Proceedings of Second International Seminar, Pile Foundations, Nanyang Technological Institute, Singapore, November 28 - 30, 12 p.

Peck, W.A., Neilson, J.L., Olds, R.J., and Seddon, K.D. 1992. Engineering geology of Melbourne. Proceedings of the Seminar on Engineering Geology of Melbourne, Melbourne, Australia, 16 September 1992, Balkema, Rotterdam, 327 p.

Standards Australia. 2009. AS 2159: Piling – Design and installation. Standards Australia, Sydney, Australia.

Topolnicki, M. 2017. Uplift control of jet grouted bottom plug by friction mobilized along embedded anchoring elements. Grouting 2017: Proceedings of the Fourth International Conference on Grouting, Deep Mixing, and Diaphragm Walls, Geotechnical Special Publication No. 289, pp. 82 - 91.

Yanni, J. 2016. On the long-term behaviour of tension loaded piles in natural soft soils. PhD thesis, Norwegian University of Science and Technology, Trondheim, Norway, 176 p.

 © Deep Foundations Institute 2026

CHALLENGES IN CONSTRUCTION OF HS2 DIAPHRAGM WALL SHAFTS

Simon Kavanagh, Intrafor Hong Kong Ltd., China, +852 9847 6588, si.kavanagh@vsl-intrafor.com
Neil Taylor, VSL Systems UK Ltd., London, United Kingdom, neil.taylor@vsl.com

ABSTRACT

High Speed 2 (HS2), Britain's new high-speed railway, is the biggest current transport infrastructure project in the country. The C1 contract crossing the Chilterns includes a requirement for 16 km of tunnel requiring 4 x 18.2 m internal diameter vent shafts constructed using diaphragm walls, up to 78.5 m deep. Pre-treatment grouting was required at all sites to mitigate the risk of major support fluid losses in weathered chalk strata. Post treatment grouting at break in break out blocks and shaft base plugs were also required. Geology comprised superficial deposits over structureless chalk including dissolution features; erosional features later backfilled with sands / gravels and alluvial deposits. Shaft design included the requirement for soft eyes to allow TBMs to shave the side of the shaft. Demanding verticality tolerances of 1 in 300 to 1 in 400 were required. Management of bentonite density influenced the rate of excavation. Milled joints resulted in increased bentonite contamination from chalk fines and concrete fines in closing panels. This paper discusses the logistical, geological and practical constraints that were identified during project preparation and overcome during execution of the specialist geotechnical works for the 4 shafts, and details the considerations implemented to address the key challenges that arose.

Keywords: Diaphragm Wall, Circular shafts, Chalk, Bentonite, Reinforcement, Concrete

INTRODUCTION

The Central 1 (C1) Main Works Civils contract for the High Speed Rail 2 project in the United Kingdom was awarded to the Align Joint Venture (JV) comprising Bouygues Travaux Publics, Sir Robert McAlpine and Volker Fitzpatrick, covering a significant section of the railway between the Chiltern Tunnel and the West Midlands, involving 16.04 km of 9.1 m internal diameter tunnels, several bridges, and complex structures like the Colne Valley Viaduct. The scope included the construction of 4 no. diaphragm wall shafts for intervention and tunnel ventilation.

The C1 Contract Design was undertaken post award by design team Align D, a Joint Venture of Ingerop Rendel Ltd, Jacobs and Bouygues Travaux Publics. Planning and construction of the diaphragm wall shafts gave rise to several logistical, geological and practical constraints that had to be addressed and overcome during execution of the specialist geotechnical work.

The shafts were located along the tunnel route as shown in Figs.1 and 2.

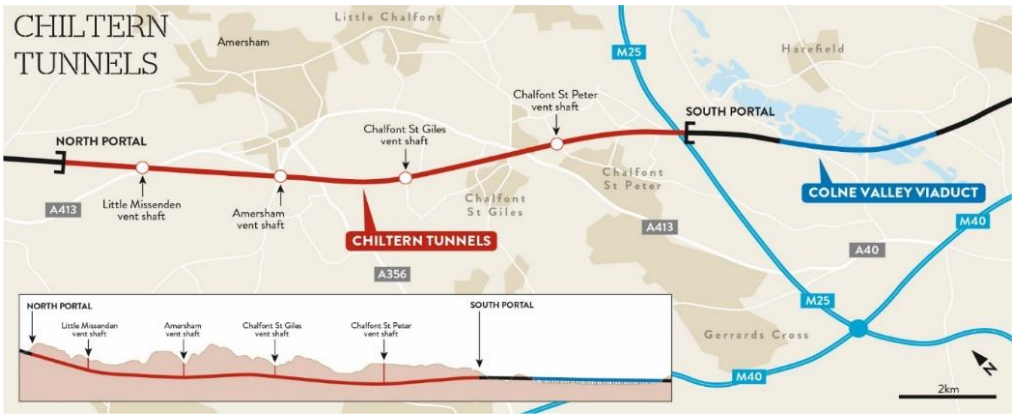


Fig. 1. Alignment of C1 Chiltern Tunnels showing shaft locations

 © Deep Foundations Institute 2026

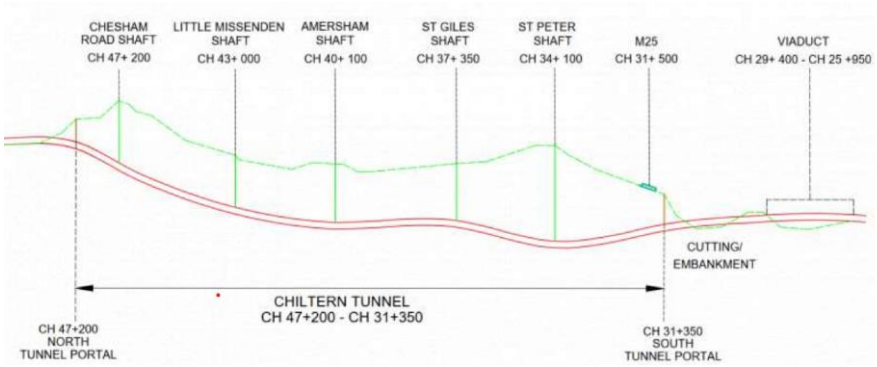


Fig. 2. Schematic alignment of C1 Chiltern Tunnels showing shaft chainages

Design for C1 was conducted in three stages, firstly Stage 1 (Scheme design), primarily used to estimate construction costs and detailed design fee. Design at Stage 1 was carried out to a sufficient level to allow confidence that a particular design solution could be developed to full design. Then Stage 2 detailed design commenced where the Stage 1 design was developed to a full design with Specifications, Construction Drawings and sequencing being issued.

To comply with HS2 project requirements for complex assets, such as these shafts, which carry considerable design risk, the third design stage required a category 3 (CAT 3) fully independent check, undertaken outside the design organisation (but appointed by the design organisation) where the HS2 standards are applied.

Discussion of the geotechnical investigation and design work undertaken for the HS2 C1 Shafts is given in the paper "Design and construction challenges of deep shafts in chalk" by Sivakumar et al. (2023).

DIAPHRAGM WALL SHAFTS

Shaft Details

The scope required permanent circular shafts 18.16 m Internal Diameter (ID) diaphragm walls with milled closing panels constructed in the sequence listed below to the wall thickness, depth and steel reinforcement content below.

Chalfont St Peter (CSP) – 1200 mm, 78.3 m deep, 79.14 kg/m3
Chalfont St Giles (CSG) – 1000 mm, 43.9 m deep, 145.06 kg/m3
Amersham (AMS) – 1000 mm, 59.6 m deep, 168.8 kg/m3
Little Missenden (LMI) – 1000 mm, 52.1 m deep, 170 5kg/m3.

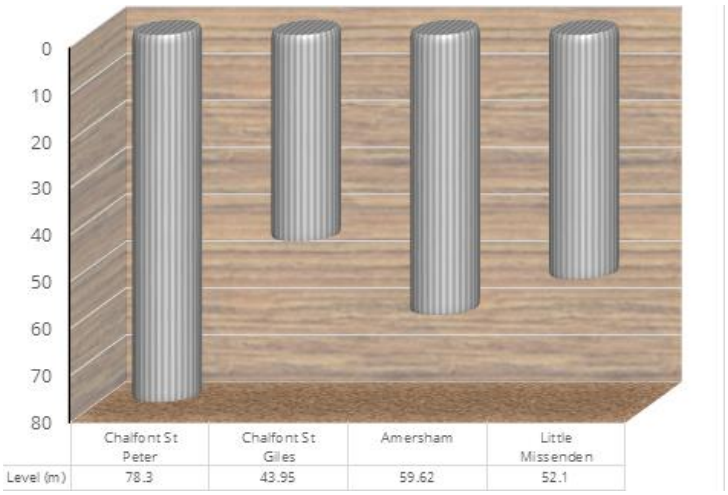


Fig. 3. Diaphragm wall shaft depths

Shaft Diaphragm Wall Details

Table 1. Principle details of diaphragm wall shafts

Founding Criteria	The structures work in skin friction. The termination criteria were determined by Align D following results from a previous pile load test, LTP1, assessing concrete to chalk friction after excavation under bentonite.
Design	The structures were designed for the tunnels to bite each side of the shaft necessitating that the shafts had to be constructed in advance of the tunnels.
Structural Concrete	C50/60
Tolerances	1:400 verticality at CSP only, 1:300 for remaining shallower shafts Setting out +/- 50 mm Cage Placement +/- 70 mm vertically, +/- 75 mm longitudinally. Coupler placement +/- 70 mm in any direction
Methodology	Grab to the base of the fill and into the structureless chalk (or a minimum of 7 m to the base of the stop-end in the closing panels). Installation of prefabricated cages using 2 service cranes. GFRP sections supported by temporary sacrificial steel frame to lift the cage from horizontal to vertical position. No excavation within 8 m of an open panel, or a panel concreted < 24 hrs.
Reinforcement	Steel cages with GFRP soft eyes where required
Site platforms	CSP platform was constructed of rolled aggregate but degraded significantly during the winter causing delay to the works. This was replaced on the other shafts by a concrete slab with cast French drain to control the overspill of bentonite and washout that was then pumped to Align's settlement and treatment tanks for later disposal.

The panel layout adopted required 16 no. panels per shaft (Fig. 4).

- 2 no. 1 bite primary panels (2800 mm)
- 6 no. 3 bite primary panels (6140-6360 mm)
- 8 no. 1 bite closing panels with milled joints. (2200 mm milled to 2800 mm)

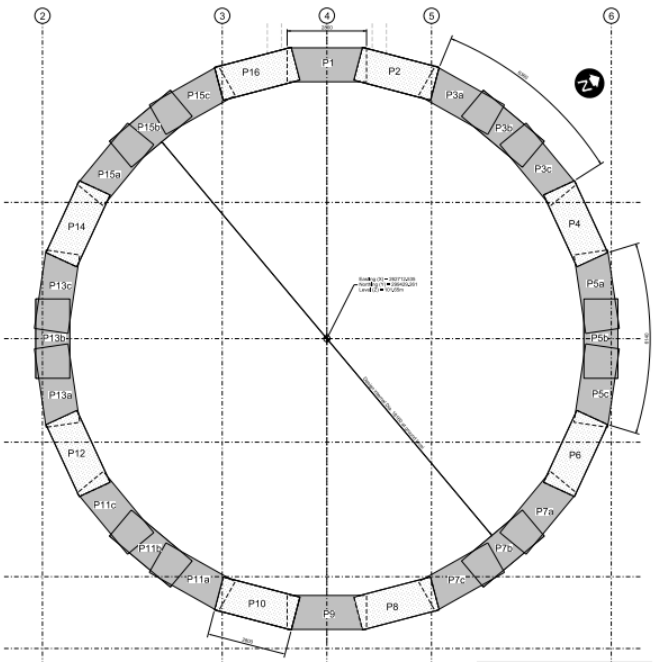


Fig. 4. Panel layout

 © Deep Foundations Institute 2026

In primary panels, a short 6 m stop-end was used to create the plane for mounting the void forming material to make the panel excavation rectangular and not trapezoidal for the 2800 m closing panels. Polystyrene and plywood were used to form the void. The use of the polystyrene created problems for the site in the dry months when the disaggregated polystyrene was blown across the site in the wind.

Generalised Ground Conditions

From the surface, a 6 m thickness of superficial deposits is underlain by structureless chalk (CIRIA C574 grades Dm or Dc) then weathered chalk (CIRIA C574 grade B and C), excavation through which resulted in a significant loss of support fluid at CSP that necessitated the grouting pre-treatment campaign on all subsequent sites. Beneath the weathered chalk, Seaford and Newhaven Chalk formations can be soft and include common dissolution features backfilled with sands/gravels/alluvial deposits. Below this the chalk becomes competent, blocky and less permeable but more transmissive. (CIRIA C574 grade A).

The Geotechnical Baseline Report provided baseline statements cover the following general geological setting, though conditions vary between each shaft location:

Table 2. Generalised Geological Summary

Material	**Thickness (m)**	**From**
Superficial Deposits: predominantly Clay-with-Flints but may contain Beaconsfield Gravel deposits. Flint maximum compressive strength 750 MPa.	6 [5.1 – 5.9]	95 m AOD
Structureless Chalk: chalk silt and gravel	5 m [4.5 to 7.5]	90 m AOD
Weathered Chalk: Seaford Chalk, predominately medium density with very closely to extremely closely spaced fractures	11m [2.4 to >14.9]	79 m AOD
Competent Chalk: comprising Lewes Nodular Chalk formation, a mixture of high and medium density chalk, displaying widely to very closely spaced fractures.	10.5m [2.4 to >14.9]	38.5 m AOD
Competent Chalk: comprising New Pit Chalk formation: a high-density chalk, displaying widely to very closely spaced fractures.	Proven to 38 m	0 m AOD
Design Groundwater Level: 80 m AOD (varies at different shaft locations)		



Fig. 5. CSG shallow geology - Weak high density white locally mottled light grey chalk

 © Deep Foundations Institute 2026



Fig. 6. CSG shaft basal geology - competent chalk

Table 3. Chalk density and other properties (BS5930)

	Low Density	**Medium Density**	**High Density**	**Very High Density**
Intact Dry Density (CIRIA C574, 2002)	<1.55 Mg/m^3	1.55 – 1.70 Mg/m^3	1.70 – 1.95 Mg/m^3	>1.95 Mg/m^3
Approximate UCS	<3 MPa	3 – 5 MPa	5 – 12.5 MPa	>12.5 MPa
BS 5930 strength term	Very Weak to Weak	Weak	Moderately Weak	Moderately Strong

PRE TREATMENT

When excavating at the first (CSP) shaft, large losses of bentonite arose at the heavily fractured weathered chalk interface of the initial panels. Because of the low water table at approximately 30 m below Working Platform Level, open fissures in the chalk above the water table allowed the bentonite support fluid to flow a significant distance into the surrounding strata due to the lack of restraining pressure from groundwater. As a result, pretreatment fissure grouting to form a grout curtain was required at each of the four remaining shaft locations before further diaphragm wall works were carried out. This added some 30–70 working days to the construction programme at different shafts.

The shafts were located within a Groundwater Source Protection Zone (SPZ 2) classified as a Principal Aquifer (Seaford and Newhaven Chalk Formations [undifferentiated]). Environmental concerns arose because the chalk is used as an aquifer to extract drinking water. Turbidity monitors were used to check bentonite or cement content in abstracted water. However, the volumes of grout and the distance the grout may travel raised concerns due to potential leaching of Chromium Cr (III) from cements.

Grout holes were drilled with water flush using 133 mm diameter drill rods to the designed toe of the diaphragm wall, at 2–2.5 m spacing around the shaft perimeter. Due to overhead power line restrictions, some drilling was restricted to 6 m headroom. Casing was installed in 2 m lengths. Stage grouting was carried out using packers below the cased length. Drill deviations of up to 2% were anticipated and achieved.

Injected grout volumes ranged from 95 to 400 m3 per shaft, up to 19% of rock volume at and below structureless chalk, substantially above planned grout intakes. A bentonite cement grout was injected

 © Deep Foundations Institute 2026

using packers or, at the end of casing, with closed head with > 1 bar pressure to a maximum a depth of 78 m.

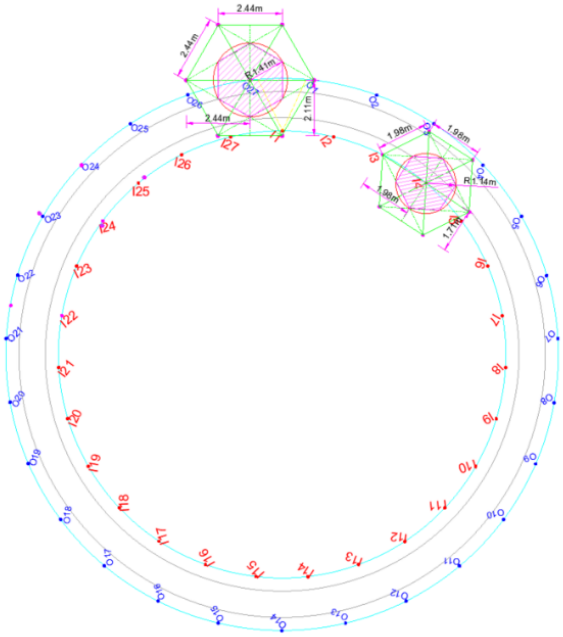


Fig. 7. Shaft grout pre-treatment layout

Termination criteria for the cement bentonite grout are noted below.

Table 4. Pre-treatment grouting termination criteria

Parameter	**Outer boreholes (Spacing 2.44m)**	**Inner boreholes (Spacing 1.98m)**
Maximum Injection Volume Per Stage, for each grout mix [Vmax]	18% consumption (as % of rock volume) at 2.44m c/c = 920 litres / m	18% consumption (as % of rock volume) at 1.98m c/c = 610 litres / m
Max Sustained Pressure [Pmax]	0.25 bar / metre + line losses	0.25 bar / metre + line losses
Target Pressure for Low flow termination set at 80% of Pmax	0.20 bar / metre + line losses	0.20 bar / metre + line losses
Low flow at Target Pressure [L/F]	Less than 5 litres / minute	Less than 5 litres / minute
Observation	Surfacing or Ground Heave	

The pretreatment grouting successfully minimised the risk of substantial bentonite loss during diaphragm wall excavation. In addition to pre-treatment grouting, post-treatment grouting, also drilled from the surface, was undertaken around the Break in Break Out (BIBO) block either side of each shaft, adit and base plug.

CONSTRUCTION METHODOLOGY AND LOGISTICAL CONSTRAINTS

Diaphragm wall construction was carried out working 24 hours per day (two shifts), 5 days per week. The available work area for each shaft was quite restricted. Reinforcement cages were fabricated off site and delivered “just in time” to minimise the need for on-site storage. The bentonite plant and spoil pits, (sunk into the working platform using precast L shaped elements) occupied a sizeable proportion of the footprint. Arrangements were made to minimise the space required for bentonite treatment by decanter and desilter. The limited working space resulted in challenging logistics and required coordination of use of loading areas.

 © Deep Foundations Institute 2026

At CSP, the original working platform was constructed of 6F5 off site processed hardcore recycled aggregate, but this was found to be no longer free draining after contamination. This delayed the diaphragm wall, and the start of grouting works at CSP. After this and the Early Warning Notices that the incident generated, all subsequent working platforms were provided using a concrete slab for the working areas where cranes were to be tracked. This worked well for the remainder of the shafts and was effective in increasing the machine efficiency, partly because no downtime was required for platform maintenance.

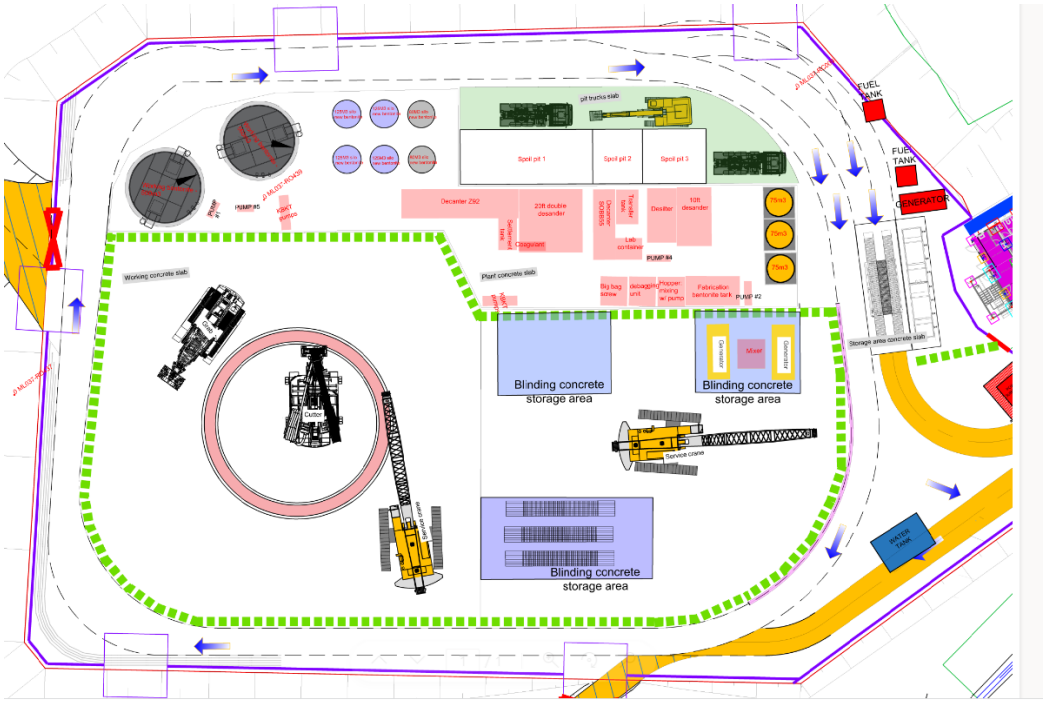


Fig. 8. CSG - Full site installation (green line delineates the extent of the structural slab)

Key plant used included:

- 1 no. MC96 base crane & BC40 Cutter frame
- 1 no. MC76 base crane & hydraulic grab
- 1 no. HS8100 as a service crane
- 1 no. 90t service crane

At CSP and CSG sites, production was hindered by cage availability issues that dictated the programme, this issue was resolved by the time the AMS and LMI shafts commenced. At all shafts, one of the biggest challenges for diaphragm wall excavation was bentonite treatment resulting in the rate of excavation often being determined by management of bentonite mud density and cleaning of contamination.

The hydraulic grab was used only to open the initial 6–8 m depth of panels, to excavate the single bite primaries, to extract stop ends and occasionally to clean the panel base; the grab was purely in attendance, so its utilization is so low. Despite this, it was considered not cost effective to remove the grab crane, which would then have required use of the service crane for intermittent grabbing operations. If sufficient working space is available, the critical path of excavation runs through the cutter for all the diaphragm wall shafts.

Excavation rates in the chalk were highly variable as anticipated. Closing panels showed more consistent excavation rates whilst milling concrete at the panel joints. The slower excavation rate of closing panels allowed more time to manage bentonite density / pollution. Average Cutter production achieved is shown in Table 5.

 © Deep Foundations Institute 2026

Table 5. Cutter excavation rate per panel type

Panel Type	Unit	CSP	CSG	AMS	LMI	Avg. all shafts
Primary	m3/hr	2.98	5.42	4.73	7.8	5.23
Closing	m3/hr	3.04	2.68	1.93	5.26	3.23

The above allows comparison of the differential in excavation rate between the primary and closing panels (assuming similar geology). Each shaft had two single bite primaries with the remainder of primaries being 3 bites.

BENTONITE TREATMENT AND DISPOSAL

Chalk is a very soft rock with a very variable flint concentration and can be dug easily. Chalk disaggregation increases with time during agitation in contact with water. Due to the centrifugal pumps used during the return of the bentonite fluid to and within the treatment plant, and the turbulence of the pipeline system, the chalk is further broken down.

The TBM team of Align conducted trials of agitating chalk slurry to determine the reduction of particle size distribution (PSD) with time during agitation. These showed a significant change in PSD with time and a sharp increase of particles passing at 63µm.

Chalk dilution in bentonite slurry test			
Time in cement mixer [min]	% > 6 mm	% 6 mm to 63 µm	% < 63 µm
5	68,0%	3,2%	28,8%
10	53,0%	7,0%	40,0%
20	36,0%	14,4%	49,6%
30	27,5%	18,1%	54,4%
60	15,5%	23,7%	60,8%

Fig. 9. Chalk particle dilution in bentonite (Align trials 2020)

For the diaphragm wall bentonite separation plant, this meant that 60% of return fluid would pass a 16 µm sieve and so be required to be handled by the hydro-cyclones and centrifuge working in decanting mode, thinning some of the circulating fluid (constrained by plant throughput capacity) for reuse.

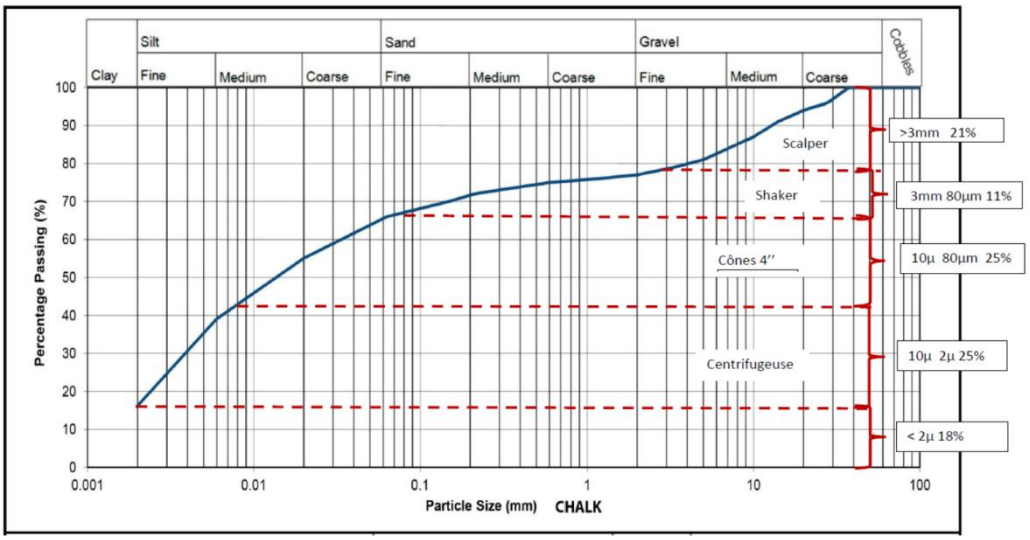


Fig. 10. PSD curve and treatment stage for bentonite mud containing chalk (generalised)

 © Deep Foundations Institute 2026

The result was that the standard treatment plant normally used on a site milling “hard rock” would not be suitable for HS2 unless the project accepted disposal of the full panel volume of bentonite mud upon completion of each panel which would have been very expensive.

Pollution of the bentonite support slurry arose from chalk fines from milling and mud circulation through centrifugal pumps associated with the cutter, in addition to concrete fines from milling the closing panels.

A 20 ft Recycler fabricated for the project used a gravity feed rather than using a base tank for storage and recycling. This limits sedimentation and therefore maintenance of the storage tanks and reduces the reduction of the particle size by reducing the number of cycles through the pumps.

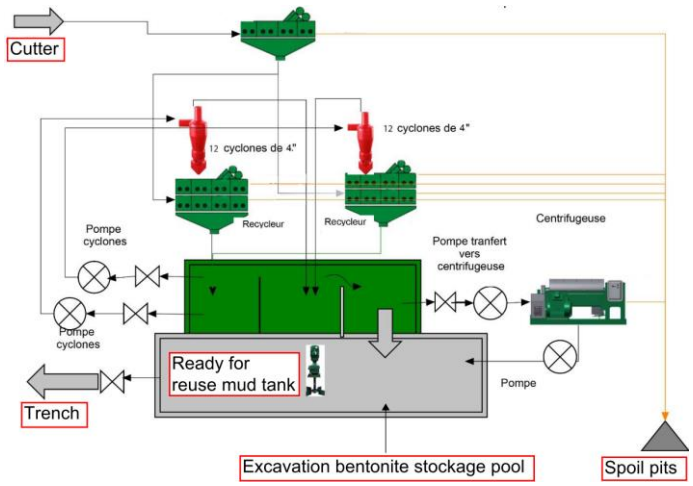


Fig. 11. Bentonite mud treatment process

By introducing 2 no. centrifuges to the site arrangement, it was much easier to manage the bentonite density in real time. The Solids Controls Step Oil Tools SOB55 was used in decanting. The Flottweg Z92 centrifuge operates at higher flow rates and was used for bentonite dewatering prior to disposal off site.



Scalper and primary screen, 1.4 and 2.8

Secondary screen,

Desilting screen after cyclones, 137.5 to 165

Output from centrifuge

Fig. 12. Bentonite treatment outputs

The centrifuge was limited to 8 µm by purely mechanical decantation (50 m3/hr). Addition of polymer allowed reduction to 2 µm (30 m3/h).

Bentonite management concentrated on the pollution of chalk particles and not the pH as this is easily resolved and quite common in all diaphragm wall projects in varying geologies. Hence, it was important to control mud parameters and monitor density. The team, at times, pushed for production

rather than slowing the cutter progress to match the available mud treatment rate. During panel excavation, bentonite was diluted with fresh mud to ensure excavation could be completed and mud density be managed later using the available centrifuge capacity when the cutter was not operating.

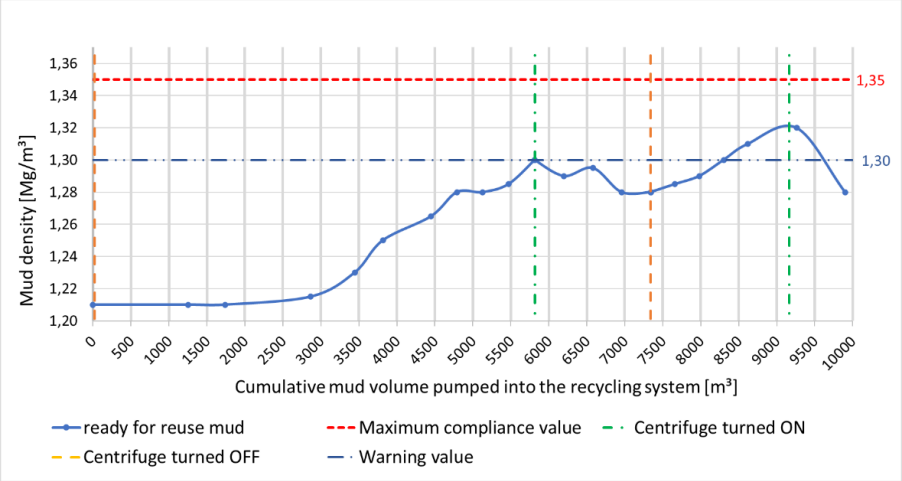


Fig. 13. Mud density evolution (with volume)

The bentonite treatment plant was managed by experienced specialist civil engineering and oilfield mud technicians. Other than losses to the ground, bentonite mud was only disposed of at the end of construction of the diaphragm wall at each shaft.

At CSP, 6300 m3 of excavation was completed but only 400 m3 of mud disposed off site. Without the centrifuges the project would have needed to dispose approximately 9500 m3 of mud at much greater cost than the cost of the centrifuges and consumables. Reusable mud was transferred to the next shaft site on completion of each shaft. Because of the bentonite recycling, post pre-treatment losses were limited to 5% of the excavated volume per day of operation.

The sludge generated by diaphragm wall excavation was treated at the surface using a mobile plant to segregate solid material for disposal and recover water to reuse in bentonite production. As dewatering changes the physical characteristics of the waste by removing water and reducing volume, this is considered a waste treatment process, therefore an environmental permit is required to be held by the waste producer and waste manager.

Each shaft was classified as a site and required separate deployment submissions. The deployment describes the process, the environmental setting and the management and monitoring conditions to be implemented. The application process is straightforward, but the Environment Agency's (EA) review process can take more than one month with requests for further details. Since the operations cannot be initiated until the Deployment Letter has been issued, timely preparation and application are important to ensure there is no delay in the beginning of the operations. The process was always managed without significant issues.

During operations, the EA can undertake inspections. Inspections to the mobile plant were always included as part of the wider EA site visit and led by the Client, Align. Operations were always compliant.

REINFORCEMENT CAGES DESIGN AND FABRICATION

Shop drawings were underdeveloped at Stage 1 design with the intent to allow maximum flexibility for specialist contractor input. However, the final shop drawing development process became very time consuming, typically > 3 months. The design allowed for only very limited mirroring of cages and fabrication struggled to achieve the designed density of links and couplers. Initial design for

hooked bars was proposed to be replaced by Terminator Couplers, but these were not widely nor readily available and so this was not adopted.

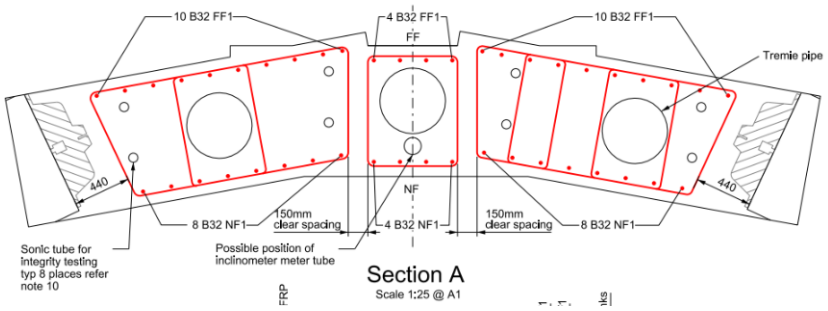


Fig. 14. Three cage primary panel reinforcement CSP

The initial design drawings required 3 cages in each of the 3 bite primaries. This was delivered at Chalfont St Peter, but problems arose with clearance and cages getting stuck on descent, with only 2 service cranes this was quite risky. The cage layout was changed to 2 cages with a crank for CSG, AMS and LMI.

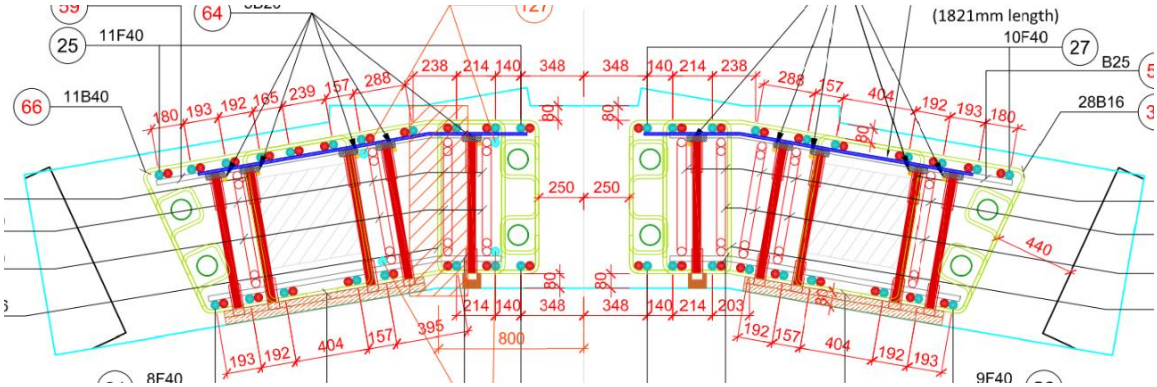


Fig.15. 2 x cranked cage primary panel arrangement CSG, AMS and LMI

Cages are fully welded, which must be done under factory conditions to maintain CARES (Certification Authority for Reinforcing Steel) certification. The requirement for an elliptical soft eye shape was more complex to set out and construct rather than just a square soft eye resulting in non-uniform rigidity to the cage. To overcome this the design called for a temporary plate U-bolted to the front side of the GFRP, which was required to be removed during installation. At least a couple of plates were left on as they were caught by the TBM.

The UK is predominantly a piling dominated foundation market using automated cage production. There are only 4 suppliers with capacity for diaphragm wall cage production, all were invited to submit proposals for supply, shop drawing, fabrication and delivery of cages. At this time the reinforcement fabrication market was facing increased demand for diaphragm wall cages during the initial phases of HS2 with four other diaphragm wall projects being built concurrently. The other projects' cage requirements were much greater than the C1 shafts so could better leverage scale.

Cage fabrication procurement raised numerous problems, partly due to a relatively small fabrication volume. Initially, a fabricator was selected for CSP though they were also already delivering another diaphragm wall project such that C1 shaft cages would have to slot into a very tight schedule without disrupting the ongoing project. The supply and fabrication at remaining shafts were not awarded at that time as the supplier could not demonstrate ability to meet the required programme.

Reinforcement cage works were let as an NEC3 Supply Contract to be back-to-back with the diaphragm wall contract. The supplier's limited experience of this contract led to even the most minor

 © Deep Foundations Institute 2026

changes from Align D interrupting the shop drawing production and, therefore, because of the supplier's already full production schedule, each change caused a production delay and movement to the back of the fabrication queue.

Design development was particularly challenging and for all parties and the selected fabricator could not meet the CSP cage programme leading to a contractual dispute. At CSG the diaphragm wall construction programme was predominantly driven by cage availability rather than excavation speed.

The decision was taken during construction at CSP to re-tender the remainder of the cage fabrication work and not continue with the initial fabricator for the next shafts. Consequently, the order for reinforcement cage supply and fabrication for CSG was not confirmed until 1 month before the start on site, which meant that the CSG shaft construction programme was dictated by cage availability.

For the remaining shafts, supply and fabrication of cages was subcontracted to a French company though they did not hold CARES equivalent certification leading to a lengthy process to get the cage fabrication approved under the French equivalent AFCAB (Association Francaise de Certification Armature Beton). Fabrication quality was not as good, but supply was not an issue and minor changes to shop drawings did not send cages to the back of the queue. The fabricator promised to match fit cages during fabrication but clashes of splicing bands during splicing still arose on site.

For CSG, shop drawing production was given to a different service provider, whilst the process between Align D and other stakeholders was made much easier, all design and drafting errors that prevented generation of a Bar Bending Schedule were treated as Compensation Events.

Due to production delays, the final 2 closing panels for CSG shaft were let to another fabricator who stated that they could meet the production schedule. Whilst the detailing was very professional, cages were again late in delivery.

For AMS, LMI and the North Portal diaphragm wall works, cages were fabricated in Paris with cut and bend conducted in Northern Spain. Whilst not desirable from an environmental perspective, this secured delivery to programme. It did however make off site cage inspection before delivery impractical.

Other fabrication issues included spacers and GFRP being shipped to the fabricators directly as they did not want to manage these aspects outside of their standard supply chain. Retaining brackets for sonic tubes were at times poorly located and were often removed during installation.

Approval of the AFCAB certification, equivalent to CARES, of AMS, LMI and NP diaphragm wall cages was not finally granted until early 2023 well after the walls were complete.

OTHER CHALLENGES AND MITIGATIONS

Concrete was provided by Align JV with a wastage allowance of 8% of theoretical volume and only 30-minute waiting time allowance. The concrete batching plant was located at the South Portal. Maintenance of an adequate delivery rate became poorer as the delivery location moved further north, resulting in an Early Warning Notice that the rate of delivery was having an adverse impact on the rate of concrete rise during a pour. Compliance with BS EN 1538; clause 8.8.3.13 was a problem. A minimum delivery rate was discussed in contract negotiations but only carried forward to the contract to the extent of compliance with SPERW and the EFFC/DFI Guide for Tremie Concrete.

An NCR was raised for each shaft to record that the concrete delivery rate for diaphragm wall panels was below the acceptable standard affecting rate of rise during the pours such as the example below.

"The rate of concrete delivery to P11 on 14/04/21 fell below the requirements of BS EN 1538; clause 8.8.3.13 which states: 'In order to ensure concrete integrity, the rate of concrete rising over the full

height of the panel should not be less than 3 m/h'. During the concreting, rates as low as 2.4m/hr were observed. This may affect the quality of the concrete placed in Panel 11."

The concrete mix design approved by Align JV from mix trials prior to the subcontract award for this scope for use in the diaphragm walls is shown in Table 6.

Table 6. Key Concrete Mix design parameters for HS2 C1 Diaphragm Walls

MATERIAL SUMMARY SHEET

Supplier	Tarmac		**Material**	Ready Mixed Concrete
Designation	C50/60 CIIIB 620mm Flow		**Date Submitted**	05.08.20
ALIGN MATERIAL APPROVALS CHECK LIST				
Concrete Design (Chalfont St Peter Diaphragm Wall)				
	Specification	**Actual**	**Comply**	**Remarks**
Minimum Cement Content kg/m^3	380	**470**	Yes	Suppliers Concrete Design Certificate
Maximum Cement Content kg/m^3	550		Yes	
Cement Class	CIIIA / CIIIB	**CIIIB**	Yes	
Minimum Percentage GGBS	40	**70**	Yes	
Contractor Preferred Consistence Class	Target Flow 620+/-50mm	**Target Flow 620+/-50mm**	Yes	
Contractor 6 Hour Consistence Retention	F5 Flow (540-640mm)	**580mm**	Yes	
Contractor 12 Hour Consistence Retention	Min. 400mm Flow	**550mm**	Yes	
Maximum Free water/cement ratio	0.50	**0.38**	Yes	
Maximum nominal aggregate size mm	20	**20**	Yes	
Compressive Strength Class	C50/60	**C50/60**	Yes	
Exposure Class	XC2	**XC2**	Yes	
Design Chemical Class	DC-1	**DC-1**	Yes	
Chloride Content By Mass of Cement (%)	Max 0.30%	**0.11%**	Yes	Suppliers Calculation
Sulfate content by Mass of Cement (%)	Required	**1.05**	Yes	
Total Alkali Content kg/m^3	3.50	**1.32**	Yes	
Other Requirements				

Problems were identified concerning concrete mix stability. In the early hours following the completion of concreting, there was frequently excessive latency noted on the surface of the concreted panel. The latency could be seen welling up in real time. Upon excavation inside the shafts, bleed paths were revealed showing no fines content in these channels. Upon further visual inspection, these did not appear to be continuous, and no defects were identified on the sonic logs. It was therefore assumed that this was some form of pressure filtration that caused the flow of water to the perimeter of the pour. Where the water could not penetrate the substrate, it moved vertically.

D Wall Reinforcement Cage Spacers (All Shafts)

Experience has shown that trapezoidal shaped precast concrete spacers allow the cage to move down the excavation surface without making too much impact on the finished walls. Efforts at the launch of the diaphragm wall works to get approval to use precast concrete spacers for cages failed. As a result, the standard spacers provided in the UK for piling projects, which are 8 mm steel covered in plastic were used. However, due to the bentonite cake production and the soft nature of the hydrated chalk in the upper sections, the piling spacers were exposed in places after excavation. The exposed steel was considered to be a corrosion risk, which would not have arisen with use of the precast concrete spacers.



Fig. 16. "Piling" spacers exposed in wall surface and grout segregation

 © Deep Foundations Institute 2026

This required spacers to be covered with waterproofing mortar MBCC Master Emaco before the internal jump form was applied the internal concrete walls. Since repairs were completed after the completion of internal shaft excavation, these were done from man rider mounted on a surface crane.

Coupler placement by Align D was very dense and created significant problems with concrete flow around the fringes and the coupler faces resulting in poor concrete flow / caking around clusters. The coupler requirement was dictated by connection design to internal shaft structures. Once exposed by internal excavation, some of these clusters had to be jetted out and broken back to ensure that concrete quality was acceptable at the internal surface prior to waterproofing application.



Fig. 17. CSP base slab couplers



Fig. 18. Coupler grouping (after jet washing)

OBSERVATIONS AND LESSONS LEARNED

The key success of the project was in the management of bentonite density and pollution of the mud, which resulted in much lower disposal volume and costs to the project. A bespoke recycler utilising gravity between scalper and desander was developed to prevent particle cutting by centrifugal pumps that would increase mud density and reducing plant footprint.

Another benefit came from bentonite plant pipework and cable layouts being preplanned before on-site establishment to maximise efficiency, including to accommodate a desander, desilter and centrifuge in the smallest practical footprint and maximise reuse of components between sites.



Fig. 19. Typical bentonite plant pipework layout

Another success came from improvement in the engagement with the designer and ensuring the that design structural intent is better developed before commencing the detailing stage.

For a future similar project, it would be beneficial to carry out extensive pre-construction constant head testing or “light mobilisation” for pre-treatment to ensure bentonite support fluid losses are controllable from commencement.

CONCLUSIONS

The 4 no. diaphragm wall shafts required for the C1 Contract of HS2 were successfully constructed in challenging ground conditions and have now been incorporated into the permanent works. Shaft construction required extensive pre-treatment by grouting of fissures, cavities and dissolution features in the chalk as an essential measure to limit bentonite support fluid losses into the chalk, which would potentially affect ground water abstraction. Cutter excavation in chalk and milling of panel joints results in significant bentonite contamination, which requires extensive treatment and doing this greatly reduced the need for offsite disposal of contaminated material.

Construction of the early shafts was driven mostly by procurement and fabrication issues of reinforcement cages arising from the limited industry capacity in the UK for this type of work. Early specialist involvement in the reinforcement design and detailing process is essential. The efficiency of cutter excavation machinery (which was on the critical path) is enhanced by provision of a concrete working platform.

ACKNOWLEDGMENTS

The authors wish to acknowledge our client Align JV, the project developer High Speed Two Limited (HS2), our Joint Venture partner in delivery of these works, Keller Ltd. and the whole team at VSL Systems UK Ltd who contributed their time and skills to successfully deliver this project.

REFERENCES

Design and construction challenges of deep shafts in Chalk. R. Sivakumar, A. Maheetharan, M. Bevan & I Thomas. International Tunnelling Association (ITA) and AITES World Tunnel Congress 2023, Athens, Greece.

 © Deep Foundations Institute 2026

TWO-TIERED SHEET PILE WALL SYSTEMS: DESIGN, EXECUTION AND FIELD PERFORMANCE

Suresh Kumar Paluri, WSP Australia Pty. Ltd., Australia, suresh.paluri@wsp.com
Su Kwong Tan, WSP Australia Pty. Ltd., Australia, sukwong.tan@wsp.com

ABSTRACT

This paper presents a detailed investigation into the design, construction, and performance of two-tiered temporary cantilevered sheet pile walls, with specific focus on two recent infrastructure projects where this system was successfully implemented. The two-tiered configuration offers a practical solution for deep excavations (up to 6 m) in constrained urban environments, where traditional support systems may be limited by spatial, geotechnical, or logistical constraints. Through comparative analysis of the selected case studies, this paper explores key engineering challenges, including soil-structure interaction, tiered wall stability, construction sequencing, and groundwater management. Survey monitoring results were reviewed to assess wall performance against design expectations and assessment of ground movement impacts on the adjacent infrastructure. The findings highlight critical considerations for optimising wall geometry, retaining systems, and tier spacing to ensure structural integrity and construction efficiency. Lessons learned and best practices are summarised herein to guide future applications of multi-level temporary shoring systems in complex geotechnical settings.

Keywords: soil-structure interaction, displacement, construction sequencing

INTRODUCTION

Temporary earth retention systems are critical components in the construction of deep excavations, particularly in urban infrastructure projects where space constraints, complex ground conditions, and existing assets demand flexible and reliable support solutions. Among these, sheet pile walls are a widely used method for temporary shoring due to their rapid installation, cost-effectiveness, and adaptability to varying site conditions. While single-tiered sheet pile walls are well documented and commonly applied, two-tiered configurations are less frequently utilised and remain underrepresented in published technical literature. This paper aims to address this knowledge gap by presenting and analysing two recent infrastructure projects in Perth, Western Australia, where two-tiered temporary sheet pile wall systems were successfully employed. The first case study (Site 1) focuses on the Malaga Pedestrian Bridge, constructed as part of the Tonkin Highway upgrade. The second case study (Site 2) involves the Belmont Pedestrian Bridge, located within the Belmont Park redevelopment precinct. In both projects, the two-tiered sheet pile system was selected to accommodate relatively deep excavation requirements adjacent to live traffic corridors and existing infrastructure, while ensuring minimal ground movement and maximum safety. Through detailed examination of these case studies, this paper explores the engineering design considerations, construction methodologies, geotechnical challenges, and field performance monitoring of the two-tiered systems. The outcomes contribute valuable insights into the practical application of multi-level sheet pile walls in real-world settings, with the goal of informing future projects where such systems may offer strategic advantages.

MALAGA PEDESTRIAN BRIDGE – TONKIN HIGHWAY (SITE 1)

Project Background

The Tonkin Gap Project, located ~8 km east of Perth between Collier Road and Dunreath Drive, forms part of a 2019 infrastructure package. As part of the MEL (Morley–Ellenbrook Line) development, a new footbridge was required to connect Ballajura with the future Malaga Train Station. The Tonkin Gap Alliance (TGA) was responsible for the design and construction of this single-span arch footbridge over Tonkin Highway, spanning approximately 85 m without intermediate support to accommodate future rail infrastructure. Due to site constraints, temporary works were necessary at Abutment 2 (illustrated in Fig. 1). A two-tiered temporary sheet pile wall system was adopted over a single-tier alternative for economic reasons, spatial constraints, and to avoid conflicts with existing

 © Deep Foundations Institute 2026

services. The original single-sheet design required soil anchors that would have clashed with services and extended beyond the project boundary.

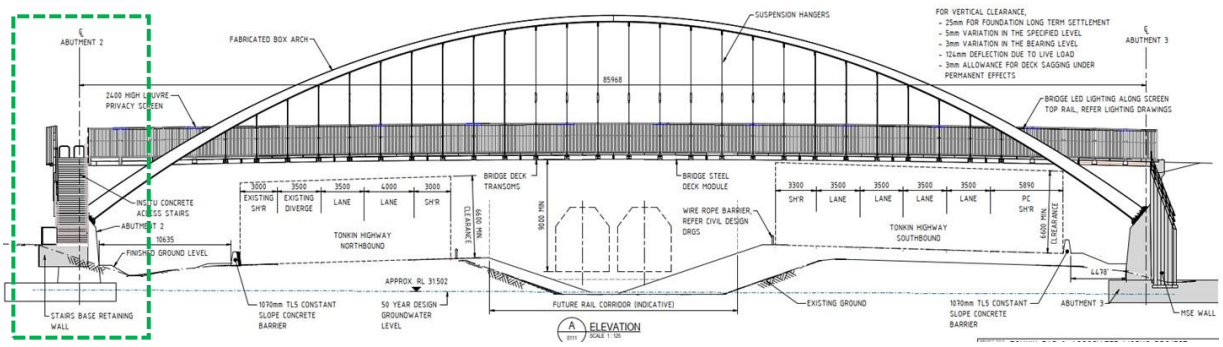


Fig. 1. Malaga Pedestrian Bridge over Tonkin highway

Site Conditions

The generalised subsurface stratigraphy at the bridge site comprises medium dense to very dense Bassendean Sand extending to around RL 16 m AHD overlying dense to very dense sand with interbedded medium dense to dense sands and very stiff to hard clays (Guildford Formation). Figure 2 illustrates geological long section at the bridge location. Based on the CPT testing, we note that at a couple of locations, shallow refusal has been encountered. This could be due to the presence of variable cemented sand locally referred to as Coffee Rock. The geotechnical parameters inferred at the Abutment 2 location are provided in Table 1. The design groundwater level at the bridge site is about RL 31 m AHD on the west side (i.e., Abutment 2) of the Tonkin Highway.

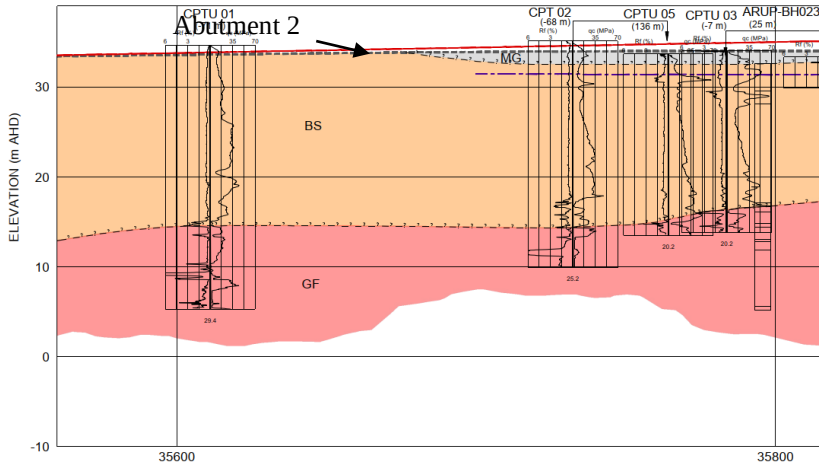


Fig. 2. Geological long section at the bridge location.

Table 1. Geotechnical Parameters inferred at the Abutment 2 location

Units	γ_{sat}[kN/m^3]	c' [kPa]	ø' [^{0}]	E' [MPa]	n [-]
BS - Bassendean sand (MD)	18	0	33	50	0.2
GF - Guildford formation sand (D- VD)	20	0	38	100	0.2

Notes: γ = unit weight; c' = drained cohesion; ø' = drained friction angle; E' = drained Young's modulus; n = Poisson's ratio;

Sheet Pile Wall Analysis and Design-Numerical Modelling

The contractor installed a two-tier sheet pile wall at Abutment 2, designed with a total retained height of 4.7 m (2.1 m for upper-tier, 2.6 m for lower-tier). During partial excavation, deflections of ~50 mm

 © Deep Foundations Institute 2026

were observed at the upper-tier sheet pile wall top, and ~15 mm at the existing noise wall (1 m behind the piles), raising stability concerns.

In response, WSP (Engineer of Record) was engaged to independently review the temporary works design and provide remediation advice.

Construction timeline (as per contractor):
- Upper tier sheet pile wall installed; top of platform level at RL 35 m AHD.
- Excavation in front of upper-tier sheet pile wall to RL 32.9 m AHD
- Lower-tier sheet pile wall installed
- 4 no. additional sheet piles were installed on the northern end of the wall to minimise over spill
- Large vibrations were induced to try and drive the sheet piles.
- Survey monitoring indicated 20 mm deflection in top tier sheets and maximum 3 mm deflection in noise wall
- 4 no. sheet piles pre-augured and installed to the southern side of the upper-tier sheet pile wall with no monitoring survey undertaken
- Commenced excavation to lower tier to RL 31.5 m AHD but paused when groundwater encountered, which was (circa 500 mm) higher than expected. Survey undertaken on sheet piles and larger movements reported.
- The required excavation level to the lower sheet piles is RL 30.3 m AHD
- Backfilled lower tier fully to RL 32.9 m AHD and daily monitoring undertaken

A site inspection, together with a review of the temporary works design, was carried out by Engineer of Record to assess the site conditions and identify the causes of the movements observed in both the sheet pile wall and the existing noise wall.

The review concluded that the temporary works design did not adequately consider the cumulative deflections from the two-tiers sheet pile wall arrangement. Although global stability was addressed via embedment depths, the design had not considered how deflections in the lower-tier sheet pile wall contributed to additional movement in the upper tier sheet pile wall. This deflection at the upper-tier sheet piles was compounded by construction sequencing, lower-tier deflections, lateral loads from the nearby noise wall, and higher-than-expected groundwater levels. The reliance on limit equilibrium software alone was insufficient for this complex scenario. Furthermore, the lateral load from the noise wall located just 1 m behind the upper-tier sheet pile wall was effectively transferred directly onto the sheet pile wall, as the design did not account for the actual load path through the noise wall foundation.

The temporary works design did not fully address the effects of dewatering on wall deflections, particularly the interaction between lower-tier sheet pile wall movements and additional displacements in the upper-tier sheet pile wall during dewatering. To assess these effects, a detailed analysis using PLAXIS (2021) was undertaken, incorporating the staged two-tier excavation and modelling the noise wall foundation under the following conditions:
- 12 kN/m lateral load and 20 kNm moment at the top of the noise wall pile
- 5 kPa surcharge behind the wall
- Dewatered profile with 0.9 m bulk excavation level in front of both sides of the sheet pile wall

Preliminary analysis showed that deflections in the lower-tier sheet pile wall significantly influenced movements in the upper-tier sheet pile wall and affected the stability of the adjacent noise wall. Without a temporary prop, upper-tier sheet pile wall deflections could exceed 120 mm, but reduce to ~45 mm with propping. The analysis confirmed that, unless the lower-tier sheet pile wall was propped or both tiers strengthened, excavation to RL 30.3 m AHD would result in excessive deflections and increased lateral movement of the noise wall. Considering site constraints and the project schedule, the adopted solution was to structurally enhance both tiers and revise the construction sequence to better control deflections and minimise impacts on the noise wall.

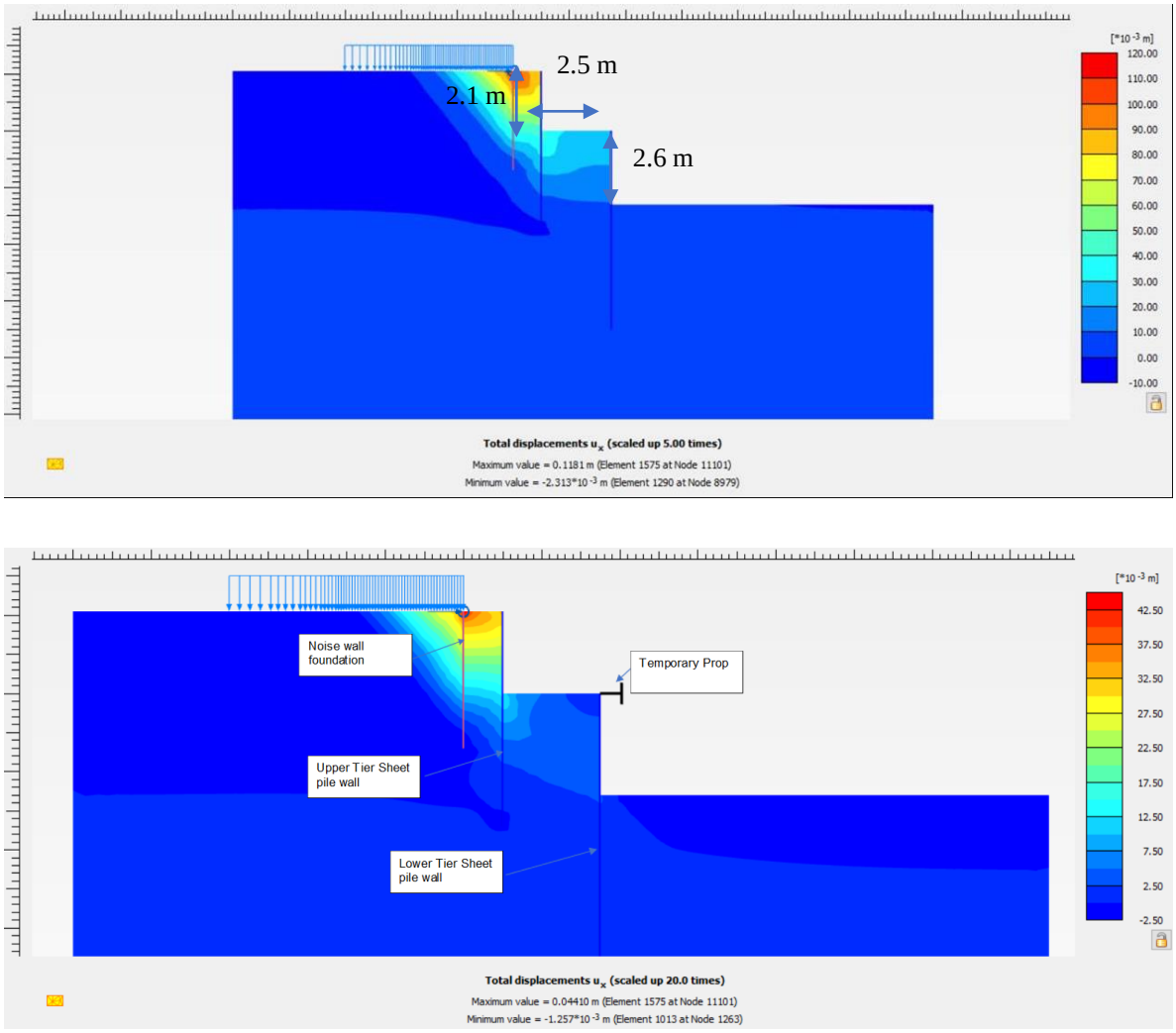


Fig. 3. Without temporary prop (top) and with temporary prop (bottom) to the lower tier sheet pile wall

The preferred option was to strengthen the sheet pile wall using UC sections in order to minimise the deflections of the temporary sheet pile wall and the existing noise wall posts. As such, the existing sheet pile wall with combined UC sections and the existing noise wall foundation were modelled in PLAXIS 2D to assess the combined effect with each stage of excavations together with dewatering. Figure 4 shows the modelled stiffened sheet pile wall.

The following considerations were made in the assessment:

- The existing noise wall foundation comprises 750 mm diameter piles, of length 3.5 m, spaced 4 m c/c
- The existing groundwater encountered was approximately 0.5 m above the final planned excavation level. The groundwater was assumed to be lowered to a minimum of 0.5 m below the final excavation level using dewatering spears
- 5 kPa surcharge loading behind noise wall
- The combined sheet pile and UC section properties (Moment of inertia: 0.0001345 m^4/m)
- Steel Grade 355 MPa
- Combined section properties to the length of the existing sheet piles and only UC section properties for the additional 1 m below the existing upper tier sheet pile as the proposed length of the UC section is 7 m
- The following noise wall loadings were adopted:
  - SLS loading (Lateral=3.57 kN/m, Moment=9.25 kNm/m)
  - ULS loading (Lateral=5.25 kN/m, Moment=13.7 kNm/m)

 © Deep Foundations Institute 2026

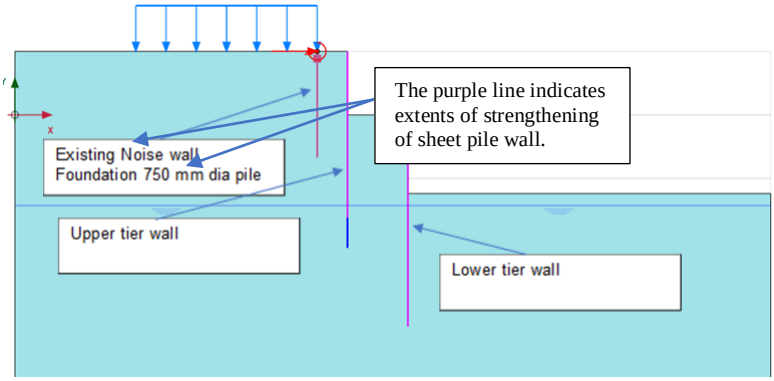


Fig. 4. Final excavation stage with schematic arrangement of stiffened sheet pile wall

Results of the assessment are provided in Table 2 below. The unfactored bending moment (BM) and shear force (SF) envelopes at the final stage in the model are provided for upper-tier and lower-tier sheet pile wall for the structural engineer to assess the adequacy of the combined sheet pile and UC sections.

Table 2. Estimated unfactored BM and SF

	Upper-tier Sheet Pile Wall	Lower-tier Sheet Pile Wall
Unfactored BM (kNm/m)	56	70
Unfactored SF (kN/m)	34	35

Table 3. Calculated deflections vs. measured deflections

Modelled Sequence/Staging	Calculated Deflections		Measured Deflections	
	Upper tier wall (mm)	Lower tier wall (mm)	Upper tier wall (mm)	Lower tier wall (mm)
Stage 1 excavation with *18 kN/m lateral load and 13.7 kNm moment	25	-	23	-
Stage 2 excavation to 0.5 m above the final excavation level	33	13	38 **	11 ***
Stage 3 backfill to the lower tier (current condition)	33	13	38 **	11 ***
Stage 4 install UC section and adopt combined section properties together with dewatering	34	15	NM	NM
Stage 5 excavation to final level with ULS wind loading on noise wall				
UCs at 4 m c/c upper and lower	50 to 55	25 to 30	NM	NM
UCs at 2 m c/c upper and 4 m c/c lower	45 to 50	25 to 30		
UCs at 2 m c/c upper and lower 2m c/c	40 to 45	20 to 25		
Stage 5 excavation to final level with SLS wind loading on noise wall				
UCs at 4 m c/c upper and lower	40 to 45	20 to 25	NM	NM
UCs at 2 m c/c upper and 4 m c/c lower	35 to 40	20 to 25		
UCs at 2 m c/c upper and lower 2m c/c	35 to 40	15 to 20		

Notes: NM (Not measured)
**The maximum ULS lateral load on the noise wall, as advised by the structural engineer, is 5.25 kN/m. However, a higher load of 18 kN/m was adopted in the model to match observed deflections of the upper-tier sheet pile wall, accounting for additional movement caused by strong wind loads and vibrations during hard driving of sheet piles at the southern end.*
***Calibration was based on measured readings at SP12 to reduce variability from excessive vibrations during southern sheet pile installation.*
****For the lower-tier sheet piles, movements at SP14 and SP15 were negligible and deemed unrepresentative. Therefore, only SP16 readings were used for assessment.*

The Plaxis 2D model has been calibrated to account for the deflections that have already occurred in respective stages of excavation and adopted to predict the anticipated additional movements for the remaining stages of excavations.



Fig. 5. Site pictures during the stages of work. Early stage (left), at completion (right)

Measured readings at SP12 were used for calibration to minimise variability caused by potential excessive vibrations during southern sheet pile installation, although no vibration monitoring was undertaken. Despite this, the calculated additional deflections are considered applicable to all upper-tier sheet piles. Higher deflections near SP11 and SP13 are attributed to vibrations from adjacent sheet installations at both ends.

Table 4 presents the calculated and estimated additional deflections. With UC posts installed at 2 m centres (top and bottom tiers), and a measured deflection of 12 mm at noise wall location NW3 (post stage 5), the total estimated deflection at NW3 is approximately 14 to 19 mm.

Table 4. Calculated deflections and estimated additional deflections in sheet pile wall

Stages	Calculated Deflections (mm)		Estimated Additional Deflections (mm)	
	Upper Tier	Lower Tier	Upper Tier	Lower Tier
Stage 3 – Measured	38	11	-	-
Stage 5 (2m c/c UC posts – Upper & Lower) – SLS	35 to 40	15 to 20	+2 mm	+9 mm
Stage 5 (2m c/c UC posts– Upper & Lower) – ULS	40 to 45	20 to 25	+ 7 mm	+14 mm

To mitigate excessive movement and potential destabilisation of the noise wall, the panels directly behind the sheet piles were removed prior to excavation. The affected noise wall posts were realigned using push-pull methods and vacuum excavation behind the foundations. Grout injection was then undertaken to stabilise the noise wall foundation and fill any potential voids.



Fig. 6. Picture at completion and after successful reinstatement of the noise wall panels (behind Abutment 2)

BELMONT PEDESTRIAN BRIDGE – BELMONT PARK (SITE 2)

Project Description

The site is located in Burswood, within the Town of Victoria Park, adjacent to Belmont Racecourse. The project forms part of a broader development plan involving land subdivision, new local roads,

and apartment construction. Due to site constraints, temporary works were required for the bridge piers and abutments spanning the Graham Farmer Freeway. This case study focuses on the temporary works at Abutment 2, as shown in Fig. 7.

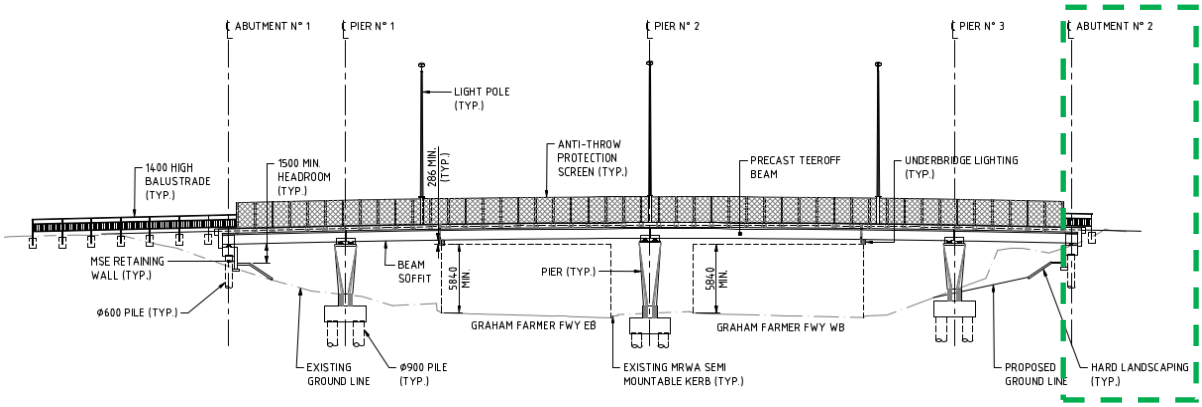


Fig. 7. Belmont Park Pedestrian bridge over Graham Farmer Freeway

Site Conditions

The geological model for the project area was developed using project-specific geotechnical investigation results, historical data, and published sources. Table 5 summarises the geological units, while Fig. 8 shows a long section along the proposed alignment. Near-surface geology consists of interbedded stiff clays and medium dense sands of the Sandy Channel Deposits (Perth Formation, formerly Guildford Formation). Controlled and uncontrolled fill materials overlay most of the site at varying depths. The design groundwater level is assumed at RL 2.1 m AHD.

Table 5. Geotechnical parameters inferred at the Abutment 2 location (Belmont bridge)

Elevation (m AHD)		Units	γ_{sat}[kN/m^3]	c' [kPa]	Su[kPa]	ø' [^{0}]	E' [MPa]	n [-]
10.5	1.5	CF – Controlled Fill	18	-	-	35	90	0.2
1.5	0	UF – Uncontrolled Fill	18	-	-	33 to 34	40	0.2
0	-5.0	SCD(c) – Fines Dominated Sandy Channel Deposits	19	-	30	-	60	0.2
-5.0	-	SCD(s) – Sand Dominated Sandy Channel Deposits	19	5	-	35	90	0.2

Notes: γ = unit weight; c' = drained cohesion; Su = undrained shear strength; ø' = drained friction angle; E' = drained Young's modulus; n = Poisson's ratio; Elevation (From/To)

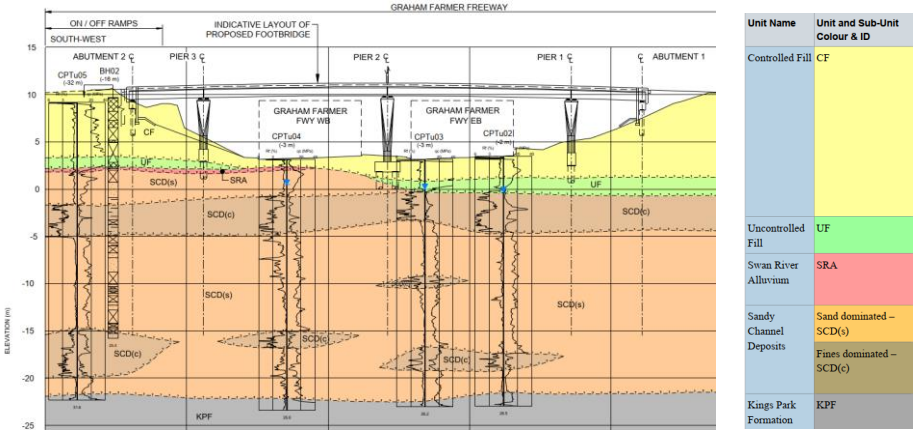


Fig. 8. Geological long section at the bridge location

 © Deep Foundations Institute 2026

Sheet Pile Wall Analysis and Design-Numerical Modelling

The following design assumptions were used in the assessments:
- Abutment 2 piling platform at RL 10.5 m AHD; Pier 3 at RL 4.5 m AHD.
- At abutment level, piling rig tracks assumed perpendicular to slope; at Pier 1 level, tracks parallel to slope/Graham Farmer Freeway.
- Piling rig dimensions and loads from Table 6 used; piling rig loads govern and are more critical than crane loads.
- Minimum 3.1 m offset of piling rig from slope crest.
- Sheet pile SCH5-750, bending stiffness 1.32E+04 kPa/m^4, moment capacity 160 kNm.

Table 6. Piling rig dimensions and loads

Plants	**Dimensions**	**Applied Ground Bearing Pressure (kPa)**
Crane – Single 92T Liebherr LTM 1750-9.1	Outrigger legs centre to centre – 12 m	245
Piling Rig – BG33H	Track length – 5.64 m Track Width – 0.8 m	350

Notes: To account for the plane strain effects in modelling, an equivalent 75 kPa over the full track length of 5.64m was used when the tracks are parallel to the model's plane

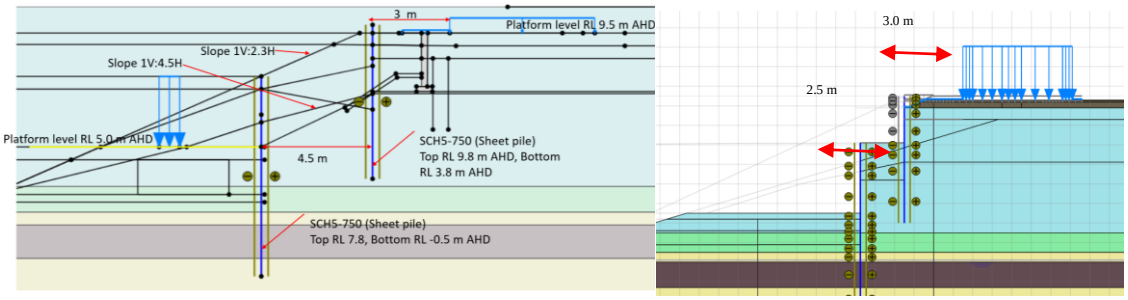


Fig. 9. Original design configuration (left), as-constructed configuration modified due to site constraints (right)

Due to changes in the construction sequence and ongoing monitoring results, a re-analysis of the temporary works was undertaken using PLAXIS 2D and Slide 2. The updated assessment aimed to estimate wall deflections, bending moments, shear forces, and global stability.

Revised Construction Sequence Based on Site Constraints

Due to changes in the installation sequence and configuration of the upper and lower-tier sheet pile walls at Abutment 2 and Pier 3, monitoring results showed greater deflections than originally predicted. These increased movements are attributed to the following deviations from the original design sequence:
- Over-excavation of 0.6 m to RL 3.6 m AHD, increasing the retained height of the lower-tier sheet pile wall from 2.8 m to 3.4 m
- Increased fill level of approximately 1.0 m between the upper and lower-tier sheet pile walls
- Construction-induced earth pressures behind the upper-tier sheet pile wall due to heavy compaction up to RL 9.9 m AHD, not accounted for in the original design
- Reduced separation between upper tier and lower tier sheet pile wall due to changes in pile location

Following the revised construction sequence, geotechnical remediation assessments were undertaken with the following constraints:
- Limit top of piling platform (compacted crushed limestone) level to RL 10.3 m AHD.

- Maintain a minimum 1.5 m offset from the crest of the platform to the upper-tier sheet piles, sloping down to RL 9.9 m AHD.
- Position crane/piling rig no closer than 3 m from the upper-tier sheet piles, using steel mats to spread the imposed loads.
- No excavation permitted at the lower working platform; it must remain no lower than RL 4.5 m AHD during abutment pile construction.
- Calibration between PLAXIS 2D modelled and measured sheet pile deflections was used to estimate incremental deflections for future activities.
- Only handheld compactors allowed within 2.5 m of the sheet piles.

Based on the above, outcomes of the geotechnical assessments are summarised in Table 7.

Table 7. Measured deflections vs. calculated deflections

Stages	Description	Measured Deflection (mm)		Calculated Deflection (mm)		Expected Incremental Lateral Movement from stage 0 (mm)	
		(UT2)	(LT2)	(UT2)	(LT2)	(UT2)	(LT2)
Initial	Upper working platform at RL 9.9 m AHD, lower working platform at RL 4.5 m AHD	56	45	57	47	-	-
1	Place compacted crushed limestone to RL 10.3 m AHD with crest of limestone at a minimum offset of 1.5 m from the sheet pile	NM	NM	58	48	< 2	< 2
2	Rig / Crane loading with steel mat at 3 m offset from the sheet pile	NM	NM	83	67	20 - 25	20 - 25
3	Remove rig load	NM	NM	85	68	< 2	< 2

Note: UT2- Top of Upper Sheet Pile, LT2- Top of Lower Sheet Pile, NM-Not monitored

A sensitivity analysis was conducted by varying the separation distance between the upper and lower sheet piles, while keeping all other parameters constant. Results show that deflections in both tiers decrease sharply as spacing increases from 1 m to approximately 3.5 m. Beyond this, deflection reduction plateaus, indicating diminishing returns. Notably, deflections slightly increase beyond 5 m spacing, suggesting potential loss of wall stiffness or stability. A spacing of approximately 4.5 m (as per design) is considered optimal, as illustrated in Fig. 10, as it: (i) minimises deflections effectively, and (ii) offers a more cost-effective solution than closer spacings.

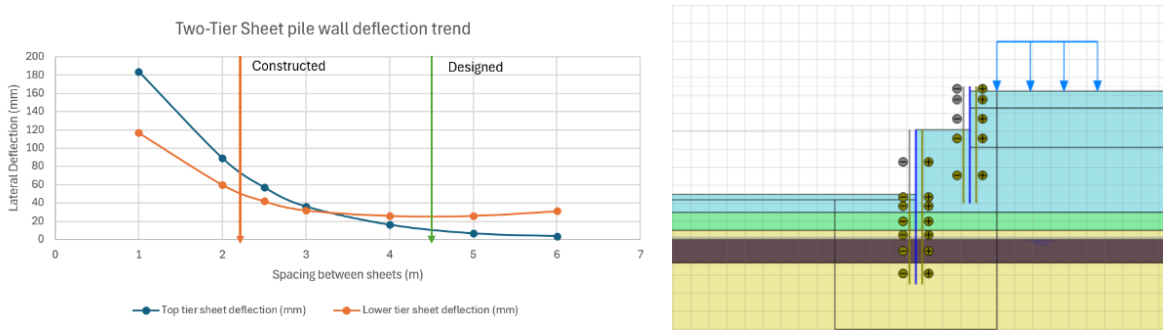


Fig. 10. Required optimal spacing between the sheet pile tiers

 © Deep Foundations Institute 2026

CONCLUSIONS AND LESSONS LEARNED

The following are the conclusions and lessons learned from the above-mentioned two case studies.

- In two-tier cantilever sheet pile systems, while the upper-tier can provide restraining effect to the lower-tier deflections, interaction between tiers may induce unintended load paths and localised stress concentrations. Accurate structural modelling is critical to avoid excessive bending, deflection, or overstressing.
- Underestimating load-bearing capacity or ignoring tier interaction risks excessive settlement or sheet pile wall failure. Use of appropriate geotechnical modelling software is essential.
- Early-stage collaboration with geotechnical designers can lead to more efficient, integrated temporary and permanent design solutions.
- Installation methods and sequencing are critical; incorrect depths or alignment can compromise effectiveness and integrity of the proposed retaining system.
- Potential ground movement and vibration effects on nearby infrastructure must be considered, especially during pile driving.
- Inadequate temporary dewatering can increase wall pressures and compromise stability.

ACKNOWLEDGEMENTS

The authors would like to acknowledge the clients, Main Roads Western Australia (MRWA), BMD Constructions (main contractor) and the Tonkin Gap Alliance (TGA), for permission to publish this paper. I also particularly grateful for the assistance provided by Su Kwong Tan for the review of the analysis. The authors acknowledge the use of OpenAI's ChatGPT for assistance in grammar correction and language refinement during the preparation of this manuscript.

REFERENCES

CIRIA, *C760: Guidance on Embedded Retaining Wall Design*, 2nd ed., London, UK: CIRIA, 2017

NAVFAC. (1982). *NAVFAC DM-7.2: Foundations and Earth Structures*. Naval Facilities Engineering Command, Alexandria, VA.

PLAXIS 2D, Version 2024.01, Delft, Netherlands: Plaxis bv, 2024

USACE. (1994). *Design of Sheet Pile Walls* (EM 1110-2-2504). U.S. Army Corps of Engineers, Washington, D.C

 © Deep Foundations Institute 2026

PILE DRIVING IN SOFT GROUND: MEASURES TO MITIGATE IMPACT ON EXISITING INFRASTRUCTURE

Jawad Zeerak, EIC Activities, Melbourne, Australia, jawad.zeerak@eicactiv.com.au
Gerard Quigg, CPB Contractors, Melbourne, Australia, gerard.quigg@cpbcon.com.au
Dobu Ungureanu, CPB Contractors, Melbourne, Australia, dobu.ungureanu@cpbcon.com.au

ABSTRACT

This paper presents a case study of pile driving in soft clay from a freeway project in Melbourne, Australia. The paper presents an overview of finite element modelling and full-scale field trials to inform design and construction. Given the presence of soft soils to significant depth, precast concrete driven piles were considered a cost effective and suitable foundation construction methodology for the proposed freeway bridges. Modelling showed that as large group of new piles were installed the soft soils would displace laterally, the magnitude of lateral displacement needed to be assessed. This mechanism was not well understood in the industry during the design phase leading to further assessment, field trials, model validation and monitoring during the construction phase. This study presents methods to predict ground movement, field trials and monitoring undertaken to validate modelling predictions and back analysis of monitoring data to inform selection of suitable mitigation measures for piling operations.

Keywords: precast concrete driven piles, soft ground, ground movement, full scale field trials, finite element analysis

INTRODUCTION

Driven precast concrete piles are displacement piles (AS 2159, 2009), meaning that their installation causes soil displacement equivalent to the embedded volume of the pile. Where the soil profile is granular or comprises clay of reasonable strength (generally stiff or better), the soil displacement results in a zone of compacted material surrounding the pile and the geotechnical design can take advantage of this and adopt somewhat higher design parameters (compared with a drilled, non-displacement pile). However, when such piles are driven through soft clay, such as Coode Island Silt (CIS), the mechanism of soil displacement is different. The soil volume change during pile installation through soft clay such as CIS is effectively nil, and consequently, the volume of displaced material will correlate directly to the volume of the driven pile. The magnitude of this displacement (heave and lateral movement) and subsequent ground movement is generally dependent on the type and size of piles, size of pile group and soil type.

The typical pile group considered in this paper, shown below, comprised groups of 12 to 30 no. 400x400 square precast driven piles with estimated pile toe levels 30 m below ground level terminating within dense to very dense sands.

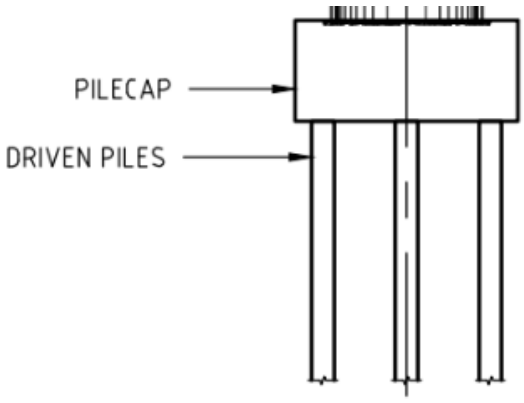


Fig. 1. Typical pile cap layout

 © Deep Foundations Institute 2026

GROUND CONDITIONS AND GROUND BEHAVIOUR

The project is located to the west of Melbourne CBD and covers an extensive area within the Yarra Delta region. The Yarra Delta, situated at the head of Port Philip Bay, is an area of Quaternary sedimentation with an intercalated flow of basalt in its eastern part. The Quaternary geological units, which together comprise the Yarra Delta, rest on an undulating plane inclined to the southwest at a low angle, which is a terrain of both steeply dipping Silurian Melbourne Formation siltstone and sandstone. A subsurface ground profile of the project area comprises typically 1 m to 5 m of historical uncontrolled fill, underlain by up to 20 m thick of CIS, which is in turn underlain by a > 2 m thick layer of firm-stiff and very stiff Fishermens Bend Silt (FBS). Moray Street Gravel, which typically comprises dense sands, is encountered below this depth where the precast driven piles are founded into. Of the geological units within the Yarra Delta, the Coode Island Silt (CIS), which is a locally well-known soft soil, is of main interest of this paper. A general subsurface ground profile of the project area is provided in Fig. 2.

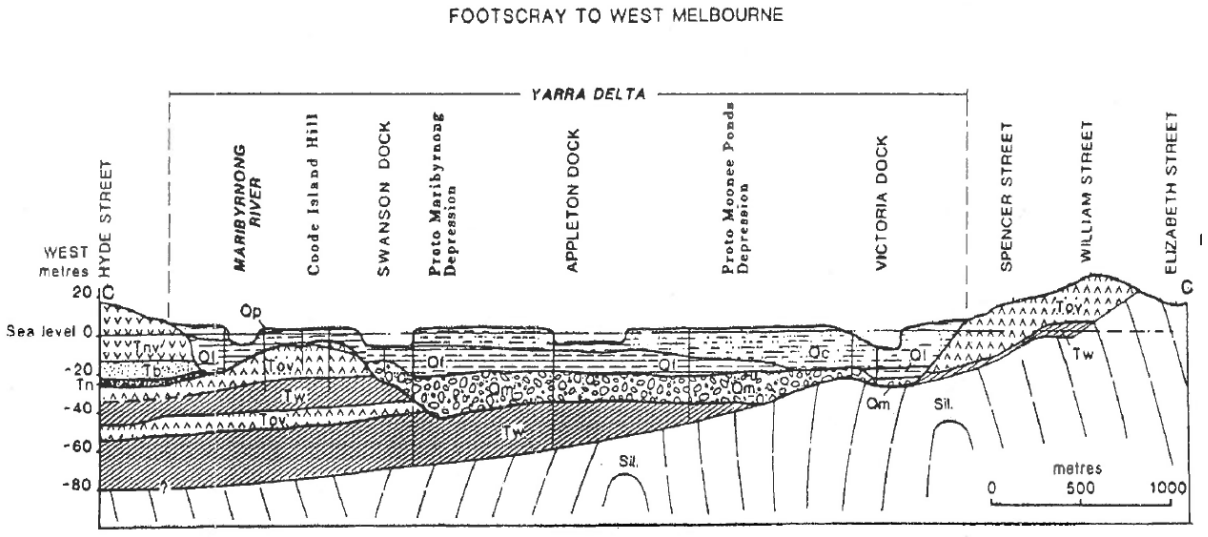


Fig. 2. Geotechnical section Yarra Delta (J.L. Neilson, 1992)

GROUND MOVEMENT DUE TO PILE DRIVING

Where ground conditions comprise granular soils or cohesive soils of firm or better consistency, the pile driving process will create a zone of highly compacted material immediately surrounding the pile. In these conditions, soil displacements are generally limited to the immediate surrounding of the pile being driven, i.e., in these conditions, the extent of ground movement is more localised because of compaction and densification of the soil. However, when driven displacement piles are installed into soft soils such as Coode Island Silt (CIS), a different soil displacement mechanism is likely to occur. Depending on the strength and nature of the soft soil, the volume of installed piles is likely to cause displacement of the in-situ ground, which may be equivalent to the volume of driven piles. The displacement caused as a result of pile driving, likely to take place in the form of heave and/or lateral displacement of surroundings soils, can extend to considerable distances from the location of piles being driven. Where there are existing foundations or structures in the vicinity of the piles being driven, this may have an adverse impact on nearby installations, structures and assets. In such cases, where existing installations and structures exist in the vicinity of piles being installed, it is essential that a ground movement and impact assessment is undertaken.

The next section discusses the approach taken as part of this project to predict magnitude and extent of soil displacement.

 © Deep Foundations Institute 2026

PRE-PRODCUTION SITE TRIAL AND FIELD MEASUREMENT

Given the lack of available data and experience with assessment of ground movement related to pile driving locally, a pre-production trial was undertaken. As part of the trial, three out of a proposed 22-pile group of 400x400 precast piles were driven. Inclinometers were installed at varying distances from the pile group to record the ground movement during pile driving. Inclinometers were installed at 2.1 m distance from location of piles installed.

Trial piles were installed to the nominated pile founding depths, i.e., pitched piles of 33–34 m in length with driven lengths of 30.0 m. Inclinometers were installed to the siltstone rock below ~RL-40 m, i.e., to a total depth of 43 m below platform level. During the trial piling, a pre-bore depth of 9 m (min) was recommended, due to available equipment limitations on site, and pre-bore depth was limited to 3 m. Manual inclinometer readings were undertaken at both inclinometer locations at the end of each pile being driven to their nominated depths as per the sequence outlined above.

Inclinometer readings obtained from two inclinometers installed at varying distance from the location of trial piles are shown below. Each plot shows three readings; each obtained as the first 3 trial piles were driven. Axis A readings show movement perpendicular to the pile being driven, while axis B shows the readings parallel to the pile.

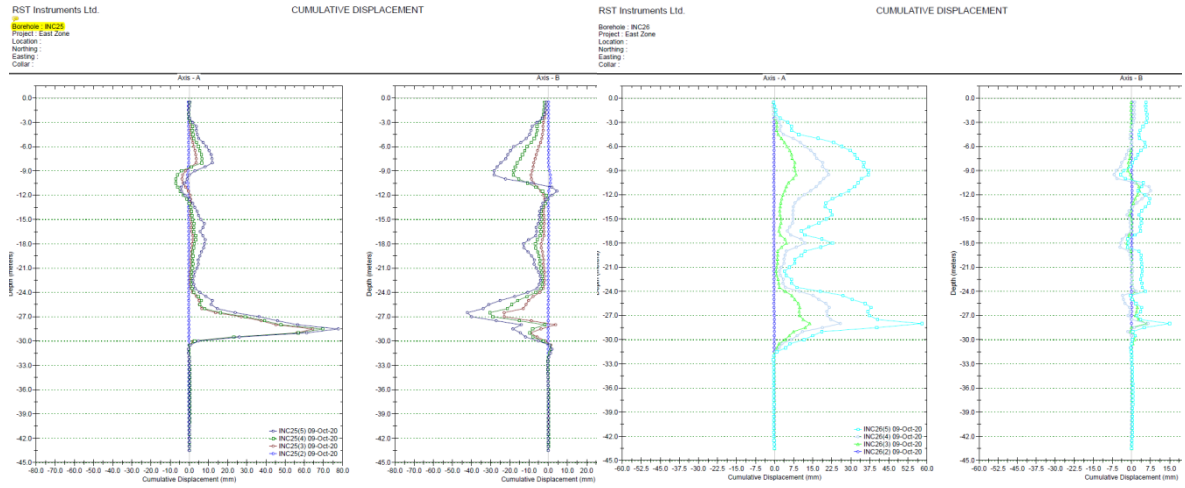


Fig. 3. Inclinometer readings for trial piling

MODEL DEVELOPMENT AND CALIBRATION

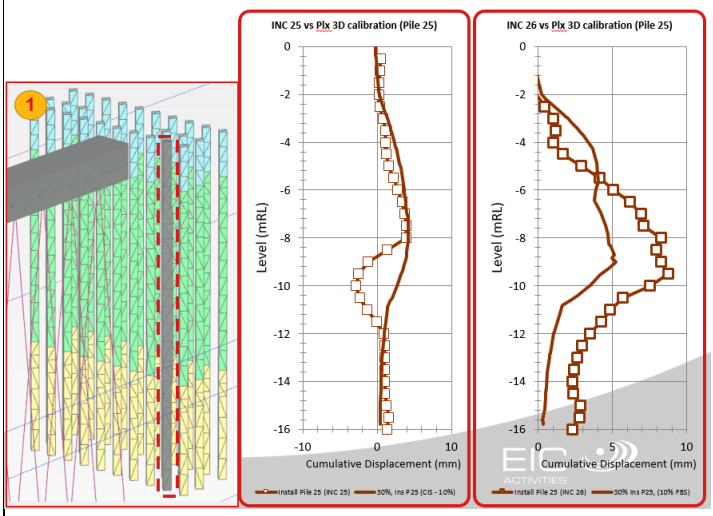
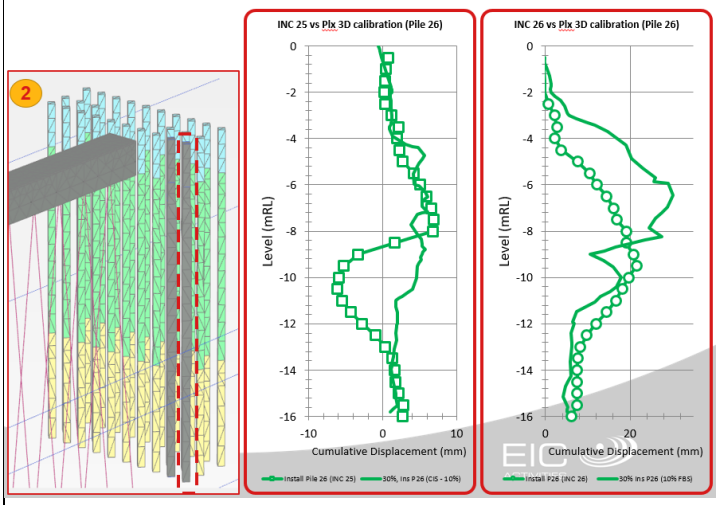
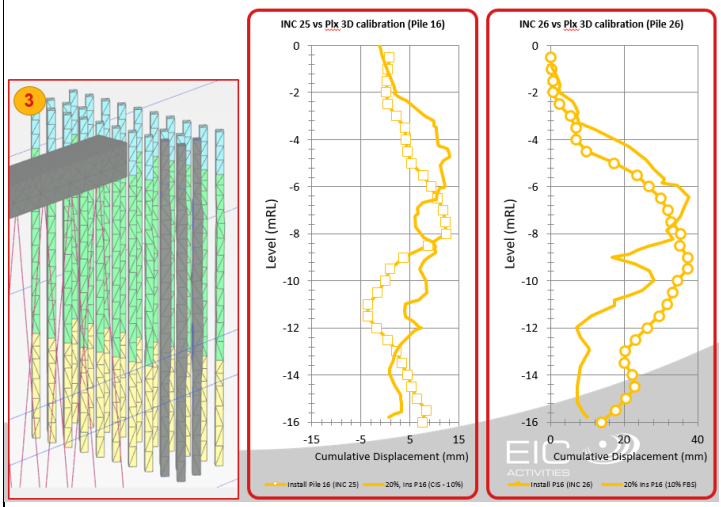
A PLAXIS 3D analysis was undertaken prior to the pre-production trials. The preliminary PLAXIS analysis was based on assumptions and a review of literature elsewhere. Results of the site-specific trial piling and inclinometer readings were used to calibrate ground movement in PLAXIS 3D. The following stages were modelled in PLAXIS 3D to replicate the site trials.

- Generate initial stress
- Install existing structure foundations
- Step 1: Install 1st pile – Review ground movements and compare against inclinometer data
- Step 2: Install 2nd pile – Review ground movement and compare against inclinometer data
- Step 3: Install 3rd pile – Review ground movement and compare against inclinometer data

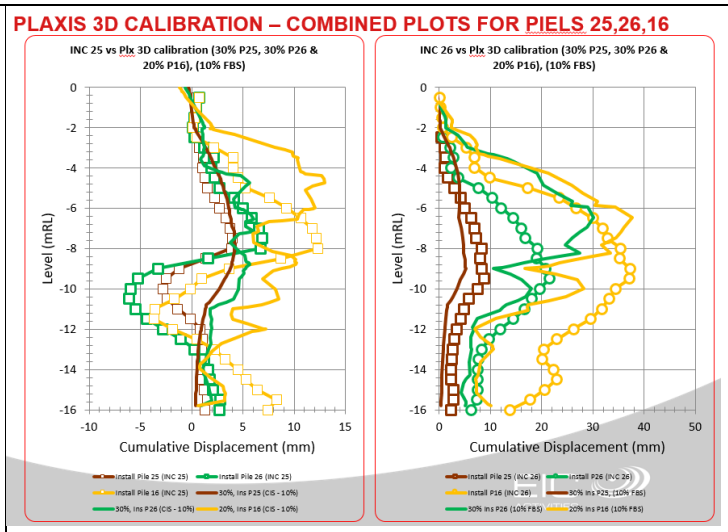
Results of the calibration modelling from PLAXIS 3D are summarised in Table **1**1 below.

 © Deep Foundations Institute 2026

Table 1 – PLAXIS 3D Calibration against Inclinometer Data

Stage	PLAXIS 3D Prediction
Step 1 – Install 1st Trial Pile	PLAXIS 3D CALIBRATION – STEP 1: INSTALL PILE 25 
Step 2 – Install 2nd Trial Pile	PLAXIS 3D CALIBRATION – STEP 2: INSTALL PILE 26 
Step 3 – Install 3rd Trial Pile	PLAXIS 3D CALIBRATION – STEP 3: INSTALL PILE 16 

 © Deep Foundations Institute 2026

Combined inclinometer vs. PLAXIS 3D plots for all three piles	

TRIAL MITIGATION OPTIONS AND PREDICTED GROUND MOVEMENT

Building on the calibrated model, the entire pile cap was then simulated in PLAXIS 3D. A similar approach as the calibration model was adopted. Previous studies and published literature indicate that there is some benefit due to "shielding effect" from the installed piles, which was adopted in the modelling.

Two cases were analyzed in PLAXIS 3D to provide an understanding of the benefits, pre-boring the soil before pile driving and installation of a steel casing before pile driving. Case 1, all piles pre-bored to 9 m and Case 2, all piles pre-bored to 9 m and also the 6 nearest piles provided with casing over the first 9 m. A casing length of 9 m was considered a maximum practical depth to which casing could be installed safely. This would also ensure driven piles through existing 'uncontrolled' fill would not generate excessive ground movement. Results and analysis approach for these two cases are presented in the next section.

CASE 1: ALL PILES PRE-BORED TO 9 M

Peak ground movements are generated within the top 10 m due to presence of the soft soil layer, which undergoes largest movements. Effectiveness of pre-boring depends on type of soil (how long the hole can remain open for) and depth of pre-bore amongst other factors. Based on past experience and the influence of groundwater on hole stability, the following pre-bore effectiveness has been considered in the PLAXIS analysis:
0 – 3.0 m: 100% effective
3 – 9.0 m: 70% effective
9 – 10.8 m: 50% effective

Predicted deflections calculated in PLAXIS 3D based on the above are presented below.

 © Deep Foundations Institute 2026

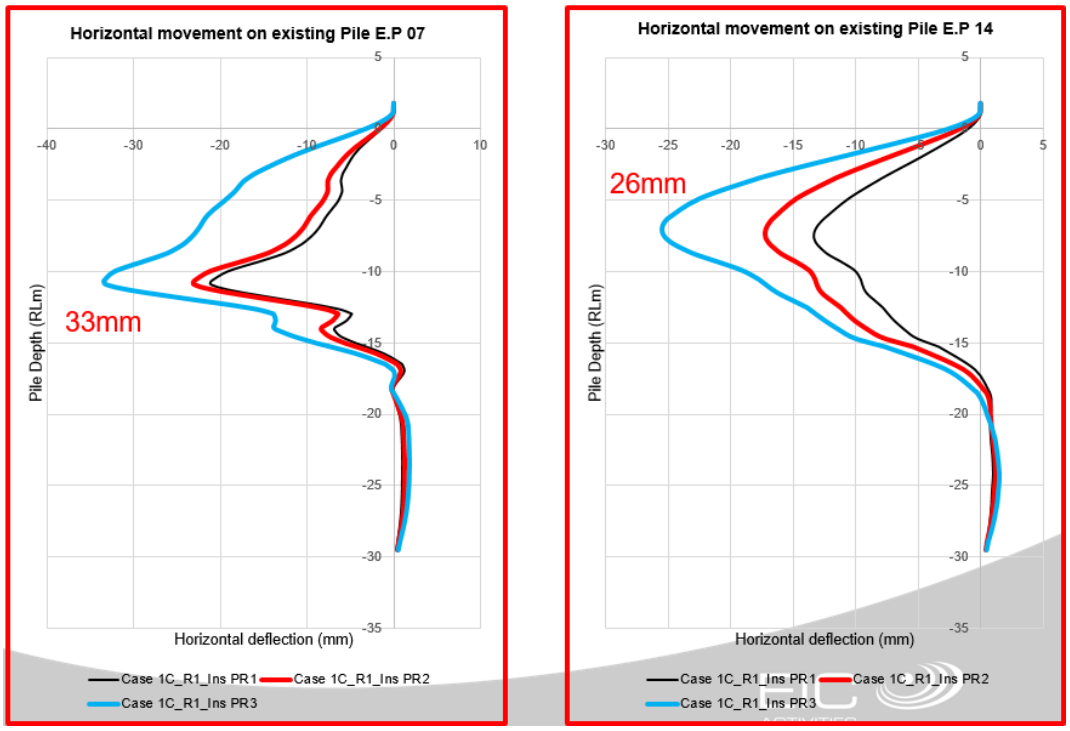


Fig. 4. Predicted pile deflection (pre-bore only)

It is noted that ground movement is likely to be much smoother than those predicted in PLAXIS 3D. The sudden changes in calculated movements are more due to modelling limitations, i.e., changed soil stiffness and stepped increases in applied movements in the finite element model.

CASE 2: ALL PILES PRE-BORED TO 9 M + SIX NEAREST PILES CASED

To understand the effectiveness of casing the piles, a second case was analyzed with the six nearest piles to the location of monitoring provided with steel casing to 10 m depth.

The following construction sequence was adopted on site:

1. Drive 12 mm thick, 680 mm inner diameter, 10.5 m long steel casing to 10 m below existing ground surface for the six nearest piles as shown above.
2. Excavate/bore out inside the casing to 10 m depth bgl.
3. Fill up the casing with water to balance hydrostatic pressure outside the casing as drilling and boring out progresses.
4. Pre-bore further 2 m locally in the middle of the casing.
5. Backfill the casing with peak sized gravels to existing surface and compact locally.

For this case, the following pre-bore effectiveness was considered in the PLAXIS analysis.
0 – 3.0 m: 100% effective
3 – 9.0 m: 70% effective (all piles)
9 – 10.8 m: 50% effective (all piles)
9 – 12 m: 100% effective (6 cased piles)

 © Deep Foundations Institute 2026

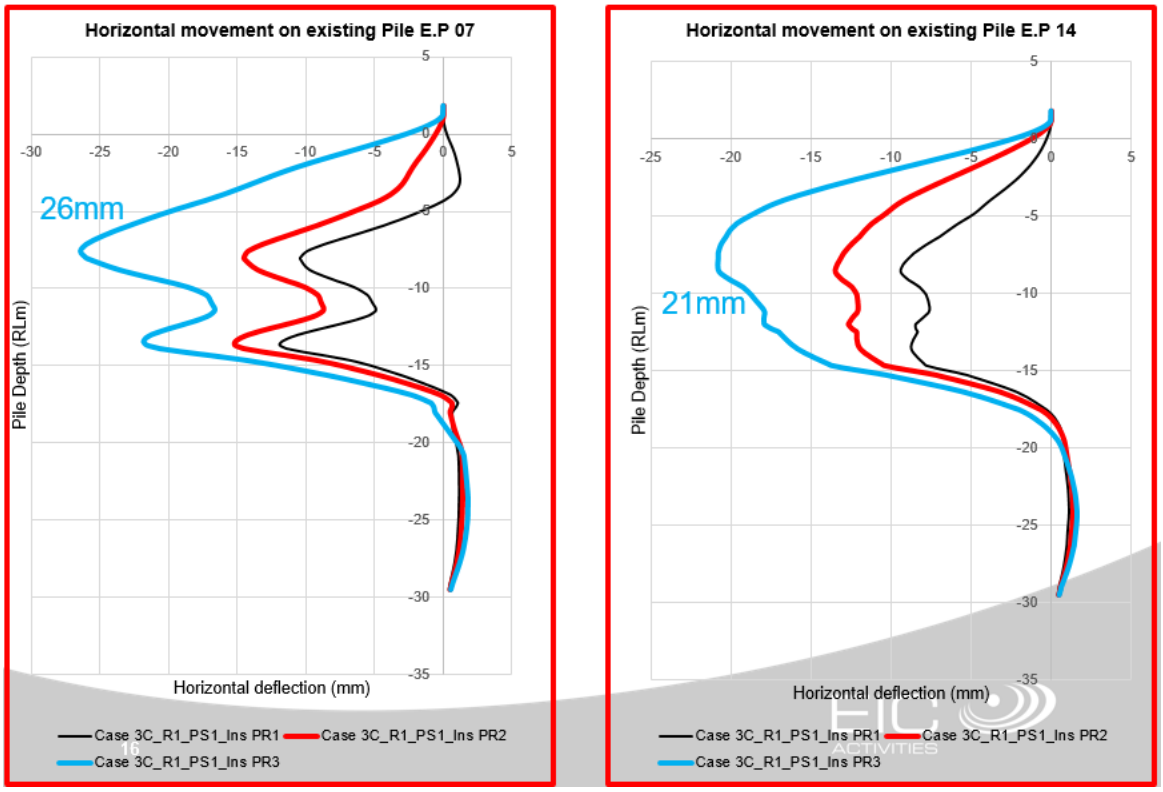


Fig. 5. Predicted pile deflection (pre-bore only + 6 piles with casing)

Based on the field trial and monitoring, the addition of a casing and pre-boring reduced the peak horizontal displacement by approximately 20%.

CASE 3: REPLACEMENT OF PRECAST CONCRETE DRIVEN PILE WITH STEEL H PILES

Further to trials using pre-boring and steel casing, additional trials were undertaken considering the replacement of precast driven piles on a one-for-one basis with low displacement steel H-piles. The chosen low displacement options were a combination of welded column sections (350WC197 and 400WC212). Theoretically the soil displacement due to pile installation is directly proportional to the cross-sectional area of the installed pile. A 400WC212 and 350WC197 have a reduced cross-sectional area compared to the 400 mm square precast driven pile, 12.9% and 15.6% of the cross-sectional area, therefore the lateral displacement caused by installation of these piles section should be reduced by a similar magnitude.

Analysis of the steel H-pile option was undertaken using Plaxis 3D like the other trials discussed above. There was a concern that the H-piles may plug as they are driven through the superficial fill, which would result in increased lateral displacement. The H-pile with a plug of soil wedged between the flanges has a gross section area approaching that of a 400 mm square PDP, and the resulting lateral displacement would likely exceed acceptable limits. The lateral soil displacement was measured using a Vertical Shape Accelerometer Array installed in an inclinometer casing to a depth of 32 m.

The installation methodology is summarised below:

1. Install inclinometer with detailed logging and sampling and obtain stable baseline readings. Install Test Pile 1 - 350WC197 with 810 mm casing through fill only. To prevent plugging of H-pile, remove fill material and possible solid obstructions in temporary casing.
2. Install Test Pile 2 – 350WC197 with 760 mm OD casing to 12 m through Coode Island Silt. Muck out material inside casing to a minimum depth of 2 m below fill or 6 m depth;

The lateral displacement at an offset of 1.7 m was measured using an inclinometer. Monitoring results indicate that the lateral displacements resulting from the installation of Test Pile – TP1 are less than 2.5 mm.

Results of Case 3 trials indicated a significant reduction in magnitude of ground movement in these conditions.

SUMMARY AND CONCLUSIONS

Case studies from pile driving trials within soft clay in Melbourne, Australia, have been presented in this paper. Ground movement predictions based on pre-production trial site data shows that large lateral ground movements can occur, especially where driving groups of piles are undertaken. Field measurements have been used to calibrate finite element modelling and develop mitigation measures to limit the impacts due to driven piles in soft clay. Adoption of mitigation measures (in this case, pre-boring, casing and replacement of concrete precast piles with H-piles) was informed by pre-production trials and calibrated finite element models. Based on the field trial and monitoring, the addition of a casing and pre-boring reduced the peak horizontal displacement by approximately 20%. Monitoring was undertaken during installation to verify the effectiveness of the mitigation measures and validate modelling assumptions. Results of the trials and modelling approach developed as part of the trials were adopted across the project with further site-specific trials, monitoring, refinement to model assumptions and adjustment to model parameters to suit local conditions.

REFERENCES

AS 2159. (2009). Piling - Design and Installation. Standards Australia.

Attari, Y., Quigley, P., Doherty, P., & Lusack, N. (2018). Predicting Pile Driving Induced Movements in Gothenburg Soft Clay. Civil Engineering Research in Ireland. Dublin: Civil Engineering Research Association of Ireland.

Chen, L. T., & Poulos, H. G. (1997). Design Charts for Analysis of Piles Subjected to Lateral Soil Movements. 8th Australia New Zealand Confernence on Geomechanics, (pp. 367-373). Hobart.

Edstam, T., & Kullingsjo, A. (2010). Ground Displacements Due to Pile Driving in Gothenburg Clay. Numerical Methods in Geotechnical Engineering, 625-630.

Edvardsson, G., & Melin-Nyholm, P. (2018). Mass Displacement Due to Pile Driving Installation in Soft and Sesntive Clay. The Influence of Pile Installation with Precast Concrete Displacement Piles has on Adjacent Areas. Gothenburg: Chalmers University of Technology.

Hagerty, J. A., & Peck, R. B. (1971). Heave and Lateral Movements Due to Pile Driving. Journal of the Soil Mechanics and Foundations Division, 1513-1532.

Hernqvist, H., & Nguyen, D. (2016). Analysis and FE-Modelling of Soil Displacement Associated to Pile Driving. A Case Study of Pile Installation at Gamlestadstorget. Gothenburg: Chalmers University of Technology.

Nenonen, P., & Ruul, J. (2011). Environmental Impact of Pile Driving. An FE-Analysis of the Displacements of the Skaran Bridge. Gothenburg: Chalmers University of Technology.

Neilson, J. L. (1992), Engineering Geology of Melbourne, Geology of The Yarra Delta, Geological Survey of Victoria.

Poulos, H. G. (1994). Effect of Pile Driving on Adjacent Piles in Clay. Canadian Geotechnical Journal, 856-867.

Rainer Massarsch, K., & Wersall, C. (2013). Cumulative Lateral Soil Displacement Due to Pile Driving in Soft Clay. Sound Geotechnical Geotechnical Reserach to Practice: Honoring Robert D. Holtz II, (pp. 463-480).

Sagaseta, C., & Whittle, A. (2001). Prediction of Ground Movements Due to Pile Driving in Clay. Journal of Geotechnical and Geoenvironmental Engineering, 55-66.

Sagaseta, C., Whittle, A. J., & Santagata, M. (1997). Deformation Analysis of Shallow Penetration in Clay. International Journal for Numerical and Analytical Methods in Geomechanics, 687-719.

Wersall, C., & Rainer Massarsch, K. (2013). Soil Heave Due to Pile Driving in Clay. Sound Geotechnical Practice: Honoring Robert D. Holtz II, (pp. 481-499).

 © Deep Foundations Institute 2026

CHALLENGES IN PILE FOUNDATION DESIGN IN NORTHL AND ALLOCHTHON

Kostas Lontzetidis, Technical Director - Geotechnical Engineering, Babbage Consultants, Auckland, New Zealand, +64204820859, kostas@babbage.co.nz
Chris Ritchie, Principal Engineering Geologist Gibb Ritchie, Auckland, New Zealand
Kori Lentfer, Principal Engineering Geologist, CMW Geosciences, Hamilton, New Zealand

ABSTRACT

Pile driving in rock formations such as Northland Allochthon presents challenges when estimating engineering properties and pile design parameters for foundation analysis. The sheared and weak nature of the Northland Allochthon can lead to rapid degradation when exposed or disturbed, causing deposits to behave as highly weathered soils. This complexity complicates the assessment of optimal design parameters for geotechnical analysis, particularly concerning skin friction, which can be overestimated in some cases when traditional methods are employed.

This paper focuses on using pile testing at two infrastructure projects (road bridges) to propose a method for estimating pile design parameters aimed at optimizing foundation design. Furthermore, it provides insights into classifying Northland Allochthon material as a rock mass, which enhances the estimation of associated engineering properties and suggests suitable pile design parameters for deep foundation analysis within this geological context

Keywords: Pile driving, Northland Allochthon, design optimization

INTRODUCTION

This paper presents a case study of two 3-span bridges constructed within the Milldale subdivision, west of Silverdale in North Auckland (Fig. 1). Building on the work of Lentfer et al. (2023), this study incorporates additional pile testing data. Both structures are founded in Northland Allochthon, a geologically complex formation that poses significant challenges for foundation design. To support foundation analysis within this formation, a geological overview of the Northland Allochthon is provided, with an accurate estimation of engineering properties relevant to deep foundation design. An extensive site investigation campaign was undertaken to develop a robust ground model for both bridge sites. This included borehole drilling, laboratory testing, as well as pile load tests to characterize subsurface conditions and inform pile design.

NOTHLAND ALLOCHTHON

The Northland Allochthon strata are part of an allochthonous (meaning removed from their formation location) mass of continental crust that was peeled from the subduction zone north of New Zealand and emplaced through low angle thrust faulting onto areas of Northland and the Silverdale area. Due to the nature of emplacement, materials are typically highly fractured or even shattered and variably weathered. Hayward (2017) describes the Northland Allochthon deposits of the Silverdale area as a series of imbricated thrusts with slivers of Northland Allochthon in a chaotic ‘heap’ between Waitemata Group units. This is observed throughout wider Milldale, including the subject sites, with observed deposits being an undifferentiated mélange of the Mangakahia and Motatau Complex units, including Whangai Formation, Hukerenui, and Mahurangi Limestone. Tauranga Group alluvium and colluvium are mapped as overlying these geologies. These are Pleistocene-aged clays and silts.

A defining feature of the Northland Allochthon is its intensely sheared and fractured fabric, often presenting as a tectonic mélange. The rock mass typically comprises tightly interlocked angular fragments with slicken sided or polished surfaces, interspersed with defects infilled by soil or calcite cement. Under reduced confining pressures materials tend to disaggregate into their constituent gravels and cobbles, reflecting limited cohesion in the absence of confinement. Upon subaerial exposure, the

 © Deep Foundations Institute 2026

rock mass exhibits rapid expansion and degradation, transitioning toward completely weathered soils over relatively short timeframes. This behaviour is particularly pronounced when the material is left exposed to atmospheric conditions without protective measures, posing challenges for both temporary works and long-term stability.

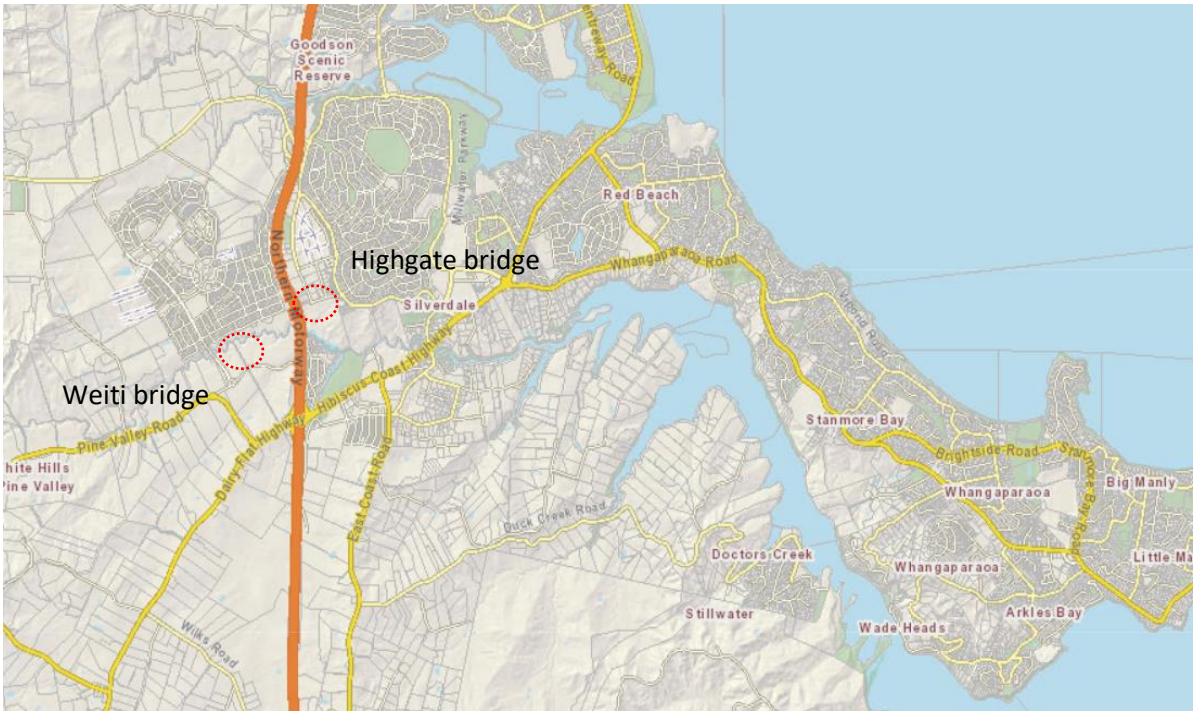


Fig. 1. Location of the two bridge sites

GROUND CONDITIONS AT THE BRIDGE SITES

Weiti Bridge

The ground conditions at this bridge comprised alluvial soils approximately 5 m thick overlying weathered Northland Allochthon mudstone. The mudstone was highly sheared and shattered and was described as extremely weak medium to coarse gravel in a matrix of clay, likely a material belonging to a Motatau Mélange. The mudstone had a horizon of completely to highly weathered material that was significantly thicker on the northern abutment (up to 15 m) overlying the moderately weathered rock mass; the weathering class was determined by the amount of clay present on defect surfaces.

Highgate Bridge

The presence of undifferentiated Mangakahia complex was confirmed by the drilling of three machine boreholes, two of which were located at the pier positions. These piers' locations lie within an area previously excavated to approximately 12 m below ground level as part of the Northern Motorway extension in 1997, known as "Lyfords Cut." Therefore, boreholes drilled during the investigation do not contain a residual soil profile, with weathered rock present from near the surface. Observations made during the Lyfords Cut excavation and subsequent investigations revealed that two different lithologies of the undifferentiated Mangakahia Complex are present at each pier: a calcareous mudstone at the western pier and a siliceous mudstone at the eastern pier. Both units are highly sheared and moderately to highly weathered.

PENETRABILITY STRENGTH INDEX

Given the fragmented and highly disrupted nature of the Northland Allochthon, recovery of intact core samples suitable for Unconfined Compressive Strength (UCS) testing was generally not feasible,

especially at the Weiti Bridge site, where core integrity was significantly compromised. In contrast, intact core samples were successfully recovered at the Highgate Bridge site, enabling UCS testing to be undertaken.

Where UCS testing was not possible, UCS values were estimated indirectly using Standard Penetration Test (SPT) data. Following the methodology proposed by Stamatopoulos & Kotzias (1993), a non-linear approach was adopted using the penetrability index "P", defined as the depth of SPT spoon penetration (in millimetres) into the rock mass after 60 blows. Figure 2 presents a classification scheme for rock strength based on penetrability values, facilitating the derivation of equivalent UCS estimates for use in foundation design.

It was observed that the UCS values derived from the penetrability index were, on average, approximately three times higher than those obtained from the laboratory UCS testing. This discrepancy may be attributed to the inherent limitations and uncertainty of the empirical correlation within the range of extremely weak to weak strength range, as well as potential deterioration or disturbance of the recovered rock sample.

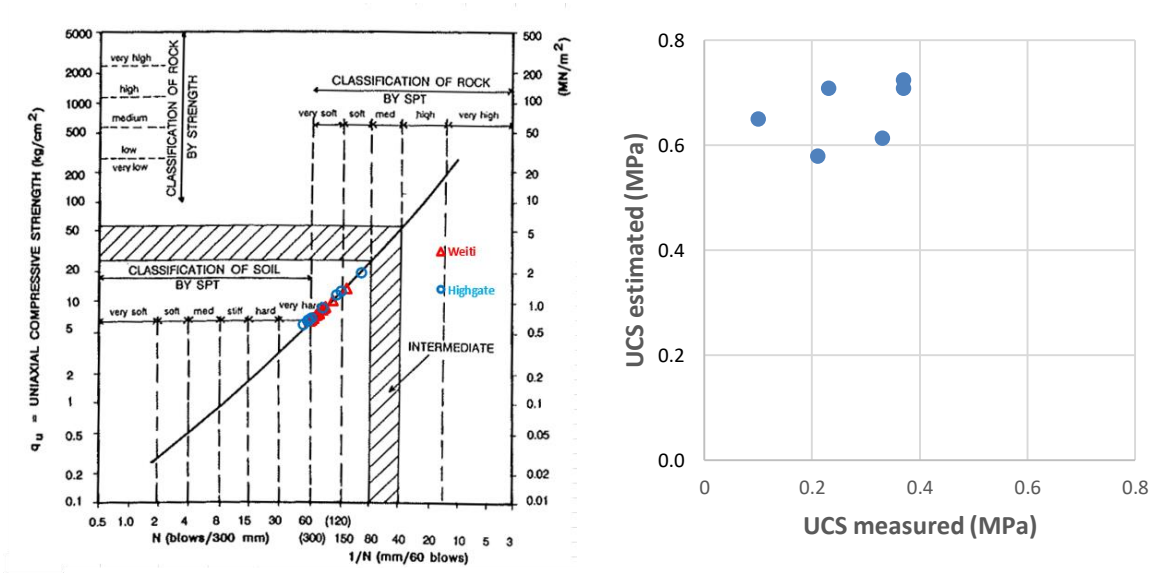


Fig. 2. UCS correlation from SPT blow count (Stamatopoulos & Kotzias 1993) and measured over estimated UCS values

PILE DESIGN IN WEAK ROCKS

As noted by Lentfer et al. (2023), when piles are founded in rock, settlement rather than ultimate capacity typically governs the design criteria. This is especially relevant for the Northland Allochthon, where the highly fractured and variable nature of the formation makes it particularly challenging to assess the ultimate capacity of driven piles. In such conditions, the absence of a widely accepted design methodology for piles in weak rock further complicates reliable foundation design.

Estimating shaft resistance for driven piles in weak rock presents further challenges. The pile driving process breaks down the surrounding rock to an unknown extent (Fleming et al., 2008), and the resulting shaft resistance depends on the grain size of the damaged material. This resistance may be significantly reduced, or even rendered negligible, due to the breakdown of the rock matrix (Tomlinson and Woodward, 2014). Several approaches have been proposed to estimate shaft resistance in weak rock.

1. Rosenberg and Journeaux (1976) established correlations between the uniaxial compressive strength (UCS) of rock and skin friction:

$$fs = \alpha \beta UCS \quad [1]$$

$$\alpha = 0.3\ UCS^{0.5} \quad [2]$$

Where: α is a reduction factor based on UCS, and β (0.35-1.0) is a correction factor related to discontinuity spacing in the rock mass (Williams & Pells, 1981).

2. Terente et al. 2017, suggested that the adhesion factor is not linear and is correlated with the UCS as follows:

$$fs = \alpha\ UCS \quad [3]$$

$$\alpha = 0.11\ UCS^{-0.5} \quad [4]$$

3. University College Dublin (UCD) rock method: Barrett and Prendergast (2020) developed a practical method to classify extremely weak to weak rock, where traditional rock mass systems often fail when these materials behave more like stiff soils. They proposed an empirical relationship linking UCS to unit shaft resistance for driven piles in weak rock, incorporating a friction fatigue model:

$$fs = \alpha_0\ UCS\ (h/D)^{-\beta}\ [1/(1 + AR)] \quad [5]$$

Where: α_0 and β are dimensionless scaling factors (calibrated as 0.71 and 0.45, respectively), h is the distance from the pile tip, D is the pile diameter (minimum h/D = 1, as lower values would result in significantly over-predicted unit shaft resistances), and AR is the area ratio of the open-ended pile.

To calibrate the dimensionless scaling factors α_0 and β, the model in Eq. 5 was applied to the seven case studies included in the study. The parameters were iteratively adjusted until the predicted shaft resistances closely matched the measured values.

4. Effective Stress Method: Chandler (1968) proposed a frictional bond model between pile and soil, where shaft resistance is a function of normal effective stress and the interface friction angle.

$$fs = K\ \sigma'_v \tan \delta \quad [6]$$

Where: K = coefficient of lateral earth pressure, σ'_v = effective overburden stress, and δ = friction angle between rock and pile wall.

5. Total Stress Method: Burland et al. (2012) considered shaft resistance as a function of UCS and effective overburden stress:

$$fs = a\ s_u \quad [7]$$

$$\text{For } s_u/\sigma'_v <= 1\ a = 0.5\ (s_u/\sigma'_v)\text{-}0.5 \quad [8]$$

$$\text{For } s_u/\sigma'_v > 1\ a = 0.5\ (s_u/\sigma'_v)\text{-}0.25 \quad [9]$$

Where: a = adhesion factor, s_u = undrained shear strength (approximated as UCS/2), and σ'_v = effective overburden stress.

Given the inherent uncertainties in characterising the Northland Allochthon for pile design, the formation represents a potentially high-risk element for proposed structures. Conducting Pile Driving Analyzer (PDA) tests offers a valuable opportunity to reassess and optimise design parameters, providing empirical data to support more reliable foundation solutions.

SHORT DESCRIPTION OF THE MILLDALE BRIDGES

Weiti Bridge

The new 3-span bridge replaced an old narrow bridge across Weiti Stream located near Silverdale. The bridge has northern and southern spans of 15 m long, a central span of 26 m long, 7 m of settlement slabs and 6 m of transition barriers at either end of the bridge. The bridge has a width of approximately 15 m, which includes two traffic lanes with a cycle lane and footpath on each side.
The specified piling design required that both the proposed abutments and the piers were each founded on 4 no. 914 mm diameter reinforced concrete piles. Permanent thick-walled steel casings (16 mm thick, 350 MPa grade) were required to be installed by driving prior to boring of the RC piles. The bridge deck was formed from precast super-tee beams.

Highgate Bridge

This bridge is a 97 m-long, three-span steel ladder deck structure with a 19.43 m-wide composite concrete deck. It features two main steel I-girders haunched over piers, connected by cross girders and topped with precast panels and an in-situ concrete slab. The bridge sits on a straight alignment with a 4.4% grade and is supported by reinforced concrete piers and semi-integral abutments founded on MSE walls and existing embankments.The piling design specified that each pier be supported by two 1524 mm diameter reinforced concrete piles. Prior to boring, permanent thick-walled steel casings, 16 mm thick and of 350 MPa grade, were driven into position to enable pile installation.

LOAD PILE TESTS RESULTS

The geotechnical specification for the piling works included high strain dynamic load testing to serve two key purposes: 1) to justify an increased strength reduction factor in calculating the design capacity of the piles, and 2) to validate pile design parameters for the Northland Allochthon, given the limited availability of reference data.

At each bridge site, two dynamic tests were conducted using a Pile Driving Analyzer (PDA), generally in accordance with AS2159, to verify the geotechnical ultimate pile capacity. Subsequent CAPWAP wave matching analyses were performed to further assess pile performance. The test arrangements are summarized in the following table.

Table 1. Pile capacity from CAPWAP analysis

Bridge	Pier/ Pile No.	Embedment Depth (m)	Hammer Weight (tone)	Drop Height (m)	CAPWAP Total Capacity (k N)	Skin Capacity (k N)	Toe Capacity (k N)
Weiti	1/8	20.5	13.5	1.75	8,650	6,100	2,550
Weiti	2/10	17.8	11.7	3.00	8,900	6,100	2,800
Highgate	2/3	21.4	14.0	1.5	13,535	11,937	1,599
Highgate	2/4	21.3	14.0	1.5	14,093	12,252	1,841

Weiti Bridge: Pile P8 was tested at end-of-drive with no wait time, while Pile P10 was tested on restrike approximately 12–24 hours after installation. Mobilization indicators confirm that both piles were fully mobilized during testing: P8 recorded a maximum head displacement of 24 mm and a CAPWAP toe displacement of 31.4 mm, while P10 recorded a head displacement of 22 mm and 29.8 mm toe displacement. These displacement magnitudes, combined with permanent sets of 9 mm/blow (P8) and 7 mm/blow (P10), demonstrate full activation of shaft and toe resistance.

Highgate Bridge: Both piles were tested on restrike approximately 24 hours after installation. Mobilization indicators confirm strong activation of resistance: P3 recorded a maximum head displacement of 16 mm and a CAPWAP toe displacement of 23 mm, while P4 recorded a head

displacement of 15 mm and 21.7 mm toe displacement. Permanent sets averaged 3 mm/blow for P3 and 2.7 mm/blow for P4, indicating not full mobilization, with shaft resistance strongly activated and toe resistance partially engaged.

We wish to highlight the notably low-end bearing values observed in the tests at Highgate Bridge, which were approximately four times lower than those recorded at the Weiti Bridge. While this trend aligns with established practice, where open-ended steel pipe piles often exhibit reduced effective end bearing with increasing diameter, the magnitude of reduction in this case is most likely influenced by the incomplete mobilization of toe resistance.

COMPARISON OF THE RESULTS BETWEEN EXISTING CORRELATIONS AND THE RESULTS FROM THE LOAD TESTS

UCS testing was conducted only at the Highgate Bridge, and comparative analyses were performed using two approaches: first, by estimating UCS values based on penetrability data, and second, by applying the actual UCS test results. This dual comparison enabled evaluation of the correlation methods under both inferred and measured rock properties.

Analysis Using Penetrability Data

Figures 3 and 4 illustrate the variation of ultimate shaft friction with depth for the Weiti and Highgate bridges, respectively. These include the values adopted in the original geotechnical design reports, those measured during PDA testing, and those derived from the analytical correlation methods outlined in previous section.

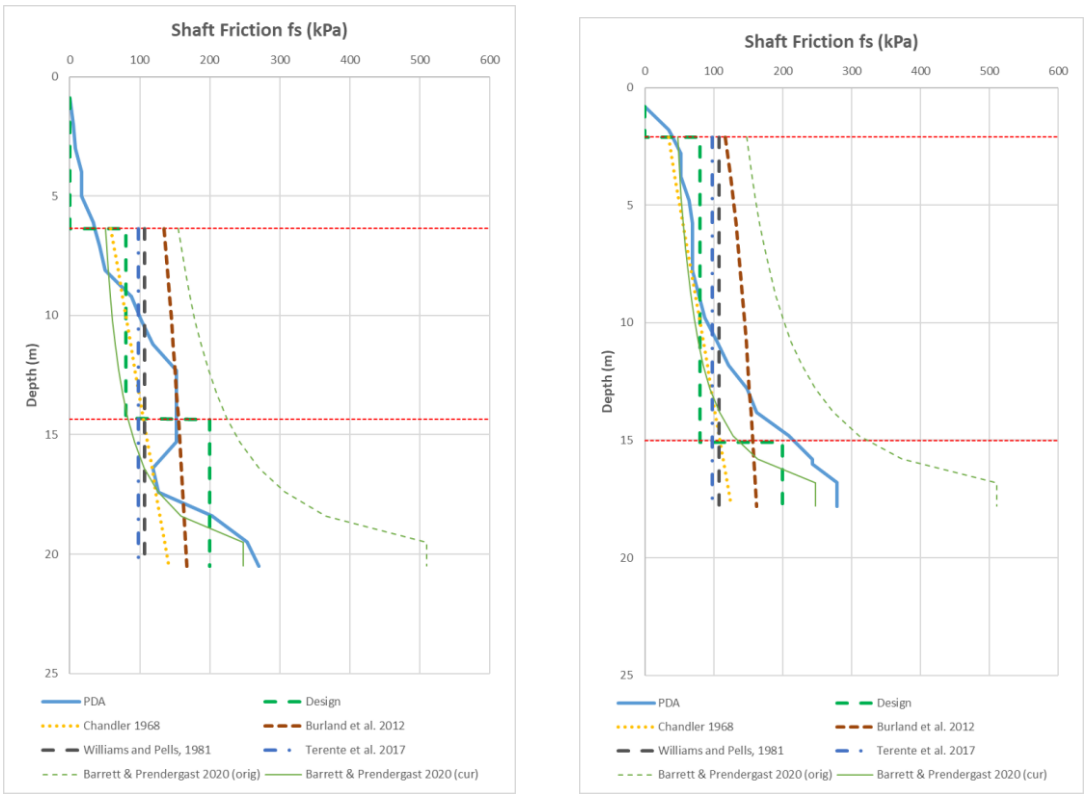


Fig. 3. Comparison of skin friction values (calculated and measured) with depth for pile P8 (left) and P10 (right), using UCS values from penetrability assessment (Weiti Bridge)

The total stress method (Burland, 2012) tends to overestimate friction values in this zone. Both approaches underestimate shaft resistance at depths exceeding 15 m for Weiti Bridge and overestimate or provide relatively accurate estimates for Highgate Bridge.

The methods proposed by Terente et al. (2017) and Rosenberg and Journeaux (1976) yield relatively accurate estimates between 10–15 m depth. However, they overpredict skin friction above this interval and underpredict it within the Northland Allochthon (depths > 15–17 m). When applying a β value of approximately 0.4, corresponding to the minimum mass factor, the Rosenberg and Journeaux method aligns closely with Terente et al.

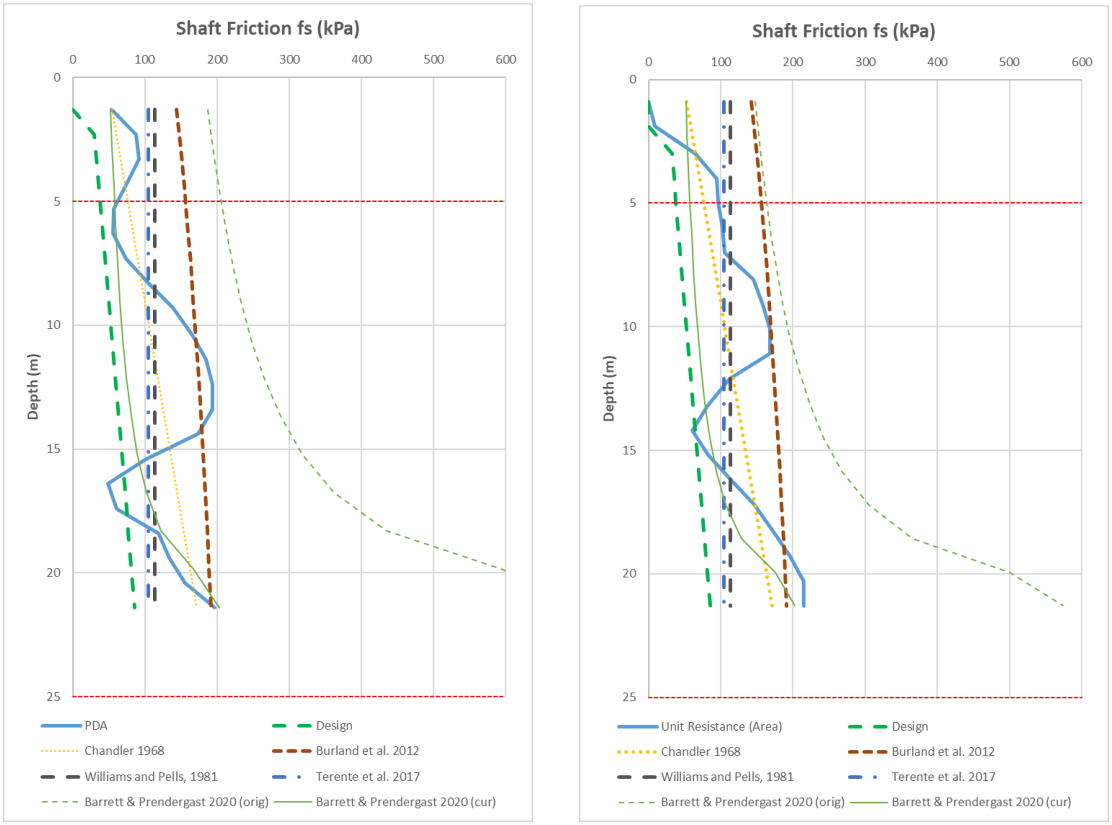


Fig. 4. Comparison of skin friction values (calculated and measured) with depth for pile P3 (left) and P4 (right), using UCS values from penetrability assessment (Highgate Bridge)

The effective stress method (Chandler, 1968) provides a reasonably accurate estimation of skin friction within the upper 12–15 m of the ground profile.

The UCD-based approach overestimates skin friction when using the original dimensionless parameters proposed by Barrett and Prendergast (2020). However, when recalibrated using pile load test data from the two bridges, with α_0 = 0.3 (0.20-0.35) and β = 0.5 (0.45-0.60), the predictions improve significantly.

Analysis Using UCS Data

Figure 5 presents the variation of ultimate shaft friction with depth for the Highgate Bridge. Owing to the relatively low UCS values, all UCS-based correlations tend to underestimate shaft resistance throughout most of the profile.

The UCD-based approach yields a reasonably accurate estimation of skin friction when applying the original dimensionless parameters proposed by Barrett and Prendergast (2020). For pile P4, a slight adjustment of the α_0 value to 0.9 further improves the prediction.

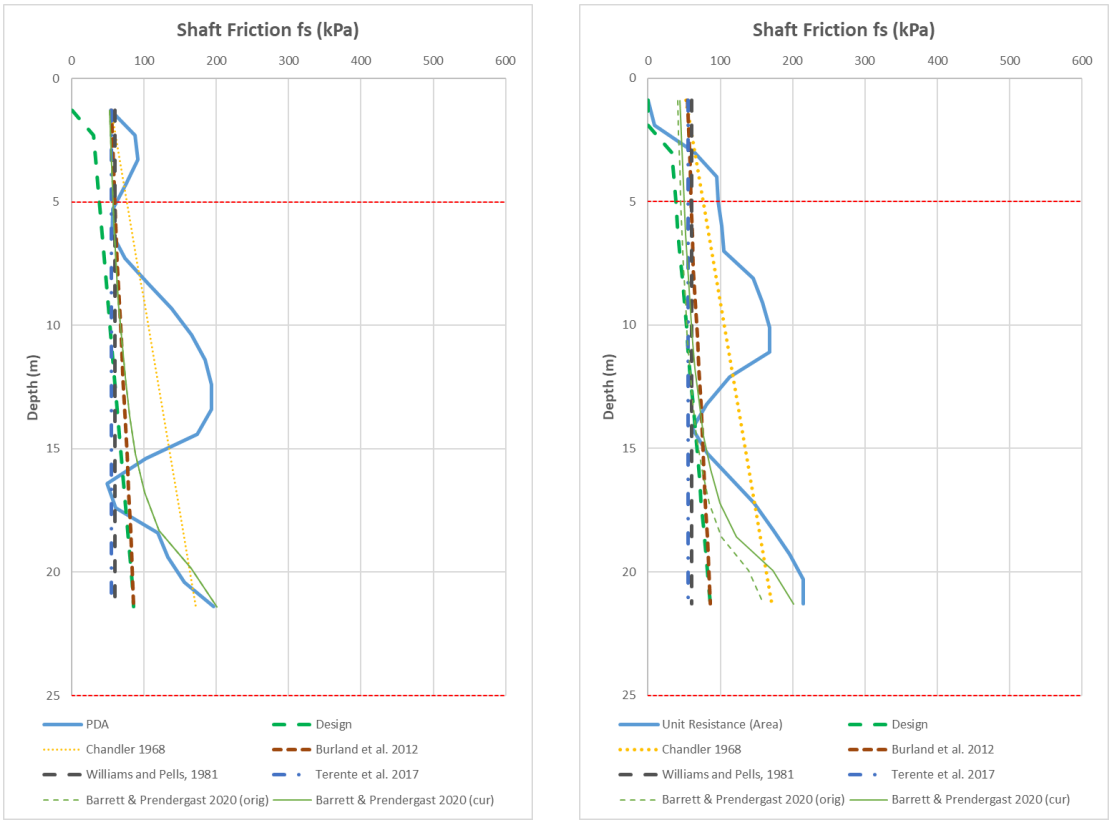


Fig. 5. Comparison of skin friction values (calculated and measured) with depth for pile P3 (left) and P4 (right) using UCS values from laboratory testing (Highgate Bridge)

CONCLUSIONS AND RECOMMENDATIONS

In this paper, various methodologies proposed by researchers for estimating the skin friction of driven piles were reviewed and critically analysed. Their applicability was assessed through Pile Driving Analyzer (PDA) tests conducted in Northland Allochthon materials.

Although several references address skin friction for driven piles, there remains a lack of direct guidance for evaluating these parameters when piles penetrate weak rock. Commonly adopted design approaches that correlate skin friction with the uniaxial compressive strength (UCS) of rock often yield inconsistent results, either overestimating or underestimating shaft resistance, and are therefore best regarded as supplementary tools rather than standalone solutions.

Current practice for estimating skin friction in weak rock typically relies on methodologies originally developed for driven piles in soils. These approaches assume degradation of the parent rock during pile installation, a phenomenon confirmed by the test results presented. However, such methods exhibit variable performance and tend to underestimate skin friction as rock depth increases.

An empirical relationship between UCS and skin friction, derived from UCD test data and incorporating fatigue effects, offers improved predictive capability, particularly when dimensionless parameters are appropriately calibrated.

To advance current practice, further case studies are essential to broaden the existing dataset and refine design methodologies for driven piles in weak rock formations, particularly when integrated with laboratory testing. Notably, the test results presented in this study show strong agreement with the findings of Barrett and Prendergast (2020) when using directly measured UCS values, rather than correlated estimates. This consistency reinforces the validity of their proposed empirical framework and the corresponding dimensionless scaling factors, α_0 and β.

ACKNOWLEDGEMENTS

The authors gratefully acknowledge the invaluable contributions of Fulton Hogan Civil, as well as the support and expertise provided by colleagues at CMW Geosciences and other personnel involved in the investigations. Their input, through shared data, insights, comments, and technical advice, was vital to the development of this paper.

REFERENCES

Barrett J. W., Prendergast L. J. 2020. Empirical Shaft Resistance of Driven Piles Penetrating Weak Rock. Rock Mechanics and Rock Engineering 53:5531–5543

Burland J., Chapman T., Skinner H.D., Brown M. 2012. ICE manual of geotechnical engineering. ICE Publishing, London

Chandler, R. J. 1968. The shaft friction of piles in cohesive soils in terms of effective stress. Civil Engineering and Public Works Review, 63, 48–51

Edbrooke, S.W. (compiler) 2001: Geology of the Auckland area. Institute of Geological and Nuclear Sciences 1:250 000 geological map 3. 1 sheet + 74 p. Lower Hutt, New Zealand. GNS Science.

East, G. R. W., & George, A. K. 2001. Roading in Northland Allochthon Terrain - Auckland and Northland - Engineering and Development in Hazardous Terrain: New Zealand - Geotechnic al Society 2001 Symposium, Christchurch, August 2001. Wellington, New Zealand: IPENZ, Proceedings of Technical Groups; 29(2), 353-364.

Fleming K. Weltman A, Randolph M, Elson K. 2008. Piling engineering, 3rd ed. Taylor & Francis, Routledge.

Hayward B. 2017. Out of the Ocean, Into the Fire. History in the Rocks, Fossils and Landforms of Auckland, Northland and Coromandel. Geoscience Society of New Zealand.

Lentfer K., Lontzetidis K., Woodward M. and Ritchie C. 2023. Pile Foundation design in Northland Allochthon Proceeding of the 14th Australia and New Zealand Conference on Geomechanics, Cairns

Pradhan, D., Lontzetidis K., and Morton D., 2019. Geotechnical Investigation and Design Report for Milldale – Weiti Bridge. AKL2019-0050AB Rev 1 CMW Geosciences.

Riddolls & Grocott Ltd, 2001. Probabilistic Techniques for Optimizing Cut Slope Earthworks, Transfund New Zealand Research Report NO. 189, 2001

Rosenberg P. and Journeaux, N.L. 1976. Friction and end bearing tests on bedrock for high-capacity socket design. Canadian Geotechnical Journal, 13, 324–333.

Stamatopoulos A. and Kotzias P.C., 1993. Refusal to the SPT and penetrability. Geotechnical Engineering of Hard Soils – Soft Rocks, 301-305.

Terente V, Torres I, Irvine J, Jaeck C 2017 Driven pile design method for weak rock. Proceedings of the 8th international conference of offshore site investigation and geotechnics. (c) 2015 Taylor & Francis Group, London, London, UK, pp 652–657

Tomlinson M., Woodward J. 2015. Pile design and construction practice. CRC Press, Boca Raton

Williams A.F. and Pells, P.J.N. 1981. Side resistance rock sockets in sandstone, mudstone and shale. Canadian Geotechnical Jou rnal,18, 502–513

Winkler, G.E, 2003. Geotechnical Engineering of the Northland Allochthon. Proceedings of the "Geotechnics on the Volcanic Edge" symposium.

 © Deep Foundations Institute 2026

SMART EXECUTION: DIGITAL INTEGRATION AND CONSTRUCTABILITY FOR DIAPHRAGM WALL AND BARRETTE DELIVERY

John Paouros, Keller, Melbourne, Victoria, Australia; +61 3 9590 2600, john.paouros@keller.com.au
Zuhaib Khan, VSL, Melbourne, Victoria, Australia; +61 3 9357 1184, zuhaib.khan@vsl.com

ABSTRACT

Delivering diaphragm wall and barrette foundation systems for major infrastructure projects involves a range of construction and risk management challenges. Large panel volumes, complex reinforcement designs and variable ground conditions require careful planning and precise execution. This paper shares insights from two major projects, which together involved approximately 3 km of alignment and excavation depths up to 45 m. The construction phase focused on delivering permanent retention and foundation structures under complex and constrained site conditions. Plaxis 3D modelling was used during early planning for temporary works design to confirm trench geometry, assess stability and define slurry performance requirements. Throughout delivery, digital tools such as TIO and B-Tronic supported real-time excavation monitoring, while 3D structural models facilitated reinforcement clash detection, rebar detailing and reduced fabrication errors. Visual inspections and digital tools helped verify cage quality prior to installation. Concrete works were tracked with mobile digital tools, and site data was consolidated into Power BI dashboards to support decision making. The use of a superlatch system for rebar splicing further improved HSEQ outcomes. This paper illustrates how constructability planning, digital integration and connected systems supported effective management of ground risk, quality and construction sequencing. It demonstrates the effectiveness of integrated tools to enhance the execution of diaphragm wall and barrette foundation systems in complex infrastructure environments.

Keywords: diaphragm wall, barrette, deep excavation, digital integration, constructability, quality control

INTRODUCTION

Diaphragm walls and barrette foundations play a critical role in the delivery of major infrastructure projects, particularly where deep excavation and ground retention are required. These systems are often constructed in dense urban settings where constrained access, stringent project requirements and challenging ground conditions, such as high groundwater or variable strata, add complexity to planning and execution. Successful delivery of these geotechnical structures relies not only on sound engineering design, but also on how effectively construction teams manage risks, coordinate activities and adapt to site-specific conditions.

As infrastructure projects grow in scale and complexity, there is an increasing need to integrate digital tools and improve their interoperability to enhance on-site coordination and construction delivery (Duarte-Vidal et al., 2021). Specialist contractors are expected to take greater responsibility for managing risks related to safety, construction quality and programme delivery. To support these responsibilities, digital tools are being more widely adopted across the construction phase (Deloitte, 2025). When used effectively, they support real-time decision making and allow site teams to proactively manage safety and productivity.

This paper demonstrates how early-stage planning and integrated digital systems supported the safe and efficient delivery of diaphragm wall and barrette foundation systems across two major infrastructure projects in Australia. It shows how the application of digital tools and constructability planning helped reduce construction risks, improve quality control and support project delivery.

 © Deep Foundations Institute 2026

PROJECT OVERVIEW

Two major infrastructure projects were delivered in urban environments, where diaphragm walls and barrette foundations served as permanent retention and foundation structures for deep excavations. Across the sites, approximately 3 km of alignment were completed, with panel thicknesses ranging from 1.0 m to 1.2 m and depths from 20 m to 45 m.

A large fleet of specialist plant was required for the execution of the project, including up to three mechanical grabs and three hydromill trench cutters operating concurrently at peak production, as shown in Fig. 1. Service cranes with lifting capacities up to 280 tonne handled heavy cages and tooling, while multiple bentonite slurry pools and associated treatment equipment enabled continuous production and fluid recycling within the constrained site footprints.

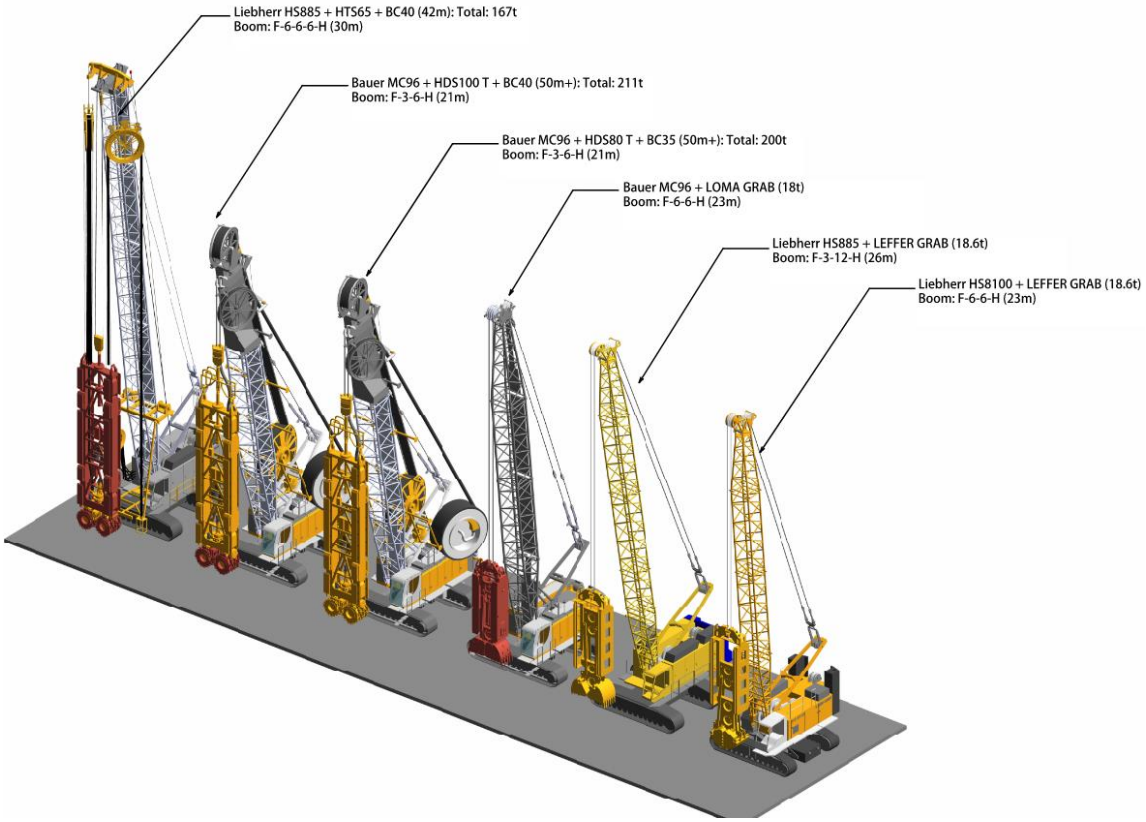


Fig. 1. Key plant used for diaphragm wall and barrette construction, including Liebherr HS885, HS8100, Bauer MC96 with BC35/BC40 cutters, LEFFER and LOMA grabs

The urban environment introduced a range of construction challenges, including limited access, constrained laydown areas, proximity to live infrastructure, adjacent sensitive structures and the public. The sites also featured variable ground conditions, adding complexity to excavation planning. These constraints affected construction methods and programme delivery, requiring careful planning and staged execution to maintain safety and meet project milestones.

Both projects presented practical opportunities to apply digital tools across planning, execution and quality control. This was driven by the need to manage site congestion, variable ground conditions and programme constraints. These challenges required close coordination between site-based personnel and engineering support teams. Digital tools supported trench stability modelling, excavation tracking, cage validation and concrete logging, helping site teams reduce construction risk and improve execution accuracy.

 © Deep Foundations Institute 2026

SITE CONDITIONS AND GEOTECHNICAL RISK

The ground conditions encountered across both project sites, one located east of Melbourne's CBD and the other west of Sydney, were variable but broadly consistent with those typically observed in deep urban excavations (Peck et al., 1992; Pells, 1985). At surface level, engineered working platforms, typically 1.0 m to 1.5 m thick, were constructed from compacted crushed rock to support heavy plant and limit surface movement. Beneath this, the subsurface profile typically comprised interbedded clays and sands with varying degrees of consolidation, strength and moisture content, reflecting complex sediment deposition at both sites.

Both sites were underlain by Quaternary alluvium, which, where thicker and saturated, presented challenges due to low shear strength and high potential for instability. Frequent variability in stiffness and permeability, even over short vertical distances, required strict control over excavation sequencing and slurry levels. At depth however, differences emerged between the two sites. At the western Sydney site, the alluvium was generally shallower, underlain by moisture-sensitive Ashfield shale, and at greater depth, Hawkesbury sandstone. In contrast, the eastern Melbourne site was characterised by thicker alluvium overlying Silurian siltstone, where the transition between the soft soils and competent rock introduced additional stability and panel misalignment risks if not carefully managed.

Across both sites, geological discontinuities observed in the rock mass such as bedding planes, joints, shear zones and faults required targeted mitigation during excavation. Weak zones in the overburden such as sand lenses were also identified as trench stability risks. These conditions were addressed during early planning and managed during excavation through active monitoring and adaptive sequencing to maintain trench stability.

Groundwater was typically encountered within the alluvial deposits, with perched water tables or localised inflows observed at depths up to 10 m below ground level. To manage trench stability risks and potential settlement of nearby structures, worst case groundwater levels were initially assumed and subsequently validated through frequent monitoring with piezometers.

TRENCH EXCAVATION AND SLURRY MANAGEMENT

Trench stability risks were addressed during early planning through numerical modelling using Plaxis 3D. The modelling assessed ground behaviour and slurry support requirements to ensure trench stability during excavation. It provided early insights into deformation and instability risks, supporting safer excavation strategies and more controlled site execution.

The Plaxis 3D analysis incorporated geotechnical data from engineering logs and laboratory testing. Ground behaviour was modelled progressively to reflect excavation conditions at varying depths, slurry levels, surcharge loads and panel geometries. The analysis produced key results such as horizontal and vertical displacements, shear strain concentrations and safety factors against failure (typically targeting values >1.2). These results also helped identify potential failure mechanisms in the upper alluvial soils, as well as lateral movement risks near sensitive structures or in zones with perched groundwater. The modelling informed the development of temporary excavation controls, including bentonite slurry criteria, excavation strategies and minimum loading distances for plant operating near open trenches. Figure 2 presents a representative failure mechanism used for one of the projects and the associated minimum plant setback distance of 2.9 m from the guide wall. It illustrates how numerical modelling was used to define safe operating limits and support smarter, risk-informed field decisions on site. This setback required the Bauer MC96 cutter crane to be offset behind the guide wall to avoid front track instability, as shown in Fig. 2.

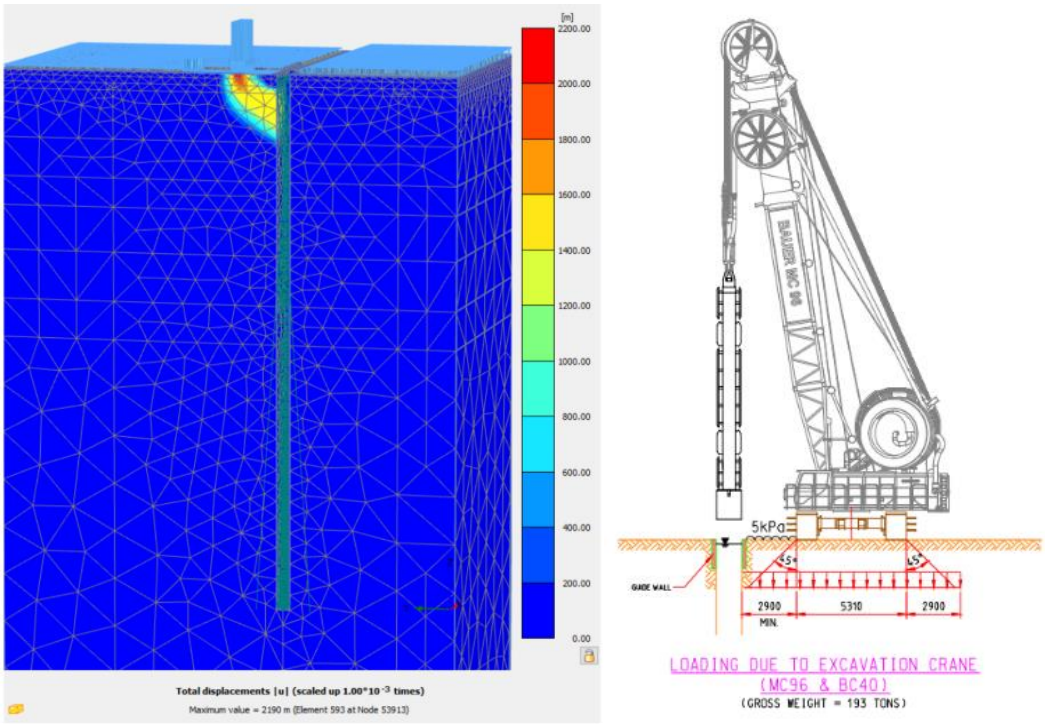


Fig. 2. Plaxis 3D trench stability failure mechanism (left) for a critical loading case with surcharge from BC40 trench cutter mounted on a MC96 crane with instability near the front track. The corresponding minimum safe loading distance from an open trench is illustrated (right)

The TIO excavation system, developed in house, was used during construction to record excavation activity, panel advancement and machine utilisation by capturing operator-entered data on a tablet. Activities such as panel excavation, trimming, stop end installation, base cleaning, bentonite recycling and de-sanding were logged by operators according to a predefined list of tasks. Engineers reviewed this data daily to assess productivity, identify delays and adjust upcoming works accordingly. In parallel, B-Tronic, a monitoring system with sensors integrated into the equipment, was used during trench excavation to continuously collect data. It supported quality assurance by capturing detailed excavation data such as panel depth, verticality and excavation rate. Engineers reviewed this to confirm conformance with design tolerances and detect anomalies in ground behaviour, particularly variable strata. Figure 3 presents a B-Tronic extract, illustrating how panel alignment (x and y deviation) and excavation progress (rate by depth) were tracked and verified during construction.

Ground movement monitoring was a key part of the excavation risk strategy, particularly near sensitive structures. Settlement and deflection were tracked during panel excavation using survey points installed on adjacent structures, while inclinometers were used post-excavation to monitor ground behaviour during the bulk excavation phase. This staged approach enabled early detection of ground movement, supporting stability control and aligning with the broader smart and safe execution strategy applied across both projects.

Effective slurry management was essential to maintain trench stability during excavation. Regular onsite testing ensured that the bentonite slurry met performance criteria such as density, viscosity, sand content, pH and fluid loss. Where possible, slurry was reused to reduce consumption and disposal volumes. However, reuse of the slurry introduced stability risks if the slurry degraded below required thresholds, especially in permeable or fractured ground where fluid loss could compromise trench support. These risks were managed through routine performance testing of the reused slurry, along with visual checks of trench conditions during excavation. Data from digital tools such as B-Tronic also helped verify trench conditions and identify potential zones requiring tighter slurry control, ensuring stability across varied ground conditions.

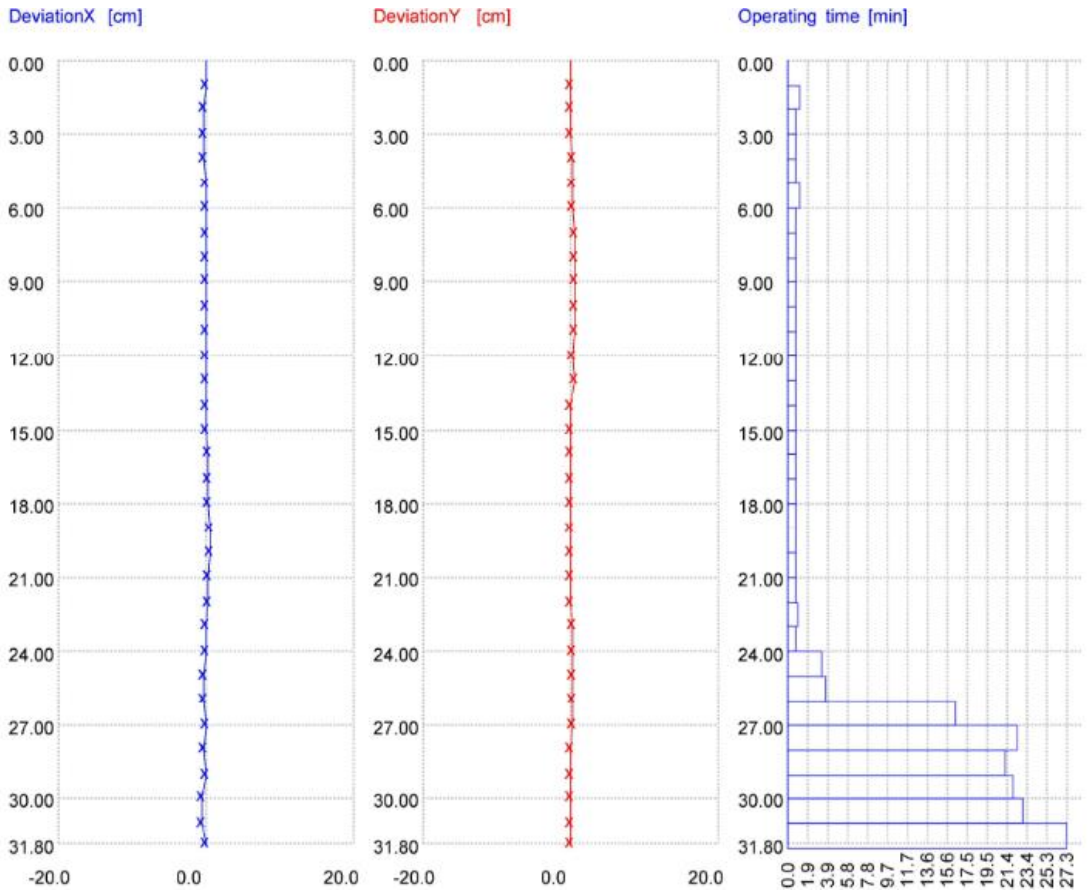


Fig. 3. B-Tronic trench verticality and penetration record during panel excavation. Blue and red lines (left/middle) indicate x and y direction deviation, while plot (right) shows excavation rate by depth

REINFORCEMENT CAGE CONSTRUCTABILITY AND INSTALLATION

Reinforcement cages required precise planning and installation due to the scale and complexity of the rebar design. Tekla Structures software was used during early planning to develop 3D cage models that helped detect clashes, validate layouts and resolve reinforcement issues prior to fabrication. The 3D models also enabled detailed planning of reinforcement elements such as coupler positions, rebar development lengths, lifting points, trapping beam locations and church bar configurations. A representative section of the model is shown in Fig. 4, illustrating the spatial arrangement of transverse and longitudinal bars, trapping bars and splice development. These details were essential not only for accurate fabrication, but also to support efficient installation and sequencing on site.

Following fabrication, the reinforcement cages were inspected using Quick Connect, a digital tool for quality verification. This tool confirmed that each prefabricated cage matched approved shop drawings and complied with all dimensional and assembly requirements. Inspection results were digitally logged to ensure full traceability. This process supported QA/QC procedures by generating photographic inspection records, verifying that the cages met installation requirements before leaving the fabrication yard.

Cages that passed inspection were fitted with a QR-coded tag linked to their corresponding shop drawing. These tags enabled site engineers to quickly access key installation details such as cage orientation, section type, splice lengths, coupler positions and RLs. This ensured correct and sequential installation on site. The process supported a smooth transition between fabrication and site activities, reducing errors and installation delays.

 © Deep Foundations Institute 2026

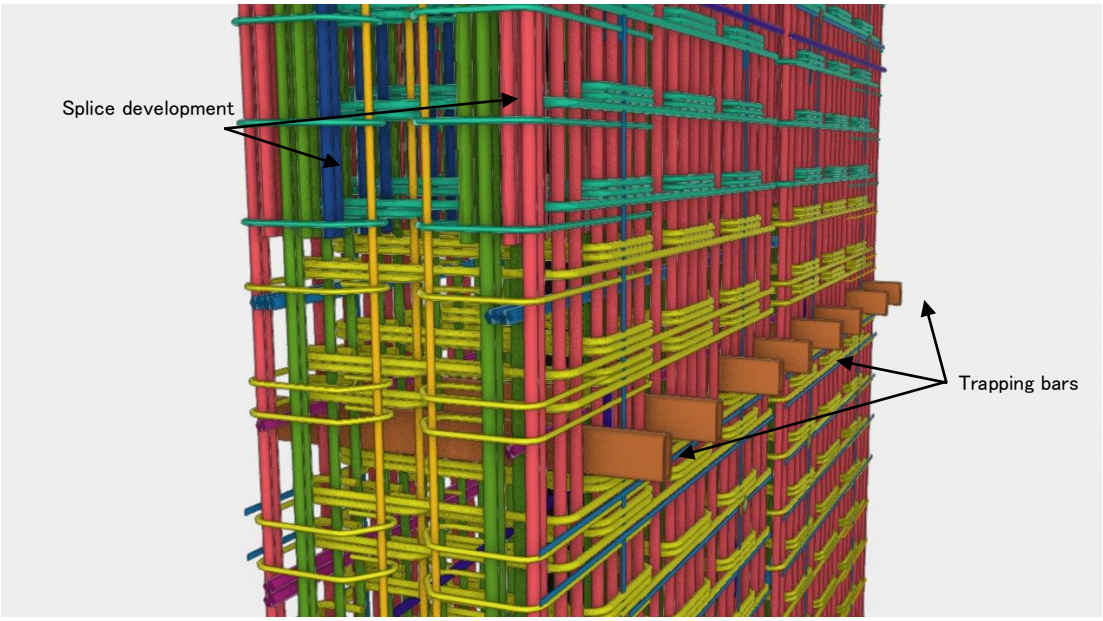


Fig. 4. Tekla Structures 3D model of reinforcement cage showing trapping bars and splice development. The image illustrates bar layout and reinforcement overlaps, supporting constructability and installation planning

Superlatch

To streamline reinforcement cage installation and reduce manual handling risks, superlatch mechanical connectors were implemented as an alternative to U-bolts on one of the projects. As shown in Fig. 5, the connectors and their receiving bands were welded to the top and bottom of cage segments, enabling fast and secure engagement during onsite assembly. This improved installation efficiency and reduced physical strain on workers.

Before connecting, alignment was confirmed using a spirit level and triangulation to ensure vertical accuracy. This method was particularly effective in areas with limited access or near adjacent structures, where traditional techniques were impractical. Superlatches also reduced construction noise by eliminating the ratcheting sounds typical of U-bolt tightening.

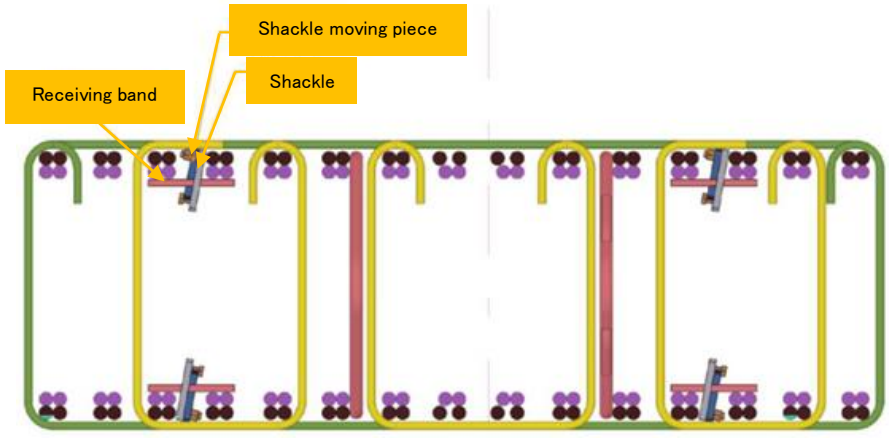


Fig. 5. Detail drawing of reinforcement cage showing welded receiving band locations for superlatch connectors

Figure 6 shows the system in use onsite, highlighting how crews completed connections with minimal manual adjustment in tight-access areas. All connections were subject to visual inspection and magnetic particle (MPI) testing to verify weld quality.

Used alongside digital tools such as structural 3D models, Quick Connect and QR-coded tags, superlatches streamlined physical assembly. Digital systems supported quality tracking and coordination across both projects.

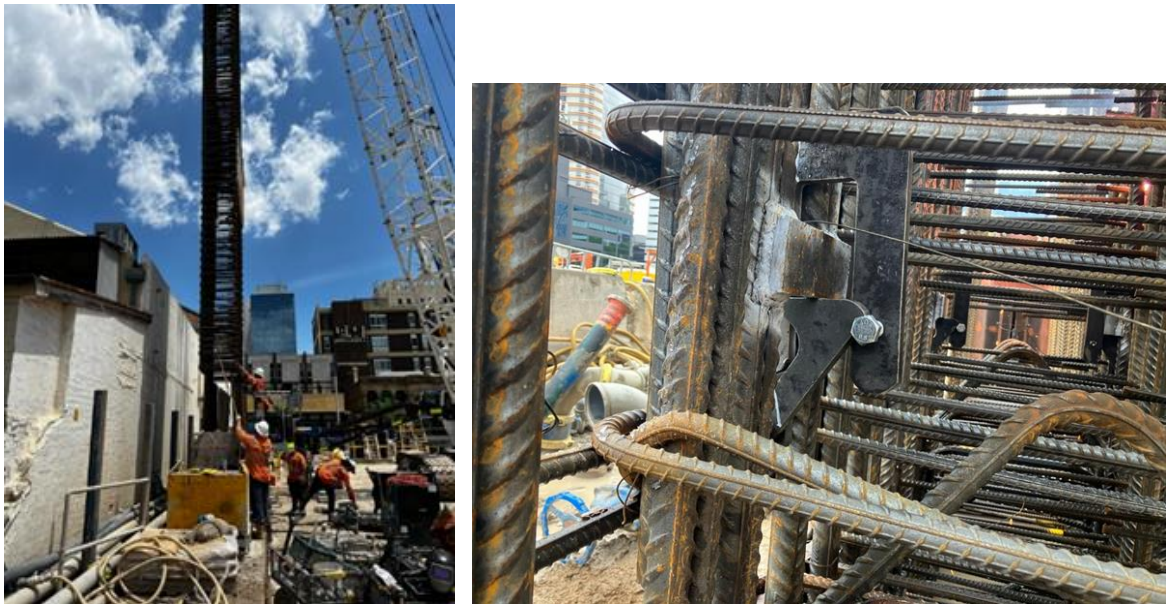


Fig. 6. On-site installation of reinforcement cages using superlatch in constrained urban environment (left) and close-up view of aligned connector and receiving band during splicing

CONCRETING AND POUR MONITORING

Concrete delivery and placement were critical construction stages that required close coordination to ensure full panel continuity and structural integrity. Pours were only scheduled once reinforcement cages were installed, slurry conditions met specification, batching was aligned with site needs and tremie pipes were positioned for uninterrupted placement. Tremie embedment was consistently maintained between 3 m and 9 m below the top of concrete to enable bottom-up placement and minimise the risk of cold joints, inclusions and slurry contamination.

To support this process, access to the supplier's digital logistics platform enabled real-time visibility of concrete batching status, truck locations and delivery timing. This allowed site teams to anticipate arrivals, coordinate tremie embedment transitions and maintain consistent delivery intervals to support uninterrupted concrete placement.

Key data including mix compliance, discharge times, concrete volumes and tremie embedment depths were captured digitally during the pour and used to support live production monitoring. Field data was automatically integrated into a live concrete displacement curve (see Fig. 7), enabling real-time tracking of pour progress and early anomaly detection.

One project used embedded sensors via thermal integrity profiling (TIP) to assess concrete quality and verify structural integrity, while the other relied on minimally invasive verification methods such as tremie placement logs, volume tracking and post-pour integrity testing (i.e., crosshole sonic logging). Both approaches enhanced traceability, enabled early anomaly detection and aligned with the broader digital QA systems implemented across both projects.

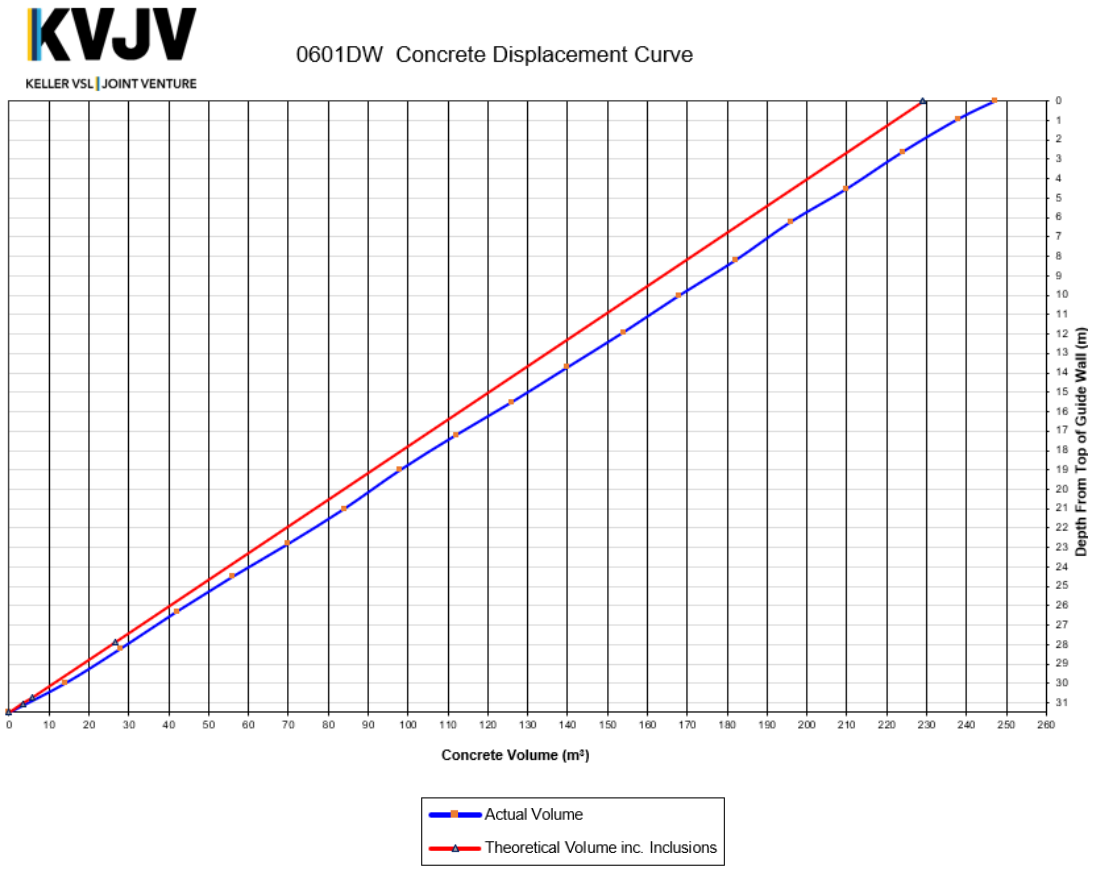


Fig. 7. Live concrete displacement curve, showing actual versus theoretical progression of concrete volume over depth

INTEGRATED DASHBOARDING

To support smart execution, a Power BI dashboard was developed to consolidate construction data from digital tools into a single platform. The dashboard offered a consistent way to track progress and generate reports, while remaining flexible enough to suit the different delivery approaches and stakeholder expectations at each site. By combining a standardised structure with site-specific adaptability, the dashboard improved the communication and coordination of activities within the project team across the two projects.

The dashboard integrated data from various digital tools used during construction. This enabled project teams to monitor construction sequencing and site performance through a unified visual interface. The dashboard tracked key metrics such as progressive excavation volumes, equipment utilisation, production rates, weekly and cumulative panel progress and production forecasts. These metrics were presented through structured visual summaries, such as weekly and cumulative excavation volumes, panel production rates, equipment-specific ultilisation charts and efficiency trends. The dashboard also provided insights into machine-level performance and near-term production forecasts, offering a clear snapshot of site progress to support planning and reporting.

Figures 8-9 illustrate key dashboard outputs used to support construction planning and stakeholder reporting. Figure 8 presents panel production progress against baseline targets, helping teams to identify delays or acceleration trends. Figure 9 displays weekly excavated volumes by machine type, alongside working hours excluding inclement weather, highlighting that higher utilisation typically corresponds with increased productivity.

 © Deep Foundations Institute 2026

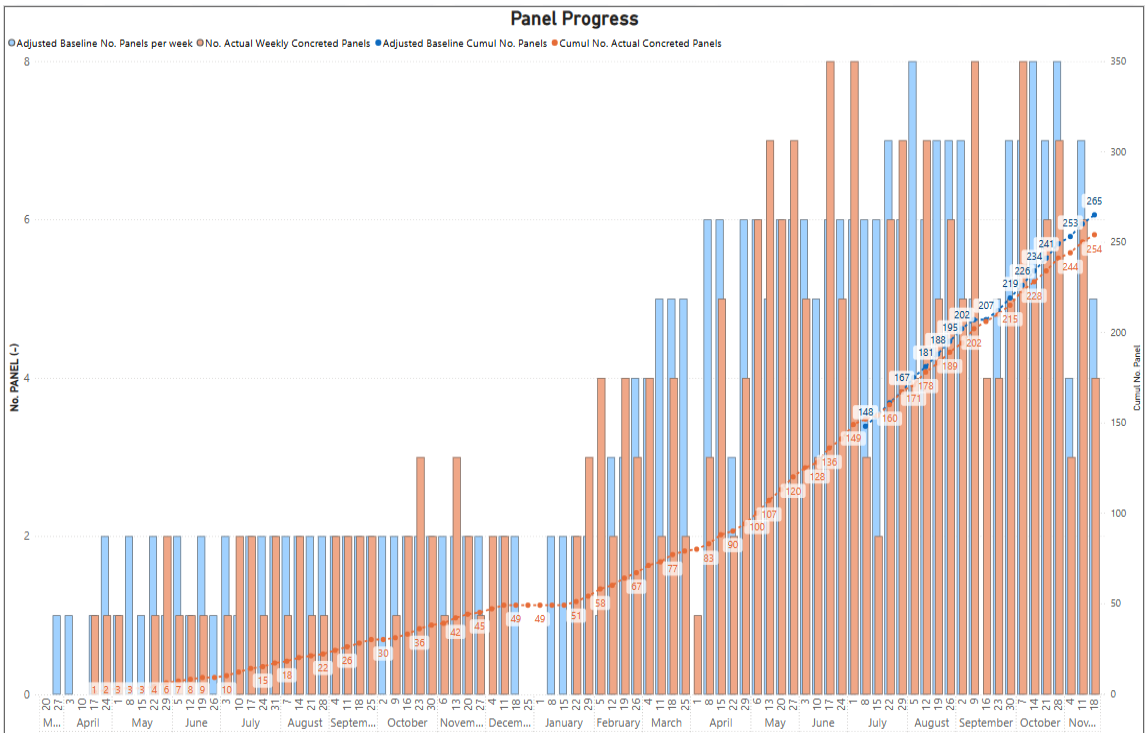


Fig. 8. Weekly and cumulative panel production progress versus baseline, used to track delivery performance

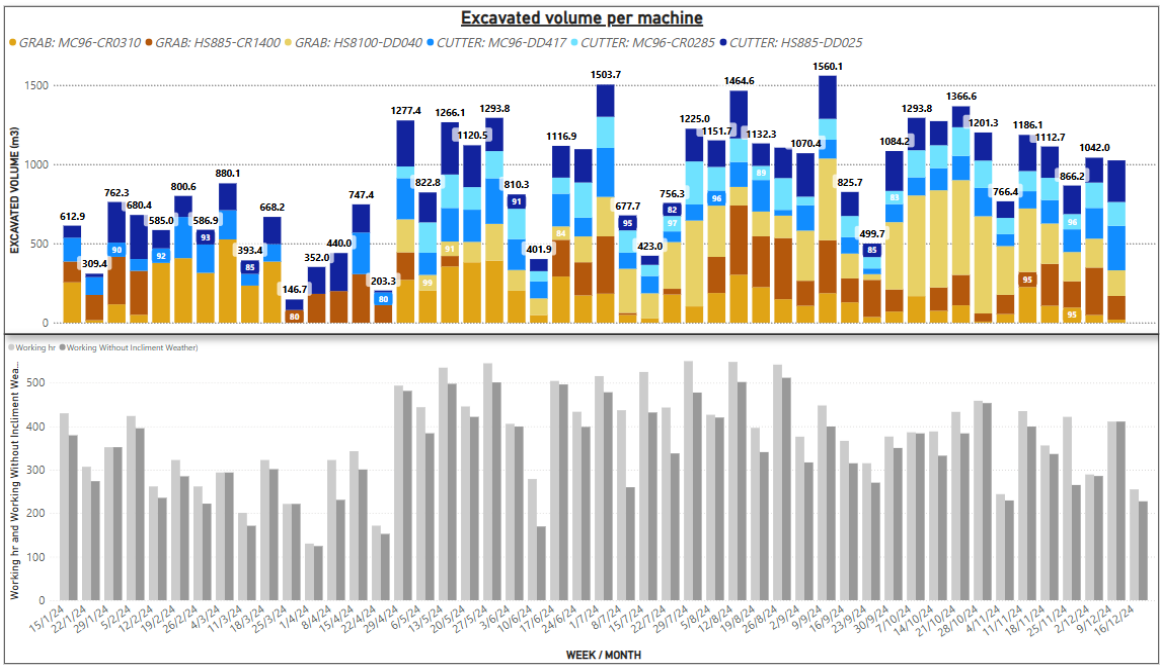


Fig. 9. Excavated volume by machine per week, showing alignment between utilisation (working hours) and productivity trends

Beyond visualising trends, the dashboards converted raw data into structured visuals that helped teams identify deviations, potential quality issues or delays. This allowed site personnel to respond proactively by adjusting execution plans as needed. The dashboards also served as a clear communication tool, presenting key metrics in an accessible format for internal reviews, planning meetings and client updates.

 © Deep Foundations Institute 2026

Despite minor differences in the digital tools used across the two projects, a standardised dashboard structure was maintained. This consistency improved the ability to benchmark performance across sites, maintain QA continuity and respond more quickly to emerging risks.

KEY LEARNINGS AND DISCUSSION

Both projects served as applied case studies for implementing smart execution methods in differing delivery environments. Together, they provided valuable insights into the benefits and limitations of digital integration in diaphragm wall and barrette foundation delivery.

Early-stage implementation of digital tools was a clear strength across both projects. Plaxis 3D enabled risk-informed trench design, improving constructability and reducing rework. Tekla Structures supported early constructability reviews for reinforcement cages, enabling clash detection and layout validation before fabrication. Field tracking tools such as TIO and B-Tronic enabled consistent excavation monitoring while reducing reliance on manual checks. Ground movement was closely monitored using survey points and inclinometers. For reinforcement cages, Quick Connect and QR-coded tags enhanced traceability from fabrication through to placement. Power BI dashboards centralised data from all construction stages, improving visibility into site progress and supporting real-time decision making.

Digital dashboards played a key role in both projects, supporting team coordination and maintaining clear communication with stakeholders. Figures 8 and 9 demonstrated how production trends and equipment performance were visualised to identify emerging delivery risks. Early warning signals, such as deviation from weekly production targets, enabled teams to adjust sequencing before delays materialised.

Despite the benefits, one of the projects faced several implementation challenges. Key digital tools were introduced midway through delivery, which delayed data consolidation and limited early visibility. This reduced the project team's ability to monitor progress effectively during critical phases. Additionally, while external systems such as concrete supplier tracking were used alongside internal tools, they were not integrated. This lack of interoperability created coordination inefficiencies and increased the risk of data inconsistencies.

These issues were significantly reduced in the other project, where digital systems were implemented from the outset. Enhanced dashboarding design, particularly for machine-specific outputs and productivity variances, enabled early identification of bottlenecks and more effective planning. Utilisation data also supported early detection of programme slippage, making the dashboard a practical tool for proactive sequencing.

Based on this comparison, the following key recommendations emerged:

- Integrate digital QA and tracking tools from early phases to ensure visibility and minimise rework.
- Prioritise interoperability between internal and external digital systems.
- Allocate sufficient time for training and system familiarisation to support user adoption.
- Evolve dashboards from basic trackers into predictive tools that support lookahead planning and adaptive sequencing.

The coordinated use of digital systems across all construction phases improved QA oversight, increased transparency and enabled faster issue resolution. These benefits were most evident in complex geotechnical and constrained work environments. When digital tools were introduced early and data was actively used to guide decision making, teams responded faster and executed more effectively.

CONCLUSION

Both projects demonstrated the advantages of early adoption of digital tools and structured QA systems in contributing to the safe and efficient delivery of diaphragm walls and barrette foundations. Despite differences in site conditions and stakeholder requirements, each project benefited from digital planning, real-time monitoring and centralised data management, which helped teams manage risk and maintain quality throughout construction.

Tools such as Plaxis 3D, Tekla Structures, TIO, B-Tronic, Quick Connect and Power BI helped overcome constructability challenges, improve traceability and streamline stakeholder communication. Embedded across excavation, cage fabrication, and concrete works, these tools gave teams greater control over quality and risk, particularly in geotechnically variable and high-pressure urban environments.

Comparing the two projects highlighted the importance of early tool adoption, cross-system integration and upskilling of site teams. Dashboards unified multiple systems and enhanced coordination across field teams and stakeholders by centralising decision-making data.

The integrated approach adopted across both projects demonstrated measurable improvements in enhancing safety, delivery speed, adaptability and quality control. As infrastructure projects become more complex, consistently applying integrated systems will be essential to managing construction risk and ensuring delivery certainty.

ACKNOWLEDGEMENTS

The authors would like to thank Keller and VSL for supporting and encouraging technical publications within the industry. They also acknowledge the colleagues whose collaboration supported the development and implementation of the digital tools and QA systems described in this paper.

REFERENCES

Deloitte Access Economics. 2025. State of Digital Adoption in the Construction Industry 2025. Melbourne: Deloitte Touche Tohmatsu.

Duarte-Vidal, L., Herrera, R.F., Atenco, E., and Muñoz-La Rivera, F., 2021. Interoperability of Digital Tools for the Monitoring and Control of Construction Projects. Applied Sciences. 11(21), 10370.

Peck, W.A., Neilson, J.L., Olds, R.J., and Seddon, K.D., 1992. Engineering Geology of Melbourne. Rotterdam: Balkema.

Pells, P.J.N., 1985. Engineering Geology of the Sydney Region. London: Routledge.

 © Deep Foundations Institute 2026

A REVIEW OF THE EFFC/DFI GUIDE TO WORKING PLATFORMS 2ND EDITION

Stephen Buttling, National Geotechnical Consultants, Brisbane, Australia,
stephen.buttling@ngconsult.com.au
David Corke, Northwich, UK, djcorke@outlook.com
Michael Dobie, Tensar, Jakarta, Indonesia, mike.dobie@cmc.com
Martin Larisch, Larisch Consulting, Waikanae, New Zealand, mdlarisch@gmail.com

ABSTRACT

The EFFC/DFI issued a Guide to Working Platforms in December 2019. Since December 2022, the authors, and many others, were involved in the preparation of a revised Edition, Ed2, of the Guide, which was published in May 2025. This states in its opening section that "*the guide outlines tools for a practical implementation of better practices that can be adopted across the world*." However, in the opinion of the authors it does not provide adequate practical advice across a number of very important areas. These include:

- The basic calculation of the bearing capacity of a strong granular layer over a weaker subgrade, such that new platform designers will have a better understanding of what the various available calculation methods are trying to achieve, and why there is not a simple mathematical formula.
- An understanding of the behaviour of high friction angle soils and materials, which have become the preferred choice for working platform materials because of the thinner platforms that are required.
- The statements that a Design Method needs to include at least three components, and maybe four, and that they must be compatible, but no advice is offered as to how this can be achieved.
- The use of calibration in a semi-empirical method, how this is carried out, and what limitations it creates on the use of the output.
- A number of questions with regard to the determination of tracked rig bearing pressure, which was not adequately addressed.
- The subject of testing, particularly to confirm the angle of friction of the platform material.
- The statements that "The working platform is temporary works and its design must be managed as such" yet no advice is offered as to what this means or how it is to be applied.
  The shortcomings in these key areas will be identified as a caution to readers and, where space permits, alternative practical advice will be provided.

Keywords: working platforms, design, bearing capacity

INTRODUCTION

This paper has been written with specific reference to the EFFC/DFI Guide to Working Platforms, Edition 2 (Guide 2) published in May 2025, with the preparation of which the authors were involved over a number of years. It is noted that all of those involved in the revisions have significant experience of at least one aspect of working platforms, and that there are also many publications available to which reference can be made. However, it is considered that, because of the inherent complexity of the subject matter, it is necessary to wind back and start at a level suitable for those who are new to this special application. This paper will try to point out where additional information is recommended and, within the space confines allowed, will provide as much of the suggested information as possible.

In Guide 2 there is a lack of basic understanding and guidance helpful to a designer, especially a new designer. An attempt is made here to provide concise, simple, practical explanations of the derivation and application of design methods in common use, to assist designers in selecting, understanding and utilizing their chosen design method appropriately.

 © Deep Foundations Institute 2026

BEARING CAPACITY OF HOMOGENEOUS SOILS

The design of working platforms is a two-layer problem, consisting of a strong upper layer (the platform) supported by a weaker subgrade. However, as part of the design process, assessment of the bearing capacity of a homogeneous layer is also required. The bearing capacity of surface or shallow foundations, even though governed by some widely accepted design methods, is a complex subject, so before getting involved in the details it is important to understand the fundamentals. The equation below was proposed by Terzaghi (1943) for the vertical bearing capacity of strip foundations (namely the two-dimensional case, such that the foundation has infinite length):

$$q = c'N_c + \gamma D N_q + 0.5\gamma B N_\gamma \quad [1]$$

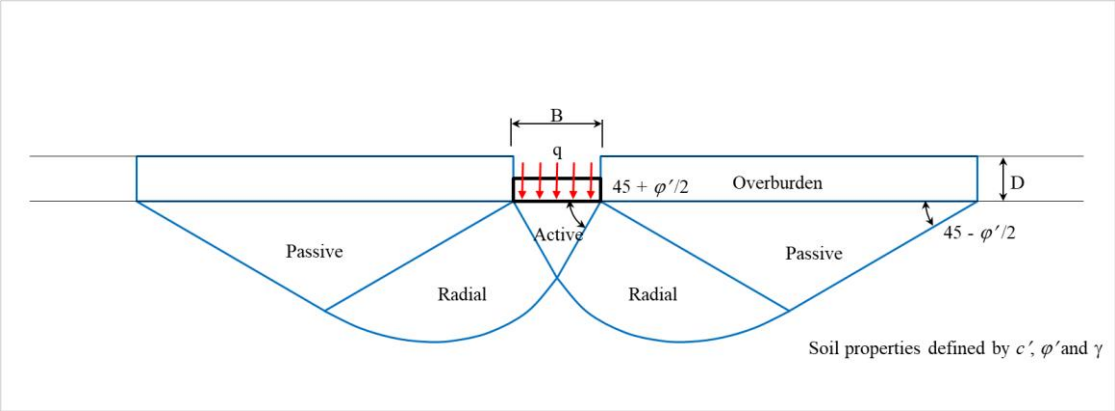


Fig. 1. Definitions for the general bearing capacity equation

As written, this solution is formulated in terms of effective stress, sometimes referred to as the drained condition. The three terms on the right-hand side predict the contributions from: the cohesion intercept of the soil; the weight of overburden above the foundation level; and the weight and frictional strength of the soil below the foundation level. All three terms may be adapted to different geometries and loading conditions by the application of factors. Shape factors (s_c, s_q *and* s_γ) are applied to take into account foundations of finite length, and inclination factors (i_c, i_q *and* i_γ) make allowance for resistance developed in directions other than vertical. The factors (N_c, N_q *and* N_γ) are referred to as the bearing capacity factors. In the cases of N_c *and* N_q closed form solutions for their values are well established as follows:

$$N_q = \frac{1+\sin\varphi'}{1-\sin\varphi'} e^{\pi \tan\varphi'} \text{ and } N_c = (N_q - 1)/tan\varphi' \quad [2, 3]$$

This leaves N_γ, but unfortunately the formulation is complex and a precise yet solvable equation to give its value over the full applicable range of φ' cannot be established. Various authors, including Meyerhof (1963), Brinch Hansen (1970) and Vesic (1973) (as used in BR470), have developed solutions, but these are all approximations. Martin (2005) used some advanced mathematics (the Method of Characteristics) to determine a precise value of N_γ for φ' values up to 50° in increments of 10°, and offered a tabulation of values up to 60° in increments of 1°, but these were discrete values with no given numerical relationship. Salgado (2008) proposed a simple equation that "fits (Martin's) values quite well", but it is still only an approximation, and Loukidis & Salgado (2009) found that, based on numerical analyses, previous approximations were too optimistic.

Relationship of N_γ to the Angle of Friction φ'

The bearing capacity equation is used in platform design to check the "platform only" resistance to applied surface loads. In this case the equation reduces to the third term only, including a shape factor:

 © Deep Foundations Institute 2026

$$q_u = 0.5\gamma B N_\gamma s_\gamma \quad [4]$$

The value of N_γ is related to the angle of friction (or shearing resistance) of the platform material, φ', which is the standard parameter used in calculating the shear strength of frictional materials in terms of effective stress, namely under drained conditions. In everyday geotechnical usage φ' will range from about 20° for clays up to about 38° for dense sandy soils. Most geotechnical engineers will be familiar with this range of soil types, and the corresponding bearing capacity factor, N_γ, has a reasonably consistent relationship with φ', as illustrated in Fig. 2.

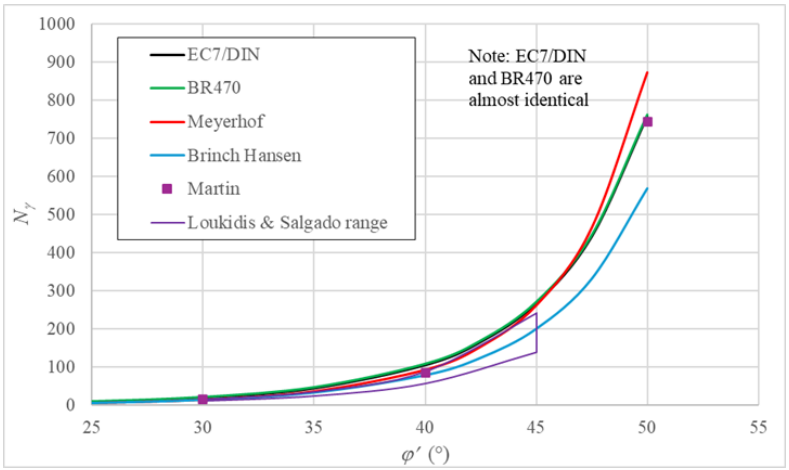


Fig. 2. Relationships between N_γ, and φ'

The problem is that, in order for working platforms over weak ground to be effective, they need to be strong, and that means that a high value of φ' is required, typically in the range of 40 to 50°. Looking again at Fig. 2, it is seen that the relationship of N_γ with φ' changes rapidly above 40° so that bearing capacity becomes more sensitive to the assumed, or measured, value. The reason for the sensitivity can be seen by comparing the slip-line fields, shown in Fig. 3, associated with the assessment of N_γ as shown in Fig. 2 for φ' values of 40°, 45° and 50°. Figure 3 also illustrates another point of which the platform designer should be aware, namely the extent of foundation soils required to generate the predicted capacities according to N_γ especially for high values of φ'. The width of the affected area more than doubles as φ' increases from 40 to 50°. This is important when considering the extent to which foundation material should have the required properties and be adequately compacted, as well as determining adequate distances between plant and the platform edge.

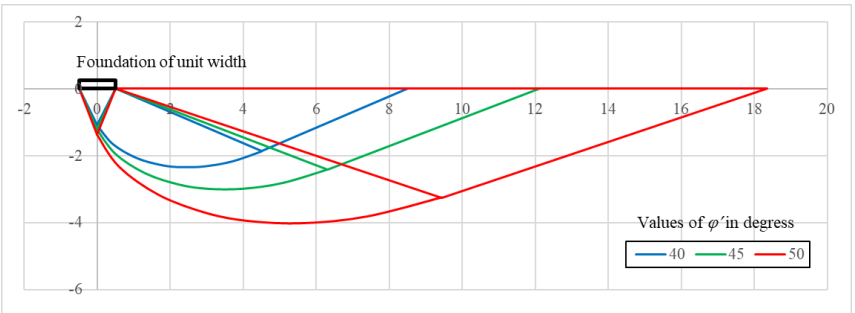


Fig. 3. Slip-line fields defined in the development of values for N_γ

Bearing Capacity for Undrained Conditions

Platform design methods also frequently require the assessment of the bearing capacity of cohesive soils under undrained conditions in which $\varphi_u = 0$, so that $N_q = 1$ *and* $N_\gamma = 0$, and the equation is simplified to:

 © Deep Foundations Institute 2026

$$q_u = s_u N_c s_c + \gamma D \quad [5]$$

It has been shown that $N_c = (2 + \pi)$ for undrained conditions and a strip foundation, and this has been found to match measured ultimate bearing capacity in practice. Shape factors (s_c) are also well defined for rectangular or circular foundations.

BEARING CAPACITY OF THE TWO-LAYER SYSTEM

When we move on to layered soils, as in a working platform over a weaker subgrade, the mathematics become even more complex, because the strength of the subgrade affects the strength of the platform. Some authors have tried to simplify the process, and sought for "an over-arching theory" (Miller, 2013), but this cannot be achieved. Where very complex mathematical equations can be reduced to something of the form $w = f(x.y.z)$, and substituting values for x, y and z gives you a value for w, we call that a "closed form solution", which can be explicitly solved. Unfortunately, sometimes the mathematics are just too complex, and there is no closed form solution. For example, we may have an integral for which there is no known answer. That is when we have to either accept a semi-empirical method, as with the bearing capacity equations, or use numerical analysis (e.g., finite element or finite difference), which makes extremely small increments to get as close as possible to the "answer", within a tolerance defined by the user. Both of these give us approximate answers, but do not provide an over-arching theory. Various approximations have been proposed for our layered soil bearing capacity problem, such as the methods of Hanna and Meyerhof (1980), T-Value (Lees, 2019), and Vrettos and Siebel (2023). While some authors have carried out numerical analyses that provide a solution for a given problem, that cannot be applied to other similar problems. Without a full understanding of these aspects, a platform designer may risk using methods that may not be applicable in certain situations, and this could lead to an overly conservative, or worse an unsafe, design. It is the authors' opinion that this risk is not identified in Guide 2 and, if used as is, increases the potential of this occurring.

The same is true of the parameter referred to as $K_p\tan\delta$, which is used in some working platform calculations. This creates the dilemma that we need these high angles of friction for economic working platform design, but the methods, and therefore the required platform thicknesses, are extremely sensitive to the values used. At the same time geotechnical engineers are likely to be unfamiliar with using and specifying values in this upper range, even to the extent that they may not be aware of the sensitivity. This includes the extent of the failure zone shown in Fig. 4. It has also been shown that, for example using the BR470 method, an increase of platform angle of friction from 45 to 50° can lead to a 30% reduction in the required platform thickness, with significant cost implications.

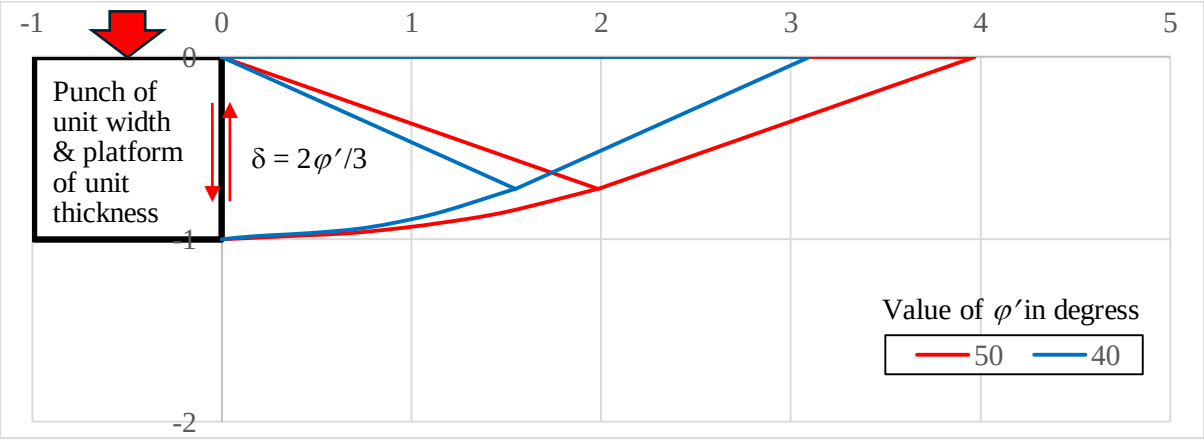


Fig. 4. Slip-line fields required to generate $K_p\tan\delta$ in punching shear methods

 © Deep Foundations Institute 2026

DESIGN METHODS

A number of methods have been developed over the years for the design of granular working platforms. They all function differently but share common components and characteristics. One of the issues, which is mentioned in Guide 2 but perhaps needs further explanation, relates to the definition of what constitutes a "Design Method". It is stated in Guide 2 that there are three essential components:

- rig track loading (input),
- the bearing capacity model, or calculation method; and
- the way in which safety is considered (factor of safety or reduction factors).
- To these could also be added:
- testing regime
- Each particular Design Method requires a prescribed combination of the necessary components.

It is important to distinguish between Design Methods, which are complete and lead to a Working Platform Design with a platform thickness, and Calculation Methods which are just one component and lead only to an estimate of ultimate bearing capacity. At the present time, in the authors' opinion there is only one complete Design Method, which is known as BR470 after the BRE Report (BRE, 2004), on which it is based. It is a semi-empirical method because the loading factors, published in the report and to be used in the method, were derived such that the method matched a set of benchmark working platform thicknesses. These were for the maximum bearing pressures and effective track lengths of seven selected rigs, on subgrades of strength ranging from the lowest the method could handle up to the highest above which a working platform was considered unnecessary. These were also for Working Platform angles of friction from 35 to 50°. This Design Method therefore has (i) the FPS Rig Track Pressure Calculation Tool V3.1 for its bearing pressure input, (ii) a calculation method using $K_p \tan\delta$ for ultimate bearing capacity, and (iii) loading factors as its approach to safety. This has since been supported by over 20 years of successful application in the UK, Australia and New Zealand. It is very important to note, with regard to what was stated earlier about understanding the process, that BR470 states clearly that "The design of working platforms for tracked plant is a geotechnical design process and should be carried out by a competent person."

There have been numerous suggestions since 2004 that BR470 is "over conservative", but the authors have come across no evidence to substantiate this. Corke and Gannon (2010) showed clearly that "conservative" platform thicknesses usually resulted from conservative estimates of subgrade or platform strength. In a specific case in Australia, subgrade parameters of φ' 32° and γ = 18kN/m^3 were proposed. The designer stated that BR470, which required a platform thickness of 970 mm for φ' = 40°, was known to be over conservative and proposed a platform of only 300 mm, which could potentially have been very dangerous. A subsequent enquiry drew the response that "970 mm was obviously conservative for medium dense sand", without noting that such a sand would not be characterized by φ' = 32° and γ = 18 kN/m^3. A rerun of BR470 with φ' = 36° and γ = 20 kN/m3 also gave a thickness of 300 mm. A published comment that "Typically the (BR470) method provides a working platform much thicker than commonly used successfully in Australian practice" has been clarified to refer to opinions expressed by main contactors, again without any supporting evidence.

While not a complete Design Method, the next method discussed is in the TWf Working Platforms: Design and construction of granular working platforms for construction plant (TWf, 2024) hereafter referred to as the TWf Guide. Its method, which uses Limit State Design principles, in accordance with Eurocode 7 (EC7, 2024), and partial factors on actions and strength based on that code. EC7 also states that "If needed, a modification of the results from the model may be used to ensure that the design calculation is either accurate or errs on the side of safety," which establishes a Model Factor. It goes on to say "If the modification of the results makes use of a model factor, it should take account of the following:

- the range of uncertainty in the results of the method of analysis;
- any systematic errors known to be associated with the method of analysis."

The authors are not aware of any work performed to establish that the method of calculation set out in the TWf Guide is either "accurate or errs on the side of safety." This would seem to require some sort of calibration, leading to a proposed model factor, which might be unity.

The BRE 470 Method and the TWf Guide Method are the only two methods listed in Appendix C of Guide 2, and it needs to be clearly understood that all the other references are to Calculation Methods. They do not generally have a bearing pressure method linked to them, nor do they have a safety approach. It is not possible to determine a safety approach without a rigorous calibration and verification procedure.

In Guide 2 a comparison has been provided, both in the guide and in the supporting reports, between up to 10 different calculation methods, based on the required platform thicknesses. This has used a standard track bearing pressure, effective length and width, together with a single value of angle of friction and weight density. Since only BR470 has a specified safety approach, the comparison has been made without any calibration or factors, which renders it meaningless.

Empirical Methods

Since there are no closed form solutions to the bearing capacity equations, all design methods are semi-empirical processes, which means that some constants in an equation have been chosen to obtain a fit to a set of data (for example the loading factors in BR470). This creates a severe limitation on the application of any such method, since it can only be used within the range of the data from which the constants were derived, and in the manner proposed and tested by the authors. Components of a semi-empirical method, such as partial factors, cannot be taken out and used in another method, as some practitioners have tried to do. Since a semi-empirical method has been calibrated, it is also not permissible to try to "improve" on the method, without going through an equivalent calibration procedure again. Miller (2013) and Miller (2020) are examples of where a modification of the BR470 method is proposed without repeating the calibration process.

Safety

BR470 established two Load Cases: Load Case 1, in which the Operator is unlikely to be able to aid recovery (such as standing, travelling and handling), and Load Case 2, in which the Operator can control the load safely, probably by reducing power such as (installing casing, drilling, extracting an auger, etc.). It then determined loading factors of 1.6 for Load Case 1 and 1.2 for Load Case 2, and how this was done will be described in the next section. It needs to also be understood that for Load Case 1 the requirement is to prevent failure in the platform and subgrade, whereas for Load Case 2 it is only to avoid failure for long enough for the plant operator to take the necessary action to prevent failure.

The TWf Guide recommends the application of partial factors in accordance with Eurocode 7, but an appropriate Model Factor has not been established, which does not meet the recommendations of EC7 as stated above. This is another example of why the TWf method cannot be considered a Design Method at this time.

CALIBRATION

BR470 Calibration

BRE produced a bearing capacity model based on the punching shear approximation as proposed by Hanna and Meyerhof (1980). Built into the Design Method are loading factors applied to the maximum predicted bearing pressures so, in order to enable the calculations to be used for working platform design, it was necessary to determine appropriate values for these factors. To assist with this requirement the FPS assembled a group experienced with the use of piling rigs and working platforms. Using the FPS rig track loading spreadsheet as input, the group considered rig operations of Standing, Travelling, Handling, Extraction and Penetrating.

 © Deep Foundations Institute 2026

In order to develop the loading factors, the FPS group calculated the rig track loading for a set of piling rigs, ranging from a mini-piling rig through medium size CFA (augercast) and rotary rigs to a large rotary piling rig. This data set, totalling over 500 scenarios for both cohesive and granular subgrades, was used by BRE to calculate required platform thicknesses using "other design methods" for subgrade strengths from 20 to 100 kPa and angles of friction from 35° to 50° for the granular working platform material. These platform thicknesses were then tabulated, reviewed and modified by the FPS team based on its collective experience, and became the benchmark of platform thicknesses that were considered safe, but still economic, and therefore should be produced by any design method. The loading factors for Case 1 and Case 2 were then adjusted over a number of cycles until it was considered that the numbers produced by BR470 matched the tabulated values, and therefore they were suitable to be used with the method. It was noted that a platform friction angle of 35° was inadequate for a number of rigs, and also noted that high friction angles have various issues as mentioned earlier. Therefore, it was decided by the FPS to limit the input angle of friction for the platform material to a maximum of 50°.

It must be understood that, while a calculation method such as the punching shear model, or the input data such as the rig bearing pressure from the FPS Spreadsheet, may of themselves be either conservative or non-conservative, any such effect is removed by the calibration process. The benchmark table of platform thicknesses was considered by the FPS panel of experts to be about right, and the loading factors were adjusted, using the ultimate bearing capacity from punching shear and the track pressures from the FPS spreadsheet, so that the required platform thicknesses were obtained, and this has been verified by the authors.

Thus, while the FPS method of calculating rig track pressures is approximate, involving several simplifications, any adverse effect of this has been removed. Therefore, it would not be acceptable, and potentially unsafe, to attempt to use track bearing pressures calculated on an alternative basis, such as the Austrian method or the EFFC/DFI simplified method referred to in Guide 2, in conjunction with the BRE design method and loading factors, or to use the FPS track bearing pressures with another design method without appropriate calibration.

Temporary Works Forum Method

TWf issued a Guide to working platforms in 2019 with an updated version published in 2024. The design method uses FPS loading for input with EC7 partial factors, but it is not known what calibration process may have been carried out to justify the calculated platform thicknesses. This is necessary because the solution to the bearing capacity equation used is approximate, and a model factor is required to account for any inaccuracies in the approximation, even if its value is unity.

RIG TRACK LOADING

Federation of Piling Specialists (FPS)

The rig track loading calculated using the FPS track loading spreadsheet was designed to be used with available information, notably the rig components and dimensions, winch/cylinder forces and suspended equipment. Wind and dynamic loading, as considered in more detailed calculations by rig manufacturers, in accordance with EN16228, are not included. Winch/cylinder forces can be adjusted to reflect requirements for a particular project for the most economic platform design. The spreadsheet calculates the variable bearing pressures along the length of a track, and then determines the Meyerhof equivalent rectangular distribution and effective track length.

It should be noted that the FPS loading is based on the rig operating on level ground, so it is important to consider the possible greater track pressures that may occur when travelling up or down a sloping ramp. BR470 warns that "*Sloping sites present particular problems for stability, which should be addressed in the design."* It is recommended that platform designers refer to manufacturers' instructions for appropriate gradients for ramps.

One aspect often overlooked is the potential risk of a rig overturning without any platform bearing capacity failure. The FPS spreadsheet calculates values for a parameter "Eccentricity Index". The spreadsheet does not provide limiting values, but Corke (2016) sets out guidance.

The disclaimer on the first page of the spreadsheet states that "the spreadsheet is intended for use only by a competent person". It has been reported that some users find the spreadsheet difficult, which has led to attempts to produce something simpler, such as the "Simplified EFFC-DFI method", the "STOPP – Machine Tipping Over", and the Austrian FSV (2002) "Platforms for Geotechnical Works RVS 08.21.02". These simplified methods have a place, such as at a preliminary stage when actual plant has not yet been selected, and provided they are adequately conservative.

The data was produced by a number of piling rig manufacturers, based on machine operating weight (including suspended equipment) on the basis of the rig working solely in extraction mode with the rig body in alignment with the rig tracks. Consequently, both tracks carry an equal load, which is the basis of the analyses in Appendix B. It has not been possible to check if the input data used by the rig manufacturers in producing this data were compatible with the FPS process. It is not possible to derive the numbers in the green columns in the tables from the numbers given in the blue columns, and thus the table cannot be verified. It is noted that various qualifications on the use of the table are provided, but it is questionable as to whether or not the advantages outweigh the risks associated with misuse.

The authors' experience over more than 15 years is that the biggest difficulty in the use of the FPS Spreadsheet is in obtaining the weight and centre of gravity of each component from the manufacturers. Guide 2 notes that piling rigs may include equipment, such as Kelly bars, drilling buckets, and augers, from other suppliers, and this is acknowledged. It has also been found that for a manufacturer to supply a consultant with the required details can be a breach of confidentiality. The simplest solution would appear to be for manufacturers to supply a catalogue with each rig, showing the weight and centre of gravity for each of their components. The manufacturers liability would then be only the accuracy of that data. It would be up to the piling contractor to identify which components they use, and to obtain similar data from any third-party suppliers. Although a certain amount of effort would be required in preparation of the catalogue, it would only be required once for each model, and this would significantly simplify the process. Since the catalogue would not indicate which components are fitted to any particular rig, it could also be issued to interested parties without breach of privacy restrictions.

Summary

With regard to rig track loading, use may be made of the UK Federation of Piling Specialists (FPS) Rig Track Pressure Calculation Tool Version 3.1. This was specifically prepared by the FPS for use with BR470, but has been adopted by the TWf Guide and may be applied to other methods subject to calibration.

The Guide 2 Appendix B track loading tables lack practical relevant data, do not represent critical design loading, are unreliable and are not considered to be appropriate for guidance or any other purpose.

TESTING

Testing, with regard to working platforms, is fraught with difficulties. It is reasonably obvious that the first requirement is to test any proposed material, but the particle size means that standard shear boxes used for Direct Shear tests cannot be used, unless the coarser particles are first removed, which calls into question the value of the test. Larger shear boxes, 300 mm square, have been used but are of limited availability. A Giant Shear Box, 1.5 m square, has also been used in the UK, but the results are

very limited. Several tests have been carried out with very large triaxial tests, 0.5 m diameter and 1 m high, which give very good results but are too expensive for routine use.

Once the material has been compacted into the platform there is an opportunity to carry out a test to confirm that the design requirements have been met, which usually means a specified angle of friction, φ'. Again, the question arises as to what test to use, because none of the available tests measure φ' directly, and rely on correlations.

The EFFC-DFI members put considerable time and effort into field trials of four in situ test methods, being Plate Load Tests (PLT), Light Weight Deflectometer (LWD) tests, and two types of dynamic cone penetrometer. One intention was to check on the simplicity of operating each test, which was reported and reviewed by the University of Stuttgart. Another intention should have been to review the correlations of the results with useful parameters but, although the correlations were published, no attempt was made to apply them, and hence to examine their variability and usefulness. It is considered that such a review would be of benefit to the piling industry, and should be included in the next edition.

Plate Load Testing

A programme of platform testing on 15 sites carried out in the UK since 2021 has shown that working platforms are more variable than it had previously been possible to quantify. The frequency of testing recommended by the TWf Guide will not be adequate to provide reliable data representing a whole site, requiring a conservative assessment of any such limited testing.

When BR470 was being developed there was considerable debate regarding the appropriate size of the plate. There was also the question of appropriate maximum test loading. The design loading (track bearing pressure multiplied by the appropriate loading factor) given by the BR470 design method was used by some as a maximum test load.

Due to the size and geometry of the loaded area of rig tracks it is not possible to carry out a single test that will prove the overall adequacy of a constructed working platform. The placed and compacted in situ platform material and the underlying subgrade need to be tested separately and independently.

If the size of the plate to be used can be minimised, the maximum possible test settlement can be achieved with the available kentledge, thus improving the reliability of the assessment of the test result. As it is commonly specified that material for working platform construction should have a maximum particle size of 75 mm, a test plate of 300 mm diameter would be advantageous. A medium size excavator that can safely provide a maximum test load of 10 tonnes is commonly used to produce the test reaction. This load equates to a maximum test pressure of approximately 1,400 kN/m^2, but even this typically results in a maximum test settlement of only a few millimetres.

Future Testing

The problem with plate load testing is that it is slow, expensive and ties up a piece of plant required to provide reaction, with typically only up to around six tests per day being achievable, which is likely why the test is not often performed. In order to address this problem, a programme of testing comparing plate load tests with Light Weight Deflectometer (LWD) testing in the UK was started in 2021 and is still under way. A LWD is a small, hand portable, device that drops a weight onto a 300 mm diameter plate (the same size as recommended for plate load testing). The output reports a surface dynamic modulus value and 60 to 80 tests can be performed in a day.

The initial objective was to see if a site specific correlation could be developed between the plate load testing and the dynamic modulus from LWD testing. A set of six plate load tests, each surrounded by four LWD tests was performed on each site in an area of 10 m x 5 m. Testing of the first few sites

shows that there was much variability, even within the test area, such that a correlation would not be achievable. Since then, testing on more sites has produced a wide range of data and a methodology is being developed that could provide a universal, rather than site specific, solution based on the use of the lower bound of the more numerous LWD dynamic modulus values. This approach is similar to the LWD requirements for road pavement sub-base testing in the UK.

TEMPORARY WORKS

This is a very wide subject, which can only be touched upon here. There seems to be a widespread belief that lower Factors of Safety apply to Temporary Works, but this surely should be restricted to situations in which the temporal variation of important parameters is taken into account. An obvious example is groundwater levels with regard to slope stability. With Temporary Works being of limited duration, the risk of an extreme event occurring during that short time is obviously reduced. However, when there are no temporal variables considered, such as when we are only concerned with the spatial variability of strength parameters, there is no logical reason for reducing the Factor of Safety, especially when there is significant risk to life, as when a piling rig topples over. Each case should be judged on its merits, as with the Load Case 1 and Load Case 2 selection.

OTHER IMPORTANT DESIGN CONSIDERATIONS

Apart from the matters dealt with above, which all relate to the components of any current or future Design Method, there are other general considerations which must be taken into account. These include, among other things, checks on global stability. This is always required as it is not checked by normal Design Methods, and is particularly relevant where working platforms are relatively small and edge effects come into play. Checking of these may lead to a requirement to cordon off certain areas as Plant Exclusion Zones.

The location of the groundwater table is extremely important for granular subgrades, and specific allowance is made for this in BR470. Where other methods are introduced, an equivalent allowance needs to be made.

Another consideration mentioned briefly under track bearing pressures is ramps. Once the revised pressures due to the inclination have been established, appropriate design needs to follow.

CONCLUSIONS

In order to understand the design of working platforms, it is first necessary to understand bearing capacity theory. The solutions to this are very complex and so require various approximations. It is therefore also necessary to have a grasp of the effect of these approximations, and how they can be minimised by calibration.

The high friction angle materials that are the first choice for working platforms because they lead to reduced thicknesses are very sensitive to the actual friction angle selected, which has a major effect on the definition of the failure surface. Their performance, testing and specification need to be well understood, and sensitivity analyses need to be carried out.

All working platform Design Methods each have a set of prescribed components which cannot be changed by the user.

Because they are based on approximate solutions, all Design Methods need to be calibrated against an accepted benchmark. The only ones currently available were prepared by the FPS in 2004, and subsequent revisions in 2009.

There are various options for the estimation of tracked rig bearing pressure, but one needs to be selected and built into the calibration of any Design Method.

 © Deep Foundations Institute 2026

Work is needed on testing to establish methods suitable for the high friction angle material required, both prior to use and when compacted into a platform.

Significant revisions to Guide 2 are required, and work should start on Guide 3 without delay.

ACKNOWLEDGEMENTS

The contribution of Scott Jacobs of Keller North America in reviewing the manuscript and providing invaluable comments is gratefully acknowledged.

NOTATION

B	Breadth of footing (track)
c'	Apparent cohesion
D	Depth of footing
q	Applied bearing pressure
q_u	Ultimate bearing pressure
q_0	Surcharge pressure
s_u	Undrained shear strength
γ	Weight density
φ'	Effective angle of friction
N_c	Bearing capacity factor on cohesion
N_q	Bearing capacity factor on depth of embedment
N_γ	Bearing capacity factor on breadth
s_c	Shape factor on cohesion
s_q	Shape factor on depth of embedment
s_γ	Shape factor on breadth
i_c	Inclination factor on cohesion
i_q	Inclination factor on depth of embedment
i_γ	Inclination factor on breadth

REFERENCES

Brinch Hansen, J. (1970) *A revised and extended formula for bearing capacity*. Danish Geotechnical Institute, Bulletin No 28, Lyngby

Corke D.J. (2016). A review of stability factor and eccentricity index for piling rigs. *Ground Engineering* December pp 23-25.

Corke, D.J. and Gannon, J. (2020). Economic design of working platforms. *Ground Engineering*, February 29-31.

Deutschen Bauindustrie e.V. (2019) STOPP - Machine turning over

EC7 (2024) *Eurocode 7: Geotechnical Design - Part 1: General rules*. BS EN 1997-1:2024

Eurocode EN 16228-4,-5:2014. *Drilling and foundation equipment — Safety, Part 4: Foundation equipment, Part 5: Diaphragm walling equipment*.

Federation of Piling Specialists. FPS Rig Track Pressure Calculation Tool V3.1 and Guidelines. fps.org.uk

FSV (2018) Platforms for Geotechnical Works. *Austrian Research Association for Roads, Railways and Transport (FSV)*; RVS 08.21.02 Edition 1, Wien.

Hanna, A.M. and Meyerhof, G.G. (1980) Design charts for ultimate bearing capacity of foundations on sand overlying soft clay. *Canadian Geotechnical Journal*, **17**, 2, 300-303

Lees, A (2019) The bearing capacity of a granular layer on clay. *Proc ICE Geotechnical Engineering*, **173**, 1, 13-20

Loukidis, D and Salgado, R (2009) Bearing capacity of strip and circular footings in sand using finite elements. *Computers and Geotechnics*, **36**, 871-879

 © Deep Foundations Institute 2026

Martin, C.M. (2005) Exact bearing capacity calculations using the method of characteristics. *In Barla, G., Barla, M. editors. Proc 11th IACMAG,* Turin, **4**, 441-450
Meyerhof, G.G. (1963) Some recent research on bearing capacity of foundations. *Canadian Geotechnical Journal*, **1**, 1, 16-26
Miller, K. (2013) *Technical note on use of BR470 in soft clay*. FPS
Miller, K. (2020) A review of Working Platform Design. *Proc Piling 2020 Conference*, ICE, London
Salgado, R (2008) *The engineering of foundations*. McGraw-Hill
Terzaghi, K (1943) *Theoretical soil mechanics*. New York, Wiley
Temporary Works Forum 2024. WORKING PLATFORMS: Design of granular working platforms for construction plant - A guide to good practice.
Vesic, A.S. (1973) Analysis of ultimate loads of shallow foundations. *Journal of the Soil Mech Div ASCE,* **99**, SM1, 45-73
Vrettos, h,C, and Seibel, E (2023) Punching shear of footings on a sand layer over clay: Calculation methods and findings from numerical parameter studies. *Geotechnik*, **46**

 © Deep Foundations Institute 2026

SHEET PILE SEAL: A LOCALLY ENGINEERED SHEET PILE SEALANT SOLUTION

Davide Cantali, Sheet Pile Solutions

INTRODUCTION AND BACKGROUND

In civil and marine construction, the inherent impermeability of steel sheet piles is often compromised by their interlocking joints, which can serve as pathways for water and soil migration. Uncontrolled seepage through these interlocks can lead to significant project risks, including the undermining of excavation dewatering, soil piping, and environmental contamination. Historically, the industry has relied on expensive secondary measures like grout curtains or deeper embedment to manage these risks.

SHEET PILE SEAL was developed as an Australian-engineered response to these challenges, providing a performance-driven, locally manufactured system designed to achieve consistent water and soil tightness under diverse geotechnical conditions. Current design frameworks, including European standards and guidelines, now recognise interlock permeability as a governing design parameter. As such, understanding sheet pile interlock permeability and improving interlock sealing performance has become central to advancing sheet pile wall reliability.

OBJECTIVES

The primary objective of this work is to validate the effectiveness of an engineered and tailored interlock sealing system. By moving away from "one-size-fits-all" generic sealants, the research demonstrates how site-specific formulations—based on groundwater pressure, geotechnical data, and pile geometry—can deliver enhanced wall integrity and long-term durability.

METHODOLOGY

The performance of the system was evaluated through a dual approach involving controlled laboratory testing and multi-site field trials:

- **Laboratory Testing:** Steel specimens (1.5 m interlock segments) were subjected to stepped hydrostatic pressure (50 kPa to 200 kPa). Leakage rates were measured and compared against unsealed baselines and traditional bitumen fillers.
- **Field Trials: Wisemans Ferry Cofferdam:** Piles were driven using vibratory methods into a marine environment to test the sealant's resilience against driving forces and tidal head differentials.
    - **The Entrance Cut-off Wall:** A sealed "test box" was constructed within a basement to verify permeability targets against unsealed configurations over a seven-day period.

KEY RESULTS

The study confirmed that the SHEET PILE SEAL system offers a significant "step change" in sealing performance:

- **Seepage Reduction:** In laboratory settings, the Bitumen-Polymer variant recorded **zero measurable flow at 100 kPa**, whereas unsealed interlocks failed rapidly, passing >1.2 L/min·m even at 50 kPa.
- **Field Reliability:** In the Wisemans Ferry trial, the sealed sections remained dry under a 2.0 m head, reducing leakage from 20 L/min·m (unsealed) to **less than 0.1 L/min·m**.
- **Constructability:** Field observations proved the sealant remains intact and relatively continuous following impact or vibratory driving, with a high softening point (~72°C) preventing "wash-out" or flow in hot climates.

 © Deep Foundations Institute 2026

Sealing Method	Max. Effective Pressure	Typical Leakage (r)
Unsealed	Negligible	> 10^{-7} m/s (Very High)
Traditional Bitumen	~100 kPa	~ 10^{-8} m/s (Moderate)
SHEET PILE SEAL (Bitumen-Polymer)	~150 kPa	~ 10^{-9} m/s (Very Low)
SHEET PILE SEAL (Hydrophilic)	~300 kPa	~ 10^{-10} m/s (Near Zero)

CONCLUSIONS

The SHEET PILE SEAL system provides a reliable, locally manufactured solution for high-performance water and soil retention. Its ability to be cold-applied in the field or yard without pre-heating simplifies logistics while meeting stringent environmental standards, including certification for contact with potable water. By eliminating the uncertainty of interlock leakage, this engineered approach expands the versatility of steel sheet piling for critical infrastructure, mining, and flood protection projects.

 © Deep Foundations Institute 2026

CIRCULAR ANCHOR PULLOUT CAPACITY IN SAND OVERLAIN BY CLAY: EXPERIMENTAL AND NUMERICAL INSIGHTS

S. Goodall, Douglas Partners Pty Ltd, Warabrook, NSW, Australia, Sean.Goodall@douglaspartners.com.au
C. Lloyd, Douglas Partners Pty Ltd, Warabrook, NSW, Australia, Chris.Lloyd@douglaspartners.com.au
J. Murphy, Douglas Partners Pty Ltd, Warabrook, NSW, Australia, Jonah.Murphy@douglaspartners.com.au
O. Buzzi, The University of Newcastle, Callaghan, NSW, Australia, Olivier.Buzzi@newcastle.edu.au
R. Merifield, Douglas Partners Pty Ltd, Warabrook, NSW, Australia, Richard.Merifield@douglaspartners.com.au

ABSTRACT

Circular anchors, such as helical anchors, are widely used in geotechnical engineering owing to their ease of installation and ability to resist both tensile and compressive forces. However, their pullout performance in layered soils remains an area of ongoing research. This study investigates the pullout capacity of circular anchors embedded in sand overlain by soft clay. An experimental and numerical study has been conducted with an aim to assess the effects of anchor embedment depth and soil shear strength. Whilst the current study is ongoing, the results provide insights into the influence of soil layering on anchor behaviour, with variations in failure mechanisms observed depending on the relative embedment and strength of the clay and sand layers. This study contributes to the understanding of circular anchor performance and offers some practical insights for engineers working with layered geotechnical conditions.

Keywords: circular anchors, layered soils, experimental, numerical

INTRODUCTION AND BACKGROUND

Circular screw anchors, such as helical steel screw piles, are increasingly used in both temporary and permanent geotechnical works due to their rapid installation and minimal environmental disturbance. However, their performance in layered soil profiles remains a topic of ongoing investigation, particularly in cases where a soft clay layer overlies stronger materials such as dense sand. In these conditions, uplift capacity is often governed by complex interactions between the anchor and the surrounding soil strata, posing challenges for both design and construction.

Douglas Partners Pty Ltd, in collaboration with The University of Newcastle, Australia, is conducting a study on the uplift performance of circular anchors embedded in sand overlain by weak clay. The research combines numerical and analytical modelling with a program of controlled scale model experiments. Future stages will focus on developing preliminary design charts, formulating an analytical model, and undertaking field-scale testing, enabling the preliminary findings presented in this paper to be revisited and further refined.

The motivation for this work arises from practical geotechnical challenges encountered on Kooragang Island, located at the mouth of the Hunter River in Newcastle, New South Wales. This reclaimed industrial island, approximately 10 km long and 3 km wide, was created through extensive dredging and sand infilling operations commencing in the late 1950s. Today, Kooragang Island is a strategically significant precinct, supporting coal stockpiling and export, ammonium nitrate and fertiliser production, and waste storage linked to the region's steelmaking history.

The subsurface profile across much of the island typically comprises about 2 m of dredged sand overlying a 2 m to 3 m thick layer of normally to slightly over-consolidated soft to firm clay. Beneath this lies a medium dense to dense sand stratum extending to depths of 10 m to 20 m, underlain by stiff to very stiff clay, with bedrock often deeper than 40 m to 50 m. This sequence poses notable design and construction challenges, particularly where uplift resistance is a governing factor.

 © Deep Foundations Institute 2026

Historically, structures such as lattice towers and other industrial facilities have been supported on driven timber piles or small-diameter grout-injection piles terminating in medium-dense to dense sand. The use of helical screw anchors has generally been discounted due to concerns over bearing capacity and pullout resistance in the dredged sand, particularly the risk of punching failure into the underlying soft clay and insufficient embedment to mobilise adequate uplift resistance. Additional constraints include refusal of screw piles within the upper about 1 m of the deeper medium-dense to dense sand layer, often requiring pre-boring, which can reduce both the economic viability and performance of the foundation system. While anchors founded in this deeper sand may meet compressive loading requirements, uncertainty frequently remains around their uplift performance due to the influence of the overlying soft to firm clay.

Previous studies (Shiau et al., 2003; Salimi Eshkavari et al., 2019a; Goodall and Merifield, 2023) have demonstrated the detrimental effects of weak layers on the bearing capacity of shallow foundations. However, to the authors' knowledge, very few studies have focused on the specific case of a circular anchor embedded in sand beneath weak clay. One recent study (Cheng et al., 2024) on plate anchors suggests that the presence of a weak clay layer overlying sand can have detrimental effects on the pullout capacity, similar to those observed for shallow footing systems.

In the absence of full-scale testing or advanced numerical modelling, current design practice offers limited guidance, leaving engineers without a reliable, cost-effective design methodology for such conditions. This study seeks to address this gap by integrating experimental model testing with advanced finite element modelling, ultimately aiming to inform practical design approaches for circular anchors founded in sand overlain by weak clay.

PROBLEM DEFINITION

The uplift capacity of anchors is commonly expressed in terms of a breakout factor, which is a function of the anchor geometry, embedment depth, overburden pressure, and the shear strength of the surrounding soil (Merifield et al., 2001). For numerical modelling and analysis, the ultimate uplift capacity q_u is often expressed in a form analogous to Terzaghi's bearing capacity equation for shallow footings:

$$q_u = \frac{Q_u}{A} = \gamma H N_\gamma \quad [1]$$

Where N_γ is referred to as the breakout factor, γ is the unit weight of the soil, and A is the effective anchor area. In the authors' experience, Equation (1) is frequently used to back-calculate breakout factors from observed or computed ultimate anchor loads, whether obtained through physical model testing, analytical models or numerical simulations.

In uniform, homogeneous soils, the failure mechanism of anchors under uplift is typically classified as either shallow or deep, depending on the embedment depth and resultant failure surface geometry. Several researchers have proposed the existence of a transitional regime between shallow and deep failure modes. For instance, Andreadis et al. (1981) and Ghaly and Hanna (1994) observed that failure mechanisms for circular anchors may evolve gradually with increasing embedment depth. In contrast, other authors (e.g., Baker and Kondner, 1965; Meyerhof and Adams, 1968; Murray and Geddes, 1987; Dickin, 1988; Sakai and Tanaka, 1998) have proposed a more abrupt shift in behavior, suggesting a critical depth that marks an instantaneous transition from shallow to deep failure.

More recent studies investigating shallow footings on layered soils, such as sand over clay (Salimi Eshkavari et al., 2019a and Goodall and Merifield, 2023) and sand over sand (Salimi Eshkavari et al., 2019b), indicate that transitional failure mechanisms are plausible for shallow footing in layered conditions. These findings indicate the potential for complex and non-binary failure behaviors in stratified soils.

 © Deep Foundations Institute 2026

In the context of circular anchors embedded in a layered profile, such as soft clay overlying sand, the following conceptual classifications are proposed:

- Shallow failure occurs when the failure surface propagates fully to the ground surface, typically associated with lower embedment ratios (low *H/D*);
- Deep failure occurs when shear zones are confined around the anchor and do not reach the surface, typically observed at higher *H/D* ratios (beyond some threshold value, κ *H/D*); or
- Transitional failure refers to mechanisms where the failure surface partially extends toward the surface but does not fully emerge, representing an intermediate state between shallow and deep modes.

These distinctions are important for both understanding failure mechanisms and developing appropriate analytical models for anchors in layered soil profiles. A schematic of the general problem definition is provided in Fig. 1.

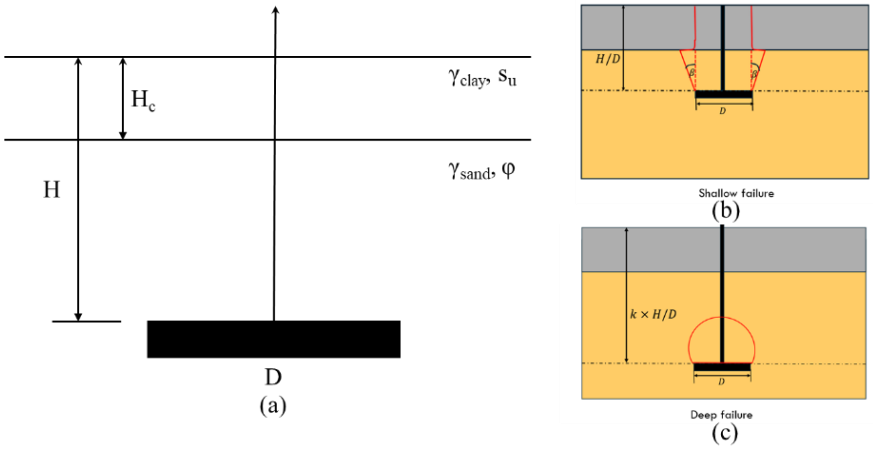


Fig. 1. (a) Problem definition, (b) Shallow failure, (c) Deep failure

NUMERICAL STUDY OF ANCHORS

Finite element limit analysis (FELA) was conducted using OptumG2 (Optum CE) to evaluate the lower and upper bound limit loads for circular anchors.

The lower bound solution is obtained by generating a statically admissible stress field in which stress discontinuities may occur between elements. By enforcing stress boundary conditions, equilibrium, and the yield criterion, the collapse load is maximised subject to constraints on allowable stresses. In accordance with the lower-bound theorem, any admissible stress field that satisfies equilibrium without violating the yield surface provides a safe estimate, and the highest such value represents the optimal lower bound. The upper bound solution is derived from a kinematically admissible velocity field that satisfies compatibility, the imposed velocity boundary conditions, and the flow rule. The internal rate of energy dissipation, arising from plastic yielding and velocity discontinuities, is equated to the external work rate, thereby establishing a strict upper bound on the true collapse load. The overall aim is to minimise the difference between the lower and upper bounds.

Adaptive meshing was employed in all analyses, with representative upper bound meshes for two H/D cases shown in Fig. 2. These meshes broadly mirror the failure mechanisms, as the adaptivity algorithm refines elements in regions of high plastic shear dissipation. This approach provides an effective balance between computational efficiency and accuracy, where mesh adaptivity based on plastic shear dissipation is generally found to be the most robust and efficient strategy for limit analysis.

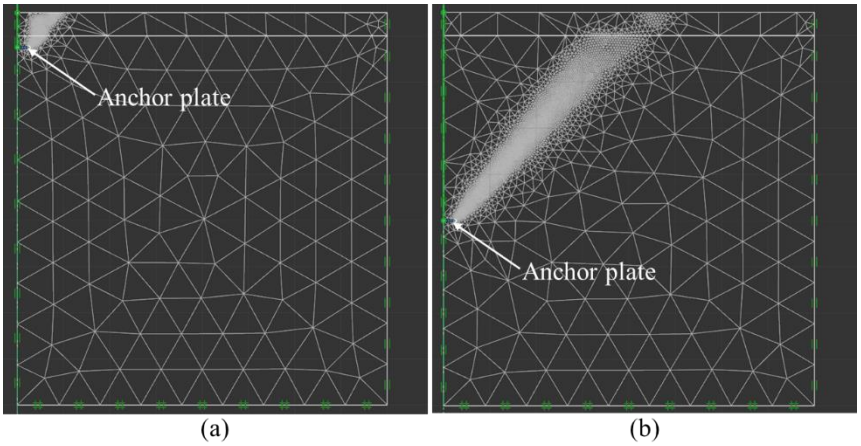


Fig. 2. Typical upper bound mesh: (a) Anchor H/D = 1.5, (b) Anchor H/D = 9

The stratified soil profile was modelled using the Mohr–Coulomb failure criterion for the sand layer and the Tresca model for the clay. An associated flow rule was adopted throughout. This assumption is considered reasonable for this class of problem, which involves a semi-infinite domain and a freely deforming ground surface, conditions under which non-associativity tends to have limited influence. The anchor was modelled as a weightless, rigid, and rough plate element. A zero-tension condition was applied to the plate interfaces, meaning the anchor could break away from the soil beneath it. The shaft of the anchor was not modelled. Given the axial symmetry of the problem, an axisymmetric formulation was adopted, modelling half the anchor width, and installation effects were not considered.

The ultimate bearing capacity was taken as the average of the lower and upper bound solutions. The relative error in the computed solutions was evaluated and was generally found to be less than about 5%.

EXPERIMENTAL STUDY OF ANCHORS

Two types of custom-built chambers were employed in the experimental study. The first was a cylindrical chamber comprising a vertically oriented PVC pipe with an internal diameter of 250 mm and an overall height of 460 mm. A square plastic base plate (300 mm × 300 mm × 20 mm) was sealed to the bottom of the pipe using silicone, with corner holes to allow for alignment and fixation. The second apparatus was a rectangular soil chamber with internal dimensions of 276 mm (W) × 600 mm (L) × 600 mm (H). The front face of the chamber was constructed from 12 mm thick Perspex to allow visualization of the failure mechanism in the sand during testing, while the remaining walls were made from 12 mm thick PVC. A 20 mm gravel drainage layer was installed at the base, incorporating a valve and hose outlet to enable controlled specimen saturation and to minimize air entrapment. An illustration of the two test chambers is provided in Fig. 3.

For the cylindrical chamber, model anchors were fabricated from 5 mm thick stainless steel, machined to diameters of 30 mm and 45 mm. In contrast, testing in the rectangular chamber employed a single anchor with a 25 mm semi-circular cross-section, aided by a purpose-built anchor guide to prevent eccentric loading and anchor rotation. In all tests, the anchor was installed horizontally and pulled vertically, with varying embedment depths considered.

The soil profile in both chambers consisted of a lower sand layer overlain by a consolidated clay layer. In the rectangular chamber, thin slices of dry kaolin clay were positioned along the Perspex face at 10 mm vertical intervals to aid in visualizing the failure surface, as shown in Fig. 4. Anchor installation was not simulated in any of the tests. Instead, each chamber was partially filled with sand until the model anchor target embedment depth was reached. The anchor was then placed and secured, after which the sand was gradually backfilled in 10 mm increments.

Anchor pullout testing was conducted using a LoadTrac II triaxial machine, which enabled precise control of the pullout rate and continuous measurement of axial force and displacement. The same device was also used to apply vertical stress during clay consolidation. During anchor pullout, sand deformation via the horizontal clay markers was recorded using a camera for image analysis of failure modes. Load-displacement data were recorded continuously to determine ultimate pullout capacity for each test.

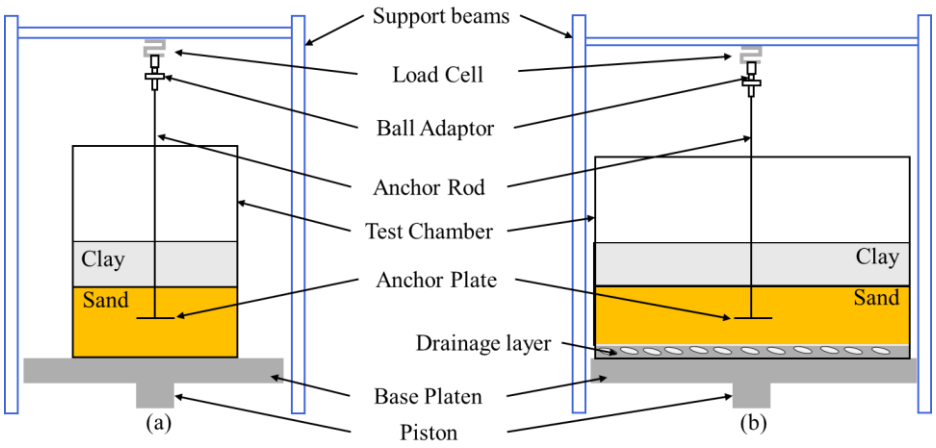


Fig. 3. Experimental apparatus (a) cylindrical test chamber, (b) rectangular test chamber

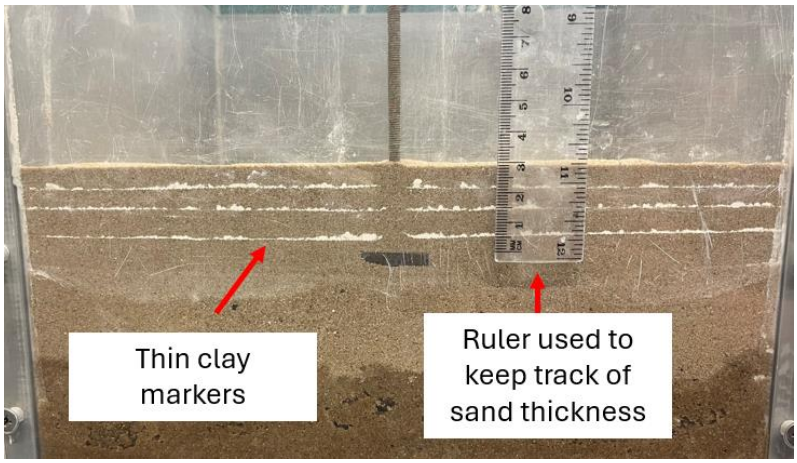


Fig. 4. Rectangular test chamber showing thin clay marker

SOIL PROPERTIES

In all tests, Stockton Beach Sand was used and deposited using a modified pluviation technique. The sand had a relative density of approximately 10%, a void ratio of 0.66, a specific gravity of 2.65, and a unit weight of approximately 19.2 kN/m³ to 19.5 kN/m³. Based on the Unified Soil Classification System, the material was classified as a poorly graded silty sand (SP). An effective friction angle of 30° was adopted, consistent with the findings of Ajalloeian (1996), who conducted extensive laboratory characterisation of this sand.

The clay layers used in the testing comprised commercially available fire clay and kaolin clay. The undrained shear strength was controlled by varying the vertical consolidation pressure, applied through a perforated plate. Following anchor pullout, shear vane testing was conducted to estimate the average undrained shear strength for each test. Measured strengths ranged from approximately 2.3 kPa to 12.4 kPa. The bulk unit weight of the clay was estimated after each test to be about 12.3 kN/m³ to 16.4 kN/m³.

 © Deep Foundations Institute 2026

RESULTS AND DISCUSSION

Benchmarking and Comparisons with Published Data

To the authors' knowledge, no previous studies have specifically investigated the behavior of circular anchors embedded in sand overlain by weak clay. As such, there is a lack of published data for direct comparison with the present study in the context of layered soil conditions. Nevertheless, several studies provide useful benchmarks for evaluating the current numerical and experimental results. For instance, circular anchors in uniform clay have been investigated by Das et al. (1994), Yu (2000), Merifield (2003) and White et al. (2008); circular and plate anchors in uniform sand by Das and Seeley (1975), Rowe (1978), Ghaly and Hanna (1994), Merifield (2002) and Merifield and Sloan (2006); and plate anchors in sand overlain by clay by Cheng et al. (2024). The results of the benchmarking have been presented in terms of the breakout factor N_{c0} for uniform clays as defined by Merifield (2003) and N_γ for uniform sands and clay over sand as given by Equation 1. Results from the current study, compared with some of the above-mentioned published data, are shown in Fig. 5.

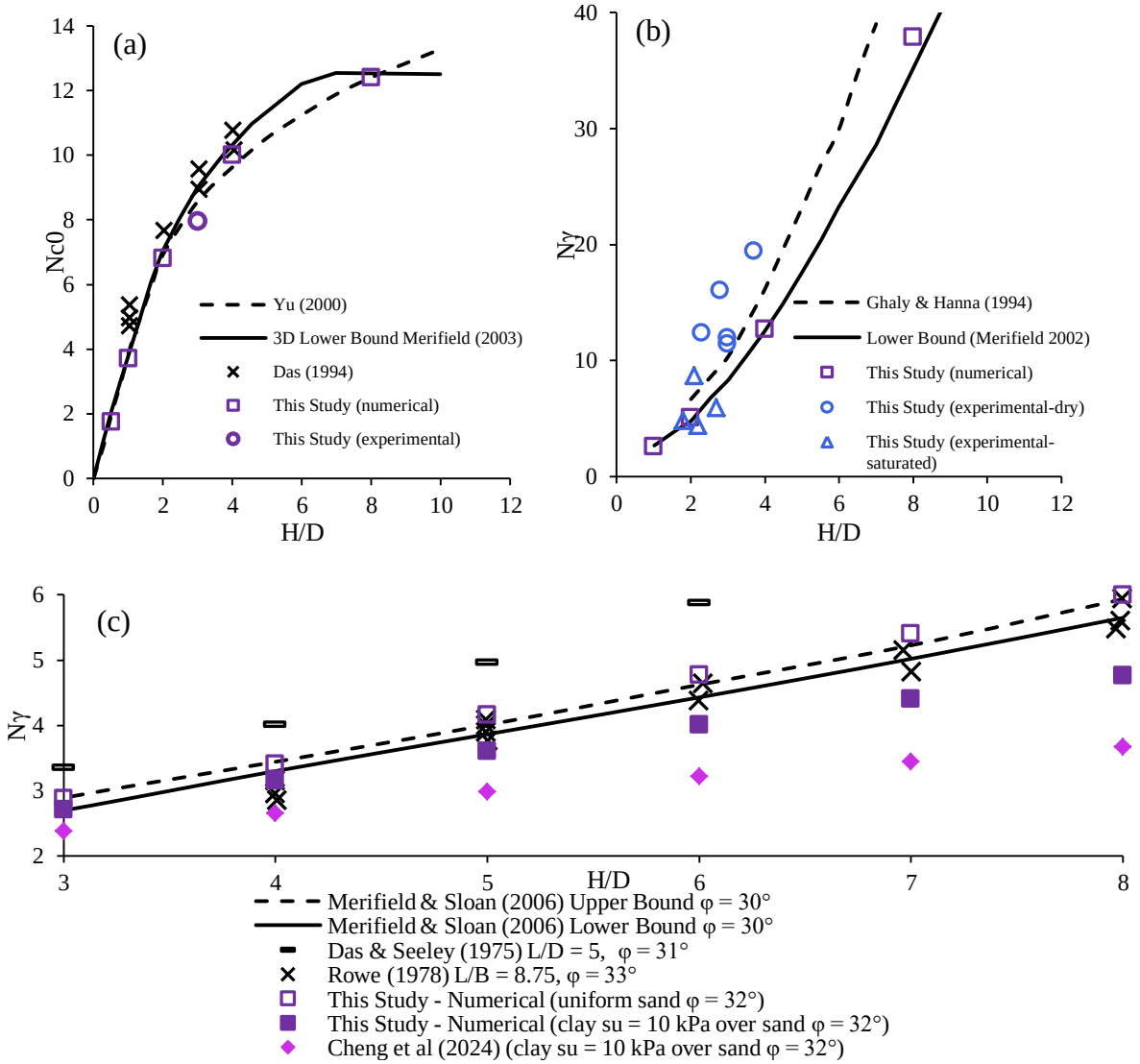


Fig. 5. Comparisons with published data: (a) Circular anchor in uniform clay, (b) circular anchor in uniform sand φ = 30°, (c) plate anchor in uniform sand and sand overlain by clay

Results from the present study show reasonable agreement with the majority of published data. However, when compared with the recent work of Cheng et al. (2024), the breakout factors predicted by the current limit analysis are generally higher. This difference can be attributed, in part,

to the distinct methodologies employed. Specifically, the limit analysis framework used herein provides rigorous upper and lower bounds on the ultimate pullout capacity. In contrast, Cheng et al. (2024) adopted a displacement-based finite element approach, defining the ultimate pullout load at the point where the anchor displacement reached 0.3 times its width. In the authors' opinion, reliance on displacement-based finite element analysis for this application may lead to the phenomenon known as "numerical locking." This occurs when the load displacement response remains artificially stiff due to limitations in the constitutive formulation or mesh refinement, resulting in a continually increasing load displacement curve without a clear peak, hence making it difficult to define the maximum pullout capacity of an anchor. Furthermore, if peak resistance occurs at displacements less than the criterion (i.e., a peak followed by a residual constant), by virtue of the criterion, the ultimate pullout capacity may be underestimated. This highlights the importance of both the failure criterion and constitutive assumptions when interpreting results from displacement-based analyses.

Numerical and Experimental Comparisons

The variables considered in the model anchor tests and numerical analysis are summarized in Table 1, with a comparison of the experimental results and FELA predictions shown in Fig. 6.

Table 1. Summary of test variables for experimental and numerical tests

Test Number	H/D -	H_c/H -	s_u (kPa	φ' (deg)	γ_{sand} (kN/m^3)	γ_{clay} (kN/m^3)
1	1.2	0.67	6.6	30	19.5	16.4
2	2.2	0.38	2.5	30	19.5	16.4
3	2.2	0.44	5.2	30	19.5	16.4
4	3.1	0.32	3.9	30	19.5	16.4
5	4.1	0.22	4.5	30	19.5	16.4
6	5.0	0.18	3.6	30	19.5	16.4
7	1.4	0.64	10.3	30	19.5	16.4
8	2.3	0.39	12.4	30	19.5	16.4
9	3.1	0.32	11.0	30	19.5	16.4
10	3.2	0.47	9.8	30	19.2	12.3
11	2.5	0.54	9.8	30	19.2	12.3
12	3.2	0.53	9.8	30	19.2	12.3
13	3	0.46	9.8	30	19.2	12.3

Although some scatter is evident between the measured and numerically estimated pullout capacities, the FELA results are generally within ±25% of the experimental values. This level of agreement aligns with previous comparisons between numerical or analytical predictions and physical model tests. For example, White et al. (2008) compared uplift resistance data from 115 model tests on buried anchors and pipelines in sand against a limit-equilibrium-based predictive method. Across a relative embedment ratio range of approximately 1 to 8, predicted-to-measured capacity ratios varied from 0.6 to 1.8, most being within ±30%. Likewise, Salimi Eshkavari et al. (2019a) applied FELA to estimate the ultimate bearing capacity of strip footings on sand overlying clay, benchmarking against experimental data from Okamura et al. (1996) and Das and Dallo (1984), as well as a limit equilibrium approach after Okamura et al. (1998). Despite some variability, their FELA predictions typically fell within ±20% of the experimental and limit equilibrium results.

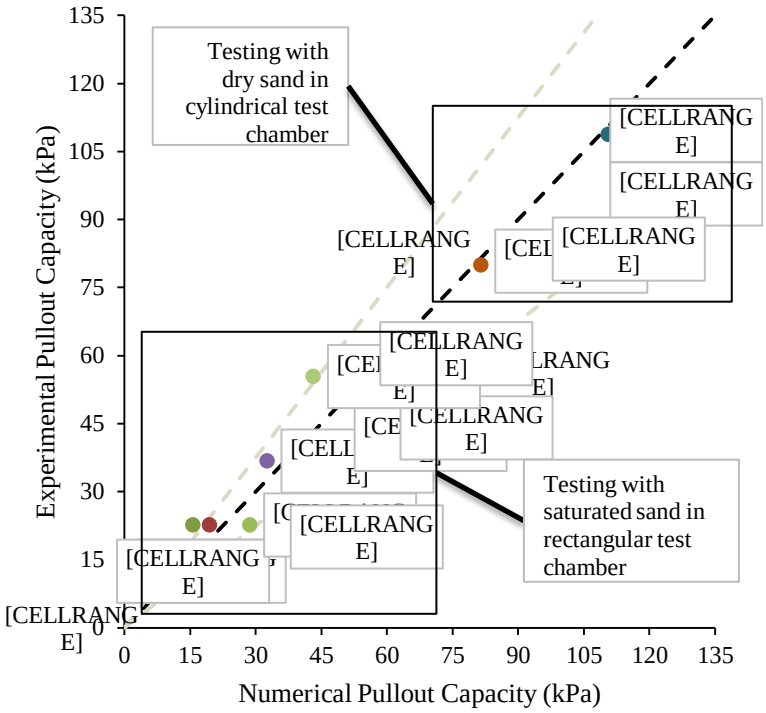


Fig. 6. Comparisons of experimental and numerical results

During anchor pullout testing in the rectangular chamber, sand deformation was recorded using high-resolution video to facilitate image-based analysis of failure mechanisms. The failure angle, β (refer to Fig. 1), was determined from the footage for each test at the point corresponding to the peak resistance force. While β is being used in the development of an analytical model by the authors, the recorded imagery also provides valuable qualitative insight into the failure mechanisms, allowing a comparison with the numerically simulated modes from the FELA, as shown in Fig. 7. Importantly, the observed experimental failure mechanisms were found to compare favorably with those predicted by the FELA simulations. The general form, extent, and transition of failure modes between shallow and deep behavior generally aligned well between both approaches.

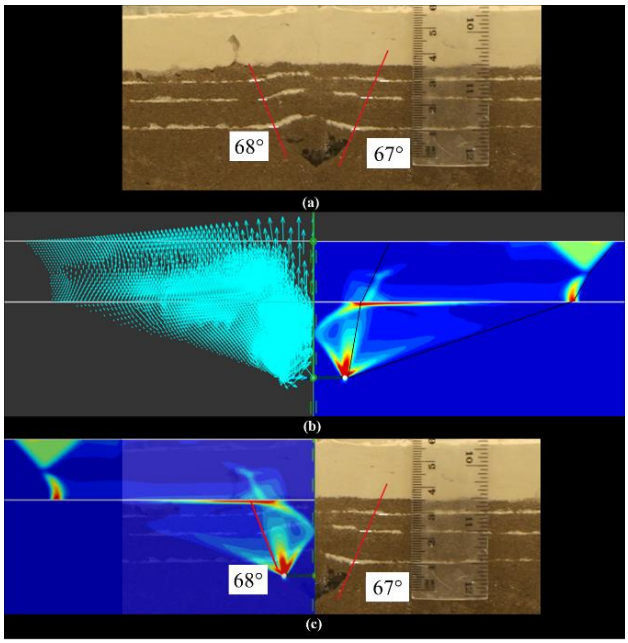


Fig. 7. Test 3 – (a) Observed failure in model test, (b) FELA velocities and shear dissipation contours, (c) FELA shear dissipation contours and observed failure in model test

 © Deep Foundations Institute 2026

The experimental observations indicated for low embedment ratios, where shallow failure was predominant, a distinct and consistent failure angle was clearly discernible. In contrast, for transitional and deep failure cases, the deformation was more diffuse, and no constant failure angle could be identified. Notably, in deep anchor scenarios, the failure mechanism was not observed to extend to the ground surface, consistent with the development of a subsurface failure envelope.

Preliminary Insights Into the Effect of the Weak Layer

The FELA has been extended beyond the initial comparisons with experimental results to consider a broader range of material parameters and anchor geometries for parametric analysis. This has included analyzing problems with undrained shear strengths ranging from 5 kPa to 25 kPa, sand friction angles between 30° and 45°, and embedment ratios of up to 9.

The analyses completed to date indicate that the presence of a weak clay layer overlying sand has the potential to adversely affect the magnitude of the ultimate pullout capacity of anchors significantly. The numerical results suggest that this effect is most pronounced for higher sand friction angles, generally in the range of 35° to 45°, where the overlying clay exhibits comparatively low undrained shear strengths (typically less than about 10 kPa). Under these conditions, reductions in ultimate pullout capacity of approximately 10% to 30% have been observed for layered soil profiles relative to equivalent anchors embedded in uniform sand, even for relatively large embedment ratios of up to around 5. This response is broadly consistent with a punching-type failure mechanism and is similar to behaviors reported for shallow foundations on layered soil profiles (Shiau et al., 2003; Salimi Eshkavari et al., 2019a; Goodall and Merifield, 2023). For lower sand friction angles, typically in the range of 30° to 32°, the influence of the overlying clay appears to be comparatively minor for the range of parameters examined to date, even for comparatively small anchor embedment. In these cases, the ultimate anchor capacity is largely governed by the shear strength of the sand layer.

In certain scenarios, the ultimate pullout capacity of anchors in layered clay over sand profiles is observed to exceed that of the corresponding uniform sand case, in some instances by up to a factor of approximately two. This behavior is generally confined to cases within the mid to upper bound range of undrained shear strengths considered in the study. The effect is evident across loose to dense sand conditions but is more pronounced for loose sands. The influence of the overlying clay layer on ultimate pullout capacity is also embedment dependent and tends to diminish with increasing anchor embedment via a power-law type decay, characterized by a relatively rapid reduction in effect at shallow embedment, followed by a progressively more gradual attenuation with depth.

While further investigation is ongoing, the analysis suggests that this behavior tends to occur where the undrained shear strength of the near-surface clay exceeds the shear strength that would otherwise be mobilized in the sand close to the ground surface in the uniform profile. This outcome is likely to be attributed to the low effective stresses present in shallow sand, which limit the mobilization of sand shear strength in the uniform case. In addition, the presence of the clay layer tends to promote a more extensive failure mechanism, characterized by a failure surface that extends further laterally than that observed in the uniform sand case. This increases the extent of the mobilized shear failure envelope and, consequently, the overall mobilized resistance. An alternative explanation is that the analyses may be overpredicting limit loads in some cases due to confinement or boundary effects. These potential influences are currently being examined and will be addressed in subsequent stages of the study.

CONCLUSIONS AND FUTURE WORK

This study combined FELA and scale model testing to investigate the uplift performance of circular anchors in sand overlain by weak clay. While the study is ongoing, the current body of work provides new insight into stratified profiles where a weak layer overlies stronger material, a scenario

with limited published data. FELA predictions were generally within ±25% of experimental capacities, consistent with other benchmark studies, and image analysis confirms close agreement between observed and simulated failure mechanisms.

Numerical studies, whilst ongoing, have indicated that there are situations where the overlying weak clay layer can have a detrimental effect on the ultimate bearing capacity, which is consistent with observations in other studies.

Future work will focus on developing an analytical model for anchor pullout capacity in sand overlain by weak clay, supported by further numerical studies examining the influence of key parameters such as sand and clay shear strength, anchor geometry, embedment ratio, boundary effects and numerical formulation. Additional investigations will also consider loading rate effects, installation influences, and cyclic behavior. Field-scale testing is planned to validate both the laboratory and numerical findings, with the ultimate aim of establishing a practical and reliable design methodology for circular anchors in layered soils.

ACKNOWLEDGEMENTS

The authors acknowledge the support of Douglas Partners Pty Ltd and The University of Newcastle, Australia.

REFERENCES

Ajalloeian, R. 1996. An experimental study of finite pressuremeter length effects in sand. PhD thesis. University of Newcastle, Australia.

Andreadis, R., Harvey, R.C. and Burley, E. 1981. Embedded anchor response to uplift loading. Journal of Geotechnical and Geoenvironmental Engineering, ASCE, 107(1), 59–78.

Baker, W.H. and Konder, R.L. 1965. Pullout load capacity of a circular earth anchor buried in sand. Highway Research Record, 108, 1–10.

Cheng, L., Wang, Q., Han, Y. and Wu, Y. 2024. Pullout behavior of strip plate anchors in clay overlying sand. Ocean Engineering, 306, 1–13.

Das, B.M., and Dallo, K.F. 1984. Bearing capacity of shallow foundations on a strong sand layer underlain by soft clay. Civil Engineering for Practicing and Design Engineers, 3, 417–438.

Das, B.M. and Seeley, G.R. 1975. Breakout resistance of shallow horizontal anchors. Journal of Geotechnical and Geoenvironmental Engineering, ASCE, 101(9), 999–1003.

Das, B.M., Shin, E.C., Dass, R.N. and Omar, M.T. 1994. Suction force below plate anchors in soft clay. Marine Georesources and Geotechnology, 12, 71–81.

Dickin, E.A. 1988. Uplift behavior of horizontal anchor plates in sand. Journal of Geotechnical and Geoenvironmental Engineering, ASCE, 114(11), 1300–1316.

Ghaly, A. and Hanna, A. 1994. Ultimate pullout resistance of single vertical anchors. Canadian Geotechnical Journal, 31, 661–672.

Goodall, S.J. and Merifield, R.S. 2023. Working platforms and bearing capacity assessments of sand overlying clay using finite element limit analysis. Australian Geomechanics, 58(3), 117–139.

Merifield, R.S. 2002. Numerical modelling of soil anchors. PhD thesis. University of Newcastle, Australia.

Merifield, R.S., Lyamin, A.V., Yu, H.S. and Sloan, S.W. 2001. Pullout capacity of earth anchors. In Proceedings of the 15th International Conference on Soil Mechanics and Foundation Engineering, Istanbul, 1203–1206.

Merifield, R.S., Lyamin, A.V., Sloan, S.W. and Yu, H.S. 2003. Three-dimensional stability analysis of plate anchors in clay. Journal of Geotechnical and Geoenvironmental Engineering, ASCE, 129(3), 243–253.

Merifield, R.S. and Sloan, S.W. 2006. The ultimate pullout capacity of anchors in frictional soils. Canadian Geotechnical Journal, 43(8), 852–868.

Meyerhof, G.G. and Adams, J.I. 1968. The ultimate uplift capacity of foundations. Canadian Geotechnical Journal, 5(4), 225–244.

 © Deep Foundations Institute 2026

Murray, E.J. and Geddes, J.D. 1987. Uplift of anchor plates in sand. Journal of Geotechnical and Geoenvironmental Engineering, ASCE, 113(3), 202–215.
Okamura, M., Takemura, J., and Kimura, T. 1996. Centrifuge model tests on bearing capacity and deformation of sand layer overlying clay. Soils and Foundations, 37, 73–88.
Okamura, M., Takemura, J., and Kimura, T. 1998. Bearing capacity predictions of sand overlying clay based on limit equilibrium methods. Soils and Foundations, 38, 181–194
Optum G2 [Computer software]. 2023. Optum CE. Copenhagen, Denmark.
Rowe, R.K. 1978. Soil–structure interaction analysis and its application to the prediction of anchor behavior. PhD thesis. University of Sydney, Australia.
Sakai, T. and Tanaka, T. 1998. Scale effect of a shallow circular anchor in dense sand. Soils and Foundations, 38(2), 93–99.
Salimi Eshkevari, S., Abbo, A.J. and Kouretzis, G. 2019a. Bearing capacity of strip footings on sand over clay. Canadian Geotechnical Journal, 56, 699–709.
Salimi Eshkevari, S., Abbo, A.J. and Kouretzis, G. 2019b. Bearing capacity of strip footings on layered sands. Computers and Geotechnics, 114.
Shiau, J.S., Lyamin, A.V. and Sloan, S.W. 2003. Bearing capacity of a sand layer on clay by finite element limit analysis. Canadian Geotechnical Journal, 40, 900–915.
White, D.J., Cheuk, C.Y. and Bolton, M.D. 2008. The uplift resistance of pipes and plate anchors buried in sand. Géotechnique, 58(10), 771–779.
Yu, H.S. 2000. Cavity expansion methods in geomechanics. Dordrecht.

 © Deep Foundations Institute 2026

GEOTECHNICAL DESIGN CHALLENGES FOR SOLAR FARM TRACKER PILES IN REACTIVE CLAYS

S. Goodall, Douglas Partners Pty Ltd, Warabrook, NSW, Australia, Sean.Goodall@douglaspartners.com.au

ABSTRACT

Australia's climate is defined by its extremes. Frequent droughts, variable rainfall, and intense solar exposure, making it a prime candidate for solar energy generation. However, the geotechnical conditions that accompany these climatic features present unique challenges for foundation design, particularly for solar tracker systems commonly supported on shallow driven I- or H-section piles. In regions underlain by reactive clays, ground movements associated with soil moisture fluctuations can lead to uplift forces during wet phases and reduced lateral or vertical support during dry periods. This paper reviews some key foundation design aspects when considering the long-term performance of pile-supported solar arrays.

Keywords: unsaturated soil, solar, piles, expansive soil

INTRODUCTION

In Australia, commercial-scale solar is a relatively recent development, with the first large facility commencing operation in 2012. Growth since then has been rapid: by March 2021, solar farms were generating almost 7 GW of capacity, around twenty times the 2016 market, and had become the largest contributor to the nation's renewable energy mix. Forecasts now suggest that in some Australian states, solar could supply up to 90% of electricity by 2035.

Since inception, the Australian Renewable Energy Agency has invested over $1 billion in solar research, driving major advances in photovoltaic technology, battery storage, and above-ground infrastructure. Yet, to the authors' knowledge, only one funded research project, led by Professors David Airey (University of Sydney) and Mark Jaksa (University of Adelaide), with some of their research recently becoming available (Thomas and Airey 2024; Thomas and Airey 2025), is directly addressing foundation behavior of solar farm piles, with an Australian Research Council grant of just $250,000. This imbalance is striking; billions are directed to the above ground technology, while the foundation systems, often a significant portion of capital cost and a key geotechnical risk, remain comparatively under-researched.

Despite the absence of substantial government funding, the design assumptions and theoretical methods underpinning solar farm pile foundations have begun to receive greater attention (Kristinof and Collingwood, 2019; Lee et al., 2019; Dissanyake et al., 2020; Tran, 2020; Kelly et al., 2021; Surjadinata et al., 2021; Goodall and Merifield, 2021; Goodall et al., 2024). Many of these studies note that solar farm piles are frequently designed with greater permissible movement limits than conventional structures, encouraging shallow-embedment strategies that can reduce upfront costs. While financially attractive, such designs can expose projects to significant geotechnical risks, including material loss from erosion and the challenges of reactive soils. In the authors' experience, some engineers and designers continue to adopt aggressive shallow pile embedment designs without adequately addressing these risks or accounting for the long-term uncertainties associated with climate variability and foundation behavior. Such short-term savings in several Australian renewable projects have already resulted in costly rectification works to both solar farms and related infrastructure.

This paper presents some of the challenges and risks associated with solar farm piles founded in reactive clay considering recent developments and experiences. While written from an Australian perspective, many of the issues discussed are of broader relevance.

 © Deep Foundations Institute 2026

BACKGROUND

Soil Reactivity and Surface Movements

In Australia, soil reactivity is classified using AS 2870 (2011) site classification procedures, which quantify potential surface movement due to seasonal moisture change. While developed for residential structures, these principles are often applied to large-scale infrastructure such as solar farms. The classification is based on the design site surface movement, y_s (Equation 1), representing a value with less than a 5% chance of exceedance over a 50-year design life:

$$y_s = \frac{1}{100}\sum_{n=1}^{N}\left(I_{pt}\overline{\Delta u}h\right)_n \quad [1]$$

Here, I_{pt} is the instability index (%/pF), $\overline{\Delta u}$ is average suction change (pF), h is layer thickness (mm), and n is the number of layers in the design depth of moisture change. The instability index is derived from the soil shrinkage index, I_{ps}, obtained via laboratory testing, index correlations, or expert visual-tactile assessment.

For solar farms, the 50-year design basis is likely to be conservative relative to their nominal 25–30-year lifespan. However, with piles representing a major capital cost, and historical evidence of energy assets operating beyond their initially proposed design life, there is a growing need to consider foundation performance for potential reuse. This is complicated by the vast and variably characterized footprints of solar farms, where sparse investigation points can mask critical reactivity variations. In Australian practice, the shrink–swell test (AS1289.7.1.1, 2003) is the most common reactivity assessment, determining the shrink–swell index, *Iss* (%Δ/pF) from shrinkage (ε_{sh}) and swelling (ε_{sw}) strains (Equation 2):

$$I_{ss} = \frac{\varepsilon_{sh} + \frac{\varepsilon_{sw}}{2}}{1.8\text{pF}} \quad [2]$$

The swell component is halved to account for lateral restraint (Fityus et al., 2005). Expansivity ranges from low (1%/ΔpF to 2 %/ΔpF) to very high–extreme (6 %/ΔpF to 8 %/ΔpF). The relationship between I_{ps}, I_{pt} and I_{ss} is given in Equation 3:

$$I_{pt} = \alpha I_{ps} \approx \alpha I_{ss} \quad [3]$$

Where α is a lateral restraint factor defined in AS 2870 (2011). The shrink–swell test's advantage over less common methods (e.g., core or loaded shrinkage) is its ability to capture both shrink and swell behavior without direct suction measurement, and retaining some of the soils structure / fabric, providing a practical and representative basis for estimating reactive site movement.

Climate Considerations and Suction Depth

The depth of moisture change H_s, also commonly referred to as the active depth or depth of suction change, is critical in determining site surface movement, as it defines the depth to which soil suction varies due to climatic influences at the surface (Fityus and Delaney, 2001). In Australian practice, H_s is commonly estimated from the Thornthwaite Moisture Index (*TMI*), with broad-scale climatic zone mapping developed by numerous authors (e.g., Fityus et al., 1998; Barnett and Kingsland, 1999; Fox, 2000, 2002; Chan and Mostyn, 2008; Fityus and Buzzi, 2008; Karunarathne et al., 2016; Jackson 2022; Karim et al., 2024). AS 2870 (2011) provides some guidance on correlating *TMI* to H_s, but the *TMI* maps themselves are interpolations of point data, many of them decades old, and therefore may not reflect current climate, site-specific conditions and future climate.

A fundamental concern is that *TMI*, and by extension H_s, is based on a long-term average, intended to represent natural variability over time. While this may be reasonable for typical residential development, where buildings and ground cover often mitigate moisture ingress and associated

volume change, solar farms are fully exposed, extend over large areas, and generally lack protective ground cover. As a result, they are more susceptible to extreme wetting and drying events. Under these conditions, piles may experience suction changes well beyond those implied by the average-based *TMI*. This approach to averaging is also contrary to most other design practices, such as wind loading according to AS 1170.2 (2021) or earthquake loading AS1170.4 (2018), which is based on peak events to ensure robustness in structures. For example, AS 1170.2 uses the design gust wind speed rather than the long-term mean wind speed. In many Australian regions, the design gust can be 1.5 to 2.0 times the mean wind speed, translating to a notably greater wind load pressure for design. Designing for the mean in this instance would be unacceptable, yet *TMI*-based active depths are, by definition, an average, meaning designs inherently exclude the worst-case climatic events that piles may face over their service life.

Where average values are adopted, whether from broad-scale maps or site-specific assessments, in the authors opinion, designers should critically assess the implications of basing designs on an average rather than peak conditions. In the authors' experience, a simple first step is to review the *TMI* record over time, comparing the spread of values to the mean. Alternatively, basic probabilistic methods can be applied to estimate the probability of exceeding the average *TMI* value under consideration. This concept is further explored in a later section of this paper.

Additionally, the *TMI* does not capture site-specific anthropogenic influences, such as past irrigation practices or the number of wet-dry cycles a pile may experience. Even seemingly minor changes, such as the removal of trees to construct solar arrays, can significantly alter ground moisture and suction profiles. This effect was clearly demonstrated by Crilly and Driscoll (2000), who monitored surface heave following tree removal at a reactive soil site at Chattenden, England, underlain by London Clay. They reported that in the absence of trees, the typical seasonal fluctuation in ground movement ranged between about 20 mm to 40 mm (representing the free surface movement), while in the presence of trees the fluctuation increased to about 60 mm to 100 mm. Of particular concern, however, was the behaviour observed after tree removal: the site experienced appreciable heave of around 150 mm, which accumulated progressively over eight years and based on their data, was still continuing at the time of their publication.

Climate change adds further uncertainty to *TMI*, with studies showing that *TMI* zones and active depths can shift over time (Lopes and Osman, 2010; Sun et al., 2017), potentially moving piles from below to within the active zone, significantly increasing their exposure to reactive soil movements. A recent study by Karim et al. (2024) investigated projected changes in *TMI* across Australia under future climate conditions. The study considered three climate scenarios broadly corresponding to low, medium, and high atmospheric CO_2 concentrations. Further detail on these scenarios is provided in Karim et al. (2024). Despite some of the limitations and simplification in their study, future projections indicate a continued drying trend across much of the continent, with areas currently classified as arid or semi-arid expanding under all scenarios considered. For the eastern states, whilst the changes where not as pronounced, the study still indicated an average reduction in *TMI* of approximately 10 to 20 units compared to the current climate. From a design perspective, this implies that solar farms designed and constructed based solely on historical or current climate data may be exposed to increased future soil reactivity. In practical terms, this may manifest as increases in H_s, which translates to an increase in characteristic surface, potentially resulting in shrink–swell or cyclic jacking movements of piles exceeding those allowed for in design, exacerbation of desiccation cracking, or the emergence of desiccation-related issues in areas where such mechanisms were not previously considered critical.

Desiccation Cracks, Gilgai Phenomena and Soil Jacking

Reactive clay soils are prone to desiccation cracking when prolonged drying causes volumetric contraction. The potential for cracking depends on the soil's shrinkage and strength characteristics and is strongly influenced by local climate. For example, many coastal areas of New South Wales, with regular rainfall and moderate seasonal variation, may rarely experience the deep drying needed for

significant cracking. In contrast, inland regions of Australia, which are common locations for solar farms, can undergo extended dry periods, producing deep, wide, and closely spaced cracks. It is also noteworthy to point out that many solar farms in Australia are constructed on sheep grazing pastures, where livestock grazing is often continued as a practical means of grass management around the panels and to promote the mixed use of developed land. However, observations of dyke / levee performance in the Netherlands (Molenaar, 2020) have shown that overgrazing by sheep can exacerbate desiccation cracking by exposing the clay surface. This suggests that allowing livestock to manage vegetation around solar arrays may contribute to, or intensify, desiccation cracking, and that agricultural land use should therefore be considered at the design stage.

Cracks can close during rewetting, but if they become filled with debris or soil, expansion of the crack is restrained, forcing the ground to heave and form undulations. This is locally known as *Gilgai* and is illustrated in Fig. 1a. This process, well documented over decades, has been linked to the "jacking" of lightly loaded, shallowly embedded infrastructure such as electricity / telegraph poles, fences, pavements, and rail formations. Given the comparable loading and embedment of solar farm piles, similar issues may arise in Gilgai-prone soils. In many agricultural areas where solar farms are built, the potential for Gilgai is often concealed by grading or cultivation. Nonetheless, indicators can include uneven vegetation growth, displaced fence posts, undulating pavements, and visible surface cracking. Hallsworth et al. (1955) and the Department of Primary Industries (2001) indicate that mounding typically re-establishes on cycles of approximately 2 years to 11 years, implying that Gilgai may develop or re-emerge after a geotechnical investigation has been completed. Preliminary assessment may draw on agricultural databases, such as published soil landscape maps, and targeted microvariability studies in test pits; however, in many cases, the most reliable insight often comes from local knowledge, such as farmers and geotechnical practitioners with long-term experience of the area.

Gilgai may also be discernible in satellite or aerial imagery where it typically manifests as irregular patterns of shallow depressions and low mounds, giving the ground surface a hummocky or "pock-marked" appearance. Following rainfall, these depressions can also present as clusters of small, transient ponds or zones of preferential water ponding. An example of Gilgai identified from aerial imagery is shown in Fig. 1b. An obvious limitation of this approach, however, is that such imagery represents only a snapshot in time and is only effective when it coincides with periods in which Gilgai is actively expressed at the ground surface.

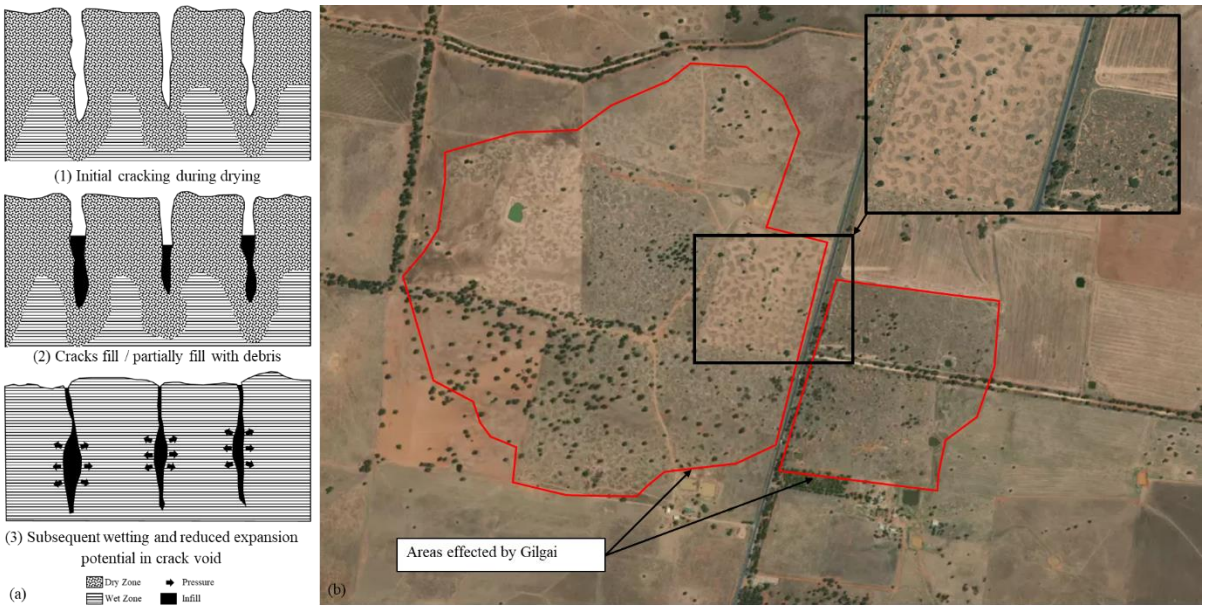


Fig. 1. (a) Simplified schematic of Gilgai formation (adapted from Gustavson, 1975), (b) Giglai affected area identified in central west New South Wales from aerial imagery

In Australian geotechnical practice, crack depth (H_c) for undisturbed reactive soils is commonly estimated as 0.5 times H_s in accordance with AS2870 (2011), while a value of zero is sometimes adopted for new cuts and fills. Alternatively, Wijesooriya (2012) and Rathnaweera and Kodikara (2015) proposed a simplified numerical model to estimate crack depth based on soil strength, suction, and climatic conditions (Fig. 2). For the soil types and conditions assessed, the model predicted crack depths of approximately 1 m to 2 m during the driest period (typically January in Australia) in semi-arid regions, increasing to around 3 m in arid regions. In the context of AS 2870 (2011), which defines an H_s of 4 m for semi-arid areas, these values represent about 25–50% of the active depth, with depths on the order of 75% appearing plausible in arid settings.

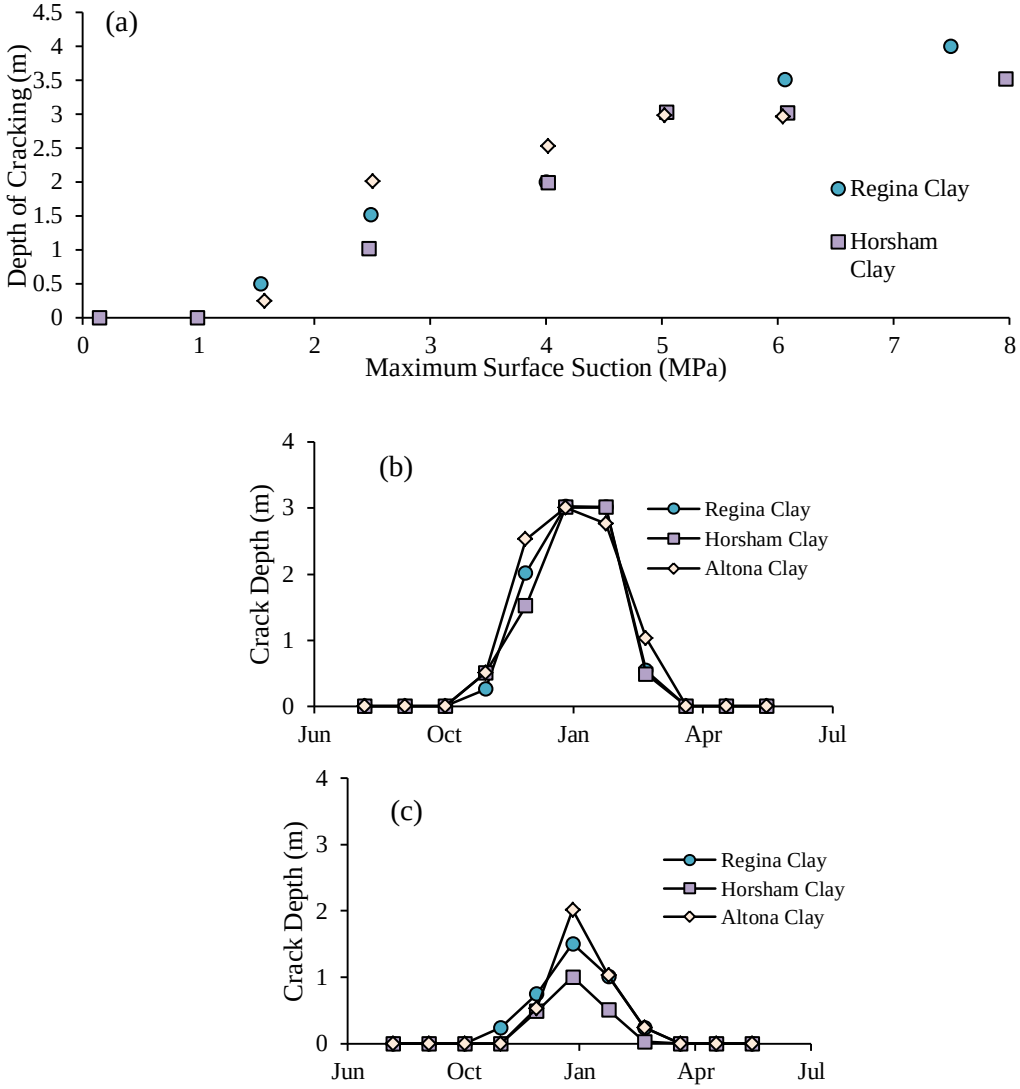


Fig. 2. Depth of cracking for various clays and climatic regions adapted from Wijesooriya (2012) and Rathnaweera and Kodikara (2015): (a) Predicted depth of cracking with climatic conditions, (b) predicted depth of cracking for an arid area, (c) predicted depth of cracking for a semi-arid area

With regards to crack width, there is no standard guidance for estimating this, which reflects the difficulty of obtaining reliable measurements to establish a method from. Some attempts have been made in the literature, however, predicting crack behaviour is inherently complex, requiring elasto-plastic unsaturated soil analysis and an understanding of climatic influences. Laboratory and numerical studies can assist, but scale effects and the inability to fully replicate soil behaviour mean that field observation remains critical.

 © Deep Foundations Institute 2026

In addition to desiccation cracking and Gilgai formation, soil jacking is another phenomenon observed in reactive clay profiles that is not well understood. In the author's experience, the soil jacking mechanism involves uplift on the pile shaft during swelling, either in the later stages of the wetting phase or earlier when soil or debris fills desiccation cracks at the soil–pile interface (similar to the Gilgai mechanism). Where piles are not sufficiently anchored below the active zone, this process can progressively 'jack' piles upwards. While initial uplift following installation and first wetting is often the largest anticipated movement, subsequent seasonal cycles have the potential to produce additional cumulative movements, which may lead to differential displacement between piles over the design life of a solar farm.

Data from Cameron and Walsh (1981) and Fityus and Delaney (2001) demonstrate that maximum upward movements do tend to occur in the first wetting phase after installation, with further albeit smaller upward displacements detected in later wetting cycles. These observations lend weight to the hypothesis that soil jacking can result in incremental uplift of piles with shallow embedment, even though the magnitudes per cycle are relatively small (typically 1 mm to 5 mm per wet cycle observed in Cameron and Walsh 1981 and Fityus and Delaney 2001). Over decades, these movements could accumulate to values that may exceed serviceability criteria for solar farm foundations (e.g., on the order of 60 mm to 150 mm additional movement for shallow pile embedment, assuming annual cycles with uplift increments of approximately 2 mm to 5 mm over a 30-year design life).

The risks posed by soil jacking remain difficult to quantify. Published data is sparse, geographically limited, and generally derived from short-term studies. While some authors argue the phenomenon is unlikely except under extreme climatic conditions, such conclusions often rely on oversimplified assumptions or one-dimensional shrinkage interpretations. Furthermore, the frequency of wetting–drying cycles over a pile's life remains uncertain. Available data suggests possible annual or multi-year cycles (Hallsworth et al., 1955; Fityus et al., 2004), but long-term patterns across different climates and soil types have not been rigorously established. In summary, engineering experience and current data indicates that soil jacking is a credible mechanism with the potential to compromise the long-term performance of shallow-driven piles in reactive clays. However, the magnitude, frequency, and universality of cyclic heave remain poorly understood, representing a significant source of uncertainty and risk in the design and serviceability assessment of solar farm piles.

ASSESSING THE IMPACTS OF REACTIVE CLAY ON SOLAR FARM PILES

Climate Considerations and Thornwaite Moisture Index

A key parameter in the geotechnical assessment of solar farm piles is the depth H_s, as it directly influences predicted vertical pile movements, axial forces, and crack depth that, in turn, govern the design toe depth of piles. However, the reliability of any such methodology to account for any of these effects ultimately depends on an appropriate assessment of the specific site conditions and risk profile of the project. As previously noted, both the depth of moisture change and the *TMI* are typically considered in terms of average values. To illustrate the implications of adopting average parameters in design, a case study adapted from Bamunawita et al. (2022) is presented. While their work extended to a statistical framework for estimating solar farm pile movements, the underlying theoretical soil-pile interaction model assumed down-drag during the drying phase. In the present author's experience, such behaviour is rarely, if ever, observed for piles founded in reactive clays, largely due to lateral soil contraction away from the soil-pile interface during drying. Downward pile movement may still occur during drying, however, this is more plausibly attributed to shallow embedment, where shrinkage of the soil beneath the pile toe governs the response, rather than the soil 'dragging' the pile down. Whilst it is not the focus of this paper to critique their analysis of pile movements, it raises questions about the reliability of their reported probability distributions for pile movement.

Bamunawita et al. (2022) reported climate data for two New South Wales weather stations (WS1 and WS2) sourced from the Australian Bureau of Meteorology. WS1 was reported to be approximately 10 km north and WS2 approximately 50 km north of a proposed solar farm site. The dataset spanned 25 years (1996–2020 inclusive). *TMI* was calculated by Bamunawita et al. (2022) using the method of

Mitchell (2013). Figure 3 shows the resultant *TMI*, the *TMI*–H_s relationship from AS 2870 (2011), a simplified curve fit to the AS 2870 step function (proposed in this study), and the resulting H_s values from *TMI*. Comparison between the AS 2870 (2011) step function, and the proposed simplified curve, shows differences typically within ±10 %, which is considered reasonable in this context. If considering average *TMI* values, WS1 indicates about –4 and WS2 about +17, which under AS 2870 (2011) correspond to design H_s values between 1.5 m and 1.8 m, which is broadly consistent with the 1.8 m proposed by Bamunawita et al. (2022). They supported this with a theoretical analysis of suction profiles, however, only 8 suction profiles from the 25-year dataset were presented.

A simplified method to investigate the temporal and spatial variability of H_s is to compute *TMI* for each weather station and then apply the proposed simplified curve fit (Fig. 3b) to estimate H_s from *TMI* as a function of time. Using this method, the average H_s over the full record was found to be 2.4 m for WS1 and 1.9 m for WS2. While Bamunawita et al. (2021) considered the WS1 data and nominated 1.8 m as the more relevant value due to its closer proximity, the average H_s method suggests otherwise. Specifically, the proposed alternative indicates that their adopted H_s for WS1 could be underestimated by approximately 30% to 40 %, with potentially significant implications for predicted vertical pile movements. Although Bamunawita et al. (2021) prioritised the dataset from 10 km away on the basis of distance, solar farms are typically large-scale developments, often spanning 1000s of hectares and extending tens of kilometres. In the author's experience, such projects are characterised by varied topography, unique site features and geology, making it questionable to exclude climate datasets solely on the basis of proximity. In many cases, more distant datasets may still provide valuable insight into the broader regional climatic behaviour relevant to design and risk assessment.

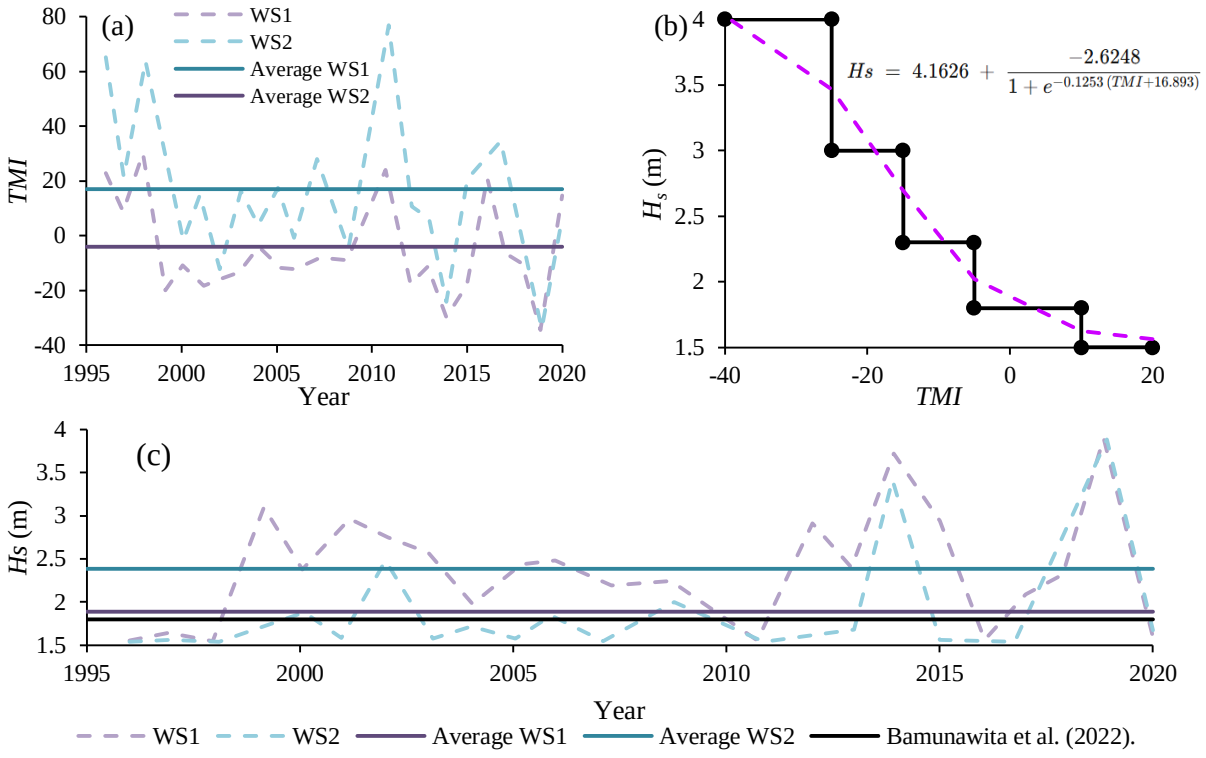


Fig. 3. (a) TMI for WS1 and WS2, (b) *TMI*-H_s relationship from AS2870 with proposed curve fit, (c) estimated H_s based on *TMI* data from Bamunawita et al. (2022) and proposed *TMI*-H_s relationship

Another key observation is the variability of conditions over time. As shown in Fig. 3 (a) and (c), from 2000 to around 2009-10, the *TMI* and derived H_s values for both stations remained relatively stable, despite notable differences when comparing the stations. However, after 2010, the *TMI* exhibits pronounced fluctuations, and in some years leading to significant increases in H_s above the long-term

 © Deep Foundations Institute 2026

averages. This underscores the limitations of relying solely on average values for design. In the author's view, it is these extremes, rather than the average values, that should govern design decisions, or as a minimum influence how risks are assessed, particularly given the high uncertainty in the long-term performance of solar farm piles and the potentially widespread consequences if tracker system movement limits are exceeded.

Rather than relying solely on visual inspection of the *TMI* and H_s trends, further analysis of the data from both weather stations can be evaluated using simple probability theory. The resulting histograms, together with descriptive statistics for *TMI* and H_s derived from the proposed curve fit, are presented in Fig. 4. The data can then be evaluated using two approaches. First, the probability of the *TMI* value being less than the average value of –4, as reported by Bamunawita et al. (2021), can be assessed, which would indicate the potential for a deeper suction depth. Alternatively, the probability of H_s exceeding 1.8 m, also proposed by Bamunawita et al. (2021), can be examined. Visual inspection suggests that neither histogram in Fig. 4 is likely to be normally distributed, except perhaps the *TMI*. Accordingly, for the present analysis, both datasets were transformed using a Johnson Transformation (JT) following Chou et al. (1998), as shown in Fig. 5. While some variability remains in the transformed data, the overall distribution fit is considered sufficient for probability estimation.

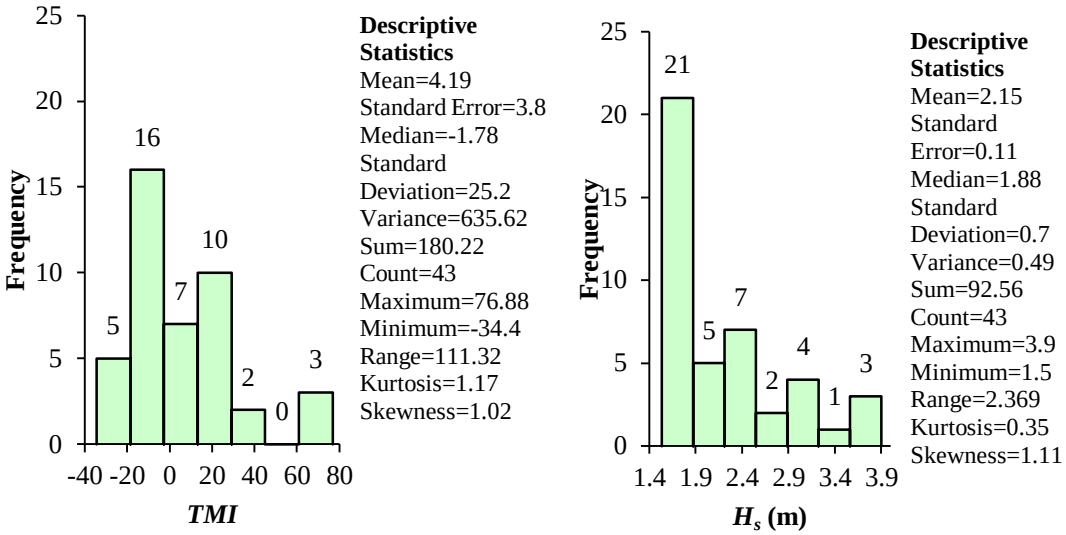


Fig. 4. Histograms for *TMI* and H_s

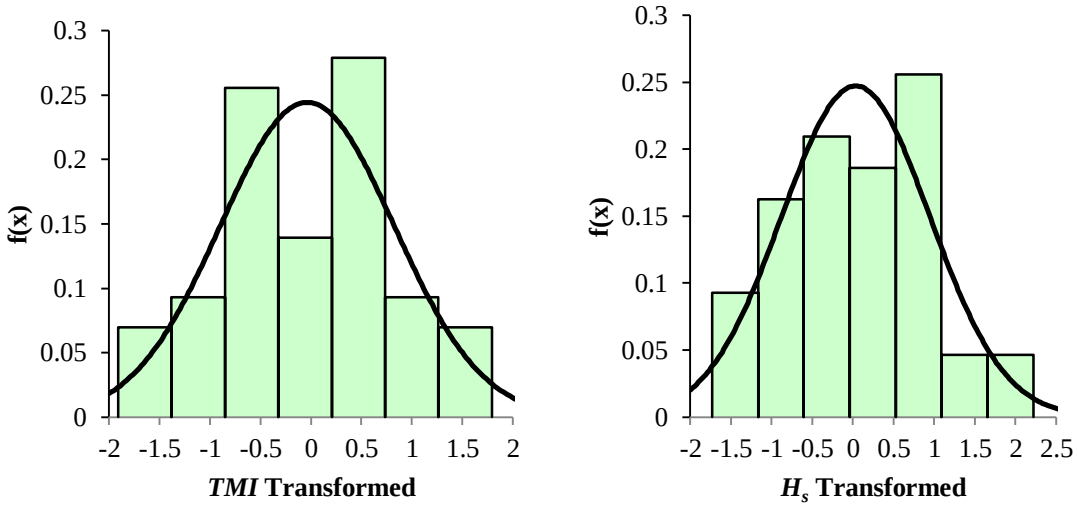


Fig. 5. Normalized histograms and probability density functions for transformed *TMI* and H_s

 © Deep Foundations Institute 2026

Based on the transformed datasets, the probability of a deeper H_s or a lower *TMI* can be determined using standard normal probability methods. This allows the generation of probability curves for both *TMI* and H_s, as illustrated in Fig.6. For comparison, results are presented for three cases: the JT-transformed data, *TMI* assumed to be normally distributed, and H_s assumed to be lognormally distributed.

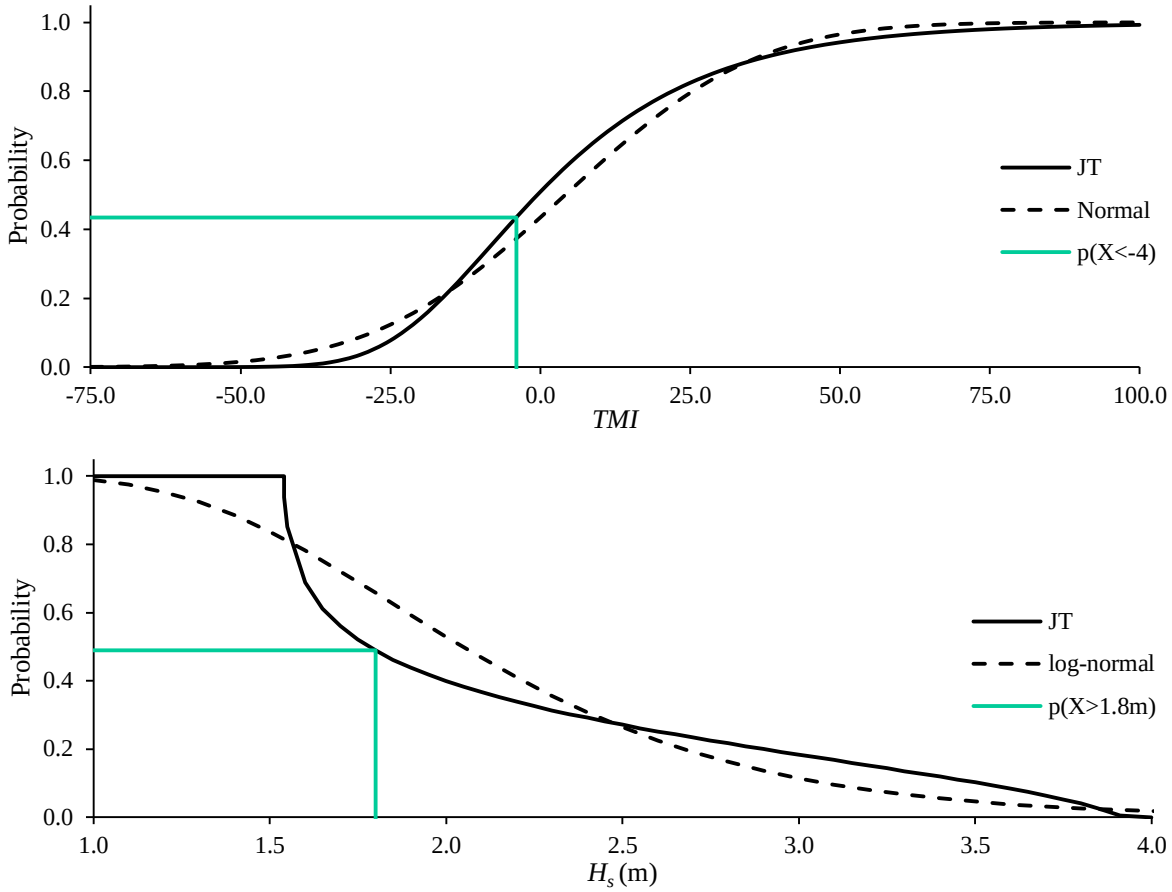


Fig. 6. Probability plots for *TMI* and H_s

From Fig. 6, it is evident that if a *TMI* of –4 is adopted as the average design value, there is about a 0.43 probability, based on the 25-year dataset, that the *TMI* will be lower. Likewise, for H_s, if a design value of 1.8 m is selected, there is around a 0.49 probability that the suction depth will be greater. It should be noted that a limitation to using curve fits and transformed data is that the conversion functions are sometimes invalid or discontinuous outside the original dataset. Another limitation is that conditions have been imposed on the simplified *TMI*-H_s relationship such that the H_s value is taken as asymptomatic for *TMI* greater than +10 or less than -25. Such limitations are evident in the probability plot for H_s.

Given that the founding depth and long-term performance of solar farm piles are intrinsically linked to the adopted *TMI* and H_s values, the above probabilities should warrant serious consideration. It is also noted that the above analysis does not explicitly account for the potential effects of climate change, which represents a key limitation of the assessment. Based on the findings of Karim et al. (2024), and for a typical *wet temperate* region as implied by the Bamunawita et al. (2021) study, there remains potential for future increases in H_s. However, such increases in a *wet temperate* region are expected to be relatively minor and would remain dependent on the specific climate scenario adopted.

While other parameters, such as soil reactivity, soil shear strength, and underlying geology, also strongly influence the interaction of the ground and piles, and while exceedances in the H_s may not

always translate to performance issues, the author's experience suggests that few, if any, Australian solar farm designs have undertaken even this simple level of probabilistic risk assessment. In most other engineering contexts, such high probabilities would be considered unacceptable unless the design could clearly demonstrate negligible impacts, or the asset owner explicitly accepted the associated risks alongside robust and practical contingency measures.

Vertical Pile Movement and Axial Forces Due to Swelling Soil

Goodall and Merifield (2021) developed a simplified, chart-based method for estimating vertical movement and peak axial load in shallow-embedded solar farm piles founded in swelling ground. The method was derived from a finite element parametric study and relies on input parameters typically available from routine geotechnical investigations, including soil shear strength, soil stiffness, the active depth, estimated free surface movement (as defined in AS 2870, 2011), as well as pile stiffness and geometry. A key assumption in the method concerns the form of the ground movement profile, which represents a simplification of a relatively 'natural' suction profile, where the maximum surface movement occurs at the surface and reduces linearly to zero at the active depth. The study outcomes were distilled into a series of design charts that enable rapid estimation of normalized vertical movement and peak axial tension load, with the problem definition and an example chart presented in Fig 7.

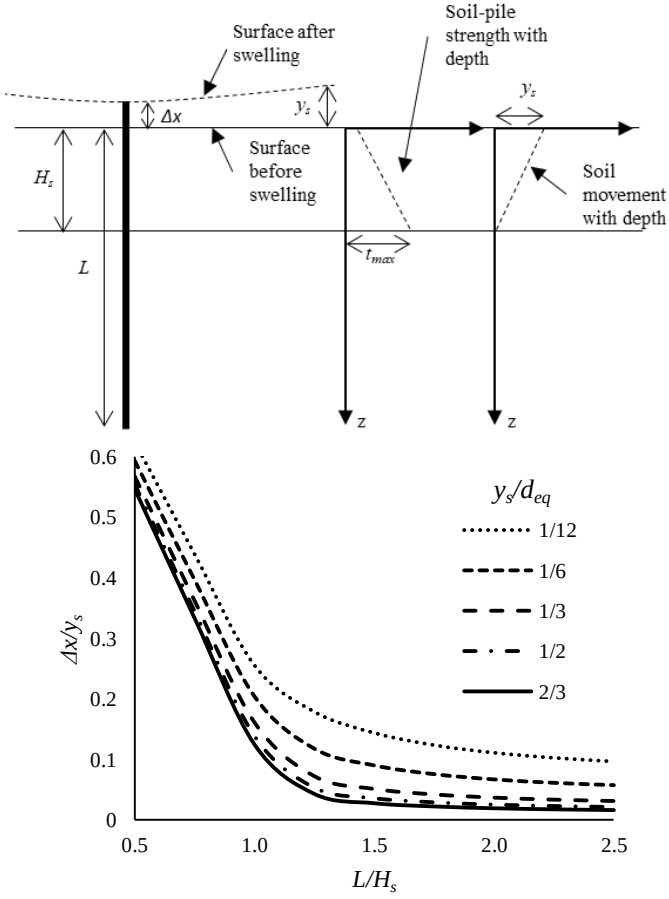


Fig. 7. Left – Problem definition of a pile in swelling soil. Right – Example chart from Goodall and Merifield (2021) for dimensionless pile stiffness of 125 and dimensionless soil stiffness of 100

Since the publication of Goodall and Merifield (2021), available literature and case studies have been further reviewed and compiled to support the validation of the proposed design charts, with the results summarized in Table 1. To date, 20 case studies have been examined, encompassing over 50 different length-to-active-depth ratios across a range of ground and moisture conditions. The dataset spans full-scale and model-scale testing, boundary element modelling (BEM), finite element modelling (FEM),

analytical methods, and p–y approaches. Each case study has been analyzed using the method of Goodall and Merifield (2021), with results collated in Table 1. Where L is the length of the pile, E_s is the elastic modulus of the swelling soil, Δx is the upward pile movement, y_s is the free surface movement, P_{max} is the peak axial load in the pile, T_{max} is the maximum uplift load due to the swelling soil within the active depth. A full explanation of assumptions and problem definition is provided in Goodall and Merifield (2021).

Table 1. Database of piles in swelling soil compared with Goodall and Merifield (2021)

				Published Data		Goodall and Merifield	
Author	**Study Type**	L/H_s	E_s/t_{max}	$\Delta x/y_s$	P_{max}/T_{max}	$\Delta x/y_s$	P_{max}/T_{max}
Cameron and Walsh (1981)	Field	0.83 1.5	100-200	0.36 0.05	-	0.34 0.05	-
Meintjes and Pellissier (1994)	Field	1.6	100-200	0.18	0.65	0.13	0.58
Kilsby et al. (1996)	Field	1.25	200-300	0.10	-	0.07	-
	FEA			0.08	-	0.07	
Kim and O'Neil (1998)	Field	2.5	200-300	0.11	0.96	0.01	0.85
Mohamedzein et al. (1999) Site 1	Field	0.3 0.7 1.0	200-300	0.57 0.13 0	-	0.70 0.40 0.13	-
	FEA	0.3 0.7 1.0		0.41 0.20 0.07	-	0.70 0.40 0.13	-
Mohamedzein et al. (1999) Site 2	Field	0.25 0.5 0.75 1.0	200-300	0.61 0.25 0.13 0	-	0.78 0.52 0.30 0.10	-
	FEA	0.25 0.5 0.75 1.0		0.41 0.26 0.14 0.09	-	0.78 0.52 0.30 0.10	-
Crilly and Driscoll (2000)	Field	3	200-300	0.03	0.97	0.02	0.7
Fityus and Delaney (2001) (east)	Field	0.6 0.9 1.2 1.8	100-200	0.43 0.14 0.12 0.05	-	0.48 0.23 0.08 0.04	-
Fityus and Delaney (2001) (west)	Field	0.6 0.9 1.2 2.1	100-200	0.46 0.29 0.09 0.04	-	0.48 0.23 0.08 0.03	-

 © Deep Foundations Institute 2026

Hong (2008) using data from Kim and O'Neil (1998)	p-y model	2.5	200-300	0.36	0.81	0.01	0.85
Hazzan and Sarsby (2010)	Field	0.8	100-200	0.45	-	0.39	-
Nelson et al (2012) using data from Mohamedzein et al. (1999) Site 1	BEM	0.3 0.7 1.0	200-300	0.65 0.40 0.11	-	0.70 0.40 0.13	-
	FEA	0.3 0.7 1.0		0.54 0.28 0.21	-	0.70 0.40 0.13	-
Nelson et al (2012) using data from Mohamedzein et al. (1999) Site 2	BEM	0.25 0.5 0.75 1.0	200-300	0.59 0.43 0.28 0.10	-	0.78 0.52 0.30 0.10	-
	FEA	0.25 0.5		0.54 0.33	-	0.78 0.52	-
Nelson et al. (2012) using data from CSU Test Site	Field	1.9	100-200	0.14	0.86	0.03	0.74
	FEA			0.06	0.68		
Liu et al. (2019) using data from CSU Test Site	Field	1.9	100-200	0.14	0.86	0.03	0.74
	Analytical			0.07	0.66		
	Benvenga (2005) cited in Liu et al. (2019)			0.42	-		
Liu (2019) using data from Fan (2007)	Model test	1	100-200	0.09	0.91	0.12	0.64
	FEA			0.14	0.78		
	Analytical			0.13	0.55		
Kelly et al. (2021) using data from Fityus and Delaney (2001)	BEM-Stochastic	0.6 0.9 1.2	100-200	0.55 0.36 0.24	-	0.48 0.23 0.08	-
Bamunawita et al. (2022)	BEM-Stochastic	0.85	100-250	0.43	-	0.2	-
da Silva Burke et al. (2022)	Field	2.4	100-200	-	0.57	-	0.7

While some published studies did not provide complete datasets of measured soil shear strength and stiffness, informed estimates were made using the available information together with engineering judgement. For most soils, the stiffness-to-strength ratio from Goodall and Merifield (2021) typically falls between 100 and 200, though higher values of 200 to 300 (or greater) are possible where abnormal moisture conditions exist or swelling is constrained at boundaries (some of which is present in the case studies reviewed). Recent work by Thomas and Airey (2025) has advanced understanding of soil-pile interface behavior under partial saturation, although the method proposed by Goodall and Merifield (2021) continues to provide a practical and robust framework for preliminary assessment. This is supported by the generally good agreement observed with available case-study data, with predictions typically tending towards the conservative side. Greater scatter is evident in case studies influenced by atypical moisture conditions, which are unlikely to conform to the assumed linear ground-movement profile inherent to Goodall and Merifield (2021). Nevertheless, for ground movements associated with typical climatic variation, the method demonstrates a reliable and practical basis for preliminary design. As additional high-quality data emerging from Thomas and Airey (2025) become available, it is proposed that the Goodall and Merifield (2021) framework be further reviewed and refined to explicitly account for the effects of partial saturation, while retaining its underlying simplicity and practical applicability.

Lateral Analysis and Accounting for a Crack at the Soil-Pile Interface

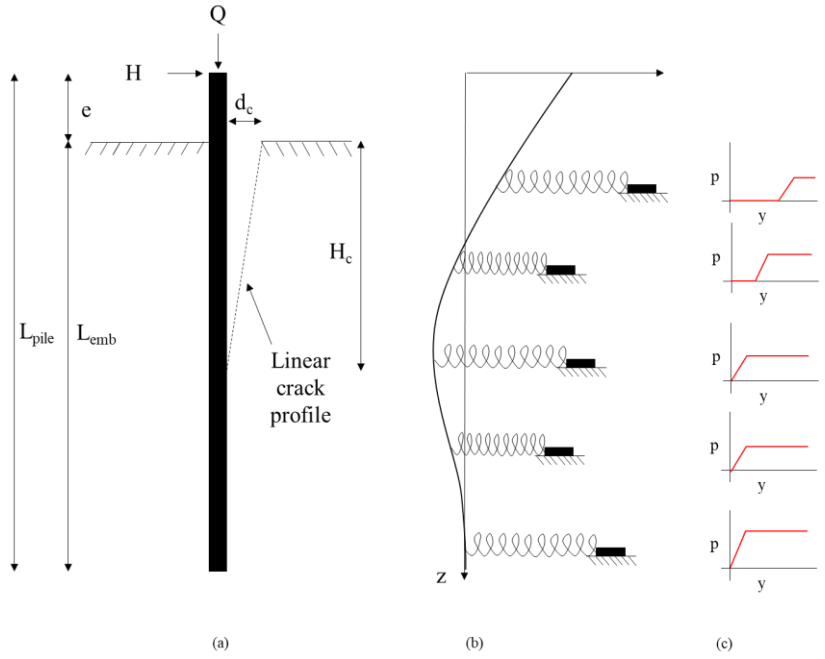
Goodall et al. (2024) have developed a simplified *p–y* method to evaluate the effect of a desiccation crack at the soil-pile interface. Figure 8 illustrates the problem definition and a sample curve set for various normalized pile displacement profiles. The approach uses linear elastic-perfectly plastic *p–y* curves and incorporates parameters commonly determined during geotechnical investigations, such as soil shear strength and stiffness (E_{soil}). Other key parameters include crack width (d_c) and depth (H_c), albeit slightly more challenging to determine or obtain during site investigations. The method also includes a procedure for extending the *p–y* relationship to a simplified unsaturated soil model following the work of Khalili (2018).

To the author's best knowledge, since Goodall et al. (2024), no other studies have specifically examined the effect of a crack at the soil-pile interface for laterally loaded piles in reactive soils. As such, there is no published data against which the *p–y* method can be directly compared when considering cracking at the soil-pile interface. However, Goodall et al. (2024) were able to benchmark their approach against other available solutions that assume no crack at the soil-pile interface. For instance, Poulos and Davis (1980) present boundary element method (BEM) solutions, while other widely adopted approaches include other *p–y* methods such as Matlock (1970), as well as three-dimensional finite element modelling (e.g., Plaxis 3D). The results are typically expressed in terms of the pile flexibility factor (K_r as defined by Poulos and Davis, 1980) and normalized plots of lateral pile displacement (ρ). Results from Goodall et al. (2024) under the no-crack condition, when compared with these published solutions and methods, as shown in Fig. 9, show reasonable agreement.

Thomas and Airey (2024) have examined a similar problem through scale model testing, focusing on piles subjected to repeated wetting and drying cycles. Their study program has incorporated moisture content measurements before each stage and photographic records to track the evolution of surface cracking in the soil, with selected images presented in Fig. 10. These laboratory results were complemented by three-dimensional finite element analyses in ABAQUS, adopting the Cam-Clay model assuming the effective stress parameter χ is equal to the degree of saturation and soil-water characteristic curves to simulate partially saturated conditions. The numerical framework captured variations in stiffness and suction-related strength gains, and allowed for soil-pile separation, but could not explicitly represent desiccation crack formation within the soil mass, which is a well-known limitation of continuum approaches.

Whilst it is noted that laboratory scale tests and numerical models calibrated using the laboratory results are unlikely to fully capture the complex behaviors expected in the field, the findings from Thomas and Airey (2024) highlight an important duality central to pile behaviour in expansive clays.

On one hand, matric suction during drying phases can temporarily enhance lateral resistance and stiffness of the soil. On the other, the initiation of desiccation cracks, particularly at the soil-pile interface, can negate these benefits and lead to a reduction in capacity and resistance. Similar behaviors were observed by Goodall et al. (2024), whereby the presence of a crack at the soil-pile interface led to a magnification of the pile displacement and peak bending moment. Goodall et al. (2024) noted that in some instances, the increased bending moment (M), even under working load conditions, may approach the yield moment (M_p) of the pile section, as shown in Fig. 11.



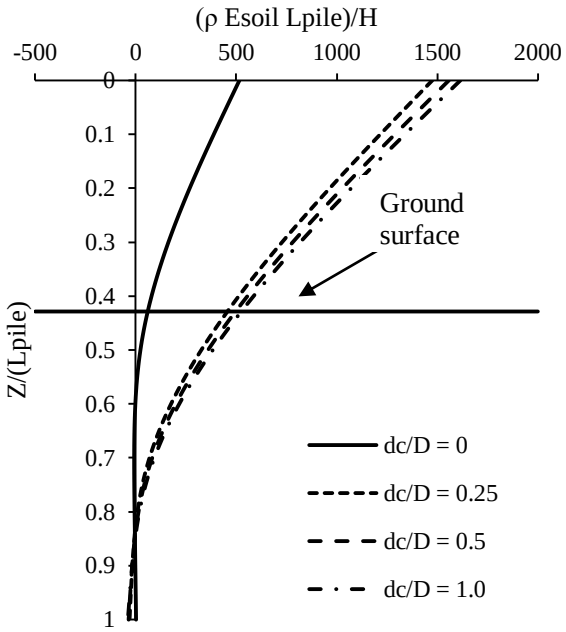


Fig. 8. Left – (a) Problem definition of a pile with a crack at the interface, (b) idealization of pile with springs and (c) p-y curves along pile. Right – Example of analysis from Goodall et al. (2024) for dimensionless pile displacement with various cracks width (d_c) at the soil-pile interface normalized to pile width (*D*)

 © Deep Foundations Institute 2026

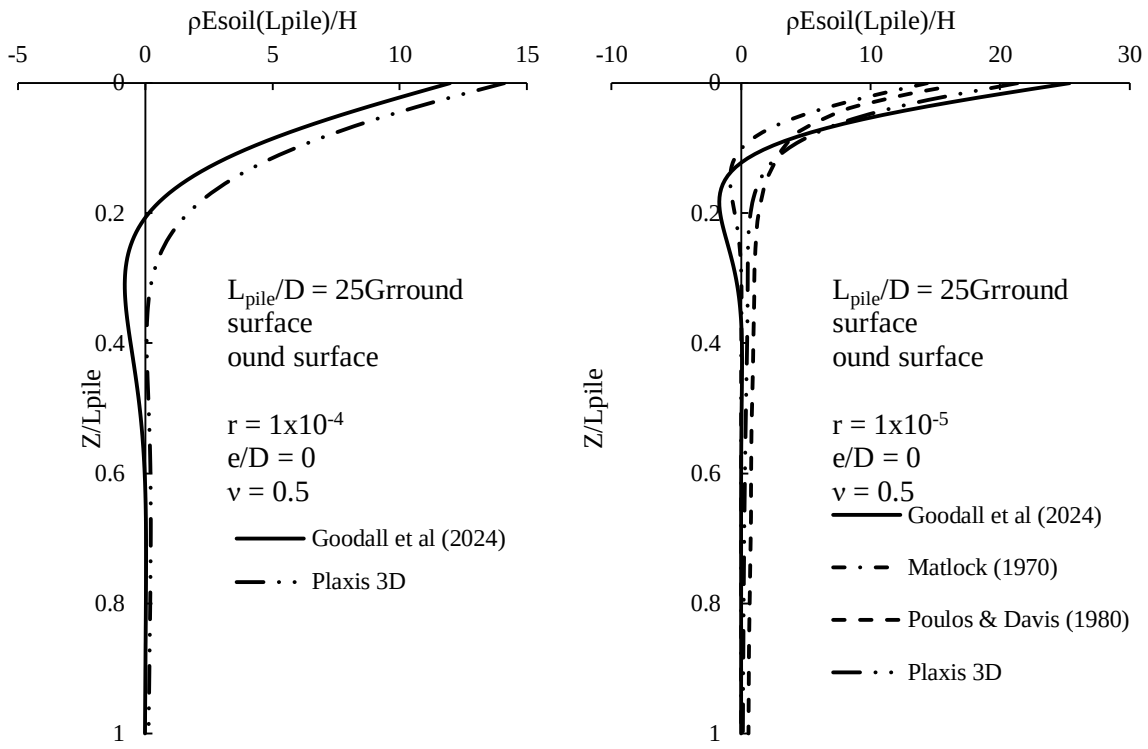


Fig. 9. Normalized pile displacement from Goodall et al. (2024) compared with other methods and published solutions without a crack at the soil-pile interface

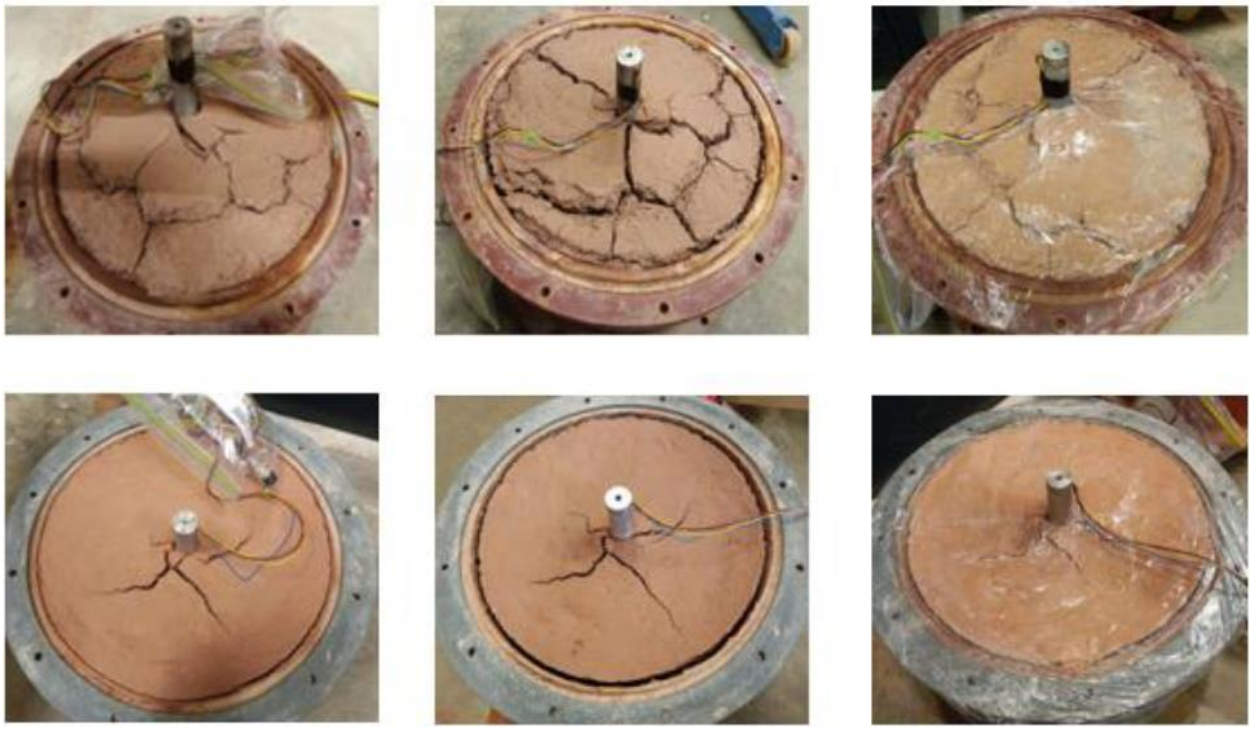


Fig. 10. Model tests and piles through different wet-dry phases (Thomas and Airey, 2024)

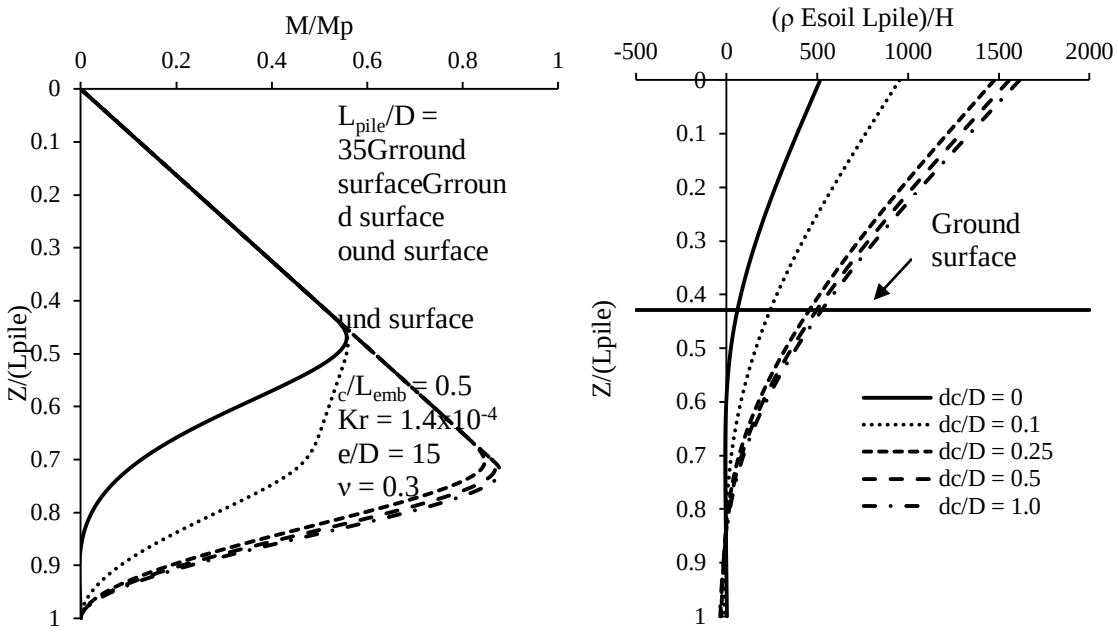


Fig. 11. Effect of crack at soil-pile interface for a typical H-pile subjected to a 10 kN lateral load, adapted from Goodall et al. (2024): Left – Ratio of pile moment to yield moment of pile section. Right – normalized lateral pile displacement

It should also be recognized that, depending on the pile section properties and ground conditions, solar farm piles may be susceptible to buckling due to lateral loading (Lee et al., 2019). Kelly et al. (2021) noted that, owing to their relatively low section properties, interior array piles are generally unlikely to experience buckling below ground level unless the soil softens, whereas larger sections used to support motors or located along array boundaries in stiffer ground are more prone to such failure. The presence of a crack at the soil-pile interface, or widespread and deep desiccation cracking, may alter this behavior by reducing lateral support along the shaft, thereby increasing the likelihood of buckling.

Understanding the presence and effects of desiccation cracking is important, as Goodall et al. (2024) and Thomas and Airey (2024) indicate that it can amplify pile displacements under lateral loading (e.g., wind loading), which may have potential implications for torque tube performance. In addition to greater displacement, bending moments are also expected to increase, driven by three key factors: (i) the amplified displacement itself, (ii) increased load eccentricity above the pile's point of fixity, and (iii) the higher ground stiffness associated with the soil's unsaturated state. Goodall et al. (2024) highlighted that, depending on crack geometry, current design practice may not adequately account for conditions where desiccation cracking extends deeper than about 0.5 times the active depth, as specified in AS 2870 (2011), or where crack widths at the soil-pile interface exceed approximately 10% of the pile width (i.e., about 15 mm to 20 mm for typical solar farm piles).

CONCLUSIONS

This study has highlighted several critical risks and uncertainties influencing the geotechnical performance of solar farm piles installed in reactive clay soils. Vertical ground movements driven by shrink–swell behaviour remain insufficiently characterised, with mechanisms such as soil jacking and Gilgai development presenting persistent challenges. Reliance on broad-scale *TMI* mapping further compounds uncertainty, as it may inadequately capture local climatic, soil moisture and variability across the vast footprints typical of solar farms. This is further complicated by the uncertainty around future climate and how this may lead to changes in the *TMI*.

Desiccation and cracking at the soil-pile interface can markedly reduce lateral confinement, increase pile displacements under lateral loading, and magnify bending moments. Current design practice is unlikely to fully account for these effects, particularly where cracking at the soil-pile interface extends

deeper than approximately 0.5 times the active depth or where crack widths exceed roughly 10% of the pile width.

These issues are further exacerbated by the limited availability of long-term, field-scale performance data for shallow-embedded piles, despite the rapid growth of the industry. Collectively, these factors underscore the need for more rigorous characterisation, monitoring, and design approaches for solar farm foundations in reactive clay environments.

As we transition to a society dependant on renewable energy, the industry faces a central challenge: balancing cost efficiency with long-term resilience. Reducing pile lengths in solar farm design can deliver immediate financial savings, yet such decisions should not be made without a full appreciation of the potential consequences. Unless asset owners clearly understand and accept the long-term risks along with practical contingencies, these short-term savings may translate into increased maintenance requirements and performance limitations over the life of the project.

A key issue for geotechnical practitioners is that the growth of solar farm development has far outpaced the acquisition of essential field data, leaving design methods heavily reliant on theoretical frameworks. While these frameworks provide valuable insight, their limitations necessitate a cautious and conservative approach to foundation design. At present, comprehensive site investigations, combined with local engineering experience and careful field observations, remain the most reliable means of understanding and managing the geotechnical risks associated with solar farm foundations. Ground risks need to be explicitly assessed by engineers and designers and clearly communicated to developers and asset owners. More emphasis is needed on whole-of-life performance, rather than prioritizing rapid deployment at minimal costs. In reactive soils, the suitability of shallow embedment remains uncertain, and in the absence of robust case-history data, there is a pressing need to refine predictive models, deepen understanding of soil-pile interaction under variable moisture regimes, and adopt demonstrably robust designs where risks cannot be reliably mitigated.

ACKNOWLEDGEMENTS

The author acknowledges the support of Douglas Partners Pty Ltd, with particular mention of Richard Merifield and Caitlyn Todd, who have been deeply involved in the ongoing study and investigation of the mechanics and geotechnical risks associated with solar farm pile foundations.

REFERENCES

AS/NZS 1170.2, 2021. Structural design actions—Part 2: Wind actions. Standards Australia, Sydney.

AS 1170.4, 2024. Structural design actions—Part 4: Earthquake actions in Australia. Standards Australia, Sydney.

AS 1289.7.1.1, 2003. Methods of testing soils for engineering purposes—Method 7.1.1: Soil reactivity tests—Determination of the shrinkage index of a soil (shrink–swell index). Standards Australia, Sydney.

AS 2870, 2011. Residential slabs and footings. Standards Australia, Sydney.

Bamunawita, C., Dissanayake, P. and Kelly, R., 2022. Solar farm tracker pile movements in expansive clay. Proceedings of the 20th International Conference on Soil Mechanics and Geotechnical Engineering (ICSMGE 2022), Sydney, Australia, pp. 5151–5156.

Barnett, I.C. and Kingsland, R.I., 1999. Assignment of AS 2870 soil suction change profile parameters to TMI-derived climatic zones for NSW. Proceedings of the 8th Australia–New Zealand Conference on Geomechanics, Hobart, Australia, pp. 149–155.

Cameron, D.A. and Walsh, P.F., 1981. Timber pile foundations for residential foundations in expansive soils. Proceedings of the 5th Australia–New Zealand Conference on Geomechanics, Adelaide, Australia, pp. 165–169.

Chan, I. and Mostyn, G., 2008. Climatic factors for AS 2870 for the metropolitan Sydney area. Australian Geomechanics, 43(1), pp. 17–28.

 © Deep Foundations Institute 2026

Chou, Y.-M., Polansky, A.M. and Mason, R.L., 1998. Transforming non-normal data to normality in statistical process control. Journal of Quality Technology, 30(2), pp. 133–141.
Crilly, M.S. and Driscoll, R.M.C., 2000. The behaviour of lightly loaded piles in swelling ground and implications for their design. Proceedings of the Institution of Civil Engineers – Geotechnical Engineering, 143(1), pp. 3–16.
da Silva Burke, T.S., Jacobsz, S.W., Elshafie, M.Z.E.B. and Osman, A.S., 2022. Measurement of pile uplift forces due to soil heave in expansive clays. Canadian Geotechnical Journal, 59, pp. 2119–2134.
Dissanayake, P.N., Bamunawita, C. and Kelly, R., 2020. Challenges in design of solar farm tracker foundations in expansive clay. Symposium on Geotechnical Aspects of Renewable Energy, Adelaide, Australia, pp. 63–69.
Department of Primary Industries, 2001. SOILpak—Southern dryland farmers: Reader's note, Part D. NSW Government, Australia.
Fan, Z.-H., Wang, Y.-H., Xiao, H.-B. and Zhang, C.-S., 2007. Analytical method of load-transfer of single pile under expansive soil swelling. Journal of Central South University of Technology, 14(4), pp. 575–579.
Fityus, S.G. and Buzzi, O., 2008. On the use of the Thornthwaite Moisture Index to infer depths of seasonal moisture change. Australian Geomechanics, 43(4), pp. 69–76.
Fityus, S.G. and Delaney, M.G., 2001. Timber pile foundations for expansive soils. Australian Geomechanics, 36(2), pp. 51–56.
Fityus, S.G., Smith, D.W. and Allman, M.A., 2004. Expansive soil test facility near Newcastle. Journal of Geotechnical and Geoenvironmental Engineering, 130(7), pp. 686–695.
Fityus, S.G., Cameron, D.A. and Walsh, P.F., 2005. The shrink–swell test. Geotechnical Testing Journal, 28(1), pp. 1–10.
Fityus, S.G., Walsh, P.F. and Kleeman, P.W., 1998. The influence of climate, as expressed by the Thornthwaite Index, on the design depth of moisture change in clay soils in the Hunter Valley. Proceedings of the Australian Geomechanics Society Conference, Springwood, Australia.
Fox, E., 2000. A climate-based design depth of moisture change map of Queensland and the use of such maps to classify sites under AS 2870-1996. Australian Geomechanics, 35(4), pp. 53–60.
Fox, E., 2002. Development of a map of Thornthwaite Moisture Index isopleths for Queensland. Australian Geomechanics, 37(3), pp. 51–59.
Goodall, S.J. and Merifield, R.S., 2021. Pile design for solar farms and reactive clay sites in Australia. Australian Geomechanics, 56(3), pp. 87–103.
Gustavson, T.C., 1975. Microrelief (gilgai) structures on expansive clays of the Texas Coastal Plain—Their recognition and significance in engineering practice. PhD thesis, University of Texas at Austin, USA.
Hallsworth, E.G., Robertson, G.K. and Gibbons, F.R., 1955. Studies in pedogenesis in New South Wales VII: The gilgai soils. European Journal of Soil Science, 6(1), pp. 1–31.
Hazzan, B.Sh. and Sarsby, R.W., 2010. Field measurements of the behaviour of lightly loaded piles in swelling clay. Proceedings of the 63rd Canadian Geotechnical Conference (GEO2010), Calgary, Canada, pp. 296–299.
Hong, G.T., 2008. Earth pressures and deformations in civil infrastructure in expansive soils. PhD thesis, Texas AandM University, College Station, USA.
Jackson, S.D.F., 2022. Thornthwaite Moisture Index and climate zones in the Northern Territory. Australian Geomechanics, 57(3), pp. 69–85.
Karim, Md. R., Devkota, B., Rahman, Md. R, M. And Nguyen, H.B.K., 2024. Thornthwaite moisture index and depth of suction change under current and future climate – An Australian Study. Journal of Rock Mechanics and Geotechnical Engineering, 16, pp. 1761-1775.
Karunarathne, A.M.A.N., Gad, E.F., Disfani, M.M., Sivanerupan, S. and Wilson, J.L., 2016. Review of calculation procedures of Thornthwaite Moisture Index and its impact on footing design. Australian Geomechanics, 51(1), pp. 85–95.
Kelly, R., Huang, J., Poulos, H.G. and Stewart, M.G., 2021. Geotechnical and structural stochastic analysis of piled solar farm foundations. Computers and Geotechnics, 132, Article 103985.
Khalili, N., 2018. Guidelines for the application of effective stress principles to shear strength and volume change determination in unsaturated soils. Australian Geomechanics, 53(1), pp. 37–47.

Kilsby, A.G., Cameron, D.A. and Symons, M.G., 1996. Soil–pile interface treatments on bored piles in expansive clay. Proceedings of the 6th Australia–New Zealand Conference on Geomechanics, Christchurch, New Zealand, pp. 412–417.

Kim, M.H. and O'Neill, M.W., 1998. Side shear induced in drilled shaft by suction change. Journal of Geotechnical and Geoenvironmental Engineering, 124(8), pp. 771–780.

Kristinof, R.E. and Collingwood, B., 2019. Challenges and opportunities in solar farm construction. Proceedings of the 14th Australia–New Zealand Conference on Geomechanics, Perth, Australia, pp. 1289–1294.

Lee, C., Ng, C. and Kelly, R., 2019. Predicting in-ground buckling instability of steel H-beam piles through nonlinear analysis. Proceedings of the 14th Australia–New Zealand Conference on Geomechanics, Perth, Australia, pp. 267–272.

Liu, Y., 2019. Interpretation of load transfer mechanisms for piles in unsaturated expansive soils. PhD thesis, University of Ottawa, Canada.

Liu, Y., Vanapalli, S.K., Nyambere, C.-F. and Mohamoud, H., 2019. Numerical simulation of the mechanical behaviour of single piles in expansive soil. ISSMGE International Journal of Geoengineering Case Histories, 5(1), pp. 12–25.

Lopes, D. and Osman, N.Y., 2010. Changes in Thornthwaite Moisture Index in Victoria from 1948–2007 and the effect on seasonal foundation movements. Australian Geomechanics, 45(1), pp. 37–48.

Matlock, H., 1970. Correlations for design of laterally loaded piles in soft clay. Proceedings of the Offshore Technology Conference, Houston, USA, pp. 577–594.

Mitchell, P.W., 2013. Climate change effects on expansive soil movements. Proceedings of the 18th International Conference on Soil Mechanics and Geotechnical Engineering, Paris, France, pp. 1159–1162.

Meintjes, H.A.C. and Pellissier, J.P., 1994. An experimental pile in deep residual expansive clay. Proceedings of the 13th International Conference on Soil Mechanics and Foundation Engineering, New Delhi, India, pp. 487–492.

Mohamedzein, Y.E.-A., Mohamed, M.G. and El Sharief, A.M., 1999. Finite element analysis of short piles in expansive soils. Computers and Geotechnics, 24(3), pp. 231–243.

Molenaar, F., 2020. Numerical analysis of the influence of desiccation cracks on the stability of Dutch river dykes. MSc thesis, Delft University of Technology, Netherlands.

Nelson, J.D., Thompson, E.G., Schaut, R.W., Chao, K.-C., Overton, D.D. and Dunham-Friel, J.S., 2012. Design procedure and considerations for piers in expansive soils. Journal of Geotechnical and Geoenvironmental Engineering, 138(8), pp. 945–956.

Poulos, H.G. and Davis, E.H., 1980. Pile foundation analysis and design. John Wiley and Sons, New York.

Rathnaweera, S. and Kodikara, J., 2015. Modelling of stable desiccation crack depths due to cyclic wetting and drying. Proceedings of the International Conference on Geotechnical Engineering, Colombo, Sri Lanka, pp. 315–318.

Sun, X., Li, J. and Zhou, A., 2017. Assessment of the impact of climate change on expansive soil movements and site classification. Australian Geomechanics, 52(3), pp. 39–50.

Thomas, H.S. and Airey, D.W., 2024. Performance and stability of short piles in cracked desiccated soil. Proceedings of the 15th Australia–New Zealand Young Geotechnical Professionals Conference, Australia.

Thomas, H.S. and Airey, D.W., 2025. Effect of partial saturation on shear strength of a high plasticity clay and soil–structure interface. Canadian Geotechnical Journal, advance online publication.

Tran, M.N., 2020. Geotechnical considerations from two renewable energy projects. Symposium on Geotechnical Aspects of Renewable Energy, Adelaide, Australia, pp. 135–144.

Wijesooriya, R.M., 2012. Modelling of desiccation crack depths in clay soils. PhD thesis, Monash University, Australia.

 © Deep Foundations Institute 2026

INFLUENCE OF TREMIE PIPE EMBEDMENT ON CONCRETE FLOW IN BORED PILE CONSTRUCTION

Thomas Mitchell, Swansea University, Swansea, United Kingdom
Chris Barker, Ove Arup and Partners Ltd, London, United Kingdom
Christopher Wilkes, Ove Arup and Partners Ltd, London, United Kingdom
Chenfeng Li, Swansea University, Swansea, United Kingdom

ABSTRACT

Numerical modelling based on Computational Fluid Dynamics (CFD) has been shown to be effective for simulating the bulk-flow rheological behaviour of fresh concrete in a variety of contexts. This paper presents a parametric study examining the impact of tremie embedment on concrete flow mechanisms within bored piles. The parametric study uses the open-source CFD software OpenFOAM to model fresh concrete as a non-Newtonian Bingham fluid. A pressure-differential approach is used in the numerical model to simulate concrete flow, capturing the gravity-driven pour of the tremie method. Increased tremie embedment reduces the concrete velocity at the tremie exit, increases the total pour time, and affects the consumption rate of the previous concrete charge in the cover zone. The general concrete flow mechanism observed within the pile is not influenced by tremie embedment; instead, it is determined by the level of reinforcement in the element. For the first time, the influence of tremie embedment on concrete inflow velocity is captured.

Keywords: fresh concrete, computational fluid dynamics, bored piles, tremie embedment, concrete flow

INTRODUCTION

The tremie method is a common construction process for placing fresh concrete in submerged conditions. This approach is applied in deep foundation construction when ground conditions dictate the use of support fluids to ensure the stability of the element's sidewalls and prevent collapse. Support fluids can be broadly categorised into three types: mineral-based (bentonite clay), polymer-based (natural or synthetic), or a blend of the two (EFFC/DFI, 2019). Figure 1 shows the pouring process of cast-in-place bored piles using the tremie method. Concrete is placed by gravity feed using a hopper and a vertical tremie, which is constructed from short pipe sections to allow for variation in total length. This method reduces direct contact between fresh concrete and the support fluid as the tremie pipe remains embedded in the concrete after flow initiation. Increasing direct contact between concrete and the support fluid can increase the amount of mixing, thereby compromising the quality of the concrete (EFFC/DFI, 2024).

When initiating concrete flow, the tremie pipe should be lifted no more than 0.2 m from the base of the pile (ICE, 2016); this distance is referred to as the 'tremie initiation height'. During this first pouring stage, a minimum concrete level of 6 m should be achieved before breaking the tremie (British Standards Institution, 2010a). As the concrete level rises, the pressure differential driving the flow decreases, and thus the flow rate declines. The key parameter governing this flow rate is the tremie embedment, which is the distance between the concrete level within a deep foundation element and the exit of the tremie pipe. Industry specifications BS EN 1536 (2010a) and BS EN 1538 (2010b) state a minimum tremie embedment between 1.5 m and 3 m, with higher values to be used for larger diameter excavations. Maximum embedment depths are not specified in industry codes, but the EFFC/DFI (2024) recommend an embedment range of 3 m to 8 m. The observed flow rate typically governs the maximum embedment; when the flow rate becomes unacceptable, the contractor will break the tremie, removing sections to reduce the tremie embedment. This is visualised in Stages 2 and 3 of Fig. 1.

 © Deep Foundations Institute 2026

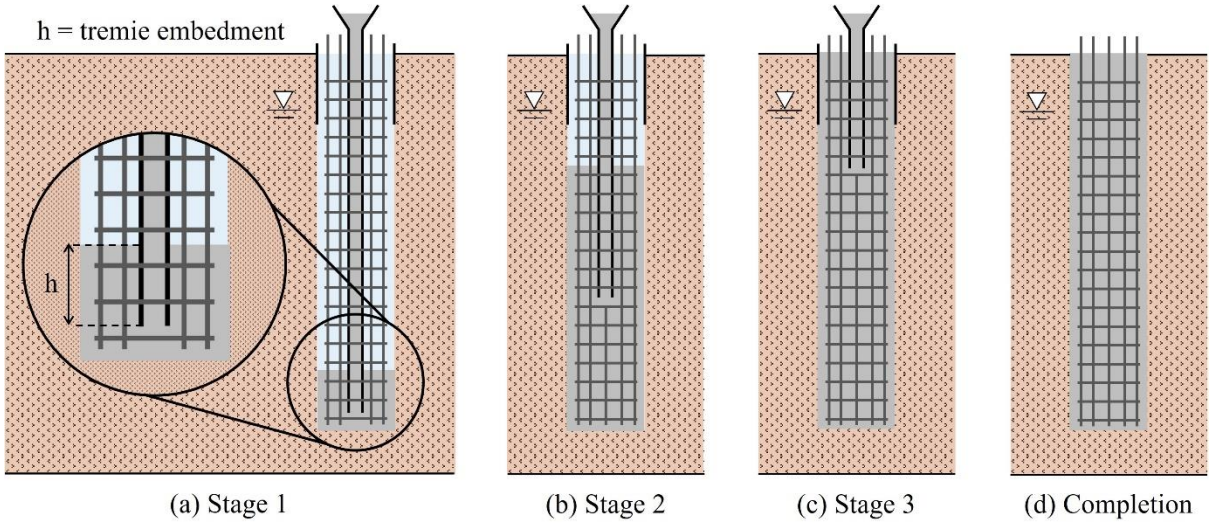


Fig. 1. The pouring process of cast-in-place bored piles using the tremie method

The concrete used in this method is commonly referred to as 'tremie concrete' and exhibits distinct fresh properties suitable for deep foundation construction. It balances high workability (Wilkes et al., 2023) to enable effective filling of the cover zone under gravity, while also providing stability to resist segregation and bleeding under significant hydrostatic pressures. Although the term 'workability' has been replaced with 'consistence' in European standards, the term remains common in the United States (Mitchell et al., 2025). Both terms are often used interchangeably to describe the concrete's ability to flow, as well as how easily it can be mixed and poured (EFFC/DFI, 2024). This paper will use the term consistence for clarity.

A variety of on-site consistence tests can be used to quantify the consistence of fresh concrete before pouring. The slump-flow test, as demonstrated by Kränkel and Gehlen (2018), can provide rheological parameters of a fresh concrete mix. The slump-flow value correlates with the dynamic yield stress, while the slump-flow velocity correlates with the viscosity of fresh concrete. The ability to quantify this information, along with the slump-flow test's simplicity and efficiency, makes it the preferred consistence test for assessing the acceptability of fresh concrete (Barker and Nicholson, 2025).

This research utilises the open-source Computational Fluid Dynamics (CFD) software OpenFOAM to investigate the influence of tremie embedment on concrete flow within bored piles, specifically by simulating cases where the tremie embedment exceeds the minimum values specified in industry standards. The final charge distributions and flow mechanisms are compared across tremie embedment values by analysing velocity vectors within the domain. The results are then used to comment on the suitability of the tremie embedment values recommended in industry codes.

MODELLING METHODOLOGY

The multiphaseInterFoam solver within OpenFOAM is used for the numerical modelling presented in this paper. This solver is capable of modelling n-phase incompressible, isothermal, immiscible flow problems and has been validated for the application of fresh concrete flow by comparing experimental results with simulations. The scales of validation include consistence tests (Fierenkothen and Pulsfort, 2017), novel laboratory-scale tests (Wilkes, 2021) and partial full-scale tests (Fierenkothen and Pulsfort, 2019; Böhle, 2013).

Modelling Concrete Rheology

Fresh concrete is modelled as a homogeneous non-Newtonian Bingham fluid. The CFD approach models fluids as a continuum and applies the fluid's rheological properties homogeneously. This approach does not explicitly capture aggregate or other particulates, nor does it capture time-

 © Deep Foundations Institute 2026

dependent properties that influence rheology, such as hydration or thixotropy. This method is selected due to the scale of the simulation, the focus on the bulk flow behaviour and the relatively short pour time modelled.

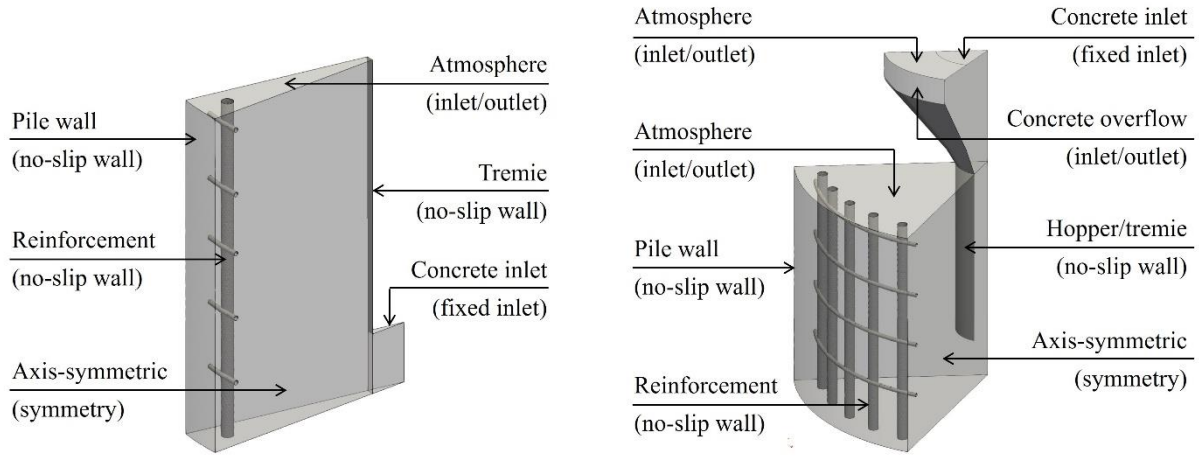
$$\tau = \tau_0 + \mu\dot{\gamma} \quad [1]$$

The constitutive model describing the relationship between the stress and strain rate in a Bingham fluid is shown in Equation 1. Where τ is the shear stress, τ_0 is the yield stress, μ is the viscosity and $\dot{\gamma}$ is the strain rate. The two input parameters for this model are the yield stress and viscosity. The yield stress is the stress required to initiate flow; the fluid behaves like a solid if the applied stress is below this value. Viscosity is a measure of a fluid's resistance to flow.

Boundary Conditions

To effectively capture the gravity-driven nature of concrete flow in the tremie method, a novel model setup is implemented. Typically, the procedure in the literature is to apply a fixed inlet boundary condition at the tremie exit, which pumps concrete at a predetermined rate (Kränkel and Gehlen, 2018; Fierenkothen and Pulsfort, 2019; Jeyaraj et al., 2023). However, understanding the variability of concrete inflow due to differences in tremie embedment is a key objective of this research, and thus, a different approach is required.

Figure 2 compares the gravity-driven boundary conditions implemented within this research with the typical fixed-inlet models used. For clarity in the figure, the pile models are shown in a shortened form. Concrete enters the hopper via the concrete inlet at a fixed rate. The hopper and tremie fill with concrete until the concrete level reaches the overflow, at which point it can exit the domain. If the concrete inlet velocity is sufficient, this setup maintains a constant fluid head within the hopper and tremie. With this model setup, the concrete flow is driven by the hydrostatic pressure within the system, arising from the varying concrete levels in the tremie and in the pile.



(a) Fixed-inlet model boundary conditions (b) Gravity-driven flow boundary conditions

Fig. 2. Comparison of fixed-inlet (a) and gravity-driven (b) boundary conditions

Model Geometry and Study Parameters

The baseline geometry of the cases modelled in this research is a pile with 1.5 m diameter and 8 m depth. The tremie pipe has a diameter of 250 mm. The reinforcement cage is constructed with 40 mm diameter vertical bars at 100 mm clear spacing and 16 mm diameter horizontal bars at 200 mm clear spacing. The cover zone is 75 mm. These values were selected based on standard geometries as described in SPERWall (ICE, 2016).

The aforementioned parameters remain constant across all simulated cases, with the only variable being the total length of the tremie, and thus the tremie embedment. Tremie embedment values of 3 m, 2 m, 1 m and 0 m are investigated within this paper. EFFC/DFI (2024) recommend a minimum embedment of 3 m, so this research aims to examine the impact of exceeding this value on concrete flow. Figure 3 shows the initial conditions of the four cases. For each case, the left image is a 3D visualisation showing only the concrete in the left half of the domain, while the right image is a 2D slice taken through the centre of the pile.

The cases are initialised with a 7 m^3 charge of concrete in the pile, corresponding to a concrete level of 3.96 m, denoted by the light grey regions in Fig. 3. The pouring of a second concrete charge, also 7 m^3, is then simulated. Both concrete charges have identical rheological properties, calibrated to a mix design with a slump-flow of 590 mm (Wilkes, 2021). The Bingham properties corresponding to this slump-flow are as follows: τ_0 = 54 Pa, μ = of 35.8 Pa·s, and ρ = 2400 kg/m^3. The remaining volume within the excavation is filled with support fluid, coloured light blue in Fig. 3. The Bingham properties of this fluid correspond to a clean bentonite slurry, with values of τ_0 = 7 Pa, μ = 0.03 Pa·s, and ρ = 1075 kg/m^3 (Wilkes, 2021).

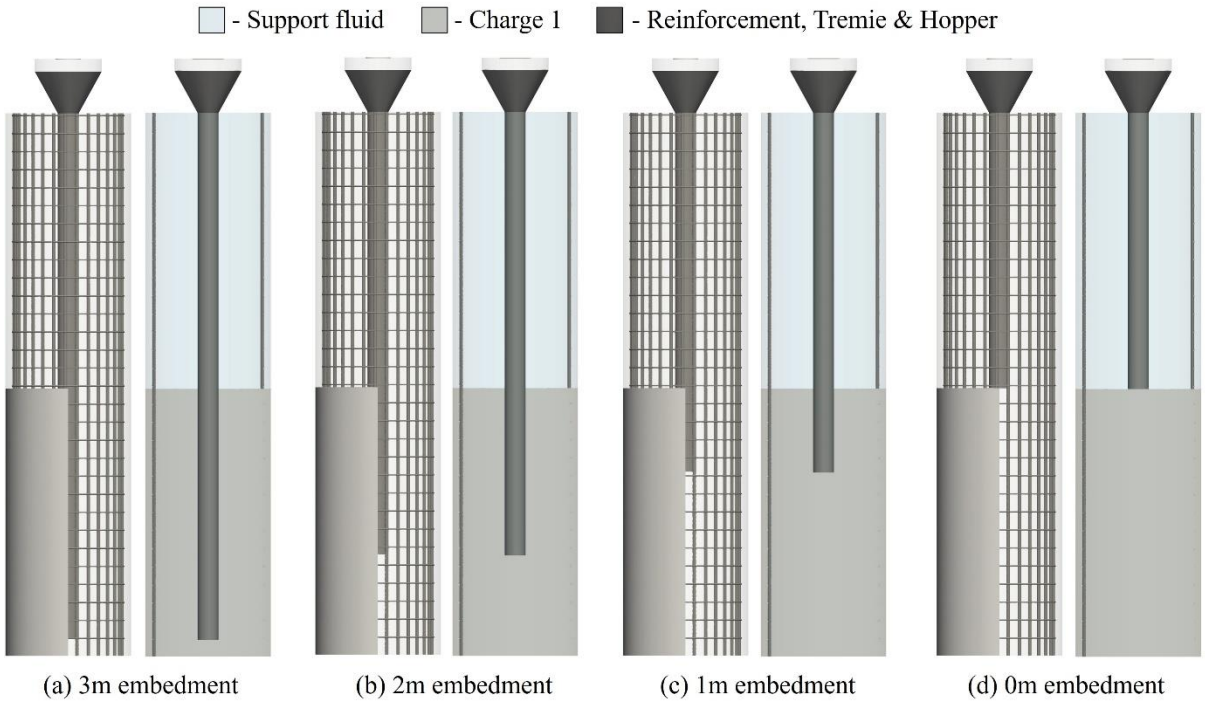


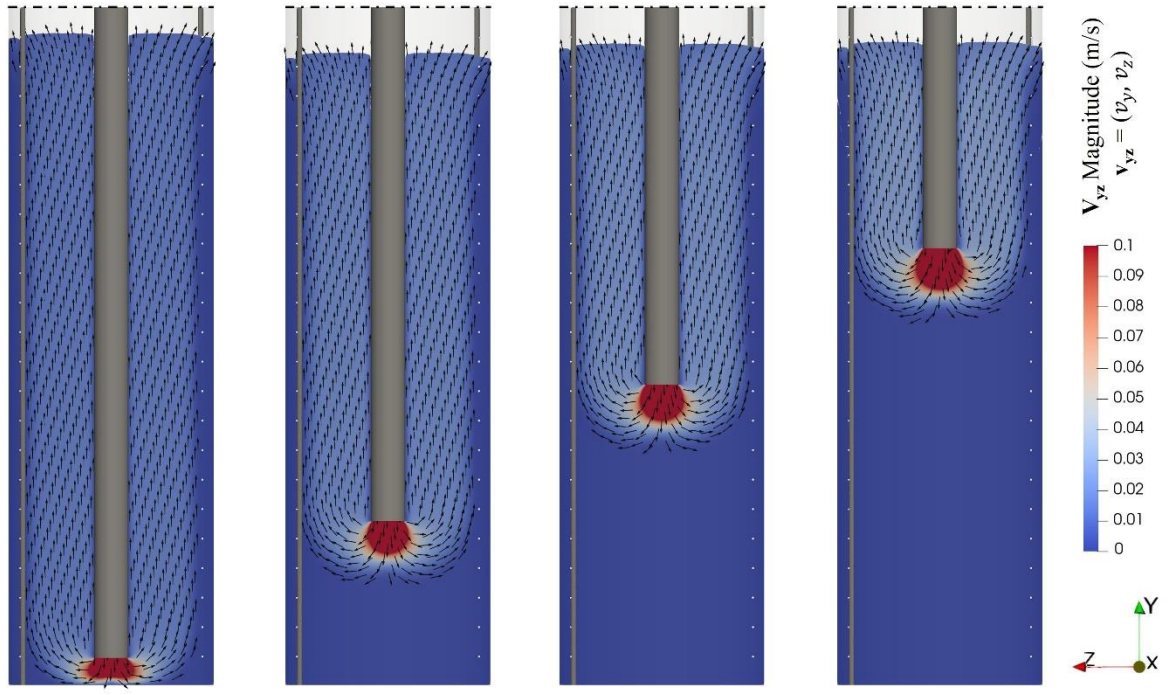
Fig. 3. Initial conditions for all simulated tremie embedment values

RESULTS AND DISCUSSION

Flow Mechanisms

Figure 4 shows a central cross section through the pile, with the velocity magnitude represented by colour and the velocity vectors shown as black arrows. The velocity vectors show the in-plane components (v_y, v_z) of the 3D velocity **v** = (v_x, v_y, v_z). The vectors are assessed at a concrete level of 4.7 m. It is shown that the bulk-flow mechanism is not affected by tremie embedment and remains consistent across all cases. Concrete exits the tremie and spreads radially up to the reinforcement cage but does not enter the cover zone. Concrete flow is restricted within the reinforcement cage, with purely vertical flow observed until the concrete reaches the interface region. At this point, the horizontal component of flow grows, and the concrete fills the cover zone. Mitchell et al. (2026) determined that the bulk-flow mechanism of concrete is determined by the level of reinforcement within the pile, with which the observations from this work agree.

 © Deep Foundations Institute 2026



(a) 3m embedment t = 160s | (b) 2m embedment t = 120s | (c) 1m embedment t = 100s | (d) 0m embedment t = 80s

Fig. 4. Velocity magnitude and vectors at a concrete level of 4.7 m for all embedment values

Charge Distribution

The final distribution of both concrete charges at the end of the pour is visualised in Fig. 5. As in Fig. 3, the right image of each case is a 2D slice through the centre of the pile. The left image is a 3D view, with the left half visualising both concrete charges and the right half visualising only the second. The final charge distribution varies significantly with different tremie embedment levels. The observed trend is that charge two enters the cover zone earlier as tremie embedment is decreased. For both 3 m and 2 m embedment, charge two does not enter the cover zone before the pour is completed. In the case of 3 m embedment, there is still a head of charge one of 1.28 m from the interface region. With 2 m embedment, charge two is much closer to being consumed within the cover zone, with a charge one head of 0.14 m from the interface region. For both 1 m and 0 m embedment, charge two is observed to be consumed in the cover zone. This consumption begins 5.34 m from the pile base with 1 m embedment, and 3.85 m with 0 m embedment. If the pouring process were modelled for deeper piles, in all four cases, charge two would eventually enter the cover zone, just at different depths and times.

By comparing the charge distribution after the pour with the initial concrete distribution, it can be shown that the volume of charge one being displaced is highly dependent on the tremie embedment, leading to the variations in charge distribution previously described. In Fig. 5, for each embedment value, the regions of charge one that are displaced during the pour are highlighted in the left images, while the locations where this displaced concrete ends up are highlighted in the right image. Effectively, all concrete above the tremie exit within the reinforcement case is displaced, along with a semi-ellipsoid volume beneath it. This semi-ellipsoid has a horizontal semi-axis of approximately 0.627 m (the distance between the pile centre and the inside of the reinforcement cage) and an average vertical semi-axis of 0.55 m (the depth at which the second concrete charge penetrates the first). This "penetration depth" remains relatively constant, with variations between all cases of less than 0.04 m. As previously described, the concrete at the interface region is slowly consumed into the cover zone before being replaced by the concrete below. Therefore, as tremie embedment increases, the volume of concrete that must be consumed into the cover zone before the subsequent charge reaches the interface region also increases, thus increasing the time taken for the fresh charge to enter the cover zone.

 © Deep Foundations Institute 2026

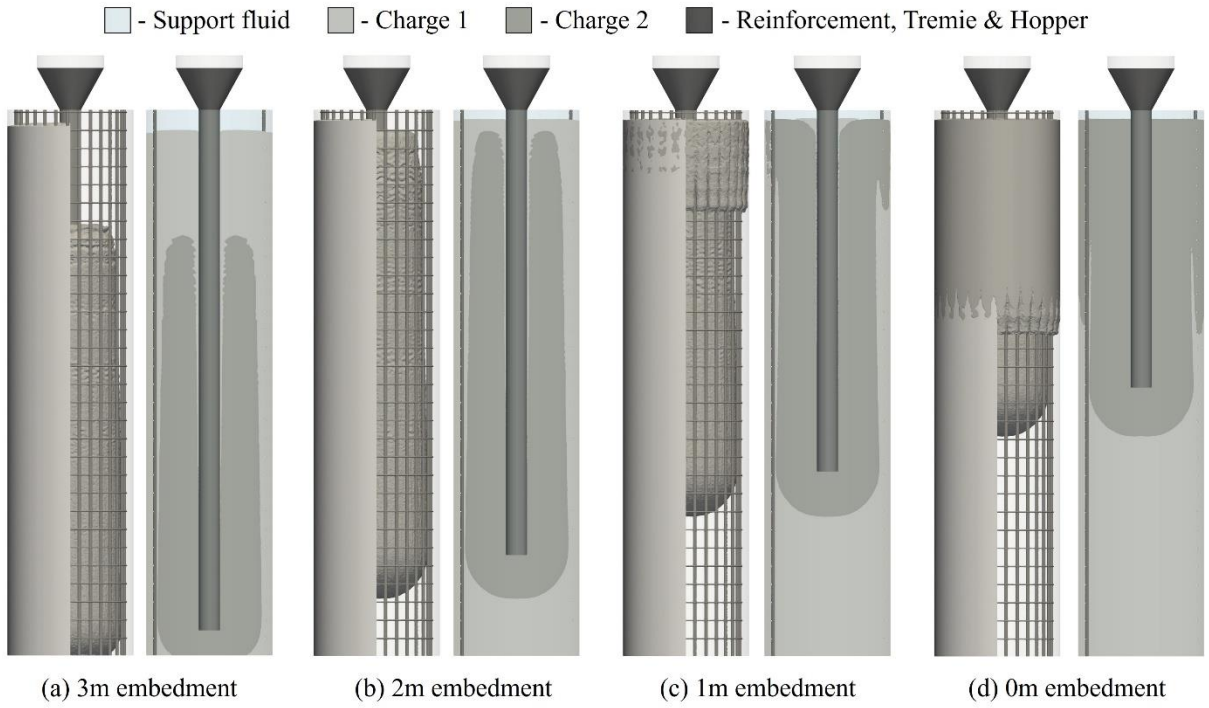


Fig. 5. Final charge distributions for all simulated tremie embedment values

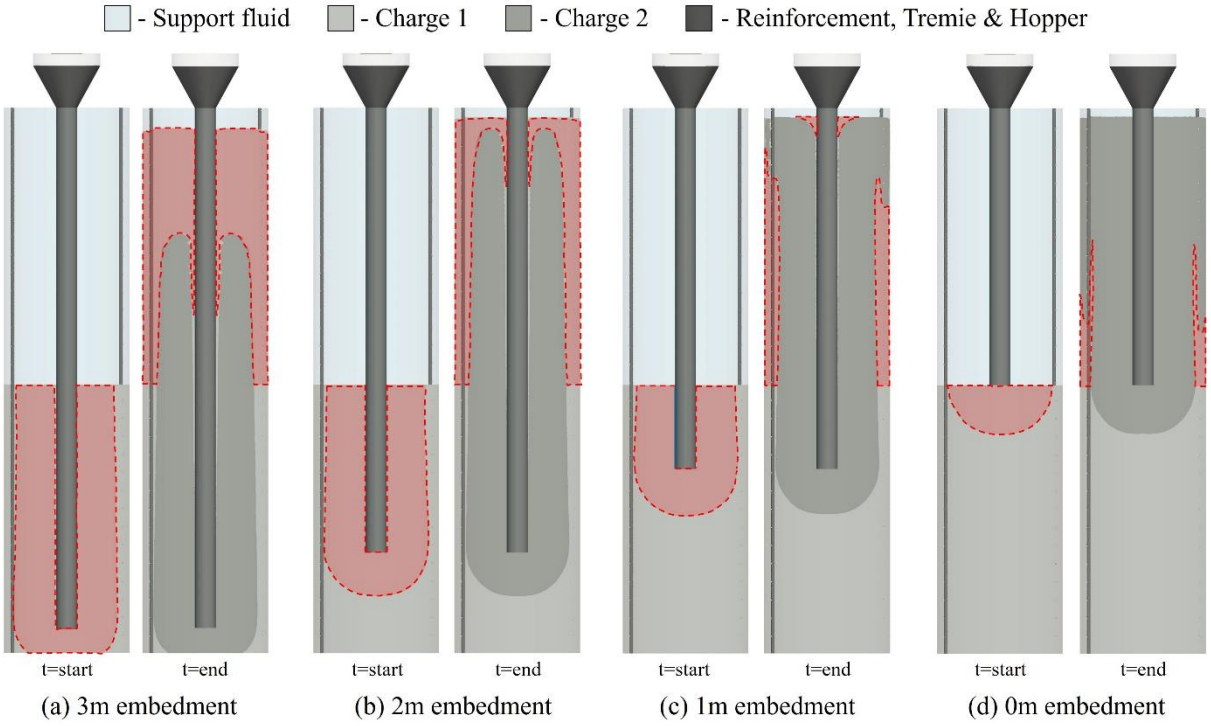


Fig. 6. Volume conservation of displaced concrete

Pour Times

The use of a gravity-driven model in this research makes the concrete flow rate an observable, time-dependent property. Figure 7 plots the average concrete velocity from the tremie outlet throughout the duration of the pour. The general flow profile shown can be split into three distinct stages: acceleration, between labels (a) and (b), deceleration, between (b) and (c) and settling, between (c)

and (d). The labels are applied to the 3 m embedment case, but this flow profile applies to all cases. At the beginning of the pour, the tremie is filled with stationary concrete (point a). After initiating flow, the concrete accelerates until a maximum velocity is reached (point b). As concrete flows into the pile, the height of the concrete within the pile increases, while the height of the concrete in the tremie remains constant. Therefore, the pressure differential driving the flow gradually decreases, reducing the velocity between stages (b) and (c). At point (c), the total volume of charge two has entered the system, and concrete stops being pumped into the hopper. The concrete level within the tremie begins to decrease, causing a more rapid deceleration of flow until hydrostatic equilibrium is reached at point (d), completing the pour.

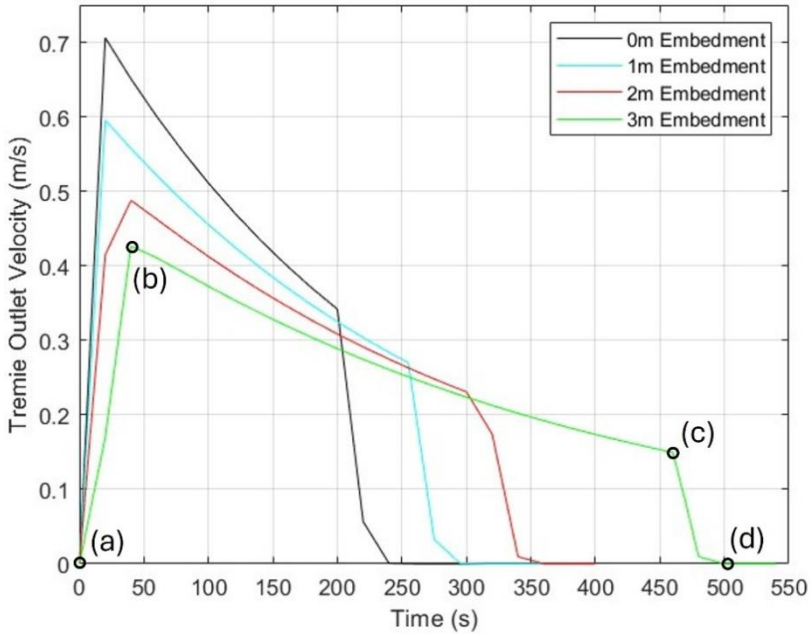


Fig. 7. Average concrete velocity at the tremie outlet over the duration of the pour

Reducing the tremie embedment leads to higher maximum and sustained velocities throughout the pour, resulting in shorter pour times. Pour times range between 240 and 500 seconds, and maximum velocities range between 0.425 and 0.707 m/s. The pressure differential at the exit of the tremie drives concrete flow; a comparison of these hydrostatic pressures for 3 m and 0 m embedment is shown in Fig. 8. The pressure differential at the tremie exit, ΔP, is calculated as shown in Equation 2. Where $P_{i,T}$ is the hydrostatic pressure inside the tremie, P_i is the hydrostatic pressure inside the pile, g is gravitational acceleration, ρ_c is the density of concrete, ρ_{sf} is the density of support fluid, $h_{c,T}$ is the height of concrete inside the tremie, h_{sf} is the height of support fluid, h_h is the hopper height, and h_e is the embedment length.

$$\Delta P = P_{i,T} - P_i, \text{ where } P_{i,T} = \rho_c g\, h_{c,T}, \text{ and } P_i = \rho_{sf} g\, h_{sf} + \rho_c g\, h_e \quad [2]$$

Substituting in $h_{c,T} = h_h + h_{sf} + h_e$ and rearranging these equations yields a relationship for ΔP that is solely dependent on gravitational acceleration, the height of the support fluid, and the difference in densities between the concrete and the support fluid, as shown in Equation 3.

$$\Delta P = g h_{sf}(\rho_c - \rho_{sf}) \quad [3]$$

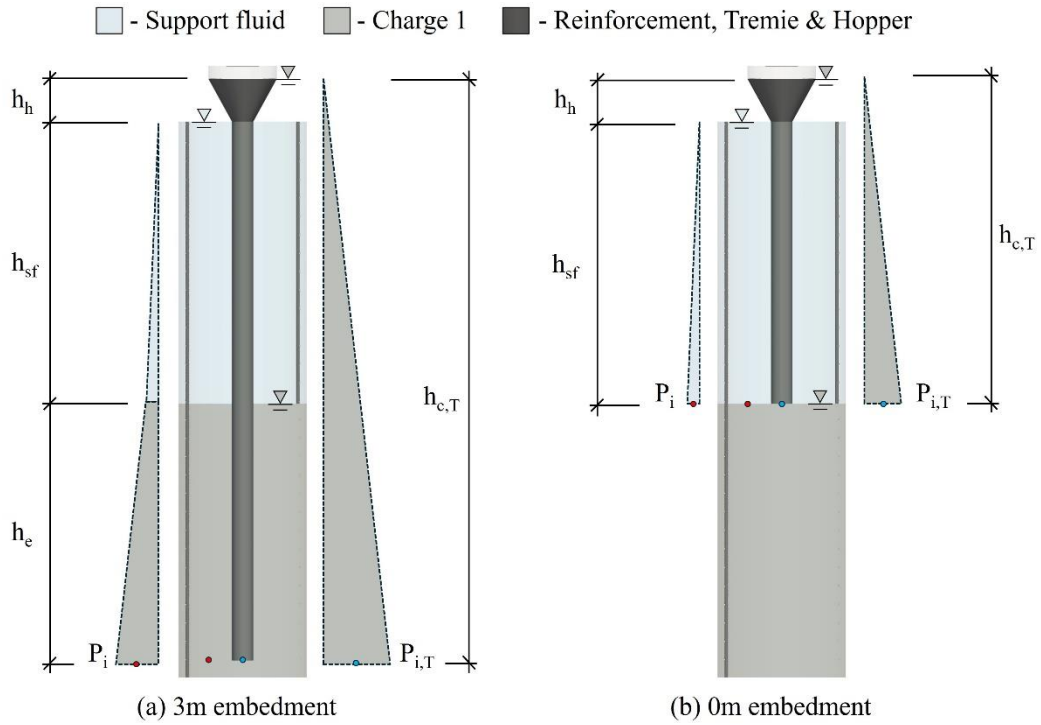


Fig. 8. Comparison of hydrostatic pressures at the tremie exit for 3 m and 0 m embedment

Interestingly, the term for tremie embedment cancels out; reducing the tremie embedment does not increase the pressure differential. To initiate concrete flow, the weight of concrete in the tremie must overcome the hydrostatic fluid pressure, the resistance of concrete already poured, and the friction between the concrete and the inside surface of the tremie (EFFC/DFI, 2024). Using a shorter tremie pipe to reduce embedment would reduce pipe friction and, more significantly, the volume of previously placed concrete that needs to be displaced by the fresh concrete, as shown in Fig. 6. Initially, the concrete within the pile is at rest. As it is a non-Newtonian Bingham fluid, for this concrete to be displaced, stress above the concrete's yield stress must be applied. Overcoming this yield stress for a greater volume of concrete absorbs more energy from the fresh concrete, reducing its maximum velocity and thus increasing pour time.

The minimum tremie embedment values are specified in industry codes and guidelines to ensure that the tremie is continuously submerged in concrete. Failure to achieve embedment would result in concrete being poured directly into the support fluid, increasing mixing between the concrete and the support fluid and compromising the quality of the concrete within the element. Concrete level is measured with simple equipment, typically a weighted tape, which relies on the operator to determine when it contacts the concrete region by touch. Due to the somewhat subjective nature of this technique, the measurements will include some degree of error. The 3 m minimum embedment ensures that there is a buffer to allow for this error. The risk of using even smaller tremie embedment values is that the actual embedment may be lower than predicted, and, in the worst case, the tremie could end up not embedded at all.

CONCLUSIONS

Within this research, numerical modelling was conducted to assess the influence of tremie embedment on concrete flow within bored piles. It has been found that the level of tremie embedment does not influence the bulk flow behaviour of fresh concrete within bored piles. The bulk flow behaviour is dependent on the level of reinforcement within the pile, as discussed by Mitchell et al. (2026). As all piles simulated in this study were fully reinforced, the consumption flow mechanism of concrete into the cover zone was consistently observed.

However, the embedment value influences the rate at which subsequent concrete charges are consumed into the cover zone. Concrete above the tremie exit must be displaced and consumed into the cover zone before the next charge can enter the cover zone. As tremie embedment decreases, the volume of concrete above the tremie exit also decreases, increasing the rate at which the fresh concrete charge enters the cover zone. Regardless of the tremie embedment, the fresh concrete penetrates approximately 0.55 m into the previous charge before the flow is redirected, leaving all concrete below this point unaffected by the subsequent pour.

Reducing the tremie embedment has been found to increase the maximum outflow velocity and thus decrease the total time required to complete the pour. This increase in flow rate is not due to a higher pressure differential, but rather to the reduction in concrete volume that must be displaced. Overcoming the yield stress of concrete already in the pile removes energy from the inflowing concrete; if there is a larger volume to displace, the flow rate therefore decreases.

While the premise of faster pour times sounds promising, as previously discussed, going below the recommended embedment significantly increases the likelihood of having insufficient embedment due to inaccurate concrete level measurements. Therefore, it is recommended that contractors maintain a minimum tremie embedment of 3 m.

ACKNOWLEDGEMENTS

The authors gratefully acknowledge the support from the Engineering and Physical Science Research Council's (EPSRC) ICASE grant 2456652 and the financial and technical support from industry partner Arup.

REFERENCES

Barker, C. and Nicholson, D., 2025. Review of slump-flow concrete testing from four UK projects. Ground Engineering.

British Standards Institution, 2010a. BS EN 1536:2010+A1:2015: Execution of special geotechnical work, bored piles.

British Standards Institution, 2010b. BS EN 1538:2010+A1:2015: Execution of special geotechnical work, diaphragm walls.

De Schryvey, R. and El Cheikh, K. and Lesage, K. and De Schutter, G., 2018. CFD implementation of time-dependent behaviour – application for concrete pumping. Symposium on Concrete Modelling, Netherlands.

EFFC/DFI Concrete Task Group, 2024. Guide to Tremie Concrete for Deep Foundations, 3rd Edition.

EFFC/DFI Support Fluids Task Group, 2019. Guide to Support Fluids for Deep Foundations, First Edition.

Fierenkothen, C. and Pulsfort, M., 2019. Investigations on fresh concrete flow mechanisms in bored piles based on CFD simulations. Proc. ECSMGE on Soil Mechanics and Geotechnical Engineering, Reykjavik.

Institution of Civil Engineers, 2016. ICE Specification for Piling and Embedded Retaining Walls.

Jeyaraj, J. A. and Perez, A. and Zayed, A. and Mullins, A. G. and Tejada-Mertinez, A. E., 2023. Computational Fluid Dynamics Modeling of Concrete Flows in Drilled Shafts. Fluids, Vol 9.

Kränkel, T. and Gehlen, C., 2018. Rheology and workability testing of deep foundation concrete in Europe and the US. Research Report No. 20-F-0107, Technical University of Munich.

Mitchell, T. and Li, C. and Barker, C. and Wilkes, C., 2026. Understanding concrete flow mechanisms in deep foundation construction using numerical modelling. Proc. International Conference on Soil Mechanics and Geotechnical Engineering, Vienna.

Wilkes, C. 2021. Modelling tremie concrete placement in deep foundations, PhD Thesis, University of Cambridge.

 © Deep Foundations Institute 2026

APPENDIX

The following demonstrates how Equation 3 can be obtained from Equation 2.

$$\Delta P = \rho_c g\, h_{c,T} - \rho_{sf} g\, h_{sf} - \rho_c g\, h_e$$

$$\Delta P = g(\rho_c h_{c,T} - \rho_{sf} h_{sf} - \rho_c h_e)$$

Substituting in: $h_{c,T} = h_h + h_{sf} + h_e$

$$\Delta P = g(\rho_c(h_h + h_{sf} + h_e) - \rho_{sf} h_{sf} - \rho_c h_e)$$

$$\Delta P = g(\rho_c(h_h + h_{sf} + h_e - h_e) - \rho_{sf} h_{sf})$$

$$\Delta P = g(\rho_c(h_h + h_{sf}) - \rho_{sf} h_{sf})$$

$$\Delta P = g h_{sf}(\rho_c - \rho_{sf}) + g\rho_c h_h$$

In full-scale piles, $h_h << h_{sf}$ and so the second term can be assumed to be negligible.

$$\Delta P = g h_{sf}(\rho_c - \rho_{sf})$$

 © Deep Foundations Institute 2026

DEVELOPMENT OF REGULATORY FRAMEWORK FOR THE DESIGN OF DEEP FOUNDATIONS AND GROUND IMPROVEMENT IN NEW ZEALAND

Alexei Murashev, WSP, Wellington, New Zealand, +6444717000, Alexei.Murashev@wsp.com
Kiran Saligame, MBIE, Christchurch, New Zealand, +6449170199, Kiran.Saligame@mbie.govt.nz
Nigel Lloyd, NZTA, Wellington, New Zealand, + 6448945200, Nigel.Lloyd@nzta.govt.nz

ABSTRACT

Soft and liquefiable soils are a significant concern in New Zealand (NZ) due to the country's seismicity. NZ experiences approximately one magnitude 7 and ten magnitude 6 earthquakes each decade. The use of deep pile foundations penetrating through poor soils into competent materials is very common. On many projects, ground improvement is used to prevent liquefaction and lateral spreading. Over the last decade, major advances have occurred in NZ's regulatory and technical framework for deep foundations and ground improvement, driven by lessons learned from the Canterbury and Kaikōura earthquake sequences. National research programmes have resulted in significant updates to the industry guidance for pile foundations and liquefaction mitigation. These developments have improved design consistency, clarified seismic performance expectations, and strengthened integration between geotechnical hazard characterisation and foundation design. Recent WSP case studies demonstrate measurable improvements achieved under the updated regulatory framework, including reductions in liquefaction vulnerability, improved stiffness uniformity beneath major structures, and enhanced seismic resilience of infrastructure. Quantitative outcomes, such as settlement reduction, increased lateral spread resistance, and material optimisation through advanced soil-structure interaction analysis illustrate the practical benefits of contemporary design approaches. Key lessons learned include the importance of early seismic hazard definition, site-wide mitigation strategies, and integrated structural–geotechnical design. These insights support ongoing refinement of NZ's national standards and contribute to long-term infrastructure seismic resilience.

Keywords: New Zealand, piling, ground improvement, foundations, design, seismic, guidelines, standards

INTRODUCTION

NZ earthquakes in the last ten years caused 186 deaths and an economic loss of NZ$42 billion. After the 2010–2011 Canterbury Earthquakes Sequence, 10,000 homes required rebuilding and 3,500 were demolished. Around 1,354 commercial buildings were demolished. In the 2016 Kaikōura Earthquake, a total of 904 road bridges were affected and two reached the life-safety limit state, suffering severe damage; more than 40 buildings were severely damaged, and several were demolished. Reliable deep foundations and ground improvement systems are central to achieving seismic resilience in NZ, particularly in regions underlain by soft or liquefiable soils. However, the engineering challenge extends beyond general seismic hazard: the key issue is how NZ's high seismicity has driven the evolution of foundation design philosophy, regulatory reform, and improved geotechnical–structural integration. While deep piles founded in competent materials tend to perform well, recent earthquakes revealed critical vulnerabilities within complex soil profiles such as liquefiable sediments beneath or around bearing layers which can induce excessive settlements, lateral displacements, and structural distortion. These lessons have directly influenced the transformation of NZ's regulatory framework over the last decade. New regulatory documents and design methodologies now place greater emphasis on advanced soil–structure interaction analysis, liquefaction characterisation, and site-wide mitigation strategies. These innovations reflect NZ's shift from prescriptive engineering practices toward performance-based seismic design. Ground improvement techniques in NZ aim to mitigate the effects of settlement and low bearing capacity of soft soils as well as liquefaction and lateral spreading. The purpose of this paper is to summarise the development of NZ's regulatory framework for deep foundations and ground improvement; examine how lessons from recent earthquakes have informed design reforms and present case studies demonstrating implementation of modern guidance on major infrastructure projects.

 © Deep Foundations Institute 2026

DAMAGE IN RECENT EARTHQUAKES

Recent NZ earthquakes have highlighted instances where pile foundations and ground improvement systems underperformed, causing significant disruption to road, rail, and harbour assets as well as buildings. As summarised earlier, the 2016 Kaikōura event affected approximately 904 road bridges and led to severe damage to more than 40 buildings; several major structures, including the BNZ Harbour Quay Building and AMI Stadium, were ultimately demolished. Observed damage modes included differential settlement due to spatially variable stiffness, lateral spreading demands on foundations, and loss of drainage efficiency in granular inclusions, all of which compromised structural performance. For example, the piled BNZ Harbour Quay Building on Wellington's waterfront founded on liquefiable reclamation fills with partial stone column improvement sustained irreparable damage involving both the foundation system and the superstructure, leading to demolition (Fig. 1; Siddiqui et al., 2019). Only a portion of the footprint (≈25% adjacent to the shoreline) was treated to mitigate lateral spreading, which introduced substantial stiffness non uniformity across the building plan. The resulting eccentricity between the centre of mass and centre of rigidity promoted torsional response under shaking and contributed to the observed damage. Available information indicates the building was designed and consented in line with the prevailing standards at the time; however, key deficiencies included reliance on partial footprint improvement, and inadequate control of plan stiffness variability. At Christchurch's AMI Stadium, both the foundation system and superstructure were damaged beyond repair. Stone columns intended to mitigate liquefaction reportedly lost drainage effectiveness due to sand infiltration during earthquake loading (Fig. 1).



Fig. 1. BNZ Harbour Quays Building, Wellington, (left) and AMI Stadium, Christchurch, (right) before and during demolition

The facility is understood to have been designed to the applicable standards of its era; however, observed performance suggests that the assumed drainage and post shaking pore pressure dissipation were not fully achieved in practice, and that liquefaction demands were underestimated for the as built soil profile. Transport assets also experienced geotechnical and structural impacts, including embankment settlements and bridge damage attributable to liquefaction and lateral ground movement (Fig. 2).

 © Deep Foundations Institute 2026



Fig. 2. Seismic damage to NZTA's Mororimu rail overbridge in Kaikoura Earthquake: left – settlement of approach embankment (Mason et al., 2017); right – cracking below knee joint of central pier column (Cubrinovski and Bray, 2017)

Engineering lessons learned: (i) Ensure deliberately controlled stiffness across the full structural footprint; partial ground improvement should be avoided or explicitly justified by analysis; (ii) adopt holistic, site wide mitigation where liquefaction and lateral spreading hazards exist; (iii) explicitly validate drainage and post shaking pore pressure dissipation assumptions for granular inclusions (e.g., stone columns) under seismic sequences; (iv) integrate geotechnical and structural models to capture complex soil–structure interaction; (v) the earthquake damage highlighted the need for national research programmes to update the industry guidance for pile foundations and ground improvement.

REGULATORY FRAMEWORK

NZ's regulatory framework for deep foundations and ground improvement has undergone substantial evolution, shaped by both historical institutional practice and the lessons learned from recent seismic events. Early state-delivered engineering under the Public Works Department (PWD) and Ministry of Works (MoW) provided a de facto national practice baseline; however, modern regulation is now centred on the NZ Building Code, associated Verification Methods, Earthquake Geotechnical Engineering Modules, and specialist NZ Transport Agency's (NZTA) guidance. This shift reflects the transition from prescriptive, government led standards to a more distributed, performance-based regulatory system. The shift is led by the following organisations: Ministry of Business, Innovation & Employment (MBIE) leads regulatory development and issues Verification Methods (e.g., B1/VM2); MBIE and NZ Geotechnical Society (NZGS) co-develop the Earthquake Geotechnical Engineering Modules; NZ Society for Earthquake Engineering (NZSEE) contributes seismic expertise to the Modules and seismic assessment guidelines; NZ Earthquake Commission (EQC) funds research and supports data collection (e.g., NZ Geotechnical Database); NZTA provides sector-specific guidance (e.g., Bridge Manual) that serves as an alternative compliance path; NZGS and NZSEE provide technical leadership and practitioner guidance. The first NZ standard with recommendations on design of simple pile foundation systems – NZS 3604 "Timber-framed buildings" was published in 1978. NZS3604 is a technical standard that sets out specifications and methods for designing and constructing light timber-framed houses and other low-rise buildings including their foundation systems. The standard allows the construction of code-compliant buildings up to three storeys high (two full storeys and a third storey in the roof space) on good ground without the need for specific structural engineering and has been updated multiple times since 1978. The first edition of NZS 3101 Code of practice for the design of concrete structures was published in 1982. NZS 3101 provides recommendations for the design of concrete piles, including detailing requirements for reinforced concrete piles and pile caps. The key aspects covered by NZS 3101 include ensuring the foundation can support design loads, including earthquake loads, and addressing potential overstrength actions.

For many years NZ did not have geotechnical standards or guidelines for the design of pile foundations or ground improvement. The first edition of NZ Building Code Verification Method B1/VM4 – Foundations was published in 1992. On 28 July 2025, MBIE published Verification Method B1/VM2 – Geotechnical Design of Foundations Second Edition, which replaced B1/VM4.

The document outlines the procedures for the ultimate limit state design of foundations, including pile foundations, to comply with NZ Building Code. However, it doesn't cover the determination of soil parameters, serviceability limit state deformations or ground improvement. Additionally, it assumes general ground stability and does not apply to foundations on slopes or specific soil types like soft materials, loose sands or liquefiable materials. The document has been amended multiple times since 1992 and is currently being reviewed by MBIE.

In 2002, AS/NZS 1170.0 Structural Design Actions – General Principles was published. NZS 1170.5 Structural Design Actions – Earthquake Actions – NZ was published in 2004. The two standards specified static and seismic design actions for structures, including their foundation systems. NZS 1170.5 replaced the old NZS 4203 – Code of Practice for General Structural Design and Design Loadings for Buildings, published in 1992 that sets out in limit state format requirements for general structural design and design loadings for buildings, including their foundation systems. The minimum structure performance requirements are set in the NZ Building Code. The design of pile foundations and ground improvement in NZ must comply with these legal minimum requirements and requires close collaboration between geotechnical and structural designers, as well as the Building Consent Authorities (BCAs). The structure of the NZ regulation framework is shown in Fig. 3. Compliance with the Building Code can be achieved via the MBIE Compliance Documents or through Alternative Solutions. The MBIE Compliance Documents are accepted means of compliance with the Building Code clauses. Verification Method B1/VM2 provides an accepted pathway for meeting NZ Building Code Clause B1 Structure. An Alternative Solution, in contrast, is a means of demonstrating compliance with the performance requirements of the Code using approaches not covered by the Compliance Documents. International design standards and guidelines as well as the NZTA Bridge Manual (NZTA, 2022) with recent amendments, are commonly used as an alternative design framework for pile foundations and ground improvement in NZ. NZTA Bridge Manual Section 6 “Site stability, foundations, earthworks and retaining walls” covers geotechnical design of pile foundations and ground improvement. Section 6 was developed prior to the publication of several key MBIE/NZGS Modules (NZGS and MBIE, 2021). In the absence of more contemporary guidance at the time, it inadvertently became a de facto reference for a broad range of geotechnical practices, including site investigations, liquefaction assessment, and the design of deep foundations and ground improvement. While this supported consistency in practice, it also highlights the need to align earlier guidance with current standards to ensure best-practice outcomes.

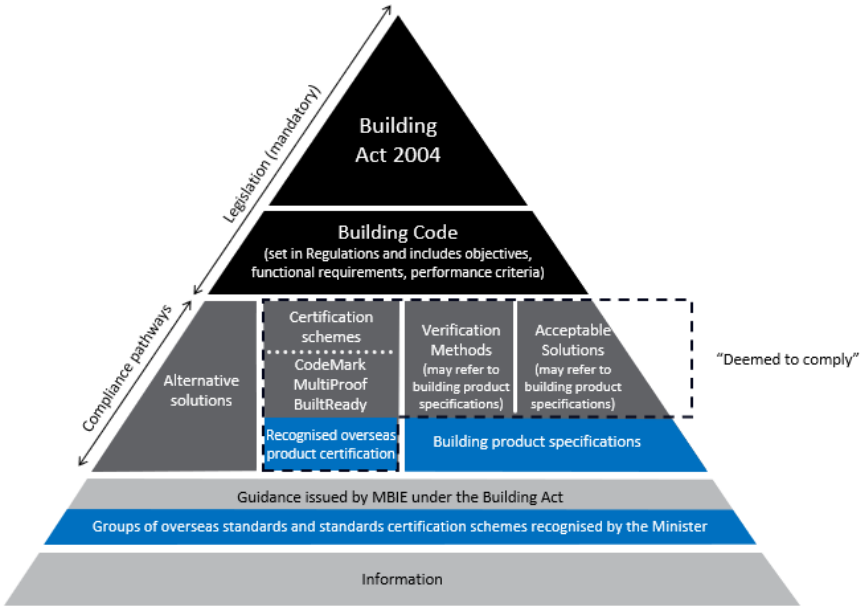


Fig. 3. NZ regulation framework showing ways to comply with the Building Code

 © Deep Foundations Institute 2026

Lack of advanced geotechnical design standards in NZ resulted in unreliable geotechnical design and damage to structural foundation systems, including pile foundations and ground improvement, in earthquakes and other natural disaster events. To advance the NZ geotechnical design framework for pile foundations and ground improvement, MBIE, EQC, NZGS, NZSEE and NZTA have been funding multiple research and standard development projects in recent years. MBIE, NZGS and the NZSEE have put substantial effort into the preparation of the Earthquake Geotechnical Engineering Standards (Modules), which specify seismic hazard as well as geotechnical design methods and requirements for foundation systems, including pile foundations and ground improvement (NZGS and MBIE, 2021). The structure of the updated revision of MBIE / NZGS Modules is shown on Fig. 4. The purpose of the Modules is to improve the overall NZ national geotechnical design practice and to promote a consistent approach.

The Modules provide information on main design principles but are not detailed design handbooks. Module 4 covers the design of foundations, including pile foundations. Modules 5 and 5A provide advice on design and construction of ground improvement (Murashev and Keepa, 2022). The Modules are classified as Section 175 Guidance under the NZ Building Act and can be used to demonstrate compliance with the NZ Building Code. Through its Research Programme, NZTA has invested in innovative research that addresses critical knowledge gaps in the design of pile foundations and ground improvement. NZTA projects relating to geotechnical practice included: Development of NZTA Bridge Manual Section 6 (Geotechnical); Guidance for the design of integral bridges; Design guidance for piled bridges in NZ for liquefaction and lateral spreading effects (Murashev et al., 2014); and Examples of analysis of piled bridges at sites prone to liquefaction and lateral spreading. NZGS prepared and published several guidelines, including Construction specification for bored and driven piles. MBIE, NZSEE and NZGS have developed guidelines for seismic assessment of existing buildings, divided into sections C1 through C10 (MBIE, 2017). Sections C1 to C4 provide the foundational aspects of the Detailed Seismic Assessment (DSA) process, including the overview (C1), assessment procedures (C2), earthquake hazard and loading (C3), and geotechnical considerations (C4).

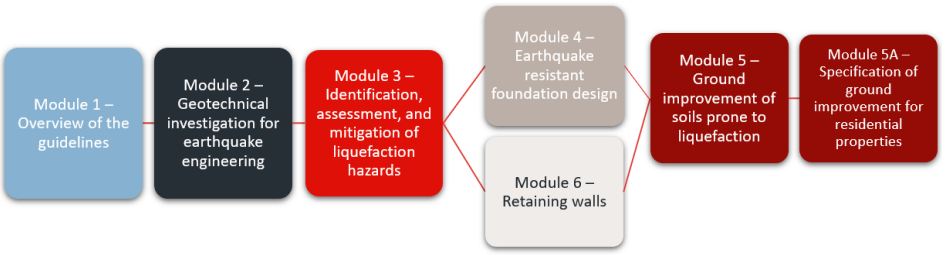


Fig. 4. Structure of 2021 Earthquake Geotechnical Engineering Modules

Section C4 covers pile foundations, particularly in the context of how they perform under seismic loading. In developing these NZ documents, a wide range of international standards, guidelines, research, and case studies were reviewed to ensure alignment with state-of-the-art design practices, particularly those from high seismicity regions such as Japan, California, and Chile.

While MBIE oversees building control and geotechnical data stewardship through the NZ Geotechnical Database, Land Information NZ plays a complementary role in managing geospatial datasets, ensuring their discoverability and integration with land-related regulatory functions. The MBIE/NZGS Modules address critical aspects such as soil strength, settlement, liquefaction and lateral spreading, soil–structure interaction, and foundation performance. These considerations are integral to seismic design and are especially relevant given NZ's high liquefaction susceptibility. Recent submissions on NZ Technical Specification TS 1170.5 Structural Design Actions (Earthquake Actions NZ) have highlighted concerns about its alignment with Verification Method B1/VM1-Structural Design of Buildings and the Earthquake-Prone Building legislation. Practitioners have called for clearer guidance to avoid inconsistent strengthening practices and to ensure sustainable retrofit outcomes. As noted by NZGS, the proliferation of documents has led to practitioner

uncertainty, often raising the question: “Which document should I use, and when?” This underscores the need for harmonised guidance and clearer compliance pathways. The 2022 update of the National Seismic Hazard Model (NSHM) has increased seismic hazard parameters across many NZ regions directly impacting geotechnical design, particularly for pile foundations and liquefaction-prone sites. The effects of the increased seismic hazard include triggering liquefaction, cyclic softening, lateral spreading and seismic-induced slope instability in lower return period events subsequently increasing design demands on piling systems. Recent collaborative initiatives, such as the NZGS, NZSEE, MBIE and NZTA conferences, have provided informal updates and opportunities for alignment to support practitioners navigating the evolving regulatory landscape. Recent WSP projects where innovative piling and ground improvement solutions have been applied based on the current regulatory framework are discussed below.

GROUND IMPROVEMENT ON NZTA PROJECTS

Non-piled MSE bridge abutments such as Reinforced Earth (RE) walls and, more recently, geogrid-reinforced soil (GRS) walls have been used on NZTA state highway projects in NZ. Only geosynthetic products certified by NZTA can be used in MSE walls and geogrid-reinforced rafts on NZ state highway projects. Quite often MSE bridge abutments need to be founded on soft or liquefiable ground. Ground improvement and preloading are commonly used to avoid the need for very deep and costly piled bridge abutments. Shallow soft soil layers are normally replaced by geogrid-reinforced granular rafts or improved by in-situ mass stabilisation (IMS) – mixing in-situ soils with liquid cement grout (Fig. 5). If non-liquefiable soft soils extend to a substantial depth, preloading and surcharging are normally used. Alternatively, fully built GRS bridge abutments founded on soft soils can be preloaded using a system of steel beams and stressed anchors that penetrate through the soft soil layer into competent bedrock at depth, as shown in Fig. 6. For MSE bridge abutments founded on liquefiable soils, stone columns or cutter soil mixing (CSM) lattice ground improvement have been used to mitigate liquefaction potential of soils beneath MSE bridge abutments. A typical CSM lattice is shown in Fig. 9.

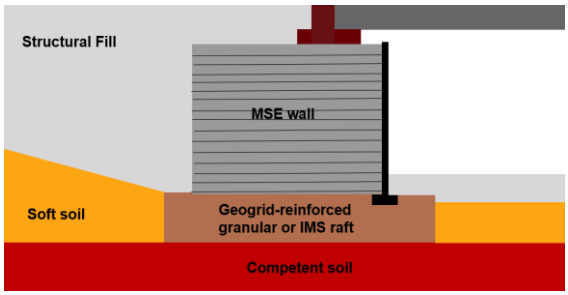


Fig. 5. Shallow ground improvement beneath MSE bridge abutment



Fig. 6. Preloading of MSE bridge abutment using ground anchors

These methods are selected based on site-specific geotechnical conditions, performance requirements, constructability constraints, and cost considerations. While structures founded on poor ground may not initially meet bearing capacity, deep-seated stability, or settlement criteria, the ground

improvement methods described above enhance soil strength and stiffness, enabling designers to satisfy these critical geotechnical performance requirements. The current editions of the NZTA Bridge Manual and the MBIE/NZGS Modules provide a robust and consistent basis for the design of bridge abutments on liquefiable ground.

COMPLEX GROUND IMPROVEMENT FOR TE KAHA – CANTEBURY'S MULTI-USE ARENA

Te Kaha is a new, permanently covered multi-use arena under construction in Christchurch. The $683 million facility will seat 30,000 for sporting events and up to 36,000 for concerts (Fig. 7). The site is located in Christchurch's central city and has a well-documented history of liquefaction during recent seismic events. Extensive seismic hazard assessments, geotechnical and hydrogeological investigations, and detailed design studies were undertaken to support the development of a robust foundation system. The adopted foundation system comprises a dense grid of Rammed Aggregate Piers (RAPs) overlain by stiff reinforced concrete rafts and intersecting grillage beams, forming an integrated load-transfer platform (Murashev, 2024a). Three foundation options were evaluated during concept design: (i) shallow foundations with ground improvement, (ii) deep piled foundations, and (iii) a hybrid system. Shallow foundations alone were ruled out due to insufficient bearing capacity and unacceptable liquefaction risk. The selected solution involved an up to 12 m-thick improved crust formed by RAPs, supporting a network of reinforced concrete grillage beams and raft foundations designed to distribute loads and control differential settlement. To resist uplift and seismic overturning, "tension RAPs" were used—these included steel base plates and vertical bars extending through the column into the overlying concrete elements. The design process included: (i) pre- and post-improvement liquefaction triggering assessments; (ii) 3D settlement modelling to derive equivalent Winkler spring stiffnesses for structural analysis; (iii) bearing capacity and deep-seated stability checks under static and seismic conditions; (iv) 3D finite element (FE) modelling of soil–structure interaction; and (v) geotechnical peer review of the structural FE model to confirm correct application of soil parameters. A total of 8,331 RAPs, including 1,092 tension RAPs, were installed to depths of 6–12 m across the 6.8-hectare site. The 600 mm diameter RAPs were constructed within the structural foundation footprint at an average rectangular spacing of 1.85 m. An artist's impression of Te Kaha and a 3D image of the structural foundation system are shown in Fig. 7. Post-improvement CPT data confirmed that the target level of densification had been achieved, with significant reductions in liquefaction triggering potential. In addition, settlement monitoring during and after construction validated the predicted performance of both the improved ground and the structural foundation system. This project demonstrates the successful application of the current ground improvement design framework, particularly the MBIE/NZGS Modules, to meet stringent seismic performance requirements on a large-scale, high-profile public facility.

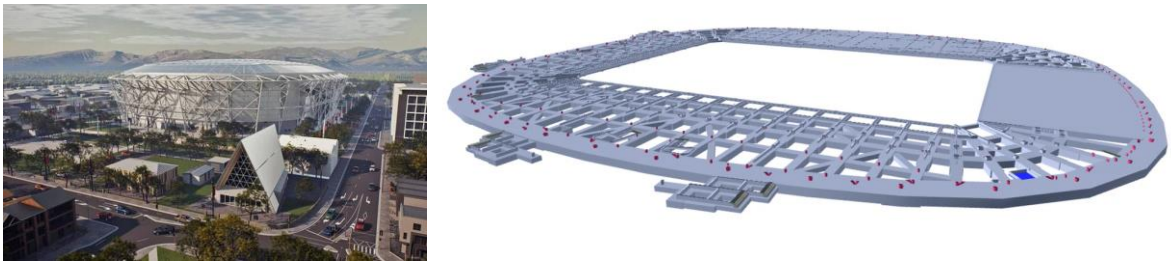


Fig. 7. Artist's impressions of Te Kaha (images sourced from www.Te-Kaha.co.nz) – left; 3D image of the reinforced concrete foundation (improved soil crust beneath the foundation is not shown) – right

INNOVATIVE RESIN INJECTION GROUND IMPROVEMENT

The Waterloo Water Treatment Plant (WTP) in Wellington is a critical post-earthquake lifeline asset, supplying approximately 40% of the region's potable water. The facility is founded on soils

susceptible to liquefaction and cyclic softening, posing a significant risk to operational continuity during seismic events. Any ground improvement solution had to be implemented while maintaining full operational continuity of the plant, including protection of sensitive infrastructure and buried services. Extensive site characterisation was undertaken, including field investigations and advanced laboratory testing (e.g., cyclic triaxial tests) to assess liquefaction potential and deformation characteristics. Multiple seismic strengthening options were evaluated, with a focus on constructability, performance, and minimal disruption. Expanding polyurethane resin injection was selected as the most suitable ground improvement method due to its low invasiveness, rapid installation, and ability to target specific zones beneath existing structures (Murashev et al., 2023).

The resin expands rapidly upon injection, often to several times its original volume, displacing and compacting adjacent soils, thereby increasing strength and stiffness and reducing void ratios (Fig. 8). A full-scale resin injection trial was collaboratively designed and executed by WSP, Mainmark, and Wellington Water to refine the injection methodology and quantify achievable improvements in soil performance. The trial included real-time monitoring of floor and wall heave, as well as deformation of critical pipelines, to ensure that injection pressures did not compromise structural or operational integrity. The trial demonstrated a significant reduction in liquefaction triggering potential, as evidenced by pre- and post-injection CPT data. Predicted seismic settlements were reduced by over 50%, and bearing capacity checks confirmed compliance with MBIE/NZGS Module 4 criteria. While the short-term improvements in soil strength and stiffness from resin injection are well documented, its long-term performance, particularly regarding durability and resistance to cyclic degradation under repeated seismic loading, remains an active area of research. Although resin injection typically involves higher unit costs than conventional ground improvement methods, it offers a valuable retrofit solution for critical infrastructure. When designed in accordance with MBIE/NZGS Modules, resin injection is especially advantageous in settings where traditional techniques are impractical due to limited access, sensitivity to vibration, or operational constraints.

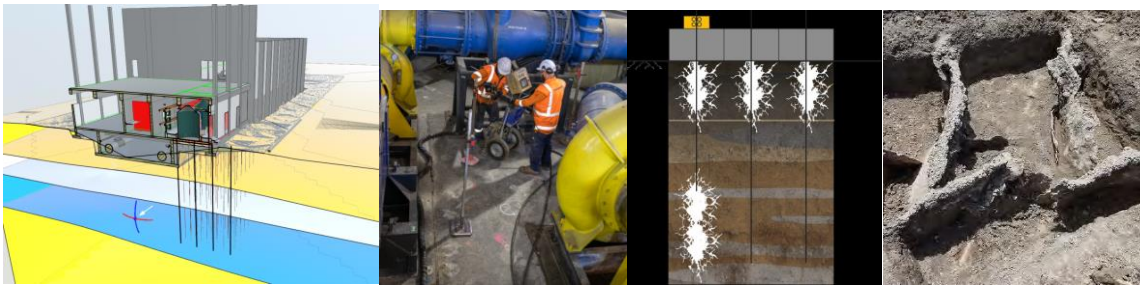


Fig. 8. Left to right: 3D injection model; injection in progress; injection illustration; exposed resin veins

INNOVATIVE SOIL – STRUCTURE INTERACTION ANALYSIS FOR PORT STRUCTURES

In NZ ports, particularly those built on reclaimed land, liquefaction and lateral spreading are significant seismic hazards. Lyttelton Port in Christchurch and Port of Wellington (CentrePort) have experienced severe liquefaction and lateral spreading during past earthquakes, which resulted in damage to the ports' infrastructure. Several NZ port companies have undertaken major resilience and redevelopment programs (Terry et al., 2021). Many of NZ ports' reclamation fills have now been improved by stone columns, vibrocompaction, anchored sheet pile walls, cutter soil mixing and deep concrete barrettes. For new wharf structures, complex soil–structure interaction effects are normally considered. This often involves dynamic time-history 2D and 3D numerical modelling of the wharf structures as well as improved and unimproved ground, using non-linear material models. A typical example of a 3D FE model of a cutter soil mixing (CSM) lattice ground improvement for a new wharf structure founded on liquefiable ground and zones of high shear stresses in CSM lattice walls due to seismic lateral ground movement analysed using time history approach is shown on Fig. 9 (Okada et al., 2025). The 3D finite element analysis was carried out in accordance with the principles of the

MBIE/NZGS Modules, using Plaxis 3D (v2023.1) with a compliant base and free-field lateral boundary conditions to simulate realistic seismic ground response. The CSM lattice was modelled as cement-stabilised soil using a Mohr-Coulomb constitutive model. Liquefiable soils were modelled using the UBC3D-PLM constitutive model, calibrated to match CPT-based cyclic resistance. Rayleigh damping was applied to achieve ~2% critical damping at the site's fundamental frequency. The model was benchmarked against 2D PM4Sand results and validated using empirical methods and published centrifuge data.

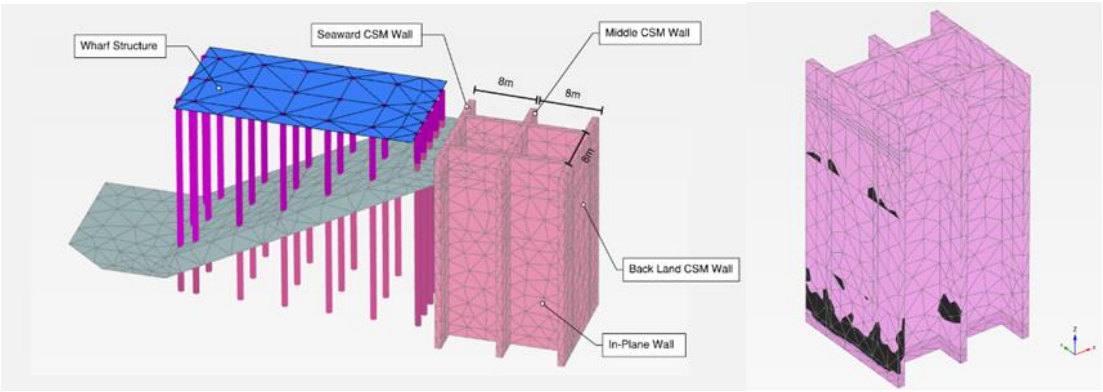


Fig. 9. Left – 3D FE model; right – high shear stress zones in CSM lattice from time-history analysis (reclamation fill was modelled but is not shown)

Advanced time-history FE analysis enabled designers to assess the stress–strain behaviour of piles, revetments, CSM lattice panels, reclamation fill, and natural ground, allowing them to optimise the design to minimise material use and increase seismic resilience of the wharf.

ADVANCED FE ANALYSIS OF SECANT PILE WALLS

Numerical modelling such as FE analysis is widely used to design secant pile walls. For many years, NZ common practice was to represent steel-reinforced concrete element in FE analysis by the means of defining a shell or plate elements with equivalent averaged mechanical properties, often assuming linear elastic performance of the plate. This assumption is deficient because it does not consider plastic deformation of steel and cracking of concrete and overlooks the complementary properties of steel and concrete—steel provides tensile strength and ductility, whereas concrete excels in compressive behaviour. From 2023–2024, more detailed FE modelling of secant pile walls, where the steel and the concrete are modelled as materials with non-linear stress-strain properties, became more common. This design methodology was used to optimise the design of the buried wet well secant pile wall for the Porirua Wastewater Peak Flow Facility (Murashev et al., 2024b), in accordance with MBIE/NZGS Modules' principles. The site soils and the concrete of the piles were modelled as 3D volume elements. The steel H-beams used as reinforcement for the primary piles were modelled as beam elements. The concrete portion of each secant pile was modelled as a cluster of 3D volume elements assigned a Mohr-Coulomb constitutive model in accordance with Bentley's guidelines for concrete (Hadzijanev Ardiac, 2009). The H-beams were modelled with Plaxis 3D's embedded beam elements having elastoplastic behaviour. We used a relatively fine mesh discretisation around the secant pile wall to capture the sharp stress gradients in the concrete and surrounding soil—the concrete "cluster" was meshed with volume elements 0.2 m in size, whereas a coarser mesh was used farther away in the native ground. The concrete and soil elements share nodes at their contact to simplify the model. Lateral model boundaries were placed sufficiently far from the excavation and treated as rollers; the base of the model was fixed in all directions. The FE modelling enabled the designers to analyse the stress-strain state of the ground and concrete of the primary and secondary piles as well as the H-beams and to optimise the design. Cost savings of 15–20% were achieved through reduced reinforcement tonnage and concrete volume compared to the initial design based on simplified methods.

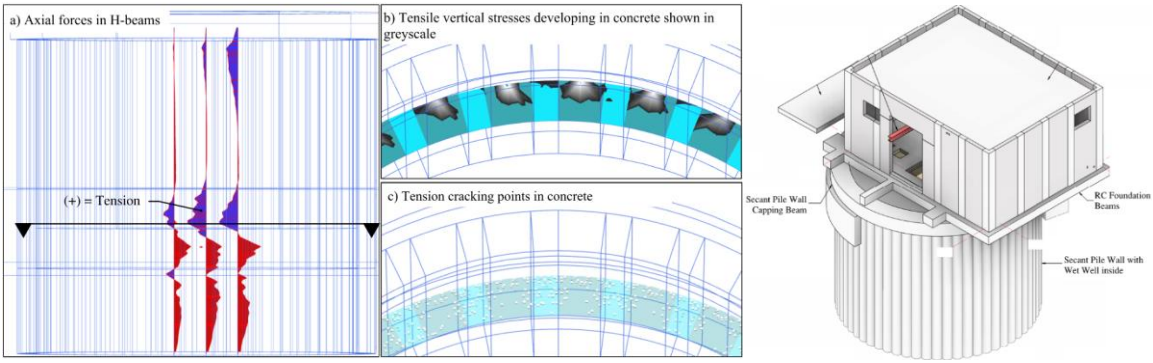


Fig. 10. Results of FE analysis (a, b, c), 3D view of the buried wet well (d)

NON-VIBRATING STONE COLUMNS AND LARGE DIAMETER BORED PILES

On many NZ projects, ground improvement is carried out next to existing buildings, retaining walls, bridges, underground services, etc. While stone columns often appear to be the most cost-effective solution, conventional stone columns often cannot be used because of high ground vibration levels during installation that may cause damage to nearby structures and underground services. Traditional stone columns are formed using vibro-replacement, which relies on powerful vibration to displace soil and compact stone. In recent years, the use of Non-Vibrating Stone Column (NVSC) in NZ's sensitive environments has become more common. NVSC avoids vibration and uses an augering method instead, which is quieter and does not generate high vibration levels. NVSC has recently been used to improve liquefiable ground for two large wastewater treatment plants in Tauranga, based on MBIE/NZGS Modules' principles. Up to 1,500 stone columns were required to improve the ground at the two sites. The NVSC method was adopted because both site boundaries are very close to several existing buildings and roads as well as critical underground services. Construction of vibratory stone columns could liquefy and cause settlement of the ground and damage to the existing structures and services. Most the plants' structures were founded on shallow reinforced concrete raft foundations over the improved ground. However, the more critical wet well structures were founded on large (1.2 m–2.4 m diameter) bored piles penetrating through a large thickness of liquefiable materials into competent soil layer at 36 m–50 m depth. The piles were bentonite-supported bored piles to minimise vibration levels (Fig. 11, Murashev et al., 2026).



Fig. 11. Left to right: 3D Image of the buried piled wet well; bored piles being constructed by March Construction; McMillan Civil's NVSC rig

CONCLUSIONS

Multiple natural hazards create challenges for the design of pile foundations and ground improvement in NZ. Due to the recent research and standards development work funded by MBIE, NZTA, EQC, NZGS and NZSEE, a robust NZ geotechnical design framework for pile foundations and ground improvement is now well-established and being constantly refined. The adopted design framework has been successfully applied on many recent infrastructure projects, which substantially improved

resilience of NZ infrastructure. However, further improvements are needed to clarify the relationships between overlapping guidance documents and to provide practitioners with clear direction on which documents to apply in specific design contexts. Continued investment in harmonising national guidance and aligning it with international best practice will support more consistent, efficient, and resilient geotechnical design outcomes.

REFERENCES

Hadzijanev Ardiac, D., 2009. Mohr-Coulomb parameters for modelling of concrete structures. Plaxis Bulletin, Spring issue 2009.

Mason D., Brabhaharan P. and Saul G., 2017. Performance of road networks in the 2016 Kaikōura earthquake: observations on ground damage and outage effects. Proceedings of 20th NZGS Geotechnical Symposium, Napier.

MBIE, 2017. Seismic Assessment of Existing Buildings: Technical Guidelines for Engineering Assessments (Parts C1 – C10). Ministry of Business, Innovation and Employment, Wellington.

Murashev A., Alves P. and Munro J., 2024. Innovative design methodology for secant pile walls. Proceedings of NZSEE 2024 Conference, Wellington.

Murashev, A., Alves, P., Crosby, G., Hnat, T., Cullen, G., Duggan, J., Edwards, L. and Myburgh, D, 2023. Innovative resin injection ground improvement to build up resilience of existing water treatment plant. Proceedings of 2023 ANZ Conference on Geomechanics, Auckland.

Murashev, A., and Keepa, C., 2022. New revision of the national design guidelines for ground improvement (MBIE Module 5). Proceedings of 2022 NZSEE Conference, Wellington.

Murashev, A., Baker, S. and Fearnley, J, 2024. Challenges associated with the geotechnical design of Te Kaha – Canterbury's new Multi-Use Arena. Proceedings of 2024 NZSEE Conference, Wellington.

Murashev, A., Keepa, C., Seve, G., Scott, J., Orense R., 2017. National Design Guidelines for Ground Improvement of Soils Prone to Liquefaction. Proceedings of 2017 NZGS Symposium.

Murashev, A., Kirkcaldie, D., Keepa, C., Cubrinovski, M. and Orense, R., 2014. Development of the design guidance for bridges in New Zealand for liquefaction and lateral spreading effects. Research report 553, NZ Transport Agency, Wellington.

Murashev, A., Tan, P. and Alves, P, 2026. Challenges associated with geotechnical design of pump stations in Tauranga. Proceedings of 2026 NZSEE Conference, Wellington.

NZGS & MBIE, 2021. Earthquake geotechnical engineering practice in NZ - Modules 1 to 6.

NZTA Bridge manual SP/M/022, 2022. Third edition.

Okada W., Fairweather B., Murashev A. and Fransis G., 2025. Sulphur point – Southern wharf extension detailed design report – Geotechnical. WSP, Auckland.

Siddiqui, U., Parker, W., Davey, R., Therkleson, S. and Quincy, M., 2019. Methodologies to assess and quantify earthquake damage: A damage assessment case study of the BNZ building in Wellington following the 2016 Kaikōura Earthquake. Proceedings of 2019 Structural Engineering Society New Zealand Conference.

Terry, P., Delaney, A., Juno, W. and Keepa, C., 2021. CentrePort Wellington: Resilient regeneration activity. Proceedings of 2021 NZSEE Conference, Christchurch.

 © Deep Foundations Institute 2026

MICROPILED PRECAST FOUNDATIONS IN ENERGY TRANSMISSION INFRASTRUCTURE: A NEW SUSTAINABLE CONSTRUCTION METHODOLOGY

Bora Okumusoglu**,** Geotech (ACCIONA), Sydney, NSW, Australia,
bora.okumusoglu@geotech.net.au
Dr Matthew Sentry, Geotech (ACCIONA), Sydney, NSW, Australia, matthew.sentry@geotech.net.au

ABSTRACT

The transition to renewable energy infrastructure demands innovative solutions to address the challenges of large-scale transmission projects. This paper presents the development and implementation of a micropiled precast foundation system for energy transmission towers by ACCIONA in Australia. Designed for remote, geologically complex, and environmentally sensitive areas, this innovative foundation system is being rolled out by ACCIONA across its transmission line projects, demonstrating its scalability and potential for wider deployment across Australia's energy grid. These efforts underscore the need for adaptable and sustainable foundation solutions to support the necessary national grid expansion.

Conventional cast-in-situ concrete pile foundations require heavy machinery, large volumes of materials, frequent vehicle movements and extensive earthworks to create access roads and working platforms, all of which heavily disturb the local environment and nearby communities. In contrast, micropiled precast systems significantly reduce the construction footprint using smaller (and more mobile) drilling plant, for a reduction in on site materials, resulting in significant reduction in land disturbance and elimination for concrete agitator trucks. This system reduces the construction carbon emissions and minimises construction impacts on the environment and local communities. For transmission projects in rural areas, where community concerns are common, these benefits are critical for gaining social license and fostering stakeholder collaboration.

This paper details progress in validating the micropile technique through pilot testing and iterative design enhancements, while also addressing challenges such as securing technical approvals and managing the risks associated with adopting new technologies. Ultimately, the findings highlight the importance of aligning technical innovation with contractual diligence and social responsibility. By documenting lessons learned from early trials and approval processes, this work contributes to the broader discourse on sustainable and socially responsible infrastructure development.

Keywords: micropiles, precast foundations, transmission towers, energy infrastructure, sustainability, innovation

INTRODUCTION

Australia's Renewable Energy Targets of 33,000 GWh/year by 2030 (Regulator, 2024) require unprecedented transmission infrastructure development. Two projects in New South Wales, HumeLink and the Central-West Orana Renewable Energy Zone (REZ) exemplify this transformation, encompassing over 1,000 km of new transmission lines across 1,333 towers.

Traditional cast-in-situ bored pile foundations, while proven, present significant challenges at this scale, as a result of conservative designs increasing pile diameter, length and reinforcement quantities; heavy equipment requirements; extensive civil works; concrete supply logistics in remote areas; and substantial environmental disturbance. These limitations become particularly acute in environmentally sensitive areas where social license and regulatory compliance demand minimal impact construction methods (CEATI, 2017).

This paper presents the development and implementation of ACCIONA's innovative micropiled precast foundation system that addresses these challenges while maintaining structural integrity and economic viability.

 © Deep Foundations Institute 2026

PROJECTS OVERVIEW

HumeLink East comprises 227km of 500kV double circuit transmission lines with 471 towers, connecting the augmented Bannaby substation to an interface with HumeLink West.

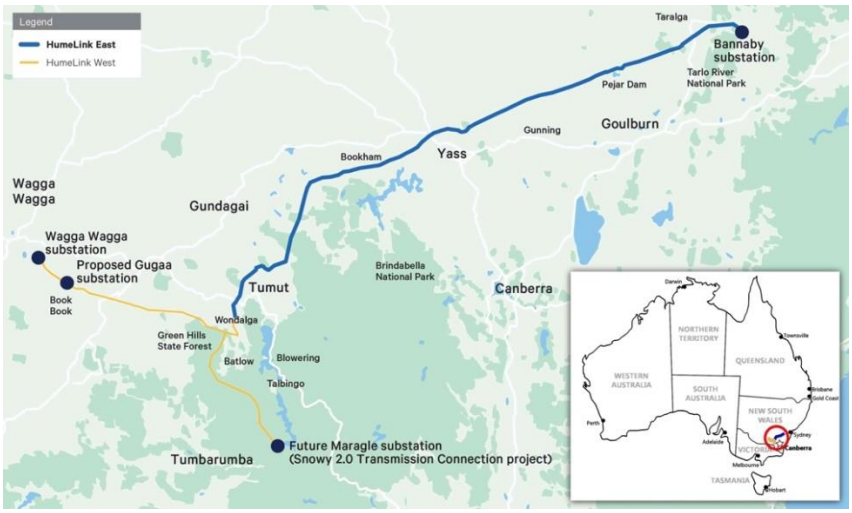


Fig. 1. HumeLink Transmission Line (Transgrid, 2024)

The Central-West Orana REZ, NSW's first priority renewable zone, includes 175km of 500kV lines (395 towers) and 159km of 330kV lines (467 towers), unlocking 4.5 gigawatts of new network capacity.

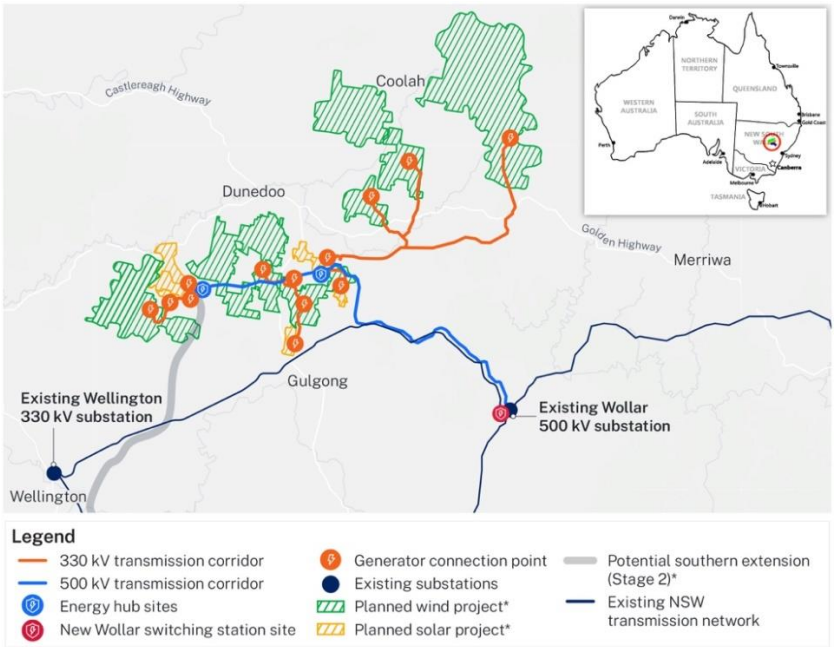


Fig. 2. Central West Orana REZ Transmission Line (EnergyCo, 2023)

GEOLOGICAL CONDITIONS

The overall geological conditions (Fig. 3) of the Central West Orana and HumeLink projects are predominantly medium to strong rock formations at an average depth of 5 m. Rock strength varies from granite and basalt (UCS values up to 200 MPa ~ 30 ksi) to weaker formations like phyllite (2–3 MPa ~ 0.3–0.5 ksi). Overburden soils transition from loose sands to very stiff clays with depth, providing favourable conditions for micropile installation.

 © Deep Foundations Institute 2026

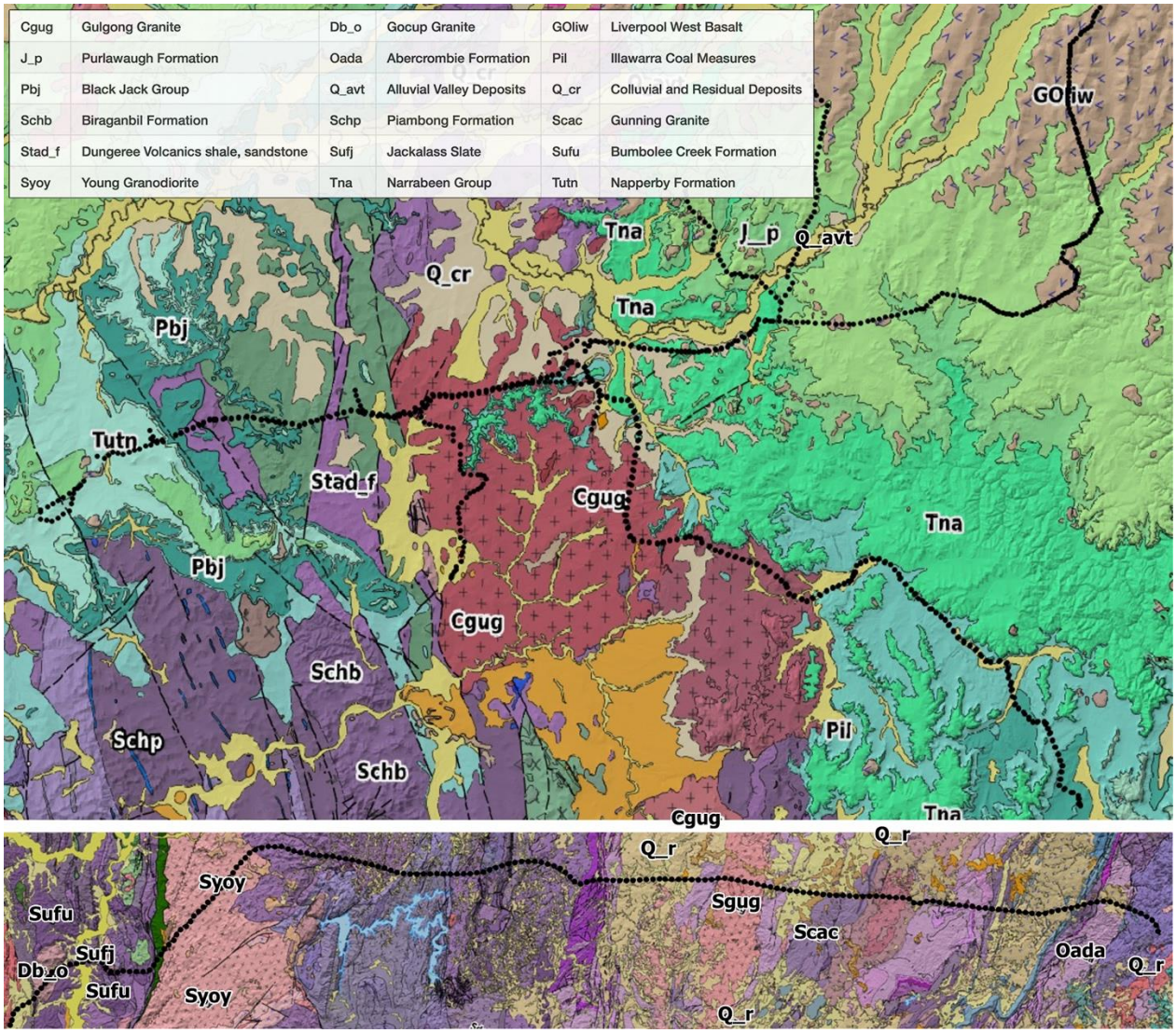


Fig. 3. Geological formations (dotted lines indicating TL alignments)

THE MICROPILED PRECAST FOUNDATION SYSTEM

ACCIONA's innovative micropiled precast foundation system was developed by ACCIONA's specialist business units ACCIONA Engineering & Design (AED) and Geotech for ACCIONA Construction Australia. The system comprises a precast concrete cap transferring loads to four micropiles. Each micropile consists of a high-strength mono bar grouted into rock, with diameters of 150–250 mm compared to 750–1800 mm for conventional bored piles.

Key advantages include:

- Smaller drilling equipment requiring minimal access infrastructure
- Elimination of concrete trucks, using only mobile grout units
- Partial early tower erection possible before micropile installation (details below)
- Reduced spoil generation and site disturbance
- Reduced construction footprint
- Enhanced safety through reduced manual handling

 © Deep Foundations Institute 2026

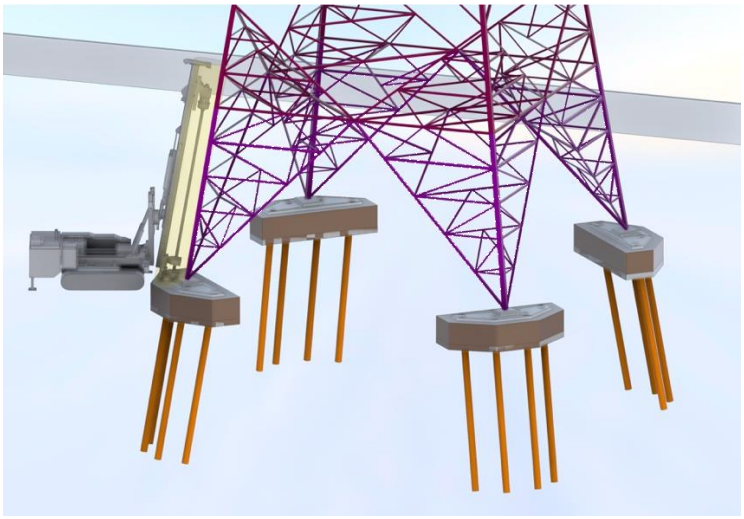


Fig. 4. One of ACCIONA's micropiled precast foundations for a transmission tower

The foundation work begins with the positioning of precast pile caps, through which the micropiles are drilled and grouted through the conical holes (Fig. 5). The unique shape of the precast cap allows for 25 m of the transmission tower to be erected before any micropiles are installed, providing flexibility in tower erection, and decoupling the piling works from the project's critical path.

The precast caps function as non-flexural members (span/depth ratio < 3), designed using strut-and-tie modelling adapted for the unique conical void geometry. Under compression, caps bear on bottom cones that wedge into micropile grout; under tension, top cones engage anchor plates for uplift resistance.

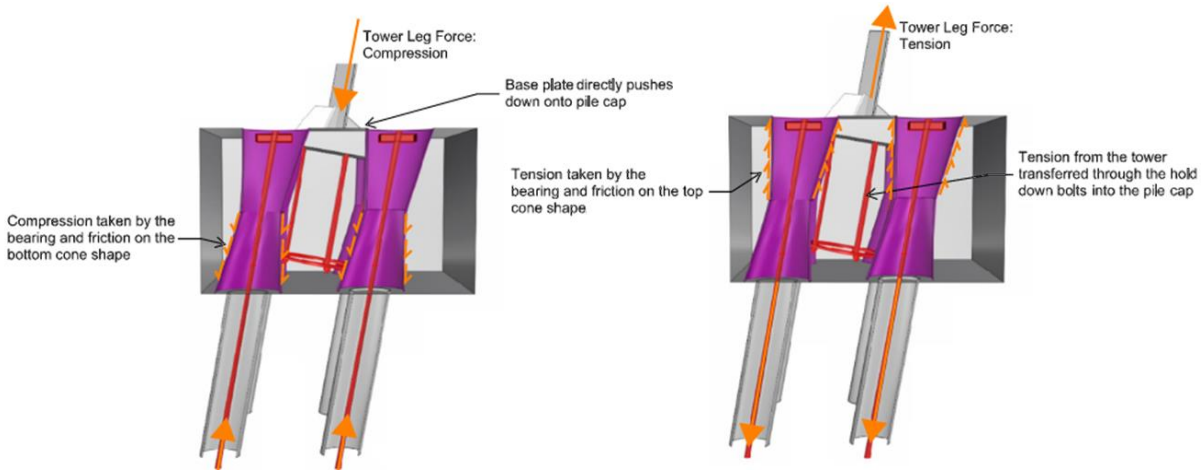


Fig. 5. Force transfer (compression and tension cases) via conical voids

Design evolution progressed from rectangular to trapezoidal caps, optimizing load distribution while meeting practical constraints: 10-tonne weight limit for transportation efficiency and 2.5 m width for road transport. Further technical details of the foundation system are provided in Okumusoglu et al. (2025).

VALIDATION AND TESTING

Four prototype caps were successfully cast by ACCIONA's precast facility (Australian Precast Solutions) for ACCIONA's Humelink East team in August 2024, validating the complex geometry and reinforcement configuration. Field trials by ACCIONA at Transgrid's Bannaby substation in September–October 2024 refined installation methodologies, including implementation of chalk line

positioning systems for achieving critical K-point tolerances for the set out and installation of the starter legs of lattice towers.

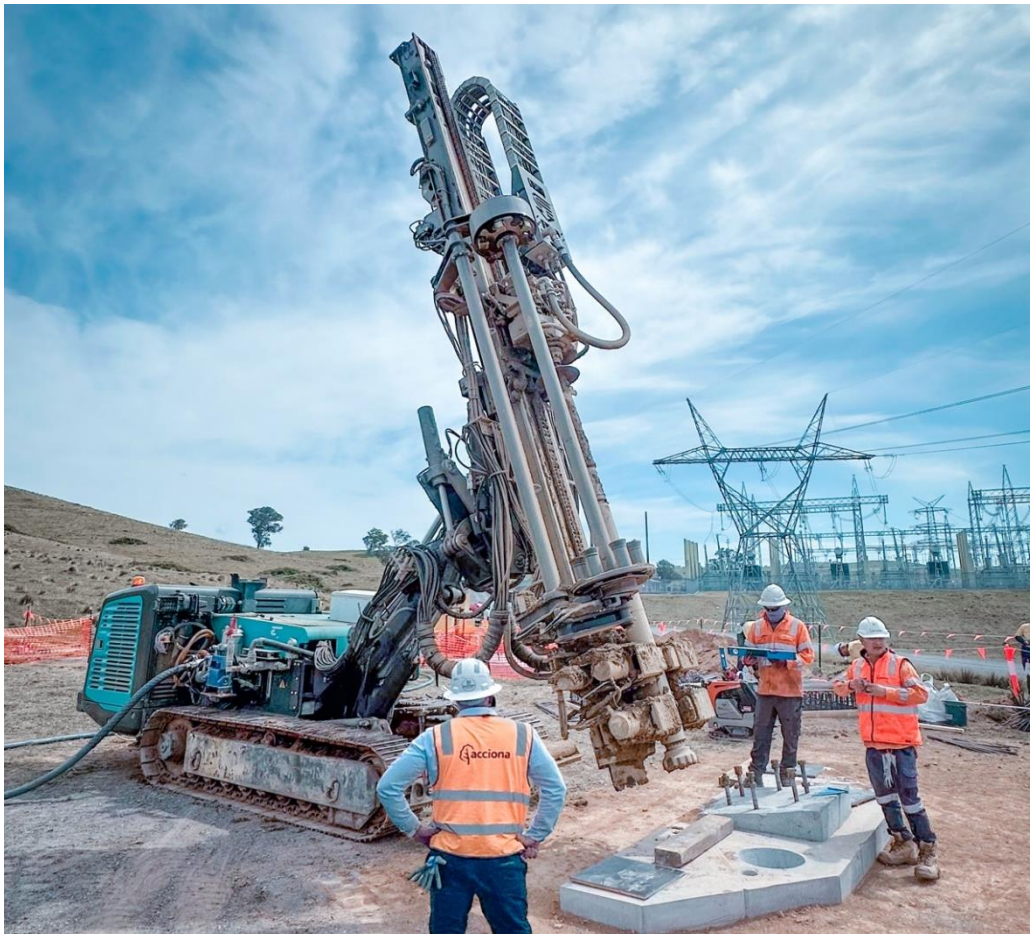


Fig. 6. In-situ trials for micropiled precast foundations

In-situ testing validated system performance by:

- Cone pull-out tests: Confirmed load transfer mechanisms between micropiles and caps.
- Tension tests: Demonstrated capacity to 1000 kN (Ultimate Limit State).
- Compression tests: Verified capacity to 1200 kN with buckling resistance validation.

All tests followed AS 2159:2009 protocols with real-time analysis using AnchorTest software (Mothersille and Okumusoglu, 2017).

ENVIRONMENTAL AND SUSTAINABILITY BENEFITS

As demonstrated below in Fig. 7, detailed carbon accounting for a 440-tower transmission line project demonstrates the following reductions:

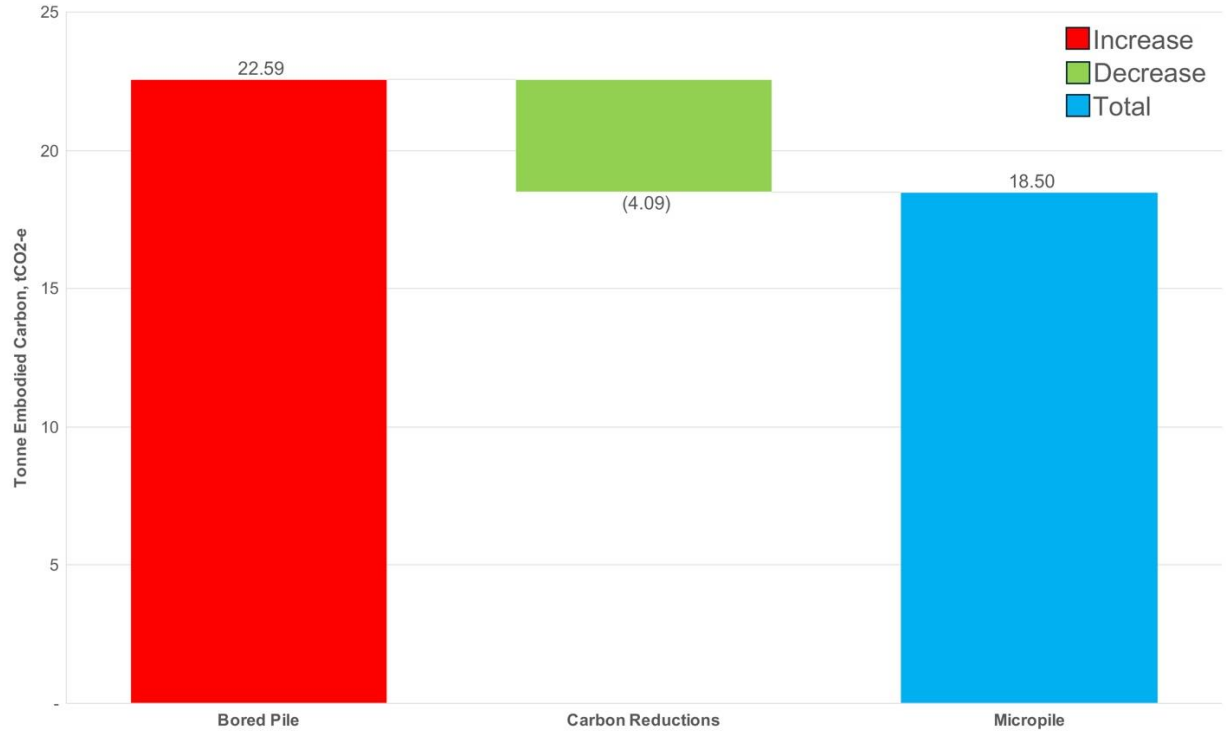
- 13% reduction in embodied carbon through reduced material quantities
- 29% reduction in fuel-associated emissions from smaller equipment and fewer vehicle movements
- 18% overall carbon footprint reduction per tower

The micropiled foundation system also reduces environmental disturbance through:

- 50% smaller working platforms compared to conventional piling,
- 50–70% reduction in temporary access tracks construction (including increases in access gradients, thus reducing required cut/fill)

- Elimination of concrete truck movements and associated contamination risks within transmission line corridor and on public roads,
- Minimisation of temporary access roads and related earthworks reducing overall environmental impact.

These benefits prove critical for maintaining social license, particularly in rural areas where community support significantly impacts project success.



Micropile+Precast
Material Quantities per Tower

	Precast			Insitu		
	Strength	Quantity	Units	Strength	Quantity	Units
Concrete & Grout	40MPa	16	m3	40MPa	9.4	m3
Steel Reo., Monobar, Casing	500MPa	2256	kg	1050MPa & 350MPa	5387.2	kg

Material	Emissions	Units
Precast concrete	0.62	tCO2-e
Insitu grout	0.37	tCO2-e
Steel	12.08	tCO2-e
Total per 4x micropiled foundation	**13.06**	**tCO2-e**

Fuel per Tower

	lt/tower	GHG emissions/tower	
Micropiling Rig + Compressor	2000	**5.44**	**tCO2-e**
TOTAL MATERIAL+FUEL		**18.50**	**tCO2-e**

Bored Pile
Material Quantities per Tower

	Insitu		
	Strength	Quantity	Units
Concrete	40MPa	54.3	m3
Steel Reinforcement	500MPa	8143.0	kg

Material	Emissions	Units
Concrete	2.11	tCO2-e
Steel	12.87	tCO2-e
Total per 4x bored piled foundation	**14.97**	**tCO2-e**

Fuel per Tower

	lt/tower	GHG emissions/tower	
Piling Rig	2800	**7.62**	**tCO2-e**
TOTAL MATERIAL+FUEL		**22.59**	**tCO2-e**

Carbon Values assumed: Concrete & Grout 0.038806947 tCO2-e per m3, Steel 1.58 tCO2-e per t, Fuel (Diesel) 2.72 tCO2-e per lt

Fig. 7. Embodied carbon reduction of foundations per tower

IMPLEMENTATION CHALLENGES AND BROADER APPLICATIONS

Introducing innovative foundation technology required comprehensive compliance mapping against existing standards, supported by extensive testing to demonstrate equivalence with established methods. Early engagement with specialist contractors, suppliers, and regulators proved essential, leading to practical refinements such as the three-stage modular reinforcement assembly for the precast element developed through steel fixer consultation.

 © Deep Foundations Institute 2026

Risk management strategies demonstrated that the micropile system reduced many conventional construction risks, particularly those related to field quality and concrete supply risk in remote locations and geological variability.

Four significant risks this system challenged included mitigating:
a) Concrete quality issues with remote concrete supply,
b) High construction traffic on local and private roads,
c) The use of large specialist plant,
d) Difficulties in achieving K-point tolerances during the in-situ placement of stubs in wet concrete.

The innovative design of a precast pile cap capable of connecting to micropiles whilst minimising its size and weight to allow two precast units to fit on one semi (four on a larger truck with two semis otherwise known in Australia as a B-double) resulted in a system that can be factory-constructed. Factory produced concrete elements are made to a higher quality standard, reducing field risks of non-conformance and structural defects.

The ability of one truck to transport up to four precast units (one tower) can remove between 14 and 31 concrete agitator trucks (agis) per tower. This is a significant reduction in daily vehicle traffic on regional public roads and construction access roads. The elimination of use of wet concrete in remote locations eliminates any risk of concrete contamination to the sensitive flora and fauna.

The precast pile cap connecting to the micropiles enables the use of piling rigs in the order of 50–67% smaller (in weight) to construct the micropiles compared to conventional bored piling rigs required to core large diameter piles (up to 1800 mm) into hard to very hard rock. Despite an increase in the number of piles (16 compared to 4 per tower), the overall spoil volume is reduced by between 72% and 95%, when compared to a bored pile solution, resulting in a significant reduction in construction time and construction waste.

The new foundation system demonstrated value for challenging sites including steep terrain, contaminated areas, and locations with strict environmental constraints. Initial cost comparisons demonstrate a 3–8% saving compared directly with conventional bored piles, but economic advantages in the order of 25–30% when accounting for global project benefits of the reduced construction footprint, reduced preliminary costs, schedule acceleration, and risk mitigation. Examples of these benefits are illustrated below in Figs. 8 and 9, which compare transmission tower construction access tracks and workbenches on steep terrain using a bored piled foundation system versus a micropiled foundation system.

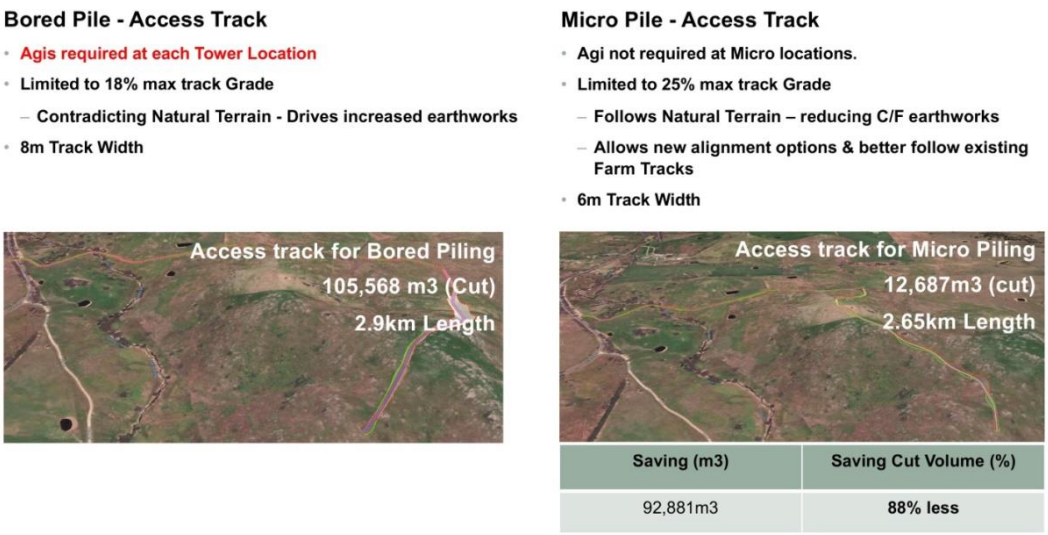


Fig. 8. Transmission tower construction access tracks

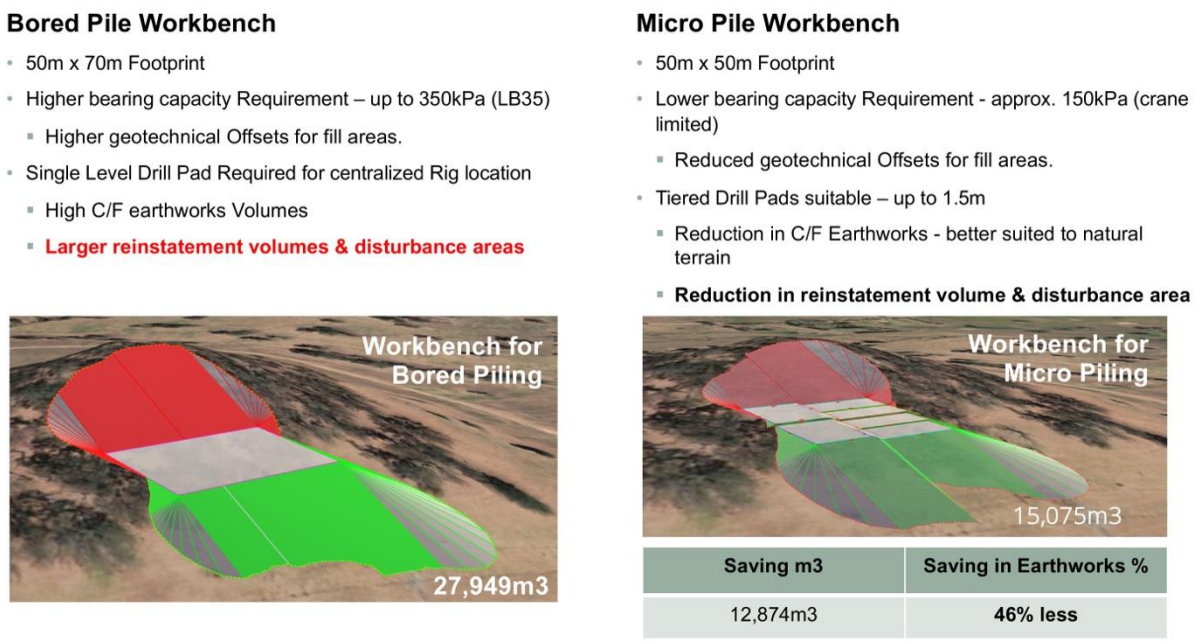


Fig. 9. Transmission tower foundation workbenches at steep terrain

LESSONS LEARNED AND FUTURE DIRECTIONS

Critical factors enabling successful implementation included:

- Early and genuine stakeholder engagement from design phase,
- Comprehensive validation through testing and field trials,
- Flexibility to iterate design based on practical feedback,
- Alignment of technical innovation with environmental and social objectives.

The importance of the O&M (Operation and Maintenance) team's ongoing feedback into this system is vital to ensuring the long-term viability (durability and longevity) of a precast pile capped micropile foundation for transmission line towers. Critical feedback during the early development focused on system security and durability, both from the environment and from wildlife perspective. The design to date addresses issues identified, but it is imperative that proactive evaluations of the system through the lenses of the operator (not just the contractor) continue to ensure the long-term validity of this innovative foundation solution.

The results of analysis from two major projects supports the use of the precast pile capped micropiled foundation solution over conventional bored pile foundations in regions of hilly to mountainous terrain or where high to very high strength rock is encountered (and not necessarily encountered at/near the surface).

Where towers are located in deep alluvial deposits or with very low to medium strength rock and are founded on flat terrain, the benefits of the precast pile capped micropiled foundation solution is limited when compared to the conventional bored pile foundation solution.

Areas for continued design and construction refinement include optimisation of reinforcement detailing, development of specialized installation techniques and tools, and integration of digital technologies for design and quality control. The potential for international transfer appears promising, particularly in countries facing similar renewable energy deployment challenges, particularly where labour costs are high.

The successful technical deployment across two major transmission line projects establishes precedents that will influence future sustainable infrastructure development, demonstrating that environmental performance and construction efficiency.

CONCLUSION

The micropiled precast foundation system represents a significant achievement in sustainable infrastructure innovation, successfully meeting all structural requirements while delivering quantified environmental benefits and enhanced construction efficiency. The carbon footprint reduction per tower, combined with dramatically reduced site disturbance, establishes new benchmarks for transmission infrastructure construction.

Beyond immediate project benefits, the innovation contributes meaningfully to Australia's renewable energy transition by enabling faster, less disruptive construction of critical transmission infrastructure. This directly supports achievement of the renewable energy targets and broader net zero ambitions.

The innovation journey demonstrates that sustainable infrastructure solutions are not only possible but practical and economically viable. The collaborative approach, bringing together diverse expertise from engineering, construction, and manufacturing, provides a model for solving complex infrastructure challenges. As the world faces multiple challenges of climate change, growing infrastructure needs and growing costs of construction, such innovations become essential for creating a sustainable future.

The micropiled precast foundation system stands as proof that innovation, sustainability, and practical implementation can work in harmony to deliver the infrastructure solutions our changing world demands. Its success rests not just in technical achievements but in contributing to a broader transformation of how we conceive, design, and build infrastructure for a sustainable future.

The authors would like to personally thank Mr Cornealius Nagel, Project Director for ACCIONA, for his commitment and drive for innovative sustainable solutions through Humelink East project, where deviations from the traditional methods of construction are challenging.

REFERENCES

AS 2159:2009. Piling - Design and installation. Committee CE-018, Piling, Standards Australia.

Centre for Energy Advancement through Technology Innovation (CEATI), 2017. Guide for transmission line foundations with least impact to environment. TODAM Report No. T153700-3310.

EnergyCo, 2023. Operational features of the project. Excerpt from an online PDF document. https://www.energyco.nsw.gov.au/sites/default/files/2023-09/cwo-rez-fact-sheet-eis-transmission-infrastructure.pdf. Accessed 18-08-25.

Mothersille, D. and Okumusoglu, B. (2017). "AnchorTest Software: Real-time Analysis of Anchor and Pile Load Tests." Proceedings of the International Conference on Ground Anchorages and Anchored Structures, London, UK.

Okumusoglu, B., Sanchez, J., Zeybek, R., Sentry, M., Nagel, C., and Alvarez, P. (2025). "Micropiled Precast Foundation Design for Transmission Line Projects in Australia." Proceedings of the DFI International Conference on Deep Foundations and Ground Improvement, Bruges, Belgium, pp. 793-807.

Regulator, C. E. (2024). The Renewable Energy Target Scheme: 2024 Administrative Report. Clean Energy Regulator, Australian Government, Canberra, Australia.

Transgrid, 2024. Division of HumeLink East and HumeLink West sections. An online figure. https://www.transgrid.com.au/humelink-east. Accessed 18-08-25.

 © Deep Foundations Institute 2026

HYBRID GROUTING FOR REMEDIATION OF TAUPO CONTROL GATE, WAIKATO RIVER

Nathan Townsend, Wagstaff Piling NZ, n.townsend@wagstaffpiling.co.nz
Russell Denny, Wagstaff Piling NZ, r.denny@wagstaffpiling.com.au
Anna Gooder, Wagstaff Piling NZ, a.gooder@wagstaffpiling.com.au

ABSTRACT

Specialised rapid-set grouting was implemented to remediate a sheet pile retaining wall located in a high-turbulence reach immediately downstream of the Taupo Control Gates on the Waikato River. The remedial methodology was developed and delivered by Wagstaff Piling NZ in collaboration with McConnell Dowell, involving a rapid gelling grout. The approach combines downstage drilling with upstage two-component (A/B) grouting—enabling real-time control of gel time for grout placement and confinement. Across a 36 m² treatment zone, >100 m³ of grout was placed between 2–12 m bgl, confirming extensive voiding. Grout-take data concentrated in the 4–12 m band indicate preferential flow paths near the sheet-pile toe; a subset of injections reached ~2,000 L, consistent with connected void networks rather than isolated cavities. Pressure records exhibited a characteristic increase-drop-rebuild sequence—gradual rise during confinement, sharp decrease on breakthrough, and subsequent rise toward peak or the 10-bar operational limit. Surface observations (local heave, cracking, lateral strain) further supported volumetric expansion as larger voids were infilled. Pressure-flow signatures with grout-take distributions provided a practical, data-based proxy for mapping void geometry, guiding rapid adjustments to mix and delivery, and preventing riverward migration. This project was an innovative solution in extreme conditions and is an example of a customised approach to drilling and grouting, used to resolve a difficult problem. Hybrid techniques such as this are not textbook solutions, combining variable techniques, although showing that with lateral thinking and drawing on experience, the most challenging conditions can be overcome.

INTRODUCTION

Wagstaff Piling NZ, in collaboration with McConnell Dowell, was engaged by Mercury NZ Limited under an Early Contractor Involvement (ECI) agreement to develop a practical remediation solution for a void that had formed in the downstream riverbank adjacent to the sheet pile wall and the Waikato River.

The Taupo Control Gates (TCG) are a critical component in regulating both normal operational flows and flood discharges to the chain of dams and hydroelectric power stations along the Waikato River. The TCG is a reinforced concrete structure measuring 27 m in length, 37.5 m in width, and 9.75 m in height, and contains six underflow gates. These gates are operated frequently throughout the day to regulate river flows for downstream hydroelectric generation, with typical operating flows ranging between 50 and 319 m³/s (Mercury, 2024).

Immediately downstream of the gates, sheet pile walls are installed along both riverbanks (Fig. 1). Over time, progressive erosion has developed along the riverbanks both upstream and downstream of the control gate structure. A sinkhole was observed on the surface directly behind the existing steel sheet pile (SSP) wall on the downstream side, likely resulting from a deeper subsurface void caused by erosion behind the SSP. Intrusive investigations confirmed the presence of this void; however, its full depth and extent remained uncertain (Fig. 2).

The voids are understood to have formed as a result of hydraulic erosion and scouring driven by flows in the Waikato River. Progressive washing out of fines behind the existing sheet pile wall has likely created highly permeable preferential flow paths, enabling continued soil loss and enlargement of subsurface voids.

 © Deep Foundations Institute 2026

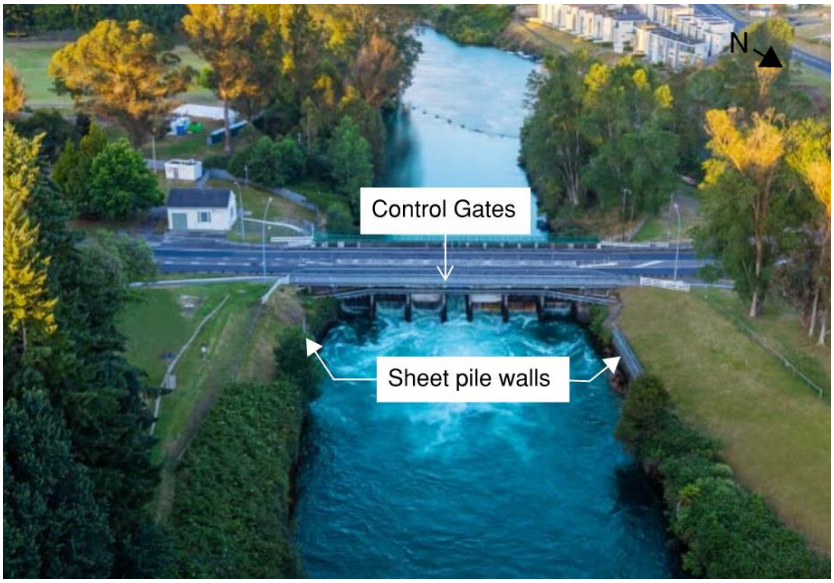


Fig. 1. Control gates on the Waikato River indicating sheet pile walls on both banks (Mercury, 2024)



Fig. 2. (Left) Location of void identified behind the upstream end of the sheet pile wall. (Right) evidence of erosion behind the sheet pile wall (McConnell Dowell, 2023)

The construction specifications required a grouting solution capable of permeating the formation sufficiently to fill existing voids while ensuring that grout migration into the adjacent river was prevented. Mercury specified a 25-year design life for the remediation works as part of its key performance requirements. In accordance with the New Zealand Dam Safety Guidelines, the Taupo Control Gates are classified as a high Potential Impact Classification (PIC) dam (Damwatch, 2021b) and are designated an Importance Level 3 structure.

Site constraints included slope stability considerations that limited the working platform to a footprint of approximately 12 m × 3 m. Minimising slope disturbance was essential. A detailed stability analysis was undertaken to evaluate excavation safety, potential ground movements, and assess machine load effects, including lateral forces acting on the existing SSP wall. The analysis also incorporated the influence of grouting-induced pressures to ensure that remediation works could proceed without compromising the structural integrity of the control gates or the surrounding riverbank.

A plan view (left) and concept of working platform (right) are shown in Fig. 3.

 © Deep Foundations Institute 2026

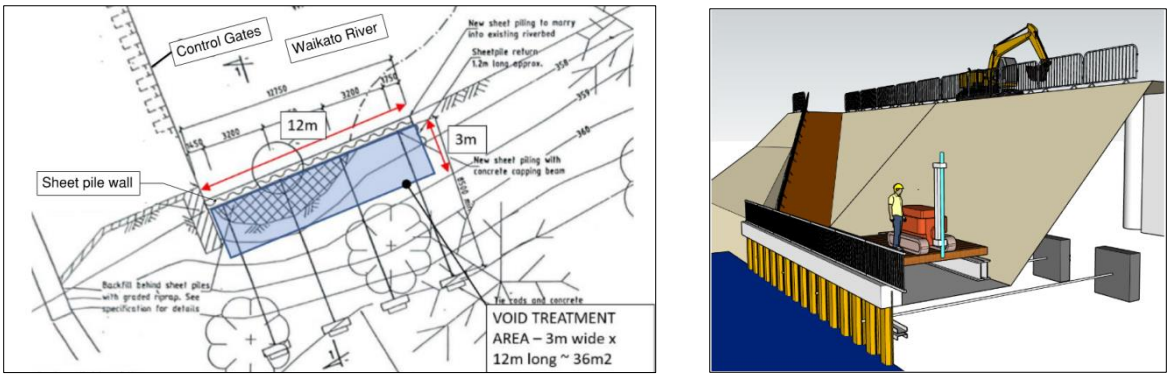


Fig. 3. (Left) Plan view of void treatment area, (right) working platform concept (McConnell Dowell, 2023)

The selected remediation approach needed to effectively stabilise and infill the void while ensuring that grout losses into the highly turbulent Waikato River were minimised.

OPTIONEERING PHASE

Concept Grout Design

During optioneering and development, Wagstaff Piling and McConnell Dowell assessed several options for both grout mix design and drilling methodology, including:

1. **Chemical Grouting:** This involved the use of hydrophobic grout designed to react with water and expand (polyether polyols and an amine-based catalyst), effectively sealing any immediate flow paths by producing a semi-flexible polyurethane foam. This would be followed by injection of conventional cementitious grout.
2. **Rapid Gelling Grout**: This approach utilised a two-part combination grout system with sodium silicate as the primary activator. The system was designed to regulate and achieve controlled gel times, ensuring the grout remained contained within the target areas.

Option two was selected due to the inert and non-active properties of sodium silicate within freshwater systems, its ability to regulate and control gel times, and the significantly lower cost compared to hydrophobic grouts.

Drilling Techniques

The drilling technique for the grout injection deployed was based on the following:

1. The need to map the formation in order to target the identified voided areas
2. The ability to alter grouting methods, i.e., upstage and downstage grouting
3. Targeted depth for grout placement

A PDC (polycrystalline diamond compact) drilling bit was selected for its versatility, as the anticipated ground conditions were largely unknown. Conventional rotary wash bore drilling techniques were used, with sodium silicate and bentonite drilling fluid.

CONSTRUCTION METHODOLGY

The selected remediation methodology comprised downstage drilling followed by upstage grouting, a well-established technique by Wagstaff Piling, and relies heavily on experience. This approach enabled real-time characterisation of the subsurface conditions during drilling, with drilling parameters providing key indicators of voided zones. These voids were typically identified by a sudden increase in penetration rate and drill head rotation, accompanied by noticeably reduced resistance on the bit.

Once the drill reached target depth at the toe of the sheet piles, the grout pump was immediately initiated, and grouting operations would commence. The system and plant arrangement were designed in such a way where fluids could be rapidly switched on or off. This was critical as the technique required grout at specific times, and if flow paths connected to the river, grout had to be immediately switched off, allowing drilling fluids (water, bentonite and sodium silicate) to remain flowing to prevent the grout from rapidly setting in the grout lines and drill string.

This methodology enabled precise placement of grout under variable subsurface conditions while maintaining control over pressures, flow paths, and material behaviour, ensuring the voided zones were stabilised without compromising the sheet pile wall or introducing grout into the river.

A stability analysis of the sheet-pile wall was completed prior to grout injection. The analysis established a maximum allowable injection pressure of 10 bar (145 psi) at the sheet-pile toe to mitigate the risk of lateral deflection of the wall and to avoid stressing the ground anchors/tiebacks that brace the SSP head. In addition, a surveyor was assigned to monitor wall deflections in real time throughout grouting operations.

Drilling the Injection Bores

A primary and secondary grouting sequence was implemented, with both sets of boreholes spaced at 1 m centres and spaced along 3 rows; Row 1, Row 2, and Row T, see Fig. 4. Primary holes were drilled and grouted first, designed to accommodate the majority of the grout take. Secondary holes, positioned between the primaries, served as verification points—minimal grout take in secondaries indicated that the primaries had effectively filled the voids.

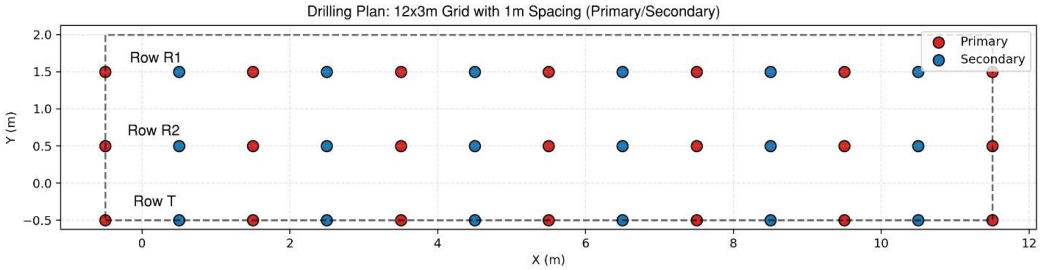


Fig. 4. Drilling locations with primary and secondary holes placed in a grid pattern

Drilling rig positioned on a primary location can be seen in Fig. 5.

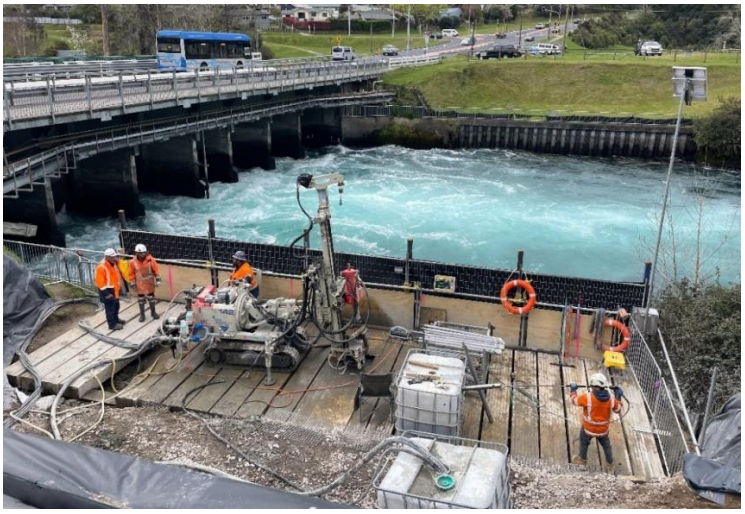


Fig. 5. Drilling rig setting up in position for grouting adjacent to the control gates, with the Waikato River in the background

 © Deep Foundations Institute 2026

Grouting Procedure and Regulation of Grout Flow and Gel Times

The upstage grouting process required precise regulation of flow rates and pressures using a dual-pump delivery system. Part A, a cementitious grout mix, was delivered via a high-pressure pump that controlled flow to the drilling rig. While Part B, a sodium silicate and bentonite mix, was supplied through a separate pump to the rig (Fig. 6).

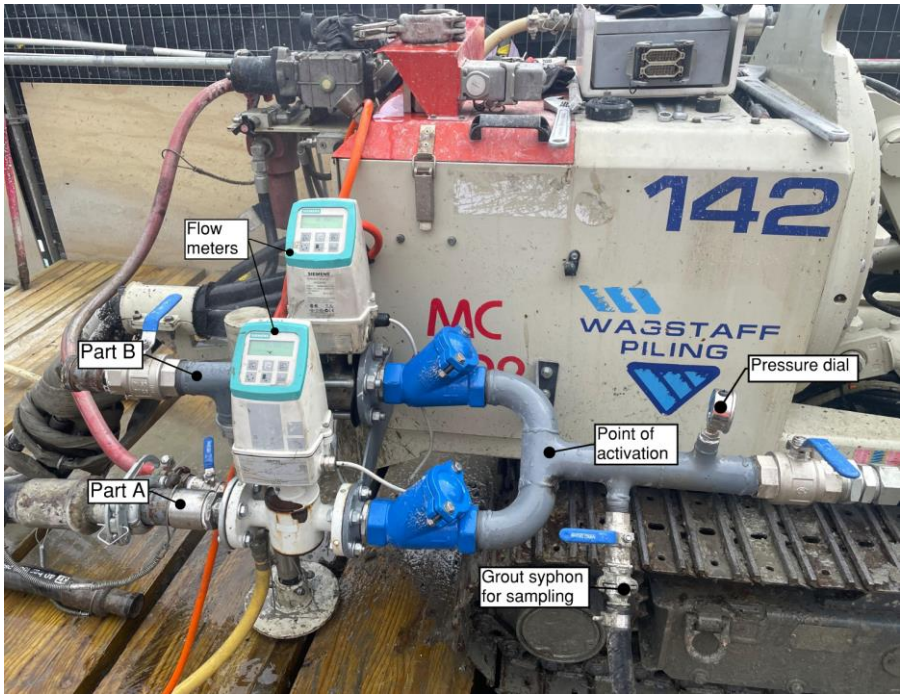


Fig. 6. Part A and Part B delivery to the drilling rig, with flow metres and pressure dials for real-time monitoring

Independent flow rate adjustments were essential to maintaining the correct Part A/Part B ratio and flow rates, enabling real-time control over grout set times. To ensure that the grout achieved the targeted set times, sampling was conducted at regular intervals. Samples were collected from a release valve positioned downstream of the Part A and Part B convergence point, ensuring that the mixed grout sampled reflected in situ conditions. Upon sampling, a timer was initiated to monitor the gelation time. The observed gel-time served as a key performance indicator, allowing for real-time adjustments to the Part A and B ratio if deviations from the set times were detected.

Grout Design and Gel Time Control

The grout design was developed by Wagstaff Piling with a focus on controlling gel and set times to ensure localised containment of the grout. Gel times were governed by the proportions of mix components and their respective flow rates. These parameters were adjusted dynamically in response to site conditions and observations, enabling real-time control of the grout's setting time. The delivery system and on-site batching setup (Fig. 7) allowed for modifications to the mix, facilitating rapid adjustments to gel times as required. In scenarios where voids exhibited high connectivity and evident flow paths, a rapid-set mix was utilised to minimise grout migration. In such instances, set times of less than five seconds were achieved.



Fig. 7. Batch plant including mixing tanks and pumps to batch, blend and deliver grout

Mechanism Between Part A and Part B

In the two component (A/B) grout system, Part A comprises cement, water, and bentonite, while Part B consists of sodium silicate (Na_2SiO_3). When the two streams converge at the mixing point on the rig, an immediate chemical reaction is triggered, resulting in:

- Formation of a cohesive gel,
- A rapid increase in viscosity, and
- Significantly accelerated setting characteristics.

This reaction is primarily driven by the calcium ions from the cement reacting with the sodium silicate to form calcium silicate hydrate (C-S-H) gel. When the sodium silicate is exposed to a multivalent cation in the cement (Ca^{2+}), the silicate molecules begin to polymerise, creating an amorphous cross-linked gel, that exhibits increased viscosity and gelation (Zhang et al., 2018). The process is further enhanced when the grout loses energy as it exits the drill bit within the formation.

The mix design of Part A and Part B are shown in Table 1, Table 2 and Table 3.

Table 1. Mix Design – Part A (75% Flow Contribution)

Component:	Mass (kg)	Specific Gravity	Volume (L)
Bentonite	18.8	2.20	0.34
Cementitious	346.9	3.15	110.1
Fly Ash	104.1	2.64	39.4
Water	592.0	1.00	592.0

Table 2. Mix Design – Part B (25% Flow Contribution)

Component:	Mass (kg)	Specific Gravity	Volume (L)
Bentonite	9.1	2.20	0.34
Water	183.2	1.00	183.2
Sodium silicate	85.9	1.38	62.5

Table 3. Combined Mix Design (Part A + Part B)

Component:	Mass (kg	Specific Gravity	Volume (L)
Bentonite	28.1	2.20	0.34
Cementitious	346.9	3.15	110.1
Fly Ash	104.1	2.64	39.4
Water	775.2	1.00	775.2
Sodium silicate	85.9	1.38	62.5

 © Deep Foundations Institute 2026

RESULTS

Grouting records show that the 36 m² treatment area behind the sheet pile wall received more than 100 m³ of grout between 2–12 m bgl (see Fig. 8), confirming extensive subsurface voiding throughout the remediation zone. Plots of cumulative grout take by drilling row revealed that Row 2 accounted for the highest demand, receiving approximately 40 m³, compared with lower but still significant volumes in Rows 1 and Row T, see Fig. 9. This spatial variation indicates that the central row was aligned with the most developed voids or preferential flow paths.

When individual injection volumes were plotted against depth, the highest grout uptake consistently occurred within the 4–12 m depth interval, identifying this band as the principal zone of erosion and loss of fines behind the sheet pile wall, see Fig. 10. This depth range also aligns with the inferred sheet-pile toe elevation and zones of highest hydraulic influence downstream of the control gates.

The distribution of per-increment injection volumes further supports the presence of highly variable voiding. Most injections were less than 600 L, forming a tight cluster associated with routine permeation or small void filling. However, a pronounced long-tail extending up to ~2,200 L was also observed, representing a smaller number of high-volume (>1,500 L) events. These outliers correspond to discrete encounters with large or interconnected voids and provide strong evidence of subsurface heterogeneity and episodic breakthrough into adjacent cavities, see Fig. 11.

Pressure responses were monitored continuously during grouting. A characteristic pattern was observed in most injections: pressures typically increased gradually with time, followed by a temporary decrease, before rising again toward a peak value or reaching the operational limit of 10 bar. This cyclic increase-decrease-increase behaviour reflects the progressive filling of voids, breakthrough into adjacent pathways, and subsequent re-confinement as the grout mobilised into new zones. Representative pressure curves illustrating this response are presented in Fig. 12.

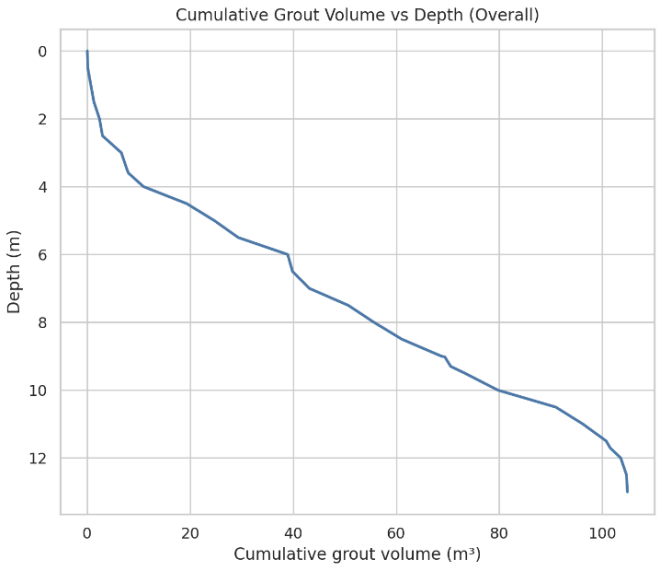


Fig. 8. Cumulative volume of grout vs. depth

 © Deep Foundations Institute 2026

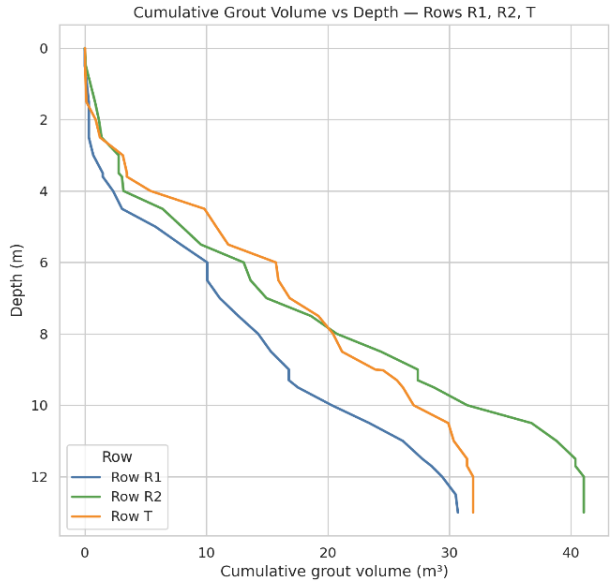


Fig. 9. Cumulative volume of grout for Rows 1, Row 2 and Row T

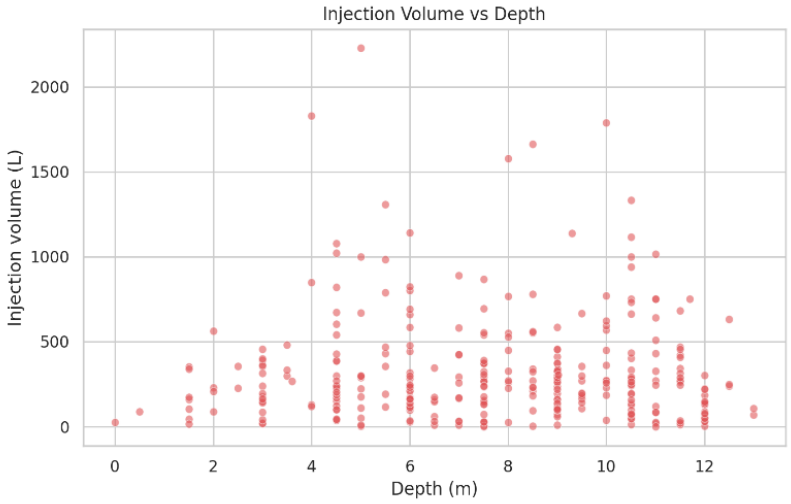


Fig. 10. Injection volume vs. depth

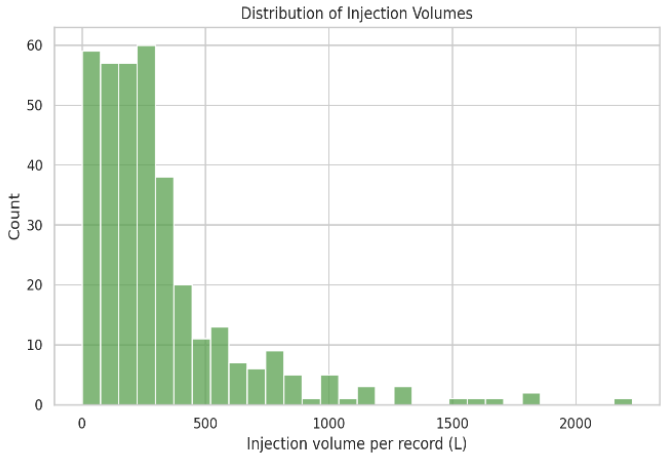


Fig. 11. Distribution of per-increment grout injection volumes

 © Deep Foundations Institute 2026

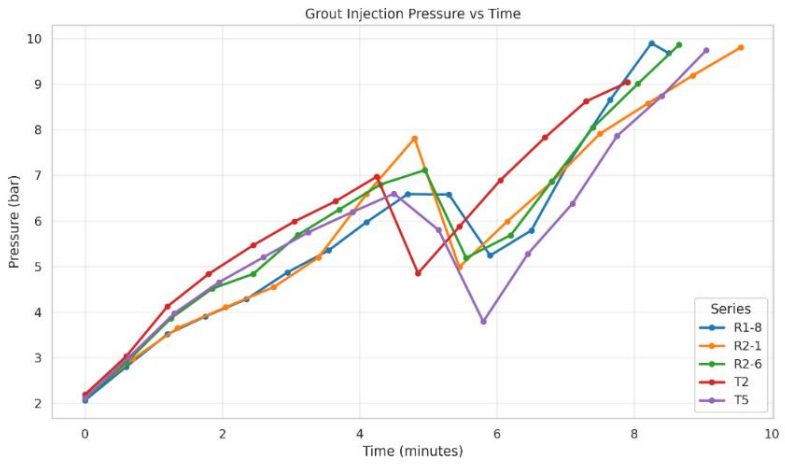


Fig. 12. Pressure vs. time plot for selected grout injection locations

SUMMARY AND CONCLUSION

The 36 m² treatment zone required more than 100 m³ of grout between 2–12 m bgl, confirming extensive, hydraulically driven voids behind the sheet-pile wall and demonstrating the need for a targeted void-infilling approach to stabilise the structure.

Key observations and findings:

Pressure–flow behaviour as a diagnostic tool:
Pressure trends consistently showed a gradual increase, followed by a rapid drop, and subsequent re-increase, reflecting sequential filling of voids, breakthrough into adjacent cavities, and re-confinement. Flow reductions coincided with rising pressure, providing a real-time indicator of decreasing void space and grout confinement.

Pressure response as a proxy for void closure:
Low initial pressures (~2 bar) increased as available migration pathways reduced. Cyclic pressure patterns—rise, drop, rebuild—aligned with grout breaching into new void spaces. This behaviour validated the interpretation that pressure response directly reflects progressive void filling and connectivity. In parallel, primary holes generally accepted larger volumes, whereas secondary holes tended to take less grout and reached higher pressures more quickly—evidence that most void infilling occurred during the primaries, with the secondaries serving as verification of effective closure.

Grout take as a proxy for erosional patterns:
Grout uptake was concentrated between 4–12 m bgl, aligning with the depth range most affected by hydraulic scour near the SSP toe. High-take events (up to ~2,000 L) indicated encounters with large, interconnected void systems, suggesting established flow paths parallel to and immediately behind the sheet-pile wall.

Ground heave and granular dilation as field evidence:
At shallow depths, ground heave, cracking and lateral strain were observed during high-volume injections. These deflection patterns confirmed volumetric expansion and granular dilation as larger voids were filled, providing additional surface-level validation of void in-filling.

Pressure–volume interpretation:
Locations with large grout takes also displayed the most pronounced pressure cycling, indicating interconnected void networks. In contrast, smaller grout takes with smoother pressure increases

corresponded to isolated or more confined voids. Together, pressure and volume data provided reliable interpretation of void geometry and grout migration pathways.

The successful delivery of this hybrid grouting programme relied on the ability to precisely target large, hydraulically formed voids, adjust mix characteristics in real time, and prevent grout migration into the adjacent river system. The combined use of pressure monitoring, grout-volume interpretation, and field observations created an innovative methodology for understanding and treating complex subsurface void structures.

The approach is readily transferable to remediation of other critical infrastructure applications, such as dams, bridge abutments and foundations, marine structures (breakwaters, wharves, quay walls), cut-off walls and impermeable barriers, where targeted void control under active hydraulic conditions is critical to long-term stability.

ACKNOWLEDGMENTS

The authors would like to thank McConnell Dowell for their collaboration and strong team culture during the project, also Greg Anderson (Wagstaff Piling) for site engineering support.

REFERNCES

Mercury. (2024). The Taupo Control Gates. Mercury NZ. https://www.mercury.co.nz/about-us/renewable-energy/hydro-generation/taupo-control-gates

McConnell Dowell, 2023. Taupo Control Gates, ECI Design Report – Separable Portions 1 & 2 MCD Design Reports

Zhang, W., Li, S., Wei, J., Zhang, Q., Liu, R., Zhang, X., & Yin, H. (2018). *Grouting rock fractures with cement and sodium silicate grout*. Carbonates and Evaporites, 33(2), 211–222. https://doi.org/10.1007/s13146-016-0332-3

 © Deep Foundations Institute 2026

INSTALLATION OF LARGE DIAMETER STEEL PILES IN VERY HIGH STRENGTH ROCK

Michael Wilkinson, CPEng, Austral Construction, Australia
Mark Johnson, Austral Construction, Australia

ABSTRACT

The Dampier region in northern Western Australia presents many challenges including remote location, temperature extremes, big tide cycles and cyclones. Notwithstanding, the region has seen significant investment in infrastructure for the export of iron ore, LNG, salt and fertiliser. The rugged coastline of Dampier consists of ancient geology that poses a unique challenge to designers and constructors alike. The region has a rich history of marine construction and piling with a broad spectrum of challenges with constructability. This paper focuses on the construction equipment and methods employed on a recent project in the region that required large diameter steel piles to be installed in challenging ground conditions.

The project required a solution that could handle varying ground conditions including reclaimed land (large rock fill), soft sediments, sedimentary rock and very high strength rock, whilst achieving the design actions (compression and lateral loads). Traditional construction techniques such as driven or bored piles were not feasible, so Austral Construction (contractor) worked with a global network of experts and suppliers to plan, procure, mobilise and execute the project using pile installation technology that had not been used in Australia previously.

Keywords: Dampier, piling, innovation, very high strength rock

INTRODUCTION

The Dampier region in northern Western Australia poses many challenges to designers and constructors. Marine infrastructure is required to perform under a wide variety of load cases exacerbated by cyclone activity and large tide cycles inherent in the region. Historically, the marine infrastructure in Dampier has been supported on bored piles or steel driven piles, that are installed using drive-drill-drive (DDD) and/or tension anchoring to achieve the design load capacity.

The subject project was located at the Parker Point iron ore facility on the Burrup Peninsula (Fig. 1). The project presented a challenging geotechnical risk profile, which is common for the region. Typical ground conditions consisted of rock fill overlaying sedimentary rock transitioning into igneous granite ranging in strength up to 170 MPa. The shallow and variable rock head meant that all piles needed to be installed into the very high strength rock to achieve the design capacities. The piling scopes consisted of 1219 mm diameter steel piles with a wall thickness of 20 mm installed as the main structural element in a land-backed marine offloading facility. Two types of piles were installed on the project:

1. Fitted with clutches to form a clutched contiguous wall (55 piles installed).
2. Standalone mooring piles with no clutches (3 piles installed).

CONSTRUCTABILITY CONSIDERATIONS AND EQUIPMENT SELECTION

The area is an existing causeway built in the 1960s. The vertical levels are expressed as a Reduced Level (RL) using the regional Chart Datum (CD) as per Australian industry practice on marine projects. A summary of the geotechnical conditions is as follows:

- Platform level RL +5.0 m CD to RL -10.0 m CD: FILL, Gravelly Boulders comprising of basalt and gabbro. Sand and fines present
- RL -10.0 m CD to -11.5 m CD: Calcrete, fine grained calcareous matrix with fine to medium gravel sized clasts of shell, coral, mudstone and granite. High strength, UCS 32 MPa

 © Deep Foundations Institute 2026

- RL -11.5 m CD to termination: Granite, medium to coarse grained with large pinkish phenocrysts of potassium feldspar surrounded by an overall grey quartz, plagioclase feldspar and biotite mica matrix. Very high strength, UCS 107 MPa.

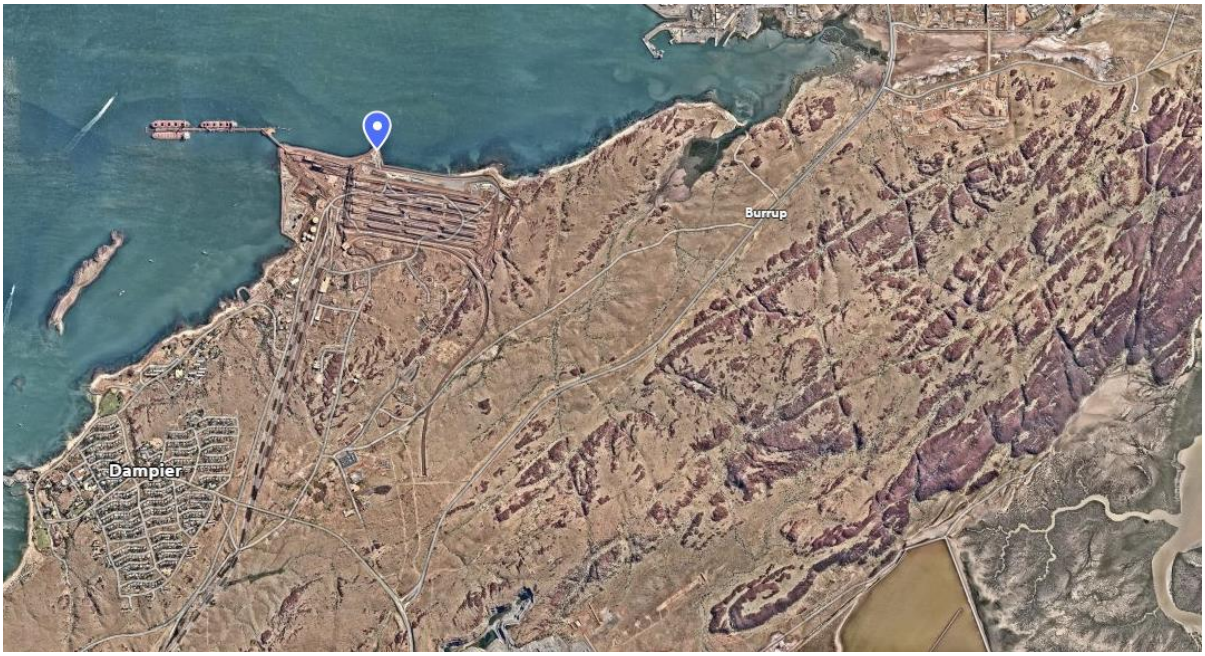


Fig. 1. Project locations (Image Credit: Nearmap)

To achieve the required embedment (nominated as 2 m in very high strength rock) the contractor had to develop and propose an installation method. Drawing from domestic and overseas experience, a method consisting of a reverse circulation down-the-hole hammer (DTH) coupled with an integrated ring bit was proposed. The system is shown in Fig. 2. This combination had the ability to progress through the overburden layers and socket into the rock strata without changing equipment or tooling. Furthermore, the ring bit can cut an annulus to allow the clearance of clutches to form the clutched contiguous wall. After extensive collaboration with the client and designer, the pile installation methodology was approved and employed on the project.

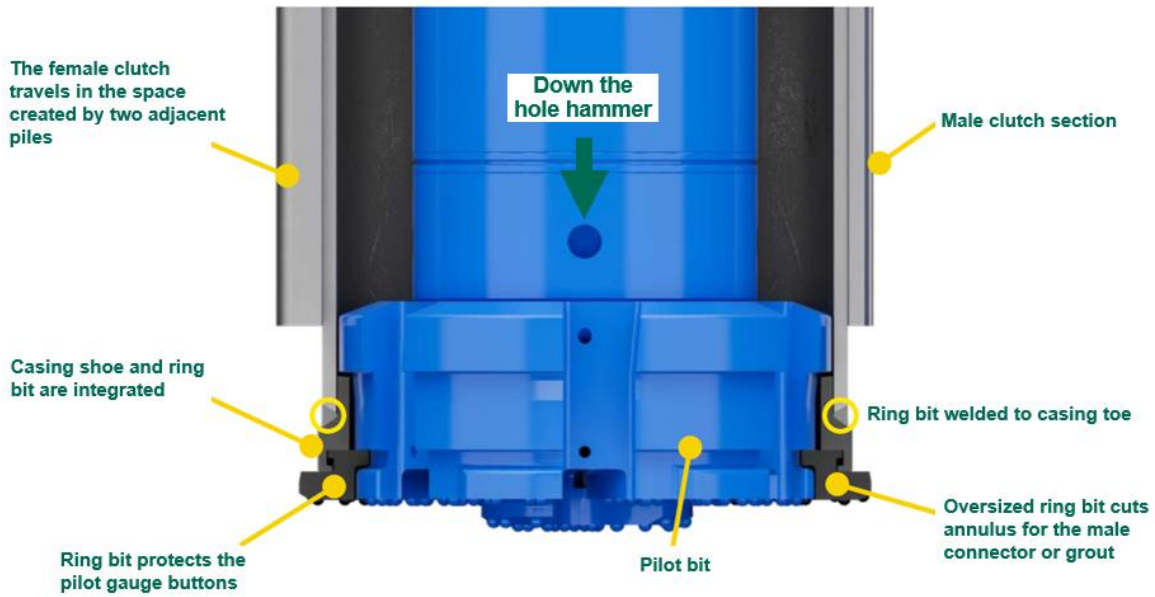


Fig. 2. Integrated ring bit system (Image Credit: Mincon)

 © Deep Foundations Institute 2026

PROJECT EXECUTION

The required equipment was procured from around the world and delivered to Dampier. To achieve the required working radius, a Liebherr LR1300 crawler crane fitted with a Liebherr LRH600 piling leader was used for the land-based piling, as shown in Fig. 3. The installation rig required a supporting spread of equipment consisting of multiple high-volume compressors and a spoil management system. Careful planning of the work area was required to fit all the equipment and maintain safe access for personnel and delivery of materials.



Fig. 3 - LR1300 crane with LRH600 leader

During the installation of a pile, multiple variables were monitored and adjusted as the ground conditions changed. The key variables are air pressure, air volume (flow rate), bit rotation speed, bit torque and bit weight (total weight on the cutting face). These variables must be closely monitored during the drilling process to ensure the system can achieve consistent production rates and avoid blockages or jamming up. In areas where the piles were installed through the working platform and fill layers, the bit weight and air management were particularly important. The bit weight needed to be sufficient to overcome the skin friction developed by the loose fill layer, clutch friction and ratcheting effect of the rocks in the fill but not enough to cause the bit to bog down. The supply of air needed to be constantly adjusted to have enough volume and pressure to clear the cuttings effectively. Too much air supply would cause the system to become unstable and prone to blockages and jamming.

Sampling of the drill cuttings was the best way to identify the material and correlate with the drill records and geotechnical investigation reports. The piling engineer and supporting geotechnical engineers were able to build a level of confidence to set the acceptance criteria for when the rock socket could be terminated based on the competency of the rock. A representative drill cutting sample of the granite encountered across the site is shown in Fig. 4.

 © Deep Foundations Institute 2026



Fig. 4. Drill cutting sample of granite

To correlate the penetration rates with the visual sample logging, a sample of 11 clutched piles closest to a geotechnical investigation borehole location were compared. The penetration rate vs. pile toe depth for each pile was recorded and plotted to see the trend (Figu.5). The general geotechnical profile has been marked on the chart for reference.

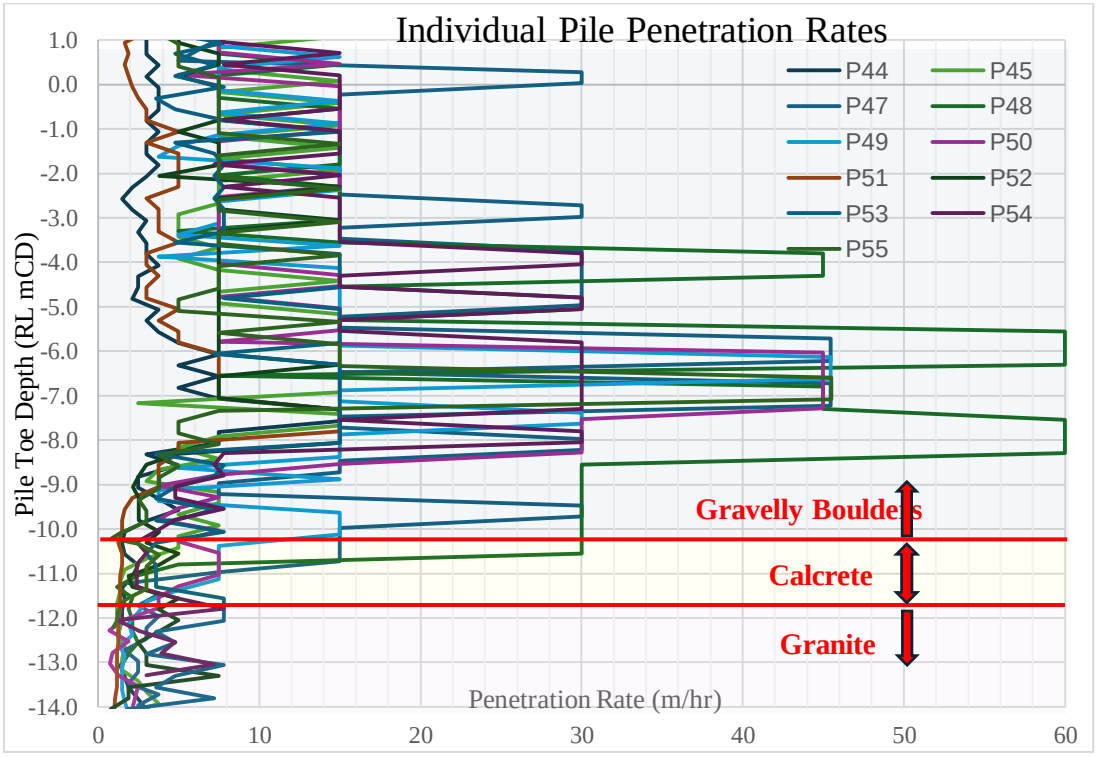


Fig. 5. Individual pile penetration rates

To establish the general trend, the penetration rates of the 11 piles were averaged. The minimum and maximum value of each averaged data point were plotted to show the variability in the penetration rates in the different ground conditions. The results are shown in Fig. 6. This shows that as the pile progressed through the fill layers, a large spread of penetration rates was observed, which was in line

with the observed inconsistent performance of the system in those layers. Noting that, the fill layers were, in their own right, very challenging drilling conditions. When the natural rock layers were encountered at approximately RL -10.0 m CD (15 m below ground level) the penetration rate slowed but was more consistent, indicated by the narrower band between the minimum and maximum values. Once granite was encountered, the penetration rate stabilised and the system performed very well.

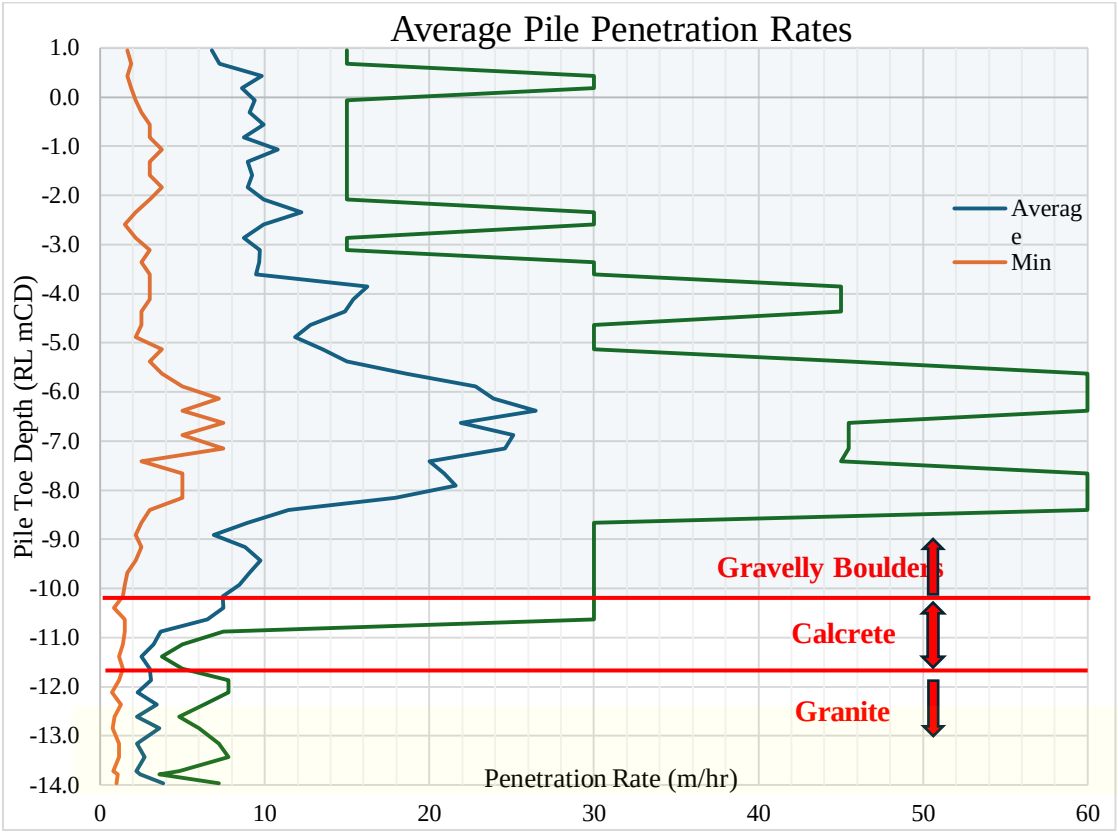


Fig. 6. Average pile penetration rates

From the 11-pile sample group, the average production rate in the fill layers was 10 m/hour and 3 m/hour in the calcrete/granite (raw drilling time). The progression through the fill layers, whilst at face value presents faster than the rock layers, encountered more issues and start/stop events due to the variable nature of the fill. More consistent progression was observed in the rock layers with minimal blocking or jamming observed.

The wear on the tooling was observed to be greater in the fill layers where the rate of progression was variable and more stoppage events occurred. Once the natural rock layers were encountered, less wear on the tooling was observed though the rate of progression was slower.

Careful alignment of the clutches and positional control was required during the installation of the clutched piles to ensure the clutches were not overstressed, potentially leading to declutching. Clutch alignment frames and the LRH600 leader were used to control the verticality and rotation of the pile during installation. This proved effective with all clutches maintaining integrity during the subsequent stages of construction including backfilling, tie-rod installation, concrete capping beam installation and finally, dredging of the berth pocket in front of the wall.

CONCLUSION

The integrated ring bit pile installation system has proven to be effective in installing both clutched and standalone piles the challenging ground conditions in Dampier, Western Australia. With proper monitoring and control of the key inputs, the system can effectively progress through a range of

 © Deep Foundations Institute 2026

ground conditions without changing tooling. The rate of penetration is highly variable in fill material with the most consistent production achieved in the natural, very high strength rock profile. The initial capital outlay on equipment and materials was higher when compared to traditional techniques (driven or bored piles). However, the performance during the construction phase provided an overall time and cost saving. In addition, the method generally presents a lower risk profile in both design and constructability in challenging ground conditions. Based on the performance of the technology on this project, the system would have broader applications where challenging/varying ground conditions are present. Collaboration between the designer and piling contractor is critical in developing an efficient and effective solution for the success of the project.

ACKNOWLEDGEMENTS

The successful execution of the project would not have been possible without the tireless work of the project teams, suppliers and support from the broader Keller group.

 © Deep Foundations Institute 2026

A CONSOLIDATED EARTH PRESSURE MODEL FOR GEOTECHNICAL STABILITY DESIGN OF EMBEDDED CANTILEVER WALLS

Chi-Kuen S. Yuen, Transport for New South Wales, NSW, Australia, +61400699232, Stanley.Yuen@transport.nsw.gov.au
Min Cai, FSG Geotechnics and Foundations, Queensland, Australia, mcai@fsg-geotechnics.com.au
Wai Liew, Transport for New South Wales, NSW, Australia, Wai.Liew@transport.nsw.gov.au
Ching M. Tan, CMT Engineers, Queensland, Australia, cmtan@cmtengineers.com.au

ABSTRACT

Ensuring adequate embedment for geotechnical stability is a critical aspect in the design of embedded cantilever retaining walls. This study aims to present a consolidated earth pressure model that unifies the stability assessment of both propped and free cantilever walls, addressing the shortcomings found in traditional embedment design approaches. The suggested method provides a stable reference for calculating stability by taking both horizontal force and overturning equilibrium conditions into account, making sure that designs meet the Australian Standard AS 5100.3 requirements. Application of the model to a typical 5 m deep excavation scenario demonstrates its ability to deliver consistent and economical embedment depths across a range of soil conditions, including both long-term (effective stress) and transient (total stress) cases. The results show that the consolidated model provides reliable factors of safety, and overcomes limitations of several widely used industry methods, particularly under undrained conditions. The study concludes that the proposed methodology improves design reliability, optimizes embedment in accordance with Australian Standard requirements, facilitates converging wall load calculations at stability limits for structural designs, and is readily automatable. These attributes provide significant advantages for large-scale infrastructure, industrial, commercial, and building and construction projects.

Keywords: Embedded retaining wall, free cantilever wall, propped cantilever wall, geotechnical stability calculation, Australian Standard AS 5100.3

INTRODUCTION

Embedded cantilever retaining walls are widely used in civil infrastructure, including basements, bridge abutments, and urban grade separation projects. Determining the appropriate embedment depth is critical for ensuring geotechnical stability and structural safety. Despite multiple earth pressure formulations in the past century, current practice still lacks a unified embedment design framework that (i) uses a constant reference design load independent of embedment, (ii) treats below-Limit Equilibrium Depth (LED) pressures as stabilizing capacity rather than added load, (iii) conforms to the design requirements of AS 5100.3, and (iv) considers both horizontal force and rotational equilibriums, which is essential for converging wall load calculations for both propped and free walls under effective- and total-stress conditions.

This study addresses these challenges by introducing a consolidated earth pressure model that unifies the stability assessment of both propped and free cantilever walls. The primary objective is to provide a reliable and economical methodology for embedment design, compliant with the requirements of the Australian Standard AS 5100.3. The proposed model refines the evaluation of limiting earth pressures and establishes a consistent reference for stability, overcoming limitations of previous methods. To demonstrate its effectiveness, the model was applied to a typical 5 m deep excavation in dry, uniform soil. Results show that the consolidated approach yields consistent factors of safety and reduces embedment requirements by up to 15% compared to traditional methods, without compromising safety or compliance. The model performs robustly under both effective stress and undrained conditions, and its stepwise calculation process is well suited for automation.

In summary, the consolidated earth pressure model enhances design reliability, improves cost-effectiveness, and facilitates straightforward integration into automated design workflows. The model

 © Deep Foundations Institute 2026

is internally consistent allowing calculation of converging wall bending moments and shear forces for structural designs. These benefits make it highly suitable for major civil infrastructure projects, addressing a significant gap in current geotechnical design practice.

DESIGN ISSUES WITH THE CURRENT METHODS

Numerous models for cantilever wall embedment design have been proposed in the literature (e.g., Bica and Clayton, 1989), yet no single model has achieved universal acceptance due to inherent conceptual differences. Most are derived from variations of the free earth and fixed earth support models, as illustrated in Fig. 1 for propped and free cantilever walls respectively. While these models are suitable for limit equilibrium calculations, they exhibit limitations when applied to determine embedment depths that satisfy consistent stability requirements.

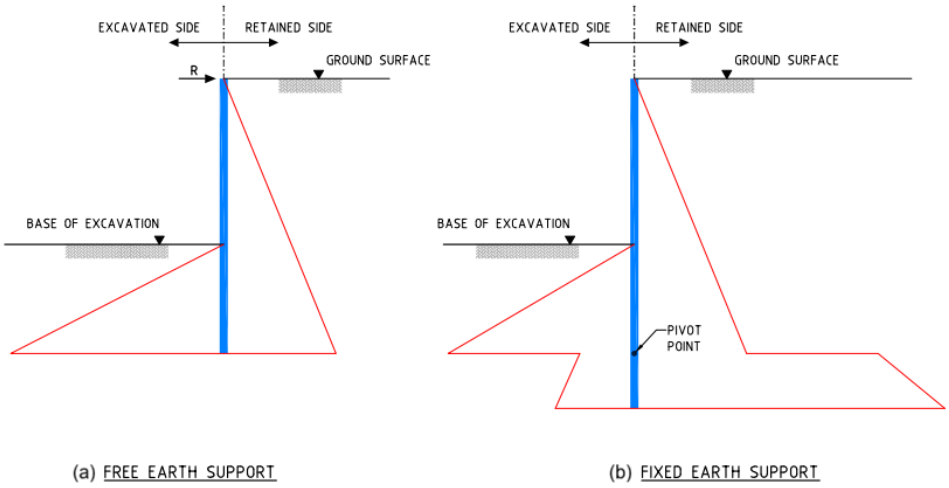


Fig. 1. Conventional earth pressure models for propped and free embedded cantilever walls

A key issue lies in the use of active earth pressures on the retained side as both the design load and the reference for restoring capacity. As embedment depth increases to meet stability demands, the calculated 'active' earth pressure also increases, even though the retained soil conditions remain unchanged. This creates a feedback loop where increasing embedment appears necessary to counteract artificially inflated loads, undermining the validity of the stability assessment. Furthermore, most existing models are not well-suited for transient loading conditions and often struggle when using total stress parameters. The use of a variable design load as a reference for stability calculations can lead to failure in determining embedment depth for certain transient cases. Consequently, the resulting embedment depths do not yield consistent factors of safety and may not accurately reflect the true stability of the wall.

In Australia, major civil infrastructures like embedded retaining walls are usually designed according to AS 5100.3 for geotechnical design. The design resistance strength $R_{d,g}$ is calculated as ϕ_g x $R_{u,g} \geq E_d$ (see Eqn. [5]), where the geotechnical reduction factor ϕ_g, with values determined from the standard, is applied to the ultimate capacity $R_{u,g}$. For a 5 m excavation in this study, ϕ_g is set at 0.55 (effective stress) and 0.80 (transient undrained). The minimum embedment is then proportioned to resist the design action effect E_d, equating to the overturning moment from a specific point appropriate for the support type under consideration. The horizontal forces are also considered for overall wall equilibrium.

While this requirement is relatively straightforward to apply for propped cantilever walls, it becomes more complex for free cantilever walls due to stress reversal caused by a restoring moment couple within the embedded wall section. Because the effective resisting components must also be factored, this internal moment interaction introduces ambiguity that can lead to inconsistent designs and

 © Deep Foundations Institute 2026

inaccuracies in embedment depth calculations. Given that these cantilever walls often span long, continuous distances around developments, it makes optimization of embedment depth economically significant.

THE WYDIWYG METHOD – A CONSOLIDATED EARTH PRESSURE MODEL

The WYDIWYG (acronym for What You Design Is What You Get) model has demonstrated suitability for the embedment depth design of cantilever walls (Yuen, 2019; Yuen and Liew, 2023). Given its effectiveness, it is appropriate to consolidate this earth pressure model into a general framework for embedment depth design, incorporating necessary refinements. This development addresses previously identified design challenges and offers a refreshed approach to an enduring engineering problem.

The model integrates several essential features to address the identified challenges:
1. Utilises Limiting Earth Pressures as a foundation
2. Establishes a Defined Reference for Stability
3. Revises definitions of Loads and Resistances

Model Based on Limiting Earth Pressures

Assuming the wall structure is adequately designed, its stability depends on the restoring capacity of the ground. In this context, adopting limiting earth pressures is appropriate. Numerical methods such as the Finite Element Method (FEM) typically only assess earth pressures mobilized under equilibrium conditions, making them suitable for serviceability evaluations but less effective for ultimate capacity assessments.

The proposed earth pressure model addresses this by considering the ultimate limit state (ULS) of the ground when deriving restoring capacity (see Fig. 2 and 3a). Notably, both propped and free cantilever walls share the same earth pressure framework, making a consolidated model for embedment stability a logical progression. The model includes a toe reaction R, which simplifies calculations for free cantilever walls, an approach supported by experimental evidence (Rowe, 1951; Yuen and Liew, 2023). For propped cantilever walls, the reaction R is relocated near the top of the wall.

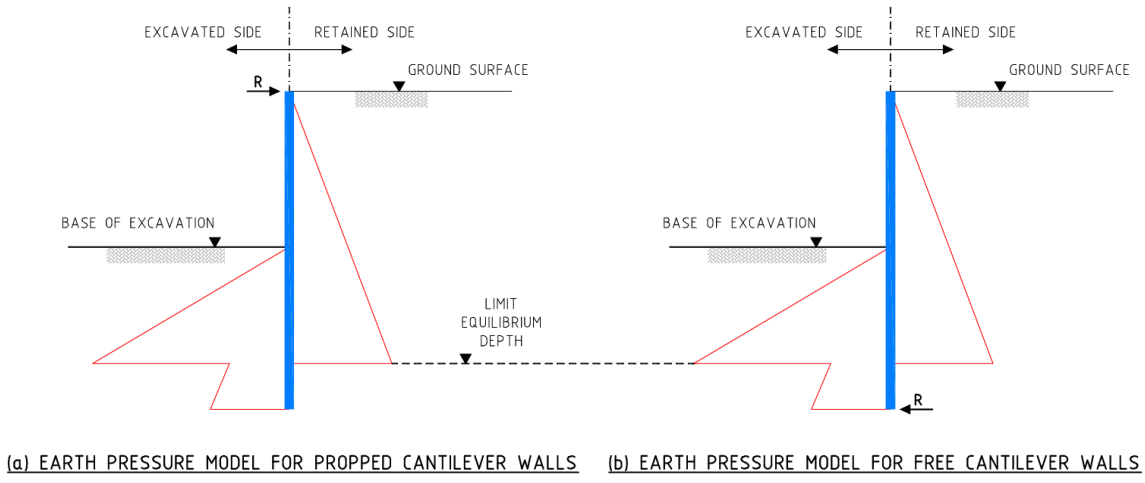


Fig. 2. New consolidated earth pressure models for propped and free embedded cantilever walls

 © Deep Foundations Institute 2026

Model with a Defined Reference for Stability

Traditional models often treat active earth pressures derived from wall geometry as design loads. This conservative approach fails to account for the unintended consequences of increasing design loads in stability calculations. To address this, the WYDIWYG model introduces a multi-stage process for both propped and free cantilever walls.

The first stage extends to the limit equilibrium depth (see Fig. 2), where earth pressures are balanced. The active pressure at this depth represents the maximum disturbing load for a given retention scenario and serves as a consistent reference for stability assessment. Importantly, this design load remains unchanged even as embedment increases beyond the equilibrium depth, reinforcing the model's consistency.

Model Redefines Loads and Resistances

Below the limit equilibrium depth, additional earth pressures develop on both sides of the wall as embedment increases (see Fig. 3b). It is essential to reconsider the role of these pressures, not as loads or resistances in isolation, but as contributors to overall stability. Yuen (2022) emphasized that these pressures should be viewed as stabilizing forces rather than fabricated loads as they can lead to unnecessarily deep embedment due to inflated design loads.

The model evaluates the net earth pressure, the difference between pressures on either side of the wall, which consistently enhances stability and aligns with engineering expectations. For propped cantilever walls, the model concludes with a net passive pressure on the excavation side, eliminating the need for active loads below the equilibrium depth (see Fig. 2a). The toe reaction R is at the support near top of the walls.

For free cantilever walls, the model introduces a restoring moment couple formed by passive pressures below the embedded section and a toe support R on the retained side (see Figs. 2b and 3c). This simplifies rotational stability calculations. However, the embedment determined at this stage is interim, and additional depth is required to satisfy horizontal equilibrium. An extra step (see Fig. 3d) shows optimization of final embedment while maintaining the previously established stability level. This step allows both rotational and horizontal force balance of the model and ensures convergency calculations of the wall loads at limiting stability condition.

EMBEDMENT DESIGN USING THE WYDIWYG MODEL

The WYDIWYG model simplifies the complex process of embedment design for cantilever walls by breaking it down into a series of manageable steps. This approach not only aids in explaining the methodology but also isolates key variables, allowing them to be resolved individually or through quadratic equations. Although the process may appear lengthy, it is well-suited for automation and can be efficiently implemented using spreadsheets or design software.

Overview of the Earth Pressure Model

Figure 3 presents a schematic of the earth pressure model used for calculating embedment in free cantilever walls. For simplicity, only forces derived from earth pressures are shown, though surcharge and other loads can be incorporated using the same design principles. The calculation is divided into:

- Two steps for propped cantilever walls
- Three steps for free cantilever walls

The first two steps are common to both wall types. For propped walls, the support point is typically near the top of the wall. In contrast, for free cantilever walls, the depth of the artificial toe support changes with increasing embedment and must be accounted for in the calculations.

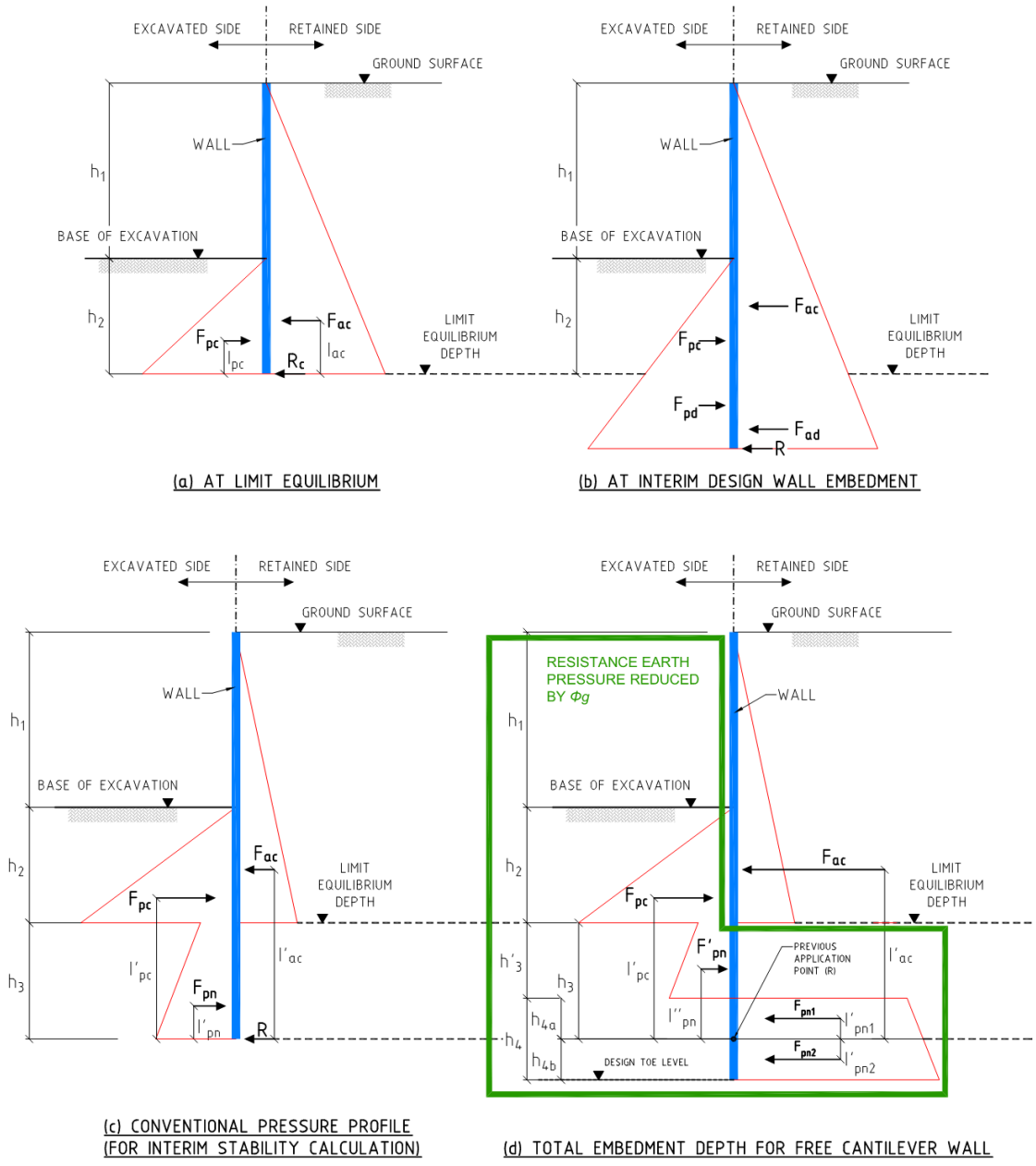


Fig. 3. Typical earth pressure development in embedment calculations for free cantilever walls

Step 1 – determine limit equilibrium depth (h_2)

This step establishes the depth at which the resisting moment from passive earth pressures equals the disturbing moment from active earth pressures, see Fig. 3a:

$F_{pc} \times l_{pc} = F_{ac} \times l_{ac}$, ➔ $l_{pc} = (F_{ac} \times l_{ac}) / F_{pc}$

Where F_{ac}, F_{pc} are active and passive forces at limit equilibrium; l_{ac}, l_{pc} are the lever arms from LED.

Assuming friction-only materials:

$l_{pc} = h_2 / 3$, rearranging the mathematical formula, $h_2 = 3 \times l_{pc}$ and substituting l_{pc}:

$h_2 = 3 \times \{(F_{ac} \times l_{ac}) / F_{pc}\}$ [1]

Where h_1 and h_2 are the retention height and embedment at the limit equilibrium depth respectively

Equation [1] is a function of h_2 and can be uniquely solved.

Step 2 – determine additional embedment for stability (h_3)

Refer to Fig. 3c, this step calculates the extra embedment h_3 required to mobilize sufficient resistance from net earth pressures to meet the desired Factor of Safety (FoS). The net pressure is the available resistance, being the difference between passive and active pressures below the limit equilibrium depth.

Considering moment equilibrium about the toe reaction point R:

FoS (Factor of Safety) = $\{(F_{pc} \times l'_{pc}) + (F_{pn} \times l'_{pn})\} / (F_{ac} \times l'_{ac})$

From geometry:

$l'_{pn} = (2 \times P_{pnt} + Pp_{nb}) / (P_{pnt} + P_{pnb}) \times h_3 / 3$

Where F_{pn} is the net force from below the limit equilibrium depth; P_{pnt}, P_{pnb} are the top net pressure and bottom net pressure from below the limit equilibrium depth respectively; l'_{pc}, l'_{pn}, l'_{ac} are the lever arms from the new wall base; h_3 is the additional embedment for stability.

Equating and solving for h_3:

$h_3 = 3 \times (F_{oS} \times F_{ac} \times l'_{ac} - F_{pc} \times l'_{pc}) \times (P_{pnt} + P_{pnb}) / \{F_{pn} \times (2 \times P_{pnt} + P_{pnb})\}$ [2]

For propped walls, the total embedment is $h_2 + h_3$, and the overall wall height H is $h_1 + h_2 + h_3$.

Step 3 - final embedment adjustment for toe reaction (for free cantilever walls)

An additional step is required for free cantilever walls to account for the simplified toe reaction. Figure 3d illustrates optimization of the final embedment by taking moment about the toe reaction R. This moment point should not be confused with the pivot point shown in Fig. 1b in the conventional free earth support model. This strategic step is a mathematical way to consider horizontal force equilibrium whilst keeping the same rotational FoS as in Step 2 above. It ensures converging wall bending moments and shear forces to be calculated accurately from the factored earth pressure diagram.

Let: $h'_3 = h_3 - h_{4a}$, where h_{4a}, h_{4b} are the additional embedment components

For horizontal force equilibrium:

$(F_{pc} + F'_{pn}) / FoS = F_{ac} + (F_{pn1} + F_{pn2}) / FoS$ [3]

For moment equilibrium about point R:

$FoS = (F_{pc} \times l_{pc} + F'_{pn} \times l''_{np} + F_{pn2} \times l'_{pn2} - F_{pn1} \times l'_{pn1}) / (F_{ac} \times l_{ac})$ [4]

Where F'_{pn}, F_{pn1}, F_{pn2} are the net passive forces over h'_3, h_{4a}, h_{4b} respectively; l''_{np} and l'_{pn1}, l'_{pn2} are the lever arms from the toe reaction point in Step 2.

 © Deep Foundations Institute 2026

These two equations, [3] and [4], solve for the two unknowns h_{4a} and h_{4b}. With spreadsheet computation, the calculations are straightforward.

Final Embedment = $h_2 + h'_3 + h_{4a} + h_{4b}$, and wall height H = $h_1 + h_2 + h'_3 + h_{4a} + h_{4b}$.

DESIGN TO AUSTRALIAN STANDARD AS 5100.3

AS 5100.3 governs the geotechnical design of major civil engineering infrastructure projects in Australia. A fundamental requirement of the standard is:

$$\phi_g \times R_{u,g} \geq E_d \quad [5]$$

Where E_d is the design action effect; $R_{u,g}$ is the geotechnical resistance capacity; ϕ_g is the geotechnical reduction factor (effectively the reciprocal of the factor of safety, FoS)

To ensure compliance using the WYDIWYG model, it is essential to understand that the design effects E_d, whether moments or forces, are derived at the limit equilibrium condition. These effects are unique to the wall configuration and should remain constant regardless of the required stability level. They represent the disturbing actions in the design.

Unlike traditional approaches that restrict the restoring capacity ($R_{u,g}$) to a single-sided ground contribution, the WYDIWYG model recognizes that, especially for free cantilever walls, stability is influenced by earth pressure reversal below the excavation level. In such instances, the geotechnical reduction factor is applicable to several zones indicated in green, as depicted in Fig. 3d. For propped cantilever walls without pressure reversal, the reduction factor only applies to the excavated side. The WYDIWYG model improves stability assessment by including all effective resistances (including earth pressure effects) below the limit equilibrium depth, specifically the net earth pressures as integral effective components of the ultimate geotechnical capacity. This approach ensures a more comprehensive and reliable evaluation of wall stability.

Treatment of Surcharge and Water Pressures

Although previous sections did not explicitly address surcharge loads, they are treated similarly to earth pressures in the WYDIWYG model. Since surcharge effects are transferred to the wall as lateral pressures, they should be incorporated into the earth pressure profile for stability assessment. Where the surcharge loads are live loads, their contribution as resistances should be discounted.

Importantly, pressures below the limit equilibrium depth are not considered part of the design effect E_d, but rather as components that contribute to the restoring capacity. These components are subject to the same geotechnical reduction factor ϕ_g as passive earth pressures.

Water pressure treatment is another critical consideration. The WYDIWYG model applies the same principles to water pressures as to earth pressures. However, AS 5100.3 states that no reduction factor is required for water pressure components. This should include the net water pressures below the limit equilibrium depth.

Conforming Design Equations
<u>Propped Cantilever Walls</u>

- **Overturning Stability**:

$$\phi_g \times (F_{pc} \times l_{pc} + F_{pn} \times l_{pn}) + (F_{we} \times l_{we} + F_{wn} \times l_{wn}) \geq F_{ac} \times l_{ac} + F_{wr} \times l_{wr}$$

- **Horizontal Force Stability**:

$R + \phi_g \times (F_{pc} + F_{pn}) + (Fw_e + F_{wn}) \geq F_{ac} + F_{wr}$

Free Cantilever Walls

- **Overturning Stability**:

$\phi_g \times \{(F_{pc} \times l'_{pc}) + (F'pn \times l''_{pn}) + (F_{pn2} \times l'_{pn2} - F_{pn1} \times l'_{pn1})\} + (F_{we} \times l'_{we} + F_{wn} \times l'_{wn}) \geq F_{ac} \times l'_{ac} + F_{wr} \times l'_{wr}$

- **Horizontal Force Stability**:

$\phi_g \times (F_{pc} + F'_{pn} - F_{pn2} - F_{pn1}) + (F_{we} + F_{wn}) \geq Fac + F_{wr}$

Where F_{we}, F_{wn}, F_{wr} are the forces due to water pressure from the excavation side above LED, net water pressure below LED, and on the retention side above LED; l'_{we}, l'_{wn}, l'_{wr} are the lever arms measured from the point R as defined in Step 2.

PERFORMANCE COMPARISON

The effectiveness of the consolidated WYDIWYG model for both propped and free cantilever walls is demonstrated using a simple example of a 5 m deep excavation in dry, uniform soil. Two design scenarios are considered:

- Long-term condition: Effective friction angle $\phi' = 35°$, with a geotechnical reduction factor $\phi_g = 0.55$
- Transient condition: Undrained shear strength $c_u = 40$ kPa, with $\phi_g = 0.80$, and a minimum 5 kPa fluid pressure

The scenario also includes a 10 kPa laterally extensive surcharge as a permanent load applied at ground level on the retained side. The soil unit weight is assumed to be 20 kN/m³.

Model Comparison

Figure 4 shows the comparison with four common industry models, the British Code of Practice method (CP2), the Strength Factor method (SF), the Burland, Potts and Walsh method (BPW) and the British Steel Corporation method (BSC). The last one is included for completeness as it is often used in temporary works only. Figure 4a (propped, effective-stress) and Fig. 4b (free, effective-stress) show embedment decreasing with increasing strength of effective friction angle ϕ'; the consolidated model tracks BPW closely while avoiding CP2's over-embedment at low ϕ'. Figure 4c (propped, undrained) and Fig. 4d (free, undrained) demonstrate that the consolidated model continues to produce valid embedment across c_u, whereas BSC underestimates FoS due to truncation of the design effect; CP2 and BPW fail to cover the full c_u range, and SF shows significant trends to increase in embedment under both effective and total stress conditions.

The WYDIWYG model demonstrates consistency that underscores its robustness and reliability in practical applications. The approach ensures that what is designed is accurately reflected in the final outcome, reinforcing its strength as a dependable modelling framework.

 © Deep Foundations Institute 2026

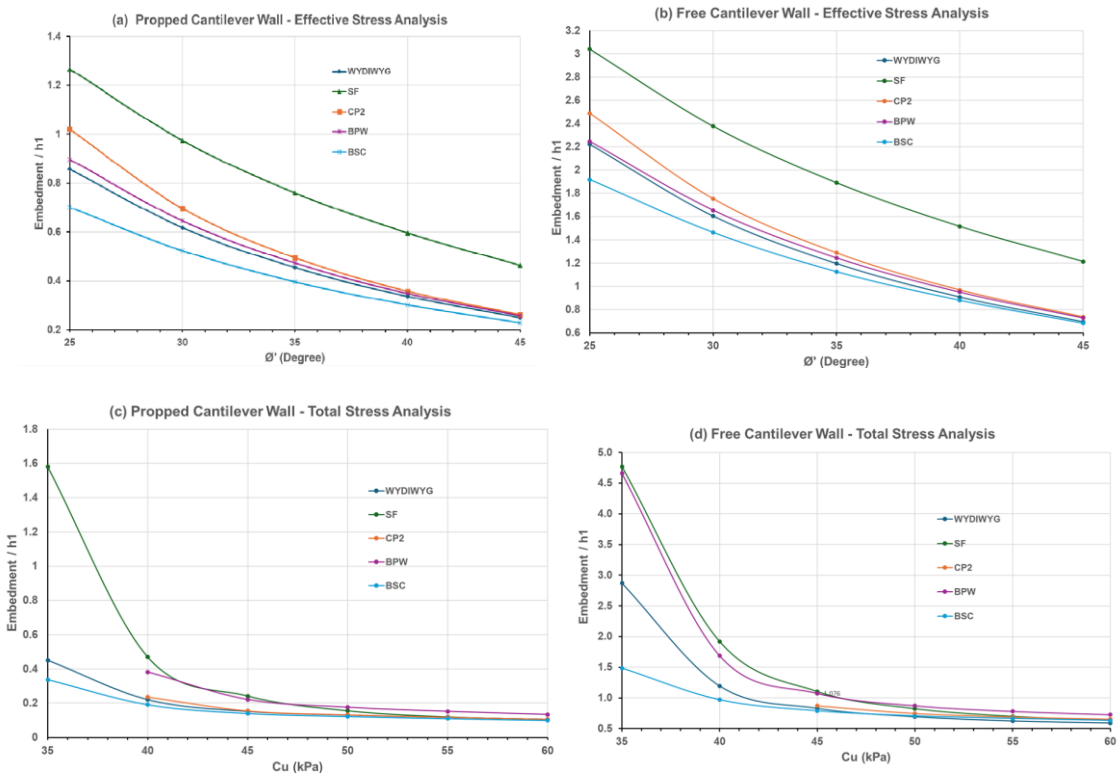


Fig. 4. Performance comparison showing effective stress analyses and total stress analyses for propped and free embedded cantilever walls

Structural Design Implications

The WYDIWYG model is primarily designed to calculate effective wall embedment. Once embedment is determined, the shear forces and bending moments for the stability case, can be correctly calculated for structural design based on the limiting earth pressure profiles factored by the selected geotechnical reduction factor. To ensure comprehensive wall design in accordance with AS 5100.3, additional load cases, such as those arising from soil-structure interaction, must also be evaluated as currently indicated in the standard. The structural design should therefore include:

- Load cases derived from the limiting stability states and other ultimate limit conditions
- Load cases relevant to other serviceability conditions

SUMMARY AND CONCLUSIONS

This paper presents a consolidated earth pressure model suitable for the embedment design of both propped and free cantilever retaining walls. The model evaluates wall stability by considering limiting earth pressures from the ground. By eliminating fictitious loads, specifically, pressures from below the limit equilibrium depth treated as disturbing forces, the model establishes a constant load reference, enabling consistent embedment calculations at any required safety level. Unlike traditional models that often overestimate embedment due to simplistic load assumptions, the WYDIWYG model clarifies the roles of active and passive pressures below LED using sound engineering principles and reinterprets them as reductions in geotechnical resistance, not as additional loads. These pressures are combined to form net effective stabilizing resistances, resulting in a more rational and consistent stability assessment. The model demonstrates robust performance across both long-term (effective stress) and transient (total stress) conditions. Through a stepwise process, it is capable to determine a most economical embedment for any chosen factor of safety through a consistent approach. Its differences become more pronounced as the design strength of materials decreases, an important consideration for major infrastructure projects. In the case of free cantilever walls, the model addresses the confusion surrounding a correct application of geotechnical reduction factors due to stress reversal. It demonstrates application of the geotechnical reduction factor to the appropriate

effective resistance components, enhancing design consistency and ensuring compliance with Australian Standard AS 5100.3. The proposed computation process considers both rotational and horizontal force equilibriums, allowing converging wall loads to be calculated for structural designs. While the model is tailored to AS 5100.3, its principles are expected to be compatible with other national and international standards, and codes of practices.

Although this paper does not explore all potential benefits of the model in the building industry, the authors are confident in its superior performance, not only in isolated long-term or transient analyses, but also in combined effective and total stress scenarios, such as those encountered in stratified ground conditions. Furthermore, while developed for cantilever retaining walls, the model is expected to be applicable to other standalone cantilever structures subjected to significant lateral loads, including signage, acoustic barriers, and pile-supported systems.

ACKNOWLEDGEMENTS

The authors would like to thank Transport for New South Wales for its permission to publish the research results. The opinions expressed in this paper are those of the authors and do not necessarily represent those of Transport for New South Wales. Thanks are also due to Kai Sheng Tan from CMT Engineers for his drafting work.

REFERENCES

Bica, A.V.D. and Clayton, C.R.I. (1989). Limit equilibrium design methods for free embedded cantilever walls in granular materials. Proc. Instn Civ. Engrs Part 1 86, No. 5, 879–989.

British Steel Corporation (1988). BSC Piling Handbook. 6th Edition (1988).

Burland, J.B., Potts, D.M. and Walsh, N.M (1981). The overall stability of free and propped embedded cantilever retaining walls, Ground Engineering, July 1981.

Civil Engineering Code of Practice No.2 (1951). Earth Retaining Structures. Institution of Structural Engineers.

Rowe, P.W. (1951). Cantilever sheet piling in cohesionless soil. Engineering, vol. 172, no. 4467.

Standards Australia (2017). AS 5100.3 Bridge Design—Foundation and Soil-Supporting Structures

WALLAP, Geotechnical design software – Earth retaining structures by Geosolve.

Yuen, C.K.S. (2019). What you design is what you get – An economical way to the stability design of propped cantilever walls. Proc. 13th ANZ Conference on Geomechanics, Perth WA Australia, Acosta Martínez and Lehane (Eds.), 483-488.

Yuen, C.K.S. (2022). Earth pressure, a load or a resistance: Formulation of the 'What You Design Is What You Get' model for stability design of propped cantilever walls. Proc. 4th International Transportation Geotechnics Vol 3, Tutumluer et al (Eds.), 541-554.

Yuen, C.K.S. and Liew, W. (2023). A simple and effective way for embedment design of free cantilever walls, Proc. 14th ANZ Conference on Geomechanics, Cairns Qld Australia.

 © Deep Foundations Institute 2026

3D FINITE ELEMENT ANALYSIS AND FIELD VALIDATION OF OLIVIER INCLUSIONS FOR RESIDENTIAL TOWERS ON SOFT GROUND

Farbod Yarmohammadi, Associate Geotechnical Engineer, CMW Geosciences, Auckland, New Zealand, +64275605567, FarbodY@cmwgeo.com
Konstantinos Lontzetidis, Technical Director, Babbage Consultants Ltd., Auckland, New Zealand, +64204820859, Kostas@Babbage.co.nz
Terry Donnelly, Director, CLL Service and Solutions, Auckland, New Zealand, +64275990227, Terry@cll.net.nz

ABSTRACT

This study presents the design, optimization and construction process of Olivier inclusion ground improvement beneath two adjacent residential towers on Mt Wellington Highway in Auckland. An Olivier inclusion is a cast-in-place, full-displacement element of concrete with a continuous helical shaft that transfers loads through a load transfer platform, which helps distribute forces between the inclusions and the soil. Fully coupled 2D and 3D finite element analyses using PLAXIS 3D were conducted, utilizing the Hardening Soil Model with Small Strain Stiffness, calibrated against site investigation data. The study closely analyzed the interaction between inclusions and tower foundations, capturing the structural response and mutual influences between neighboring inclusions. A parametric assessment of geometry, spacing, and embedment depth guided the optimization of construction methodology to achieve a safe, sustainable, and cost-effective outcome. The 3D analysis captured the interaction between the inclusions and each tower as well as the mutual interaction between the neighboring towers. Additionally, load tests on inclusions of varying lengths were conducted to validate axial stiffness assumptions across different soil layers.

Keywords: ground improvement, finite element modelling, rigid inclusions, Olivier inclusions

INTRODUCTION

Soft, compressible soils often experience substantial settlement when subjected to external load. A traditional solution to address large settlements typically involves the use of deep foundations that transfer structural loads to more stable underlying strata (Das and Sivakugan, 2018). However, because deep foundations can be both costly and time-consuming, a variety of alternative ground improvement methods have been developed to enhance the soil's ability to bear loads. Han (2015) categorized these ground improvement strategies into six principal groups: (1) densification, (2) replacement, (3) drainage and consolidation, (4) chemical stabilization, (5) reinforcement, and (6) thermal and biological treatment.

Rigid inclusions have emerged in the past years as an effective solution to improve the bearing capacity of shallow, weak soils and to reduce associated settlements (Cirión et al., 2013). Historically, early use of rigid inclusions involved driving wooden piles into the ground to enhance subgrade stiffness beneath foundations (Auvinet and Rodríguez, 2006). With technological progress, concrete columns have replaced timber ones, delivering more effective performance (Cirión et al., 2013). These inclusions do not connect directly to the structure above as their main function is to strengthen the subsoil and prepare a suitable ground for placing the foundation. The load transfer from the superstructure to the rigid inclusions through a load transfer platform (LTP) typically consists of a compacted layer of sand or gravel placed between the reinforced soil and the foundation (Auvinet and Rodríguez, 2006; Han and Gabr, 2002; Russell and Pierpoint, 1997; van Eekelen et al., 2013).

One notable development in the evolution of rigid inclusions is the Olivier rigid inclusion system, introduced in Belgium in the late 1990s. This method involves the installation of concrete columns using a displacement auger, which forms the inclusion without generating spoil. This installation method offers advantages such as reduced construction time, reduced environmental impact due to lower concrete consumption, and therefore significant time and cost-saving on projects. Olivier

 © Deep Foundations Institute 2026

inclusions have been widely adopted across Europe and internationally, particularly in projects where settlement control and enhanced bearing capacity in soft soils are essential (Raithel et al., 2008; Almeida et al., 2013).

Various design and modelling approaches for rigid inclusions have been proposed in the literature, ranging from simplified analytical methods to advanced numerical simulations (Bhasi and Rajagopal, 2015; Blanc et al., 2014; Combarieu, 1990; Mánica Malcom et al., 2016; Pérez and Melentijevic, 2015; Raithel et al., 2008). In routine practice, particularly for small-scale developments, designers often treat inclusions as isolated elements, focusing on achieving the required bearing capacity and limiting settlements for the foundation. While this approach may be sufficient for simple or isolated structures, it becomes inadequate for larger or more complex projects, especially when multiple buildings are constructed in close proximity. In such cases, ignoring the interaction between adjacent foundations and the influence on the reinforced ground can lead to unconservative designs and underestimation of settlement or load-sharing effects.

This paper outlines the design, optimization, and construction of Olivier rigid inclusions beneath two adjacent residential towers located at 80 Mt Wellington Highway in Auckland, New Zealand. Fully coupled two and three-dimensional finite element models were developed using PLAXIS 3D, incorporating the Hardening Soil Model with Small-Strain Stiffness (HS-Small), calibrated against detailed site-specific geotechnical investigation data. The analysis considered the interaction between the inclusions and the tower foundations, as well as the mutual influence between the two towers and their adjacent car parks. A series of parametric studies were undertaken to optimize the inclusion lengths across the building platforms, aiming to achieve uniform performance while maintaining cost-efficiency. Additionally, full-scale load tests were conducted on inclusions of varying lengths to verify the assumed axial stiffness across the site's heterogeneous soil profile.

PROJECT DESCRIPTION

The proposed development at 80 Mt Wellington Highway, Mt Wellington, Auckland, New Zealand, comprised two multistorey towers: an 8-storey (Building A) and an 11-storey (Building B) structure, both supported on raft foundations. The location of these towers is shown in Fig. 1.



Fig. 1. Proposed locations of Towers A and B

 © Deep Foundations Institute 2026

The anticipated serviceability pressures were approximately 110 kPa for Building A and 150 kPa for Building B. Under these loads, the unimproved ground was predicted to experience long-term settlements of up to 110 mm beneath Building A and 170 mm beneath Building B.

To mitigate these excessive settlements beneath the proposed raft foundations, CMW Geosciences undertook the detailed design of a ground improvement system beneath both towers. The adopted solution comprised an Olivier pile inclusion system installed below a 750 mm thick load transfer platform, which consisted of compacted hardfill reinforced with geogrid. Figure 1 shows the location of each of these two towers.

GROUND MODEL

Published geological maps for the area depict the regional geology as comprising Holocene alluvium (sand, silt mud and clay with local gravel and peat beds) of the Tauranga Group as shown in Fig. 2 below.

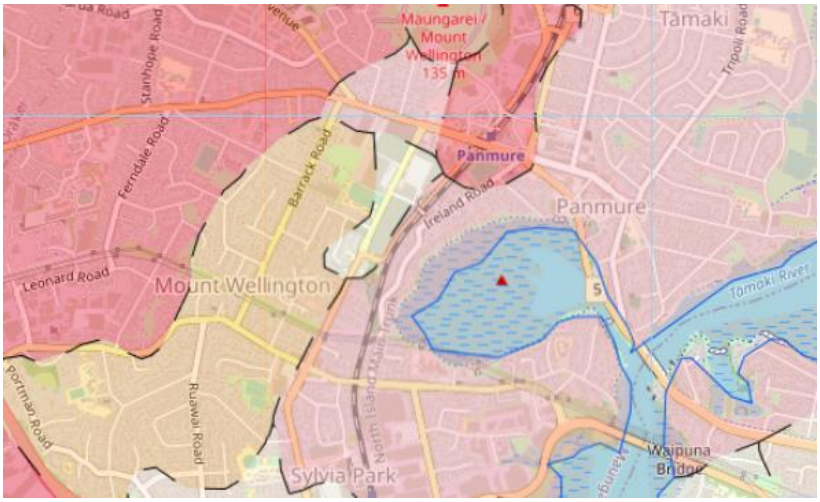


Fig. 2. Regional geology (New Zealand Geology Web Map) – Site is circled with the red dotted line

The description and distribution of the various units encountered during investigations is summarized in Table 1 below.

Table 1. Summary of strata encountered during site investigations

Unit	Depth to base (m)		Thickness (m)**	
	Min	Max	Min	Max
Fill: Gravels and Cobbles with some silt; 'medium dense', moist. Cobbles were up to 100mm in diameter, strong, subangular to angular, non-spherical, slightly vesicular basalt.	0.3	1.3	0.3	1.3
Auckland Volcanic Field Tephra / Tuff: Silts with some clay with minor lenses of gravels and cobbles. Very stiff, moist, moderately plastic.	0.9	3.2	0.2	1.5
Alluvium – Tauranga Group (Recent): Silts and sands; stiff to very stiff, moist, slightly to moderately plastic.	9.5	11.0	~7.3	10.8
Very Dense Rhyolitic Ash: Silty sand; very dense, moist,	13.5	14.4	3.0	3.5

 © Deep Foundations Institute 2026

Unit	Depth to base (m)		Thickness (m)**	
	Min	Max	Min	Max
non-plastic.				
Alluvium – Tauranga Group (Old): Silt and clays with variable sand content; soft to stiff, moist, slightly plastic. Minor lenses of fibrous peat.	34	34.6	20.0	20.2
Kawa Formation (Bedrock): Moderately to slightly weathered; fine sandstone with minor lenses of mudstone. Extremely weak to very weak, carbonised rootlets throughout.	-		>7.0	

During the investigations completed in late spring, groundwater was encountered within the Test Pits at a depth ranging from 1.7 m to 2.9 m below ground level.

Geotechnical design parameters developed from CMW investigations and rationalized for Olivier Inclusions design are presented in Table 2. The parameters used in the numerical modelling of the inclusions are presented in the subsequent section.

Table 2. Ground model and general design parameters

Geological Unit	Thickness (m)	γ (kN/m^3)	c' (kPa)	φ' (deg)	Su (kPa)	E (MPa)	fs (kPa)	fb (MPa)	v	e_o
Fill	1.1	18	0	30	-	12	0	0	0.3	2
Auckland Volcanic Field Tephra/Tuff	1.8	18	3	30	80	12	70	2	0.3	1.2
Alluvium – Tauranga Group (Young)	8.6	18	2	26	50	15	35	1	0.4	1.68
Very Dense Rhyolitic Ash	3.4	19	0	40	-	50	120	5	0.3	0.6
Alluvium – Tauranga Group (Old)	18.1	18	1	30	100	15	35	1	0.4	1.25
Kawa Formation	10+	20	40	40	-	100	500	5	0.2	1

γ = unit weight, c' = effective cohesion, ϕ' = effective friction angle, Su = undrained shear strength, E = Youngs Modulus, fs = skin friction, fb = end bearing, v = Poisson's ratio, e_0 = initial void ratio

NUMERICAL MODELLING

Fully coupled 2D and 3D finite element analyses using PLAXIS 3D were conducted, utilizing the Hardening Soil Model with Small Strain Stiffness (HS-Small) to design the ground improvement elements under the proposed towers.

The objectives of the design were the following:

- Estimating long-term ground settlements due to the different stages of the construction considering the group effect of the inclusions.

- Estimating the differential settlements across the building footprint.
- Analysing the effect of the nearby buildings (Towers A and B) on the overall building settlements.
- Analysing the effect of the proposed car park adjacent to the towers on the building settlements.
- Providing the structural engineers with the spring stiffness of the improved ground.
- Checking the bearing capacity of the bearing stratum.

The following modelling steps were undertaken in the design stage to achieve these objectives:

- Axisymmetric modelling of the rigid inclusions in PLAXIS 2D using solid volumetric elements to assess the settlement and the stresses developed within the inclusions. This axisymmetric model will be used later to calibrate the embedded beam elements used for modelling the inclusions in PLAXIS 3D.
- Small-scale modelling of one rigid inclusion in PLAXIS 3D using embedded beam elements to calibrate the embedded beams using the results of the previous step.
- Large-scale 3D modelling of the entire site using the calibrated embedded beam elements to achieve the design objectives.

After developing the calibrated large-scale 3D modelling of the site, sensitivity analyses were undertaken to optimize the length of the proposed rigid inclusions, while ensuring uniform behavior of the raft foundations under the proposed bearing pressures.

Model Dimensions

Axisymmetric model

The dimensions of the unit cell axisymmetric model were chosen according to the recommendations detailed in ASIRI (2012), presented in Fig. 3 below.

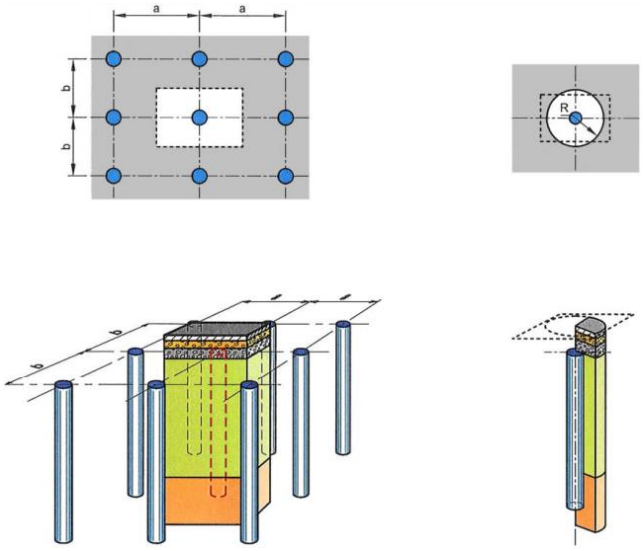


Fig. 3. Axisymmetric model representing a single mesh of a distributed load supported by a soil reinforced by rigid inclusions (ASIRI, 2012)

Using this method, the dimensions of the model were chosen so that the soil in the unit cell model represents the same area as the soil supported by a single inclusion in the 3D model (i.e., $\pi R^2 = a.b$).

Small-scale 3D model

Small-scale 3D analysis was undertaken to calibrate embedded beam elements against the unit cell model developed in the previous step. The dimensions of this model were chosen to match the actual spacing of the inclusions (i.e., a and b in Fig. 3).

Large-scale 3D models

Large-scale 3D analyses were undertaken using the calibrated embedded beam elements to achieve the objectives of the design. The model dimensions were chosen according to the size of the footprints of the proposed towers and carparks. Additionally, sensitivity analyses were undertaken to eliminate the unwanted effects of the model boundaries on the estimated building performance. As a result, a minimum 30 m distance was considered between the model boundaries and the edge of structures in the large-scale 3D models. Fig. **5** presents an example full-scale 3D model developed in PLAXIS 3D showing the location of the proposed towers and car parks.

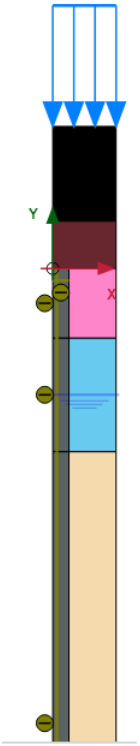


Fig. 4. Example 2D axisymmetric model developed in PLAXIS 2D using solid elements

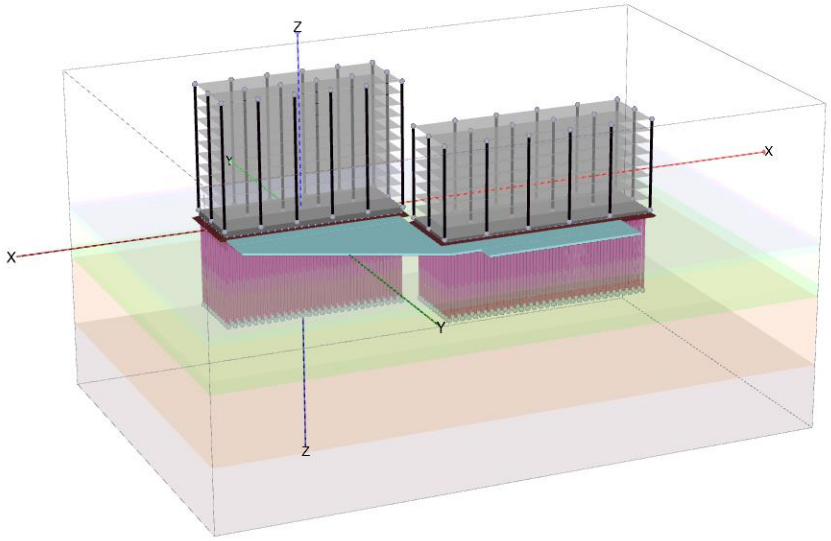


Fig. 5. Example full-scale 3D model developed in PLAXIS 3D using embedded beam elements

 © Deep Foundations Institute 2026

Material Models

Soil elements

The design uses the drained Hardening Soil model with small stiffness (HS-Small) to model the soil behavior under the building surcharge. The Hardening Soil model is an advanced model for simulating the behavior of both soft and stiff soils. In contrast to an elastic perfectly plastic model (e.g., Mohr-Coulomb) with a fixed yield surface, the yield surface of a hardening plasticity model can expand due to plastic straining. This model can distinguish between the two main types of hardening (i.e., shear and compression hardening). The original Hardening Soil model assumes elastic material behavior for the soil during unloading and reloading phases. However, the HS-Small model considers the non-linear soil behavior in smaller strains and therefore takes the soil small-strain stiffness reduction into account. Table 3 below shows the design parameters for this soil model for each geological unit. The parameters were estimated conservatively using the existing relationships in literature and PLAXIS Material Model Manual (2023).

Table 3. HS-Small parameters used in the numerical modelling

Geological Unit	**$E50_{ref}$ (MPa)**	**$Eeod_{ref}$ (MPa)**	**Eur_{ref} (MPa)**	**$\gamma_{0.7}$**	**G_{oref} (MPa)**	**m**
Fill	12	9.6	36	$1.5x10^{-4}$	15	0.5
Auckland Volcanic Field Tephra/Tuff	12	9.6	36	$1.0x10^{-4}$	120	0.7
Alluvium – Tauranga Group (Young)	15	12	45	$2.0x10^{-4}$	40	0.7
Very Dense Rhyolitic Ash	50	40	150	$2.0x10^{-4}$	150	0.5
Alluvium – Tauranga Group (Old)	15	12	45	$7.5x10^{-5}$	50	0.7
Kawa Formation	100	80	300	$2.0x10^{-4}$	150	0.5

$E50_{ref}$ = Secant drained stiffness, $Eeod_{ref}$ = Tangent stiffness for primary loading, Eur_{ref} = unloading/reloading stiffness, $\gamma_{0.7}$ = threshold shear strain at which $G_S = 0.722G_o$, $G_{o\text{-}ref}$ = reference small-strain shear modulus, m = power for stress-level dependency of stiffness

Rigid inclusions

The 2D models used solid volumetric elements to model the rigid inclusions and estimate their settlements and stresses to calibrate the 3D models. The 3D models used embedded beam elements with multi-linear axial resistance to simulate the rigid inclusions in the ground. These elements in PLAXIS 3D consist of beam elements with embedded interface elements to describe the interaction with the soil at the pile skin and at the pile foot (bearing capacity). The axial skin resistance of the beam elements was considered to be dependent on their adjacent soil layer and was calibrated using the unit cell model. Linear elastic behaviour was considered for the rigid inclusions in both 2D and 3D models. A value of 0.7 was chosen for then R_{int} value between the soil and the rigid inclusions.

Concrete slabs and geogrids

All models used solid volumetric elements to simulate the building and carpark concrete slabs under the proposed loads. Linear elastic behaviour was considered for all the concrete slabs with the elastic modulus calculated according to the concrete compressive strength after 28 days of curing.

3D geogrid elements with elastic material behaviour implemented in PLAXIS 3D were used to simulate the proposed biaxial geogrids placed under the proposed LTP to control the differential settlements between the rigid inclusions and the soil in between. Interface elements were used to simulate the interface between these elements and the adjacent soil.

Analyses stages

The following stages were used in the finite element analyses:

- Initial phase to calculate the in-situ stresses in the soil prior to impose any loads.
- Installing the rigid inclusions to the required depth.
- Installing the geogrid and the LTP.
- Installing the building slabs on top of the LTP.
- Adding the building surcharge (provided by the structural engineers) on top of the slab as a distributed load.
- Adding the slab and surcharge for the adjacent carparks (provided by the structural engineers).

LOAD TESTS

Three compression static load tests were carried out to verify the design assumptions and predicted settlements of the rigid inclusions under the proposed building loads. Sacrificial inclusions of varying lengths were installed to assess settlements for inclusions embedded in different soil strata. Test loads were applied incrementally, from 0% to 100% of the ultimate pile capacity in 17% load steps, with each load stage held for up to 60 minutes. The designed test inclusions were as follows:

- Inclusion #1: 10 m long, designed for an ultimate test load of 760 kN. Two 12 m long Olivier inclusions were installed on either side to provide the necessary reaction capacity during testing.
- Inclusion #2: 12.5 m long, designed for an ultimate test load of 1,850 kN. Two 22 m long Olivier inclusions were installed on either side to provide the necessary reaction capacity during testing.
- Inclusion #3: 15 m long, designed for an ultimate test load of 1,516 kN. Two 16 m long Olivier inclusions were installed on either side to provide the necessary reaction capacity during testing.

Three displacement gauges installed on top of each test rigid inclusion measured its movement throughout the loading process.

RESULTS AND CONCLUSION

Design Results

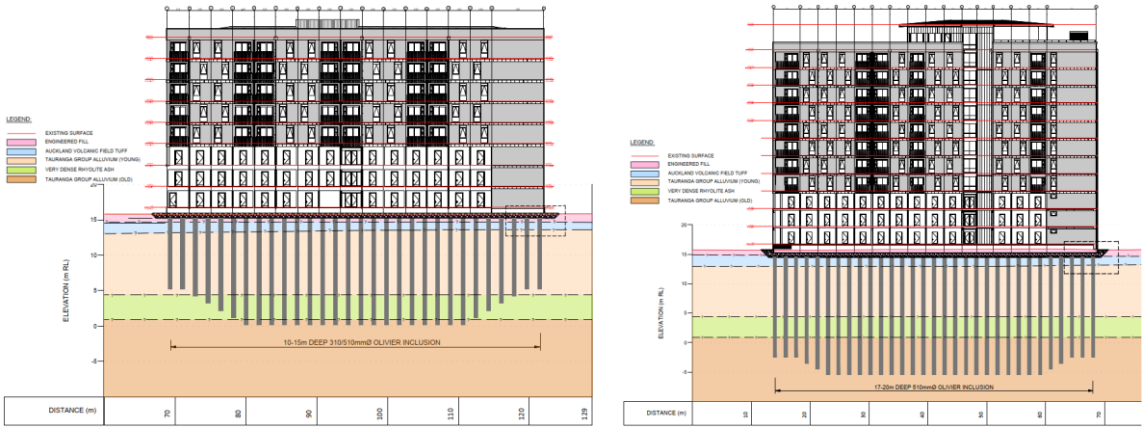
Traditional simplified design methods for rigid inclusions typically focus on the load applied to a single representative element. This often results in a uniform inclusion length beneath the raft foundation, with each element extending to a hard stratum (often rock) and relying primarily on end bearing. In this project, such an approach would have produced inclusion lengths exceeding 30 m. Using this method would also have overlooked the complex interaction between adjacent towers through the intervening soils.

The proposed 3D numerical modelling approach enabled optimisation of inclusion lengths by accounting for a more realistic load distribution across the site. Inclusions were embedded within a stiff to very stiff alluvial layer (Old Tauranga Group Alluvium) rather than extending to rock. The design incorporated variable lengths with shorter inclusions at the foundation perimeter, increasing gradually towards the centre to ensure uniform raft foundation performance under the proposed loads. Table 4 summarizes the design of Olivier inclusion for each tower, while Fig. 6 and Fig. 7 present typical cross sections of Olivier inclusion layout beneath each building and their predicted settlements.

Table 4. Rigid inclusion design summary

Tower	Slab thickness (mm)	LTP thickness (mm)	Inclusion inner/outer diameter (mm)	Inclusion spacing (m)	Inclusion length (m)	Concrete strength (MPa)	Total settlements (mm)
A	800	750	310/510	1.8	10-15	40	45
B	1500	750	310/510	1.8	16-20	50	45

 © Deep Foundations Institute 2026



(a) (b)

Fig. 6. Olivier inclusion design – (a) Building A (b) Building B

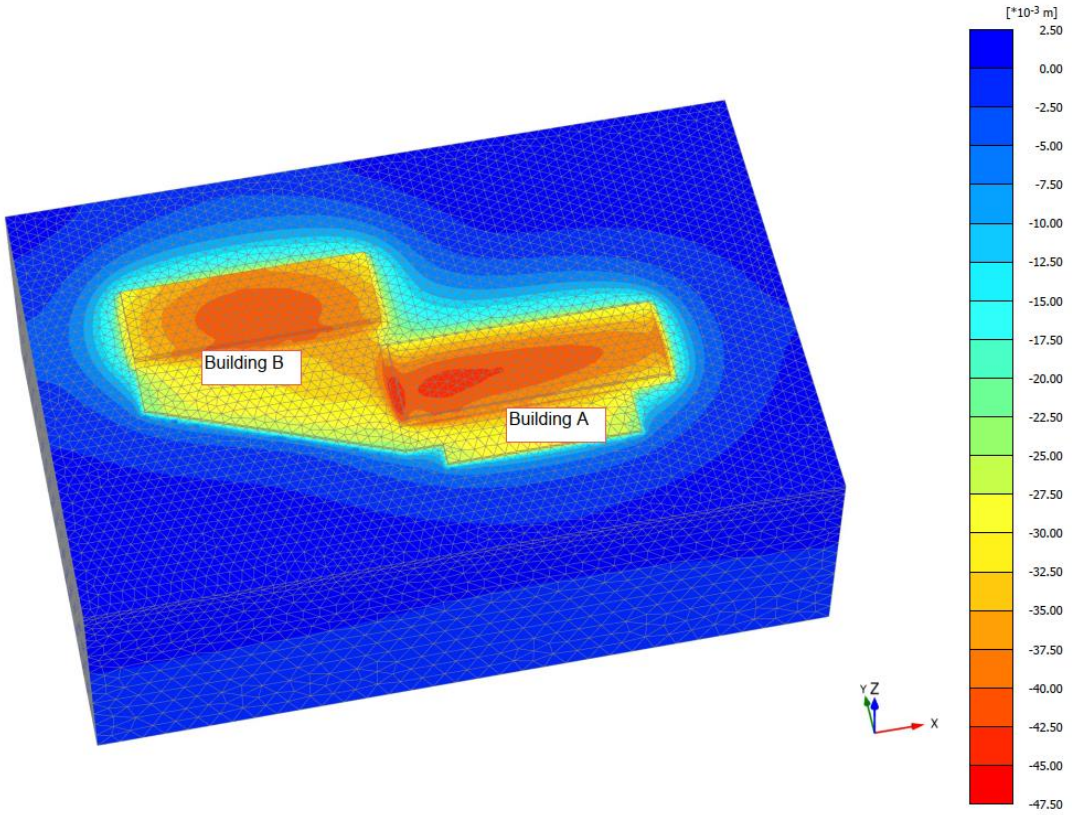


Fig. 7. Predicted building settlements after installation of rigid inclusions

Load test results

Figure 8a-c. below show the load displacement curves of the three test rigid inclusions with different lengths. These tests showed that the displacements of the rigid inclusions under the proposed serviceability loads remained under 5 mm, confirming that the design approach provided a conservative prediction of settlement. Despite these smaller measured settlements, the inclusion lengths were not reduced further in order to maintain a conservative performance margin and to account for variability in soil conditions across the site.

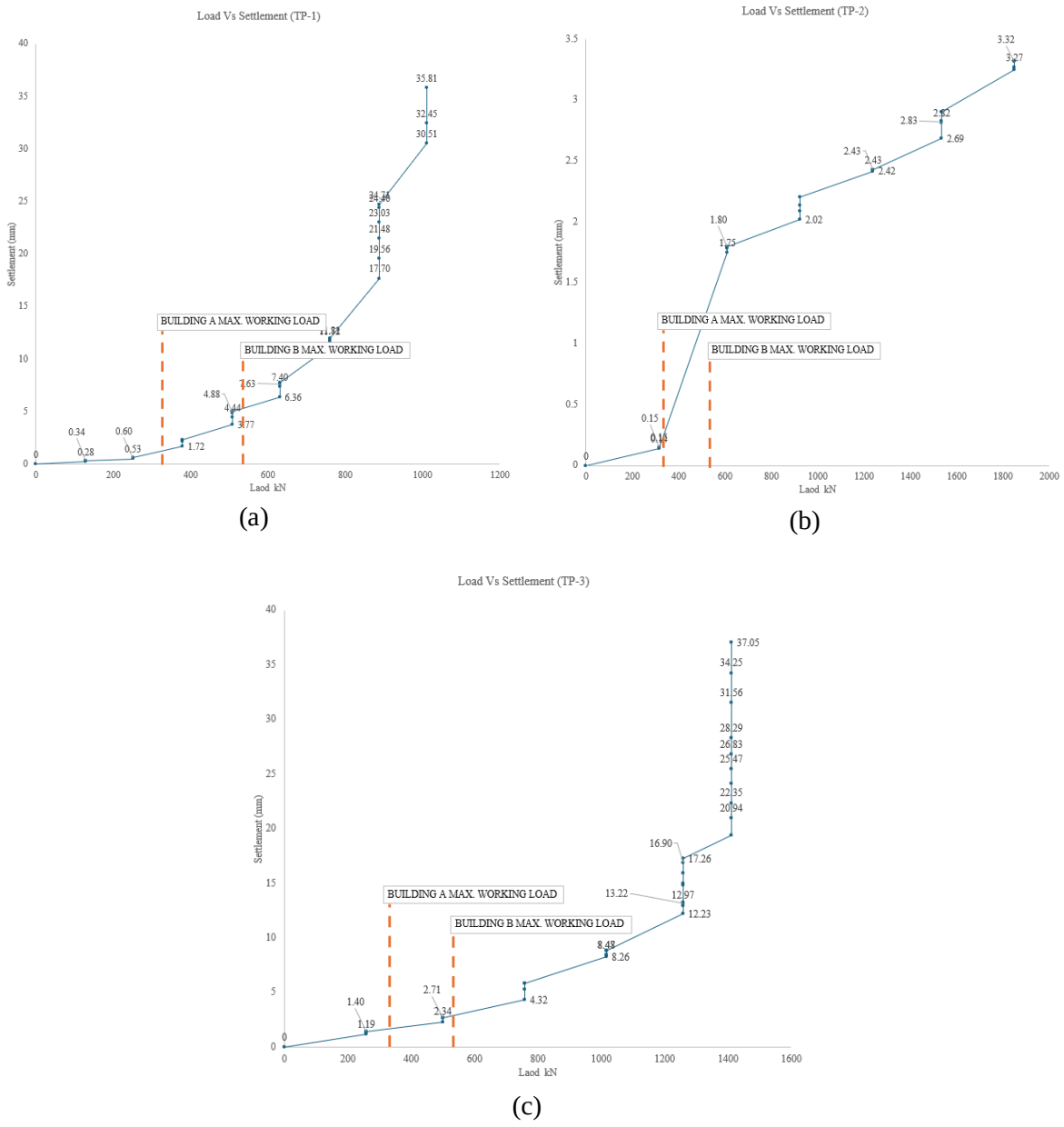


Fig. 8. Load-displacement curve of test inclusion (a) #1-10m (b) #2-12.5m (c) #3-15m

ACKNOWLEDGEMENTS

The authors thank Simplicity Living for their support and collaboration throughout this project. Their endorsement of this innovative foundation solution, alongside their support of our advanced numerical modelling approach, contributed to a more efficient and environmentally sustainable design that benefits the future of New Zealand. Authors would also like to thank Mitchell Vranjes, the structural engineering team, whose expertise and collaborative spirit enabled the successful integration of geotechnical design into the structural framework contributing to a successful outcome for the project.

REFERENCES

ASIRI, 2012. Recommendations for the design, construction and control of rigid inclusion ground improvements, Presse des Ponts et Chaussée.

Auvinet, G., and Rodríguez, J. F., 2006. Rigid inclusions in Mexico City soft soils: history and perspectives. Proc. of the Symposium Rigid Inclusions in Difficult Subsoil Conditions ISSMGE TC36.

 © Deep Foundations Institute 2026

Bentley, 2023. Plaxis 2D Material Models Manual.
Bhasi, A., and Rajagopal, K., 2015. Numerical study of basal reinforced embankments supported on floating/end bearing piles considering pile–soil interaction. Geotextiles and Geomembranes, 43(6), 524–536.
Blanc, M., Thorel, L., Girout, R., and Almeida, M., 2014. Geosynthetic reinforcement of a granular load transfer platform above rigid inclusions: comparison between centrifuge testing and analytical modelling. Geosynthetics International, 21(1), 37–52.
Cirión, A., Paulín, J., Racinais, J., and Glandy, M., 2013. Displacement rigid inclusions. Proceedings of the 18th ICSMGE, Paris, France.
Combarieu, O. 1990, Fondations superficielles sur sol amélioré par inclusions rigides verticales. Revue Française de Géotechnique, 53, 33–44.
Das, B. M., and Sivakugan, N., 2018. Principles of Geotechnical Engineering. Cengage Learning, Boston.
Han, J., 2015. Principles and practice of ground improvement. John Wiley and Sons.
Han, J., and Gabr, M. A., 2002. Numerical analysis of geosynthetic-reinforced and pile-supported earth platforms over soft soil. Journal of Geotechnical and Geoenvironmental Engineering, 128(1), 44–53.
Mánica Malcom, M. Á., Ovando-Shelley, E., and Botero Jaramillo, E., 2016. Numerical study of the seismic behavior of rigid inclusions in soft Mexico City clay. Journal of Earthquake Engineering, 20(3), 447–475.
Pérez, R. G., and Melentijevic, S., 2015. Comparative analysis of analytical and numerical calculation methods for soil improvement by rigid inclusions. In From Fundamentals to Applications in Geotechnics (pp. 1859–1866). IOS Press.
Raithel, M., Kirchner, A., and Kempfert, H. G., 2008. German recommendations for reinforced embankments on pile-similar elements. In Geosynthetics in civil and environmental engineering (pp. 697–702), Springer.
Russell, D., and Pierpoint, N., 1997. An assessment of design methods for piled embankments. Ground Engineering, 30(10).
van Eekelen, S. J. M., Bezuijen, A., and van Tol, A. F., 2013. An analytical model for arching in piled embankments. Geotextiles and Geomembranes, 39, 78–102.

 © Deep Foundations Institute 2026

GEOGRID REINFORCED TEMPORARY WORKING PLATFORMS FOR TRACKED PLANT – INSIGHTS FROM A LARGE-SCALE FIELD-TRIAL ON SENSITIVE LACRUSTINE CLAY

Jörg Klompmaker, Naue GmbH and Co. KG, Espelkamp, Germany, jklompmaker@naue.com
Lars Vollmert, Naue GmbH and Co. KG, Espelkamp, Germany, lvollmert@naue.com
Christoph Füger, Technical University of Munich, Munich, Germany, christoph.fueger@tum.de
Stefan Vogt, Technical University of Munich, Munich, Germany, stefan.vogt@tum.de

ABSTRACT

The safe operation of tracked vehicles on temporary working platforms over soft, cohesive soils presents significant geotechnical challenges. Although geogrid reinforcement is widely used to improve bearing capacity and reduce settlements, design approaches remain largely empirical. This study presents results from a large-scale field trial investigating the performance of a laid-and-welded geogrid installed over a separation geotextile to reinforce a granular working platform on soft lacustrine clay. The trial was conducted under real construction conditions during pile driving operations and was supported by extensive instrumentation. Strain gauges integrated into the geogrid measured mobilised tensile forces, while earth pressure sensors beneath a loaded track recorded vertical stress distribution at different interfaces. Multipoint settlement gauges monitored total and differential settlements to assess deformation behaviour and operational stability. This paper describes the test setup, boundary conditions, instrumentation, and selected preliminary monitoring results. The findings will be used to validate numerical models and to compare measured performance with predictions from the BR 470 guideline. The study aims to support the development of performance-based design methods for geogrid-reinforced working platforms on soft cohesive soils.

Keywords: Temporary working platforms, design guideline BR 470, geogrid reinforcement, field performance monitoring.

INTRODUCTION

Temporary working platforms are essential for the safe operation of heavy tracked construction equipment such as piling rigs and cranes, particularly in infrastructure and foundation engineering projects. When such platforms are constructed over soft, cohesive subsoils – such as young deposits formed by lacustrine clays – their stability and load-bearing capacity become decisive for design. Inadequate platform performance can lead to excessive deformations, operational hazards, or even structural failure, posing significant safety risks and economic consequences. To improve the mechanical performance of these platforms, geosynthetic stabilisation and reinforcement products – especially geogrids – are increasingly employed. Their inclusion can enhance bearing capacity, reduce differential settlements, and optimize the use of granular fill materials, thus offering economic advantages and saving of natural resources. Research carried out by Abu-Farsakh, et al. (2008) showed, that the inclusion of geogrid reinforcement in a shallow foundation over soft silty clay significantly improved the soil's bearing capacity and reduced the footing's immediate settlement. Geogrids with higher tensile modulus performed better than geogrids with lower tensile modulus. Despite these benefits, current design methods for geogrid-reinforced working platforms remain largely empirical and the limitations of their applicability are subject to discussion (Miller 2013 and 2020, Khansari et al., 2021 and 2023). Guidelines such as BR 470 provide useful frameworks but often lack rigorous validation under varying subsoil conditions, particularly for very soft, cohesive soils.

This research addresses this drawback by presenting a large-scale field trial designed to investigate the performance of a laid and welded geogrid reinforcement embedded at the base of a granular working platform constructed over soft lacustrine clay. The study combines full-scale loading by a piling rig with comprehensive instrumentation to record strain of the geogrid, earth pressure, and settlement below the tracks of the piling rig under various loading and manoeuvring conditions. The overarching goal is to assess the validity of existing design assumptions, contribute to the development of

 © Deep Foundations Institute 2026

performance-based design approaches, and support the broader adoption of geogrid reinforcement in temporary working platforms on subgrades of comparably low strength and stiffness.

WORKING PLATFORM

Subsoil

For the field trial, a working platform intensively instrumented with a wide range of sensors to measure geogrid strain, earth pressure and settlement was constructed at a test site established as part of an ongoing research project "SEBRO" in the municipality of Kolbermoor, Southern Germany (Berz et al. 2026). The test site is located within the Rosenheim basin north of the Alps, which is characterized by subsoil of soft, sensitive lacustrine clay up to a depth of 300 m deposited after the last glacial period from about 11 thousand years ago. The lacustrine clay is of low to medium plasticity including thin layers of silty sand to silt (Cudmani et al. 2022). The first step in constructing the working platform was to excavate a 0.7 m-thick surface layer of peat. Laboratory testing was conducted on three samples collected from the surface of the lacustrine clay. The measured mean dry density was 1.71 ± 0.01 g/cm³, and the mean natural water content was 21.3 ± 1.0%, resulting in near-saturated conditions (S_r = 0.99). The liquid limit and plastic limit were determined as 30.5 ± 0.8% and 19.8 ± 0.9%, respectively. Based on these results, the consistency of the samples ranged from soft to hard.

Three SPLTs Ø 300 mm were carried out based on DIN 18134 (German code). According to the code, unloading was conducted once a settlement of 5 mm was reached. Table 1 provides the deformation modulus of primary loading (E_{v1}) and reloading (E_{v2}). The measured E_{v1} of about 4 MPa and E_{v2} = 20 MPa clearly indicated that the bearing capacity of the lacustrine clay was insufficient for operating heavy machinery directly on it. FVTs were performed at depths of 0.25 m and 0.40 m below excavation level, which corresponds to the position where the geogrid was placed (see Table 2). In accordance with the planned manoeuvres of the piling rig, a plastic pipe was installed next to the planned position of the track, to keep a small area of the lacustrine clay accessible for further FVTs after the base course material had been placed and compacted. The FVTs within the pipe were carried out on the day of the field trials and two days after. The derived values of the peak shear strength c_{fv} in the field ranged from 285 kPa to 416 kPa, while the residual value c_{rv} at large displacement (after three full 360°-degree rotations of the vane) was measured between 85 kPa and 184 kPa. Lower values were recorded after construction of the working platform possibly due to soil disturbance from vibrations by the compaction of the base course material. FVTs conducted on samples in the lab showed a further decrease in shear strength, with c_{fv} = 174 kPa and $c_{r\,v}$ = 37 kPa indicating the soil's sensitivity against shear loadings as induced by sampling.

The observed scatter in shear strength may be attributed to the clay's structural sensitivity. The highest values were measured before the working platform was constructed. The second test series in the pipe was conducted after compaction of the base course material using a vibratory plate, which may have disturbed the clay. The samples tested in the lab experienced the highest rate of disturbance and thus suffered greater shear strength loss. Nevertheless, and partly in contrast to the SPLT results, the values obtained for the very top surface layer of the lacustrine clay indicated a consistency more typical of stiff to hard clay rather than soft clay. This finding is consistent with cone penetration tests (CPTu) conducted in the immediate vicinity of the working platform examined in this study. The CPTu indicated an undrained shear strength of c_u > 200 kPa in the uppermost 2 m, which then decreased to about 90 kPa at depths between 2 m and 10 m (Berz et al., 2026).

Table 1. SPLT test results on the lacustrine clay

Day of testing	Testing depth	Number of tests	E_{v1} [MPa][1]	E_{v2} [MPa]	E_{v2}/E_{v1} [-]
7 days before field trials	Surface of excavation level	3	3.9 ± 1.1	20.4 ± 1.7	5.63 ± 1.62

[1] where E_{v1} and E_{v2} are respectively the deformation modulus of Primary loading and Reloading.

Table 2. FVT test results on the lacustrine clay

Day of testing	Testing depth	Number of tests	c_{fv} [kPa] [2]	c_{rv} [kPa]
7 days before field trials	0.25 m	8	371 ± 63	126 ± 29
	0.40 m	5	416 ± 56	184 ± 15
Day of field trials and 2 days after	0.20 m	3	285 ± 20	85 ± 9
1 month after field trials	tested in cutting cylinders in the lab	6	174 ± 28	37 ± 9

[2] where c_{fv}, c_{rv} are respectively the peak and residual undrained shear strength.

Reinforced Base Course / Working Platform

Directly on the surface of the lacustrine clay, a nonwoven geotextile separator was installed to prevent intermixture of the fine clay particles with the coarse base course material. On top of the geotextile a laid and welded geogrid was placed. The geotextile had no overlap on the northern long side of the working platform (see Fig. 1). A locally available crushed dolomite rock (0/45 mm grading) was used as base course material for the working platform. Its maximum dry density (MDD) was 2.09 g/cm³ and optimum moisture content was 4.7% according to the external quality control of the quarry. The base course layer was compacted in one layer (0.3 m) using a vibratory plate of 500 kg weight. The working platform thickness of 0.3 m was determined in accordance with the BR 470 design methodology, based on the dimensions and load specifications of the piling rig used in the field trial. The achieved degree of compaction D_{Pr} was about 100% or slightly higher when comparing the MDD with in-situ testing using the Troxler density gauge (Table 3) and was slightly higher considering density measurement by using the balloon densitometer method. However, the deformation modulus E_{v2} determined by SPLT only reached values of < 40 MPa. One reason for the relatively low E_{v2} values, despite the high density D_{Pr} of the base course aggregate, is likely the transfer of stresses beneath the load plate beyond the thickness of the base course layer into the underlying lacustrine clay.

Table 3. Results of the field test for characterizing the reinforced base course

Test	Number of tests	Parameter	Result
		E_{v1} [MPa]	15.7 ± 2.6
SPLT	2	E_{v2} [MPa]	37.8 ± 2.0
		E_{v2}/E_{v1} [-]	2.46 ± 0.28
Troxler density gauge	10 at 0.15 m; 10 at	ρ_d [g/cm³]	2.09 ± 0.07
Balloon densitometer	4	ρ_d [g/cm³]	2.23 ± 0.08

Monitoring Program

For the trial-loading, a Junttan PMx22 pile driving rig (Kuopio, Finland) operated on the working platform. The dead load of the rig, including hammer weight, pile, and fuel, was 66,000 kg. The precast concrete pile moved by the rig had a length of 8 m with a square cross section measuring 0.4 m x 0.4 m. The weight of the pile was 3,200 kg. Figure 1 shows a plan view of the instrumented working platform illustrating the contact area of the chain track measuring 4.2 m x 0.9 m and the position of the various sensors. For estimating the distribution of the load induced by the piling rig during the different manoeuvres, four piezoelectric earth pressure sensors (Glötzl Gesellschaft für Baumesstechnik mbH, Rheinstetten, Germany) were installed on the surface of the lacustrine clay directly below the geotextile and geogrid (EP L1-L4; see Fig. 2, photo on the left). Five earth pressure sensors were placed close to the surface of the base course layer (EP B1-B5), positioned as near as possible beneath the chain track, after the base course layer had been laid and compacted. The highest track pressures are expected during rotation of the upper carriage at 10°–20°, 160°–170°, 190°–200°,

and 340°–350°, according to the manufacturer's manual. These specifications coincide with the DFI WP Guidelines (2025). For that reason, the position chosen for pile driving was at a rotation of 13° of the upper carriage. The sensors were distributed along the contact area of the track, with more positioned at the front in the direction of the telescopic leader at the desired position. The sensors were embedded within a thin layer of sand (0/4 mm) to protect the sensing pressure plate from angular base course particles and to ensure an evenly distributed stress for recording representative changes of the vertical earth pressure dominantly influenced by the piling rig.

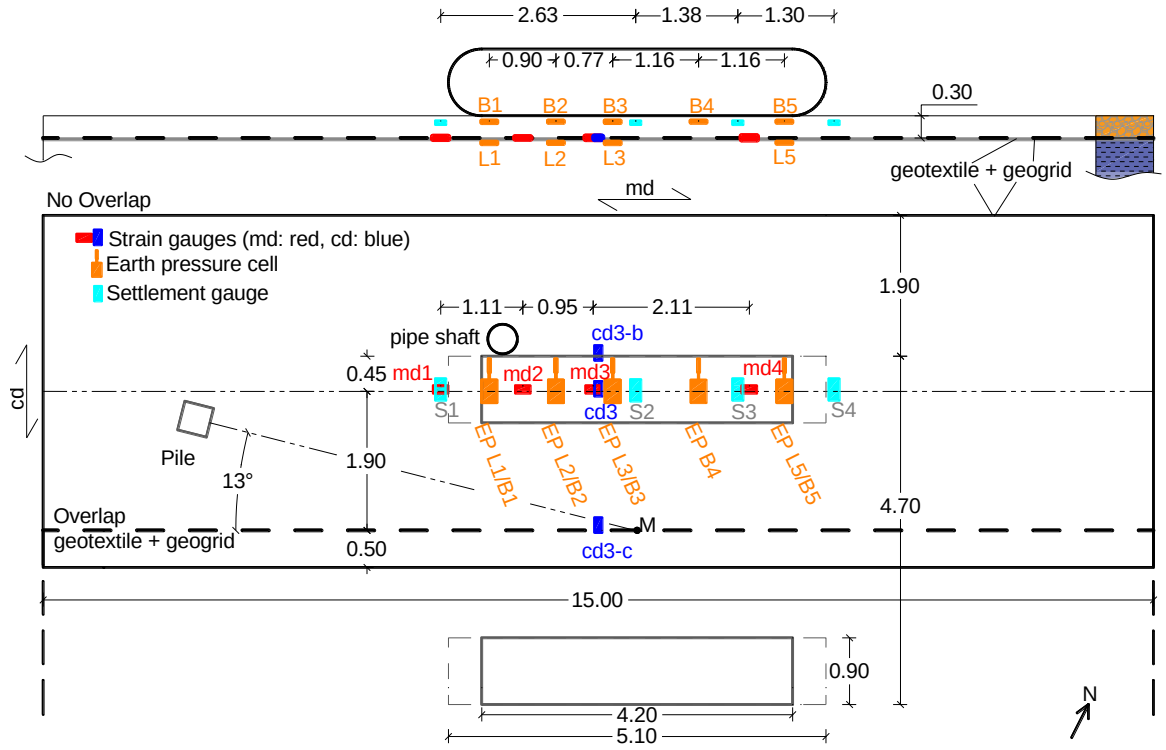


Fig. 1. Arrangement of the monitoring equipment in relation to the two tracks of the piling rig (cross section [top] and plan view [bottom])

The geogrid was equipped with strain gauges, four of them measuring strains in the machine direction (md) along the centre of the permanently loaded track of the piling rig (md1-md4), and three gauges in the cross-machine direction (cd) (cd3, cd3-b, cd3-c). The photo in the middle of Fig. 2 shows how the strain gauges were slightly covered with a thin sand layer, so that the granular particles of the working platform aggregate could still interlock with the apertures of the geogrid. Additionally, four sensors of a multipoint settlement system (Sisgeo Srl, Masate, Italy) were placed along the crawler track close to the working platform surface (S1-S4, see Fig. 2 photo on the right). This system is based on the hydrostatic measurement principle and records absolute settlement values relative to a water-filled reference tank. Two sensors were placed outside the contact area at both ends of the track. The other two sensors were placed within the contact area in the rear half of the track.

The monitoring systems were synchronized using connected measuring amplifiers with a sampling rate of 100 Hz. The data obtained from the multipoint settlement system was smoothed using a moving average filter with a window size of one second. The earth pressure sensors and the multipoint settlement system were calibrated at the factory prior to the tests.



Fig. 2. Earth pressure sensors placed at the surface of the lacustrine clay (left); placing of nonwoven geotextile with geogrid on top and protection of geogrid strain gauges by a thin sand layer (centre); and multipoint-settlement gauges installed close to the surface of the base course before protection by sand (right)

LOAD MANEUVERS BY PILING RIG

Several loading scenarios, referred to as "Load manoeuvres", were carried out during the field trial, two of which are presented in this publication. Prior to the piling rig entering the instrumented working platform, all sensor readings were initialized to zero. The first load manoeuvre, corresponding to Load Case 1 and 2 as defined by BR 470, was performed once the rig had been positioned at the designated location above the monitoring equipment, as illustrated in Fig. 1. This involved rotating the upper carriage by 176°. The precast concrete pile was then pulled toward the rig and lifted into the leader with a further rotation to 215°. Finally, the carriage was rotated back to 13°, with the pile positioned in the leader (see Fig. 3 photo sequence on the left). As the destabilizing loads can be partially mitigated by a skilled machine operator (e.g., during pile pulling, but not during pile lifting), the manoeuvre may be referred to both as Load Case 1 and Load Case 2 according to BR 470. The second load manoeuvre presented here, was carried out after the pile had been driven into the soil, with the upper carriage rotated 13° relative to the chassis. Using the winch and a slip around the pile, a pulling force of approximately 100 kN was applied (see Fig. 3, right photo). This load manoeuvre can be interpreted as a Load Case 2 scenario according to BR 470, as the operator can reduce the applied force to prevent failure of the working platform.



Fig. 3. Load manoeuvre 1: Lifting pre-cast concrete pile into position for installation (photo sequence, left) and load manoeuvre 2: Pulling after pile driving (right)

 © Deep Foundations Institute 2026

MONITORING RESULTS

Load manoeuvre 1 – BR 470 Load Case 1 and 2

Figures 4a–c show the recorded data of all monitoring systems over time during load manoeuvre 1. Figure 4a shows the signals recorded by the earth pressure transducers. The legend entries are arranged to reflect the sensor positions. During the first 25 s, the upper carriage of the piling rig is rotated. At the beginning of load manoeuvre 1, the rig's load is distributed across EP L1 to L3 and EP B3. The sensors at the rear end of the track (EP L5/B5), as well as EP B2/B3, did not record any load. EP B2/B3 are located above EP L2/L3, which registered approximately 100 kPa. This indicates that the load was transferred past the sensors EP B2/B3, likely due to an arching load-bearing effect formed by the gravel and the crawler chain. Between 0 s and 25 s, as the upper carriage turns, the load distribution gradually shifts from the front sensors to EP B5/L5, reaching about 130 kPa. From 25 s to 300 s, the operator lifted the pile into the leader. At 310 s, the upper carriage rotated back from the position as seen in Fig. 3, photo on the left, and remained in position with a rotation of 13° relative to the chassis axis, as shown in the third photo of Fig.3. During reversal rotation the maximum stress measured in EP L5 and B5 as well as in EP L1 and B1 exceeded the measured values of the first rotation due to a shift of the machine's centroid by the additional pile weight.

Figure 4b shows the results obtained from the multi-point settlement gauges. Initially, before the start of load manoeuvre 1, the settlement values ranged between approximately 10 mm and 30 mm. From this baseline, S1 recorded a slight reduction in settlement, whereas S2 and S3 indicated increasing settlements, reaching up to 40 mm at S3. The sensor S4 remained largely unaffected by load manoeuvre 1. The strain measurements (see Fig. 4c) showed negative values relative to the reference measurement taken before the rig moved onto the working platform, indicating tensile forces mobilized by the geogrid. The strain gauges reflected deformations in the geogrid consistent with the measurements from the earth pressure transducers. As the rig rotated and the stress shifted from the front to the rear of the track, tensile strain in md2 decreased. At the end of the measurement, the tensile strain had returned to a level like that at the beginning of load manoeuvre 1 (-0.3%). The strain gauges in the cross-machine direction (cd3 and cd3-b) exhibited a similar trend to md2. Strain gauge cd3, located beneath the central axis of the track, recorded the highest strain relative to the reference measurement (-0.45%).

Load manoeuvre 2 – BR 470 Load Case 2

For load manoeuvre 2, the winch of the piling rig was attached to the previously driven pile and a tensile force up to 100 kN was applied to increase the load exerted by the tracks on the working platform. In this scenario, the machine operator can mitigate destabilizing effects at any time by reducing the winch's tensile force. As in load manoeuvre 1, the sensor readings were set to zero prior to the initial movement of the piling rig onto the instrumented working platform. During the gradual increase of the tensile force of the winch up to a maximum of 100 kN, the earth pressure transducers EP L1 and B1 recorded rising values with only marginal differences between them (Fig. 5a). This reflects a stress concentration at the front of the track, increasing from below 100 kPa to approximately 240 kPa during the manoeuvre. In contrast, the readings of EP L3 decreased, indicating a reduction of the load in this area beneath the track due to the increasing tilt of the piling rig. The remaining earth pressure transducers did not show significant changes compared to the load transfer conditions at the start of load manoeuvre 2.

The tilting of the piling rig can be inferred from the readings of the multi-point settlement gauges, as shown in Fig. 5b. At S1, located at the front of the track, the settlement increased, while at S2 the settlement decreased. This corresponds to the stagnant or decreasing earth pressures recorded by EP L2 and B2 as well as EP L3 and B3. The pronounced changes in both earth pressure and settlement, despite the relatively small distances between individual sensors, indicate that tilting of the rig induces a localized load transfer, resulting in simultaneous loading and unloading beneath the track. The strain measurements at discrete points in machine and cross machine directions of the track are presented Fig. 5c. As tensile force increases in the winch, both increases and decreases in strain occur depending

on the sensor position. The strongest increase was recorded by md2, reflecting the pronounced localization of the load transfer at the front of the track. Here, tensile strain increased from -0.32% before the winch started to apply the tensile force to -0.48% at approximately 100 kN. At md1, strain also increased by about 0.07%. In contrast, significant decreases in tensile strain were observed at cd3, cd3-b and md3. This further demonstrates that, due to the changing load transfer, not only were initially loaded areas subjected to additional loading, but adjacent areas of the working platform also experienced unloading. These effects occurred within comparably short distances.

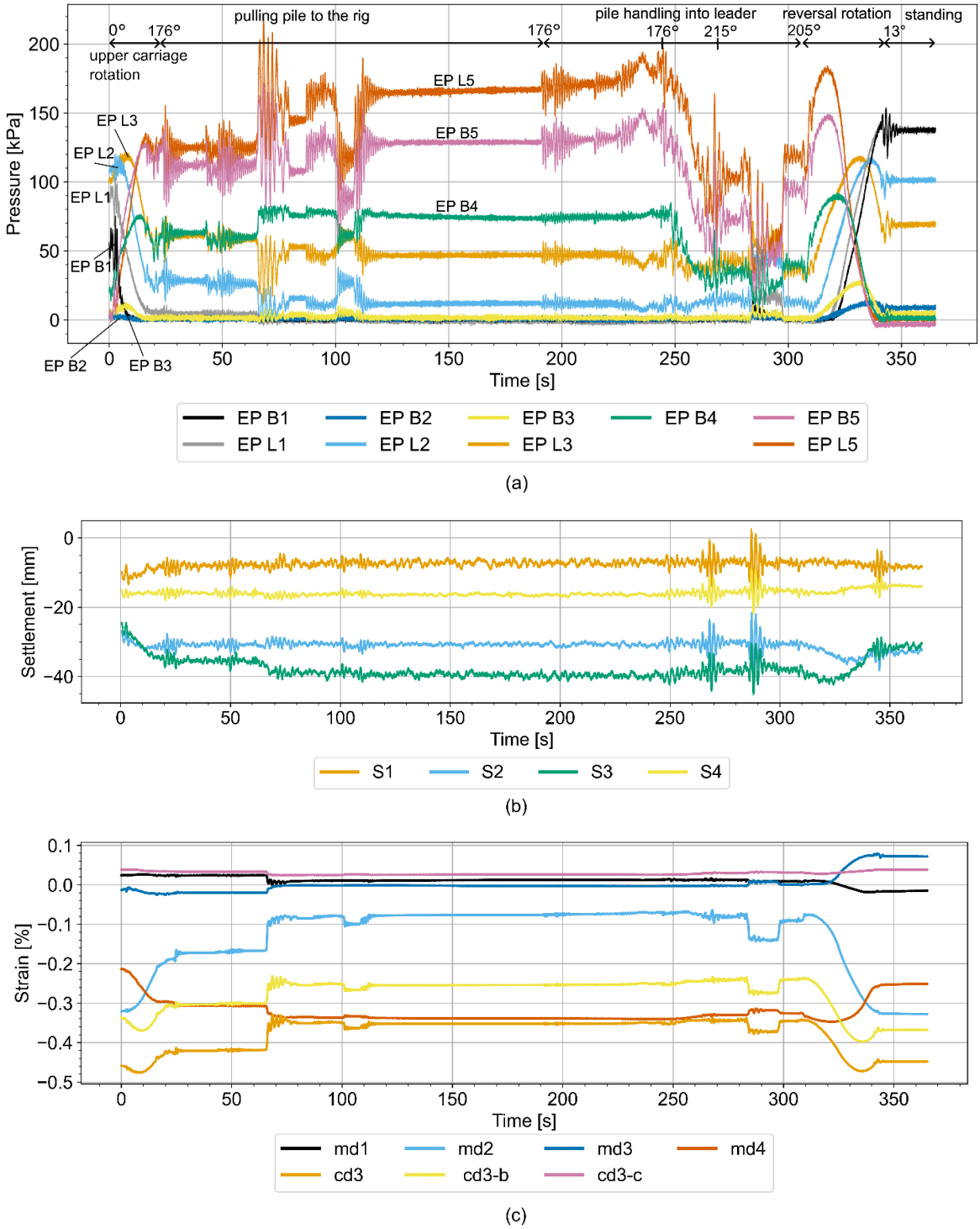


Fig. 4. Measured earth pressures with upper carriage rotation angles (a), displacements (b), and geogrid strains (c) during load manoeuvre 1

 © Deep Foundations Institute 2026

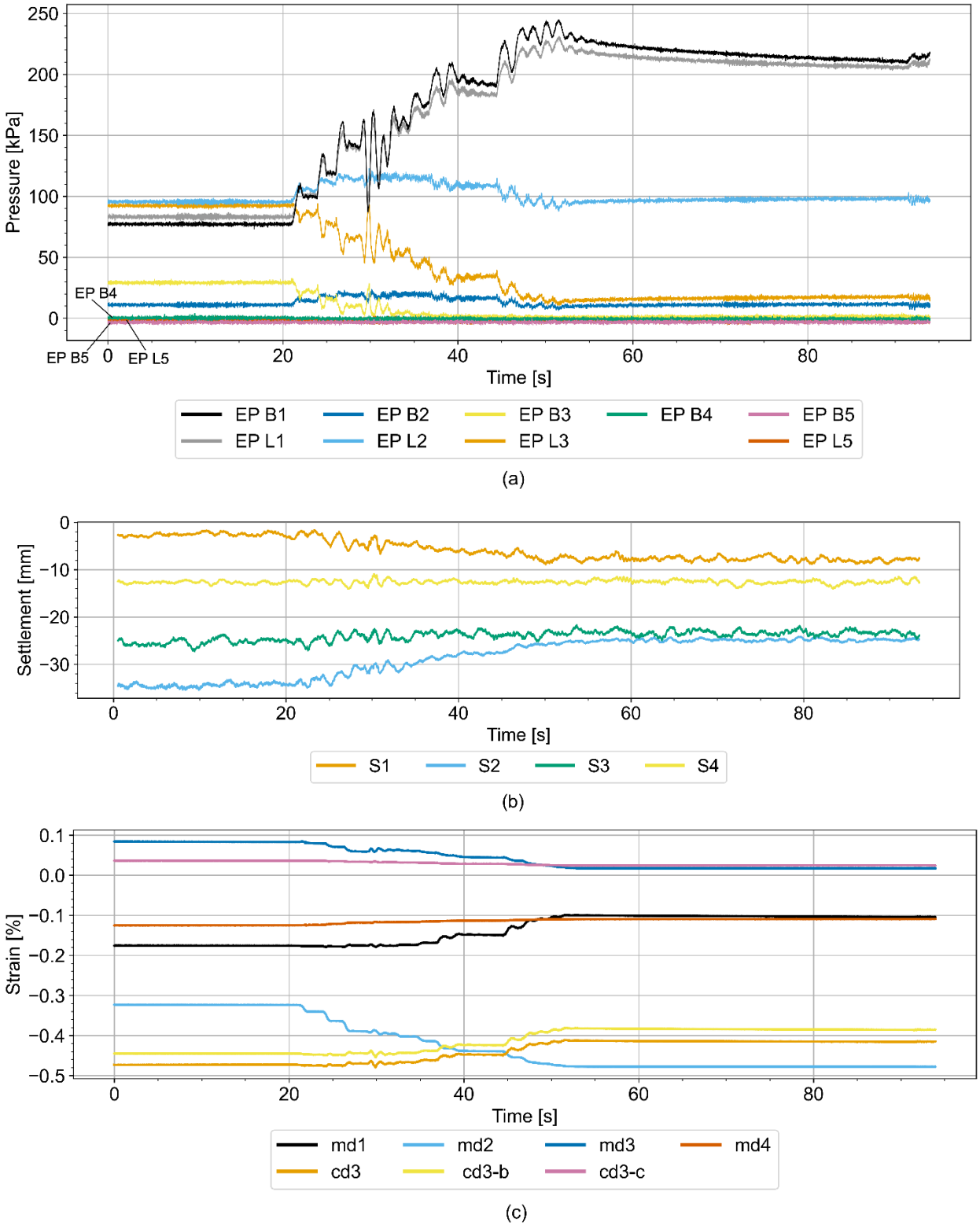


Fig. 5. Measured earth pressures (a), settlements (b), and strains (c) during load manoeuvre 2

DISCUSSION

The monitoring data obtained during the field trial provide valuable insights into the load transfer mechanisms and deformation behaviour of the geogrid-reinforced working platform under real pile driving operations. The first loading manoeuvre represented Load Cases 1 and 2 according to BR 470. Although local earth pressures increased significantly, up to 240 kPa and the settlements reached up

 © Deep Foundations Institute 2026

to 40 mm, the geogrid strains (0.25%) remained limited. A similar conclusion can be drawn from the second loading manoeuvre. In this scenario, pulling the pile with the winch is interpreted as Load Case 2, as the operator can stabilise by reducing the pulling force. However, since the rope used for load application cannot transfer compressive forces, it is arguable that, even after reducing the tensile load, the rig may continue to tilt due to excessive differential settlements. Further tilting results in increased loading of the working platform accompanied by a reduction in stiffness (softening). A skilled operator could probably still use the leader as support for the tilting rig.

Despite the limited strains measured at discrete positions, the settlement gauges recorded deformations up to 40 mm in combination with clearly visible tilting of the piling rig, indicating severe loading conditions. Further evaluation will consider the subsoil conditions, where a comparatively stiff surface crust overlies weaker layers at greater depth. These conditions are consistent with the low values of deformation modulus measured by static plate load tests.

Based on the recorded data evaluated so far, the conclusion can be drawn that the comparably high values of undrained shear strength and stiffness of the subgrade lead to limited utilization of the geogrid tensile forces (and corresponding strains) despite the relatively thin base course with only 30 cm thickness. Nevertheless, moving the piling rig directly on the lacustrine clay would inevitably cause severe rutting, critical tilting, and strong vibrations of the machine during pile driving even under dry weather conditions. In this study, the loading tests were carried out during intense rainfall, further emphasising that construction without a working platform would have been impossible. The efficient compaction of the base course material is clearly linked to the pronounced interlocking effect between the aggregate particles and the geogrid apertures.

CONCLUSION

In this paper a large-scale field trial of a geogrid-reinforced working platform on soft lacustrine clay is presented. A comprehensive monitoring program yielded valuable insights into stress transfer mechanisms, settlement behaviour, and the mobilization of tensile forces within the used laid and welded geogrid under typical loading scenarios (Load Cases 1 and 2), as considered in the BR 470 design guideline of working platforms for tracked plant. This paper outlines the layout and boundary conditions of the field trial and presents initial results derived from the comprehensive monitoring program. Based on these results, subsequent work will focus on validating and extending the experimental findings through finite element (FE) analyses. These simulations aim to reproduce the stress–strain response observed in the field under the specific loading scenarios of the piling rig and to calibrate the numerical models against the measured data. The analysis will focus on the deformation-related serviceability limit state (SLS), since in practical applications failure is often governed by tilting or excessive deformation of construction equipment rather than by ultimate failure caused by geogrid rupture (ULS). The outcomes of this study will be reported in a forthcoming publication.

REFERENCES

Abu-Farsakh, M. Y., Chen, Q. Yoon, S., 2008. Use of Reinforced Soil Foundation (RSF) to Support Shallow Foundation, Technical Report FHWA/LA.07/423, Louisiana Transportation Research Center, November 2008, USA

Berz, P., Niebler, M., Cudmani, C., Miraei, M., Rebstock, D., Vogt, S., 2026. Performance of pile foundations and soil improvements in sensitive lacustrine clay by large-scale zone loading tests and loading tests on single elements. Proceedings of the 21st ICSMGE, Vienna, Austria.

BRE 470, 2004. Working platforms for tracked plant: good practice guide to the design, installation, maintenance, and repair of ground-supported working platforms. United Kingdom.

Cudmani, R., Premstaller, M., Rebstock, D., Vogt, S., 2022. Geotechnische in situ Charakterisierung von Seeton am Beispiel des Rosenheimer und Salzburger Beckens: 36th Christian Veder Kolloquium, 28th to 29th June 2022, Graz, Austria.

EFFC/DFI, 2025. Guide to Working Platforms, 2nd Edition.

 © Deep Foundations Institute 2026

Khansari A., Vollmert L., Quirk C., Klompmaker J., 2021. Prediction models for deformation and punching shear resistance of geogrid- reinforced working platforms under tracked plant. Geosynthetic International, Kansas City, USA.
Khansari A., Vollmert L., Klompmaker J., 2023. Evaluation of the available design models for the analysis of geosynthetic-reinforced working platforms. GeoAfrica 2023, Cairo, Egypt.
Miller, K. S., 2013. Technical Note on Use of BR470 in Soft Clay. Federation of Piling Specialists.
Miller, K. S., 2020. A Review of Working Platform Design. Proceedings of the Piling 2020 Conference. Institution of Civil Engineers. London.

 © Deep Foundations Institute 2026

PRAGMATIC USE OF PILE TESTING METHODS TO VERIFY DRIVEN PILE CAPACITY ON LINEAR INFRASTRUCTURE PROJECTS

Edward J. Smith, The University of Queensland, Brisbane, Queensland, Australia,
edward.smith1@student.uq.edu.au
Jim Slatter, FSG Geotechnics and Foundations, Brisbane, Queensland, Australia.

ABSTRACT

The capacity of a driven pile at end-of-drive varies as a function of several factors including the ground conditions, pile size and geometry, pile material, and installation method. Further, this capacity is known to vary with time following installation as a function of the preceding factors, pile testing protocol, loading history, and environmental conditions. Due to the range of factors that affect pile capacity, and the complex pile-soil interactions that occur during installation, many of which are time dependent, estimating pile capacity following pile installation to enable an efficient and verifiable pile design is a non-trivial undertaking. Due to this complexity, a critical component on any driven piling project is the development and application of an efficient and robust pile testing protocol to verify that the required pile capacity has been achieved. This testing protocol may allow for time-dependent effects, but such allowances should not cause unexpected delays to the construction program due to excessive waiting periods or equipment movements. The impact of these waiting periods can be particularly severe on linear infrastructure projects where structures can be distributed over a considerable distance. In this paper, a brief overview of some mechanisms that affect pile capacity are outlined, followed by a discussion on key items to be considered when developing a practical pile testing and verification regime.

Keywords: driven piles, pile set-up, pile relaxation, pile testing, dynamic testing

INTRODUCTION

Driven pile foundations are frequently used to support structures that overlie substantial depths of soft unstable strata, or where a granular layer or rock unit offering substantial end bearing occurs at depth (Fleming et al., 2008). The installation of pre-formed piles alleviates issues relating to bore stability and may enable more efficient construction staging. Depending on the pile type, it can also induce considerable ground disturbance within the vicinity of the pile, which gives rise to a range of complex and inter-related mechanisms that alter the ground strength and stiffness, and therefore the pile capacity. Many of these mechanisms remain active following pile installation, resulting in time-dependent variations in pile capacity, with increases referred to as set-up, and decreases referred to as relaxation (Smith, 2025). Predicting this time-dependent response, for a particular combination of ground conditions, pile type, installation equipment, loading history, and environmental conditions poses considerable difficulty (Seidel, 2015b). As a result, the development and implementation of an efficient and robust pile testing and verification regime is critical for ensuring that driven piles can be efficiently designed, constructed, and verified.

This paper is intended for those involved in projects where driven piles are being considered as a foundation option, but without specialist knowledge of the complex time-dependent response exhibited by driven piles or the key considerations required when developing practical testing protocols for this foundation type. Attention is focused on mechanisms that can substantially affect pile capacity over the first 24 to 72 hours following pile installation, as in the author's experience set-up periods beyond this time frame may have detrimental impact on project schedule and budget. Where pile relaxation has been identified by early restrike testing, or where set-up can be reliably predicted and the net benefit of longer set-up periods can be demonstrated, longer waiting periods may be needed and/or justified. Key considerations when developing a pile testing and verification regime include appropriate selection of a testing method, selection of representative piles for testing, timing of testing, and in some cases assessing the feasibility of trial pile programs.

 © Deep Foundations Institute 2026

SELECT FACTORS AFFECTING PILE CAPACITY

A selection of factors and mechanisms that contribute to the time-dependent variation in the capacity of driven pile foundations are summarized in Table 1. Whilst not exhaustive, the listed mechanisms/factors all have the potential to affect driven pile capacity during and shortly after installation. A brief description of the mechanisms is provided in the following.

Table 1: Selection of mechanisms/factors affecting the time-dependent capacity of driven pile foundations (adapted from Smith [2025])

Mechanism/Factor	Ground conditions	Inferred influence	Example references
Dissipation of positive excess porewater pressures	Cohesive (primarily)	Cause of set-up.	Poulos and Davis (1980); Randolph and Wroth (1982)
Relaxation of arching stresses	Granular	Cause of set-up.	Cathie et al. (2022); Jardine (2023)
Constrained dilation at the pile-ground interface	Granular	Cause of set-up.	Alawneh and Sharo (2019); Axelsson (2002)
Open- versus closed-ended	Cohesive	Closed-ended or plugged piles typically take longer to set-up.	Carter et al. (1979)
	Granular	Open-ended piles have a reduced tendency to set-up.	Jardine (2020); Schneider (2007)
Installation method	Cohesive	Research is inconclusive, slow-jacked piles may demonstrate greater capacity increases on disturbance from retesting.	Bond and Jardine (1991); Ghose-Hajra et al. (2015); Rausche, Robinson, et al. (2004)
	Granular	Vibrated piles have the greatest propensity for set-up, with jacked piles the least.	Lim (2013)
Retesting of piles	Cohesive	Typically enhances set-up rate, some potential for capacity reduction in higher-plasticity overconsolidated soils.	Bullock et al. (2005); Karlsrud et al. (2014)
	Granular	Reduces shaft capacity and slows the set-up rate.	Jardine et al. (2006)
Dissipation of negative excess porewater pressures	Over-consolidated cohesive or dense granular	Cause of relaxation.	Karna (2001); Ng et al. (2013), Thompson and Thompson (1985)
Ground fracturing beneath pile toe	Soft rock	Cause of relaxation.	George et al. (1976); Thompson and Thompson (1985)

Dissipation of Excess Porewater Pressures

The generation of excess porewater pressures during pile installation particularly in cohesive soils, and the subsequent increase in soil strength and pile capacity as these porewater pressures dissipate, has been recognised since at least the middle of the 20th century (Cummings et al., 1950). Sensitive normally consolidated soils typically generate larger excess porewater pressures and therefore demonstrate a greater propensity for set-up than insensitive heavily over-consolidated soils (Bond and Jardine, 1991; Poulos and Davis, 1980).

Soderberg (1962) presents the partial differential equation, which describes the dissipation of excess porewater pressures following pile installation in Equation 1, where c_h is the horizontal coefficient of consolidation, t time, and u the excess porewater pressure. The derivation assumes drainage and deformation occur only in the radial direction, which is supported by several studies (Cummings et al., 1950; Roy et al., 1981), and may be valid at a sufficient distance from the ground surface and the pile toe, and where the soil profile is uniform with depth.

$$\frac{\partial u}{\partial t} = c_h\left(\frac{\partial^2 u}{\partial r^2} + \frac{\partial u}{r\partial r}\right) \quad [1]$$

The solutions to Equation 1 are functions of the time factor T_h (Equation 2), where R is the pile radius. Randolph and Wroth (1979) indicate that for a solid impermeable pile 90% of soil consolidation occurs by the time T_h is between 20 and 60, depending on the ratio of shear modulus to undrained shear strength.

$$T_h = \frac{c_h t}{R^2} \quad [2]$$

The installation of piles in contractive granular materials also has the potential to generate positive excess porewater pressures. The dissipation of these excess porewater pressures generally occurs relatively quickly in granular soils, often being complete during, or soon after, pile installation (Axelsson, 1998; Samson and Authier, 1986). As a result, it is uncommon for set-up in granular materials to be substantially influenced by the dissipation of excess porewater pressures. The exception would be a fine-grained sand where pile capacities are compared to the EOD pile capacity; however, even in this case, the contribution from the dissipation of excess porewater pressures is likely negligible within a few hours after pile installation (Axelsson, 1998; Chow et al., 1998).

Relaxation of Arching Stresses

The development of arching stresses in the granular soils around driven, vibrated, or jacked piles, and the associated variation in radial stresses, is often cited as a contributor to set-up (Chow et al., 1998; Jardine et al., 2006). During the installation of a displacement pile, the radial stresses in the ground have a tendency to increase towards the passive state near the pile toe, with ongoing penetration often causing contraction at the pile-soil interface and a reduction in radial stresses (Jardine et al., 2013). This contraction may result from the disturbance caused by toe penetration, shear straining, and/or grain crushing. The contraction and associated stress reductions result in soil movement toward the pile, however full restoration of the radial stresses is limited by the development of increased circumferential arching stresses further afield (Fig. 1).

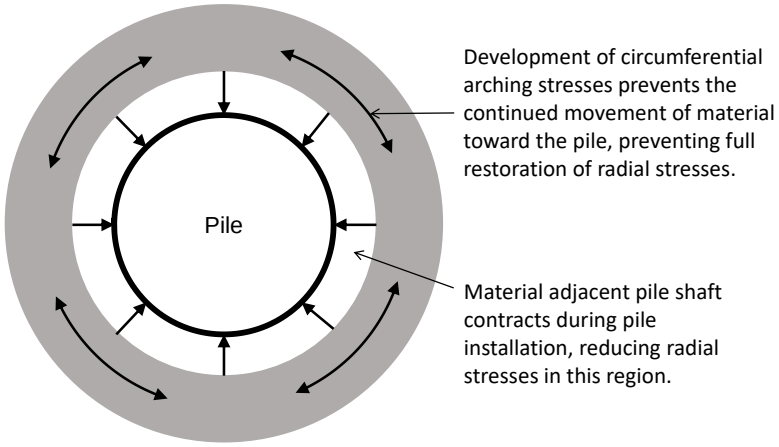


Fig. 1, Arching stresses that may develop around a pile during installation (after Smith [2025])

 © Deep Foundations Institute 2026

Friction fatigue is the term that describes the reduction in shaft resistance offered by a given soil horizon with increasing penetration of a displacement (low- and full-displacement) pile. The reduction in shaft resistance is often related to a reduction in radial stresses with ongoing penetration (the h/R effect, where h is the distance of a particular soil horizon behind the toe of the pile, and R the pile radius), which has been observed in field and laboratory studies using instrumented piles installed into granular soils (Jardine et al., 2013; Lehane et al., 1993). The magnitude of the reduction is affected by installation method, cyclic loading, and particle strength (Smith, 2025). At the conclusion of pile installation, the soil adjacent the shaft is left in an overconsolidated state, with a tendency to dilate on static loading (Yang et al., 2010).

Over time the increased circumferential stresses relax, the soil moves toward the pile, and the radial stresses acting on the pile increase, thereby increasing the axial capacity. This mechanism is likely most active in the first 30 days following installation (Cathie et al., 2022; Jardine, 2023), however ongoing capacity increases have been observed for years following installation (Chow et al., 1998). Reliable and broadly applicable predictive methods are not yet available.

Constrained Dilation at Pile-Soil Interface

Set-up in granular materials has also been attributed to increased stiffness and dilation at the pile-soil interface, resulting in increased normal stresses and mobilised pile resistance during loading (Axelsson, 2002; Cathie et al., 2022; Karlsrud et al., 2014). Lehane et al. (1993) describes the change in stress as a result of a given amount of dilation, δh, using Equation 3, where G is the shear modulus and R the pile radius (Fig. 2). Equation 3 suggests that increased dilatancy or shear stiffness, or reduced pile radius, will result in improved constrained dilation and greater radial stresses being imparted on the pile. Increases to either δh (e.g., overconsolidated soil, corrosion) or G (e.g., soil ageing) with time would lead to set-up (Axelsson, 2002).

$$\Delta\sigma'_{\mathrm{r}} = 2\delta h \frac{G}{R} \qquad [3]$$

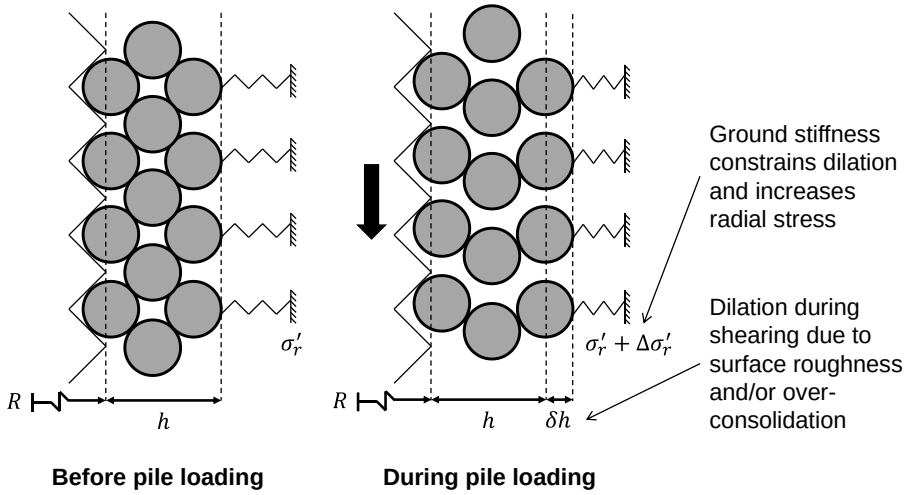


Fig. 2. Constrained dilation during pile loading (after Axelsson [2002])

Open- Versus Closed-Ended piles

Open-ended piles allow soil to enter the pile during installation, however with increasing penetration and the accumulation of resistance on the pile interior there is a tendency for partial plugging (i.e., reduced upwards soil movement relative to pile penetration) or full plugging (i.e., no interior soil movement relative to pile penetration) to occur. The tendency for a pile to plug is also affected by the

nature of the loading, with dynamic loading being less likely to cause plugging due to the inertia of the plug, which must be overcome, and the difference in wave speed for the plug material compared to the pile material (De Nicola and Randolph, 1997).

Carter et al. (1979) used cylindrical cavity expansion theory to compare the effect of driving open-ended unplugged plugs with that of closed-ended piles into cohesive soils. When compared to closed-ended piles, open-ended piles:

- Generated excess porewater pressures over a smaller radial distance.
- Dissipated excess porewater pressures sooner.
- Developed lower long-term radial effective stresses and consolidated undrained shear strengths.

Where plug formation occurs earlier in the installation sequence, the more the ground response will tend toward that expected of a closed-ended pile.

For granular soils, Kraft (1991) indicates that open-ended piles cause smaller changes in radial stresses compared to closed-ended piles, with associated reductions in pile capacity. Schneider (2007) used theoretical analysis and interpretation of a database comprised of approximately 80 pile load tests (diameters between 0.3 and 2 m) to demonstrate that open-ended piles develop smaller shaft resistances than closed-ended piles. Regarding set-up in granular soils, both grain crushing and stress redistribution are affected by whether the pile toe is open or closed (Cathie et al., 2022; Jardine, 2020). Typically, greater set-up rates (relative to an earlier test) are observed for closed-ended piles (Long et al., 1999; Schneider, 2007).

Installation Method

Jacked, driven, and vibratory pile installation methods subject the surrounding soil to different loading rates, loading energies, and number of loading cycles all of which have the potential to affect the set-up exhibited.

The effect of installation method on pile capacity and set-up in granular soils is fairly consistent across the literature. Vibrated piles demonstrate lower capacities at end of installation with a greater propensity for set-up compared to driven piles, and likewise when comparing driven and jacked installation (Bittar et al., 2023; Lim, 2013). This response is typically attributed to the greater number of load cycles imparted by vibratory (or driven) installation compared to driven (or jacked) installation methods, with the cyclic degradation creating a greater propensity for time-dependent capacity increases (Lim, 2013).

Research on the effect of installation method for pile capacity and set-up in cohesive soils is less conclusive. The broad conclusions that can be drawn from a limited number of studies indicate:

- In soils susceptible to sliding failure (typically high-plasticity with a high proportion of platy particles, Lupini et al. [1981]) slow-jacked (50 to 100 mm/min) piles develop smaller resistance than either fast-jacked (400 to 600 mm/min) or driven piles due to the formation of continuous, polished failure surfaces near the pile-soil interface (Bond and Jardine, 1991).
- Slow-jacked piles may demonstrate increased set-up with retesting as the disturbance and failure mode approaches that of a driven pile (Bullock, 1999; Jardine, 1985). However, piles tested at a lower displacement rate than that during installation may demonstrate lower capacities if a transition to sliding failure occurs (Jardine, 1985).
- The effect of vibratory driving on set-up is unclear. Intuitively the higher number of load cycles caused by vibratory installation (or small hammer energies) would lead to greater cyclic degradation, smaller EOD capacities and larger propensity for set-up (Ghose-Hajra et al., 2015), however this is not always supported by the literature (Rausche, Robinson, et al., 2004).

  In the author's experience with onshore linear infrastructure projects, the most cost-effective driven pile designs are those that demonstrate capacity at, or soon after, pile installation.

Considering the effect of installation method on pile capacity and set-up, the following suggestions are made with regards to pile installation best practice to facilitate this outcome:

- Where possible, use fixed leader piling rigs to minimize the potential for pile whipping during driving. Pile whipping refers to the lateral pile movements that occur during driving due to a combination of some or all of, lateral hammer movement relative to the pile head, eccentric loading of the pile, or significant unrestrained pile length above-grade (particularly in slender piles). Pile whipping may contribute to gap formation and loss of shaft resistance (Nowacki et al., 1992). Whilst there is no consensus on the relative effect of pile whipping relative to other causes for reduced near surface shaft resistance (e.g., cyclic loading, friction fatigue, reduced kinematic constraint), it almost certainly doesn't enhance shaft resistance and should be avoided where possible.
- Avoid vibratory pile installation where possible (in the context of other project constraints), and if required, to assist in pitching piles, should be used to a minimum. Research on whether initially vibrated piles that are then subject to impact driving achieve similar capacities to solely impact driven piles is inconclusive (Bittar et al., 2023; Mosher, 1987), however it almost certainly doesn't enhance shaft resistance and should generally be minimised.
- Ensure drivability studies that adequately capture the range of expected ground conditions are undertaken and appropriately sized hammers are selected to avoid premature refusal, and ensure the required geotechnical resistances can be mobilised.
- Minimise surface anomalies or changes in pile geometry that result in the creation of small gaps between the pile and the soil (e.g., proud external welds in spiral tubular piles, or poorly detailed pile splices that contain elements which are proud of the pile surface).

Retesting of Piles

The additional disturbance caused by the retesting of piles (i.e., more than 1 test) following installation has the potential to affect set-up trends (Bullock, 1999).

Studies that have examined the effect of retesting piles in cohesive soils generally suggest either no effect (Bittar et al., 2022), or a beneficial increase in pile capacity that is generally attributed to a pre-shearing effect (Bullock et al., 2005). In some high-plasticity, overconsolidated soils there is a potential for decreased capacity that may be affected by the displacement rate during the test (Jardine, 1985; Karlsrud et al., 2014).

The majority of studies examining the effect of prior testing on set-up trends in granular soils indicates that retested piles have a lower capacity, set-up at a slower rate than 'fresh' piles, and exhibit stiffer, more brittle response to loading (Jardine et al., 2006; Karlsrud et al., 2014).

Negative Excess Porewater Pressures

Dense granular or overconsolidated cohesive soils tend to develop negative excess porewater pressures and associated increases in effective stress as they dilate during shearing. This behaviour is often deemed to contribute to the relaxation of piles installed in such materials, with the reductions in effective stress as the negative excess pore pressures dissipate causing a reduction in pile capacity over time (Rausche, Moses, et al., 2004). The time for dissipation of these negative pore excess pore pressures in silts and fine sands is typically comparable to or exceeds the pile installation time, such that they are likely to contribute to driving resistance during installation, and result in relaxation when tested at restrike (Yang, 1970). Coarse sands are more permeable and less likely to exhibit relaxation behaviour (Yang, 1970). The author acknowledges that there is some contention as to the viability of this mechanism (Thompson and Thompson, 1985), however negative excess porewater pressures have been measured during pile installation (Bond and Jardine, 1991), and pile relaxation has been observed in dense sands and over-consolidated silts (Karna, 2001; Ng et al., 2013). Having an awareness for the propensity for pile relaxation in these conditions is advisable.

Ground Fracturing Beneath Pile Toe

A considerable portion of observed pile relaxation is documented for cases where the pile toe is embedded into soft rock such as mudstone or shale (George et al., 1976; Thompson and Thompson, 1985). The observed relaxation is typically attributed to fracturing, water ingress and associated deterioration of the rock beneath the pile toe (Rausche, Moses, et al., 2004). It is important to determine the extent of this relaxation before certifying a pile as having met the design requirements. Several authors recommend that pile testing is completed at least 1 week following EOD (Foundation QA, 2006; Goble and Likins, 1996) in order to assess relaxation. In the author's experience these sorts of testing and validation delays can result in significant time and cost impacts on linear infrastructure projects, when applied on a widespread scale. Should relaxation be identified through initial and/or routine restrike testing, a carefully considered testing and verification regime would need to be developed which considers overall design efficiency, assesses the likely long-term relaxation potential, and addresses the need to construct the foundations in a timely manner. It is advisable to limit design end-bearing to readily achievable/demonstrable resistances when materials are known to be susceptible to relaxation at the toe, as high end-bearing requirements can necessitate repeated redriving of piles. This can be particularly problematic where piles are arranged in large groups, where previously installed piles can be affected by driving or testing of adjacent piles.

PRACTICAL PILE TESTING PROTOCOLS

The development of a robust and efficient pile testing regime is essential for the reliable and cost-effective execution of a driven pile foundation project. The development of this regime should address:

- The selection of a reliable pile testing technique.
- The number and proportion of piles to be tested.
- A regime for selecting the piles to be tested at each structure.
- The waiting period to be allowed between EOD and subsequent testing (restrike testing).

Pile Testing Method

The verification of driven pile axial capacity can be undertaken using static, dynamic, and/or rapid testing methods. The merits and limitations of each method have been discussed by various authors (Poulos, 2017; Randolph, 2003; Rausche, 2019; Seidel, 2015a, 2015b), and can be broadly summarized as follows:

- **Static Load Testing:** Involves loading the pile in increments against a reaction (e.g., reaction piles, kentledge, ground anchors) over an extended duration to obtain an essentially static load-displacement response, with the ultimate capacity typically identified as the load supported at a given head displacement. Often used as the benchmark against which other testing methods are compared, however engineers need to be cognizant of and correct for the interaction of the reaction system with the test pile. The test is relatively time consuming and costly to prepare for and undertake, and information regarding the distribution of resistance along the pile is not available unless the pile is instrumented. Furthermore, as static tests are performed after initial driving of the pile, the results are influenced by time dependent effects and developing a relationship between EOD driving behavior and static test results is not necessarily straight forward.
- **High-Strain Dynamic Testing:** Involves attaching accelerometers and strain gauges to the pile to capture the stress wave propagation following a hammer impact. The imparted downward stress wave interacts with the ground and reflects upward waves, captured over the full pile length. This response from the ground can be modelled using the one-dimensional wave equation and appropriate selection of ground resistance and stiffness parameters to provide an estimated compressive resistance. The ground parameters are iteratively modified until near-optimum correspondence between the measured and simulated stress wave is obtained. The dynamic test can be undertaken relatively quickly using equipment already utilized as part of pile driving

operations, with a demonstrable history of closely approximating the results of static load tests. Due to the number of parameters involved in stress wave modelling the assessed resistance distribution is not unique. Interpretation must therefore be undertaken with due consideration to the whole-of-project test results and the available geotechnical information to ensure the dynamic testing program provides meaningful and reliable insights into the relationship between the pile capacity, imparted energy, and the pile movement. A significant advantage of dynamic testing is that it can be performed at EOD and can therefore be easily correlated with pile driving behavior. Restrike testing can also be undertaken to assist with understanding time dependent effects thereby facilitating the development of a robust pile verification procedure.

- **Rapid Load Testing:** Involves the application of a downward force on the pile head through carefully designed combustion against a reaction, or dropping of a cushioned mass in a guide frame. The duration of impact is such that the whole pile is maintained in compression for a defined minimum duration. Compared to static load testing, preparation and testing can typically be undertaken relatively quickly. Dynamic stress wave effects are also reduced compared to dynamic testing due to the slower loading velocity, and maintaining the entire pile in compression, such that there is less difficulty in obtaining the static resistance from the test. It is however important to note that rapid load tests typically require a reaction load of 5% to 10% of the test load compared to 1.5% to 2% for dynamic testing and therefore require larger testing infrastructure and support on site.

Due to the time and cost associated with static load testing, it is typically only feasibly applied to 0.5 to 1% of piles on a project (Rausche, 2019; Seidel, 2015b). Further, given the pseudo-static nature of the test and being conducted a significant time after installation, the results are not well suited to the development of EOD acceptance criteria (Seidel, 2015b). However, it is acknowledged that static load testing may still feature in a pile testing program if calibration of dynamic test results is deemed necessary and/or to meet regulatory requirements.

In the author's experience, the use of driving equipment already mobilized to site to undertake high strain dynamic testing along with the relatively short time to prepare and undertake the dynamic tests, typically allows 3 to 15% of piles on the project to be tested, giving statistically significant insights into the performance and reliability of the foundation system (Collingwood, 2006; Seidel, 2015b). Further, if the foundation design is to incorporate the benefits of set-up, the capacity and resistance distribution at end of (or soon after) installation need to be assessed, which is only practical with dynamic testing (Kirsch and Plaβmann, 2002; Rausche, 2019; Seidel, 2015b). These attributes allow dynamic test results to directly inform driven pile acceptance criteria. When undertaken using best practice by competent pile testing engineers, these benefits mean that high strain dynamic testing should be considered as the preferred testing methodology for driven pile foundations.

The remaining discussion in this section refers to high strain dynamic testing as this is seen as being the most practical and appropriate means of developing a robust pile acceptance criteria on large scale pile driving projects.

Number and Proportion of Piles to Be Tested

The number of piles to be tested for a given structure will vary as a function of,

- The project size and the number of piles supporting the structure (Collingwood, 2006; Rausche, 2019).
- The quality of the site investigation and the geotechnical complexity of the site (Kirsch and Plaβmann, 2002; Rausche, 2019; Seidel, 2015b).
- The experience of the designer and the reliability of the design methods adopted (Rausche, 2019; Standards Australia, 2009).
- The extent to which the pile design has been optimised (i.e., the proportion of the ultimate capacity which is utilized in the design capacity) (Rausche, 2019).

- The type and quality of construction control and monitoring undertaken during installation/construction (Seidel, 2015b; Smith, 2009).

Building projects typically test 3 to 15% of installed piles, however for linear infrastructure projects in Australia, where 1 or 2 tests per pier/abutment are nominated, a far higher testing rate may occur (Collingwood, 2006). Where this situation arises, the benefits of higher testing rates for foundation reliability should be incorporated into the assessment of the reduction factor adopted (e.g., Standards Australia [2009]). Further, where the site is geotechnically complex, or the design method adopted is less reliable, a higher testing rate may be adopted.

It is also imperative that dynamic pile testing and further analysis (for example using CAPWAP) is undertaken by competent engineers, with due consideration for the geotechnical conditions and the testing database already established for the site. If pile tests are undertaken in isolation, and adopt parameters which are not geotechnically credible, then it is unlikely that a reliable relationship between energy input, pile capacity, and pile movement (ECM relationship) can be established (Seidel, 2015a). The establishment of this relationship is critical for determining pile acceptance criteria (for both tested piles and untested piles) in a consistent manner. Where pile testing indicates there may be a need for considerable modification to the ECM relationship, or a unifying ECM relationship is not established for the site, higher testing rates may be required.

Selecting Piles for Testing

The selection of piles for testing will be informed by the experience of the designer and contractor for the given installation equipment, pile type and geometry, and expected ground conditions, in addition to the monitoring data collected during pile installation.

It is typically advisable to undertake testing on the first pile for a given pile group/abutment/pier on any project. The early availability of this information will assist in:

- Creating an initial database for development of the project/structure ECM relationship (Seidel, 2015a).
- Avoiding pile damage by confirming that the stresses developed within the pile section are within acceptable limits.
- Identifying issues that may arise due to considerable degradation of pile resistance during installation (Komurka et al., 2017; Rausche, 2019). These issues could be rectified with increased pile lengths or allowance for some set-up period; the sooner this information is available the more effectively the risk to project budget and/or schedule can be managed.
- Confirming the magnitude of any expected relaxation such that subsequent piles can be driven to a higher EOD capacity to account for the relaxation response (Rausche, 2019).

Any delay to pile testing (i.e., not testing the first pile at a structure) heightens the risk of damaging piles (as the driving stresses are not yet validated to be within acceptable limits), limits the ability to which deleterious time-dependent effects can be effectively managed, and increases the risk that piles will need to be restruck to confirm that they meet acceptance criteria.

Detailed driving records should be maintained for all piles, as a minimum, recording penetration, set, temporary compression for the final 10 to 20 blows, hammer mass, and drop height. Some monitoring systems on the market are able to infer or estimate impact energy, however at this stage the only method of directly measuring energy transferred to the pile is via PDA monitoring. Typically, PDA testing should be used to develop an understanding of the impact efficiency of the hammer and these data are then used in conjunction with other monitoring data to estimate impact energy for non-tested piles. Where monitoring records suggest that a given pile may demonstrate the lower bound capacity for the given pile group/abutment/pier, or a considerable deviation from the established ECM relationship, testing of this pile is recommended (Collingwood, 2006; Standards Australia, 2009).

Waiting Period Before Testing

The waiting period to be adopted before undertaking restrike testing will vary based on the capacity demonstrated by the pile at EOD, the propensity for set-up/relaxation, and the construction program or sequence.

In the author's experience restrike testing of approximately 30% of tested piles is generally prudent. Restrike testing should be conducted early in the project to understand time dependent effects on pile capacity. Where initial restrike testing indicates there may be a propensity for relaxation, sufficient time for this relaxation to fully develop should be allowed for it to be properly characterised. The required waiting time could be known from local experience, or from a series of restrike tests early in production piling. In the absence of this information, pile testing should be completed at least 1 week following EOD (Foundation QA, 2006; Goble and Likins, 1996).

For cases where insufficient capacity is demonstrated at EOD, a waiting period that allows any set-up response to develop may allow the pile to demonstrate capacity without significantly increasing embedment (Goble and Likins, 1996). For production piles, a waiting period of 24 hours (Collingwood, 2006; Rausche, 2019; Smith, 2009), or at most 96 hours (Komurka and Arndorfer, 2009) is typically allowed. Longer waiting periods of a week or more are occasionally documented (Goble and Likins, 1996; Kirsch and Plaβmann, 2002; Smith, 2009). However, for linear infrastructure projects where foundations are spread over a substantial distance, the inefficiencies introduced by extended waiting periods are amplified by the delay from remobilizing equipment to a given pile. Unless the net benefits of extended waiting periods have been demonstrated during the design phase, and allowances made in the construction program, waiting periods beyond 24 hours (or at most 72 hours) should be avoided. Designers should be cognisant of the factors which may give substantially reduced capacities at EOD compared to typical design procedures (e.g., sensitive soils, long piles, vibratory installation), and adjust the design accordingly.

The trends demonstrated by pre-production pile driving programs over extended set-up periods, in conjunction with testing of production piles after short set-up periods, may allow the capacity increases associated with extended set-up periods to be utilised without requiring testing of production piles at these times (Rausche, 2019). However, as will be discussed in the following section, the feasibility of undertaking pre-production trial pile programs to the extent where set-up trends can be confidently predicted across the large geological footprint of a linear infrastructure project is questionable.

Feasibility of Pre-Production Trial Pile Programs

Pre-production trial pile programs undertaken using the anticipated production equipment on the anticipated production pile (geometry, material, length, embedment) are occasionally considered as a means of:

- Confirming and/or optimizing the parameters adopted in design (Fleming et al., 2008).
- Confirming the suitability of the driving system to achieve the required embedment without damaging the pile (Komurka et al., 2017; Smith, 2009).
- Understanding the set-up/relaxation response that may develop for the specific circumstances to be expected during production (Komurka et al., 2017; Rausche, 2019).
- Developing an acceptance criteria for production piles (Rausche, 2019; Smith, 2009).

  Trial pile programs are typically only feasible on large projects, where the efficiency gains can be realised over a significant number of piles and therefore justify the cost of the program (including equipment mobilization, early site access, pile cost if not installed at a production location, etc.) (Rausche, 2019). The design must also be at a stage where there is reasonable confidence in the structure location, pile type and geometry to be adopted, and installation equipment to be used. Significant changes after conducting the trial program may limit the applicability of the results. As such, obtaining a justifiable net benefit from a trial program typically requires that,

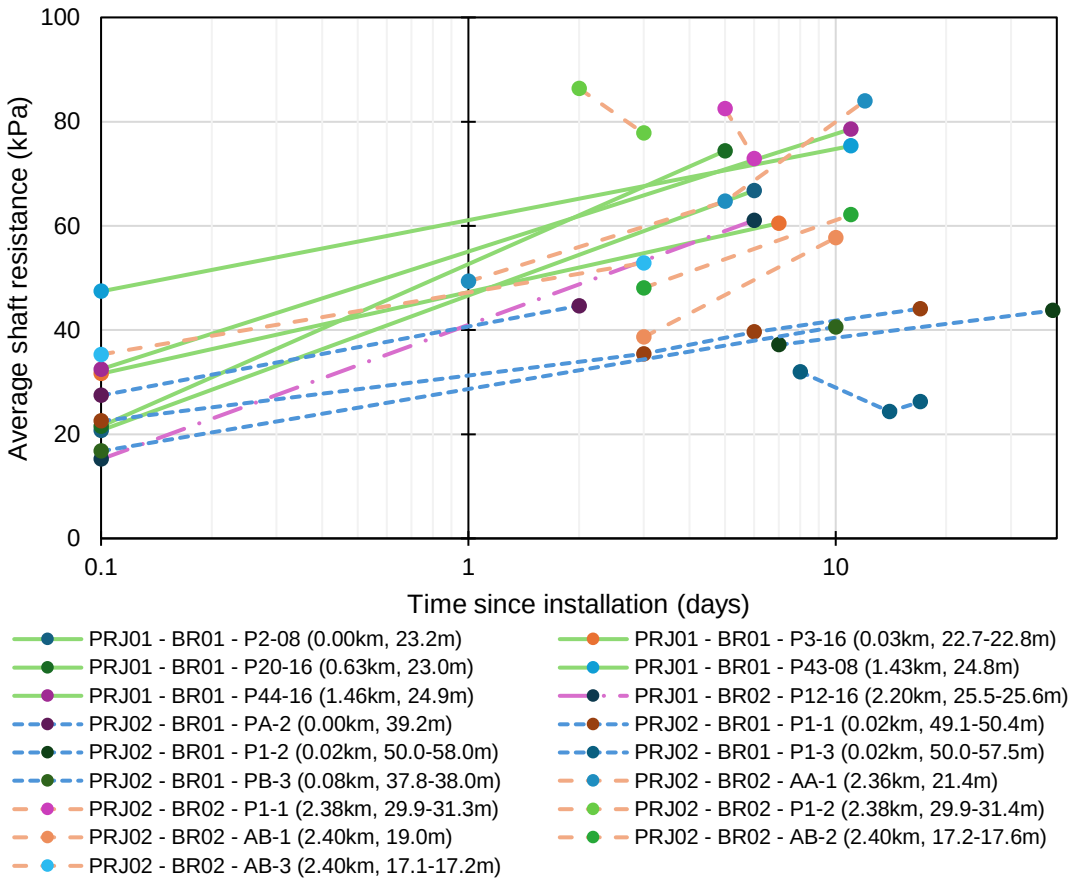
- The program is well coordinated between client, designer, contractor, and testing engineers. This coordination allows the potential benefits of a trial program to be identified early in design and then be organized in a timely manner. It also encourages a best-for-project mindset with a unified focus on the areas with greatest potential to benefit the project and a commitment to realise these benefits during construction.
- The program is thoughtfully designed to give results that can be applied to production pile acceptance. Whilst static load testing may often be referred to as the benchmark pile test, the vast majority of the trial pile program should involve dynamic testing to understand the ECM relationship for the site, which will ultimately be used to determine pile acceptance.
- The pile density relative to project footprint is relatively high (e.g., building projects, multi-level interchanges), such that the utility of any given test pile is increased.

In these situations trial pile programs can lead to reductions in project timeline and cost (Komurka and Arndorfer, 2009; Komurka and Theiss, 2018). However, for linear infrastructure projects occurring over far larger geological footprints, and where the trial program may only be conducted at a limited number of locations, the utility of the results is reduced and the costs are more difficult to justify.

The variability in EOD capacity and subsequent set-up even on land development projects is well documented (Komurka et al., 2017; Kristinof and Thorn, 2017). As a further demonstration of some of the variability which can occur on linear infrastructure projects, a selection of pile test results are presented in Fig. 3 from projects described in Table 2. The following are noted when inspecting Fig. 3,

- Pile shaft resistance was assessed using PDA testing with CAPWAP analysis. Average shaft resistance is calculated as mobilized shaft resistance divided by embedded shaft area (open-ended piles consider the exterior shaft area only). No attempt has been made here to isolate and analyse trends based on individual soil layers.
- For testing undertaken on the same day as EOD, the time since installation has been arbitrarily set at 0.1 days. The available shaft resistance can be highly variable shortly after pile installation and this may explain some of the scatter observed in the shaft resistances plotted at 0.1 days.
- At PRJ02 the set-up rate (as an absolute value) is larger at BR02 compared to BR01, likely affected by the change in geological setting. Variability in set-up trends is also observed through the slightly more uniform geological conditions at PRJ01.
- A selection of piles from PRJ02 (e.g., BR01 P1-3, BR02 P1-1, BR02 P1-2) show a reduction in capacity shortly after testing. These piles were subject to redriving (as opposed to restrike testing), which appears to have temporarily reduced the shaft resistance and which is expected to recover over time.

The overarching conclusion from Fig. 3 is that shaft resistance mobilized at EOD and subsequent set-up rates can be highly variable even for similar pile embedment in similar geological conditions. The uncertainty is further increased as geological heterogeneity increases. As a result, if set-up is to be incorporated as part of a pile acceptance procedure it should be based on a lower-bound trend established from a significant number of tests early in a project, and then validated progressively as the project proceeds. For large linear infrastructure projects where geological conditions can vary considerably along the alignment, care should be taken to ensure any set-up trend adopted is appropriate and properly validated for the geological conditions at a given pile location.



Note: First bracketed term is distance from reference pile (BR01 P2-08 for PRJ01, BR01 PA-2 for PRJ02), second bracketed term is pile embedment.

Fig. 3, Selection of pile test results demonstrating variability in EOD capacity and subsequent set-up

Table 2: Summary of projects associated with data in Fig. 3

Project ID	Structure	Ground conditions	Typical pile type
PRJ01	BR01	Holocene age alluvium overlying Quarternary age alluvium overlying sedimentary rock (siltstone, mudstone, sandstone, conglomerate). Typically 6–13 m thickness very soft to stiff medium to high plasticity clay, 0–10 m thickness soft to very stiff low to medium plasticity silt/clay, 5–25 m thickness medium dense to very dense sand/gravel, overlying sedimentary rock.	550 mm octagonal pre-stressed concrete piles
	BR02		
PRJ02	BR01	Holocene age alluvium. Typically 3–5 m thickness of very loose to loose sand/soft to firm clay, overlying 16–28 m thickness of loose to medium dense alluvial sand interbedded with soft to stiff high plasticity clay layers, overlying stiff to hard cohesive materials interbedded with medium dense to very dense granular materials.	900 mm steel tubes, open-ended, 20 mm wall, 32 mm driving shoe
	BR02	Pleistocene age alluvium. Typically 3–6 m thickness very stiff to hard low to medium plasticity clay, 2–8 m thickness loose to medium dense sand, overlying very stiff to hard medium to high plasticity clay.	

 © Deep Foundations Institute 2026

SUMMARY AND CONCLUSIONS

The capacity of a driven pile at EOD and with time following installation varies as a function of several complex and inter-related factors. It is important for designers to consider these effects as they can have implications for the required pile length, the construction sequence, and the project timeline. Predicting the time-dependent response, for a particular combination of ground conditions, pile type, installation equipment, loading history, and environmental conditions also poses considerable technical difficulty. Due to this complexity, a critical component on any pile driving project is the development and application of an efficient and robust pile testing regime to verify that the required pile capacity has been achieved and will be maintained or exceeded over time. In the author's experience, such protocols typically utilize high strain dynamic testing, applied early in the pile installation sequence for a given pile group, and should rely on a waiting period typically no more than 24 to 72 hours. Where pile relaxation is expected to occur, or where set-up can be reliably predicted and the net benefit of longer set-up periods can be demonstrated, longer waiting periods may be justified. Whilst designing piles to account for time dependent capacity increases (set-up) can theoretically offer material savings, one must consider whether the associated program delays and verification risks associated with a long term restrike program offset (or outweigh) potential material savings. Further, pre-production trial program piles can present considerable benefits in certain specialized circumstances, however their utility on linear infrastructure projects is typically limited due to the reduced pile density relative to project footprint, and any potential benefits must be thoroughly considered before undertaking such work.

ACKNOWLEDGMENTS

The first author prepared this manuscript during their studies at The University of Queensland, which are supported by the Australian Government Research Training Program Scholarship and the National Industry PhD Program.

REFERENCES

Alawneh, A. S., and Sharo, A. A. (2019). Estimation of long-term set-up of driven piles in sand. *Geomechanics and Geoengineering*, *15*(4), 281-296. https://doi.org/10.1080/17486025.2019.1641630

Axelsson, G. (1998). *Long-term Increase in Shaft Capacity of Driven Piles in Sand*. 4th International Conference on Case Histories in Geotechnical Engineering St Louis, Missouri, USA.

Axelsson, G. (2002). *A Conceptual Model of Pile Set-up for Driven Piles in Non-cohesive Soil*. International Deep Foundations Congress 2002, Orlando, Florida. https://doi.org/10.1061/40601(256)6

Bittar, E., Huang, B., Lehane, B., and Watson, P. (2022). *Pile ageing in clay to support life extension of offshore platforms*. 20th International Conference on Soil Mechanics and Geotechnical Engineering, Sydney, Australia.

Bittar, E., Lehane, B., Watson, P., Shonberg, A., and Deeks, A. (2023). *Effect of installation mode, pile shape and cycling on the ageing of shaft friction of mild steel piles*. 9th International Offshore Site Investigation Geotechnics Conference - Innovative Geotechnologies for Energy Transition, London, UK. https://doi.org/10.3723/WXLP8612

Bond, A. J., and Jardine, R. J. (1991). Effects of installing displacement piles in a high OCR clay. *Géotechnique*, *41*(3), 341-363. https://doi.org/10.1680/geot.1991.41.3.341

Bullock, P. J. (1999). *Pile Friction Freeze: A Field and Laboratory Study* [PhD, University of Florida]. Florida, USA.

Bullock, P. J., Schmertmann, J. H., McVay, M. C., and Townsend, F. C. (2005). Side Shear Setup. II: Results from Florida Test Piles. *Journal of Geotechnical and Geoenvironmental Engineering*, *131*(3), 301-310. https://doi.org/10.1061/(Asce)1090-0241(2005)131:3(301)

 © Deep Foundations Institute 2026

Carter, J. P., Randolph, M. F., and Wroth, C. P. (1979). *Some aspects of the performance of open- and closed-ended piles*. Numerical methods in offshore piling, London, UK. https://doi.org/10.1680/nmiop.00865.0020

Cathie, D., Jardine, R., Silvano, R., Kontoe, S., and Schroeder, F. (2022). *Pile setup in sand - the "PAGE" joint industry project*. 11th International Stress Wave Conference, Rotterdam, The Netherlands.

Chow, F. C., Jardine, R. J., Brucy, F., and Nauroy, J. F. (1998). Effects of Time on Capacity of Pipe Piles in Dense Marine Sand. *Journal of Geotechnical and Geoenvironmental Engineering*, *124*(3), 254-264. https://doi.org/10.1061/(Asce)1090-0241(1998)124:3(254)

Collingwood, B. (2006). Precast driven piles in the Melbourne Region - A brief overview of current practice. *Australian Geomechanics*, *41*(3), 7-16.

Cummings, A. E., Kerkhoff, G. O., and Peck, R. B. (1950). Effect of Driving Piles into Soft Clay. *Transactions of the American Society of Civil Engineers*, *115*(1), 275-285. https://doi.org/10.1061/taceat.0006327

De Nicola, A., and Randolph, M. F. (1997). The plugging behaviour of driven and jacked piles in sand. *Géotechnique*, *47*(4), 841-856. https://doi.org/10.1680/geot.1997.47.4.841

Fleming, K., Weltman, A., Randolph, M., and Elson, K. (2008). *Piling Engineering*. CRC Press. https://doi.org/10.1201/b22272

Foundation QA. (2006). *PDA Training Module 5 - Case method and soil resistance*, Foundation QA.

George, A. B., Sherrell, F. W., and Tomlinson, M. J. (1976). The behaviour of steel H-piles in slaty mudstone. *Géotechnique*, *26*(1), 95-104. https://doi.org/10.1680/geot.1976.26.1.95

Ghose-Hajra, M., Jensen, R., and Hulliger, L. (2015). *Pile setup and axial capacity gain for driven piles installed using impact hammer versus vibratory system*. International Foundations Congress and Equipment Expo 2015, San Antonio, Texas. https://ascelibrary.org/doi/abs/10.1061/9780784479087.095. https://doi.org/10.1061/9780784479087.095

Goble, G., and Likins, G. (1996). *On the Application of PDA Dynamic Pile Testing*. 5th International Conference on the Application of Stress-wave Theory to Piles, Orlando, Florida, USA.

Jardine, R. (1985). *Investigations of pile-soil behaviour, with special reference to the foundations of offshore structures* [PhD, University of London]. London, UK.

Jardine, R. (2023). *The 6th ISSMGE McClelland Lecture: Time-dependent vertical bearing behaviour of shallow foundations and driven piles*. 9th International Offshore Site Investigation Geotechnics Conference - Innovative Geotechnologies for Energy Transition, London, UK. https://doi.org/10.3723/GIRI9226

Jardine, R. J. (2020). Geotechnics, energy and climate change: the 56th Rankine Lecture. *Géotechnique*, *70*(1), 3-59. https://doi.org/10.1680/jgeot.18.RL.001

Jardine, R. J., Standing, J. R., and Chow, F. C. (2006). Some observations of the effects of time on the capacity of piles driven in sand. *Géotechnique*, *56*(4), 227-244. https://doi.org/10.1680/geot.2006.56.4.227

Jardine, R. J., Zhu, B. T., Foray, P., and Yang, Z. X. (2013). Measurement of stresses around closed-ended displacement piles in sand. *Géotechnique*, *63*(1), 1-17. https://doi.org/10.1680/geot.9.P.137

Karlsrud, K., Jensen, T. G., Lied, E. K. W., Nowacki, F., and Simonsen, A. S. (2014). *Significant ageing effects for axially loaded piles in sand and clay verified by new field load tests*. Offshore Technology Conference, Houston, Texas, USA. https://doi.org/10.4043/25197-MS

Karna, U. L. (2001). *Characterization of Time-Dependent Pile Capacity in Glacial Deposits by Dynamic Load Tests* [PhD, New Jersey Institute of Technology]. New Jersey, USA.

Kirsch, F., and Plaβmann, B. (2002). *Dynamic Methods in Pile Testing: Developments in Measurement and Analysis*. International Deep Foundations Congress 2002, Orlando, Florida, USA. https://doi.org/10.1061/40601(256)61

Komurka, V., and Arndorfer, R. (2009). *Driven Pile Cost Comparison for Two Large Wisconsin DOT Bridge Projects*.

Komurka, V., and Theiss, A. G. (2018). *Savings from Testing the Driven-Pile Foundation for a High-Rise Building*. International Foundation Congress and Equipment Expo 2018, Orlando, Florida, USA. https://doi.org/10.1061/9780784481622.008

Komurka, V., Walton, W., Rusk, R., and Hannigan, P. (2017). *High-Capacity Driven Pile Foundation for a 33-Story High-Rise in Milwaukee, Wisconsin, USA*. DFI 42nd Annual Conference on Deep Foundations, New Orleans, Louisiana, USA.

Kraft, L. M. (1991). Performance of Axially Loaded Pipe Piles in Sand. *Journal of Geotechnical Engineering*, *117*(2), 272-296. https://doi.org/10.1061/(Asce)0733-9410(1991)117:2(272)

Kristinof, R., and Thorn, M. (2017). Setup of Driven Pile Capacity with Time in Soft Marine Sediments. *Australian Geomechanics*, *52*(3), 1-9.

Lehane, B. M., Jardine, R. J., Bond, A. J., and Frank, R. (1993). Mechanisms of Shaft Friction in Sand from Instrumented Pile Tests. *Journal of Geotechnical Engineering*, *119*(1), 19-35. https://doi.org/10.1061/(Asce)0733-9410(1993)119:1(19)

Lim, J. K. (2013). *Time and Scale Effects on the Shaft Friction of Displacement Piles in Sand* [PhD, The University of Western Australia]. Western Australia, Australia.

Long, J. H., Kerrigan, J. A., and Wysockey, M. H. (1999). Measured Time Effects for Axial Capacity of Driven Piling. *Transportation Research Record*, *1663*(1), 8-15. https://doi.org/10.3141/1663-02

Lupini, J. F., Skinner, A. E., and Vaughan, P. R. (1981). The drained residual strength of cohesive soils. *Géotechnique*, *31*(2), 181-213. https://doi.org/10.1680/geot.1981.31.2.181

Mosher, R. L. (1987). Axial Capacity of Vibratory-Driven Piles versus Impact-Driven Piles. *Transportation Research Record*(1277), 128-135.

Ng, K. W., Roling, M., AbdelSalam, S. S., Suleiman, M. T., and Sritharan, S. (2013). Pile Setup in Cohesive Soil. I: Experimental Investigation. *Journal of Geotechnical and Geoenvironmental Engineering*, *139*(2), 199-209. https://doi.org/10.1061/(ASCE)GT.1943-5606.0000751

Nowacki, F., Karlsrud, K., and Sparrevik, P. (1992). *Comparison of recent tests on OC clay and implications for design*. Recent large-scale fully instrumented pile tests in clay, London, UK.

Poulos, H. G. (2017). *Tall Building Foundation Design*. CRC Press. https://doi.org/10.1201/9781315156071

Poulos, H. G., and Davis, E. H. (1980). *Pile Foundation Analysis and Design*. Wiley.

Randolph, M. F. (2003). Science and empiricism in pile foundation design. *Géotechnique*, *53*(10), 847-875. https://doi.org/10.1680/geot.2003.53.10.847

Randolph, M. F., and Wroth, C. P. (1979). An Analytical Solution for the Consolidation Around a Driven Pile. *International Journal for Numerical and Analytical Methods in Geomechanics*, *3*(3), 217-229. https://doi.org/10.1002/nag.1610030302

Randolph, M. F., and Wroth, P. (1982). Recent developments in understanding the axial capacity of piles in clay. In. Cambridge, UK: Cambridge University Engineering Department.

Rausche, F. (2019). *Combining Static and Dynamic Loading Test Results of Piles*. 10th International Conference on Stress Wave Theory and Testing Methods for Deep Foundations, San Diego, California, USA.

Rausche, F., Moses, F., and Goble, G. G. (2004). Soil Resistance Predictions from Pile Dynamics. In *Current Practices and Future Trends in Deep Foundations* (pp. 418-440). https://doi.org/10.1061/40743(142)24

Rausche, F., Robinson, B., and Likins, G. (2004). *On the Prediction of Long Term Pile Capacity from End-of-Driving Information*. GeoTrans 2004: Current Practices and Future Trends in Deep Foundations, Los Angeles, California, USA. https://doi.org/doi.org/10.1061/40743(142)5

Roy, M., Blanchet, R., Tavenas, F., and Larochelle, P. (1981). Behaviour of a sensitive clay during pile driving. *Canadian Geotechnical Journal*, *18*(1), 67-85. https://doi.org/10.1139/t81-007

Samson, L., and Authier, J. (1986). Change in pile capacity with time: case histories. *Canadian Geotechnical Journal*, *23*(2), 174-180. https://doi.org/10.1139/t86-027

Schneider, J. A. (2007). *Analysis of Piezocone Data for Displacement Pile Design* [PhD, University of Western Australia]. Western Australia, Australia.

Seidel, J. (2015a). *Enhanced Use of Dynamic Pile Testing in Foundation Engineering*. 12th Australia New Zealand Conference on Geomechanics, Wellington, New Zealand.

Seidel, J. (2015b). *Overview of the Role of Testing and Monitoring in the Verification of Driven Pile Foundations*. 12th Australia New Zealand Conference on Geomechanics, Wellington, New Zealand.

 © Deep Foundations Institute 2026

Smith, B. (2009). *Dynamic Pile Testing - Construction Control and Design Verification*. International Foundation Congress and Equipment Expo, Orlando, Florida, USA. https://doi.org/10.1061/41021(335)75

Smith, E. J. (2025). Broad Synthesis of Factors and Mechanisms Contributing to Time-dependent Increase in Axial Capacity of Driven, Jacked, and Vibrated Piles. *Geotechnical and Geological Engineering*, *44*(1). https://doi.org/10.1007/s10706-025-03432-4

Soderberg, L. O. (1962). Consolidation Theory Applied to Foundation Pile Time Effects. *Géotechnique*, *12*(3), 217-225. https://doi.org/10.1680/geot.1962.12.3.217

Standards Australia. (2009). AS2159-2009 - Piling - Design and installation.

Thompson, C. D., and Thompson, D. E. (1985). Real and Apparent Relaxation of Driven Piles. *Journal of Geotechnical Engineering*, *111*(2), 225-237. https://doi.org/10.1061/(ASCE)0733-9410(1985)111:2(225)

Yang, N. C. (1970). Relaxation of Piles in Sand and Inorganic Silt. *Journal of the Soil Mechanics and Foundations Division*, *96*(2), 395-409. https://doi.org/10.1061/jsfeaq.0001394

Yang, Z. X., Jardine, R. J., Zhu, B. T., Foray, P., and Tsuha, C. H. C. (2010). Sand grain crushing and interface shearing during displacement pile installation in sand. *Géotechnique*, *60*(6), 469-482. https://doi.org/10.1680/geot.2010.60.6.469

DOWNHOLE MAGNETIC GRADIOMETRY FOR ESTIMATING THE LENGTH OF EXISTING PILES

Joshua Valencic, Douglas Partners, Sydney, NSW, Australia, +6128878 0660,
Joshua.Valencic@douglaspartners.com.au
Bruce McPherson, Douglas Partners, Sydney, NSW, Australia, +6128878 0660,
Bruce.McPherson@douglaspartners.com.au
Jeremy Hill, Douglas Partners, Sydney, NSW, Australia, +6128878 0660, Jeremy.Hill@douglaspartners.com.au

ABSTRACT

The reuse of existing piled footings in the absence of as-built documentation requires investigation and geotechnical assessment. To assess the geotechnical capacity of existing piles, an understanding of the length (i.e., founding depth) is necessary. One method of investigating the pile toe depth is via the downhole magnetic gradiometry (DMG) method. This research has built on the work of prominent authors (Packer et al. 2022 and Carlos et al. 2022) to investigate the magnetic fields of N24 steel reinforcing bars (i.e., a pile cage), on the basis of a specific signal pattern (traditionally assumed to be the 'lower most peak'). For the field-testing trials that form the basis of the current research, the bars were 3 m in length and were placed in an ungrouted 100 mm diameter hole (the 'model' pile). Cased boreholes were installed at 0.5 m, 2 m and 3 m offsets from the edge of the model pile. This research presents 15 data sets, involving variations in offset distance and bar orientation. The findings demonstrated that the lower most gradient peak is an acceptable method of estimating the base of the steel bars, albeit slightly conservative (e.g., 2.7 m vs 3.0 m actual length). The findings also demonstrated a maximum interpretable borehole offset of around 2 m for 'best-case' conditions, although this should be reduced to 1.0 m or a maximum of 1.5 m for more realistic conditions. Some combinations of bars led to inconclusive results, typical of many non-unique geophysical problems.

Keywords: Pile length assessment, downhole magnetic gradiometry, magnetometry pile reuse.

INTRODUCTION

Increased land values and carbon emission reduction/sustainability goals have resulted in an increased focus on the reuse of existing pile foundations in Australia. In many cases, building owners will look to add additional levels on existing buildings, which will also necessitate the investigation and assessment of piles to cater for increased loadings for in-service structures. Several geophysical methods as well as pulse-echo sonic integrity testing have been adopted to determine the length of existing piles. In cases where the pile head is not available for testing, geophysical methods are typically preferred. Downhole magnetic gradiometry (DMG) is a robust testing method that has a proven track record, in addition to a dual benefit from the need to undertake borehole investigations adjacent to the subject pile The DMG method is not without major limitations in both the test method and the interpretation of the results, which is presently an active area of research worldwide.

This paper describes research that builds on the work of several recent authors (Packer et al., 2022; Santos et al., 2022), which in turn build on the original papers produced by Jo et al., (1999 and 2003). This research includes data from R&D work undertaken by Douglas Partners from a project involving the reuse of existing piles. The research fieldwork was undertaken in November 2024. The data from this research was collected as part of a master's thesis at the University of NSW (UNSW).

The goal of the research is to improve established interpretation methods, specific to estimating the toe depth of existing piles. This research (including potential further work) is critical in increasing the reliability and trustworthiness of DMG testing results, ensuring good project outcomes for the construction and development industry sectors. Furthermore, a good understanding of the limitations of the testing method, and therefore avoiding undesirable outcomes due to incorrect interpretation or inconclusive investigation results, is essential in maintaining client trust.

 © Deep Foundations Institute 2026

BACKGROUND

Reuse and Investigation of Piled Footings

Investigations for estimating the length of an existing pile are commonly required for geotechnical assessment of:

- reuse of existing footings for a new building;
- adding floors to the top of an existing building;
- upgrading of an existing building where there is an increased loading imparted on the foundation piles as a result of new dead, live or seismic loads;
- large excavations adjacent to an existing building that may partially undermine footings/piles and/or where finite element modelling is required to estimate stresses and strains caused by deep excavation adjacent to a building;
- where an excavation well below a building (e.g., tunnelling or microtunnelling) needs to occur but must avoid existing piles; and
- other reasons for which estimating the geotechnical capacity of piles in the absence of as-built drawings is required.

The need for pile length investigations has increased over time, especially due to the scarcity and price of land within major capital cities, resulting in the need to build vertically. Due to the significant increase in land value in high density cities (such as Sydney, Australia) land owners are looking to maximise gross floor area (GFA) or gross lettable area (GLA) by building additional levels on existing buildings (McPherson and Hill, 2022). There are numerous examples of projects in Sydney where detailed engineering drawings of the building footing system are no longer available, primarily because of the age of the building. Councils are also requiring developers to provide off-street parking, necessitating the need for basement parking levels. In both cases there is a need to determine the depth of foundation and/or shoring piles.

Another aspect is the concept of designing ‘lean and green’ with faster construction times (idea coined by Berry et al., 2024). The embodied carbon of the construction of new piled footings includes (but is not limited to) emissions associated with the:

- mining and processing of the raw materials required for concrete and steel manufacturing and transporting of concrete;
- manufacturing and transporting of steel reinforcement;
- onsite construction related activities such as the operation of cranes, excavators, concrete agitator trucks and piling rigs; and,
- disposal of spoil generated, in addition to treatment of potentially contaminated soil.

The Greater London Plan was released in 2014 and provided a guideline for the planning and construction of new developments within London in the U.K. The plan outlines that all new developments need to consider reusing existing footings and foundations, or keeping them wherever possible (Patel, 2024). One of the main reasons for this is the carbon emissions resulting from the construction of new footings. Some estimates indicate that the proportion of the embodied carbon of a building can be up to 40% for the below ground concrete footings (Patel, 2024). There are several case studies from London and other areas in the U.K. where footing reuse has successfully been undertaken (Berry et al., 2024; Gasparre et al., 2024; Morrison and Ganesharatnam, 2024; Packer et al., 2022).

The European Federation of Foundation Contractors (EFFC) and Deep Foundations Institute (DFI) have created an online tool (V5 - uploaded: 09/01/2023) for the calculation of carbon emissions for piling projects, which can assist with determining the embodied carbon for several different project proposals (e.g., bored piles, displacement piles or soil mixing).

Downhole Magnetic Gradiometry (DMG)

There are several established methods for determining the length of a pile (e.g., sonic echo or pile integrity testing using stress wave methods, coring through shaft), all of which generally require access to the top of the pile. For situations where a column, capping beam or other superstructure is above the pile and/or the top of the pile is buried, alternative methods such as parallel seismic are required. These methods are explained at length in Packer et al. (2022), each with a list of pros and cons.

One option is to lower a magnetometer tool down a borehole installed adjacent to the existing pile to attempt to detect the base of the steel reinforcement cage. The method is commonly referred to as downhole magnetic gradiometry (DMG), but also downhole magnetics or magnetometry by other authors. The testing equipment consists of two individual magnetometers that are spaced at a fixed distance, which measures a magnetic gradient (i.e., change in magnetic field over distance). Many versions of the DMG testing equipment exist, with different arrangements and offset distances between the two magnetometers. The magnetic gradient versus depth is typically shown in nanoteslas/m (nT/m). The advantage of using a gradiometer is that measurements are relative, meaning that diurnal drift measurements are not required. Another advantage is that the gradiometer is less sensitive to background 'noise', as the measurements are relative between two points.

The downhole magnetics method involves the lowering of a fluxgate magnetometer down a cased borehole to take measurements of the vertical magnetic field intensity generally expressed as nT for absolute measurements or nT/m for gradiometer measurements (Santos et al., 2022). The method seeks to identify the base of the reinforcement cage of a piled footing, by determining the depth where there is a peak in the vertical magnetic gradient (or vertical derivative) (Coe et al., 2019; Dong et al., 2011; Packer et al., 2022). The method assumes that the reinforcement continues to the base of the pile, and therefore in the case of reinforcement curtailment (which is sometimes designed by a structural engineer to only extend to below the depth of zero lateral / shear stress), provides an estimate of the minimum pile depth.

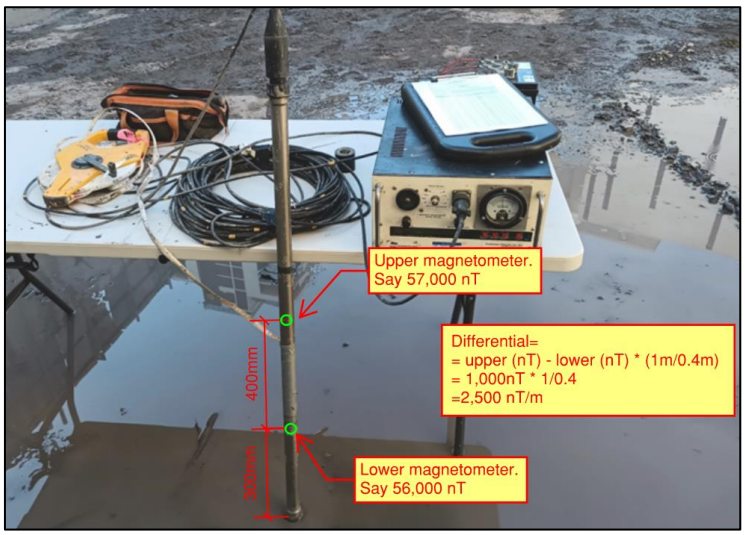


Fig. 1. DMG testing equipment, showing approximate location of magnetometers

The first paper to mention using a downhole magnetometer to measure the length of an existing pile was by Jo et al. (1999). The paper outlines a programme of testing for an existing pile and demonstrated a depth of 11.5 m using the "lower most peak" method. The paper discusses and illustrates the magnetic susceptibility concept, whereby the earth's magnetic field induces a secondary field within the steel pile or steel reinforcement. This is contrary to other authors who postulate that the remnant magnetisation prevails over the induced field (Santos et al., 2022), and is therefore a point of contention.

Jo et al., (1999) was then followed up by another paper by Jo et al., (2003) where trial testing was undertaken on a 4.5 m long driven steel H beam pile, where the lower most peak method was used to demonstrate the pile toe, within a borehole (for the magnetometer) at a distance of 1.0 m from the edge of the pile. This was then replicated on an existing bridge driven steel pile of unknown length, to confirm an interpreted depth of 22.8 m.

There are many case studies where the method has been used to investigate the length of existing piles in the absence of ground truth or calibration (Coe et al., 2019; Dong et al., 2011; Santos et al., 2022). Examples of where the depth of the pile is known prior to testing (i.e., purposely constructed for the aim of testing or calibrating the method) are far more limited (Jo et al., 2003; Packer et al., 2022, Sun et al., 2009). Other than Packer et al. (2022), the field trials were very limited and often included only testing one or two piles, with no sensitivity testing undertaken. The findings from the 'controlled' field trials were generally successful, however, the results indicated a range of results, and strongly recommended further controlled experiments or field trials.

An example of investigating shoring piles in Sydney was undertaken by McPherson et al. (2022) where a combination of side mounted sonic echo (pile integrity testing) and DMG testing were undertaken on shoring piles. Access to the pile tops was not possible due to the presence of a capping beam (and building) on top of the tested piles. The two testing methods generally indicated similar pile depths for rock socketed shoring piles. The results of the investigation were used for finite element numerical modelling (in Plaxis) to provide outputs to demonstrate that excavation of a basement would result in tolerable deflection limits and not compromise the stability of an existing multistorey building adjacent to a new development site.

Although the peak vertical gradient is the most common interpretation of the base of steel (Fig. 2), there are several different interpretation methods including: lower most peak of the vertical gradient, mid-point between peak vertical gradient and background signal (Jalinoos et al., 2006), inversion of gradient (Scarano Hemsi et al., 2022) and the zero crossing intercept. Jo et al. (2003) first postulated a "valley between two ridges" (i.e., peak gradient), which has been restated by many papers in more recent years. It is clear that the lowermost peak method is the most commonly used, but far from ubiquitous.

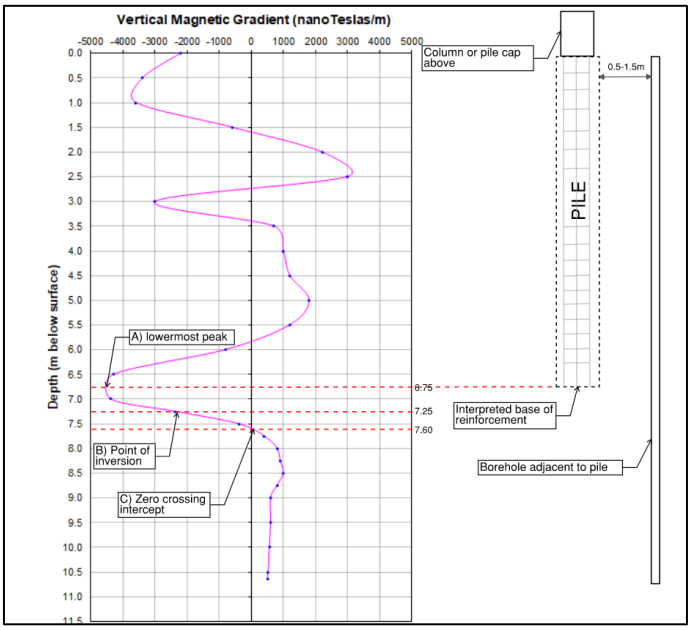


Fig. 2. Example downhole magnetics data showing peak, inversion and zero crossing intercept. Conventional base of reinforcement interpretation shown at 6.75 m depth. Borehole offset (from edge of pile) is approximately 1 m

 © Deep Foundations Institute 2026

An often-cited case study (Packer et al., 2022) included the construction of several test piles as part of a larger existing footing reuse project (i.e., 8000 existing driven piles), consisting of four driven cast insitu piles that were 'blind' tested by five different testing contractors in Bristol, U.K. The experiment included several testing methodologies, and downhole magnetometry was shown to be one of the most accurate, with length errors ranging from 100 mm to 2000 mm (for piles ranging from 5.32 m to 8.59 m depth). The experiment used driven piles with large steel driving shoes, which is not considered like-for-like with respect to conventional steel reinforcing cages for cast-in-situ pile types, and it is likely that the testing results were of a higher quality due to this aspect.

A general consensus between DMG studies is that the cased boreholes generally need to be installed as close as possible to the edge of the pile, ideally within 1 m (Santos et al., 2022, Packer et al., 2022). Where superstructure above the pile prevents a drill rig from drilling closer, 1.5 m to 2 m can be attempted but with generally poorer quality data resulting (Packer et al., 2022). The maximum distance between the testing borehole and edge of pile is not generally not well established, but tends to range from 1 m to 2 m (Jo et al., 2003), and up to 3 m (Jo et al., 1999). The amplitude of the signal typically attenuates as the inverse cube of the distance from the probe (Packer et al., 2022).

Due to the elongated shape of a longitudinal bar, previous authors have assumed a simple magnetic dipole (Jo et al., 2003; Santos et al., 2022), with a theoretical positive and negative end. Due to the complex nature of a reinforcement cage, there may be several individual longitudinal bars each with different magnetic field orientations, in addition to the presence of lapped lengths and ligatures.

Previous attempts at theoretically modelling this using Matlab has been made (Santos et al., 2022), and it was shown that analytical solutions are non-unique. Forward modelling of field-testing data was undertaken to back calculate a reinforcement cage with several sections of heterogenous ferromagnetic features (e.g., different magnetic intensity and magnetisation direction facing up or down). The paper concludes that the lower most peak method works well in most cases but can fail in others predominantly due to the fact that two or more numerical models (with different pile lengths) may fit the observed data. They also suggest multiple points of data are required as part of the pile length interpretation/assessment, including: DMG testing for multiple piles at a specific site, review of as-built drawings and supplementing with additional testing methods (e.g., parallel seismic, sonic echo/stress wave pile integrity testing).

METHODOLOGY

Experimental field testing was undertaken within an active construction site at a new aged care facility on the Central Coast, approximately 80 km north of Sydney, Australia. DMG and sonic echo integrity testing had already been undertaken for several existing piles at the site already with apparently good quality results. The development included the construction of a new multi-storey building (with new piled footings). However, the previous builder had constructed the piles but did not keep (or was not willing to provide) records. When the builder at the site changed hands at the Principal's request, the depths of the piles were unable to be confirmed for regulatory approval.

A tracked drilling rig was used to drill several 100 mm diameter boreholes using conventional auger drilling methods. One 'model' pile and three adjacent boreholes, to accommodate the magnetometer sensor, were drilled and constructed. The model pile was drilled to a depth of 3.0 m below the ground surface. The three test boreholes were drilled at offsets of 0.5 m, 2 m and 3 m from the edge of the model pile. The model pile hole was supported using 100 mm diameter PVC casing and the three test boreholes were cased using 50 mm diameter PVC casing. Due to the presence of extremely and highly weathered rock with some high strength, iron-cemented bands, the boreholes were not taken down to 5 m depth as initially planned.

A section diagram and plan showing the arrangement of the experiment are shown in Fig. 3. Initially it was proposed to drill four test boreholes, however, an obstruction at 3 m depth for the 1 m offset borehole, meant this hole was terminated early, and DMG data was not acquired. Five 3 m-long N24

steel deformed bars were purchased from a local steel supplier in Sydney. The steel supplier obtained their bars from the Infrabuild steel mill at Rooty Hill in Sydney.

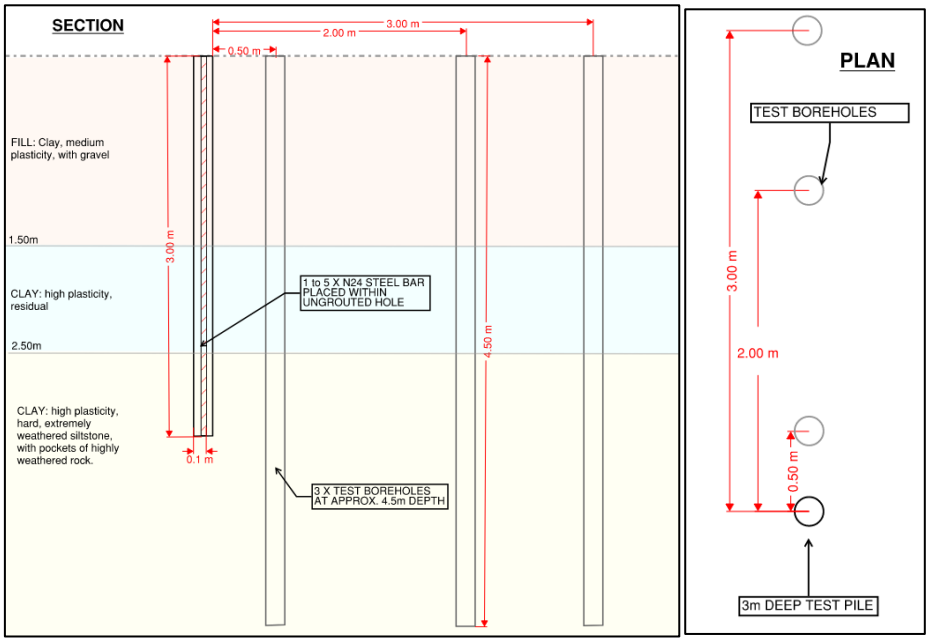


Fig. 3. Experiment setup, showing section (left) and plan view (right)

The DMG testing was undertaken using a Schonstedt GAU-20 gradiometer. The gradiometer has a 46 mm outer diameter with two magnetometers spaced at 400 mm. The sensor is attached to a survey tape, with readings being manually recorded at ground level using an analogue control unit. To undertake the testing, numerous unique arrangements of bar quantities and orientations (i.e., vertically flipping bars) were carried out, each representing the 'model' pile. Five bars of 3.0 m length were used for the testing. Ten combinations of a single bar were undertaken within the 0.5 m offset borehole (e.g., Bar 1 up, Bar 1 down…). Each bar was assigned with a reference 'up' and 'down' side.

SINGLE BAR RESULTS

A sample of the single bar data is shown in Fig. 4. The DMG test results from the 0.5 m offset borehole (Table 1) show that the lowermost peak method indicated a range of interpreted pile toe depths ranging from 2.20 m to 3.05 m. The average of the results was 2.76 m, or 2.83 m excluding the outlier from Bar B4. These results are generally within 10% of the pile depth. The lowermost peak method has slightly underestimated the model pile depth, which for most projects is a conservative approach. The point of inversion and zero crossing intercept methods indicated an average model pile length of 3.14 m and 3.41 m, respectively. Although these results appear good at first glance, we know that the point of inversion and zero crossing intercept methods depend on the wavelength of the signal, which becomes wider with distance from the pile, rendering such methods increasingly less accurate at offsets of more than 0.5 m.

Multiple Bar Results

Based on the single bar results, each end of each bar was marked as either positive (+ive) or negative (-ive) depending on the polarity of the lower most peak gradient. Five different experiment arrangements were undertaken for the multiple bar model pile testing (Table 2). Data sets 11 to 13 indicated a 'best-case' scenario consisting of all +ive bar ends facing downwards with testing at 0.5 m, 2 m and 3 m offset from the edge of the pile. Data sets 14 and 15 included two additional data sets for a 0.5 m offset, with alternative bar arrangements comprising some +ive and -ive facing down. Each row has been colour coded to match the graphs shown in Fig. 5.

 © Deep Foundations Institute 2026

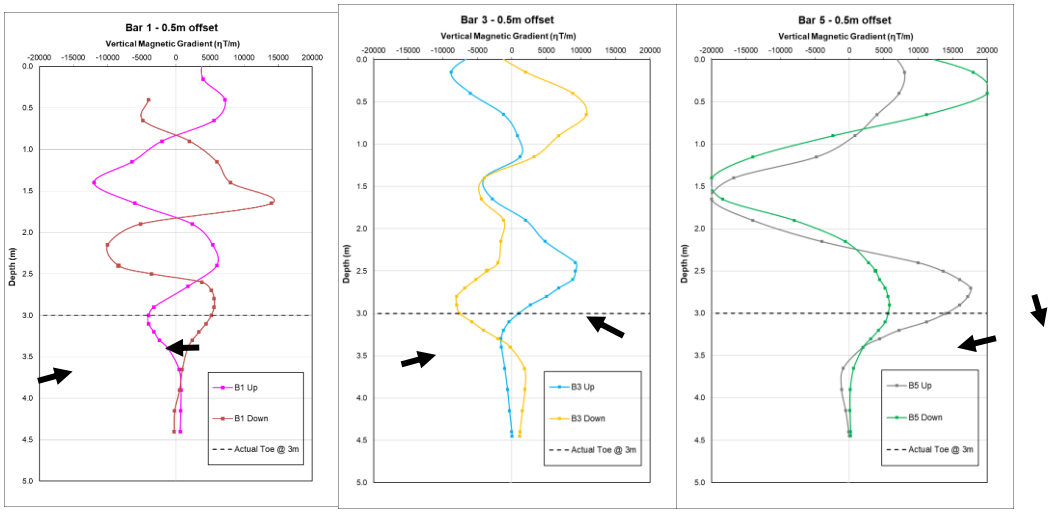


Fig. 4. Example single bar data from Bar 1, 3 and 5. Lower most peak method shown with black arrow

Table 1: Depth of interpreted 3m deep model pile according to each testing stage at 0.5m offset

Data set	Bar	Borehole offset (m)	Interpreted depth to base of 'model pile' (m)		
			a) Lowermost Peak Gradient	b) Point of Inversion	c) Zero crossing intercept
1	Bar 1 Up	0.5	3.05	3.30	3.65
2	Bar 1 Down	0.5	2.85	3.20	3.65
3	Bar 2 Up	0.5	2.50*	3.15	3.30
4	Bar 2 Down	0.5	2.90	3.30	3.50
5	Bar 3 Up	0.5	2.50	2.80	3.05
6	Bar 3 Down	0.5	2.90	3.20	3.40
7	Bar 4 Up	0.5	2.20*	2.70	2.95
8	Bar 4 Down	0.5	2.85	3.20	3.50
9	Bar 5 Up	0.5	2.70	3.20	3.50
10	Bar 5 Down	0.5	2.90	3.30	3.65
Average Depth (m)			**2.76 (2.83 ex. B4 Up)**	**3.14**	**3.41**

Notes: * = data unclear or anomalous

Table 2: Multiple bar results from five cases

Data set	Bar	Borehole offset (m)	Interpreted base of model pile (m)		
			a) Peak	b) Point of Inversion	c) Zero crossing intercept
11	B1 to B5, +ive down *Best Case Conditions*	0.5	2.70	3.10	3.45
12		2.0	2.90	unclear	unclear
13		3.0	unclear	unclear	unclear
14	B1 to B5, half +ive, half -ive down	0.5	2.70	3.15	3.5
15	B1 to B4, half +ive, half -ive down	0.5	2.00 – 2.60*	3.00	3.40

Notes: 1. Colour as shown on Figure 5

 © Deep Foundations Institute 2026

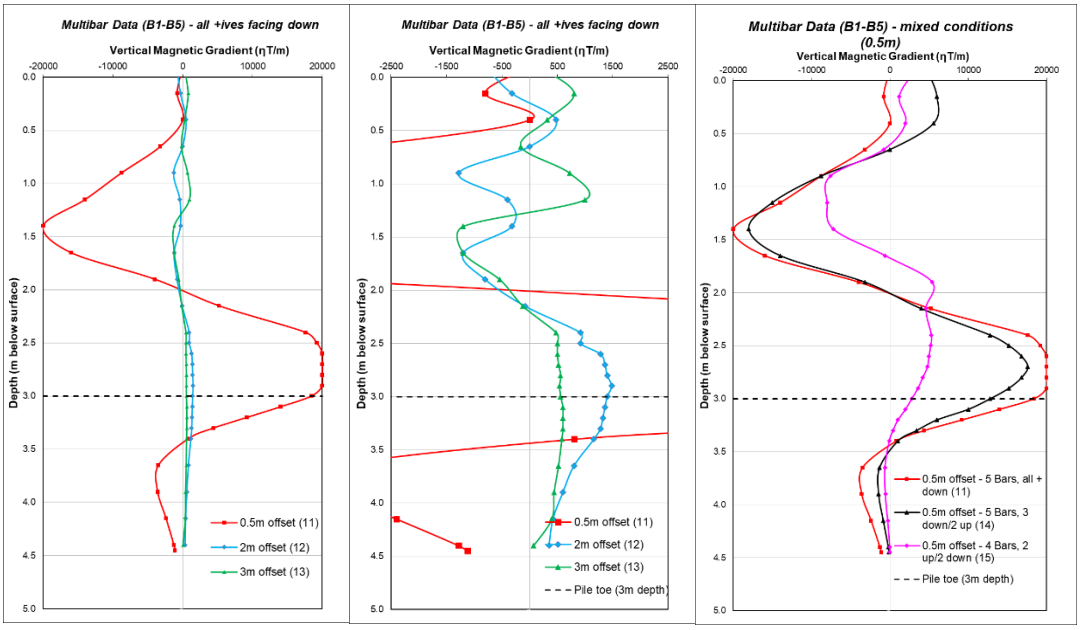


Fig. 5. Data sets 11 to 13. B1 – B5, all positive sides down (best case scenario), natural x- axis scale (left) and amplified scale (middle). Data sets 11, 14 and 15 (right) showing mixed case results

The results from data sets 11 to 13 (Fig. 5) indicate a clear pile toe peak at around 2.7 m depth for the 0.5 m offset borehole, however, the amplitude of the peak drops off rapidly with distance from the pile and is much smaller for the 2 m and 3 m offset cases. The 0.5 m data clips beyond the working range of the instrument (>20,000 nT), however, the peak is generally identified as the midpoint between the total clipped extent. A peak at around 2.9 m depth has been inferred for the 2 m dataset, however, it is not a clear signal and the data quality is poor. For the 3 m dataset, a gradient peak is not visible, and at best, a range of possible pile toes has been interpreted (2.5 m to 3.4 m). The 3 m data set would generally be considered inconclusive and would likely require further investigation. For the point of inversion and zero crossing intercept methods, the data sets for both 2 m and 3 m offsets are inconclusive, highlighting the issue with these methods.

The mixed case results (Fig. 5; right-most graph) introduce two new experiment changes. For data set 14, half of the bars are flipped such that some -ive sides are facing down. A resulting reduction in the amplitude of the peak gradient is apparent, causing the data to no longer be clipped. The data quality for set 14 is good, a clear peak at 2.7 m depth can be seen (same as set 11). For data set 15, B5 is removed from the model pile, resulting in inconclusive results with no clear gradient peak (and hence pile toe) apparent. A possible range of around 2.0 to 2.6 m depth may be interpreted, but further investigation would be necessary for this case due to lack of clear peak.

DISCUSSION

The individual steel bars appear not to be simple magnetic dipoles (with a clear peak at either end, as numerical modelling undertaken by others has assumed) but rather includes complex ferromagnetic fields with two or more dipoles along the length of the bar. The individual bars indicated a high range of variability, however, when the bars were tested as a group or ‘cage’, the lowermost gradient peak (interpreted pile toe depth) was shown to be the same as the average of the interpreted depths for the individual bars (i.e., 2.7 m and 2.7 m). This is broadly consistent with conventional magnetic field theory, which states that that individual magnetic fields are vectors (direction and magnitude) and are added together via a vector sum and super-positioning.

Previous authors have stated a maximum borehole offset ranging from less than 1 m, up to 3 m from the edge of the pile. It is commonplace for large offsets between the existing (‘test’) pile and the

borehole and thus the magnetometer (e.g. >2 m), due to tight access and minimum clearances necessary for a drilling rig. The requirement to get a 'quick' answer with whatever tools and budget are available, can sometimes lead to inconclusive results, resulting in the need for further investigation, highlighting the importance of properly understanding the limitations of the DMG testing method. Logically, reducing the distance between the pile and the borehole, maximises the chances of successful testing results.

The decay or dissipation of a magnetic field over a given distance (i.e., over a radius within a hypothetical sphere) is known to follow the inverse cube law (Packer et al., 2022). It is a reasonable assumption to expect that the decay of the magnetic gradient will be proportional to the decay of the absolute magnetic field. The results from data sets 11 to 13, and data from Packer et al. (2022) (results rebased to 20,000 nT/m) have been plotted on Fig. 6, in addition to a line representing the inverse cube and inverse square formulas. The results indicate that the best-case conditions for the specific test site fall around the inverse cube. With comparison to the Packer (2022) data, it can be seen that data falling well below the inverse cube line is evident (e.g., result for 1.3 m offset distance) and is likely to be pile (e.g., bored pile with reo. cage, or driven steel H pile) and/or site specific. By comparing the decay results from Fig. 6 and the peak gradient from Fig. 5, it is clear that the maximum borehole offset is probably around 2 m for this experimental setup. However, it is noted that the maximum offset could vary either way depending on a number of variables (e.g., strength of remnant magnetisation, quantity of steel in the piles, sensitivity of measuring equipment and magnetisation of surrounding material). Assuming more realistic field conditions, a maximum offset distance of less than 1.5 m is considered more appropriate, but it should be kept as small as reasonably practicable (i.e., closer to 1 m).

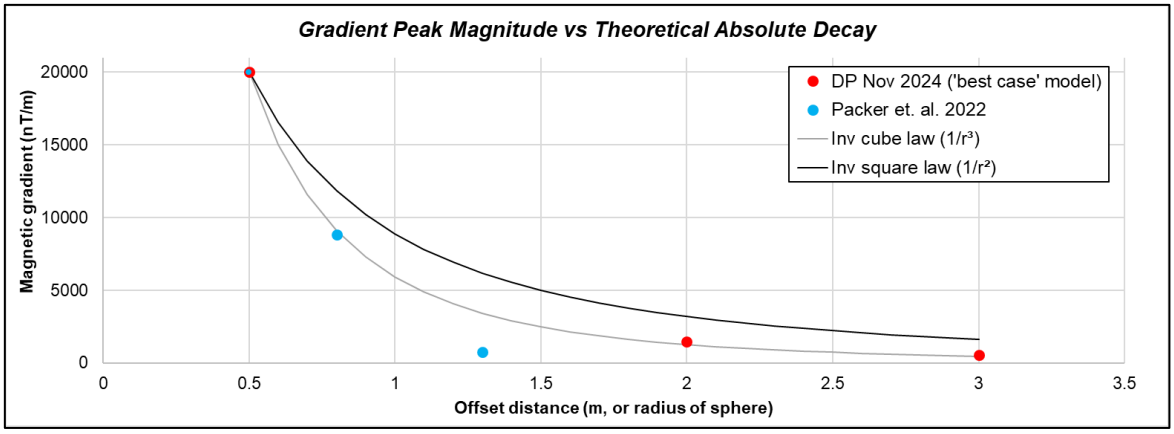


Fig. 6. Dissipation of magnetic field (as a function of measured gradient) vs. distance plotted against inverse cube law and inverse square law

For the single bar results, a significant range of pile depths was interpreted, however, once this was averaged out over 5 bars, the anomalies and inconclusive gradient peaks tended to 'filter' out. This was evident by the average single bar depth (around 2.7–2.8 m) versus the pile toe depth seen in data sets 11 and 14 (2.7 m), both with 5 bars installed with the positive end downward (i.e., at the base of the pile). It is clear that in most cases, the lower most peak is the most appropriate method (albeit slightly conservative, giving a shorter pile length) of estimating the pile toe depth, although multiple data points are necessary to substantiate a high level of confidence in the results (e.g., at least 3 different piles tested via DMG to establish a trend, coring through a subset of the tested piles, review of as-built drawings, parallel seismic, sonic echo/stress wave testing).

CONCLUSION

Downhole magnetic gradiometry (DMG) has risen in popularity over the last 10 years for determining the length of existing pile foundations for reuse or building upgrade projects. Sustainability and carbon offset objectives are likely to see an increasing need for pile investigation methods, as is

occurring in U.K. and other countries. For example, the Greater London Plan was released in 2014 and provides guidelines for the planning and construction of new developments where it is necessary to consider re-using existing footings and foundations.

Notwithstanding the limitation of the method being reliant on steel reinforcement extending to the full depth of the pile, DMG provides a valuable means of investigation, particularly for in-service piles where the pile head is not accessible for testing. The method can provide accurate information on as-built pile length but obtaining accurate data depends on several factors that were not previously well understood.

By undertaking an experimental field trial using several 3 m-long N24 steel reinforcement bars, this research has produced data that assist in testing previously untested hypotheses from other DMG studies. This research has built on the work of several previous authors (Packer et al., 2022; Santos et al., 2022) to investigate the magnetic fields of several N24 bars on the basis of the lowermost peak pile toe interpretation method.

The findings suggest that in most circumstances that the borehole should be located no more than 2 m away from the edge of the pile. For best results, it has been shown that an offset distance of 1 m to 1.5 m can give a good balance between signal quality and safe drilling rig access.

The findings demonstrate that the lowermost peak method is an acceptable interpretation method for estimating the pile toe depth, and probably a conservative approach. It should be noted that previous authors have occasionally obtained questionable investigation results using the method (Packer et al., 2022; Santos et al., 2022), so where possible, multiple DMG tests on different piles should be undertaken for any single site for increased reliability.

REFERENCES

Berry, A., Patel, D., Faber, F., Bond, L., Brook, J., Kaussen, J., 2024. Managing piling obstruction risk intelligently for reinvention of a UK brutalist building. Proc. Inst. Civ. Eng. - Forensic Eng. 177, 75–86. https://doi.org/10.1680/jfoen.22.00028

Coe, J.T., Kermani, B., Nyquist, J., 2019. Evaluation of Unknown Bridge Foundations Using Borehole-based Nondestructive Testing Methods: A Case Study in Urban Settings. J. Environ. Eng. Geophys. 24, 299–315. https://doi.org/10.2113/JEEG24.2.299

Dong, P., Sun, B., Fan, J., Wang, L., 2011. Determining Lengths of Reinforcements in Bored In Situ Concrete Piles Using the Magnetic Method. J. Environ. Eng. Geophys. 16, 37–46. https://doi.org/10.2113/JEEG16.1.37

Foss, C., Leslie, K., and, W.S., 2015. A moving 3 component fluxgate magnetometer to measure remanent and induced magnetizations in drill core. ASEG Ext. Abstr. 2015, 1–3. https://doi.org/10.1071/ASEG2015ab067

Gasparre, A., Crilly, M., Harland, S., Atkinson, G., 2024. Strip footings for the extension of a piled building. Proc. Inst. Civ. Eng. - Forensic Eng. 177, 95–103. https://doi.org/10.1680/jfoen.22.00030

Hashemi, A., Yazdanpanah Qaraei, P., Dehghani, M., Taheri, H., 2024. Optimum design and manufacturing of the lifting cylindrical electromagnets considering magnetic, thermal, and mechanical limitations. Int. J. Interact. Des. Manuf. IJIDeM 18, 2345–2357. https://doi.org/10.1007/s12008-023-01491-6

Jalinoos, F., Gibson, A., Diehl, J., 2006. Determination of unknown length of sheet piles using three geophysical logging methods. Geophysics.

Jo, C.H., Cha, Y.H., Choi, J.H., 2003. A borehole magnetic logging tool for estimating unknown foundation depths. 3rd Int. Conf. Appl. Geophys. 1–5.

Jo, C.-H., Hyun-Key, C., Kwang-Ho, C., 1999. Borehole Magnetics for the Estimation of Unknown Foundation Pile Depth. J. Korea Inst. Struct. Maint. Insp. 1999, 161–167.

 © Deep Foundations Institute 2026

McPherson, B., Hill, J., 2022. Existing Pile Length Assessment Using Geophysical and Low Strain Testing Methods. Presented at the DFI-PFSF Piling & Ground Improvement Conference, ICC, Sydney, Australia.

Morrison, P., Ganesharatnam, L., 2024. Driven pile foundation reuse in East London, UK. Proc. Inst. Civ. Eng. - Forensic Eng. 177, 87–94. https://doi.org/10.1680/jfoen.22.00033

Packer, M.L., d'Agostino, S.J., Schreiner, H.D., 2022. Systematic field test of non-destructive techniques for driven cast in situ pile lengths. Proc. Inst. Civ. Eng. - Geotech. Eng. 175, 49–61. https://doi.org/10.1680/jgeen.20.00171

Patel, D., 2024. Editorial: Themed issue on reuse of foundations and structures. Proc. Inst. Civ. Eng. - Forensic Eng. 177, 73–74. https://doi.org/10.1680/jfoen.2024.177.3.73

Santos, M.C.D.S., Mendonça, C.A., Souza, T.D.J., Hemsi, P.S., Gandolfo, O.C.B., 2022. Borehole magnetometry to determine the depth of reinforced foundations in telecommunication towers. GEOPHYSICS 87, EN33–EN43. https://doi.org/10.1190/geo2021-0281.1

Scarano Hemsi, P., De Souza Santos, M.C., De Jesus Souza, T., Gandolfo, O.C.B., Alberto Mendonça, C., 2022. Borehole Magnetometry Test for Evaluating a Caisson's Reinforced Depth: Experimental Results and Theoretical Modeling. Geotech. Test. J. 45, 20–37. https://doi.org/10.1520/GTJ20200300

 © Deep Foundations Institute 2026

SEISMIC PERFORMANCE EVALUATION FOR PILE-RAFTED GENERATION III NUCLEAR POWER PLANT

Meng Chu, Shanghai Nuclear Engineering Research & Design Institute Co. Ltd., Shanghai 200233, China
Weiming Gong, Key Laboratory of Concrete and Prestressed Concrete Structures of Ministry of Education, College of Civil Engineering, Southeast University, Nanjing 211189, China
Zhenkun Ding, Shanghai Nuclear Engineering Research & Design Institute Co. Ltd., Shanghai 200233, China
Jie Yang, Shanghai Nuclear Engineering Research & Design Institute Co. Ltd., Shanghai 200233, China
Dong Feng, Key Laboratory of Concrete and Prestressed Concrete Structures of Ministry of Education, College of Civil Engineering, Southeast University, Nanjing 211189, China, super_sage@163.com
Yu Ren, Shanghai Nuclear Engineering Research & Design Institute Co. Ltd., Shanghai 200233, China
Ziduan Shang, Shanghai Nuclear Engineering Research & Design Institute Co. Ltd., Shanghai 200233, China
Yugang Sun, Shanghai Nuclear Engineering Research & Design Institute Co. Ltd., Shanghai 200233, China
Bing Li, Key Laboratory of Concrete and Prestressed Concrete Structures of Ministry of Education, College of Civil Engineering, Southeast University, Nanjing 211189, China

ABSTRACT

This study evaluates the seismic performance of pile-rafted foundations in Generation III nuclear power plants (NPPs), emphasizing steel-concrete-steel (SCS) structures and small modular reactors (SMRs). SCS structures maintain integrity under static and seismic loads, with steel plates remaining elastic and concrete cracking controlled at 0.3g safe shutdown earthquake (SSE) levels. Large-scale shaking table tests were conducted to investigate the seismic response characteristics of the sandy sites – pile-rafted foundations – SMR structures system. The results demonstrated that the pile-rafted foundations effectively filtered high-frequency components of seismic loads, significantly reducing acceleration sensitivity, and enhancing the overall seismic performance. In a nuclear island building test model, a horizontal acceleration amplification effect was most pronounced in external plant and internal nuclear equipment components, while an internal steel containment vessel component exhibited a weaker acceleration amplification effect due to the top weight. Seismic response spectrum analysis further revealed that the combined action of pile-rafted foundations and superstructures significantly altered the frequency characteristics of the test model, underscoring the critical role of pile foundations in improving the seismic performance of SMR structures. The new findings of this study provide important theoretical and technical supports for the modular design as well as seismic performance evaluation and optimization of NPP in non-rock sites.

Keywords: Nuclear power plant, steel-concrete-steel structure, pile-rafted small modular reactors, shaking table test, seismic performance

INTRODUCTION

In recent years, modular steel-concrete-steel (SCS) structures have been widely adopted in major engineering projects, such as nuclear power plants (NPP), due to their excellent mechanical properties, particularly for the construction of two-dimensional components like walls, floors, and shells [1-6]. SCS structures are primarily categorized into single-sided SCS structures, used for horizontal components (e.g., floors and domes), and double-sided SCS structures, suitable for vertical components (e.g., walls and cylinders) [7]. Compared to traditional reinforced concrete (RC) structures, SCS structures exhibit superior load-bearing capacity, ductility, integrity, and exceptional

 © Deep Foundations Institute 2026

resistance to impact and penetration. Stress distribution analysis at typical locations of a nuclear reactor building revealed that, under seismic loading, the concrete cracked due to tension, but the steel plates did not reach yield strength, indicating that the SCS structure maintains excellent seismic performance at a 0.3g safe shutdown earthquake (SSE) level. Additionally, the steel plates in SCS structures serve as formwork during concrete pouring, significantly enhancing construction efficiency.

Leveraging these advantages, the United States pioneered the application of SCS structures and modular construction techniques in the design of AP1000 NPP, such as the Vogtle NPP in Georgia [6, 8]. Subsequently, SCS structures have been successfully implemented in some projects like the Sanmen NPP in Zhejiang and the Haiyang NPP in Shandong, China, achieving remarkable technical and economic benefits and becoming a defining feature of generation III NPP. Currently, other types of generation III nuclear power units in China are also gradually adopting modular SCS structures. Furthermore, generation IV NPP, including advanced light water reactors (ALWR) and small modular reactors (SMRs), are considering SCS structures as primary shielding and protective components.

Notably, SMRs have emerged as a significant trend in nuclear technology development, garnering attention in countries such as China, Canada, and the United States. SMRs can meet a broader range of power demands, providing small-scale combined heat and power solutions for developing countries, remote areas, and off-grid regions, while also supporting hybrid nuclear-renewable energy systems [9]. Moreover, the deployment of SMRs contributes to global climate change commitments by facilitating the transition to a low-carbon future, including the phase-out of traditional coal-fired power generation, deep decarbonization of heavy industries, and the transformation of industrial infrastructure toward clean energy [10]. Additionally, SMRs offer advantages such as modular design, compact size, and lower construction costs, demonstrating significant technical potential in specific application scenarios [11].

Earthquakes, as critical external natural hazards, have always been a central focus in nuclear safety research during the design, construction, and operation of NPP [12-13]. The seismic performance of nuclear facilities must be rigorously evaluated, as their failure could lead to severe public safety and societal risks. Particularly, research on the seismic performance of SMR plants in non-rock sites has become a key aspect of nuclear engineering safety assessments. Furthermore, the interaction mechanisms among soil sites, pile group foundations, and reactor buildings under seismic loading are highly complex [14-19]. In-depth studies in this field are essential to ensure the seismic safety and stability of SMR structures in non-rock sites.

Based on this context, this study also conducted large-scale seismic simulation shaking table tests on SMR models under non-rock site conditions, aiming to provide critical references for the seismic performance evaluation and optimization of pile-supported nuclear island buildings in such sites. The findings offer essential technical support for the seismic design, construction, and operation of NPP in non-rock sites, further bolstering confidence in the safe expansion of nuclear power projects to these sites across the global.

SEISMIC PERFORMANCE EVALUATION OF PILE-RAFTED SMR VIA SHAKING TABLE TEST

SMR offer greater flexibility in site selection due to their inherent safety features. Particularly for heating-type SMR, deployment near user areas such as industrial parks or residential zones is common to minimize heat loss and ensure heating efficiency. However, these potential sites often have complex site conditions, typically consisting of non-rock sites or even deep soft soil layers. Under seismic loading, the seismic response of soft soil sites is significantly stronger than that of rock sites and often exhibits pronounced nonlinear effects.

Pile foundations, as a deep foundation type with excellent seismic performance [20-25], can effectively enhance the ability of reactor buildings to withstand strong earthquakes in non-rock sites. Their application in SMR foundation design has garnered increasing attention. As NPP are special

infrastructure with extremely high safety standards, a comprehensive evaluation of the seismic response characteristics of SMR structures with pile foundations is essential. Therefore, conducting large-scale shaking table tests to study the seismic soil-pile-structure interaction of pile-supported SMR buildings in non-rock sites is of great significance for assessing the safety of nuclear power generation [25].

Large-Scale Seismic Simulation Shaking Table Test System

A series of shaking table tests in this study were conducted on the Tang Zhongying Seismic Experimental Platform at Southeast University. The primary test equipment was a large-scale seismic simulation shaking table manufactured by SERVOTEST, UK. The table measures 6.0 m × 9.0 m (expandable to 9.0 m × 9.0 m) and has a maximum payload capacity of 120 t, as shown in Fig. 1.

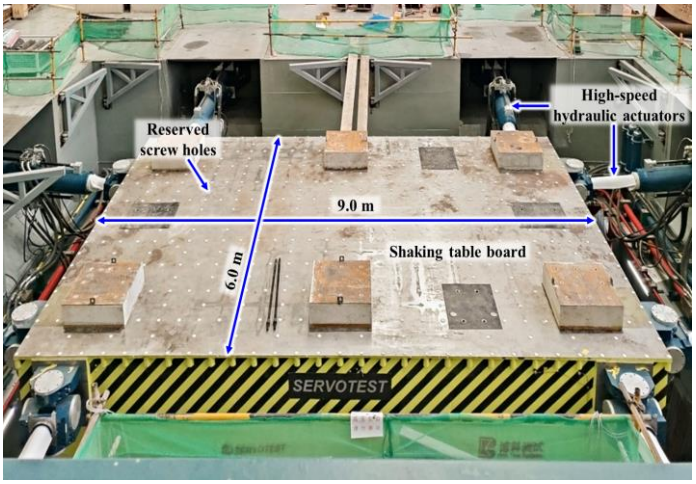


Fig. 1. Large-scale seismic simulation shaking table test system at Southeast University

The shaking table is equipped with high-performance hydraulic actuators, enabling high-speed motion in three directions and six degrees of freedom. It also features an advanced Pulsar digital control system and a high-precision Pacific 6000 data acquisition system, capable of effectively simulating near-fault ground motions. This system is suitable for seismic simulation studies of engineering structures, electromechanical equipment, and transportation infrastructure. The main technical parameters of the shaking table test system are listed in Table 1.

Table 1. The main technical parameters of large-scale seismic simulation shaking table test system.

Item name	**Measurement range**
Table size	6.0 m × 9.0 m (expandable to 9.0 m × 9.0 m)
Vibration direction	Three directions and six degrees-of-freedoms (X/Y/Z)
Maximum load capacity	120 t
Maximum displacement	X/Y: +/-500 mm; Z: +/-300 mm
Maximum acceleration at full load	X/Y: 1.5 g; Z: 1.3 g
Maximum overturn moment	X/Y: 6,707 kN·m; Y: 6,391 kN·m (Meet simultaneously at maximum load capacity)
Maximum eccentric moment	1,500 kN·m
Maximum eccentricity	±1.25 m
Operation frequency range	0.1 ~ 50 Hz
Vibration waveform	Periodic wave/random wave/seismic wave
Control mode	Pulsar digital control system
Pacific 6000 data acquisition system	256 Channels

Innovative Large-Size, Multi-Directional Laminar Shear Soil Box

Our research team developed a large-size innovative multi-directional laminar shear soil box, which is leading in size, performance, and functionality among similar devices. As shown in Fig. 2, the soil box consists of a base, frame laminations, interlayer bull-eye bearings, energy-dissipating rods, and an external protective frame. The internal rectangular box measures 5,600 mm (length) × 3,800 mm (width) × 2,191 mm (height) and can hold over 80 tons of test soils. The box is divided into 18 laminations, each constructed from rectangular hollow steel tubes welded together. The laminations are connected by bull-eye bearings, allowing relative horizontal movement within a defined circular range, with a lamination spacing of 23 mm. Energy-dissipating rods are arranged around the box, and their number, diameter, stiffness, and fixing keys can be adjusted to modify the box's stiffness, reducing boundary effects on test results, and approximately simulating semi-finite foundation conditions. The external protective frame provides vertical counter-pressure and limits horizontal displacement. The combination of boundary rings, energy-dissipating rods, and the protective frame ensures triple safety for the tests.

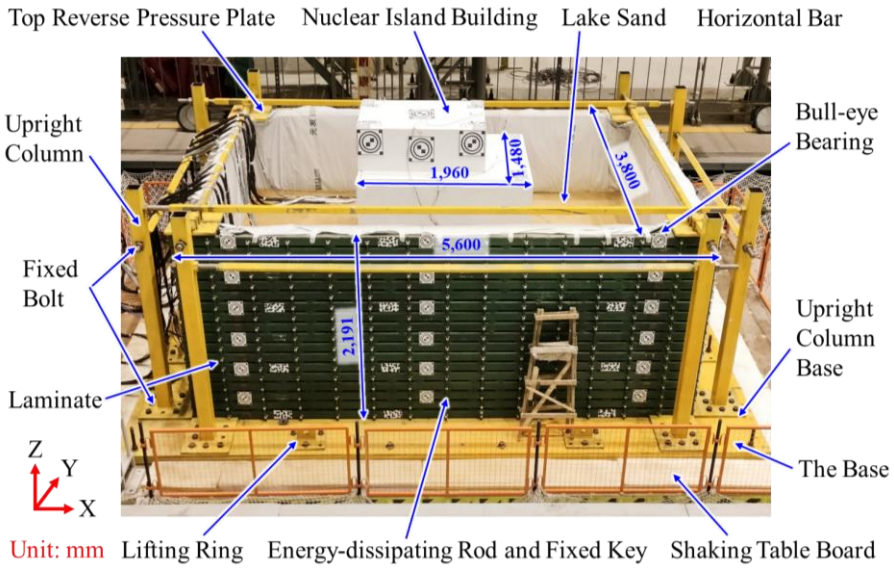


Fig. 2. Shaking table test for seismic performance of pile-rafted SMR

Design of the Shaking Table Test Program

The test began by bolting the soil box base to the shaking table platform. Rectangular frame laminations were then stacked layer by layer, and energy-dissipating rods were installed around the box. Finally, an external protective frame was assembled to ensure test safety. After laying energy-dissipating foam boards and waterproof geomembranes on the box's base and inner walls, natural lake sand was filled into the box using a layered compaction method, with a relative density parameter (D_r) of 0.818 and a filling thickness of 1,100 mm. During sand filling, 20 model aluminium pipe piles (arranged in a 4 × 5 grid) were installed, with pile ends positioned 200 mm above the box base. After completing the sand filling and pile group arrangement, the cushion cap and nuclear island building model were installed, with pile tops penetrating the cap and bolted to the building's base plate.

During the layered filling of the natural lake sand model site and the installation of the nuclear island building model, accelerometers were placed at key locations, including the model's top, interior, and within the soil layers, to monitor the time–history variations of triaxial accelerations during seismic loading. As shown in Fig. 3, accelerometers AS1 and AS10 were embedded in the test soil near the inner walls of the soil box; AS2–AS5 and AS11 were embedded in the soil between the pile group and the inner walls, with a vertical spacing of 275 mm; and AS6–AS9 were embedded in the soil within the pile group, also with a vertical spacing of 275 mm. Uniaxial accelerometers AW1–AW4 were

 © Deep Foundations Institute 2026

attached to the exterior walls of the nuclear island building model, with a vertical spacing of 573 mm. Triaxial accelerometers AN1–AN4 were attached to the nuclear equipment component inside the steel containment vessel component, with vertical spacings of 190 mm, 160 mm, and 130 mm, respectively. Triaxial accelerometers AN5–AN8 were attached to the internal steel containment vessel component, with vertical spacings of 250 mm, 250 mm, and 280 mm, respectively.

The AS and AN series sensor are triaxial accelerometers, used to monitor 3D acceleration responses in the X, Y, and Z directions. The AWX, AWY, and AWZ series sensors are uniaxial accelerometers, measuring acceleration responses in the X, Y, and Z directions, respectively. All sensors have a data acquisition frequency of 512 Hz.
\

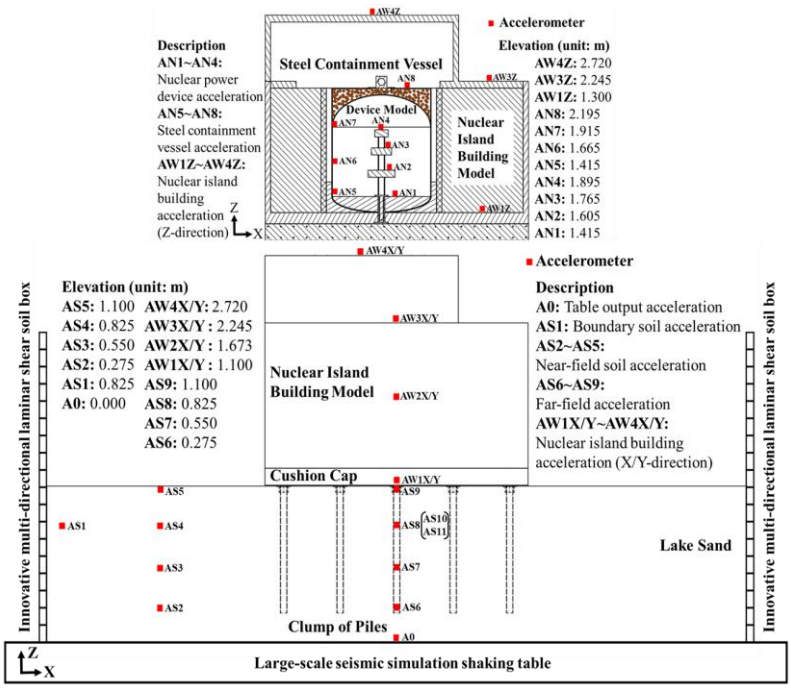


Fig. 3. Schematic diagram of accelerometer layout in shaking table test model for pile-rafted SMR

The primary objectives of this study are: (i) to verify the rationality of the boundary effects of the large-size innovative multi-directional laminar shear soil box and ensure that it does not adversely affect test results; and (ii) to investigate the acceleration response patterns at different locations (above and below ground) of the sand sites – pile-rafted foundations – nuclear island buildings system model under seismic loading and conduct quantitative analysis. To achieve these objectives, multiple test conditions and corresponding seismic loading mechanisms were designed. Three types of seismic loads were applied, i.e., the EL-Centro records, the Chi-Chi records, and an artificially synthetic excitations, each applied simultaneously in the X, Y, and Z directions.

ANALYSIS AND DISCUSSION OF SHAKING TABLE TEST RESULTS

Through large-scale shaking table tests, this study preliminarily evaluated the seismic performance of pile-rafted SMR structures. Below, the acceleration amplification effects and seismic response spectrum characteristics of the lower lake sand sites and the upper nuclear island building model under the typical Chi-Chi seismic loads are analysed and discussed.

Acceleration Amplification Effects in Lower Lake Sand Sites

The reinforcing effect of pile-rafted foundations significantly influenced the acceleration response characteristics under seismic loading. Figure 4 shows the variation of peak acceleration amplification

factors with depth in the far-field and near-field regions of the natural lake sand sites under the Chi-Chi seismic loads.

In the far-field region of the lake sand sites, the vertical (Z-direction) peak acceleration amplification effect was the most pronounced, with a surface-to-base amplification factor of 4.52. The amplification factors in the X and Y directions were similar, at 3.00 and 3.01, respectively. However, the peak acceleration amplification effect in the near-field region of the pile foundation soil was significantly weaker than that in the far-field region. In the near-field region, the Z-direction amplification factor was 2.32, while the X and Y directions were 1.23 and 1.24, respectively. The acceleration amplification factors in the near-field region were 41.28%, 41.37%, and 51.27% of those in the far-field region at the same depth for the X, Y, and Z directions, respectively. It should be noted that the Z-direction accelerometer AS3 failed to record valid data due to a malfunction.

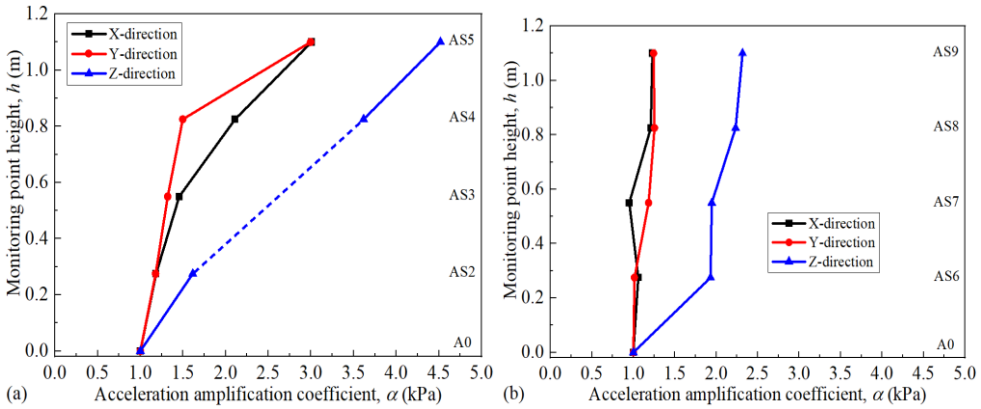


Fig. 4. Acceleration responses of the natural lake sand sites under Chi-Chi seismic loads: (a) far-field foundation soil; and (b) near-field pile foundation soil

These results indicate that under the Chi-Chi seismic loads, there is a significant difference in the acceleration amplification effects between the near-field pile foundation soil and the far-field foundation soil, demonstrating the substantial regulatory effect of pile-rafted foundations on the seismic response of sandy sites.

Acceleration Response Behaviours of Upper Nuclear Island Building Model

Figure 5 illustrates the variation of peak acceleration amplification factors with sensor height for the external plant component, internal steel containment vessel component, and nuclear equipment component inside the vessel of upper nuclear island building model under the Chi-Chi seismic load. Using the bottom of the pile cap as the elevation reference plane (elevation = 0), the analysis results are as follows:

(i) External plant component (Fig. 5a). The Y-direction acceleration amplification effect was the most significant, followed by the X-direction, while the Z-direction showed almost no amplification. The top-to-base amplification factors were 2.57 (Y-direction), 2.21 (X-direction), and 1.01 (Z-direction).

(ii) Internal steel containment vessel component (Fig. 5b). Due to the influence of the top sand-filled weight, the X-direction acceleration showed slight amplification, while the Y and Z-direction accelerations decreased, particularly with a significant reduction in the Z-direction. The top-to-base amplification factors were 1.46 (X-direction), 0.42 (Y-direction), and 0.63 (Z-direction).

(iii) Nuclear equipment component inside the vessel (Fig. 5c). The X-direction acceleration amplification effect was the most significant, followed by the Y-direction, while the Z-direction showed almost no variation with height. The top-to-base amplification factors were 2.45 (X-direction), 1.71 (Y-direction), and 1.01 (Z-direction).

 © Deep Foundations Institute 2026

Through comparison, it was found that the horizontal (X/Y) acceleration amplification effect was most significant in the external plant component, followed by the nuclear equipment component inside the vessel, while the vessel component exhibited the least amplification. The decrease in Z-direction acceleration with increasing height may be related to the sand-filled weight at the top of the vessel.

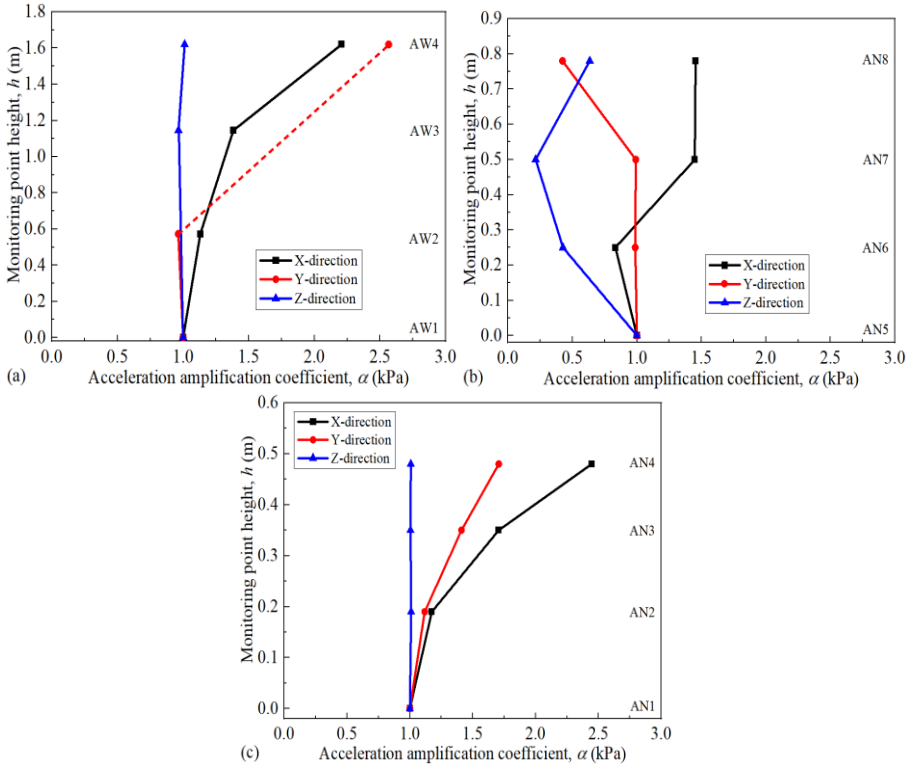


Fig. 5. Seismic acceleration responses of the nuclear island building model under Chi-Chi seismic loads: (a) external plant component; (b) internal steel containment vessel component; and (c) nuclear equipment component inside the vessel

Seismic Response Spectrum Analysis of Pile Supported SMR

According to the literature [26-30], plotting seismic response results as tripartite response spectra—including displacement (Sd), pseudo-velocity (PSv) and pseudo-acceleration (PSa) spectra—is beneficial for seismic performance evaluation. Figure 6 shows the X-direction tripartite response spectra for typical measurement points (A0, AS9, AS5, AN4, AN8, and AW4) of the pile-rafted SMR test model under the Chi-Chi seismic loads. The analysis reveals the following:

(i) Full-period band characteristics. As the structural damping ratio increases, the response spectrum amplitudes generally decrease. The structural period can be divided into three segments, i.e., short (acceleration-sensitive region, ASR), medium (velocity-sensitive region, VSR), and long (displacement-sensitive region, DSR), with boundary periods of $T_1 = 0.055$ s and $T_2 = 1.230$ s.

(ii) Lower lake sand sites. The response spectrum of the near-field pile foundation soil surface measurement point AS9 was consistent with the table output response spectrum, indicating that the combined effect of the pile-rafted foundation and the superstructure did not significantly alter the near-field region response spectrum (Fig. 6b). The response spectrum of the far-field foundation soil surface measurement point AS5 showed a significant increase in the ASR segment, stabilized in the VSR segment, and gradually decreased in the DSR segment (Fig. 6c). This suggests that the pile-rafted foundations and superstructures filtered high-frequency components of the upward seismic loads.

(iii) Upper nuclear island building model. The response spectra of the external plant component (AW4), internal steel containment vessel component (AN8), and nuclear equipment component inside the vessel (AN4) showed significantly reduced amplification effects in the ASR segment, stabilized in the VSR segment, and gradually decreased in the DSR segment (Fig. 6d-f). The

 © Deep Foundations Institute 2026

higher-order periods of nuclear equipment component fell within the ASR segment, resulting in localized acceleration sensitivity, while the external plant component and internal steel containment vessel component exhibited displacement sensitivity in the DSR segment.

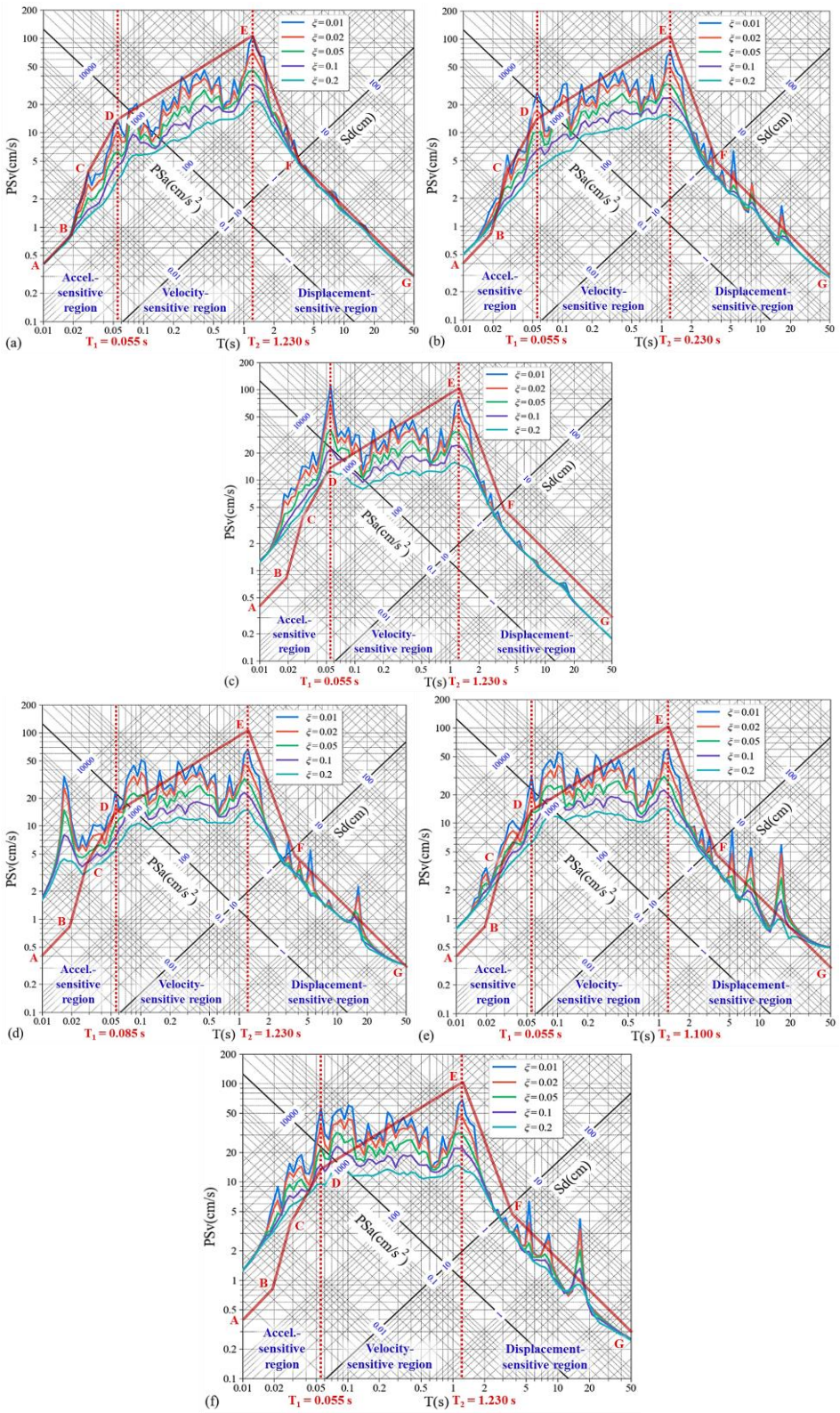


Fig. 6. X-direction tripartite response spectra for typical measurement points of the pile-rafted SMR test model under Chi-Chi seismic loads: (a) A0; (b) AS9; (c) AS5; (d) AN4; (e) AN8; and (f) AW4

 © Deep Foundations Institute 2026

In summary, non-rock lake sand sites weaken the displacement and velocity sensitivity of nuclear reactor seismic responses but enhance acceleration sensitivity. However, pile-rafted foundations effectively filter high-frequency components of upward seismic loads, mitigating the adverse effects of acceleration sensitivity. These new findings provide important technical supports for the seismic design of pile-supported SMR structures in non-rock sites.

CONCLUSIONS

This paper systematically summarizes the latest research advancements in the modular design of generation III NPP and preliminarily evaluates the seismic performance of the sandy sites – pile-rafted foundations – SMR structures system based on large-scale shaking table tests. SCS structures exhibit excellent mechanical and seismic performance under both static and seismic loads. Specifically, under a 0.3g safe shutdown earthquake (SSE) level, the steel plates remain elastic, and concrete cracking does not lead to structural failure. Shaking table tests reveal that pile-rafted foundations significantly enhance the seismic response of sand soil sites. Under seismic loading, the acceleration amplification effect in the near-field region of the pile foundation soil is much smaller than that in the far-field foundation soil, indicating that pile-rafted foundations effectively filter high-frequency components of upward seismic loads. This reduces the acceleration sensitivity of the seismic response, thereby improving the overall seismic performance of the structure. The nuclear island building model exhibits differentiated acceleration amplification effects for different components. The horizontal (X/Y) acceleration amplification effect is most pronounced in the external plant component, while the internal steel containment vessel component shows weaker amplification due to the influence of the top weight, with a noticeable reduction in the vertical (Z) direction. Seismic response spectrum analysis further demonstrates that the combined action of the pile-rafted foundations and the superstructures significantly alters the frequency characteristics of the seismic response, validating the critical role of pile foundations in enhancing the seismic performance of SMR structures.

The new findings of this study provide important theoretical and technical support for the modular design as well as seismic performance evaluation and optimization of NPP. They hold significant implications for advancing the safety and efficiency of NPP construction.

ACKNOWLEDGEMENTS

The authors would like to gratefully acknowledge the support from the Scientific Research Program of Shanghai Nuclear Engineering Research & Design Institute Co. Ltd. (SNERDI), National Natural Science Foundation of China (Grant Nos. 52378328 and 52178317), Postgraduate Research and Practice Innovation Program of Jiangsu Province (Grant No. KYCX22_0217), and the National Construction of High-level University Public Graduate Project (Grant No. CSC202206090133).

REFERENCES

[1] McKinley, B., and Boswell, L. F. (2002). “Behaviour of double skin composite construction.” *Journal of Constructional Steel Research*, 58(10), 1347-1359.

[2] Liew, J. Y. R., and Sohel, K. M. A. (2010). “Structural performance of steel-concrete-steel sandwich composite structures.” *Advances in Structural Engineering*, 13(3), 453-470.

[3] Sohel, K. M. A., Liew, J. Y. R., Yan, J. B., Zhang, M. H., and Chia, K. S. (2012). “Behavior of steel-concrete-steel sandwich structures with lightweight cement composite and novel shear connectors.” *Composite Structures*, 94(12), 3500-3509.

[4] Roberts, T. M., Edwards, D. N., and Narayanan, R. (1996). “Testing and analysis of steel-concrete-steel sandwich beams.” *Journal of Constructional Steel Research*, 38(3), 257-279.

[5] Tang, R. Y., Sun, Y. L., Wang, Y. G., Ding, R., Fan, J. S., and Nie, J. G. (2024). “Finite element analysis of single steel-plate concrete composite containment of nuclear power plant under commercial aircraft impact.” *Engineering Structures*, 321, 118998.

[6] Lin, Y. Z., Yan, J. C., Cao, Z. G., Zeng, X. Z., Fan, F., and Zou, C. Y. (2018). “Ultimate strength behaviour of S-UHPC-S and SCS sandwich beams under shear loads.” *Journal of Constructional Steel Research*, 149, 195-206.

 © Deep Foundations Institute 2026

[7] Leng, Y. B., Song, X. B., Chu, M., and Ge, H. H. (2015). "Experimental Study and Theoretical Analysis of Resistance of Steel-Concrete-Steel Sandwich Beams." *Journal of Structural Engineering*, 141(2), 04014113.
[8] Federal Register. (2011). "AP1000 Design Certification Amendment." Accessed date: 30 December 2011.
[9] Ye, Q. Z. (2022). "China's innovative development of nuclear energy." (in Chinese).
[10] Canadian Small Modular Reactor Roadmap Steering Committee. (2018). "A Call to Action: A Canadian Roadmap for Small Modular Reactors." Ottawa, Ontario, Canada.
[11] U.S. Department of Energy. (2017). "Small Modular Reactors: Adding to Resilience at Federal Facilities."
[12] Sui, Y. (2020). "Fine Research on Dynamic Response Characteristics of Nuclear Island Subjected to Beyond Design Basis Loads," Ph.D. dissertation, *Dalian University of Technology*. (in Chinese).
[13] Wang, F. (2021). "Study on the Effect of Non-rock Site on Seismic Behavior of Safety-Related Nuclear Structure," Ph.D. dissertation, *Institute of Geophysics, China Earthquake Administration*. (in Chinese).
[14] Forcellini, D. (2023). "The role of Soil Structure Interaction (SSI) on the risk of pounding between low-rise buildings." *Structures*, 56, 105014.
[15] Yang, Y., Gong, W., Cheng, Y. P., et al. (2021). "Effect of soil-pile-structure interaction on seismic behaviour of nuclear power station via shaking table tests." *Structures*, 33, 2990-3001.
[16] Zou, D., Sui, Y., and Chen, K. (2020). "Plastic damage analysis of pile foundation of nuclear power plants under beyond-design basis earthquake excitation." *Soil Dynamics and Earthquake Engineering*, 136(2), 106179.
[17] Yang, Y., Cheng, Y. P., Gong, W., et al. (2023). "Effect of cushion types on the seismic response of structure with disconnected pile raft foundation." *Structures*, 48, 1333-1345.
[18] Mostafa, Y. E., and Naggar, M. H. E. (2002). "Dynamic analysis of laterally loaded pile groups in sand and clay." *Canadian Geotechnical Journal*, 39(6), 1358-1383.
[19] Yang, J. P., Lu, Z., and Li, P. Z. (2020). "Large-scale shaking table test on tall buildings with viscous dampers considering pile-soil-structure interaction." *Engineering Structures*, 220, 110960.
[20] Yang, Y., Gong, W., Cheng, Y. P., et al. (2021). "Effect of soil-pile-structure interaction on seismic behaviour of nuclear power station via shaking table tests." *Structures*, 33, 2990-3001.
[21] Poulos, H. G. (2001). "Piled raft foundations: design and applications." *Géotechnique*, 51(2), 95-113.
[22] Poulos, H. G., and Davids, A. J. (2005). "Foundation design for the emirates twin towers, Dubai." *Canadian Geotechnical Journal*, 42(3), 716-730.
[23] Clancy, P., and Randolph, M. F. (1993). "An approximate analysis procedure for piled raft foundations." *International Journal for Numerical and Analytical Methods in Geomechanics*, 17(12), 849-869.
[24] Sonoda, R., Matsumoto, T., Kitiyodom, P., et al. (2009). "Case study of a piled raft foundation constructed using a reverse construction method and its post-analysis." *Canadian Geotechnical Journal*, 46(2), 142-159.
[25] Zou, D., Sui, Y., and Chen, K. (2020). "Plastic damage analysis of pile foundation of nuclear power plants under beyond-design basis earthquake excitation." *Soil Dynamics and Earthquake Engineering*, 136(2), 106179.
[26] Velestos, A. S., and Meek, J. W. (1974). "Dynamic behaviour of building foundation systems." *Earthquake Engineering and Structural Dynamics*, 3, 121-138.
[27] Chopra, A. K. (2017). "Dynamics of structures: theory and applications to earthquake engineering." *Pearson Education Limited*.
[28] Rajasekaran, S. (2009). "Structural dynamics of earthquake engineering; theory and application using Mathematica and Matlab." *CRC Press*.
[29] USNRC. (2014). "Regulatory Guide 1.60—Design Response Spectra for Seismic Design of Nuclear Power Plants."
[30] ASCE/SEI 4-16. (2016). "Seismic analysis of safety-related nuclear structures and commentary." *American Society of Civil Engineers*.

ESTIMATION OF INSTALLATION TORQUE AND AXIAL ULTIMATE CAPACITY OF SCREW PILES IN TROPICAL SOILS USING SPT DATA

Diego Gazolli Yanez, Klohn Crippen Berger, Perth, WA, Australia, +61 488 756 153, dgazolli@klohn.com
Daniel Renosto, PierTech Systems, Chesterfield, MO, USA, +1 (385) 424-9415, drenosto@piertech.com

ABSTRACT

This study investigates the relationship between installation torque and axial ultimate capacity (compression and pullout) of screw piles installed in tropical soils, with emphasis on lateritic and residual soil conditions. The work builds upon the semi-empirical torque estimation method proposed by Yanez and Renosto (2019), which combines mechanical torque mobilisation concepts with SPT-based pile-soil resistance correlations commonly used in Brazil. A database comprising fourteen screw piles installed in two tropical soil profiles in Brazil was analysed. Standard Penetration Tests (SPT) were performed at each site, and installation torque was recorded continuously during pile installation. The proposed method was used to estimate installation torque, incorporating correction factors to account for the mechanical behaviour of lateritic soils. Tension load tests were subsequently performed on selected piles to determine ultimate axial capacity, allowing derivation of the torque-capacity correlation factor (K_t). The predicted installation torque showed good agreement with field measurements, and the K_t values derived from load testing were consistent within the analysed dataset. The results indicate that incorporating soil-specific frictional behaviour into torque estimation provides a reliable framework for correlating installation torque and axial capacity of screw piles in tropical soils. The proposed approach supports more informed design decisions regarding pile geometry, installation equipment, and safety margins in tropical environments.

Keywords: screw piles, torque, bearing capacity, tropical soils

INTRODUCTION

Screw piles are an increasingly popular foundation system due to their fast installation and suitability for both compression and tension applications. They consist of a central steel shaft with one or more helices, installed by applying torque at the pile head. Unlike most conventional piles, the installation of screw piles imposes significant torsional stresses on the pile shaft – stresses that are unrelated to the common in-service axial or lateral loads and, more often than not, governing stresses in the pile design.

Although screw piles have been used for centuries, design challenges remain. Traditional helical pile design methods, often based on Terzaghi's bearing capacity theory, can underperform in predicting screw pile behaviour, particularly in tropical soils. Empirical torque-based methods, such as those by Hoyt and Clemence (1989), have proven to be more reliable for capacity estimation (Perko 2009). However, these approaches are often proprietary, with each manufacturer adapting them to tailor specific pile geometries (e.g., round and square-shaft helical piles, spade-shaped and corkscrew pilot points, dual-cutting, octagonal, and square bladed helix with rounded corners). This has resulted in the absence of a universal design framework that incorporates both installation torque prediction and in-service performance.

Tropical soils are predominantly residual soils formed *in situ* under intense chemical weathering conditions, typical of humid tropical climates, and present distinct engineering behaviour related to their mineralogy, soil-water characteristic curves, index properties, classification systems, compaction response, and even biological activity (Camapum de Carvalho and Gitirana Jr. 2021). Within this group, an important distinction exists between lateritic and saprolitic soils, which differ in both genesis and mechanical behaviour. Lateritic soils are highly weathered materials characterised by advanced leaching of silica and enrichment in iron and aluminium oxides, resulting in a distinct pedogenetic structure and relatively high small-strain shear stiffness (Barros and Pinto 1997). In

 © Deep Foundations Institute 2026

contrast, saprolitic soils correspond to less weathered residual profiles derived from the decomposition of the parent rock, commonly preserving its original fabric and mineralogical features (Nogami and Villibor 1981). In this study, the distinction between lateritic and non-lateritic tropical soils is adopted to reflect their markedly different mechanical response during screw pile installation and load transfer mechanisms.

In tropical soils, the empirical torque-capacity relationship can present significant scatter, especially in lateritic soils, where installation torque may be disproportionately high compared to ultimate pile resistance. This can lead to underestimation of structural demands during installation and, in some cases, to premature shaft yielding if unaccounted for.

The present study applies and expands the semi-empirical torque prediction method developed by Yanez and Renosto (2019), originally validated in lateritic soils, to a broader database including non-lateritic tropical soils. Furthermore, the method is extended to estimate ultimate load capacity from torque, with adjustments to account for the higher shear modulus of lateritic materials.

The present study applies and extends the semi-empirical installation torque estimation method proposed by Yanez and Renosto (2019) to a broader dataset of screw piles installed in tropical soils. A range of piles installed in lateritic and residual soil profiles in Brazil are analysed using Standard Penetration Test (SPT) data and monitored installation torque. The method is employed to estimate installation torque while accounting for soil-specific frictional behaviour, and the resulting torque measurements are subsequently used to derive torque-capacity correlation factors from axial tension load test results. This approach allows assessment of the consistency and applicability of the torque-based framework for predicting the axial performance of screw piles in tropical soil conditions.

BACKGROUND OF TORQUE ESTIMATION ON LATERITIC SOILS

Proposed Methodology

The torque estimation approach combines a mechanical representation of torque mobilisation with semi-empirical pile capacity correlations widely used in Brazil. The force applied by the hydraulic motor at the top of the helical pile induces rotation of the pile within the ground, generating frictional resistance along the central tubular shaft and the helices. Consequently, the torque theoretically mobilized during pile installation is given by the product of the frictional shear stress acting over the pile-soil contact area and the radial distance between the pile axis and the contact surface (i.e., the lever arm).

As illustrated in Fig. 1, the contact area of the central shaft (shown in green) multiplied by the moment arm d_s results in the contribution to the reaction torque generated along the central tubular shaft. Likewise, the summation of the products of the contact areas of the helices (shown in red) multiplied by their respective moment arms, $d_{h(i)}$, represents the contribution to the reaction torque generated by the helices of the helical pile. It is assumed that the entire length of the central tubular shaft below the ground surface is in contact with the soil. In other words, any reduction in the frictional contact area in the region where the helices are welded to the central shaft was neglected. Figure 1 also shows that the soil-helix contact area was assumed to be equal to twice the projected area of the helix (corresponding to the upper and lower surfaces of the helix). Equations [1] and [2] define the geometry of the moment arms of the central shaft and the helices as functions of the helical pile geometry, whereas Equations [3] and [4] present the corresponding soil-pile contact areas of these components. The subscript "*s*" refers to the central shaft, and the subscript "*h*" refers to the helices.

$$d_s = r_s \quad [1]$$

$$d_h = \frac{r_s + r_{h,i}}{2} \quad [2]$$

$$A_s = 2\pi L_s r_s \quad [3]$$

$$A_h = 2\pi\left(r_{h,i}^2 - r_s^2\right) \quad [4]$$

Figure 1 indicates the geometrical parameters, where L_s = embedded shaft length, r_s = shaft radius, $r_{h,i}$ = i-helix radius, and f_u = maximum unit shaft resistance as per Cambefort's first law, shown in Fig. 2 (Massad 1995).

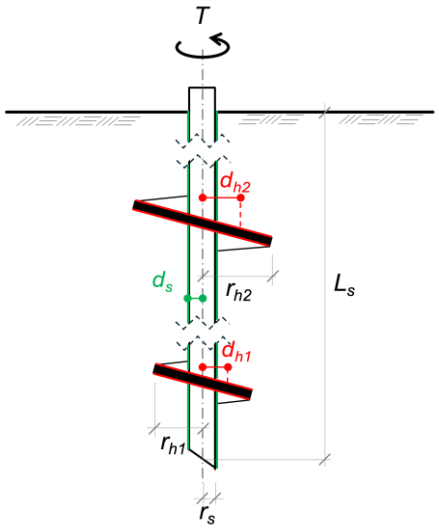


Fig. 1. Schematic illustration (not to scale) of a screw pile indicating the variables used in the analysis

Following Yanez and Renosto (2019), the torque generated by the shaft and each of the i helices is given by:

$$T_s = 2\pi L_s r_s^2 f_u \quad [5]$$

$$T_{h,i} = \pi\left(r_{h,i} + r_s\right)^2\left(r_{h,i} - r_s\right)f_u \quad [6]$$

It is worth noting that Equation [4] was published with the parameters $r_{h,i}$ and r_s inverted in the second term in Yanez and Renosto (2019). Next, it is necessary to define the soil-pile friction to be adopted. As a rule, the load-transfer functions of the soil profile would need to be known in order to perform the calculations. The Cambefort hypotheses are applied to represent these functions. During the rotation of the helical pile in the ground, it is assumed that the displacement of the pile shaft is sufficiently large to reach and maintain the maximum plateau shown in Fig. 2a. Accordingly, Equations [5] and [6] define the theoretical torque mobilized by the central shaft (T_s) and by the helices ($T_{h,i}$), respectively, as functions of the maximum unit lateral friction f_u from the first Cambefort law.

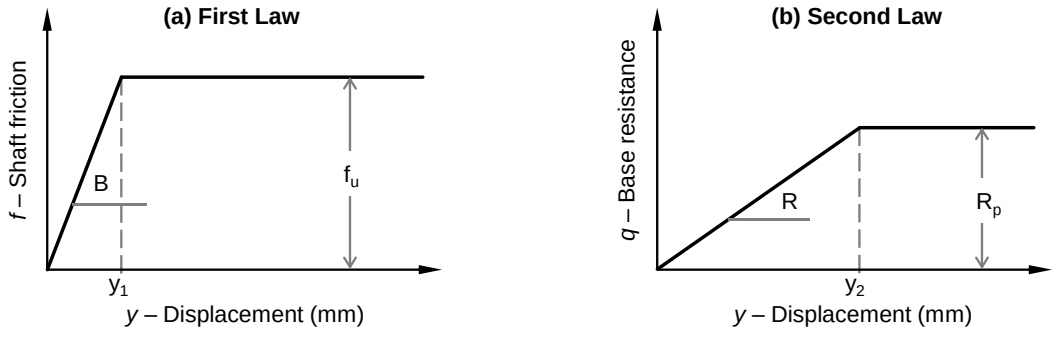


Fig. 2. Cambefort hypothesis (Massad 1995)

 © Deep Foundations Institute 2026

The Cambefort hypotheses, or laws, represent the behaviour of shaft–soil friction, or load transfer function, for a single vertical pile under axial loading. Figure 2 presents the simplified first and second laws of Cambefort (Cassan 1978, as cited in Massad 1995). The case of an isolated vertical pile subjected to axial loading can be treated using Cambefort's relationships for unit shaft resistance (f) and end-bearing resistance (q). From Fig. 2, it follows that $f = B.y$ (for $y \leq y_1$) and $f = B.y_1$ (for $y \geq y_1$) while $q = R.y$ (for $y \leq y_2$) and $q = R.y_2$ (for $y \geq y_2$).

The maximum unit shaft resistance mobilised between the screw pile and the surrounding soil is estimated from SPT data using the Brazilian semi-empirical method for single pile capacity proposed by Décourt and Quaresma (1978). The method was originally calibrated for a local SPT energy efficiency of 72% (N_{72}) and developed for precast concrete piles, and was later expanded to bored and injected pile systems of various construction methods. It is postulated that the ultimate end-bearing stress is dependent on the soil type through the coefficient K (Equation [7] and Table 1), while pile-soil adhesion is considered independent of soil type and can be determined using Equation [8] below, expressed in kPa.

$$q_p = K \cdot N_{72} \quad [7]$$

$$q_s = 10 \cdot \left(\frac{N_{72}}{3} + 1\right) \ [kPa] \quad [8]$$

Table 1. Coefficient *K* according to Décourt and Quaresma (1978)

Soil	K (kPa)
Clays	120
Clayey silts	200
Sandy silts	250
Sands	400

Lateritic Soil Characteristics

Barros and Pinto (1997) analysed the small-strain shear modulus G_0 of lateritic and saprolitic tropical soils by comparing results obtained from cross-hole testing with the N_{SPT} values from standard penetration tests (72% efficiency). Data from ten regions with lateritic and saprolitic tropical soils in the state of São Paulo, Brazil, previously published in the literature, were evaluated and compared with correlations for soils from temperate climate zones. Significant discrepancies were observed for both lateritic and saprolitic soils. According to the authors, these discrepancies are associated with the presence of cemented structure in lateritic soils, which can be broken during sampler penetration, and the high heterogeneity of saprolitic soils.

Figure 3 presents the data obtained for the tropical soils analysed. The difference between the correlations for lateritic and saprolitic soils is 3.3 times. Of particular relevance to the present study, Barros and Pinto (1997) concluded that lateritic and saprolitic soils exhibit markedly different dynamic properties, which cannot be predicted using correlations developed for temperate climate soils; and that lateritic and saprolitic soils represent distinct domains in terms of the relationship between small-strain shear modulus G_0 and N_{SPT}. In relative terms, saprolitic soils exhibit behaviour closer to that of temperate climate soils. Nevertheless, the linear correlation coefficient for saprolitic soils is 2.7 times smaller than the corresponding coefficient for temperate climate soils. The magnitude of this difference provides justification for the correction factors adopted in the present study.

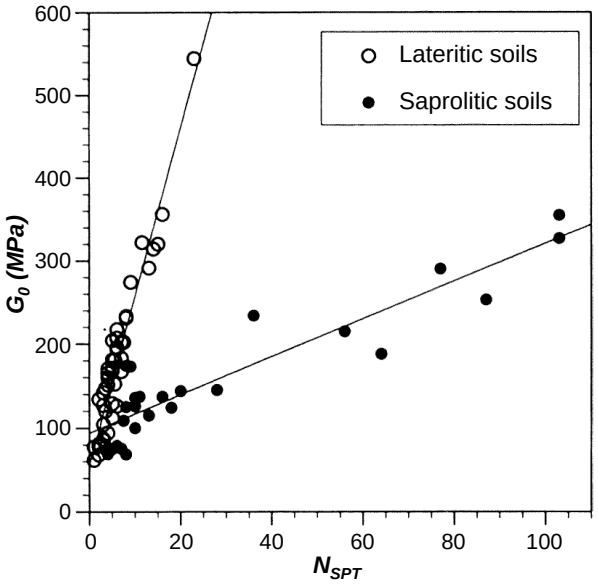


Fig. 3. Small-strain shear modulus G_0 of lateritic and saprolitic soils, highlighting the higher stiffness typically observed in lateritic materials (Barros and Pinto 1997)

The method used in this study, first published by Yanez and Renosto (2019), evaluated seven screw piles installed in Ribeirão Pires, São Paulo, at a screw pile testing site where standard penetration tests (SPT) were carried out and Miniature Compacted Tropical (MCT) tests, as proposed by Nogami and Villibor (1981), were performed to classify the local lateritic tropical soils.

Assumptions and Parameters

The pile-soil shaft resistance used in the calculation of the torque mobilised during screw pile installation is approximated by the first law of Cambefort, with the unit shaft resistance calculated using the method of Décourt and Quaresma (1978). As discussed, it is assumed that the displacement of the pile shaft during pile rotation in the ground is sufficiently large to reach and maintain the maximum plateau shown in Fig. 2a.

Equation [10] provides the pile-soil adhesion from the Décourt and Quaresma (1978) method given by Equation [8], linearly corrected to the standardised N_{SPT} value referenced to 60% potential energy of the SPT hammer, as suggested by Seed et al. (1985) and Skempton (1986), shown in Equation [9].

$$N_1 \cdot E_1 = N_2 \cdot E_2 \;\therefore\; N_{72} = N_{60} \cdot \frac{60\%}{72\%} \quad [9]$$

$$q_s = (2.77N_{60}) + 10\ [kPa] \quad [10]$$

For the purposes of this study, end-bearing resistance during pile installation was disregarded during the installation torque estimation; however, the authors acknowledge that this component can be significant if the installation crew applies excessive pull-down force with the installation equipment, meaning that the pile is actively pressed into the ground using the hydraulic system – an installation condition generally considered undesirable practice. Variations in screw pile geometry at the connections, such as bolts or shaft section enlargements, were also disregarded.

Helical piles' ultimate tension capacities were calculated from load tests results using Chin (1970), Décourt (1996; 2008), Van der Veen (1953), and Aoki (1976) extrapolation methods, summarised in Table 2, where P = any applied load, δ = the movement associated with load P and, P_u = pile ultimate capacity.

Table 2. Summary of pile load movement curve extrapolation applied methods

Method	Load-movement function	Parameters
Chin (1970)	$P = \frac{\delta}{C_1\delta + C_2}$	C_1 = slope of the straight line in the δ/Q versus movement diagram C_2 = y-intercept of the straight line in the δ/Q versus movement diagram
Décourt (1996; 2008)	$P = \frac{C_2\delta}{1 - C_1\delta}$	C_1 = slope of the straight line in the Q/δ versus movement diagram C_2 = y-intercept of the straight line in the Q/δ versus movement diagram
Van der Veen (1953)	$P = P_u(1 - e^{-C_1\delta})$	C_1 = slope of the straight line in the $-ln(Pu/P)$ versus movement diagram, $P = 0$, $\delta = 0$ included
Aoki (1976)	$P = P_u(1 - e^{-(C_1\delta + C_2)})$	$1/C_1$ = slope of the straight line in the $-ln(Pu/P)$ versus movement diagram, $P = 0$, $\delta = 0$ excluded C_2 = y-intercept of the straight line in the $-ln(Pu/P)$ versus movement diagram, $P = 0$, $\delta = 0$ excluded

Following the estimation and measurement of installation torque, the ultimate axial capacity of the screw piles was evaluated using the empirical torque-capacity relationship proposed by Hoyt and Clemence (1989)

$$P_u = K_t \cdot T \quad [11]$$

Where K_t = torque correlation factor.

CASE STUDY: ASSESSED PILES

The proposed method is based on the analysis of fourteen screw piles: seven installed at a lateritic site in Ribeirão Pires, São Paulo (Yanez and Renosto 2019), and seven screw piles installed at a mixed lateritic/residual soil site in Rio Verde, Goiás. The Rio Verde piles were constructed as part of the foundation system of cable-stayed transmission line towers, where screw piles were used primarily as inclined anchor elements to resist tensile forces. Both sites are shown in Fig. 4.

The seven screw piles tested at Ribeirão Pires (Yanez and Renosto 2019) were installed in a well-characterised lateritic soil profile, supported by SPT soundings and MCT testing confirming lateritic behaviour. Installation torque was monitored at regular depth intervals, and the proposed semi-empirical method, based on the first Cambefort law and Brazilian SPT-based shaft resistance correlations, provided a satisfactory match to the measured torque profiles when a correction factor of 3.3 was applied to account for laterisation effects. The consistency of this response across the Ribeirão Pires dataset provide the baseline against which the additional seven piles from Rio Verde are compared, demonstrating that both datasets exhibit similar trends in torque mobilisation and soil-pile interaction despite differences in site conditions and pile geometry.

In Rio Verde, piles consisted of 101.4 mm diameter and 8.1 mm thickness steel shafts with helices of 10” (0.25 m), 12” (0.3 m), 14” (0.36 m), and 16” (0.41 m) diameter as shown in Fig. 5. SPT N_{72} tests were performed every 1 m in boreholes near each pile location, and installation torque was recorded at 1 m depth intervals. The piles were installed at an inclination of 38° from the vertical, selected to match the geometry of the cable-stayed transmission tower foundations, where inclined anchors are required to efficiently resist tensile loads from the stay cables. The inclination was accounted for in the interpretation of installation depth and torque measurements, as discussed in the Results section. All piles were manufactured from VMB 350 COR steel, with a yield strength f_y = 350 MPa.



Fig. 4. Location of Rio Verde, Goiás and Ribeirão Pires, São Paulo, Brazil, indicating the site of the screw pile field testing programs. The former is situated in the Cerrado region, characterised by lateritic and residual tropical soils

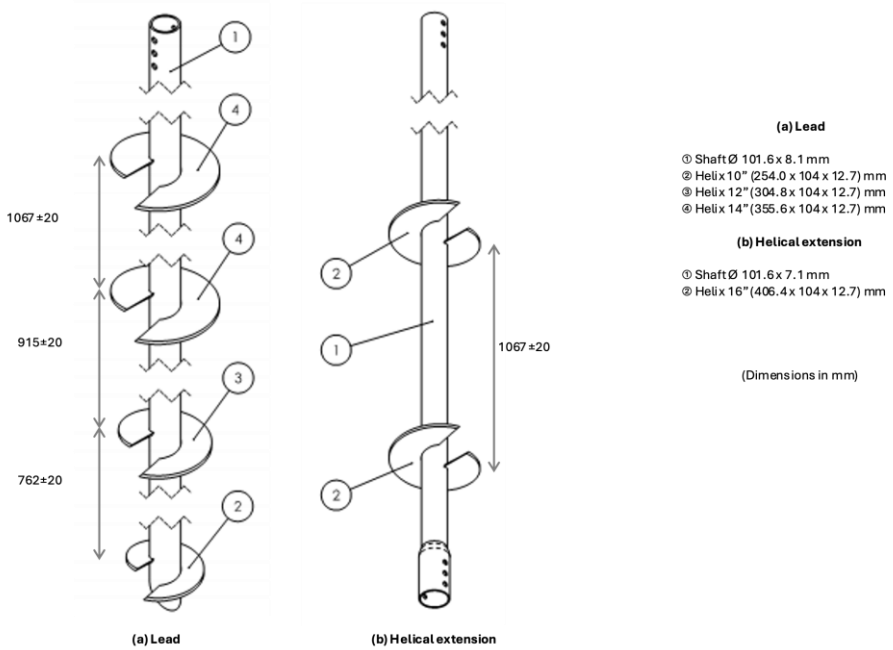


Fig. 5. Helical pile configuration and dimensions

RESULTS

Figures 6-9 present the subsurface profile, the converted N_{60} values, the measured installation torque and estimated torque for each of the piles analysed in this study. The calculations were performed on a metre-by-metre basis by subdividing the embedded shaft length and evaluating the soil-pile friction for each segment using the cited methods. The same discretization was applied at the depths of the installed helices. The soil-pile friction values obtained from the Décourt and Quaresma (1978) method were multiplied by factors ranging from 2.5 to 3.3, reflecting the differences between correlations for lateritic and saprolitic soils, as discussed in Fig. 3. The adopted values per pile are summarized in Table 4. The depth of the torque measurements was corrected for the installation inclination angle of

38°, allowing alignment with the subsurface profile shown in the figures. Groundwater was not observed in any of these locations. It should be noted that the pile inclination adopted in Rio Verde reflects project-specific structural requirements and does not affect the applicability of the proposed torque-capacity framework, which remains valid for both vertical and inclined screw piles provided installation torque is correctly interpreted.



Fig. 6. Location 158/2 soil stratigraphy with corrected N_{60} blow counts, recorded screw pile installation torque, and torque estimated from the proposed method

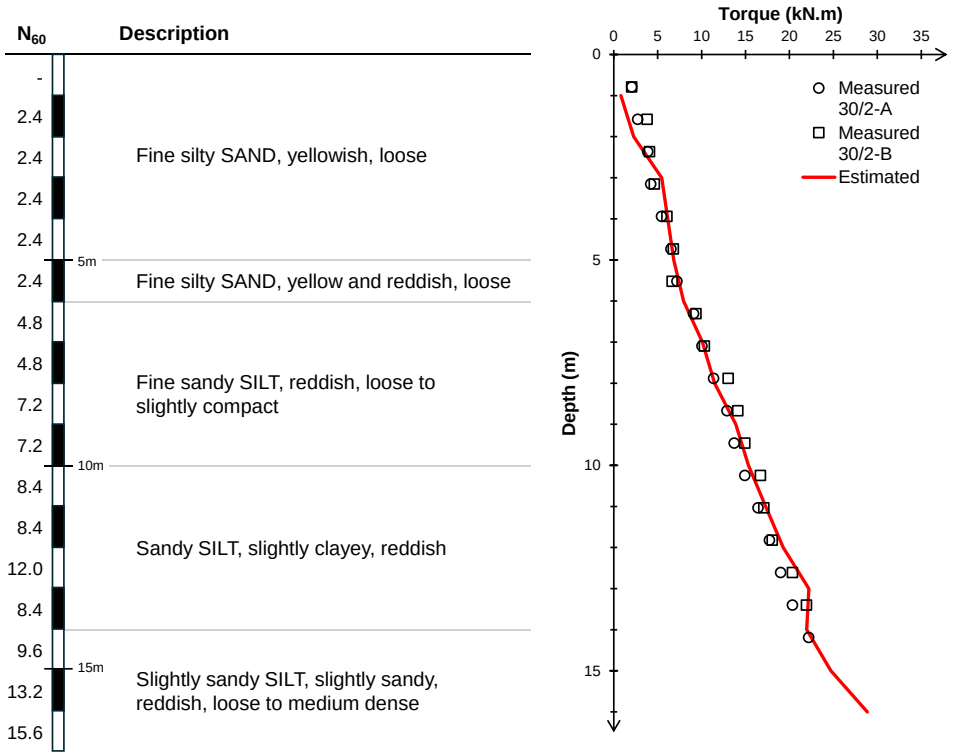


Fig. 7. Location 30/2 soil stratigraphy with corrected N_{60} blow counts, recorded screw piles installation torque, and torque estimated from the proposed method

 © Deep Foundations Institute 2026

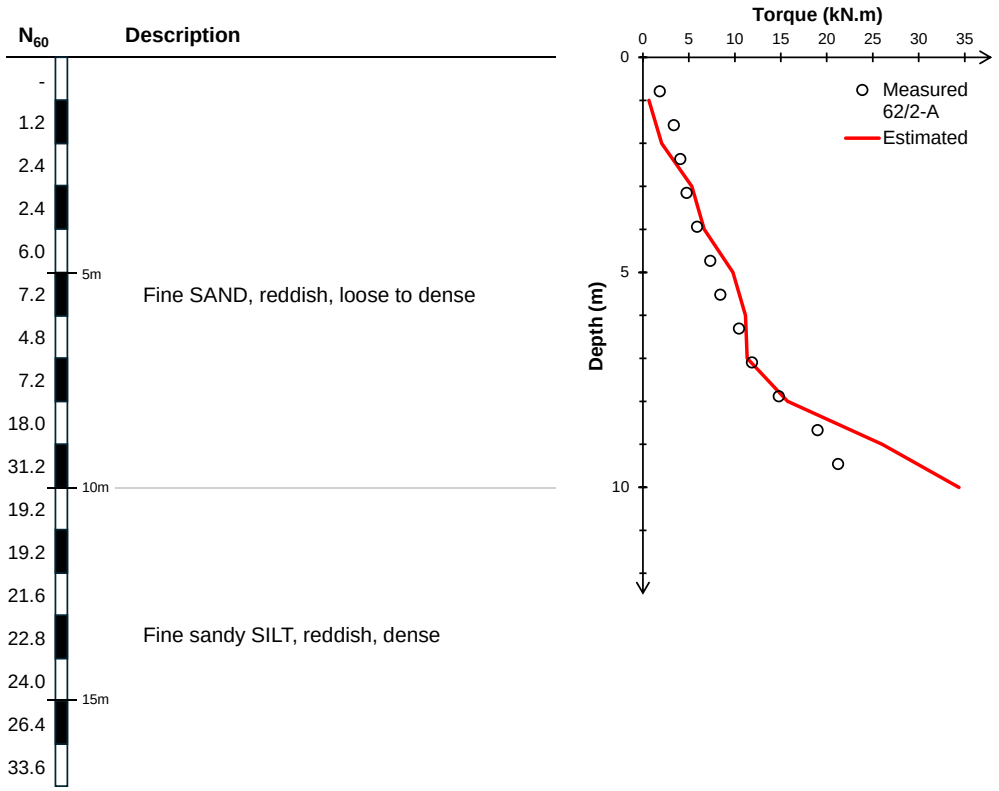


Fig. 8. Location 62/2 soil stratigraphy with corrected N_{60} blow counts, recorded screw pile installation torque, and torque estimated from the proposed method

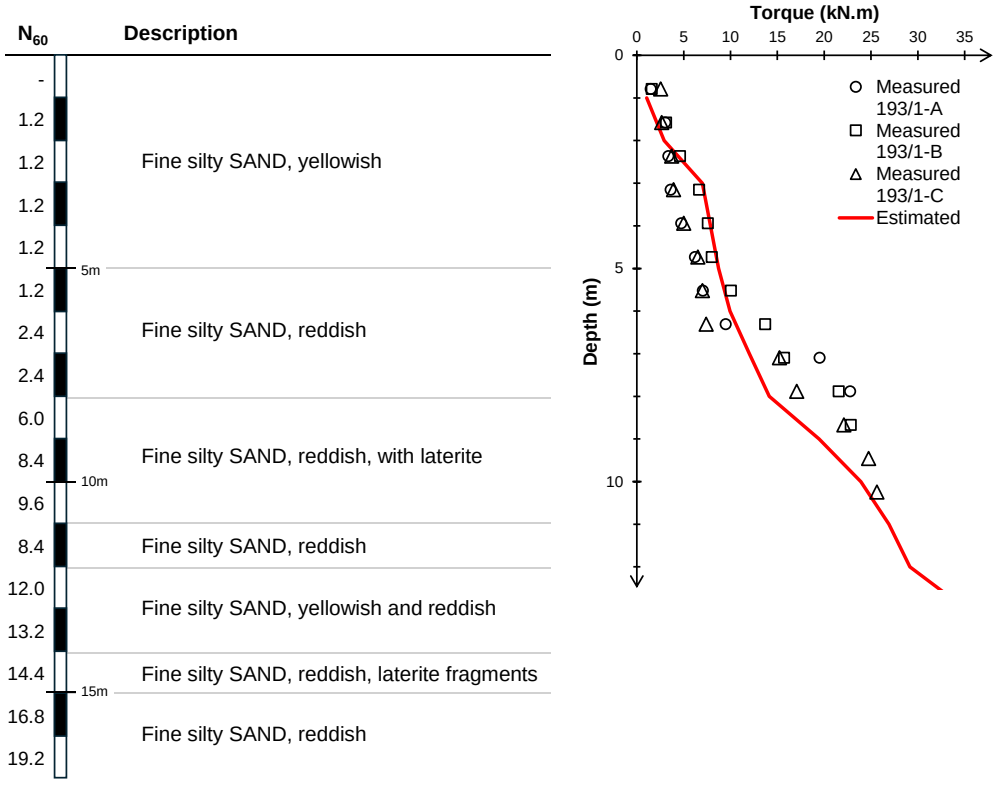


Fig. 9. Location 193/1 soil stratigraphy with corrected N_{60} blow counts, recorded screw piles installation torque, and torque estimated from the proposed method

 © Deep Foundations Institute 2026

Multi-stage tension load tests were performed on selected piles, including load-unload cycles. Ultimate capacities were determined from load tests using the extrapolation methods listed in Table 2 and results presented in Table 3. Table 3 presents extrapolated bearing capacity ranges by minimum, median and maximum, illustrated in Fig. 10.

Table 3. Summary of ultimate capacity analysis results for the screw piles

Location	Extrapolated ultimate bearing capacity (kN)						
	A [1]	B [2]	C [3]	D [4]	Extrapolation Minimum	Extrapolation Median	Extrapolation Maximum
158/2-A	754	742	540	730	540	736	754
30/2-A	594	583	475	520	475	552	594
30/2-B	563	544	475	630	475	554	630
62/2-A	558	543	465	495	465	519	558
193/1-A	562	543	475	530	475	537	562
193/1-B	605	590	495	520	495	555	605
193/1-C	635	619	505	610	505	615	635

Notes
[1] Method A: Chin (1970)
[2] Method B: Décourt (1996; 2008)
[3] Method C: Van der Veen (1953)
[4] Method D: Aoki (1976)

The load-test extrapolated bearing capacity ranges were in turn compared to the measured torque during installation in order to determine the torque correlation factor according to Equation [11]. Given the nature of estimating pile ultimate bearing capacity, the smallest calculated K_t (i.e., 19.7 m^{-1}) was then selected to calculate bearing capacity based on the estimated torque calculated using the proposed method in Equations [1] through [6]. Resulting estimates are presented in Fig. 10 and calculations shown in Table 4.

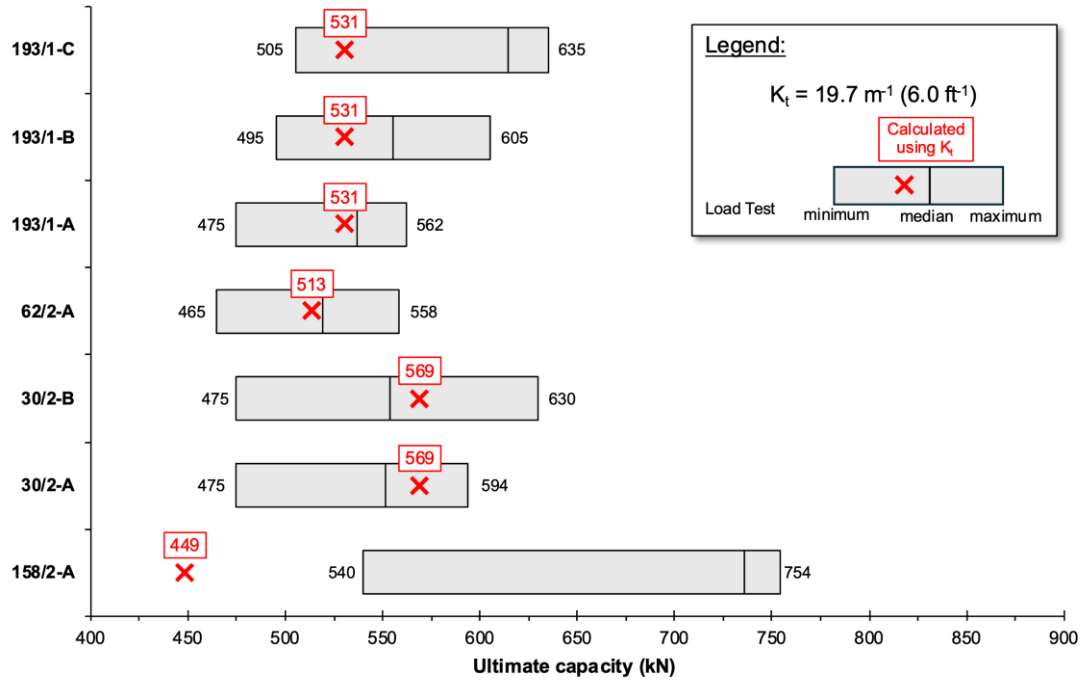


Fig. 10. Helical piles load test extrapolated ultimate capacity results compared to calculated ultimate capacity by the K_t method

 © Deep Foundations Institute 2026

Table 4. Summary of torque correlation factor and estimated bearing capacity for the screw piles

Location	Lateritic factor	Calculated K_t (m^{-1})			Torque (kN.m)		Calculated bearing capacity (kN)
		Minimum	Median	Maximum	Measured during installation	Estimated	
158/2-A	3.3	23.6	32.1	32.9	22.9	22.7	449
30/2-A	2.5	21.4	24.8	26.8	22.2	28.9	569
30/2-B	3.3	21.7	25.3	28.8	21.9	28.9	569
62/2-A	2.5	21.9	24.5	26.3	21.2	26.0	513
193/1-A	2.5	20.8	23.5	24.6	22.8	26.9	531
193/1-B	2.5	21.6	24.2	26.4	22.9	26.9	531
193/1-C	2.5	19.7	24.0	24.8	25.6	26.9	531

The torque estimation method showed good agreement with the observed behaviour of lateritic soils, in which installation torque is predominantly governed by shaft–soil friction mobilised along the pile. These results indicate that installation torque is highly sensitive to soil frictional characteristics, reinforcing the importance of explicitly accounting for soil mechanical behaviour in torque-based analyses. Within this framework, the derived K_t values demonstrate that the torque-capacity relationship remains a practical and consistent tool for assessing the axial performance of screw piles installed in lateritic conditions.

SUMMARY AND CONCLUSIONS

The results presented in this study indicate a strong correlation when using semi-empirical methods based on torque to estimate the load capacity of helical piles for lateritic soils, consistent with previous observations by Hoyt and Clemence (1989) and Perko (2009).

In particular, for tropical soils, it has been observed that the torque mobilised during the installation of helical piles tends to be higher than in saprolitic tropical soils and temperate climate soils. This paper aims to explain these observations in light of the pedogenesis of lateritic soils, characterized by a cemented microstructure, and the prior knowledge from Barros and Pinto (1997) regarding the higher shear modulus of tropical soils with respect to the corrected SPT.

Seven helical piles installed in the city of Rio Verde, Goiás, Brazil, were evaluated in terms of installation torque and ultimate load capacity inferred from tension load tests. These analyses were based on borehole profiles and measured SPT blow count and compared with the installation torque estimated according to Yanez and Renosto (2019). This method utilizes the pile-soil adhesion parameters postulated by Décourt and Quaresma (1978), multiplied by a laterization factor in the order of 3 to estimate the installation torque of a helical pile in tropical lateritic soils.

Furthermore, the measured torque was compared with the ultimate load capacity inferred by four different load test extrapolation methods to analyse the torque correlation coefficient for the assessed piles. A good agreement was observed between the ultimate load capacity and the estimated torque by the derived K_t value of 19.7 m^{-1}.

These findings highlight that, although installation torque is strongly influenced by soil friction, accounting for the soil's mechanical properties allows the K_t method to remain a practical and conservative tool for predicting axial performance of screw piles. Incorporating soil-specific frictional behaviour in design provides guidance for equipment selection, pile geometry, and safety margins, contributing to safer and more efficient screw pile applications in tropical lateritic environments.

ACKNOWLEDGMENTS

The author acknowledges Daniel Canova Renosto for providing the data, and Klohn Crippen Berger for the technical and grammatical review. They also acknowledge the use of ChatGPT for assisting in writing flow improvement.

REFERENCES

Aoki, N., 1976. Considerações sobre a capacidade de carga de estacas isoladas. Universidade Gama Filho, Rio de Janeiro, 44 p.

Barros, J.M.C. and Pinto, C.S., 1997. Estimation of maximum shear modulus of Brazilian tropical soils from Standard Penetration Test. Proceedings of the 14th International Conference on Soil Mechanics and Foundation Engineering, Hamburg, Vol. 1, pp. 29-30.

Camapum de Carvalho, J. and Gitirana Jr., G., 2021. Tropical soils: peculiarities, classification, and engineering behaviour. Soils and Rocks, 44(3):e2021068121.

Chin, F.K., 1970. Estimation of the ultimate load of piles not carried to failure. Proceedings of the Second Southeast Asian Conference on Soil Engineering, Singapore, Southeast Asian Society of Soil Engineering, pp. 81-90.

Décourt, L., 1996. A ruptura de fundações avaliada com base no conceito de rigidez. Proceedings, Seminário de Engenharia de Fundações (SEFE3), São Paulo, ABMS, CD-ROM, 10 p.

Décourt, L. and Quaresma, A.R., 1978. Capacidade de carga de estacas a partir de valores de SPT. Proceedings of the 6th COBRAMSEF, Rio de Janeiro, Vol. 1, pp. 45-53.

Décourt, L., 2008. Loading tests: interpretation and prediction of their results. Proceedings of the Research to Practice in Geotechnical Engineering, New Orleans, ASCE, pp. 452-470. http://dx.doi.org/10.1061/40962(325) 16.

Hoyt, R.M. and Clemence, S.P., 1989. Uplift capacity of helical anchors in soil. Proceedings of the 12th International Conference on Soil Mechanics and Foundation Engineering, Rio de Janeiro, Vol. 2, pp. 1015-1018.

Massad, F., 1995. The Analysis of Piles Considering Soil Stiffness and Residual Stresses. Proceedings of the Panamerican Conference of Soil Mechanics and Foundation Engineering - CPMSEF, 10, 1995, Guadalajara. Guadalajara: Sociedad Mexicana de Ingeniería Geotécnica. pp. 1199-1210.

Nogami, J.S., Villibor, D.F, 1981. Uma nova classificação de solos para finalidades rodoviárias. Proceedings of Simpósio Brasileiro de Solos Tropicais em Engenharia, Rio de Janeiro. Rio de Janeiro: COPPE/UFRJ. Vol. 1, pp. 30-41.

Perko, H.A., 2009. Helical Piles: a practical guide to design and installation. Hoboken, New Jersey: John Wiley & Sons. 512 p.

Seed, H.B., Tokimatsu, K., Harder, L.E and Chung, R., 1985. Influence of SPT procedures in soil liquefaction resistance evaluations. Journal of Geotechnical Engineering, ASCE, 111(12) 1425-1445.

Skempton, A.W. 1986. Standard penetration test procedures and effects in sands of overburden pressure, relative density, particle size, aging and over consolidation. Géotechnique, 36(3) 425-447.

Van der Veen, C., 1953. The bearing capacity of pile. Proceedings of the International Conference on Soil Mechanics and Foundation Engineering, Zürich, pp. 84-90.

Yanez, D.G. and Renosto, D.C., 2019. Análise do torque de instalação de estacas helicoidais a partir do SPT e métodos semi-empíricos de capacidade de carga. Proceedings, Seminário de Engenharia de Fundações (SEFE9), São Paulo.

 © Deep Foundations Institute 2026

SELECTING PARAMETERS FROM IN-SITU TESTS TO DESIGN PASSIVE PILES

Wei Dong Guo, Gold Coast, Australia, 61-0468635677, camsaweidguo@gmail.com

ABSTRACT

Piles used as deep foundations for high-rise buildings are often subject to passive loading due to lateral soil movement (e.g., embankment, tunnelling, deep excavation, landslide, earthquake, etc.). The design of the piled foundations will depend on selecting input parameters, in particular, from model or in-situ tests (with different sliding depths), as any tests conducted on a specified sliding depth can be hard to relate to real- world scenarios.

A 3-layer (theoretical) model (for rigid piles) and BiP (bi-portions of a flexible pile with a hinge) model can well capture the respective response of single piles and pile groups subjected to axial loading and various lateral soil movement profiles using similar sets of parameters. This paper presents a 3-layer analysis of the measured response of seven passive pile tests in five typical scenarios, regardless of the pile flexibility. The tests were conducted on model piles in moving soil with either pre-selected slip depths (surfaces) in two types of soil profiles, or on real-world piles with unknown multi-slip depths (surfaces) in two projects. The analysis provides worked examples of selecting input parameters for the practical design of piles in multiple-slip depths.

Keywords: pile groups, passive loading, slope, landslide, design parameters

INTRODUCTION

Pile foundations designed to support structures and services may be subjected to unexpected or additional loadings during their service lifetime. These loadings can be either temporary or permanent, and often occur due to adjacent construction activities, such as deep excavation, tunnelling operations, or pile driving. The foundations may also be subjected to lateral soil movement caused by sliding slopes, settling embankments, or liquefaction. Thereby, it is important to evaluate the response of piles under such circumstances.

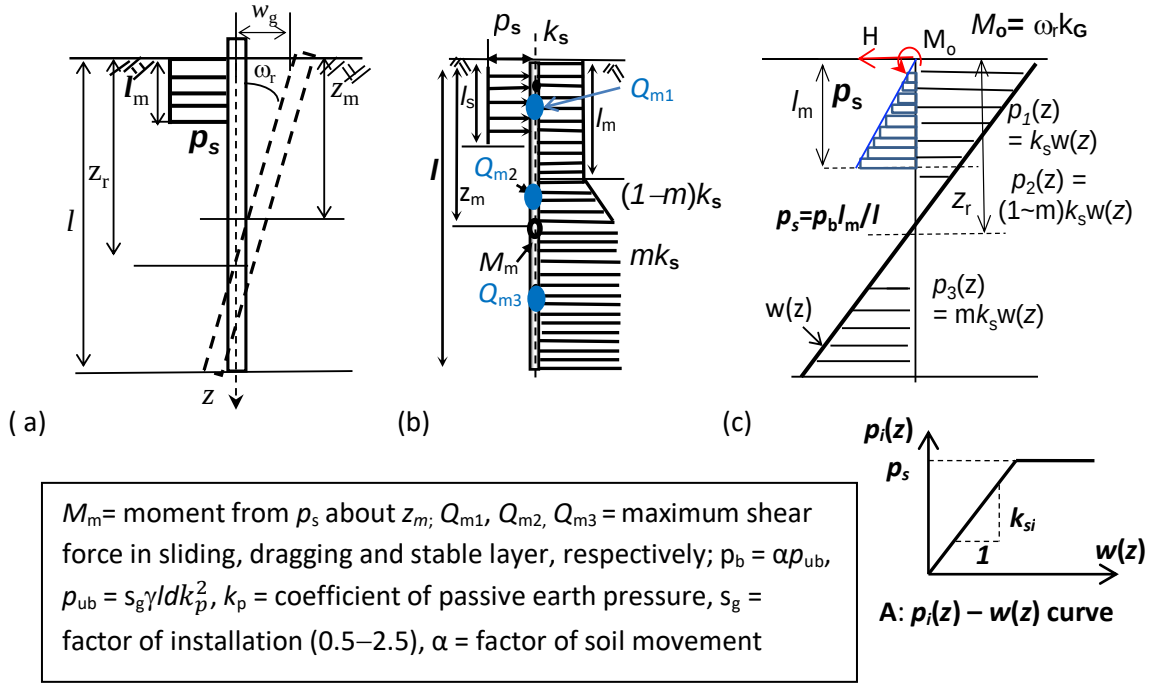
To obtain the pile response, model tests (e.g., Guo and Ghee 2004) were conducted. More recently, a number of model and field tests have been conducted to study the behaviour of piles subjected to lateral soil movements (e.g., Xiang et al., 2013; Wang et al., 2019; Zhou et al., 2019; and Yang et al., 2023). All of the tests included a 'shearing system', a loading system, and a data acquisition system. Given the diversity of loading methods, different profiles of soil movement were imposed on test piles in different sizes of shear 'box'. The pile response was generally measured using strain gauges, LVDTs, and earth pressure cells. The study reveals a deficiency of theoretical simulations for those piles. Guo (2016; 2023) developed a 3-layer model, and with this model, the author conducted simulations of over 30 slope-stabilising piles under diverse situations using a consistent set of 3–4 parameters. The simulation does not require sliding depth(s) to obtain the overall (maximum) pile response at any stage of soil movement. They are presented next for seven instrumented tests on piles, which were subjected to adjacent surcharge (Xiang et al., 2013), moving soil along a fixed slip interface (Wang et al., 2019; Zhou et al., 2019), or landslides (Yang et al., 2023). This study aims to highlight the accuracy of the selected input parameters in predicting the behaviour of real-world slope-stabilising piles.

3-LAYER MODEL AND INPUT PARAMETERS FOR SEVEN PILES

Figure 1 indicates a rotationally restrained, rigid pile (with an embedment length l) that is subjected to a moving layer (of thickness l_m) underlain by a stable, lower layer of thickness l-z_m (z_m= depth of maximum bending moment). Assuming l_m= z_m, the pile-soil system is referred to as a 2-layer model. As with laterally loaded piles, the pile-soil interaction is modelled by a series of springs distributed

 © Deep Foundations Institute 2026

along the pile shaft (Guo 2008). The spring now has a constant modulus of subgrade reaction k_s (= kd, d = pile diameter) for the sliding layer and mk_s for the stable layer, respectively. It exerts a net force per unit length (*FPUL*) p_s (= $k_s w_s$) at a soil movement $w_s > w_s^*$ (= p_s/k_s) over a sliding depth c (= αl_m, α = factor to reflect the soil movement profile) on the pile surface; otherwise, below the sliding depth (with $w_s < w_s^*$), the on-pile *FPUL* $p_i(z)$ is proportional to the local displacement $w(z)$ (see insert A, Fig. 1). Guo (2016) reveals that the moving layer may rotationally restrain free-head piles. This effect is lumped into restraining springs k_G and k_T at the pile-head and tip, respectively (Fig. 1c), and an ultimate *FPUL* value of αp_{ub}. A series of piecewise uniform p_s (= $\alpha p_{ub} l_m/l$, see Fig. 1 for all symbols) over the on-pile 'sliding' depth c produces a linear profile of soil movement w_s. The αp_{ub} value accommodates the impact of soil movement and its profile.



M_m= moment from p_s about z_m; Q_{m1}, Q_{m2}, Q_{m3} = maximum shear force in sliding, dragging and stable layer, respectively; $p_b = \alpha p_{ub}$, $p_{ub} = s_g \gamma l d k_p^2$, k_p = coefficient of passive earth pressure, s_g = factor of installation (0.5–2.5), α = factor of soil movement

Fig. 1. 3-layer model for rigid passive pile: (a) schematic pile-soil system; (b,c) p_s and k_s profile for nonlinear response (Revised from Guo 2016; 2023)

Soil movement incurs rotation of the rigid pile [with $l \geq 2.1(E_p/G_s)^{0.25}$, E_p=Young's modulus of pile body, G_s= shear modulus of soil]. The pile, with a displacement $w(z) = \omega_r z + w_g$ at depth z (below GL) rotates to an angle ω_r, a mudline displacement w_g, about a rotation depth z_r (= $-w_g/\omega_r$). The net on-pile *FPUL* $p(z)$ is given by $p(z) = k_s w(z) - p_s$ in sliding layer (depth of 0~l_m), and $p(z) = mk_s w(z)$ in stable layer, respectively. In practice, piles may have a dragging layer from depth l_m to depth z_m (i.e., a transition layer between the sliding and stable layers), resulting in a 3-layer model (Guo 2016). The transition layer is stipulated to have a linearly increasing modulus from k_s to mk_s (from depth l_m to z_m) (with new depths z_m~l for the stable layer), and the net on-pile *FPUL* $p(z)$ becomes $k_s w(z)[1+(m-1)(z-l_m)/(z_m-l_m)]$.

Closed-form expressions for rotationally restrained piles in the 2-layer and 3-layer models were developed (Guo 2014–16; 2023), and their applications to 'rigid' piles in diverse scenarios have been illustrated. To gain reliable design parameters, the author has recently conducted analyses on the measured response of instrumented slope-stabilising piles at over 20 different sites. This paper presents relevant results (see Table 1) to show the impact of selecting parameters on modelling seven piles subjected to multi-slips, including flexible piles in Sichuan and Qinghai-Tibet projects.

 © Deep Foundations Institute 2026

Table 1. Input parameters for piles in each case

Reference	l_s (m)	*Effective l* (m)	*d* (m)	*EI* (kNm^2)	γ (kN/m^3)	ϕ_s (^{o})	*c* (kPa)
Xiang et al. 2013	4.59	15.3	0.14	3.521	21.0	12	18
Xiang et al. 2013	4.41	12.6	0.14	3.521	21.0	12	18
Zhou et al. 2019	3.3	5.0	0.089	1.28?	16.8	21/34?	15
Wang et al. 2019	3.6	5.5	0.13	1.28	16.8	21/34	5
Yang et al. 2023	30(10)	40(20)	1.95	1.8×10^9	21?	21.8/23	
Ghee 2009	0.2	0.7	0.032	1.28	16.5	0	10

In-Situ Piles Subject to Two Sliding Depths

Xiang et al. (2019) conducted loading tests (see Fig. 2) in the Hongshitan ancient landslide zone, Sichuan Province. The sliding mass primarily consists of low-liquid-limit clay and blocky soil with a thickness of 8–20 m, which is underlain by interbedded sandstone and mudstone of the Mesozoic Cretaceous System. Micro steel pipe pile groups were installed to reinforce the subgrade excavation. The steel pipe piles have a *length ($l>l_c$ of 0.89 m), an* O.D. (outside diameter) *d* of 0.14 m, a wall thickness *t* of 4.5 mm and a *bending stiffness (EI) of* 3.521 kNm^2 (see Table 1). They are arranged in a rectangular pattern. The pile heads were connected together by 0.4 m × 0.4 m reinforced concrete beams. Table 1 provides the soil unit weight γ, angle of internal friction ϕ_s, and cohesion c.

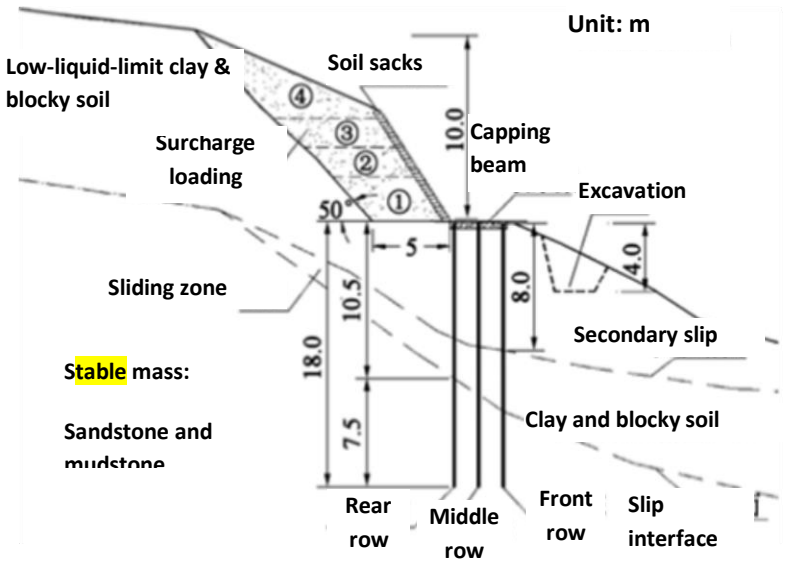


Fig. 2. Piles under surcharge (Xiang et al., 2019)

Three field tests were performed on no-pile case (M_1) and capped pipe piles (M_2, M_3). Five piles were installed in a row at a pile center-to-center spacing of 1.5–1.7 m with 2 rows (test M_2 of 10 piles) or 3 rows (M_3, of 15 piles) at a row-to-row spacing of 1.5–1.6 m. Each group was loaded in a four–stage sequence, followed by an excavation in front of the piles to induce failure. Measured data include pile deformation, soil deformation between piles, pile bending moments, and earth pressures from initial loading to ultimate failure for each test. The slip surface was identified at depths of 4.3 to 4.8 m (M_1), 6.3 to 9.0 m (M_2) and 6.5 to 8.9 m (M_3). *In the 3-layer model predictions for front-row piles, the input parameters (m, k_s, and p_{ub}) are determined (see Table 2). A sliding depth l_s of 4.59 m is adopted to gain the 'maximum' response profiles. As shown in Fig. 3, the measured response profiles are well predicted, with a notable difference between the measured earth pressure and the on-pile pressure without considering the pile flexibility. Given a series of stipulated sliding depths, the predicted maximum bending moment M_m in stable layer, M_{m1} in sliding layer, the maximum shear force Q_m*

(subscripts 1, 2, and 3 for the sliding, transition and stable layer) and pile-head displacement w_g (≈ soil movement) compare well with the measured data (see Fig. 3). The same prediction is presented in Fig. 4 for the rear-row pile. Note that Q_m (≈0.6T_m and 0.33T_m for front-row and rear-row piles) was scaled from the applied sliding thrust T_m, in light of a shadowing effect, which reduces Q_m from the front to the rear row. The predictions of rear-row piles adopt reduced values of l_s, l, and m due to the reduced slip depth compared with the front-row piles. The predictions for both piles are satisfactory.

Table 2. Input parameters for 3-layer model for each case simulation

Reference	ϕ(°)	m	k_s (kPa)	$\frac{p_{ub}}{\gamma l d k_p^2}$	p_{ub} (kN/m)	α (α_p)	
Xiang et al. 2013	$0.9\phi_s$	3.3	360	0.23	64.1	0.72	M_2 (Front)
Xiang et al. 2013	$0.9\phi_s$	2.1	150	0.60	34.7		M_2 (Rear)
Zhou et al. 2019	$0.95\phi_s$	10.9	150	1.15	93.35	0.67(3.)	
Wang et al. 2019	$0.8\phi_{s2}$	7.5	120	0.628	54.8	0.33(3.)	
Yang et al. 2023	$1.1\phi_s$	5.39	60,000	1.75	16,100		
Ghee 2009	0	5.21	2.0	4.5*	1.008	0.67	Row 3*d*
	0	5.21	2.3	4.0*	0.896		Row 5*d*

*p_{ub}/($s_u dl$) ratio for clay, determination of m, k_s, α, and p_{ub} are detailed in Guo (2016; 2023)

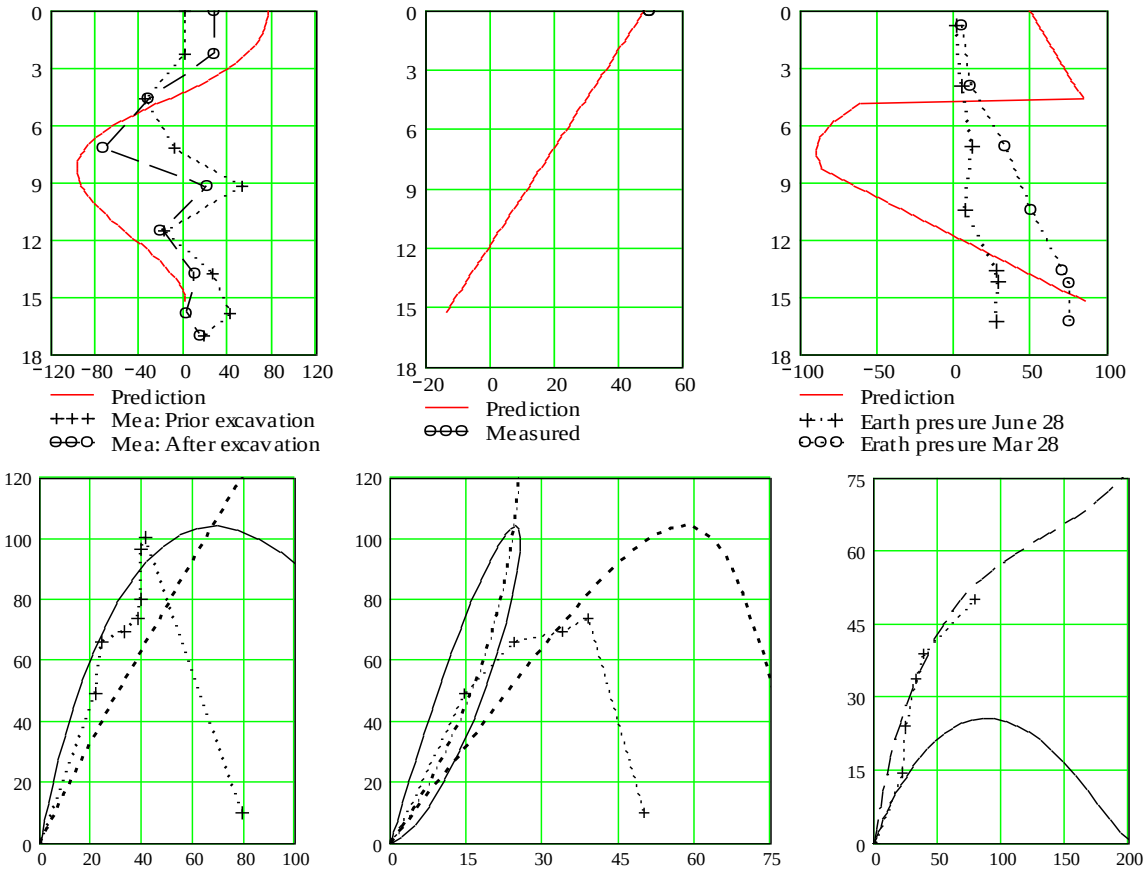


Fig. 3. 3-layer predictions versus measured (Xiang et al., 2019) response of M_2 front-row piles

 © Deep Foundations Institute 2026

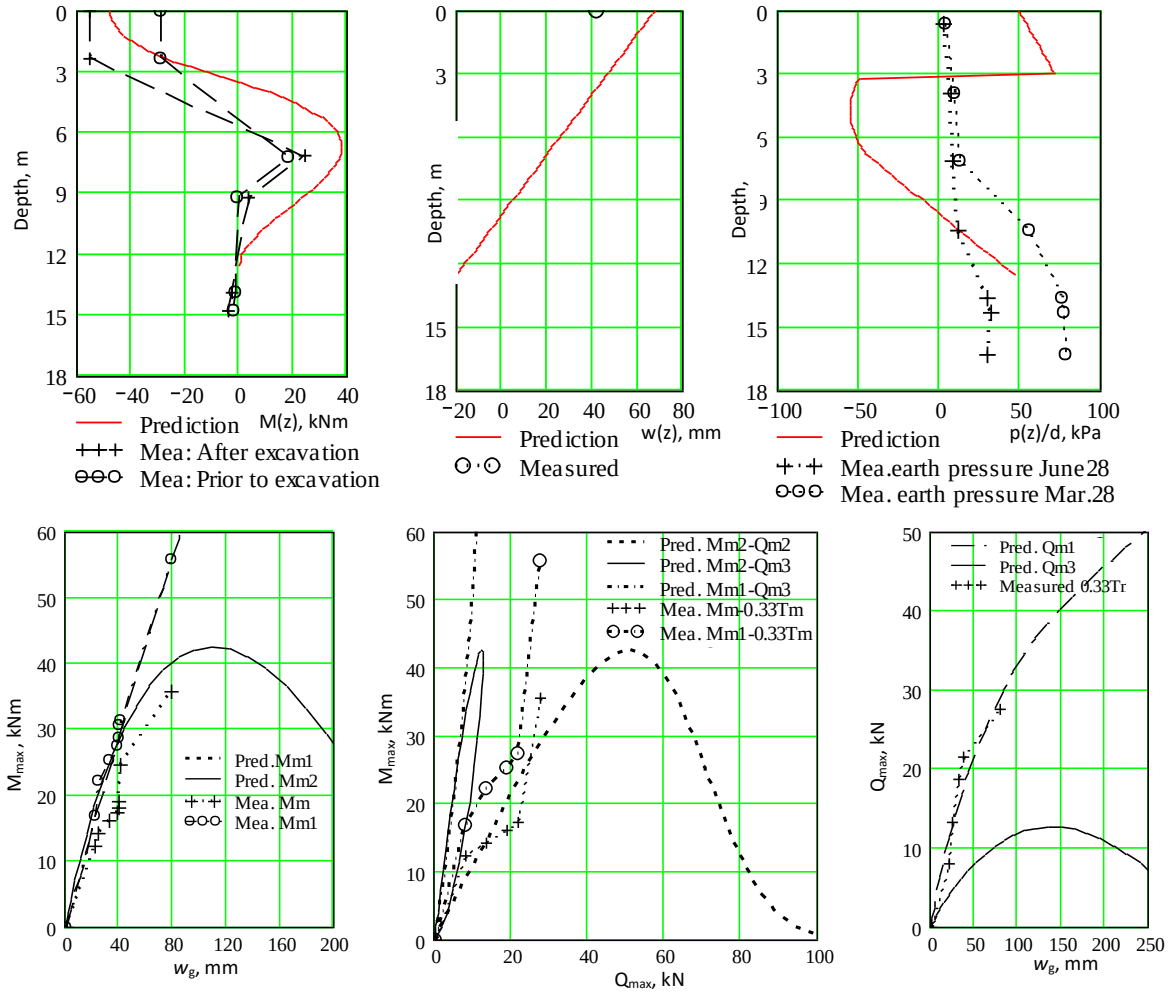


Fig. 4. 3-layer predictions versus measured (Xiang et al., 2019) response of M_2 rear-row piles

Grouting (Semi-Rigid) Micropiles with a 'Fixed' Sliding Depth

Zhou et al. (2019) proposed combining primary low-pressure grouting (pipe-borehole annulus) and multiple-stage high-pressure fracture grouting (within the pipe at weak slip zones) to form a large, root-like grout body around the pipe. This enhances the anti-sliding capacity of a single controlled-grouting steel pipe. Three model tests were conducted in a tank measuring **6.0 m (height, H) × 1.5 m × 6.5 m**, which included reaction walls, sidewalls, and loading plates (Fig. 5). They are samples without **pile,** with **single-pile single-grouting, or single-pile multi-stage grouting.** The steel pipe piles have O.D. = 89 mm, and t = 4.5 mm. **The** slope material has c = 5 kPa and ϕ_s = 34°. A slip surface was formed using saturated soft clay (weathered shale, c =15 kPa, and ϕ_s = 21°) to a thickness of 15–20 cm. The measured Q_m ($\approx 0.06T_m$) (Guo 2012) is scaled from the applied total thrust T_m. The 'measured' w_g ($\approx w_s$-40 mm) is estimated using the measured soil movement w_s (Guo 2023). The soil movement factor α is taken as 0.667, with α_p = 3 for the maximum response profile. *In the 3-layer model predictions for the single piles (*primary grouting*), for example, the input parameters (m, k_s, and p_{ub}) are determined (see Table 2). A sliding depth l_s of 3.3 m is adopted to gain the 'maximum' response profiles. As shown in Fig. 6, the measured response profiles are well predicted, with a slight difference between the measured earth pressure and the on-pile pressure for semi-rigidity of the piles. As with previous examples, the maximum M_m, Q_m, and w_g are well predicted, against the measured data (Fig. 6). A* low M_m is predicted for a given thrust, which is on the safe side. This is owing to neglecting soil resistance along the upper-pile portion, which also incurs a large pile-head deflection if taking $\alpha_p < 3$.

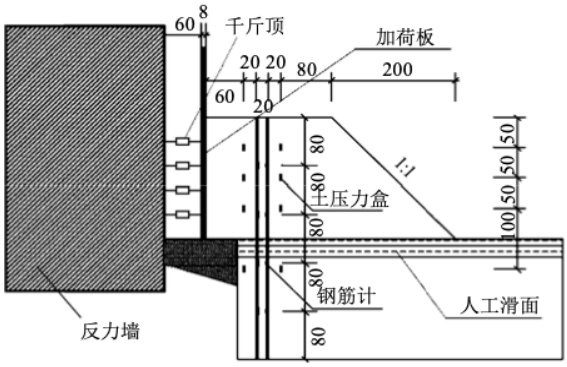


Fig. 5. Model tests (Zhou et al., 2019)

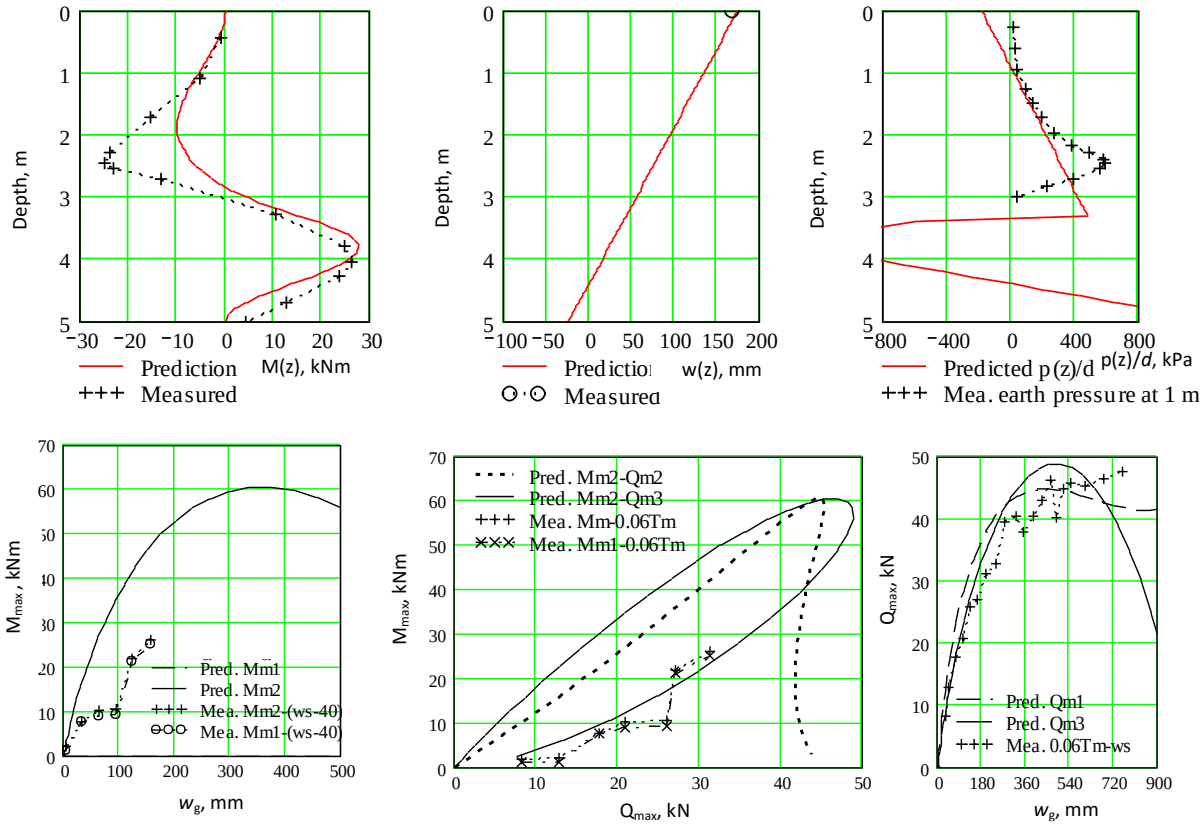


Fig. 6. 3-layer model predictions against measured (Zhou et al., 2019) response

Steel flower-pipe micropiles are integrated with *secondary grouting* (Wang et al., 2019) to enlarge grout bulbs around perforated steel pipes. In a rather similar test setting to Fig. 5, four model tests were conducted using a reinforced concrete tank (6.0 m [H] × 1.5 m × 9.48 m), including a **reaction wall**, **sidewalls** laterally supported by rubble concrete fills, and a steel **loading plate** (3.0 m × 1.45 m × 0.08 m), mounted on rollers, and with hydraulic jacks between the reaction wall and loading plate. The tests included no-pile case, single pile with primary and secondary grouting, and 3 free-head piles in a line (secondary grouting). The **fill** (sand-clay mixture) **material** is characterised by c = 5 kPa and ϕ_s = 34°. A saturated, fully-weathered shale is used to create a 0.2 m-thick a**rtificial slip surface** with c = 15 kPa and ϕ_s = 21°. The pipe pile has an O.D. of 0.89 m and a wall thickness of 4.5 mm (t) with secondary grouting holes. The piles were installed, together with 4LVDTs, 2 inclinometers, 42 earth pressure cells, and 7 pairs of on-pile strain gauges, to gain response of the unreinforced slope, and the piles.

To allow comparison with the previous example, the single pile (primary grouting) is analysed here (note that other piles exhibit a rather similar trend of response to the single pile) with *the input*

parameters (m, k_s, and p_{ub}) (see Table 2). A sliding depth l_s of 3.6 m is adopted to gain the 'maximum' response profiles. As shown in Fig.7, the accuracy of the prediction is similar to that of the last example, in comparison with the measured response profiles, the on-pile pressure, and maximum bending moment M_m, shear force Q_m ($\approx 0.03T_m$) and pile-head displacement w_g ($\approx w_s$-60 mm, at a maximum sliding movement of 160 mm). Again, a low M_m is predicted for a given thrust.

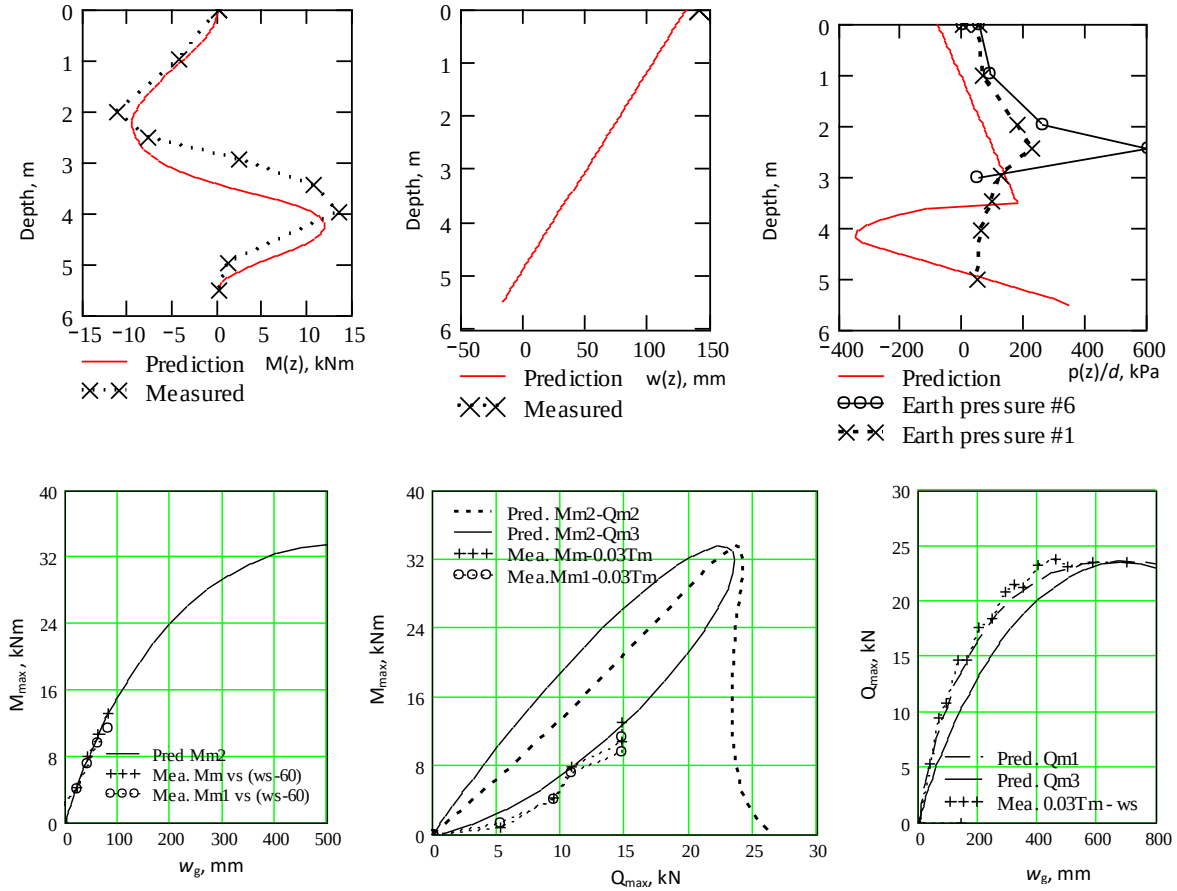


Fig. 7. 3-layer model predictions against measured (Wang et al., 2019) response

Landslide in Qinghai-Tibet Plateau (Hinge at One of Three Sliding Depths)

The Jiangdingya landslide (in Nanyu Township, Zhouqu County) is located on the northeastern margin of the Qinghai-Tibet Plateau, where accumulation landslides occur frequently. The landslide poses significant potential risks (e.g., flooding and debris flows). On July 12, 2018, the Jiangdingya H1 landslide reactivated with a sliding mass (about 4 million m³) extending over an area of 462 m × 210 m and a thickness of about 26.5 m. It consists of loose deposits (of gravelly soil and fragments of grayish-black carbonaceous slate) from the old landslide. The sliding transition layer is relatively dense with high moisture content. It crumbles into low-strength powder or mud when rubbed in dry state and softens readily upon contact with water. The sliding bed consists mainly of highly weathered limestone.

To stabilise the Jiangdingya H1 landslide, 39 **large-diameter (**3.0 m × 4.0 m in cross section**) reinforced piles** were installed to a depth of 40 m (into the sliding bed) at a pile center-to-center spacing of 5.5 m, together with three rows of prestressed anchor cables within concrete frames (at a grid spacing of 4 m × 4 m). Three piles (designated Z_1, Z_2, Z_3) at the landslide front were instrumented to monitor steel bar stress and concrete strain, together with earth pressure on the sliding-face side of the piles. The associated distribution profiles of bending moment $M(z)$ and shear force $Q(z)$ for the Z_2 pile are plotted in Fig. 8. Note that those of pile Z_1, and pile Z_3 exhibit similar response trends to pile Z_2.

 © Deep Foundations Institute 2026

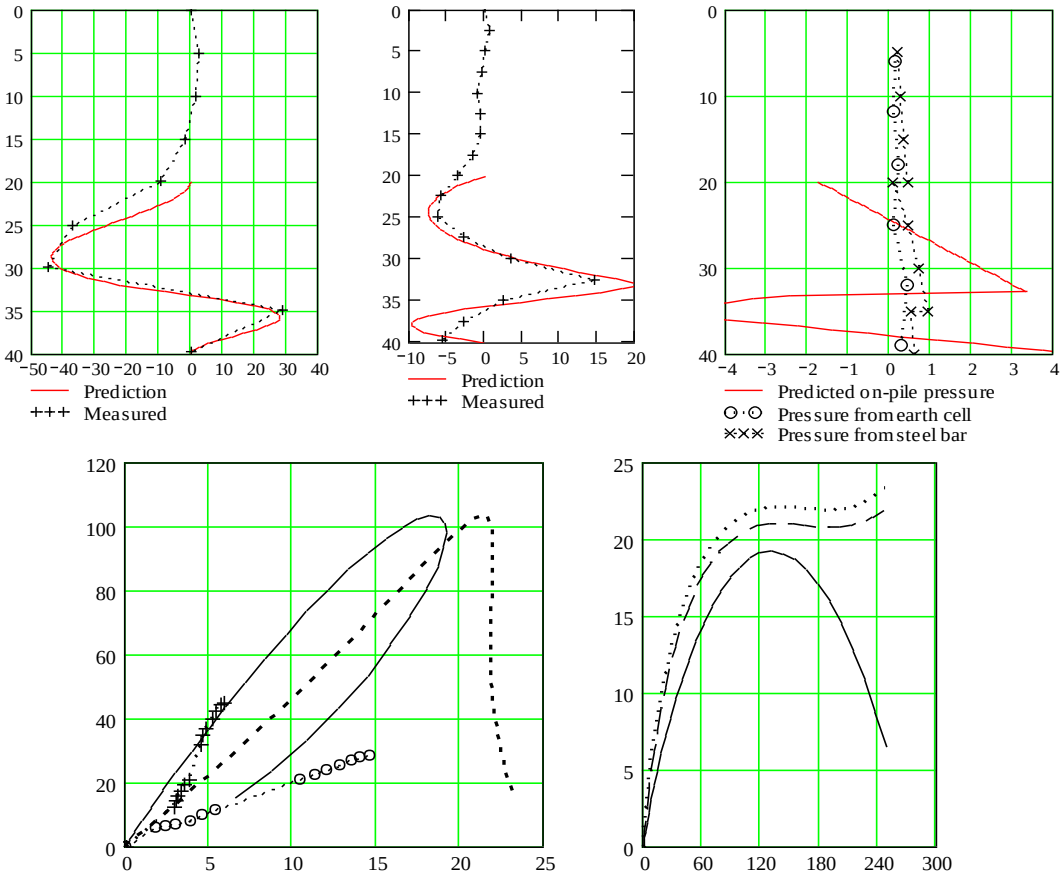


Fig. 8. 3-layer model predictions against measured (Yang et al., 2023) response

Crucially, all piles show multiple local extrema in the profiles, with **multiple slip surfaces** (at depths of 5–10 m, 20–25 m, and 30–35 m) within the reactivated landslide as revealed through field drilling. Yang et al. (2023) reiterate the difficulty in capturing the pile response using a single-slip-surface model as stipulated in relevant national code, and further state that this code is unsuitable for designing anti-slide piles with multiple slip surfaces, as it offers very different thrust (forces) and bending moments from the measured data. To meet these needs, the 3-layer model is adopted here to simulate the measured response of pile Z_2 as an example. Analysis focused on the deep sliding of 30–5m is presented herein, using an effective pile length of 20 m by taking a hinge at the sliding depth (i.e., 20 m) and without impact of anchor force H. In other words, a hinge is taken at depth of an upper sliding depth in modelling free-head, flexible piles in the underlying layer. The parameters are determined (Guo 2016; 2023, see Table 2). Note that the α value is not explicitly given as no pile deflection or soil movement is available to justify it accordingly. The predicted profiles of bending moment and shear force agree well with the measured data (Fig. 8). The evolution of measured M_m and Q_m during the slide for the depths 22.3 m and 32.4 m is well predicted. The difference between on-pile pressure and earth pressure is noted as expected for the model for flexible piles.

In the previous tests, the in-pile shear force and pile-head movement were largely deduced from estimated thrust and soil movement, which naturally lead to differences from their actual values. The difference disappears if measured shear force, pile-head displacement, and rotation (apart from bending moment) are available for each soil movement, as illustrated next.

RIGID PILES SUBJECTED TO A 'FIXED' SLIDING DEPTH

The shear box has internal dimensions of 0.8 m (H) × 0.5 m × 0.5 m (see Fig. 9, Ghee 2009). Other features are similar to those reported earlier (e.g., Guo 2013). The upper part is moved by a rectangular

loading block to generate a uniform lateral soil movement at a stable thickness l_s. The kaolin clay was used in the model tests, which has a liquid limit of 42.08%, a plastic limit of 25.54%, a specific gravity of 2.64, an average moisture content of 39.2%, and an average density of 17.5 kN/m^3. The clay was mixed (in 8 batches over 4 days) to achieve a moisture content close to the liquid limit (to prevent air voids). Moisture loss during the mixing was prevented by storing the clay in a 'storage' box (at least 14 days), in the shear box, and before installation of the pile (24 hours late). The clay thus was unconsolidated, as is accepted in laterally loaded model pile tests. After one test, the piles were removed, and the clay was left to reconsolidate under its self-weight prior to the next test. The model test pile was made of an aluminium tube measuring 1200 mm in length, 32 mm in O.D., and 1.5 mm in wall thickness, with a calculated bending stiffness of 1.28×10^6 kNmm^2. The pile was instrumented with ten pairs of strain gauges mounted along the shaft. The pile cap was fabricated from a solid aluminium block (50 mm thick) and connected to the piles via two 32±0.5 mm diameter holes.

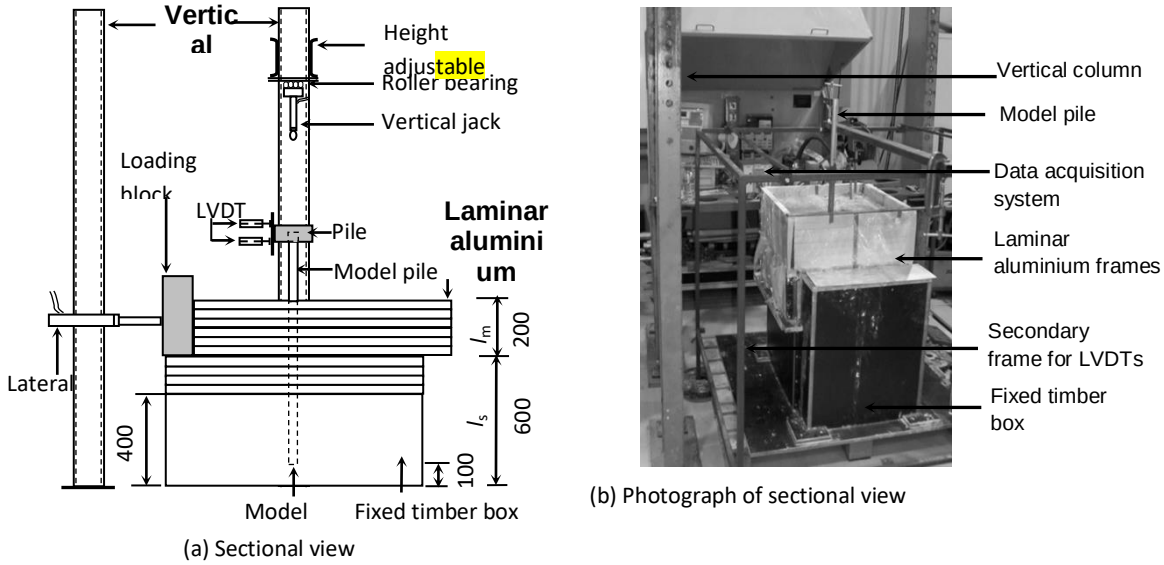


Fig. 9. Model tests on piles in clay (Ghee 2009)

A series of tests were conducted on model single piles, and two-pile groups (at a spacing of 3*d* or 5*d*, *d* = 32 mm) subjected to a uniform lateral soil movement 200 mm thick. Eight vane shear tests show an undrained shear strength of 3 kPa (single pile), 13 kPa (3*d* in-row) and 9 kPa (5*d* in-row) of the clay. All piles have embedment length, *l*, of 700 mm (see Fig. 9). The soil movement was raised by 10 mm (increments) until reaching a total of 130 mm. For each increment, strain gauge readings were used to obtain a bending moment profile *M*(*z*). The profiles were then integrated to deduce inclination ω(z) and deflection *w*(*z*) profiles or differentiated to gain shear force *Q*(*z*), and soil reaction *p*(z) profiles. The five profiles of *M*(*z*), ω(z), *w*(*z*), *Q*(z), and *p*(z) were obtained for each soil movement (e.g., Fig. 10 for a single pile).

The profiles offer the measured maximum values of w_g, M_m, ω (ration angle), and Q_m. For the two-pile in a row groups, they are plotted in Fig. 11a and b for a spacing of s = 3*d* and in Fig. 12 for s= 5*d*. The fourfold higher undrained shear strength of 13 kPa (3*d* row) compared to 3 kPa (single pile) is associated with only a 4.2% reduction in the corresponding M_{max}. Only the two-pile in row groups are analyzed herein. In light of m = 5.21, k_s = 2.0, and 2.3, $p_{ub}/(s_u dl)$ = 4.5 and 4.0, and α = 0.667, the 3-layer predictions offer the profiles of bending moment *M*(z), shear force *Q*(z), pile displacement *w*(z), and on-pile pressure *p*(z)/*d*, which agree well (see Fig. 11a) with the measured maximum response profiles at a soil movement of w_s =130 mm, with α = 1 for the short distance between the pile and loading jack position. The predicted evolution of the maximum response (bending moment, shear force, pile displacement, and rotations) during the soil movement closely match with the measured data at either pile center-to-center spacing, subjected to unknown slip depths around the pile(s). This further demonstrates the accuracy of the 3-layer model.

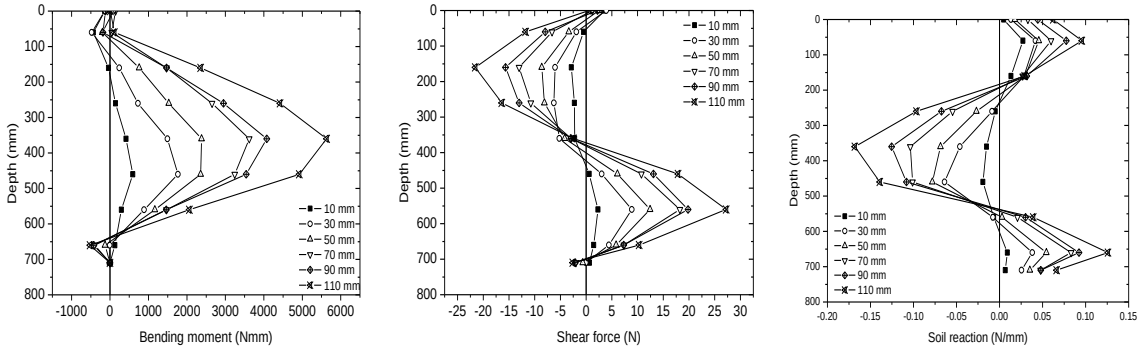


Fig. 10. Response profiles of M(z), Q(Z) and p(z) for a single pile

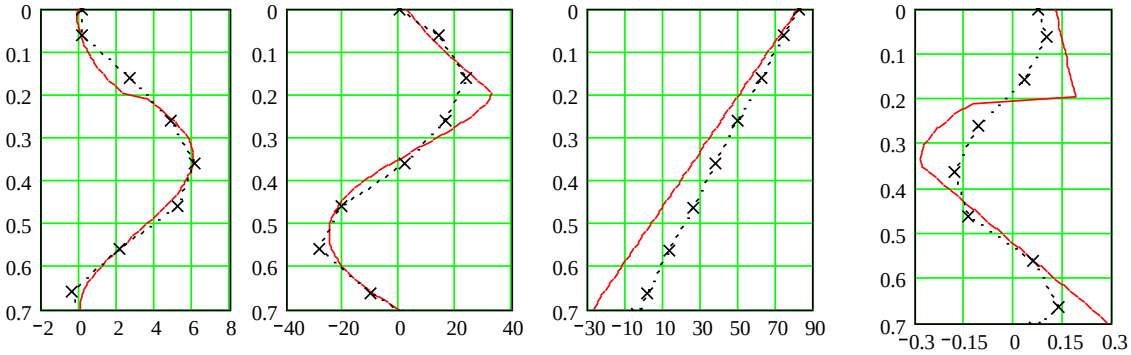


Fig. 11a. Predicted vs. measured response of a pile in 2-pile row (s = 3d)

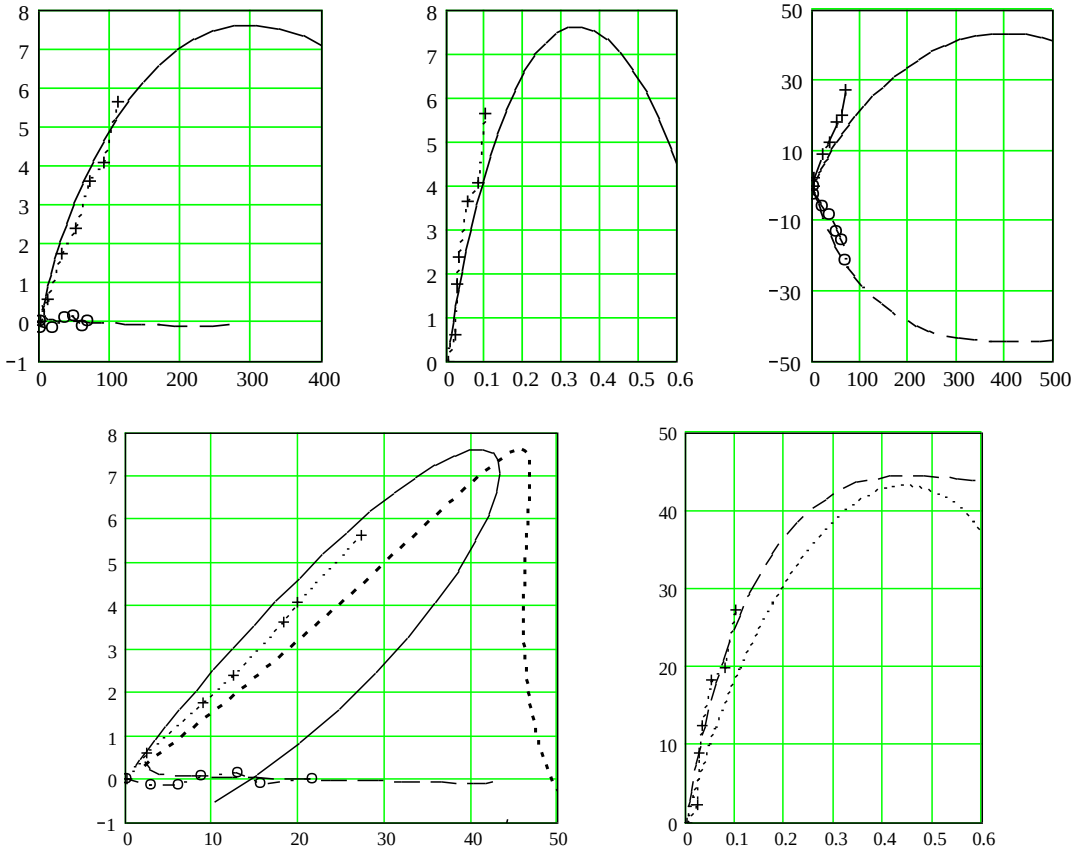


Fig. 11b. Predicted vs. measured maximum response of a pile in 2-pile row (s = 3d)

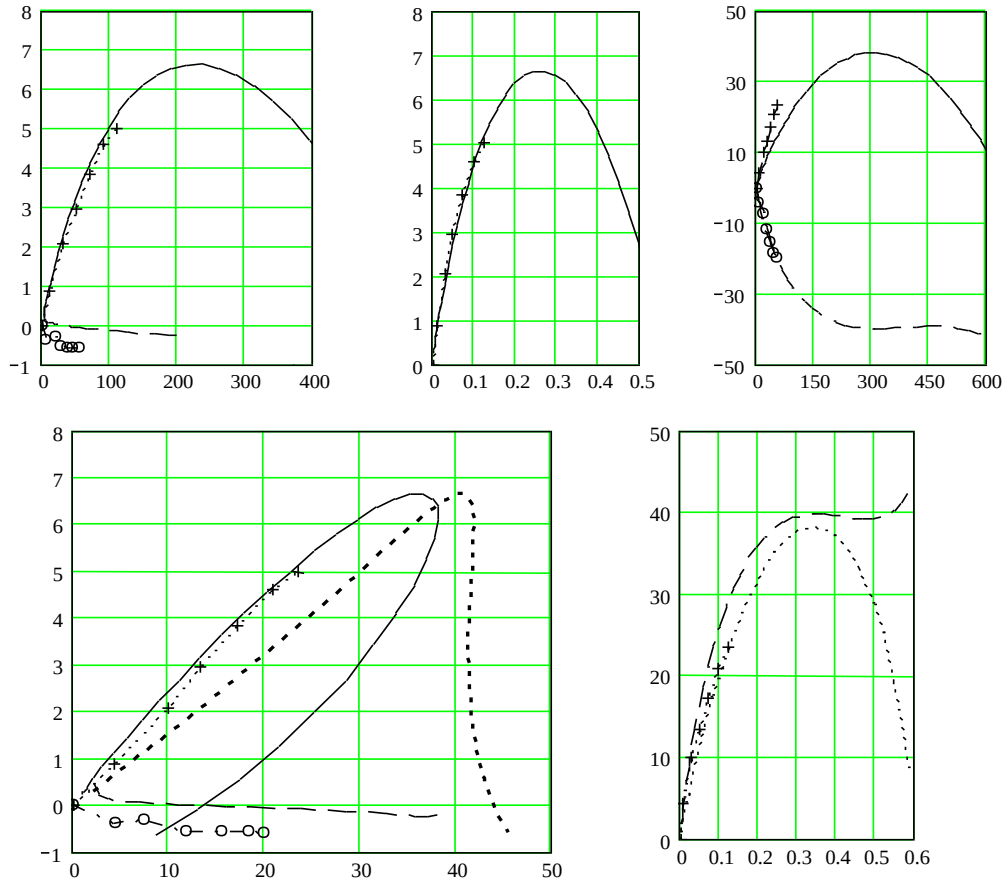


Fig. 12. Predicted vs. measured maximum response of a pile in 2-pile row (s = 5d)

CONCLUSIONS

This paper provides a 3-layer model analysis of the measured response of seven passive piles in five different scenarios. The tests are characterised by pre-selected slip depths for model piles and micropiles, or 2- or 3-slip depths (surfaces) for two real-world projects. Without specifying slip depths, the 'rigid' pile model analysis, based on a consistent set of 3-4 input parameters, offers satisfactory simulation of the measured pile response experiencing multiple slip surfaces, but for the on-pile pressure on flexible piles. The only exception is that a hinge is taken at depth of an upper sliding in modelling free-head, flexible piles in the underlying layer. A sliding depth is normally selected to determine response profiles. Additional evolution detail of in-pile shear force and pile-defection with soil movement would warrant a refined analysis of the five in-situ tested piles using BiP models. Nevertheless, the selected input parameters are deemed sufficiently accurate to design the slope-stabilising piles.

ACKNOWLEDGMENTS

The model tests were supported by Australian Research Council (DP0209027) awarded to the author during his work in Griffith University. Dr. Ghee E.H. conducted the tests.

REFERENCES

Guo, W. D. 2012. Theory and practice of pile foundations. CRC press, Taylor & Francis group.
Guo, W. D. 2023. Advanced design of pile foundations under lateral loading. CRC press, Taylor & Francis group.

Guo, W. D. and Ghee, E.H., 2004. Model tests on single piles in sand subjected to lateral soil movement. Proceedings of the 18th Australasian Conference on the Mechanics of Structures and Materials, Perth, Vol.2, pp.997–1003.

Wang, K.-Y., Li, Y-J., Li, G., and Yu, X.-G., 2019. Experimental study on the horizontal bearing capacity of vertical steel floral tube micropiles with twice grouting, Chinese Journal of Rock Mechanics and Engineering, 38(8) 1707–1717.

Xiang, B., Ma, J.-L., He, Y.-Y., and Zhou, L.-R. 2013. Prototype tests on micro-steel pipe piles as retaining structures, Chinese Journal of Geotechnical Engineering, 35(11) 2131–2138.

Yang, X.-H., Chen, K.-Q., Zhang, W.-X., Ding, B.-Y., and Zhu, J.-H. 2023. Monitoring of large-diameter anti-slide piles and analysis of landslide thrust in resuscitated accumulation landslides, Chinese Journal of Rock Mechanics and Engineering, 42(11) 2776–2787.

Zhou, W.-J., Wei, S.-W., and Zhang, Y.-F. 2019. Model test study on anti-sliding performance of multiple segment grouting steel-tube, Rock and Soil Mechanics, 40(11) 4412–4420.

 © Deep Foundations Institute 2026

RATE-AWARE PILE DESIGN IN GLACIOGENIC SILTS: FROM FABRIC TO SERVICEABILITY

Ri Hong Kee, A O'Sullivan Geotechnical Engineering (AOS), Auckland, New Zealand, cyrus@aosullivan.co.nz
Andy O'Sullivan, AOS, Auckland, New Zealand, andy@aosullivan.co.nz
Sergei Terzaghi, AOS (Australia), Katoomba, NSW, Australia, sergei@aosullivan.com.au

ABSTRACT

Sensitive glaciogenic silts often exhibit high small-strain stiffness (G_0) in the intact state yet contractive, strain-softening behaviour once fabric is disturbed or loading rates are high. This paper synthesises investigation, monitoring and testing from instrumented railway bridge foundations to propose a practice-ready workflow. Co-located dual-rate CPT ($v_{CPT-u} \approx 20$ mm/s; $v_{CPT-S} \approx 3$ mm/s) reconciled with seismic DMT (sDMT) provides a rate-aware, effective-stress interpretation to infer the state parameter ψ and to map installation-induced destructuration via ΔV_s ("damage meter"). Field verification demonstrates critical installation effects: controlled vibratory penetration mobilized significantly higher, more uniform unit shaft resistance ($\tau_s \approx 36kPa$) compared to impact driving ($\approx 10kPa$) and achieved superior set-up rates (~1.1 vs ~0.27 kPa/day). Post-installation sDMT data confirmed a 20–30% V_s reduction adjacent to impact-driven piles, while vibratory installation left the surrounding silt fabric largely intact. Transient settlements of adjacent foundations during vibratory works were bounded ($\approx 5\,mm$) and stabilized rapidly. The resulting design guidance advocates for a shaft-dominated resistance model at the Serviceability Limit State (SLS), with toe resistance reserved for Ultimate Limit State (ULS) reserve. This approach is verified via segmental, multi-energy PDA/CAPWAP interpretation and supported by state- and structure-aware constitutive models—including PM4Silt, NorSand, and structured hypoplasticity—to rigorously assess cyclic and seismic performance. This integrated methodology bridges the discrepancy between conventional analytical predictions and observed performance, enhancing foundation reliability in sensitive, metastable glaciogenic silts.

Keywords: glaciogenic silt, rate effects, state parameter (ψ), vibratory vs. driven installation, PDA/CAPWAP

INTRODUCTION

Modern railway infrastructure demands robust foundation performance even in challenging ground conditions. However, pile foundations in certain fine-grained deposits—notably glaciogenic silts—continue to present complex soil–structure interaction problems. These soils are often fabric-dependent and highly rate-sensitive, meaning their engineering response is tied to their depositional microstructure and the loading rate. Many such silts (e.g., glaciolacustrine deposits) have an open, lightly cemented structure with high porosity, which can be metastable under moisture conditions (Jefferies and Been, 2016; Shuttle and Cunning, 2007). When the fragile inter-particle bonds in these silts are broken (for instance, by loading or wetting), the soil structure can collapse, leading to abrupt volume reduction and differential settlements (Jefferies and Been, 2016). This inherent collapse potential and contractive tendency pose serious challenges for geotechnical design, as evidenced by widely reported issues in sensitive glaciogenic silts and related metastable silt formations worldwide (review perspectives in Musso et al., 2018; Shuttle and Cunning, 2007). Such soils are found globally—from loess plains in Asia and North America to varved glacial silts in Europe—and are well recognised as problematic, requiring careful consideration to ensure foundation resilience.

Conventional design approaches often struggle to reliably predict serviceability performance in these sensitive silt deposits. Standard analytical methods and codes typically categorise soils as either cohesive (clay) or cohesionless (sand), yet low-plasticity silts straddle this boundary and exhibit dual characteristics (Jefferies and Been, 2016). For example, in the projects motivating this paper

 © Deep Foundations Institute 2026

(overconsolidated glaciolacustrine silt, plasticity index around 7 %), design verification required parallel assessment using both drained friction parameters and undrained shear strength—reflecting a deficiency in traditional frameworks when metastable structure controls behaviour. In practice, serviceability limit state (SLS) criteria—settlements, deflections, and differential movements—often govern in such soils even when ultimate limit state (ULS) capacity is met. Unfortunately, conventional settlement methods (elastic/empirical correlations) can severely under-estimate deformations in fabric-sensitive silts, especially under long-term or cyclic service loads. Field observations from the present bridge foundations exemplify this gap: measured pier settlements in one case exceeded ~160 mm versus an SLS allowance of ±25 mm, despite conformity with conventional design checks. In extreme cases, seemingly stable silts have undergone "quick-like" subsidence when disturbed, underscoring that standard SLS checks may not be conservative for soils on the verge of structural collapse. There is hence a growing recognition that new analytical and design approaches are needed to address the gap between conventional predictions and actual performance in metastable, contractive silts (Jefferies and Been, 2016).

The performance inconsistencies observed in the field further highlight the limitations of status-quo methods. For instance, in-situ test data from sensitive silt sites often display pronounced rate effects. A standard cone penetration test (CPT) pushed at the usual rate can generate high excess pore pressures in low-permeability silt, artificially reducing the measured tip resistance; in contrast, slower penetration CPT registers higher resistance and lower u2, indicating a stronger soil when partial drainage is allowed (Shuttle and Cunning, 2007). Such discrepancies between regular and slow CPTs in the same stratum were documented at the subject sites and are consistent with partially drained silt behaviour (Jefferies and Been, 2016). This rate-sensitive behaviour complicates soil characterisation—if unrecognised, designers can undervalue stiffness/strength or misclassify the material. Another recurring field observation is the variability of pile "set-up" (time-dependent capacity gain) in silts. Following installation, some piles show substantial gains in shaft resistance over days or weeks as pore pressures dissipate and soil reconsolidates, while others show modest changes—an in-between response relative to the distinct set-up patterns often expected for sands versus clays. If construction schedules or service loads do not allow sufficient set-up time, piles may experience excessive early settlements despite satisfying ultimate capacity on paper.

Laboratory studies on these soils reinforce the field findings, clarifying the underlying soil mechanics. Undisturbed triaxial tests typically show a pronounced peak strength due to structure, followed by strain-softening as the structure collapses—hallmarks of high sensitivity (Jefferies and Been, 2016). Under cyclic or repeated loading, fabric-dependent silts may generate cumulative pore water pressure and stiffness degradation with each load cycle; the cyclic triaxial tests (conducted to ASTM D5311) showed progressive contractive response and degradation trends consistent with metastable fabric breakdown under working cyclic stresses (Azizi et al., 2020). Even when individual cyclic stress ratios were modest, repetition led to incremental effective stress loss—mechanistically aligning with serviceability drifts observed in the field. These laboratory insights help explain why conventional static analyses fall short: they do not capture cyclic fatigue, strain-rate dependency, or fabric collapse under sustained service conditions (Jefferies and Been, 2016).

Given the significant gaps identified above, there is strong motivation to pursue innovative geotechnical solutions tailored for complex soil–structure interaction in these environments. One line of investigation is to optimise pile installation methods to minimise disturbance and leverage time-dependent gains. For example, controlled vibratory installation can, in suitable soils, reduce initial shaft friction during driving (promoting penetration) while inducing beneficial stress changes and densification in the surrounding ground, potentially improving shaft resistance after reconsolidation (Massarsch and Wersäll 2017). Consistent with this mechanism, dynamic testing at the bridge sites showed higher and more uniform long-term skin resistance—and smaller SLS settlements—for piles installed with controlled vibration compared with piles installed by impact with intrusive plugs. Another crucial avenue is the deployment of advanced in-situ testing and monitoring strategies. High-resolution tools such as seismic piezocone (SCPTu), flat dilatometer and seismic dilatometer (DMT/SDMT), plus staged CPTU with dissipation pauses, resolve small-strain stiffness

and drainage behaviour to inform more reliable SLS predictions (Oberhollenzer, 2024). Similarly, cyclic load testing and high-strain dynamic monitoring during trial installations help quantify evolution from end-of-drive to fully set-up conditions, enabling design choices—e.g., accounting explicitly for set-up in SLS checks, selecting installation methods less sensitive to fabric disturbance, or improving the ground pre-installation—that improve resilience (Massarsch and Wersäll, 2017).

Objectives

In this paper, the above issues are examined through the lens of recent railway bridge projects constructed over sensitive glaciogenic silt deposits. The aim is to generalise the lessons learned and propose design enhancements that extend beyond any single site. First, the background and motivation for studying pile foundations in metastable silts are established, emphasising why standard practice can fall short. Next, a synthesis of field data is provided, highlighting key patterns (settlement trends, load-displacement behaviour, and soil test inconsistencies) observed in instrumented bridge foundations. Laboratory test results on undisturbed silt samples—including monotonic and cyclic triaxial tests—are then discussed to elucidate the soil's rate-sensitive and strain-softening nature. Building on these findings, the paper explores potential improvements in foundation design: from re-calibrating settlement prediction models to adopting installation techniques and ground-improvement measures that mitigate disturbance. Finally, an overarching discussion frames these solutions in the context of infrastructure resilience. While the case studies originate from railway projects, the implications are broadly relevant to deep foundation design in sensitive fine-grained soils worldwide. By treating the problem not as a local anomaly but as a prevalent geotechnical challenge, this study contributes to the development of more reliable and innovative design methodologies for complex soil–structure interaction in difficult ground. The insights and recommendations herein are intended to support practitioners and researchers alike in advancing foundation engineering for the next generation of infrastructure on problematic soils.

GEOLOGICAL AND GEOTECHNICAL CONTEXT

Regional Geomorphic Setting and Depositional Model

The bridge corridor is sited on late-Pleistocene glaciogenic valley-fill where glacifluvial reworking of rock-flour silts produced laterally persistent fine-grained sequences (Boulton and Dobbie, 1993). Microfabric observations consistently show angular particles arranged in anisotropic, weakly bonded packings formed by flocculation and freeze-thaw processes (Clarke, 2018). These packings display a dual character: elevated small-strain stiffness (G_0) in the intact state, yet a strong contractive undrained response once the fabric is disturbed or loading rates are high.

Generalized Stratigraphy and Groundwater

A consistent stratigraphic motif occurs along the alignment: a gravel-sand crust (approx. 4–6 m) overlies a laterally extensive silt-dominated unit encountered to at least 30–40 m depth. Penetration records indicate that this silt unit is underlain by progressively denser granular horizons, including sand and gravel lenses. While founded piles could potentially leverage these deeper, more competent strata for end-bearing, the thickness of the silt unit and the governing serviceability requirements often necessitate an optimized shaft-dominated design within the silt to manage differential settlements. The phreatic surface is shallow, typically between 2.7 m and 4.6 m below ground level.

In-Situ Signatures: Rate, Drainage and State

The in-situ response of the fines unit is governed by penetration rate and drainage. Co-located CPT-u ($v \approx 20\ mm/s$) and CPT-S ($v \approx 3\ mm/s$) exhibit systematic trends: CPT-S yields higher q_c and near-zero B_q while conventional-rate CPT-u mobilizes significant excess pore pressure and lower apparent resistance q_c (Fig. 1). These paired signatures are diagnostic of partial drainage at slow rates and undrained-to-partially undrained penetration at standard rates.

To further delineate fabric effects, the small-strain rigidity index ($K_G = G_0/q_n$) was evaluated following Robertson (2016). The K_G profiles derived from CPT-S more accurately reflect the "intact" structured stiffness, whereas the K_G values from CPT-u show a marked reduction, highlighting the sensitivity of the silt fabric to standard penetration energy. Interpreted critical void ratios for the stress range imply that the shallower–intermediate silts reside above the CSL ($\psi > 0$), consistent with the observed contractive tendency in element tests and enhanced cyclic fragility (Thevanayagam, 2000; Thevanayagam et al., 2002). These data rationalise silts that appear "stiff" in situ when intact but soften rapidly once structure is mobilised or disturbed.

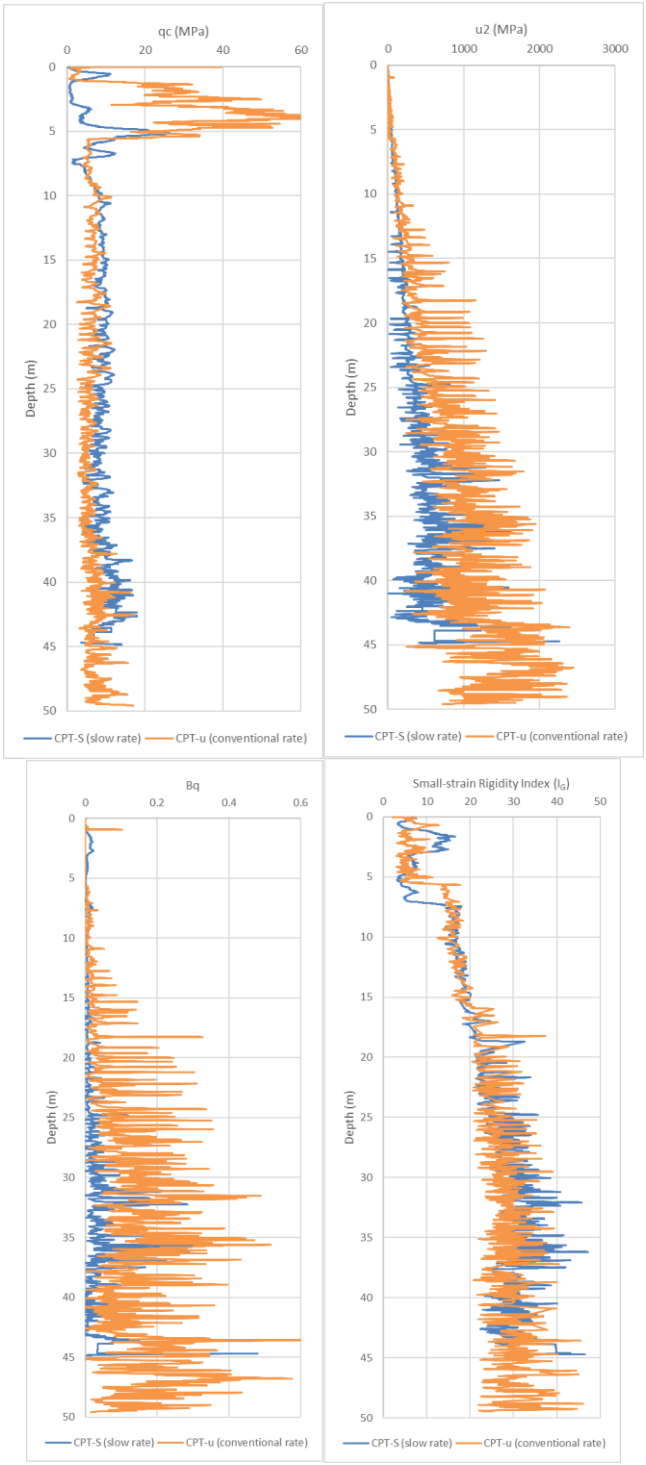


Fig. 1. Dual-rate CPT overlay in the fines-dominated unit (CPT-u vs CPT-S)

 © Deep Foundations Institute 2026

Index Properties, Grading and State

Laboratory classification and particle-size evidence indicate fines-rich, low-plasticity silts with broad silt gradation and minimal clay content. Measured natural water contents are in the high-20s to mid-30s (percent), with void ratios ranging approximately 0.72–0.77 at one site and 0.88–0.96 at another; plasticity index is generally < 7 % and in several cases undetermined because of dilatant behaviour during testing. Interpreted critical void ratios for the stress range imply that the shallower–intermediate silts reside above the CSL ($\psi > 0$), consistent with the observed contractive tendency in element tests and with enhanced cyclic fragility under undrained loading paths. These data also rationalise an apparently paradoxical field observation: silts that appear "stiff" in situ when intact (high small-strain stiffness, respectable q_c) but soften rapidly once structure is mobilised or disturbed.

Small-Strain Stiffness From sDMT/MASW and Fabric Sensitivity

Baseline seismic dilatometer (sDMT) surveys indicate shear wave velocities (V_s) in the intact silt typically on the order of 200–350 m/s. Re-profiling after foundation works demonstrates the role of installation-induced destructuration: high-energy impact driving produces a narrow annulus of reduced V_s (20–30% reduction), whereas controlled vibratory installation largely preserves the intact V_s in the surrounding fines. Critically, the V_s profile—and the resulting G_0—reflects the elastic stiffness of the soil skeleton and is independent of the CPT penetration rate, providing a neutral "damage meter" to delineate disturbed bands and calibrate working-strain moduli for settlement analysis.

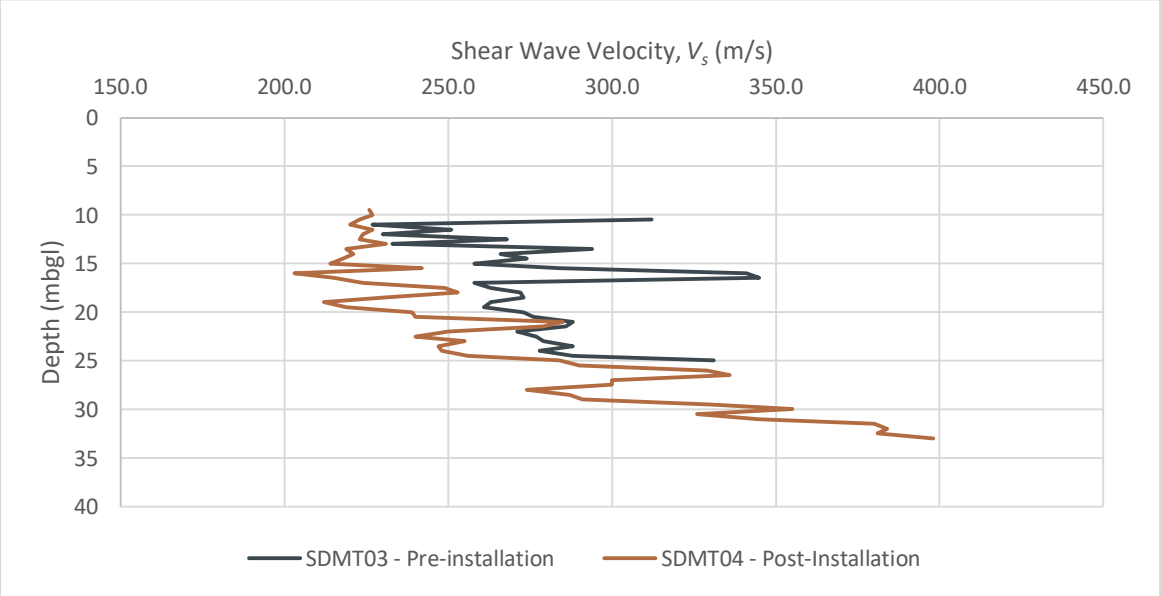


Fig. 2. Small-strain stiffness from sDMT (pre/post installation)

Element Behaviour: Monotonic and Cyclic Response

Monotonic undrained compression on undisturbed silt exhibits a structured peak followed by strain softening and an evolution of pore pressure characteristic of metastable, fabric-dependent materials tending toward a denser state upon shearing. Cyclic triaxial evidence brackets two end-member responses tied to state and confinement: at shallow/intermediate depth with $\psi > 0$ and lower p', cyclic mobility can be reached within tens of cycles at $CSR \approx 0.5$; at higher confinement and smaller ψ, the same material may remain stable for $>7{,}000$ cycles at $CSR \approx 0.02$ with negligible strain growth. This bifurcation reflects state control rather than classification control of cyclic resistance in fines; it aligns with the dual-rate CPT signatures and with the tendency of intact silt to appear "strong" under partially drained probing yet degrade rapidly when cycled undrained at adverse state.

 © Deep Foundations Institute 2026

Synthesis: Implications For Analysis and Design

Taken together, the glaciogenic fines present a coherent mechanistic picture:

- Open, lightly bonded microfabric with void ratios above the CSL yields $\psi > 0$ at shallow-intermediate depth; intact material shows high small-strain stiffness but is contractive under undrained monotonic and cyclic paths.
- Shallow groundwater and low permeability enforce rate-dependent in-situ signatures; CPT-S partially drains and preserves fabric, while conventional CPT-u tends toward undrained penetration, excess pore-pressure generation, and destructuration beneath the tip.
- Baseline V_s provides G_0 for working-strain modelling; ΔV_s after construction resolves the depth and severity of destructuration bands adjacent to installed foundations.
- Monotonic and cyclic triaxial behaviour is consistent with positive ψ at shallower levels and smaller ψ at depth; cyclic resistance is state-controlled and should be assessed accordingly.

For subsequent sections, three practical consequences follow. First, site characterisation must include co-located dual-rate $CPT - u/CPT - S$ within the silt and baseline sDMT to establish $\psi(z)$ and $G_0(z)$, with repeat sDMT post-installation to quantify destructuration. Second, rate-aware parameter selection and state-parameter interpretation are required to avoid bias in stiffness/strength derivation for $t - z/q - z$ modelling and cyclic checks. Third, because destructuration reduces G_0 and unit shaft resistance in disturbed bands, installation method becomes a design variable; vibratory methods that preserve fabric and lateral confinement can produce higher, more uniform shaft resistance and faster setup than impact driving in these silts, as resolved by segmental PDA/CAPWAP trends and ΔV_s mapping.

FIELD EVIDENCE OF PERFORMANCE AND INSTALLATION EFFECTS

Monitoring Strategy and Construction Context

A staged construction programme enabled side-by-side observation of two installation regimes across the same glaciogenic fines unit described in Section 2: (i) controlled vibratory penetration of steel casings and (ii) conventional impact driving. Instrumentation comprised settlement targets on adjacent legacy piles and track-adjacent benchmarks, accelerometers for vibration, and high-strain dynamic testing (PDA) with segmental CAPWAP interpretation on selected production piles. Seismic dilatometer (sDMT) profiling was performed before and, in targeted locations, after installation to quantify small-strain stiffness changes attributable to destructuration (ΔV_s). The monitoring spanned abutment and pier zones to capture any transverse asymmetry in ground response, and results were interpreted against the depositional/structural framework established in Section 2.

High-Strain Dynamic Testing: Segmental Trends and Set-Up

Dynamic testing resolved clear method effects on shaft development and time-dependent set-up:

- Unit shaft resistance at test: Vibro-installed segments mobilised a mean τ_s of $\approx 36\ kPa$, triple the $\approx 10\ kPa$ observed for driven segments at comparable depths.
- Set-up rate: Vibro-installed segments exhibited faster strength gain (~1.1 kPa/day) relative to driven segments (~0.27 kPa/day).
- 13-day Comparative Set-up: Review of the set-up evolution (Fig. 4) indicates that while vibratory piles reached a stable resistance plateau within roughly a week, impact-driven piles tested at 13 days still exhibited significantly lower unit shaft resistance. This suggests that the initial remoulding and destructuration from impact driving create a “recovery lag” that is not observed in fabric-preserving vibratory installations.

 © Deep Foundations Institute 2026

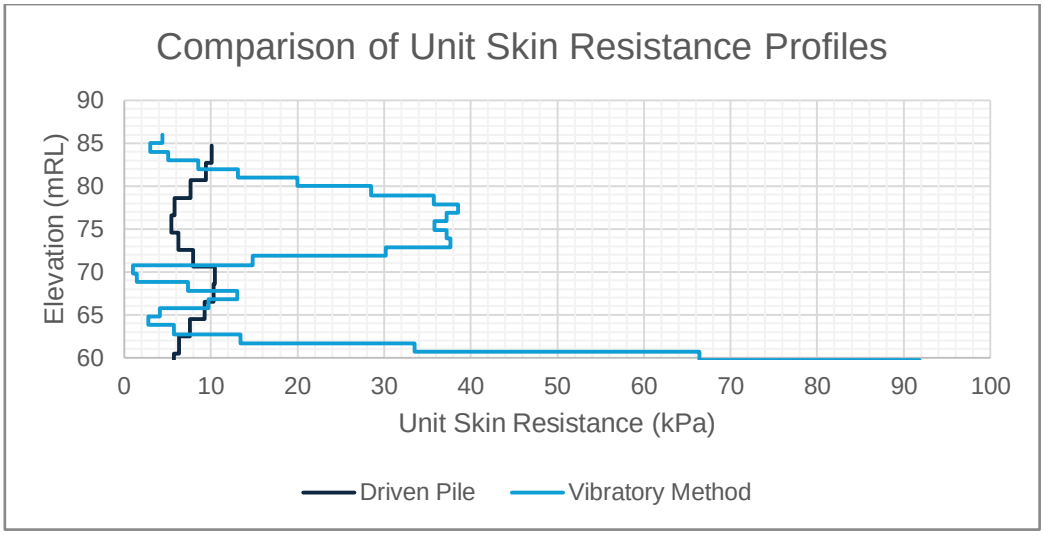


Fig. 3. Segmental unit shaft resistance by installation method

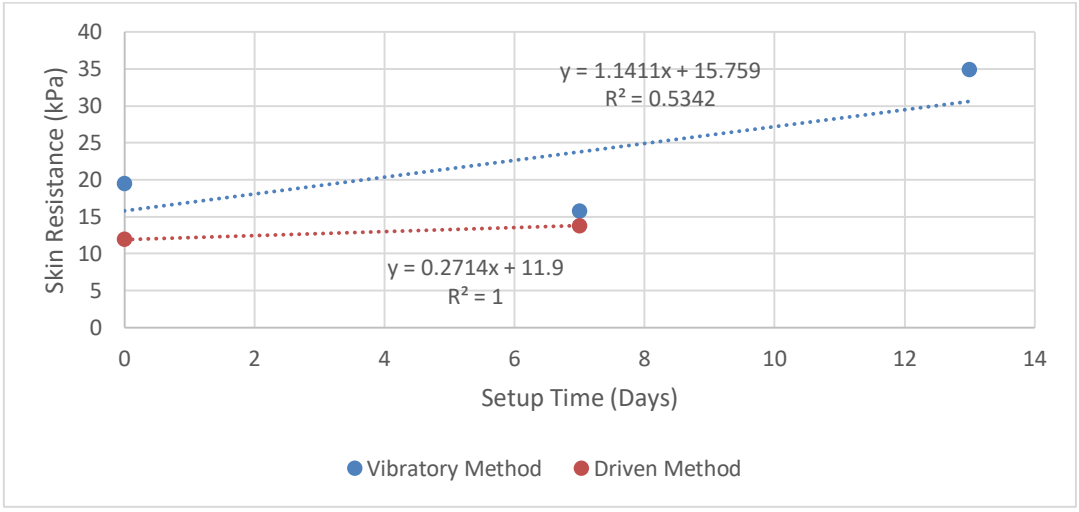


Fig. 4. Evolution of unit shaft resistance (set-up)

Settlement Response During Vibratory Installation

Instrumentation recorded maximum settlements of approximately 5 mm on adjacent piles during vibratory installation, with stabilisation within weeks. The patterns were consistent with densification of the loose granular crust and upper silt band. Procedures focused on continuous geophone surveillance and frequency management to avoid resonance windows, successfully bounding vibration exposure while preserving the densification benefits of vibratory penetration.

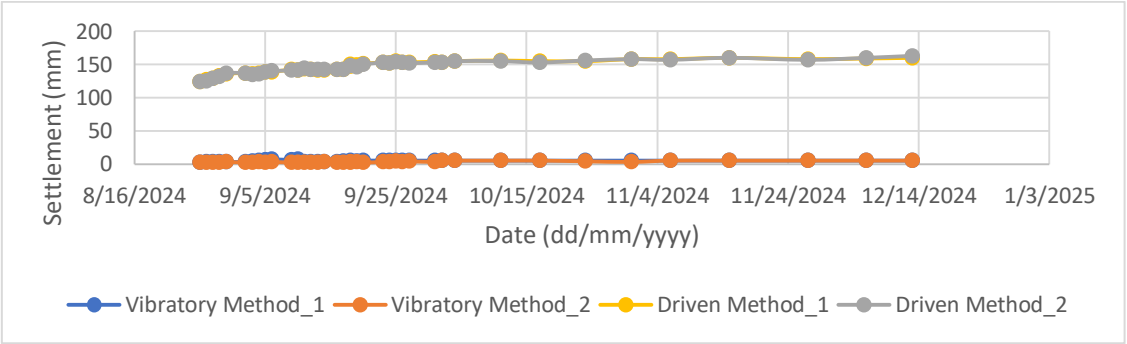


Fig. 5. Settlement of adjacent piles during vibratory and driven installation (time history)

 © Deep Foundations Institute 2026

Early Service Observations and Cyclic Demand Envelope

To assess serviceability under traffic, the cyclic stress ratio (CSR) from train passages was estimated at ≈ 0.025. In situ, the intermittent nature of axle loads provides frequent opportunities for pore-pressure dissipation, supporting stable shakedown at the operational CSR, which explains why post-installation settlements remained bounded during early operation.

Bridging Field Evidence to Analysis Choices

The monitoring and dynamic-testing dataset implies three design-relevant inferences that are distinct from the material description in Section 2:

- Installation method is a first-order design variable. In the fines-dominated unit, vibratory penetration yielded higher and more uniform initial shaft resistance and faster set-up than impact driving. For serviceability, a shaft-dominated design is robust; toe resistance should be treated as ULS reserve only, given the observed softening in the toe influence zone.
- Acceptance must be segmental and rate-aware. Dynamic capacity near the toe is biased low if taken from single-energy CAPWAP alone in strain-softening silts. The adopted protocol—multi-energy restrikes, segmental interpretation, and ΔV_s checks from repeat sDMT—proved reliable and is recommended for future works on similar glaciogenic fines.
- Construction-induced ground movements are predictable and manageable. The observed ~5 mm settlement envelope during vibratory installation is consistent with densification of the shallow granular crust and upper silt band. With symmetric staging and frequency management, those settlements can be kept uniform across the track formation, minimising operational impact.

DESIGN INTERPRETATION AND ANALYSIS FRAMEWORK

Rate-Aware State Interpretation

Design inputs were derived from a rate-aware synthesis of the dual-rate CPTs and seismic stiffness profiles in the fines unit. Conventional-rate CPT-u ($\approx 20\,mm/s$) within the silt was treated as partially to fully undrained, with excess pore pressure and destructuration depressing q_c; the slow-rate CPT-S ($\approx 3\,mm/s$) provided the partially drained counterpoint and the better proxy for intact structured response. Effective-stress groupings ($e.g., Q(1 - B_q) + 1$) were used to infer the depth-varying state parameter $\psi = e - e_c(p')$. This interpretation underpins the cyclic resilience checks and the serviceability settlement envelopes. The state-based approach follows current practice for fines-rich silts and was cross-checked against the element test endpoints for consistency with the site-specific CSL.

Small-Strain Stiffness and Destructuration

Seismic dilatometer (sDMT) shear-wave velocities V_s provided $G_0 = \rho V_s^2$ profiles in the intact silt. Repeat sDMT where high-energy impact driving had occurred indicated a local V_s reduction of order 20–30 %—a measurable destructuration band—whereas vibratory installation left Vs essentially unchanged. For analysis, the measured ΔV_s was used directly to scale working-strain moduli in $t - z/q - z$ settlement calculations and to set lower-bound unit shaft resistances in disturbed bands.

Shaft-Dominated Serviceability; Toe As ULS Reserve

Given (i) the contractive, strain-softening tendency of the disturbed silt near the toe, (ii) the higher, more uniform τs observed for vibratory segments, and (iii) the larger displacements required to mobilise base resistance, the Serviceability Limit State (SLS) is treated as shaft-dominated, with toe resistance serving as reserve for Ultimate Limit State (ULS) only. Segmental PDA/CAPWAP results and staging-pile back-analysis support lower-bound τs envelopes of ~23.5–25 kPa for disturbed bands and ~36 kPa where fabric is preserved, with distinct time-dependent set-up trends by method.

 © Deep Foundations Institute 2026

Constitutive Choices Proportional to Consequence

For screening-level settlement and global stiffness checks, HSsmall can be used with G0 from sDMT and modulus decay tied to measured ΔVs. For cyclic and seismic serviceability, and wherever installation history matters, adopt state- and structure-aware models (PM4Silt; structured hypoplastic clay; NorSand for ψ-based monotonic bounds) so that cyclic mobility, pore-pressure generation, and destructuration can be represented without ad-hoc tuning. Calibrate against: (i) $\psi(z)$ from CPT-u/CPT-S; (ii) $G_0(z)$ and $\Delta V_s(z)$ from sDMT; (iii) measured segmental τs and log-time set-up rates.

NUMERICAL MODELLING: MINIMUM REQUIREMENTS FOR RELIABLE SLS PREDICTRION

Model Set-Up

1. Ground profile and state: Use the generalized stratigraphy and groundwater from Section 2, with $\psi(z)$ interpreted from paired CPT-u/CPT-S; assign $G_0(z)$ from baseline sDMT. Reduce G_0 locally in the observed ΔV_s band adjacent to impact-driven elements; leave unchanged adjacent to vibratory installations.
2. Interfaces and $t-z/q-z$: Derive initial τs envelopes from segmental PDA (vibratory: mean ~36 kPa; impact-driven: mean ~10 kPa) and apply log-time set-up consistent with field restrikes (≈ 1.1 kPa/day vs ≈ 0.27 kPa/day). Where acceptance relies on post-installation V_s recovery, scale τ_s with the measured ΔV_s ratio.
3. Constitutive selection:
   - HSsmall for envelope settlements;
   - PM4Silt for cyclic/earthquake response of the silt;
   - structured hypoplastic clay to represent bonding and destructuration where ΔV_s bands are material;
   - NorSand for ψ-consistent monotonic bounding and CPT back-analysis.

Calibration Targets

(i) Monotonic: reproduce strain-softening and pore-pressure evolution from undrained triaxial tests in the positive-ψ range;
(ii) Cyclic: match cyclic mobility at $CSR \approx 0.5$ for shallow high-ψ material within 10–30 cycles, and stable response for $> 7{,}000$ cycles at $CSR \approx 0.02$ at depth;
(iii) Installation history: replicate the measured ΔV_s drop around impact-driven elements and the near-zero ΔV_s around vibratory installations;
(iv) PDA/CAPWAP: match segmental τ_s at EOD and after restrike at two energies.

CONCLUSIONS

Rate, state and fabric jointly control performance in the glaciogenic silt. Slowed, partially drained CPT-S consistently shows higher qc and near-zero B_q than conventional CPT-u, confirming rate sensitivity and intact-fabric effects (Fig. 1). Small-strain stiffness from sDMT is high in the intact state, but repeat profiling after impact driving reveals narrow destructuration bands with Vs reductions of ~20–30 %, whereas vibratory installation leaves V_s essentially unchanged (Fig. 2). These signatures match the observed service response and frame a state-based design approach.

Installation method is a first-order variable. Segmental PDA/CAPWAP shows higher and more uniform unit shaft resistance for vibro-installed segments ($\approx 36\,kPa$) versus driven segments ($\approx 18\,kPa$), and faster set-up ($\sim 1.1\,vs\,\sim 0.27\,kPa/day$). The lowest resistances occur in the toe-proximal zone irrespective of method—consistent with local strain-softening and the well-known toe bias in inverse dynamics. These outcomes were documented at BR89 and in our companion study, and they anchor a shaft-dominated SLS design with toe treated as ULS reserve.

 © Deep Foundations Institute 2026

Construction-stage movements during vibratory works were transient and manageable (envelope ≈ 5 mm) and stabilised within weeks. Resonance windows can transiently amplify particle velocities; in practice, continuous monitoring and slight frequency/sequence adjustments were effective controls. Together, the field and interpretation evidence support a rate-aware, fabric-preserving workflow: co-located CPT-u/CPT-S to infer ψ, pre/post sDMT as a "damage meter" (ΔV_S), segmental multi-energy PDA/CAPWAP for acceptance, and state-/structure-aware constitutive models for cyclic checks.

REFERENCES

ASTM International, 2011. ASTM D5311-11: Standard Test Method for Load-Controlled Cyclic Triaxial Strength of Soil. ASTM International, West Conshohocken, PA. doi:10.1520/D5311-11.

Azizi, A., Musso, G., and Jommi, C., 2020. Effects of repeated hydraulic loads on microstructure and hydraulic behaviour of a compacted clayey silt. Canadian Geotechnical Journal. doi:10.1139/CGJ-2018-0505.

Balachandran, S., and Kanagaratnam, G., 2019. Microfabric and mechanical response of glaciogenic silts. Engineering Geology, 252, 10–22.

Bayraktaroglu, H., et al., 2023. NorSand updates for structured soils. Computers and Geotechnics, 157, 105309.

Boulanger, R.W., and Ziotopoulou, K., 2018. PM4Silt (Version 2): A sand-like silt plasticity model for earthquake engineering. Report UCD/CGM-18/01, University of California, Davis, Center for Geotechnical Modeling.

Boulanger, R.W., and Ziotopoulou, K., 2023. PM4Silt user update. Soil Dynamics and Earthquake Engineering, 169, 107611.

Boulton, G.S., and Dobbie, K.E., 1993. Consolidation and microstructures of glacial sediments. Journal of Geology, 101(5), 559–570.

Clarke, B., 2018. Small-strain stiffness and bonding in sensitive fines. Géotechnique, 68(12), 1057–1072.

Goble, G.G., Rausche, F., and Likins, G.E., 1980. The analysis of pile driving—A state-of-the-art. Proceedings of the First International Conference on the Application of Stress-Wave Theory on Piles, Stockholm, Sept. 10–13, A.A. Balkema, pp. 131–161.

Hardin, B.O., and Black, W.L., 1969. Closure to "Vibration modulus of normally consolidated clay." Journal of the Soil Mechanics and Foundations Division, ASCE, 95(SM6), 1531–1537.

Hardin, B.O., and Drnevich, V.P., 1972. Shear modulus and damping in soils: measurement and parameter effects. Journal of the Soil Mechanics and Foundations Division, ASCE, 98(SM7), 667–692.

Høeg, K., et al., 2000. Undrained behaviour of silt and tailings. Canadian Geotechnical Journal, 37(6), 1237–1248.

Jefferies, M., and Been, K., 2016. Soil Liquefaction: A Critical State Approach (2nd ed.). CRC Press, Boca Raton.

Mašín, D. (2007). A hypoplastic model for clays with explicit structure. Géotechnique, 57(4), 311–326.

Massarsch, K.R., and Wersäll, C., 2017. Fundamentals of vibratory driving. Geotechnik, 40(1), 1–16.

Musso, G., Azizi, A., and Jommi, C. (2018). Issues in sensitive glaciogenic silts and related metastable silt formations. (Refers to perspective reviews in Shuttle and Cunning, 2007).

Niemunis, A., and Herle, I., 1997. Hypoplastic model with intergranular strain. Mechanics of Cohesive-Frictional Materials, 2(4), 279–299.

Oberhollenzer, S., 2024. Influence of soil structure on CPTu and SDMT: case study from Onsøy (SMA² Award Paper). Proceedings of the 7th International Conference on Geotechnical and Geophysical Site Characterization (ISC-7), Barcelona.

Obrzud, R., and Truty, A., 2018. The Hardening Soil model: Theory and applications. ZSoil.PC White Paper, Lausanne.

Robertson, P.K., 2009. Interpretation of cone penetration tests—A unified approach. Canadian Geotechnical Journal, 46(11), 1337–1355.

 © Deep Foundations Institute 2026

Robertson, P.K. (2016). Cone Penetration Test (CPT) - A Unified Approach for Soil Behavior Type and State.
Shuttle, D.A., and Cunning, J., 2007. Liquefaction potential of silts from CPTu. Canadian Geotechnical Journal, 44(1), 1–19.
Shuttle, D.A., and Cunning, J., 2008. Discussion: Liquefaction potential of silts from CPTu. Canadian Geotechnical Journal, 45(1), 142–145.
Thevanayagam, S., 2000. Liquefaction potential and equivalent granular void ratio. Journal of Geotechnical and Geoenvironmental Engineering, 126(2), 149–156.
Thevanayagam, S., Shenthan, T., Mohan, S., and Liang, J., 2002. Undrained fragility of silty soils: state and fabric effects. Proceedings, ASCE Geotechnical Special Publication No. 124, 77–94.

 © Deep Foundations Institute 2026

A SYSTEMATIC APPROACH TO FOUNDATION SELECTION FOR REMOTE TRANSMISSION LINE PROJECTS: THE INVESTIGATIVE DRILLING METHOD

Masoud Manafi, Correspondence Author, Research and Development Department, Civil Group (Aust), 50-54 Bennet Avenue, Melrose Park, SA, Australia; manafigs@tcd.ie; ORCID: 0000-0002-5998-1478
Ben Juett, Research and Development Department, Civil Group (Aust), 50-54 Bennet Avenue, Melrose Park, SA, Australia; bjuett@civgroup.com.au
Ben Evans, Research and Development Department, Civil Group (Aust), 50-54 Bennet Avenue, Melrose Park, SA, Australia; bevans@civgroup.com.au
Michael Turner, Research and Development Department, Civil Group (Aust), 50-54 Bennet Avenue, Melrose Park, SA, Australia; mturner@civgroup.com.au

ABSTRACT

This paper outlines a detailed methodology for selecting the optimal foundation systems for transmission line structures in remote and diverse geological landscapes. The Investigative Drilling (ID) Method, utilising a Measurement While Drilling (MWD) technique, employs a systematic approach that integrates geotechnical investigation, constructability evaluation, and environmental factors into a single decision-making framework. This framework is developed based on field experience gained from numerous transmission line projects across Australia. The methodology addresses the specific challenges of remote transmission line projects by tackling factors such as limited access to site locations, geological diversity, and logistical challenges. Major transmission line projects can benefit by reducing costs and environmental impacts while enhancing construction efficiency with customised foundation solutions, with case studies suggesting the potential to lower costs by 10% or more compared to less investigated projects. This research indicates that early detailed geotechnical assessments enable efficient foundation construction, minimising environmental impacts and boosting project success. This paper explains both the theoretical and practical aspects of its methodology, introducing a logical model to select site-specific foundations suitable for different infrastructure projects within challenging environments.

Keywords: transmission line foundations, foundation selection, geotechnical investigation, remote construction, investigative drilling method, decision matrix, environmental impact mitigation

INTRODUCTION

Selection of suitable foundation systems for transmission line structures poses considerable engineering challenges, particularly in remote areas characterised by complex and poorly understood geotechnical conditions. Extensive power transmission line projects, usually located in remote areas, have substantial constructability challenges concerning accessibility to the site, equipment mobilisation, as well as materials supply (Pall et al., 2020). The practical feasibility and economic viability of different foundation types in construction projects depend upon a variety of factors, including buildability, cost, and site conditions (Alsanabani et al., 2023). Therefore, most of these transmission line projects, especially those to remote areas, tend to encounter problems in acquiring enough geotechnical information because of logistical challenges and environmental limitations (Kandaris et al., 2018; Thompson et al., 2009).

Various studies and established geotechnical principles emphasise the critical importance of comprehensive geotechnical investigations in foundation selection for infrastructure projects (AASHTO, 2022; Clayton, 2001). Understanding ground behaviour and its associated uncertainties within the reliability-based design framework can facilitate more optimised foundation design and construction. By better characterising soil and rock properties, engineers can reduce design conservatism and make more informed decisions regarding material usage (Phoon and Kulhawy, 2008). The significance of geotechnical data for infrastructure projects, including transmission lines, is well-recognised for identifying risks and ensuring cost-effective decision-making (AASHTO,

 © Deep Foundations Institute 2026

2022). Nonetheless, numerous transmission line projects, particularly in isolated regions, frequently face challenges in obtaining sufficient geotechnical data because of logistical limitations and environmental constraints (Kandaris et al., 2018; Thompson et al., 2009). This data scarcity can lead to increased knowledge uncertainty (AASHTO, 2022), frequently necessitating more conservative design approaches. Such conservatism can lead to higher initial construction costs. Additionally, insufficient subsurface investigation increases the risk of encountering unforeseen ground conditions, which can cause construction delays and further cost escalation as unexpected problems arise during the project (AASHTO, 2022; Clayton, 2001). Thus, the variability of soil and rock conditions within project corridors requires a systematic approach to foundation selection that balances engineering requirements with economic constraints.

Table 3-5 of AASHTO (2022) specifies that for poles, masts, and towers, a minimum of one boring at each foundation location is required, extending to a depth of at least 9 m below the anticipated top of the foundation in soil or 3 m of rock coring, whichever is shallower. This recommendation aims to provide sufficient subsurface data for foundation design and risk assessment. However, the practical implementation of this requirement in electric transmission line projects often deviates due to the high costs and time-consuming nature of conventional investigation methods. This difference is especially evident when transmission lines stretch across vast, isolated areas, making thorough conventional evaluations at every foundation site logistically difficult and economically challenging. The spacing of structures along linear infrastructure projects, such as transmission lines, can be considerable, and the cumulative cost and time investment of adhering strictly to the recommended investigation frequency using traditional drilling and sampling techniques become significant project constraints. This practical reality often necessitates a more risk-informed approach, potentially involving a lower density of conventional investigation points supplemented by other less invasive methods or reliance on conservative design parameters.

Traditionally, geotechnical engineers have relied upon a suite of ground investigation methods to characterise site conditions. These conventional techniques, including the excavation of trial pits, the advancement of boreholes with Standard Penetration Tests (SPTs), and the execution of Cone Penetration Tests (CPTs), along with laboratory analysis of recovered samples, have served as the foundation of subsurface exploration for decades. However, the increasing complexity and scale of modern infrastructure projects, particularly electrical transmission systems, have raised the demand for efficiency and the need for continuous and reliable ground profiles. This requires the use of advanced techniques like Measuring While Drilling (MWD), which has become a significant breakthrough in geotechnical site characterisation, enabling more thorough stratigraphic profiling (Reiffsteck et al., 2018).

MWD represents a dynamic approach to subsurface investigation. It involves the continuous, real-time monitoring and recording of various drilling parameters as a borehole is advanced into the ground (Reiffsteck et al., 2018). This is achieved through the integration of sensors directly into the drilling equipment, allowing for the collection of data on key operational parameters such as the Penetration Rate (PR), the torque applied to the drill bit, the thrust force exerted, the rotation speed (RPM) of the drill string, the pressure and flow rate of the drilling fluid or air flush, and the holdback pressure used to control the drilling process (BS EN ISO 22476-15, 2016; Reiffsteck et al., 2018). Modern MWD technology, such as Investigative Drilling (ID) rigs, increasingly incorporates sophisticated computerised systems and high-frequency sensors, enabling the acquisition of accurate and detailed data throughout the drilling operation (Duthy and Juett, 2020; Huang et al., 2025a). Figure 1 demonstrates several ID rigs utilised in electric transmission lines across Australia.

Duthy and Juett (2020) discuss the advantages of the ID method for geotechnical investigations, particularly for projects necessitating a large number of footings, such as transmission lines, wind farms, and solar farms. The ID technique offers a key advantage over traditional drilling methods: it is generally much more productive and cost-effective in these environments. This approach enables the exploration of all structural locations, rather than just a limited few, leading to considerable cost savings and reduced project risks associated with unforeseen ground conditions. For example, a 20 m-

deep ID method drill hole can be completed in about 30 minutes or less. In contrast, a 20 m-deep drill hole advanced by rotary hollow flight auger drilling in soil and then diamond coring in rock could take up to one day to complete. The ID method constantly measures and logs various drilling parameters in real-time while the bore advances. This process provides ongoing data streams that deliver essential insights into subsurface conditions and stratigraphy. Simultaneously, the ID method retrieves disturbed samples from known depths, allowing for the visual and tactile evaluation of ground layers (see Fig. 2). This process aids in identifying lithologies, stratigraphic sequences, and estimating strengths. While the disturbed nature of the samples means in-situ structure cannot be assessed, the synthesis of continuous drilling parameters data, driller's observations, and disturbed sample logging by a geotechnical engineer provides a reasonable indication of the ground profile at each location. Accordingly, bulk samples (see Fig. 2a) and sub-samples (see Fig. 2b) can be collected for geotechnical and geo-environmental laboratory tests such as Particle Size Distribution (AS 1289.3.6.1, 2009; AS 1289.3.6.3, 2003), Atterberg Limits (AS 1289.3.3.1, 2009; AS 1289.3.4.1-2008, 2016; ASTM D4318-17e1, 2017; Manafi, 2019; Manafi et al., 2022), Contaminant Screening (AS 1289.4.2.1, 2020; AS 1289.4.3.1, 2021; AS 1289.4.4.1, 2017), and many other tests applicable to disturbed samples.

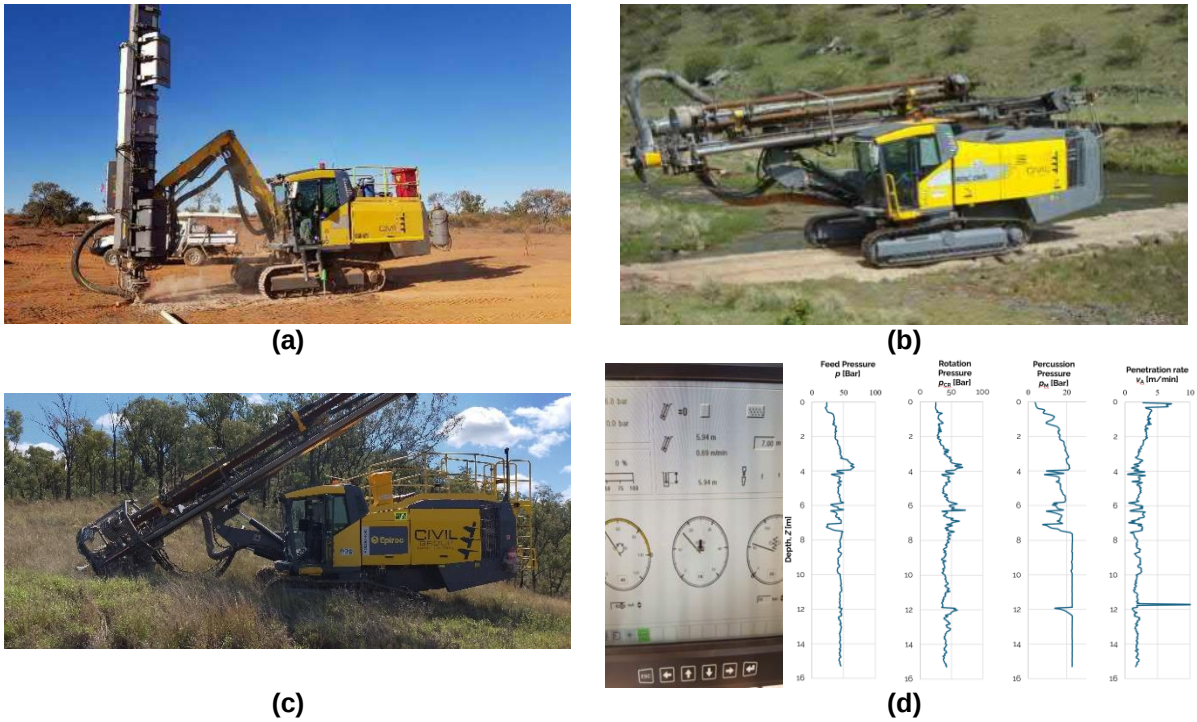


Fig. 1. Utilised ID rigs in electric transmission lines across Australia. (a) Atlas Copco D9C - Top Head Hammer; (b) Atlas Copco D65 - Down Hole Hammer; (c) Epiroc D65 - Down Hole Hammer; (d) Data Acquisition System and Some Data Plots

Decisions made at the initial stages of the design process for piling and foundation construction hold a significant influence on their subsequent successful construction. Consequently, early engagement of relevant parties, particularly specialist contractors, enables the provision of practical advice before finalisation of the design (ICE, 2016). These comprehensive, location-specific data increase confidence in making proper footing design, including bored pile design assignments, among the most common foundation types. The ID method is established as a highly adaptable and unique geotechnical investigation tool for geotechnical projects due to its extensive coverage, continuous data collection, and sample recovery capabilities. Furthermore, following drilling of the approximately 150 mm diameter boreholes used in the ID method, they are commonly monitored overnight primarily to determine the depth of the stabilised standing water level. This period also allows for observations regarding the stability of the borehole walls. These holes can also be used for standpipe installations

 © Deep Foundations Institute 2026

to determine long-term groundwater levels. These additional observations are highly beneficial and practical for the actual foundation construction.



(a)

(b)

Fig. 2. Recovered samples during ID boring. (a) Sample board, recovered samples at 1m intervals; (b) Sub-sample collections

Despite these insights, current industry practice often lacks a structured methodology for integrating geotechnical data with practical considerations in foundation selection for transmission line projects. This paper aims to address this gap by introducing a multi-phase approach that systematically evaluates geological, logistical, and environmental factors to determine the most appropriate foundation solution for each transmission tower location, utilising the ID method. Accordingly, the objectives of this paper are to:

1. Present a comprehensive foundation selection methodology that considers both technical and practical realities;
2. Demonstrate the value of early and detailed geotechnical investigation in optimising foundation design;
3. Introduce a logical assessment model for foundation selection that can be applied to diverse projects with various ground conditions;
4. Illustrate the application of the methodology through a case study example from a major transmission line project.

MULTI-PHASE GROUND INVESTIGATION PROCESS

The proposed method utilises a structured, multi-phase approach to ground investigation, aimed at refining understanding of subsurface conditions while minimising unnecessary expenditure progressively. This approach aligns with recommendations for staged investigation processes that allow for adaptation based on emerging information, as advocated in established site investigation practice (Clayton et al., 1995). The methodology comprises four distinct phases.

 © Deep Foundations Institute 2026

Preliminary Desktop Study

The initial phase involves a comprehensive evaluation of existing geological data, including regional geological maps, past site investigations, and remote sensing information. This stage sets the geological context for the project, highlighting potential geotechnical risks. GIS-based analysis is used to create initial geological profiles along the transmission corridor. Specific activities include:

- Review of geological maps and historical ground surveys;
- Analysis of satellite imagery and aerial photography for terrain assessment;
- Examination of existing transmission line design parameters;
- Development of preliminary site models to guide field investigation;
- Preliminary positioning of the tower structures.

Pre-ID Method Field Investigation

Following the desktop study, targeted site reconnaissance is conducted to validate desktop findings and assess additional factors that may influence foundation selection. This phase emphasises visual examination of surface conditions, environmental and cultural heritage features, and access constraints. As noted by CEN. E.N. 1997-2 (CEN. E.N. 1997-2, 2007), preliminary site investigation should focus on identifying potential geotechnical hazards and establishing the variability of ground conditions. The reconnaissance typically involves:

- Assessment of terrain and ground surface conditions;
- Identification of potential environmental and cultural heritage constraints;
- Evaluation of site access for equipment mobilisation and subsequent investigation/construction;
- Preliminary mapping of geological features visible at the surface;
- Refine positioning of the tower structures.

ID Method Field Investigation

The core of the methodology involves a detailed initial subsurface investigation using the ID technique for every structure at the beginning of the field intrusive investigation, followed by several conventional field investigations to provide a clear understanding of the underground conditions. This is accomplished by creating tailored site investigation protocols that tackle the specific challenges of remote transmission line projects. This is especially important for ensuring extensive coverage and adapting investigations to the various dispersed tower locations. It includes the strategic placement of conventional boreholes to align with the proposed configurations of tower foundations at each location. The ID method allows for continuous data acquisition during drilling and the recovery of disturbed samples from known depths. These samples, though disturbed, enable the determination of lithology and stratigraphic sequence, as well as the estimation of approximate strengths and weathering grades of the subsurface layers. The protocols emphasise the synthesis of information from multiple sources, including ID method drilling metrics (such as advance rate, penetration thrust, rotation rate, torque, and flush pressure), the driller's log, and the engineer's field log of recovered samples. Additionally, post-drilling observations, such as monitoring the stabilised standing water level and assessing the stability of borehole walls overnight, are common practices within these protocols. Evaluating the data gathered using the ID method and comparing it with a historical database of ID parameters previously correlated with verified ground conditions from conventional testing on comparable projects allows for more focused and optimised planning of subsequent conventional investigations by anticipating subsurface conditions. It is assumed that the historical database of ID parameters and corresponding conventional test data provides a reliable basis for correlating the ID data with ground conditions in comparable geological settings. This approach combines ID and conventional drilling methods with specialised in-situ and laboratory testing to characterise subsurface conditions at each tower location (AASHTO, 2022; AS 1726, 2017; ASTM D420-18, 2018; BS 5930, 2015; BS EN ISO 22476-15, 2016).

Complementary standard geotechnical tests like SPT, CPT (where soil conditions permit), and rock coring/RQD are integrated, typically in a limited capacity (e.g., 10% of structure locations, depending on the complexity of the site ground condition), for calibration and verification purposes. During the data analysis, some inconsistencies may be noted in the correlation of ID parameters in specific ground materials, which require further refinement through targeted conventional testing.

Data Analysis and Reporting

The final phase of ground investigation integrates field and laboratory data to develop comprehensive geotechnical models for each tower location. These models serve as the foundation selection basis and include:

- Stratification models indicating layers of soil and rock;
- Engineering parameters for design calculations;
- Groundwater conditions and potential seasonal fluctuations;
- Identification of key design and construction constraints;
- Foundation recommendations along with supporting reasons.

FOUNDATION SELECTION FRAMEWORK

Based on the geotechnical investigation, a systematic framework will be established to assess and select the most suitable foundation types. This framework extends beyond the traditional bearing capacity considerations to include constructability, environmental impact, and economic factors. The approach draws on decision-making methodologies and integrates quantitative assessment techniques to inform decision-making. Key evaluation criteria include:

1. **Technical Suitability**: Assessment of foundation capacity to resist vertical, lateral, and overturning loads under various conditions;
2. **Constructability**: Evaluation of construction feasibility considering equipment access, material logistics, and installation challenges;
3. **Environmental Impact**: Analysis of ground disturbance, habitat disruption, and remediation requirements;
4. **Economic Factors**: Consideration of material costs, installation time, and long-term maintenance requirements.

RESULTS

Logical Assessment Model for Foundation Selection

The integration of geotechnical data with practical considerations results in a systematic and thorough assessment model for foundation selection. This model offers a structured approach to evaluating foundation options for transmission towers in remote locations, ensuring that all relevant factors are meticulously considered.

The model utilises a matrix-based evaluation system, where foundation types are assessed against site-specific criteria. For each tower location, potential foundation options are scored across multiple parameters, including:

- Geotechnical suitability (e.g., bearing capacity, settlement potential);
- Installation feasibility (e.g., equipment requirements, access constraints);
- Environmental impact (e.g., footprint size, ground disturbance);
- Material and logistics considerations (e.g., concrete requirements, transportation);
- Construction time and seasonal constraints;
- Long-term performance and maintenance requirements.

Scoring is conducted on a normalised scale, with weighting factors applied to reflect project priorities. This approach enables a transparent comparison of foundation alternatives, facilitating informed decision-making. Figure 3 illustrates the logical assessment model structure, demonstrating the clear

relationship between evaluation criteria and decision outcomes. To ensure consistency in the evaluation process and minimise subjectivity, a scoring rubric is utilised to assign values to each criterion. Table 1 defines the guiding principles for assigning a Low (1), Moderate (3), or High (5) suitability score across the key assessment categories.

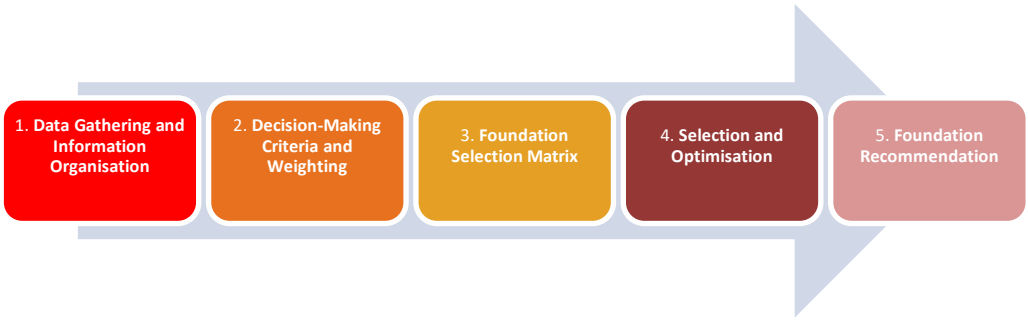


Fig. 3. Logical assessment process for foundation recommendation

Table 1. Scoring Rubric for Foundation Suitability Assessment

Score / Suitability	Technical Suitability	Constructability	Environmental Impact	Economic Factors
1 - Low Suitability	Foundation capacity is marginal or requires significant over-design to meet safety factors; high settlement risk.	Requires specialised equipment not readily available; extensive access track construction required; significant safety hazards.	High level of ground disturbance; permanent footprint in sensitive areas; extensive remediation required.	High comparative cost (>20% above baseline); long installation duration leading to program delays.
3 - Moderate Suitability	Meets design capacity with standard safety factors; acceptable settlement within tolerances.	Standard equipment is required, but there are some logistical constraints; moderate access upgrades are needed.	Moderate ground disturbance; temporary impact on flora/fauna; standard rehabilitation measures sufficient.	Average comparative cost; installation time aligns with standard program allowances.
5 - High Suitability	Exceeds capacity requirements; negligible settlement risk; robust performance in variable ground.	Uses standard, readily available equipment; minimal or no access track upgrades required; safe and rapid installation.	Minimal ground disturbance; negligible ecological footprint; no significant remediation required.	Low comparative cost; rapid installation significantly accelerates project schedule.

The assessment process typically evaluates the following foundation types for transmission towers:

1. Concrete pad and chimney foundations;
2. Rock-socketed foundations;
3. Driven steel piles (open-ended and closed-ended);
4. Bored cast-in-place piles;
5. Micropiles and minipiles;
6. Ground anchors and helical piles;
7. Precast concrete foundations.

 © Deep Foundations Institute 2026

Each foundation type is assessed against the established criteria, with the highest-scoring option selected as the preferred solution. In cases where multiple options achieve similar scores, additional factors such as contractor experience and equipment availability may influence the final selection. A hypothetical case example based on the Logical Assessment Model for Foundation Selection is presented in Appendix A.

Impact of Ground Investigation on Foundation Construction

The implementation of the ID method on a major transmission line project demonstrates significant benefits in terms of construction efficiency and cost-effectiveness. Comprehensive ground investigation data enabled precise matching of foundation types to ground conditions, resulting in:

1. Reduced Risk of Foundation Failure: By accurately characterising subsurface conditions, foundation designs are optimised to address specific geotechnical hazards, reducing the risk of settlement or failure, which can significantly reduce design uncertainties and associated contingency costs.
2. Optimised Design and Cost Efficiency: Robust geotechnical investigations are pivotal for catalysing optimised foundation design, translating directly into material savings and enhanced overall cost-effectiveness. Accurate site characterisation enables a departure from overly conservative designs, thereby mitigating the financial burden of unnecessary materials and potential delays due to unforeseen ground conditions. Several studies emphasise that quantifying the value of geotechnical information, particularly through reliability-based design, directly links investigation efforts to reduced construction costs and optimised foundation dimensions (Arsyad et al., 2009; Ching and Phoon, 2012; Purdy et al., 2022).
3. Improved Construction Planning: Understanding soil and rock conditions, facilitated by robust geotechnical investigations, is crucial for more effective planning of the construction process. This includes the appropriate selection of equipment and anticipation of potential challenges or risks associated with subsurface conditions. Effective planning and geotechnical risk management contribute to avoiding significant project delays caused by unforeseen ground conditions, thereby resulting in a considerable reduction in construction time compared to outcomes where inadequate investigations occur. This demonstrates a clear relationship between managing geotechnical risk and enhancing construction (AASHTO, 2022; Clayton, 2001; Duthy and Juett, 2020; ICE, 2016; Thompson et al., 2009).
4. Environmental Impact Reduction: Tailored foundation solutions, selected based on specific site conditions and environmental constraints, can minimise site disturbance and reduce the ecological footprint of construction activities. Particular examples include the selection of micropile foundations in environmentally sensitive areas where access is limited, allowing for construction methods that reduce clearing requirements compared to conventional foundations, which often require more extensive access preparation (Alsanabani et al., 2023; ICE, 2016; Kandaris et al., 2018; Thompson et al., 2009).

DISCUSSION

Tailoring Foundation Selection: Balancing Constraints and Opportunities

The research demonstrates that selecting a practical foundation for transmission line towers requires consideration of multiple interdependent factors beyond traditional bearing capacity calculations. The systematic approach presented in this paper addresses this complexity by integrating geotechnical, logistical, and environmental concerns into a unified decision-making framework.

A key finding from the implementation of the ID method is the importance of early engagement with geotechnical investigation. As noted by numerous researchers, early identification of ground-related risks allows for proactive management strategies that can significantly reduce project costs and improve outcomes such as public safety, project schedules, and performance (AASHTO, 2022; Clayton, 2001; Duthy and Juett, 2020; Purdy et al., 2022). This was particularly evident in areas with challenging ground conditions, where preliminary investigation identified potential issues that could be addressed through foundation design modifications.

The research also highlights the value of tailored foundation solutions for transmission line projects. Traditional approaches often rely on standardised foundation designs applied across entire project corridors, resulting in inefficiencies where ground conditions vary significantly. By contrast, the ID method enables foundation types to be matched precisely to local conditions, optimising both technical performance and construction efficiency.

Comparison with Traditional Approaches

The methodology presented in this paper differs from traditional approaches to foundation selection in several key aspects:

1. **Integration of Multiple Criteria**: While conventional methods typically prioritise technical factors such as bearing capacity and settlement, the ID method explicitly incorporates constructability, environmental impact, and economic considerations into the decision-making process.
2. **Progressive Refinement**: The multi-phase investigation approach enables the progressive refinement of geological models and foundation recommendations, thereby reducing unnecessary investigation costs while ensuring sufficient data for informed decision-making.
3. **Systematic Evaluation**: The logical assessment model provides a structured framework for comparing foundation alternatives, ensuring consistent evaluation and transparent decision-making.

A comparative analysis with projects using traditional foundation selection approaches reveals significant advantages of the ID method, which is considered superior for managing geotechnical uncertainty and risk in long linear infrastructure, such as transmission lines (Duthy and Juett, 2020). Conventional geotechnical investigations, particularly limited ones, can lead to unforeseen ground conditions and significant cost impacts and delays, such as the estimated direct cost exceeding AUD$20,000 per footing location for aborted work and overall project cost increases of 10% or more due to inadequate investigation (Duthy and Juett, 2020; Hytiris et al., 2014; Purdy et al., 2022). By contrast, the implementation of the ID method, as demonstrated in this paper, accurately identifies ground conditions, significantly reducing the likelihood of unexpected situations. As a result, significant savings in construction costs and delays can be achieved by proactively managing geotechnical risks.

Limitations and Future Research

While the methodology has demonstrated significant benefits, several limitations and areas for future research have been identified:

1. **Data Integration Challenges**: Considering that the ID method is a relatively new technology, limited site investigations have utilised this method around the world and hence, limited data sets are available. The integration of diverse data types, including geological, environmental, and logistical data, presents challenges in developing comprehensive evaluation models. Future research could explore improved data integration techniques, potentially incorporating machine learning approaches for pattern recognition in complex datasets (Huang et al., 2026, 2025b, 2025c, 2025d).
2. **Quantification of Environmental Impacts**: Current methods for assessing the environmental impacts of foundation construction primarily rely on qualitative assessments. Development of more robust quantification methods would enhance the evaluation framework.
3. **Long-term Performance Monitoring**: Long-term studies of foundation performance would provide valuable validation of the selection methodology. Establishing a monitoring programme for selected tower foundations could generate data to refine and improve the selection process.
4. **Application to Other Infrastructure Types**: Although developed for transmission line projects, the methodology can potentially be adapted for other linear infrastructure projects, such as pipelines, bridges, and tunnels. Research into such adaptations represents a promising direction for future work.

5. **Refinement of ID Parameter Correlations:** Further research is warranted to develop more refined and site-specific correlations between the recorded ID parameters and the key engineering properties of various soil and rock types. Establishing a robust library of these correlations, validated across diverse geological settings, could potentially reduce the reliance on the current benchmark of conventional geotechnical testing for calibration, leading to further cost and time efficiencies in the site investigation phase.

CONCLUSION

This paper presents a comprehensive methodology for selecting suitable foundation systems for transmission line structures in remote and geologically diverse terrains. The ID method provides a systematic framework for integrating detailed geotechnical investigations with practical construction considerations, enabling optimised foundation solutions that balance technical requirements with logistical constraints and environmental responsibilities.

Key findings from the research include:
1. The critical importance of early and comprehensive ground investigation in optimising foundation design and construction.
2. The value of a structured decision-making framework that incorporates multiple evaluation criteria.
3. The significant benefits of tailored foundation solutions in projects with variable ground conditions.
4. The potential for substantial cost and time savings through systematic foundation selection.

Implementation of the methodology on major transmission line projects demonstrates tangible benefits, including reduced material costs, improved construction efficiency, and minimised environmental impact. These outcomes support the proposition that a systematic approach to foundation selection can significantly enhance project delivery in challenging environments.

Future research will focus on refining the methodology, including the improved quantification of environmental impacts, the integration of digital technologies for data management, and the adaptation of the framework for other infrastructure applications. Long-term monitoring of foundation performance will provide valuable data to validate and enhance the selection process, contributing to improved industry practices in foundation engineering.

APPENDIX A - A HYPOTHETICAL CASE EXAMPLE BASED ON THE PROPOSED LOGICAL ASSESSMENT MODEL FOR FOUNDATION SELECTION

The evaluation involves scoring potential foundation options against a defined set of parameters to quantify their suitability. Scores are assigned using a numerical scale, such as the pre-defined scale (e.g., 1 - low suitability, 5 - high suitability). The parameters assessed against site-specific conditions typically include geotechnical suitability (e.g., bearing capacity, settlement potential), installation feasibility (considering equipment requirements and access constraints), environmental impact (e.g., footprint size, ground disturbance), material and logistics considerations (e.g., concrete requirements, transportation), construction time and seasonal constraints, and long-term performance and maintenance requirements. The specific score assigned for each parameter reflects an evaluation of how well a particular foundation type aligns with the site's specific characteristics, the project's constraints, and the weighted priorities, based on predefined rankings and engineering judgment.

Hypothetical Case Example: Foundation Selection for a Transmission Line Tower.

Project: Construction of a new transmission line traversing a remote mountainous region.

Site: Tower Location #123 - Situated on a steep slope with limited access for large construction equipment. Nearby presence of a stream with sensitive ecological features.

Step 1: Data Gathering and Information Organisation

- **Project Data:** Tower load requirements (wind, groundwater, seismic), as well as environmental restrictions near the stream.
- **Geotechnical Data:** ID boring indicate layered soil conditions with competent rock at depth.
- **Site Classification:** Steep slope, limited access, environmentally sensitive area.

Step 2: Decision-Making Criteria and Weighting

- **Economic Factors (Weighting: 0.2):** Initial construction cost and the potential for additional environmental mitigation measures.
- **Engineering Considerations (Weighting: 0.4):** Foundation capacity to support tower loads, taking into account the slope.
- **Environmental Impact (Weighting: 0.3):** Minimising disturbance to the stream ecosystem.
- **Construction Feasibility (Weighting: 0.1):** Equipment access limitations and suitability of foundation types for remote construction methods.

Step 3: Foundation Selection Matrix

An example of a foundation selection matrix is presented in Table A1.

Table A1. Foundation selection matrix example.

Foundation Type	Economic Factors	Engineering Considerations	Environmental Impact	Construction Feasibility
Concrete Bored Piers	Moderate	High	Moderate	Difficult (requires access upgrades)
Mass Footing with Micropiles	Low	High	High	Moderate (limited access challenges)
Helical Screw Piles	Low	Moderate	High	Easy (minimal access needs)

Step 4: Selection and Optimisation

- **Evaluation:** Each foundation type is assessed against each criterion, with scores assigned based on a pre-defined scale (e.g., 1 - low suitability, 5 - high suitability).
- **Weighted Scoring:** Scores are multiplied by their corresponding weightings.
- **Sum of Weighted Scores:** Scores for each foundation type across all criteria are summed. A calculation example is provided in Table A2.
- **Sensitivity Analysis:** The model is run with slight variations in weighting or scores to assess if the preferred option remains the same.
- **Engineer's Judgment:** Based on the analysis, Helical Screw Piles appear most favourable. However, the engineer considers the potential impact of unforeseen subsurface conditions on screw pile capacity.

Table A2. Calculation example (assuming scores)

Foundation Type	Economic Factors	Engineering Considerations	Environmental Impact	Construction Feasibility	Weighted Score
Concrete Bored Piers	3 (Moderate)	5 (High)	3 (Moderate)	1 (Difficult)	(0.2 * 3) + (0.4 * 5) + (0.3 * 3) + (0.1 * 1) = 4.1
Mass Footing with Micropiles	1 (Low)	5 (High)	4 (High)	3 (Moderate)	(0.2 * 1) + (0.4 * 5) + (0.3 * 4) + (0.1 * 3) = 4.7
Helical Screw Piles	1 (Low)	4 (Moderate)	5 (High)	5 (Easy)	(0.2 * 1) + (0.4 * 4) + (0.3 * 5) + (0.1 * 5) = 5.1

Conclusion: Given the limited access and environmental concerns, Helical Screw Piles are the recommended foundation type for Tower Location #123. This selection prioritises environmental

responsibility and construction feasibility while ensuring adequate engineering performance. The engineer will request conducting additional subsurface investigations to confirm the suitability of screw piles for the specific ground conditions at this location.

Note: This is a hypothetical example, and the actual weighting and scoring may vary depending on the specific project requirements and site conditions.

REFERENCES

AASHTO, 2022. Manual on subsurface investigations, 2nd Edition. ed. American Association of State Highway and Transportation Officials (AASHTO), Washington, DC.

Alsanabani, N.M., Al-Gahtani, K.S., Bin Mahmoud, A.A., Aljadhai, S.I., 2023. Integrated Methods for Selecting Construction Foundation Type Based on Using a Value Engineering Principle. Sustainability 15. https://doi.org/10.3390/su15118547

Arsyad, A., Jaksa, M.B., Fenton, G.A., Kaggwa, W.S., 2009. The effect of limited site investigations on the design of pile foundations, in: Proceedings of the 17th International Conference on Soil Mechanics and Geotechnical Engineering (Volumes 1, 2, 3 and 4). pp. 2671–2674. https://doi.org/10.3233/978-1-60750-031-5-2671

AS 1289.3.3.1, 2009. Methods of testing soils for engineering purposes - Soil classification tests - Determination of the plasticity index of a soil.

AS 1289.3.4.1-2008, 2016. Methods of testing soils for engineering purposes - Soil classification tests - Determination of the linear shrinkage of a soil - Standard method.

AS 1289.3.6.1, 2009. Methods of testing soils for engineering purposes - Soil classification tests - Determination of particle size distribution of a soil - Standard method of analysis by sieving.

AS 1289.3.6.3, 2003. Methods of testing soils for engineering purposes - Soil classification tests - Determination of particle size distribution of a soil - Standard method of fine analysis using a hydrometer.

AS 1289.4.2.1, 2020. Methods of testing soils for engineering purposes - Soil chemical tests - Determination of the sulfate content of a natural soil and the sulfate content of the groundwater - Normal method.

AS 1289.4.3.1, 2021. Methods of testing soils for engineering purposes - Soil chemical tests - Determination of the pH value of a soil - Electrometric method.

AS 1289.4.4.1, 2017. Methods of testing soils for engineering purposes - Soil chemical tests - Determination of the electrical resistivity of a soil - Method for fine granular materials.

AS 1726, 2017. Geotechnical site investigations.

ASTM D420-18, 2018. Standard Guide for Site Characterization for Engineering Design and Construction Purposes. https://doi.org/10.1520/D0420_D0420M-18

ASTM D4318-17e1, 2017. Standard Test Methods for Liquid Limit, Plastic Limit, and Plasticity Index of Soils. https://doi.org/10.1520/D4318-17E01

BS 5930, 2015. Code of practice for ground investigations.

BS EN ISO 22476-15, 2016. BSI Standards Publication Geotechnical investigation and testing - Field testing - Part 15: Measuring while drilling.

CEN. E.N. 1997-2, 2007. Eurocode 7 – Geotechnical design – Part 2: Ground investigation and testing.

Ching, J., Phoon, K.-K., 2012. Value of Geotechnical Site Investigation in Reliability-Based Design. Advances in Structural Engineering 15, 1935–1945. https://doi.org/10.1260/1369-4332.15.11.1935

Clayton, C.R.I., 2001. Managing geotechnical risk: improving productivity in UK building and construction. Thomas Telford, London.

Clayton, C.R.I., Matthews, M.C., Simons, N.E., 1995. Site Investigation, 2nd ed. Blackwell Science, London.

Duthy, M., Juett, B., 2020. Application of the Investigative Drilling Method to Renewable Energy Transmission Line Projects, in: Geotechnical Aspects of Renewable Energy. Australian Geomechanics Society – SA/NT Chapter, pp. 17–32.

 © Deep Foundations Institute 2026

Huang, F., Qin, H., Manafi, M., Juett, B., Evans, B., 2026. Machine learning approaches for automatic cleaning of investigative drilling data. Geomechanics and Geoengineering 21, 194–212. https://doi.org/10.1080/17486025.2025.2566311

Huang, F., Qin, H., Manafi, M., Juett, B., Evans, B., 2025a. Preliminary study on the potential of the investigative drilling (ID) method for quantitative site characterisation. Australian Geomechanics Journal 95–108. https://doi.org/10.56295/AGJ6034

Huang, F., Qin, H., Manafi, M., Juett, B., Evans, B., 2025b. Comprehensive evaluation of tree-based machine learning algorithms for soil classification from investigative drilling data. Machine Learning for Computational Science and Engineering 1, 45. https://doi.org/10.1007/s44379-025-00047-7

Huang, F., Qin, H., Manafi, M., Juett, B., Evans, B., 2025c. A Preliminary Study on the Correlations Between Drilling Parameters and Pile Capacities, in: The First International Conference on Measurement While Drilling (MWD'1). Deep Foundation Institute, pp. 81–90. https://doi.org/10.37308/MWD.060201

Huang, F., Qin, H., Manafi, M., Juett, B., Evans, B., 2025d. Data-Driven Rock Strength Classification from Investigative Drilling Using Machine Learning, in: 59th U.S. Rock Mechanics/Geomechanics Symposium. Santa Fe, New Mexico.

Hytiris, N., Stott, R., McInnes, K., 2014. The importance of site investigation in the construction industry: A lesson to be taught to every graduate civil and structural engineer. World Transactions on Engineering and Technology Education 12, 414–419.

ICE, 2016. Specification for Piling and Embedded Retaining Walls, Third edition. ed. Institution of Civil Engineers, London. https://doi.org/10.1680/icesperw.61576

Kandaris, P.M., Evans, A.E., Haldar, A., 2018. Guide for Transmission Line Foundations with Least Impact to Environment, in: Electrical Transmission and Substation Structures 2018. pp. 47–61. https://doi.org/10.1061/9780784481837.005

Manafi, M., 2019. Soil Plasticity Variability and Its Effect on Soil Classification. Geotechnical Testing Journal 42, 20170273. https://doi.org/10.1520/GTJ20170273

Manafi, M., Deng, A., Taheri, A., Jaksa, M.B., HB, N., 2022. Determining Soil Plasticity Utilizing Manafi Method and Apparatus. Geotechnical Testing Journal 45, 797–818. https://doi.org/10.1520/gtj20210235

Pall, G.K., Bridge, A.J., Gray, J., Skitmore, M., 2020. Causes of Delay in Power Transmission Projects: An Empirical Study. Energies (Basel) 13, 1–29. https://doi.org/10.3390/en13010017

Phoon, K.-K., Kulhawy, F.H., 2008. Serviceability limit state reliability-based design, in: Kok-Kwang Phoon (Ed.), Reliability-Based Design in Geotechnical Engineering. CRC Press, London, pp. 344–384.

Purdy, C.M., Raymond, A.J., DeJong, J.T., Kendall, A., Krage, C., Sharp, J., 2022. Life-cycle sustainability assessment of geotechnical site investigation. Canadian Geotechnical Journal 59, 863–877. https://doi.org/10.1139/cgj-2020-0523

Reiffsteck, P., Benoît, J., Bourdeau, C., Desanneaux, G., 2018. Enhancing Geotechnical Investigations Using Drilling Parameters. Journal of Geotechnical and Geoenvironmental Engineering 144, 04018006. https://doi.org/10.1061/(asce)gt.1943-5606.0001836

Thompson, F., Salisbury, N., Khattak, A., Hastings, A., Foster, M., 2009. Integration of optimum, high voltage transmission line foundations, in: Electrical Transmission and Substation Structures 2009: Technology for the Next Generation. pp. 94–105. https://doi.org/10.1061/41077(363)9

 © Deep Foundations Institute 2026

FAST-TRACK PILE DESIGN AND CONSTRUCTION FOR THE FITZROY RIVER BRIDGE REPLACEMENT

Hudson C. Moore, Project Geotechnical Engineer, CMW Geosciences, Perth, Western Australia, Australia, (08) 6555 4920, hudsonm@cmwgeo.com

ABSTRACT

The Fitzroy River Bridge replacement in Fitzroy Crossing, Western Australia, was a critical and urgent infrastructure project. It was led by Main Roads Western Australia following the destruction of the original bridge during flooding associated with ex-Tropical Cyclone Ellie in January 2023. The bridge is located on the Great Northern Highway, the only sealed road linking Western Australia and the Northern Territory, making its replacement vital to regional freight and community connectivity.

Due to the emergency nature of the project, geotechnical investigations could not be completed prior to the commencement of detailed design. To address this, historical pile dynamic probing data from 1972 was re-purposed using pile driveability back-analysis to estimate unit shaft and end bearing resistance. Although pile penetration testing (dynamic probing) is now considered obsolete, it provided a valuable basis for parameter estimation in the absence of contemporary subsurface data. The replacement structure is supported by open-ended steel tubular piles driven 30 to 40 m into the riverbed to withstand scour of up to 15 m below nominal riverbed level. Pile design and construction methods needed to consider a strict timeframe and particularly extreme loading conditions. Construction support included pile installation monitoring, soil and rock logging, and verification of pile capacities via pile driving analyzer (PDA) testing and case pile wave analysis program (CAPWAP) analysis (Pile Dynamics, Inc. 2023a, 2023b; AS 2159). This paper outlines the adaptive geotechnical strategies that enabled successful delivery of a resilient foundation under difficult time and information constraints.

Keywords: remote construction, disaster recovery, driven piles, weak rock, Fitzroy Crossing, dynamic pile load testing, shaft resistance parameters, foundation design, geotechnical engineering

INTRODUCTION

The new Fitzroy River Bridge (Fig. 1) is supported on 1200 mm diameter, 25 mm wall thickness open-ended steel tubular piles, driven, drilled out, and filled with reinforced concrete. The 270 m long bridge comprises eight spans (seven piers and two abutments), typically 35.3 m in length, with shorter 28.2 m spans at each abutment. Abutments are founded on three-pile groups perpendicular to the alignment, while piers are supported by four-pile groups in a rectangular arrangement. Piles were installed from a temporary causeway, with pile caps 2 m thick and founded at reduced level (RL) 98 m Australian height datum (AHD), approximately 1.5 m above the assumed nominal riverbed level.



Fig. 1. Completed new bridge after construction (left) and being tested by first flooding (right)

This paper presents the geotechnical approach to the design and construction of the new Fitzroy Crossing Bridge, which was delivered in under one year (from design commencement to bridge opening). It describes the adaptive strategies, monitoring, and verification processes applied during the project to help enable the fast-track outcome which was required by the project.

 © Deep Foundations Institute 2026

BACKGROUND

In January 2023, ex-Tropical Cyclone Ellie brought record-breaking rainfall and flooding to the Kimberley region of Western Australia. At Fitzroy Crossing, peak flood discharges in the Fitzroy River were estimated to exceed 60,000 m³/s, making it one of the largest recorded flood events in Australian history (Bureau of Meteorology, 2023).

The extreme river conditions caused extensive scour beneath the pier footings of the original Fitzroy River bridge and ultimately led to structural failure and the washing away of a significant portion of the substructure downstream. Figure 2 presents markup of the original as-built piles against the estimated scour levels following cyclone Ellie. This collapse resulted in the complete closure of the Great Northern Highway, the only sealed road link between Western Australia and the Northern Territory. The highway serves as a nationally significant freight corridor, routinely used by road trains transporting goods between Darwin, Broome, Perth, and inland mining regions. It also provides critical access to isolated Indigenous and remote communities throughout the Kimberley.

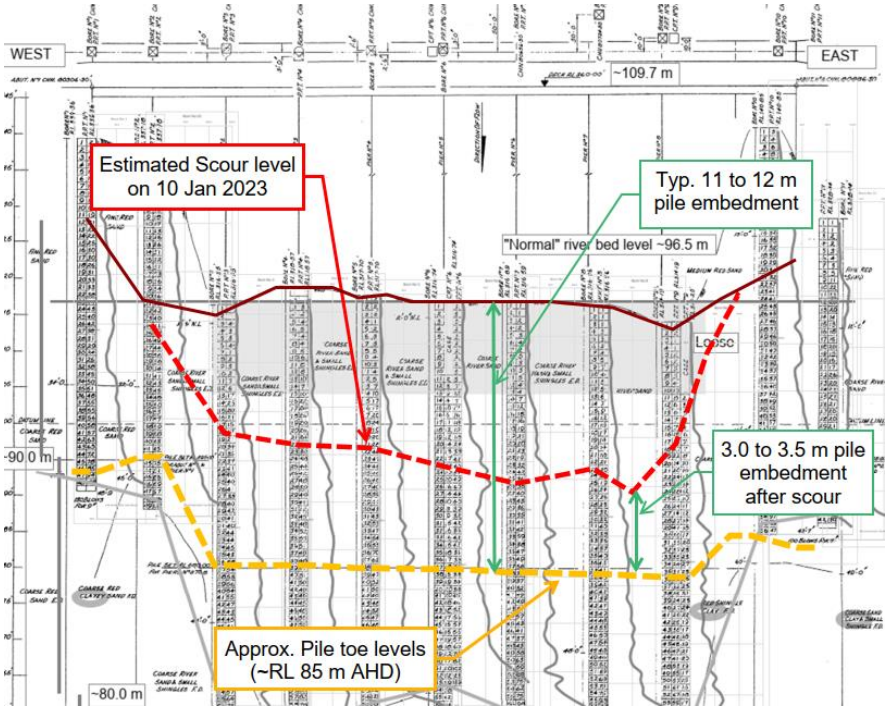


Fig. 2. Markup of original bridge pile and estimated scour levels

The loss of this crossing severed not only interstate logistics but also disrupted access to essential services, emergency response, and supply chains for several months. The strategic urgency of restoring this connection prompted an accelerated design and construction program, led by Main Roads Western Australia (MRWA).



Fig. 3. Images of flood and damaged bridge (February 2023 left and March 2023 right)

 © Deep Foundations Institute 2026

PRELIMINARY INFORMATION

The only geotechnical information available at the site was the historical section shown in Fig. 4 (with markup), which included geotechnical logs and pile penetration test results. Log descriptions were basic such as "firm grey clay" (which was inferred to be weathered bedrock) and drilling records were limited (whether it was easy/fast or slow/hard drilling was not available). The preliminary ground model used for early design was based on this limited information and interpretation of the pile penetration tests (PPTs).

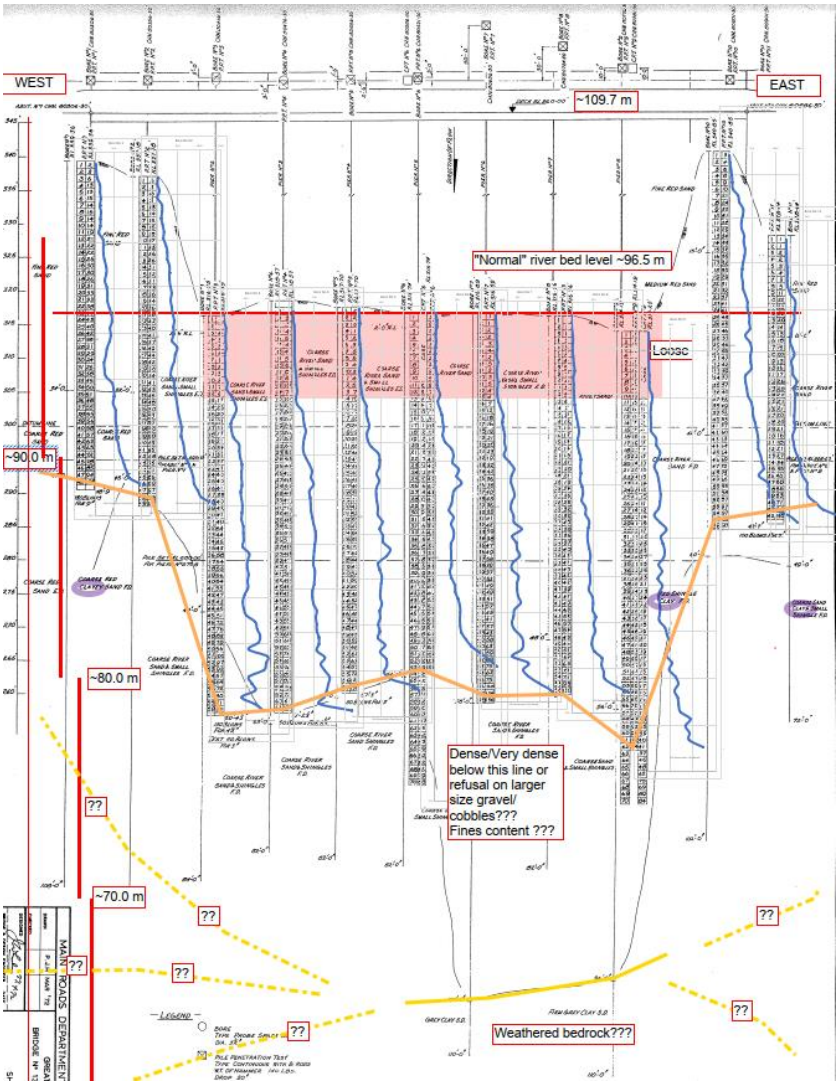


Fig. 4. Preliminary interpretive markups of historical section

PILE PARAMETER BACK ANALYSIS USING HISTORICAL DATA

Pile shaft and end bearing resistance was estimated using historic PPTs and modelled using GRLWEAP (Pile Dynamics, Inc. 2016), manually adjusting unit end and shaft resistance over depth, attempting to match the blows from PPTs by an iterative process to refine the data to match the as-built results. Figure 5 presents the back analysis with Tables 1 and 2 providing input pile parameters for the West abutment and the river channel (piers 1 to 7). The hammer energy was set to standard penetration test (SPT) energy and modelled driving a continuous 50 mm diameter steel rod (understood to be similar to the PPT setup).

 © Deep Foundations Institute 2026

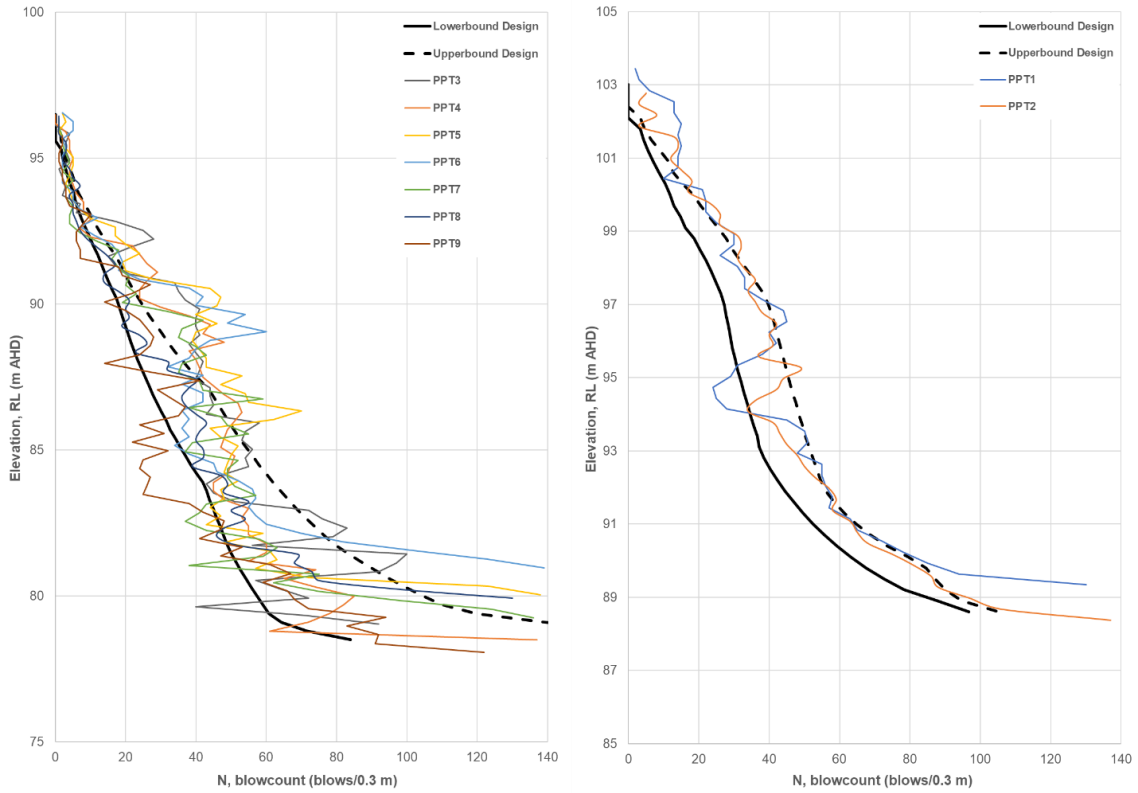


Fig. 5. Pier (left) and West abutment (right) preliminary design calibration

Table 1. River basin preliminary design profile from PPTs

Top Elevation, RL (m AHD)	Lower Unit Shaft Resistance (kPa)	Upper Unit Shaft Resistance (kPa)	Unit Toe Resistance (kPa)
96.5	1	1	0
95.9	10	10	0
91.5	20	30	1000
81.5	20	30	2000
79.5	20	30	3000
78.5	140	150	3000

Table 2. West abutment preliminary design profile from PPTs

Top Elevation, RL (m AHD)	Lower Unit Shaft Resistance (kPa)	Upper Unit Shaft Resistance (kPa)	Unit Toe Resistance (kPa)
103	12	17	0
102	20	30	0
98	12	20	1000
96	5	10	1000
93	35	40	2000
89	100	120	3000
88.5	200	200	4000

There was limited PPT information in the bedrock, but the back analysis provided very useful information in the upper 20–25 m of the riverbed and provided valuable guidance in the absence of other available information.

 © Deep Foundations Institute 2026

PILE DESIGN

Preliminary pile parameters were initially developed through back-analysis of historical pile penetration tests (PPTs) and were subsequently confirmed and refined following the geotechnical investigation. The final design was undertaken in accordance with AS2159 and AS5100.3 and also assessed against scour predictions, earthquake classification, liquefaction potential and with appropriate consideration of negative skin friction.

Following the geotechnical investigation, the pile design parameters were refined with reference to established methods to ensure reliability across the varied subsurface conditions. These included API (2011) Geotechnical and Foundation Design Considerations (referencing API, 2002), the Bustamante and Gianeselli/LCPC method (1982), and the UWA-05 (sands) and UWA-13 (clays) methods for driven piles. For rock parameters, guidance was drawn from Williams and Pells (1981), Rowe and Armitage (1984), and Randolph et al. (1998).

DRIVEABILITY ASSESSMENT / HAMMER SELECTION

A preliminary drivability assessment was undertaken using GRLWEAP 14 to evaluate the feasibility of installing 1200 mm diameter open-ended steel tubular piles. Two hammer types were modelled: the JUNTTAN HHK-16S (max energy of 235 kNm) and the larger JUNTTAN HHx350 (max energy of 350 kNm). Five design cases were assessed, covering lower-bound, upper-bound, effective stress-based, and bedrock-intercept scenarios, with a range of assumed ground profiles and soil strength parameters. The analysis estimated achievable pile lengths and refusal levels for each hammer, accounting for plugging effects and anticipated set-up. Results indicated that the HHK-16S could reach refusal above the target toe level under upper-bound conditions, whereas the HHx350 demonstrated potential to achieve design embedment in most cases. This early assessment guided hammer selection and construction methodology planning, with the recognition that assumptions would need revisiting following the geotechnical investigation and contractor engagement. Unlike axial capacity design, the adopted parameters were intentionally optimistic, representing worst-case, highest-resistance ground conditions to ensure driveability risks were adequately assessed.

PILING RISKS AND MITIGATION STRATEGIES

Given the emergency nature of the project and the need to progress design and procurement prior to completing a full ground investigation, geotechnical and construction risks required particularly careful management.

Access to the riverbed was only practical during a narrow five-month ‘dry-season’ window. See Fig. 6 for water level data collected by the department of water (DOW 2023). To avoid wet-season flooding from November to April, piling works needed to commence by May or June, requiring precise scheduling to complete critical foundation works before access was lost.

Key uncertainties at the early design stage included the absence of recent subsurface data, unknown bedrock levels and characteristics, and the potential for significant variability in soil conditions along the bridge alignment. These geotechnical unknowns were compounded by the need to predict future scour levels and assess their impact on foundation performance.

Procurement and construction planning risks also emerged due to the requirement to commit to pile sizing and hammer selection prior to investigation or finalising design. This included uncertainty regarding pile driveability, hammer energy requirements, and hazardous ground conditions (e.g., the risk of encountering obstructions such as boulders or shallow bedrock during driving).

 © Deep Foundations Institute 2026

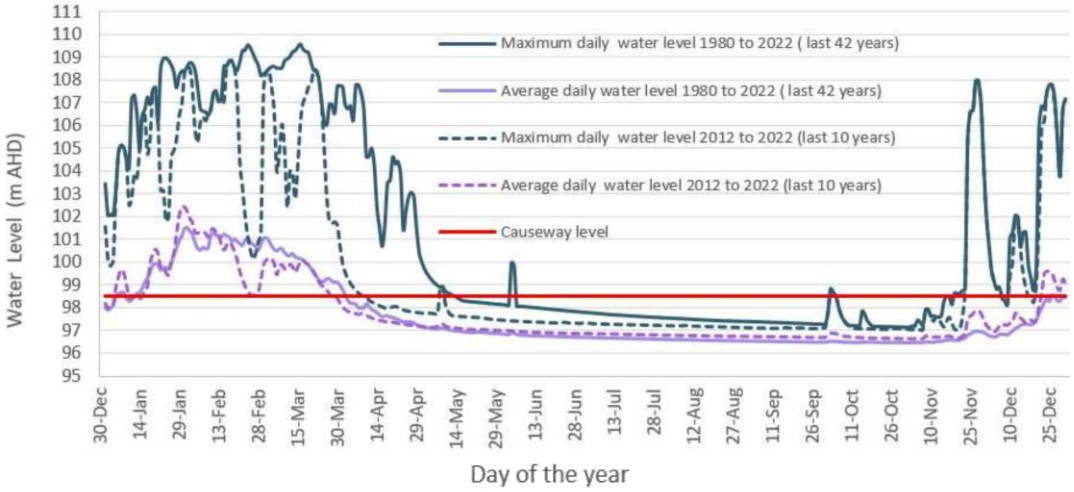


Fig. 6. Maximum and average daily recorded water levels at the bridge (BG&E Pty Ltd. 2023)

To mitigate these risks, a staged ground investigation strategy was adopted alongside a conservative preliminary design approach, allowing for longer and heavier piles, offsetting new piers from the damaged bridge, deeper potential scour, and higher geotechnical reduction factors. Construction-related risks were addressed by specifying robust pile materials, recommending contractors with appropriate experience and equipment (including high-energy hammers and drilling capability), and ensuring full-time geotechnical oversight during pile installation. These measures were essential in managing uncertainty and maintaining progress on a nationally significant infrastructure project with a compressed delivery timeline.

GEOTECHNICAL INVESTIGATION

The geotechnical investigation comprised eleven machine-drilled boreholes (BH01–BH11) to depths of 42.5–59.0 m, using sonic drilling in the unconsolidated alluvium for high recovery, transitioning to HQ3 diamond coring in competent siltstone bedrock. Standard Penetration Tests (SPTs) were generally conducted at 1.5 m intervals in soils and upper bedrock, ceasing after three SPT refusals in rock, with boreholes terminating after at least 10 m of competent bedrock was penetrated. Eight CPTs (8.7–29.7 m depth) and one seismic CPT with shear wave velocity profiling were completed, with full-depth pore pressure measurements. Laboratory testing included particle size distribution (PSD), Atterberg limits, soil aggressivity, UU triaxial tests, and UCS testing (Standards Australia 2014, 2016, 2017c, 2020). UCS values in the upper bedrock generally range from 2.5–5 MPa ('low strength' per AS1726). Limited access to the river basin and east abutment restricted early CPT coverage; however, opportunistic investigation from the riverbed during early construction of the temporary low-level crossing to the north provided valuable characterisation of channel materials. See Addendum A1 for geotechnical investigation plan.

GROUND MODEL

Subsurface conditions comprise fill, alluvial sediments and siltstone bedrock. Fill includes compacted sands and clays at the former bridge approaches and coarse causeway materials with cobbles and boulders in the river channel. Beneath this, alluvial silts, clays and sandy units transition into granular sands and gravels of the Fitzroy River basin, increasing in size and density with depth. Large cobbles and boulders are locally present, particularly near a suspected paleochannel between Piers 4 and 5.

Bedrock consists of horizontally laminated siltstone with strength increasing at depth and thickness exceeding 20 m, overlain by a thin layer (nominally 0.5 to 1.5 m thick) of weathered residual soil.

Groundwater levels correspond to river levels, ranging from about RL 96.5 m AHD at the end of the dry season to RL 110 m AHD during extreme wet season floods. Addendum A2 depicts a geotechnical section.

SCOUR ASSESSMENT

Scour depth estimates were developed using the method proposed by Annandale (2006) for non-cemented granular soils, which relates critical stream power to soil density and particle size (D_{85}). Design stream power data for the ultimate limit state (ULS) event were provided by the waterways Engineer and compared against upper and lower bound critical thresholds. PSD testing and visual assessment of borehole samples from the investigation indicated that D_{85} values for the alluvial sands and gravels between RL 81.5 and RL 85 m AHD were generally at or above the required 20–25 mm threshold. Increasing grain size with depth, observed across boreholes, supports the expectation that winnowing of finer sediments would result in a coarser riverbed surface as scour progresses.

The following general scour cases were adopted for foundation design under the ULS flood event:
1. No scour: RL 96.5 m AHD (existing riverbed level) – presented in Fig. 7 (for pier 4)
2. Moderate scour: RL 91.5 m AHD
3. Maximum design scour: RL 81.5 m AHD – presented in Fig. 7

These scenarios were considered in both axial and lateral pile design to assess structural performance across a range of embedment conditions. This assessment showed that the ultimate limit state (ULS) loads reduced as the riverbed scours out. This is due to a reduction in flow velocity from an increased river channel cross-sectional area. For example, the ULS compression for the no scour case was 8650 kN, whereas for maximum design scour it dropped to 5800 kN.

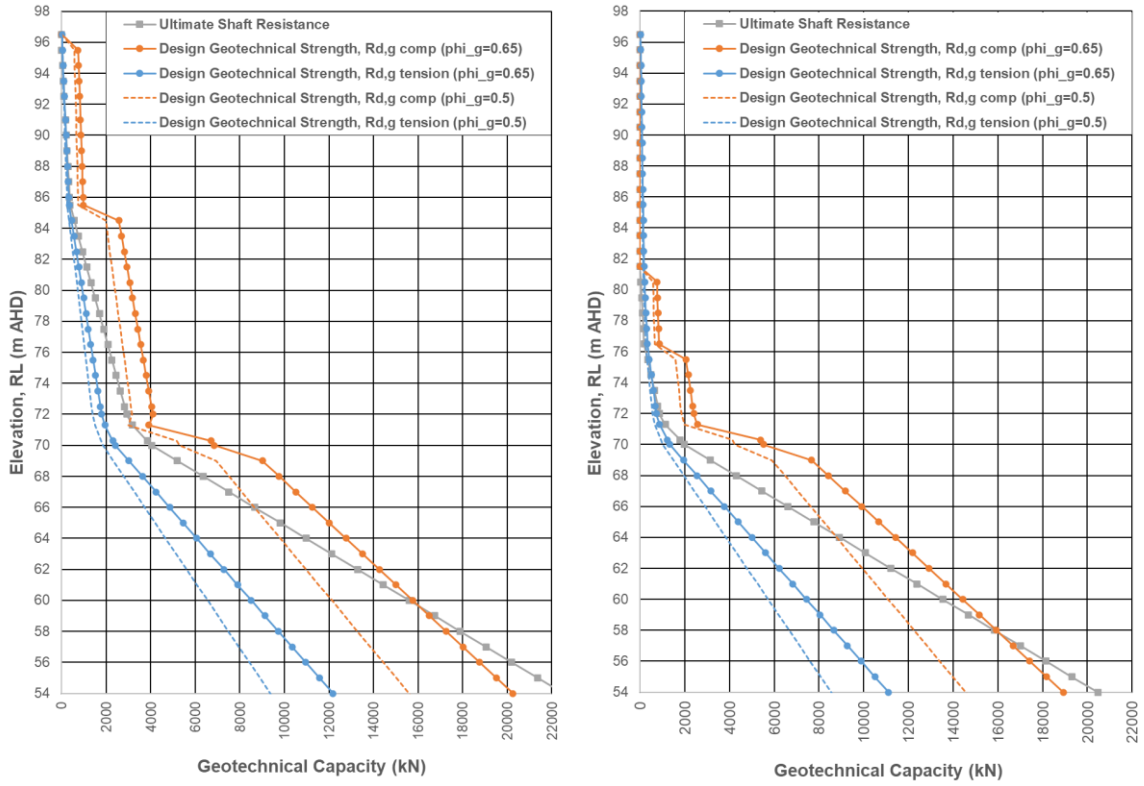


Fig. 7. Design axial capacity for case 1: no scour (left), and case 3: maximum design scour (right)

 © Deep Foundations Institute 2026

CONSTRUCTION PILE INSTALLATION MONITORING

As the Junttan HHx350 was the first commissioned hammer of its type, minor issues arose during the early stages, such as an initial failure to record blow counts on pile A1-1. This was quickly resolved, and subsequent piles were monitored with full electronic records of hammer energy and blow counts per 250 mm. This data was used to generate performance graphs, providing insight into hammer behaviour and variability in driving conditions across the site, as presented in Addendum A3 and A4. The records indicate driving conditions that are within typical ranges for natural variability of soils and rock. Zones of loose and dense material were readily identifiable, supported by spoil logging undertaken to further verify subsurface conditions. Monitoring also included key stages of piling such as casing splicing, cleaning, base checks, cage installation and concreting via tremie. A vibratory hammer (PVM40) was also employed for efficient casing installation, particularly during pitching and when advancing through alluvial deposits. At least one pile per pier or abutment was subject to formal pile testing with CAPWAP interpretation to confirm performance against design requirements.

PILE TESTING

Where feasible, both end-of-drive (EOD) and re-strike tests (RST) were carried out, with restrikes scheduled as late as possible in the construction sequence to evaluate pile 'setup'. The observed pile setup likely arises from the dissipation of excess pore pressures in the fine-grained sands, clays and siltstone bedrock whilst soil recovery and stress arching are likely to explain the pile setup in coarser grained materials. Unit Shaft resistance drawn from all pile tests throughout the project is presented Fig. 8.

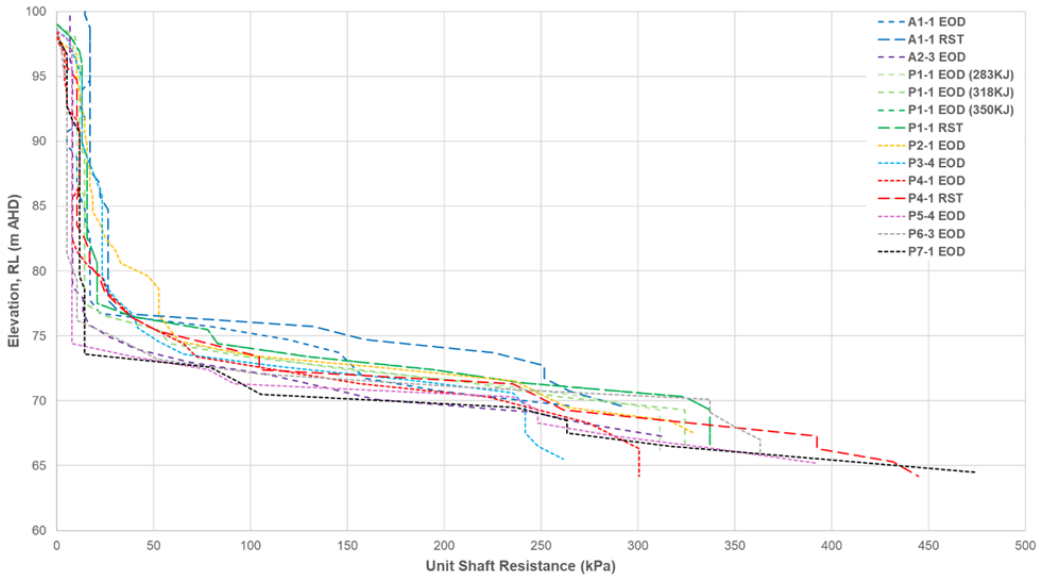


Fig. 8. Unit shaft resistance on casings from all pile tests

Following an unseasonal flood-related delay to piling works, as discussed by Toleman (2025), an opportunity for a restrike test (RST) was performed on pile P4-01 approximately 30 days after EOD. This provided valuable insight into the potential longer-term setup effects, with general increases observed across all strata: averages of 25% in the very loose sands (RL 96–80 m), 15–20% in the medium dense to dense sands and gravels (RL 80–70 m), and around 35% in the siltstone (RL 68–64 m), as shown in Fig. 9. Gravels and coarse sands from RL 92 to RL 86 and RL 79 to RL 75 showed no setup. Given the extended interval between driving and testing compared with earlier restrikes, these results are considered a more reliable indication of long-term pile capacity.

While shaft friction provided the primary component of axial capacity, end bearing was essential to satisfy Ultimate Limit State (ULS) design requirements. High-strain dynamic testing (with CAPWAP

 © Deep Foundations Institute 2026

interpretation) indicated that the 1200 mm diameter piles typically achieved a nominal end bearing capacity of 5 MN, corresponding to a unit resistance of approximately 4.5 MPa under a plugged base assumption.

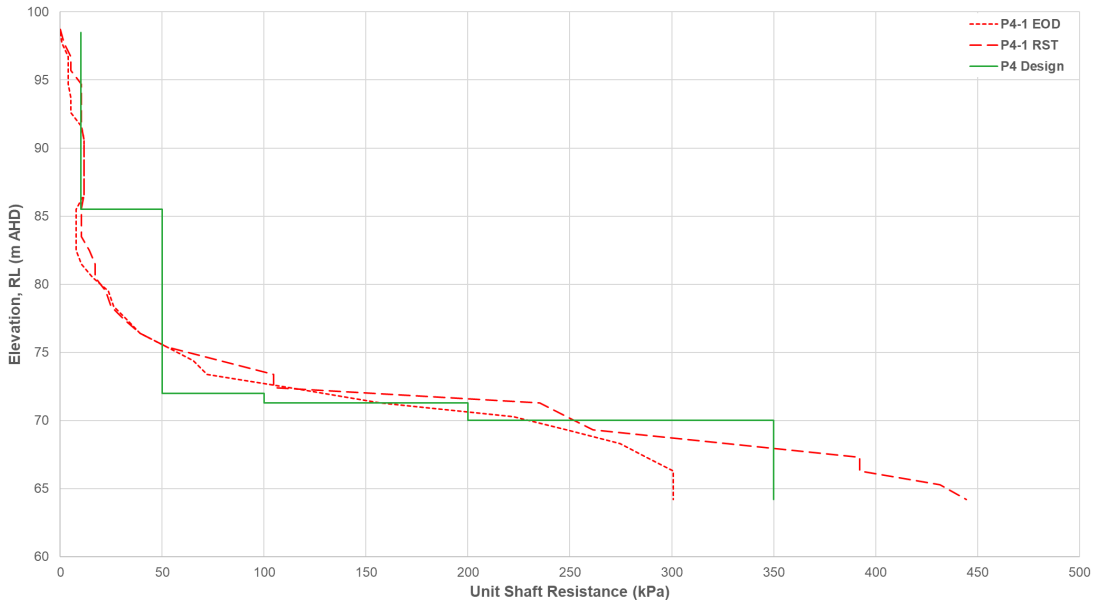


Fig. 9. Unit shaft resistance (adhesion) comparison between pier 4 design and pile testing

Pile testing further indicated that the design likely overestimated adhesion in the alluvial deposits between RL 86 and RL 80 and underestimated adhesion in the residual soils and siltstone bedrock, but overall ultimate design axial capacities were found to align closely with those derived from testing.

Testing, together with site observations, verified that installed piles satisfied design requirements. Scoured capacities were also assessed using CAPWAP-derived data and checked against design loads, with shaft resistance above the scour level omitted and a 50% reduction applied to the 5 m of soil immediately below the scour level to account for the reduced vertical effective stresses.

PILE APPROVAL PROCESS

Acceptance of installed piles involved confirming compliance with the geotechnical design, supported by field observations and construction records. The process generally included:

1. Minimum Toe Level – Confirming each pile achieves the specified embedment depth into the founding stratum, referenced to design elevations.
2. Axial Capacity – Verifying via dynamic load testing (e.g., End of Drive PDA with CAPWAP) on a representative pile that ultimate capacities meet or exceed design requirements for all scour scenarios, applying the specified geotechnical reduction factor.
3. Group Assessment – Ensuring untested piles achieve a more onerous drive set under similar hammer energy to the tested pile.
4. Subsurface Logging – Recording and comparing material descriptions and layer depths during driving/drill-out against the design ground model, noting any variability.
5. Pile Cleanliness – Cleaning base and inside of casing observed to ensure a dry, debris-free condition before concreting.
6. Construction Records Review – Reviewing driving logs, set measurements, welding, drill-out depths, grout plug placement, reinforcement installation and pour method.

Piles meeting embedment, capacity, cleanliness, and ground condition requirements were certified as acceptable in accordance with the geotechnical design.

 © Deep Foundations Institute 2026

CONCLUSION

The development of the geotechnical design relied on prompt review of limited historical records and informed qualitative judgments of the subsurface profile and parameters to guide early design choices. These preliminary assessments were later validated through investigation to satisfy industry standards and client assurance requirements, enabling compliance without disrupting the compressed construction program. Preliminary design relied on historic ground models, requiring conservative robust assumptions. The drivability back-analysis proved valuable for cross-checking early interpretations and assumptions. Driveability assessments also demonstrated the benefit of selecting the larger commercially available hammer to reduce the risks associated with embedment or load testing issues and avoided the requirement of forming rock sockets if premature refusal occurred. During construction, efficient pile acceptance relied on accurate on-site set measurements, backup driving records, and early load testing. Challenges included limited hammer energy control for correlation across pile tests, delays from pile splicing, and the need to minimise time between drilling out and concreting to prevent toe softening, which was mitigated by grout plugs. Overall, robust planning, appropriately conservative design, and adaptable site practices were key to managing unforeseen conditions and meeting tight piling timelines. Scour cases did not govern the final design due to lighter loading from the increased channel area and reduced flow velocities. However, a rigorous assessment remained crucial, as undermining of the central pier piles was the primary failure mechanism of the original bridge.

Despite all of the challenges, the bridge opened to traffic in December 2023, six months ahead of schedule. This project went on to win the national Engineers Australia's "Project of the Year" award in 2024 for standing as a remarkable example of engineering achievement.

ACKNOWLEDGEMENTS

The author would like to acknowledge the following parties, whose support and collaboration was key to the project's success: The people of the Fitzroy Valley Region
Main Roads WA – owner participant
BG&E – lead design engineer (structural, civil and waterways)
CMW Geosciences – geotechnical engineer: especially big thanks to Andrew Websper and Marc Woodward
BMD and Georgiou – main contractors
Brady Marine and Civil and GFWA – piling contractors
The author used Google Gemini to assist with reference formatting and language refinement

REFERENCES

Annandale, G.W., 2006. Scour technology: Mechanics and engineering practice. McGraw-Hill, New York, 292 p.

API, 2011. Geotechnical and Foundation Design Considerations. American Petroleum Institute, Washington, DC.

Australian Government Department of Infrastructure, 2023. Critical freight routes in northern Australia. https://www.infrastructure.gov.au. Accessed 15-07-25.

BG&E Pty Ltd. 2023. Fitzroy bridge replacement - IFC waterways assessment. Technical Report No. FBA1-WW-100-REP-01_0, prepared for Main Roads Western Australia, Perth, WA.

Bureau of Meteorology, 2023. Special climate statement: Record flooding in the Kimberley region. Australian Government, https://www.bom.gov.au. accessed 15-07-25.

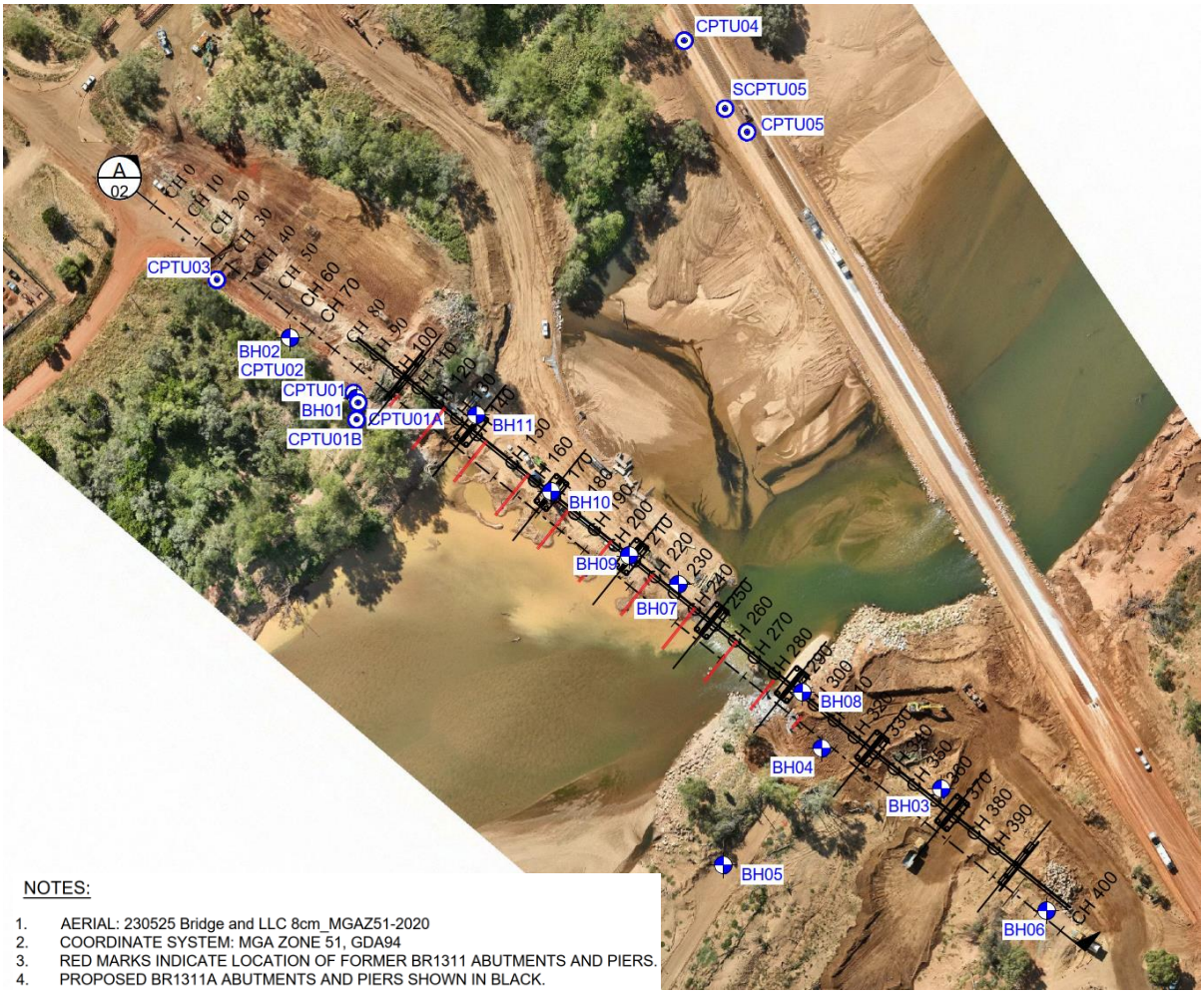
Bustamante, M., and Gianeselli, L., 1982. LCPC method for pile capacity estimation using CPT data. Laboratoire Central des Ponts et Chaussées, Paris.

Department of Water (DOW). 2023. Water information reporting portal. https://www.water.wa.gov.au. Accessed 01-02-23.

 © Deep Foundations Institute 2026

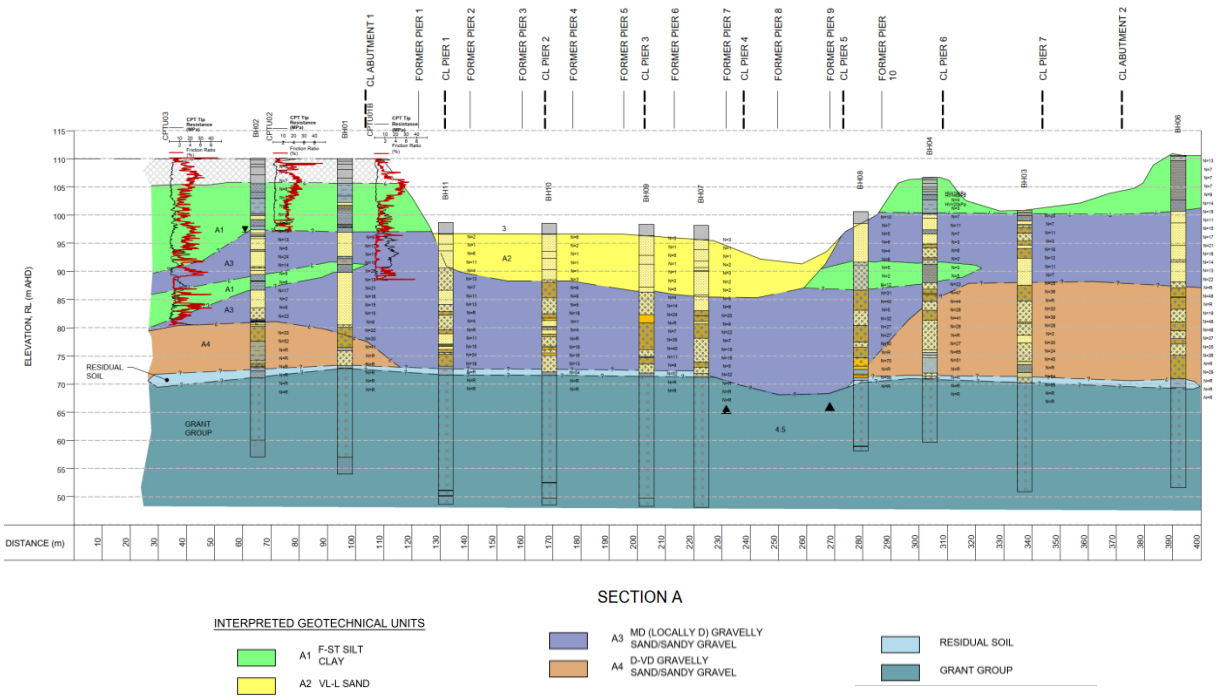
Lehane, B., Schneider, J., and Xu, X., 2005. The UWA-05 Method for Prediction of Axial Capacity of Driven Piles in Sand. In: M. J. Cassidy & S. Gourvenec (eds), Proceedings of the International Symposium on Frontiers in Offshore Geotechnics, Perth, CRC Press, pp. 683–689.
Lehane, B.M., Douglass, C., Gaudin, C., & Randolph, M.F., 2022. UWA-13 Method for Predicting the Axial Capacity of Driven Piles in Clay. University of Western Australia, Crawley, WA.
Main Roads Western Australia, 2023. Fitzroy River Bridge replacement project overview. https://www.mainroads.wa.gov.au. Accessed 15-07-25.
Pile Dynamics, Inc., 2016. GRLWEAP® Wave Equation Analysis Program – User Manual. Pile Dynamics, Inc., Cleveland, Ohio.
Pile Dynamics, Inc. (2023). Pile Driving Analyzer® (PDA) User Manual. Pile Dynamics, Inc., Cleveland, Ohio.
Pile Dynamics, Inc. (2023). CAPWAP® Wave Equation Analysis Program – User Manual. Pile Dynamics, Inc., Cleveland, Ohio.
Rowe, R. K., and Armitage, H. H., 1984. The Design of Piles Socketed Into Weak Rock (Geotechnical Research Report). Faculty of Engineering Science, University of Western Ontario, London, Ontario.
Randolph, M.F., Houlsby, G.T., and Pile-Group Team. 1998. Rock socket design parameters for pile foundations. Geotechnical Research Report G1329, Department of Civil Engineering, University of Western Australia, Crawley, WA.
Standards Australia. 2009. Piling – Design and installation. AS 2159:2009. Sydney, NSW.
Standards Australia. 2014. Methods of testing soils for engineering purposes, Method 3.1.1: Soil classification tests—Determination of the liquid limit of a soil—Casagrande method. AS 1289.3.1.1:2009. Sydney, NSW.
Standards Australia. 2016. Methods of testing soils for engineering purposes, Method 6.4.1: Soil strength and consolidation tests—Determination of the compressive strength of a specimen tested in undrained triaxial compression without measurement of pore water pressure. AS 1289.6.4.1:2016. Sydney, NSW.
Standards Australia. 2017a. Bridge design – Foundations and soil-supporting structures. AS 5100.3:2017. Sydney, NSW.
Standards Australia. 2017b. Geotechnical site investigations. AS 1726:2017. Sydney, NSW.
Standards Australia. 2017c. Methods of testing soils for engineering purposes, Method 6.1.1: Soil strength and consolidation tests—Determination of the California Bearing Ratio of a soil. AS 1289.6.1.1:2014. Sydney, NSW.
Standards Australia. 2020. Methods of testing soils for engineering purposes, Method 6.1.2: Determination of the unconfined compressive strength of a cohesive soil—Standard method. AS 1289.6.1.2:1998. Sydney, NSW.
Toleman, M. (2025). Reconnecting the North: The New Fitzroy River Bridge Project. Proceedings of the Austroads Bridge Conference 2025, Brisbane, 25–27 June 2025.
Williams, A. F., and Pells, P. J. N., 1981. Side Resistance of Rock Sockets in Sandstone, Mudstone, and Shale. Canadian Geotechnical Journal, 18(4), 502–513.

ADDENDUM A1. GEOTECHNICAL INVESTIGATION PLAN

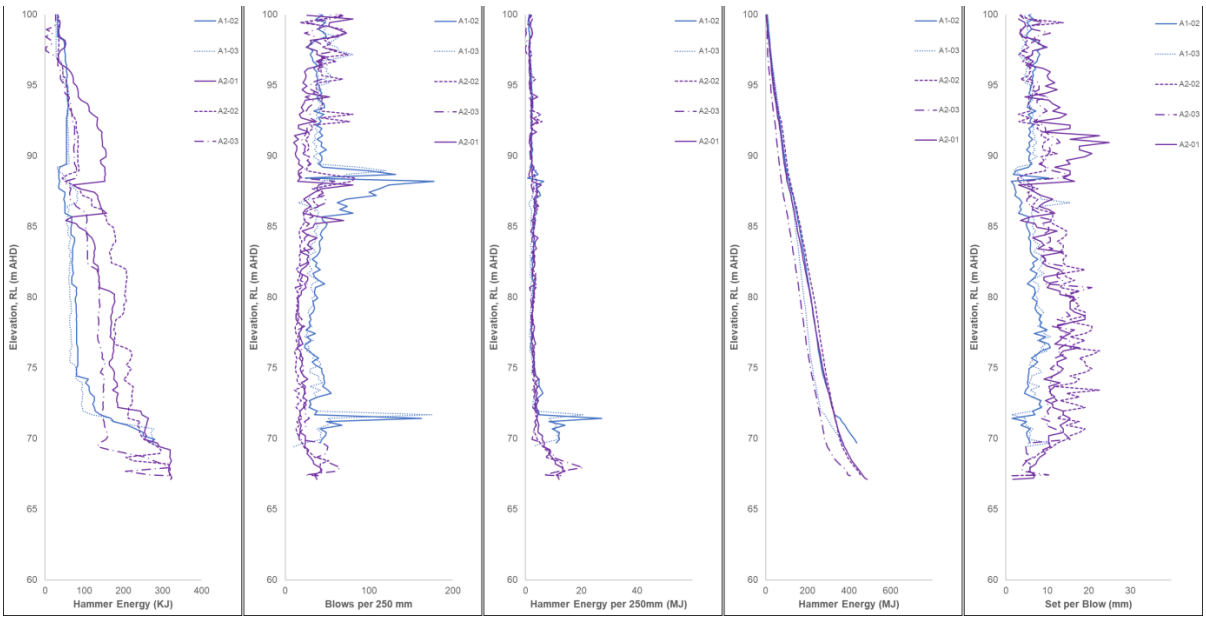


 © Deep Foundations Institute 2026

ADDENDUM A2. GEOTECHNICAL SECTION ALONG BRIDGE ALIGNMENT

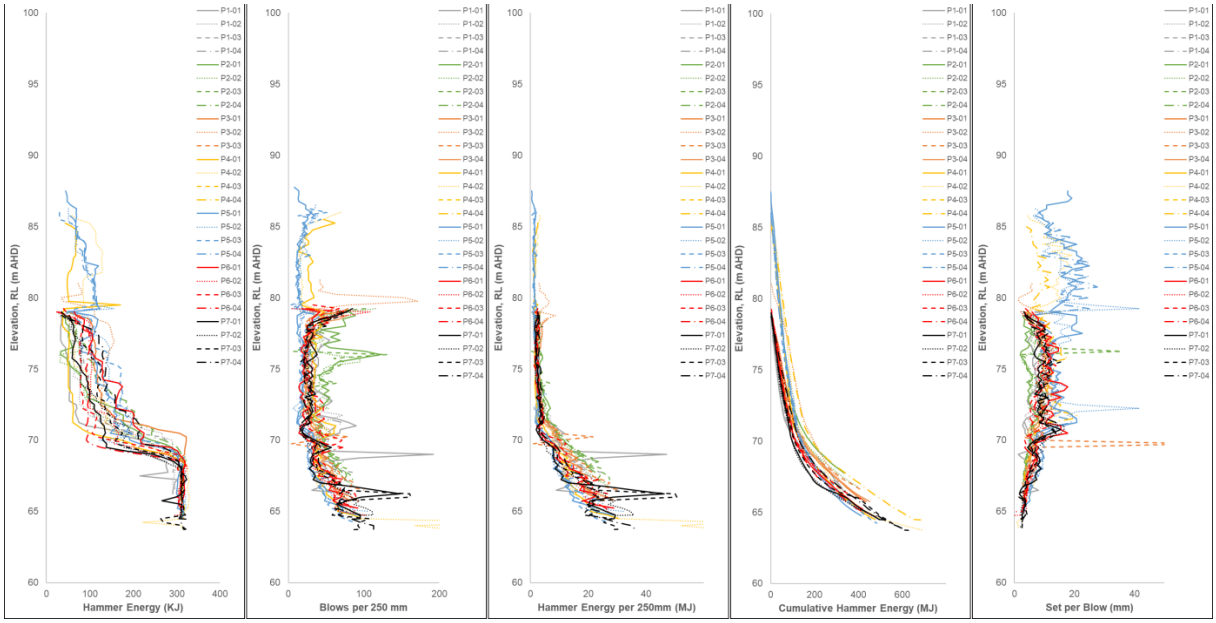


ADDENDUM A3. PILE DRIVING RECORDS FOR ABUTMENTS



 © Deep Foundations Institute 2026

ADDENDUM A4. PILE DRIVING RECORDS FOR PIERS (FROM START OF IMPACT DRIVING)



 © Deep Foundations Institute 2026

AUTOMATION IN GEOTECHNICAL ENGINEERING: AI-ENABLED FOUNDATION DESIGN WORKFLOW

WaiLeung Ng, Tetra Tech Coffey, Melbourne, Australia, +61 392907120, waileung.ng@tetratech.com
Helen Chow, JK Geotechnics, Sydney, Australia, +61 298885000, hchow@jkgeotechnics.com.au

ABSTRACT

The integration of Artificial Intelligence (AI) into geotechnical engineering is revolutionizing the way foundations are designed, enabling more efficient and consistent solutions. This paper proposes a framework using integrated AI agents that automates the end-to-end process of foundation design, starting from the interpretation of site investigation data, through geotechnical modelling and analytical calculation, to reporting. The workflow begins with the application of large language models (LLMs) to interpret site investigation data. These LLMs generate ground models that characterise subsurface conditions. From these models, the framework identifies appropriate analytical tools suited to the specific foundation types and loading conditions. Subsequently, customized AI agents perform the associated geotechnical assessments. The key feature of the framework is its ability to intelligently route design tasks. The framework also enables rapid design iteration and reducing reliance on manual procedures. To illustrate its practical application, one worked example is provided as a test module. The proposed methodology can be extended to other geotechnical scenarios, paving the way for developing a comprehensive AI-powered geotechnical engineering agent. This proof-of-concept research highlights the transformative potential of AI in geotechnical design. The proposed framework marks a step forward in the digitization and automation of foundation engineering practices.

Keywords: Artificial Intelligence, large language models, foundation, geotechnical design, automation

INTRODUCTION

Geotechnical engineering primarily involves seven key areas: desk study, investigation, analysis, design, in-situ testing, construction and monitoring. While AI cannot yet replace fieldwork unless future technologies such as robotic site investigations become viable, it holds significant promise in streamlining data interpretation, analytical evaluations, and design activities. These stages are often standardized to a degree that makes them amenable to automation. In the domain of monitoring, advanced AI applications are already being employed to monitor ground settlement and predict geohazards such as landslides.

This paper emphasizes the data interpretation, analysis, and design stages of the geotechnical workflow. Given the complexity of end-to-end automation, the authors propose a modular approach in which AI solutions are divided into smaller, task-specific agents, each designed to perform a distinct function. These modules can then be integrated into a comprehensive workflow using cloud platforms such as n8n. An illustrative framework of the overall workflow is presented in Fig. 1.

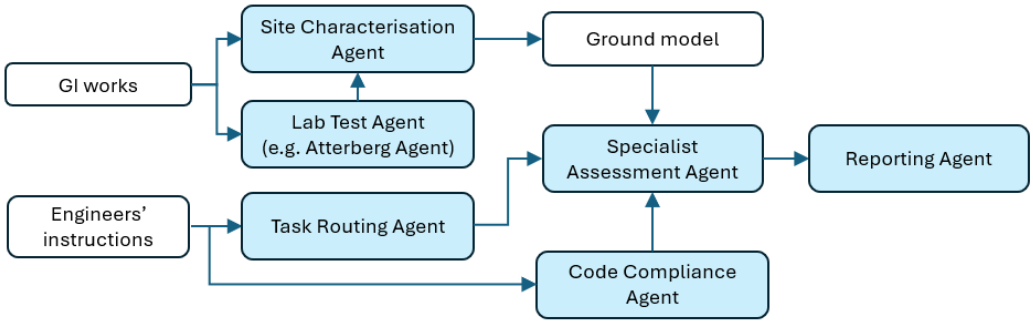


Fig. 1. Illustrative framework of the overall workflow

 © Deep Foundations Institute 2026

n8n is a workflow automation tool that enables users to integrate diverse software applications through Application Programming Interfaces (APIs) and web-based services. An API is a defined set of rules and protocols that allows software systems to communicate and exchange data. In addition to standard API integrations, n8n supports LLMs, custom logic, and scripting using JavaScript and Python, providing a flexible framework for complex data processing. As LLMs are trained on large-scale text data to understand and generate human-like natural language, these capabilities enable n8n to imitate engineers' behaviors based on user instructions and design briefs. This paper presents a prototype AI-assisted foundation design workflow using n8n to demonstrate the feasibility and benefits of such integration.

GENERAL FOUNDATION DESIGN WORKFLOW

Foundation design encompasses a broad spectrum of disciplines, including architectural, civil, structural, geotechnical and financial considerations. For clarity and focus, this paper limits its scope to routine workflows typically managed by geotechnical engineers. The process of foundation design involves ten major aspects, beginning with a desk study, progressing through the development of a geotechnical model and iterative design and ending in performance monitoring (Poulos, 2017). Depending on project complexity, Category 2 or Category 3 design methods are adopted in accordance with relevant guidelines (Poulos 1989). Sensitivity analyses and parametric studies are often necessary to address variability in subsurface conditions. These result in a design report that consolidates findings and recommendations, followed by proof testing and long-term monitoring. Within this framework, the integration of AI will be demonstrated, particularly in the stages of data interpretation, analysis, and design.

SITE CHARACTERISATION AGENT

Borehole logs are typically the first source of ground information accessible to geotechnical engineers. These logs are often stored in the gINT format, which presents detailed subsurface data. To enable efficient interpretation by AI models, this information must be transformed into a machine-readable format. Structured data formats such as Comma-Separated Values (CSV) and JavaScript Object Notation (JSON) are well suited to this task, as they support efficient processing and seamless integration into AI models. In particular, JSON is a lightweight, text-based format widely used for storing and exchanging structured data, especially in web APIs and inter-program data exchange.

For demonstration, a fictional borehole log reflecting a typical geological profile near Werribee South, Melbourne was compiled in gINT format and transformed into two separate CSV files storing the information of soil strata and Standard Penetration Test (SPT) N-values respectively. Table 1 contains information on soil strata including layer descriptions and corresponding depths. Table 2 presents SPT N-values alongside their respective depths. This conversion lays the groundwork for AI-based analysis by simplifying data ingestion.

Table 1. Soil strata of a fictional borehole log

Soil type	Depth to top of layer (m)	Depth to bottom of layer (m)
Fill: very stiff clay	0	3
Fill: stiff clay	3	3.5
Residual soil: firm clay	3.5	9
Residual soil: stiff clay	9	13.5
Residual soil: very stiff clay	13.5	14

 © Deep Foundations Institute 2026

Table 2. SPT summary of a frictional borehole log

Depth of SPT (m)	1.5	3	4.5	6	7.5	9	10.5	12	13.5
N values	28	9	8	4	5	10	14	13	20

These CSV files were retrieved via an API connection to a Google Sheet, using the n8n workflow automation platform, as illustrated in Fig. 2. Within this workflow, the AI agent (referred to as Site Characterisation Agent) tackles a core geotechnical task: assigning Standard Penetration Test (SPT) N-values to soil layers, which may contain one or multiple recorded test results. Mimicking the judgment of a geotechnical engineer, the agent intelligently determines representative N-values by averaging available data or extrapolating from adjacent layers, guided by user-defined rules or interactive prompts. This process ensures transparency and consistency while maintaining user's control throughout the interpretation.

Once the SPT N-values are assigned to each soil layer, they serve as the basis for estimating key geotechnical design parameters. For example, undrained shear strength ($S_u = 6.25 \times N$ kPa) and undrained Young's modulus ($E_0 = 250 \times S_u$) are determined accordingly. These empirical correlations are encoded as rule-based algorithms that can be easily adjusted using JavaScript or Python. Users may specify lower-bound, upper-bound, or percentile-based values to reflect project-specific risk tolerances, either as default configurations or through real-time interaction using conversation box during the workflow.

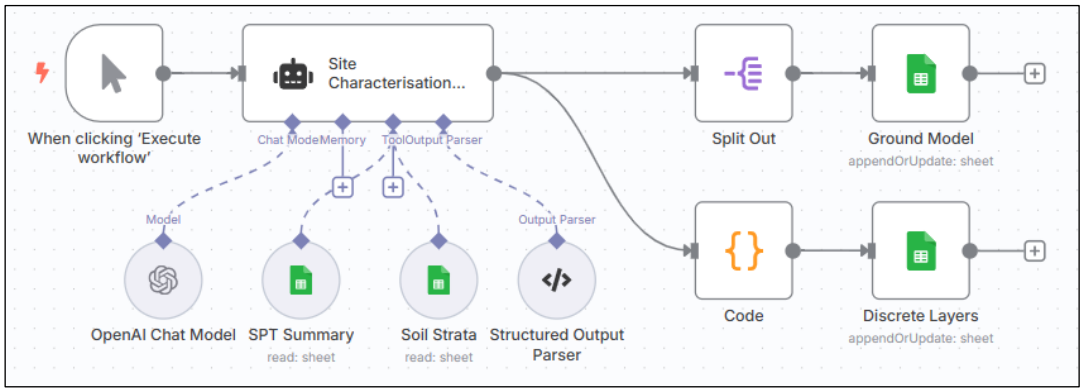


Fig. 2. Workflow diagram of Site Characterisation Agent

The output is a structured JSON array representing the interpreted ground model, including automatically assigned strength and stiffness parameters. This array is then transformed into a consolidated summary table as presented in Table 3. Readers may find the resulting values slightly too precise. It is up to users' preference to instruct the agent of the strategy of rounding off. In addition, a high-resolution dataset providing layer-by-layer data at 0.1 m vertical intervals can also be generated for analyses when discrete finite layers are required. This dataset can be exported back to Google Sheets for use in subsequent phases of the AI-assisted foundation design process.

Table 3. Summary of ground model generated by Site Characterisation Agent

Soil consistency	**Depth to top of layer (m)**	**Depth to bottom of layer (m)**	**Average SPT N values**	**Undrained shear strength (kPa)**	**Young's modulus (kPa)**
Very stiff clay	0	3	28	175	43,750
Stiff clay	3	3.5	9	56	14,063
Firm clay	3.5	9	5.7	35	8,860
Stiff clay	9	13.5	12.3	77	19,265
Very stiff clay	13.5	14	20	125	31,250

 © Deep Foundations Institute 2026

This paper demonstrates the proof-of-concept using a single borehole data. For more complex scenarios involving multiple boreholes, Li and Shi (2025) demonstrate the use of few-shot learning based on LLMs and augmented prompting strategies to generate two-dimensional cross sections from sparse site investigations. Existing commercial software such as Leapfrog also offers sophisticated algorithms for soil stratification analysis. This technology is well-developed and readily available commercially.

Correlation of Design Parameters

In addition to undrained shear strength, the drained shear strength (expressed as a friction angle, ϕ') of sandy soils can be estimated based on SPT N-values within defined soil density ranges. For example, medium dense sand with SPT N-values ranging from 10 to 30 typically exhibits friction angles between 35° and 40° (Look 2023). The Site Characterisation Agent can be configured to interpolate values within such predefined ranges, ensuring realistic and site-specific assignment of design parameters.

The Site Characterisation Agent is not limited to processing SPT data. It can also integrate results from in-situ tests such as Cone Penetration Test (CPT) and shear wave velocity, and from laboratory tests, such as the Plasticity Index (PI), which can be correlated with drained shear strengths (Mesri and Abdel-Ghaffar 1993). A complementary AI module, referred to as Atterberg Agent, automates the extraction and summarization of laboratory test data, as illustrated in Fig. 3. When a laboratory test report is uploaded to Atterberg Agent, the corresponding data in a Google Sheet is updated automatically. This update process can be manually triggered or scheduled to run periodically, with the system set to detect newly uploaded laboratory test reports in a designated Google Drive folder.

Once the Atterberg test summary is available, the Site Characterisation Agent can be extended with an additional node to access and incorporate the PI data directly from the relevant Google Sheet. With access to both field and laboratory datasets, the agent is capable of producing a comprehensive interpretation by combining SPT-based correlations and laboratory-derived parameters. Users can guide the analysis by specifying preferred correlation methods ensuring that the resulting ground model is both technically sound and tailored to project-specific requirements. The final ground model includes essential geotechnical attributes such as soil classification, depth ranges, shear strength parameters and deformation moduli. All of these parameters can be derived from a robust synthesis of field and laboratory data.

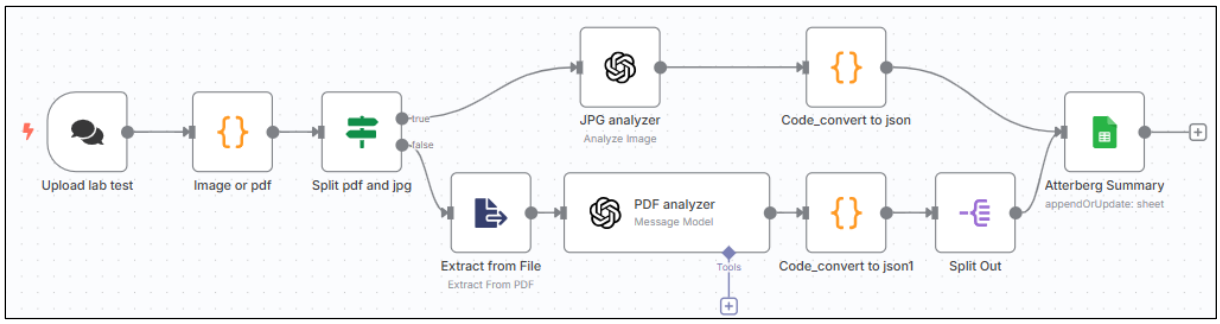


Fig. 3. Workflow diagram of Atterberg Agent

TASK ROUTING AGENT

Following the development of the ground model during the site characterisation phase, the system transitions to identifying the specific design tasks to be executed. At this point, users can submit their design briefs, thereby initiating the next stage of automation. This process activates a dedicated AI module known as Task Routing Agent, which is responsible for interpreting the content and intent of the design request.

Using a structured screening approach, Task Routing Agent analyzes the submission and determines which specialised design agent should be engaged. This process emulates the thought process of an engineer flipping through the table of contents of a technical manual to locate the most relevant chapter for solving a particular problem. In this capacity, Task Routing Agent functions as an intelligent navigator, directing the workflow toward the most appropriate specialist module within the framework.

Before initiating the handoff to a specialist agent, Task Routing Agent reformats the JSON data from the previous stage into a predefined structure. This structure corresponds to the input requirements of specific analytical spreadsheets or tools that perform each design task. For example, a pile capacity assessment typically requires a defined set of inputs, such as pile geometry, material properties and applied loading conditions. Task Routing Agent can automatically populate these parameters based on available data and identify any missing inputs. Where necessary, it can initiate additional queries to the user, enabling a multi-step dialogue to gather all required information.

Figure 4 presents a simplified illustration of this workflow. The system can be further adapted to support conversational loops that collect supplementary data, ensuring completeness before proceeding. Functionally, a Task Routing Agent operates much like a general practitioner performing diagnostic triage. It gathers the key information, identifies the nature of the design problem and issues a referral to the most suitable specialist agent for further analysis.

SPECIALIST ASSESSMENT AGENTS

After a Task Routing Agent determines the appropriate analytical method and auto-populates all necessary design parameters such as structure type, geometry and load conditions into a standardized "referral letter" (a predefined JSON array and users' instructions), a specialist assessment agent is activated to perform the detailed analysis.

The role of this agent is to synthesize the ground model provided by Site Characterisation Agent with the foundation design requirements identified by a Task Routing Agent. Using this combined dataset, the specialist assessment agent evaluates whether the subsurface conditions are suitable for the proposed geotechnical structure.

For demonstration purposes, a pile capacity assessment is presented. The analytical methodology required for this assessment is embedded within the LLM. In this example, a simple total stress alpha method is used for estimating pile shaft resistance. For more complex analytical algorithms, a code node can be added to complement the LLM's capabilities. This code node functions as a programmable environment that supports advanced computational logic.

As the ground model presented in Table 3 initially does not include pile resistance parameters, an intermediate step is required to assign them. This is achieved through the use of a helper module called Pile Design Parameter Agent. This agent is tasked with assigning appropriate values for both skin friction resistance and end bearing resistance based on predefined rules.

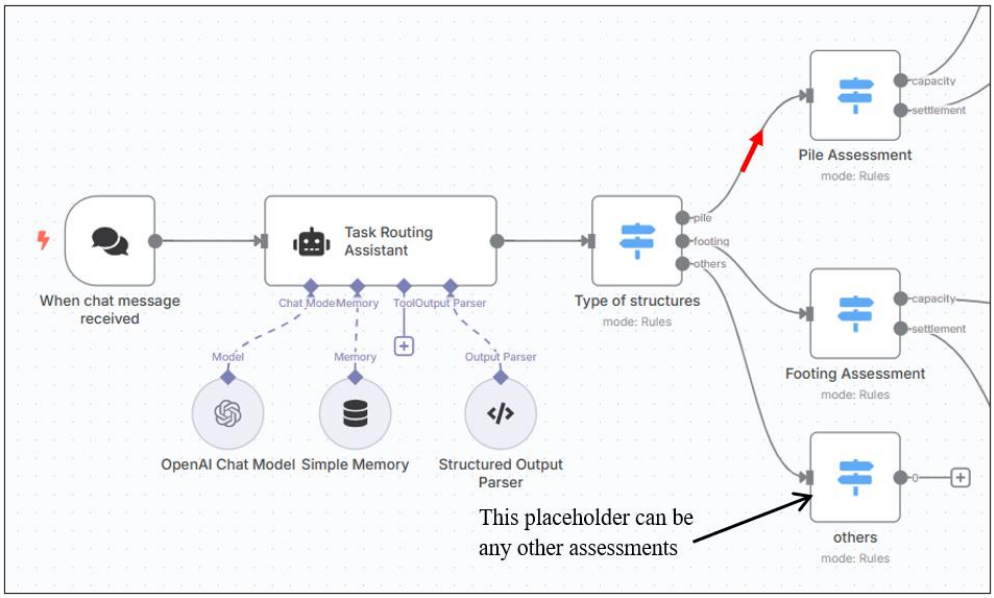
The following correlation is specified as a system prompt (primary instructions for the LLM) in Pile Design Parameter Agent to estimate pile design parameters for cohesive soils:

1. Ultimate skin friction $f_s = \alpha \times Su$
   where α is the adhesion factor = $0.21 + 0.26\ p_a/Su \leq 1$ and p_a is the atmospheric pressure (Kulhawy and Jackson 1989)

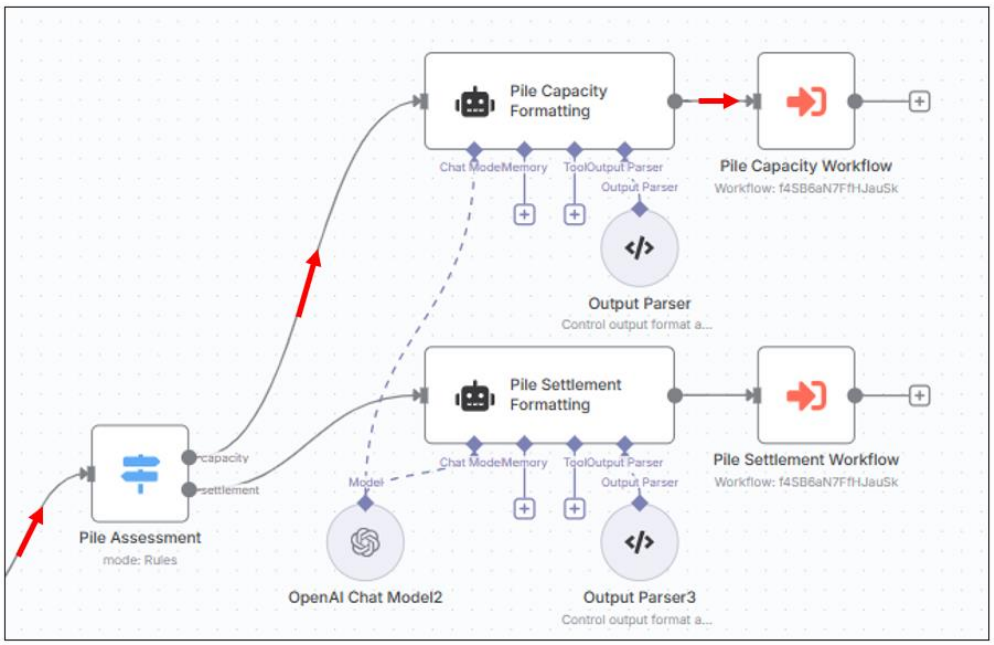
2. Ultimate base resistance $f_b = N_c \times Su$
   where Nc is the adhesion factor = $6 + L/d_b \leq 9$, L is the pile length and d_b is the pile diameter (Poulos, 2017)

 © Deep Foundations Institute 2026

Once the resistance parameters have been assigned and the Google Sheet (Ground Model) updated, the specialist assessment agent compiles all relevant information and feeds it into a LLM or a rule-based Python script to carry out the necessary calculations. The results of this assessment include ultimate shaft resistance, base resistance and total pile capacity.



(a)



(b)

Fig. 4. Workflow diagram of Task Routing Agent (split into 2 flow charts)

CASE STUDY

In this case study, a specialist assessment agent “Pile Capacity Agent” is activated in response to a user request. The structure of the Pile Capacity Agent is illustrated in Fig. 5. Given that the calculation primarily involves basic multiplication and summation along the pile depth, the LLM is sufficient to perform the assessment without the need for additional Python scripts. This agent receives a structured JSON array from the preceding Task Routing Agent, integrates data from the

Ground Model stored in a Google Sheet, and carries out straightforward numerical integration along the pile depth. The user's design prompt and the resulting calculations are summarized below.

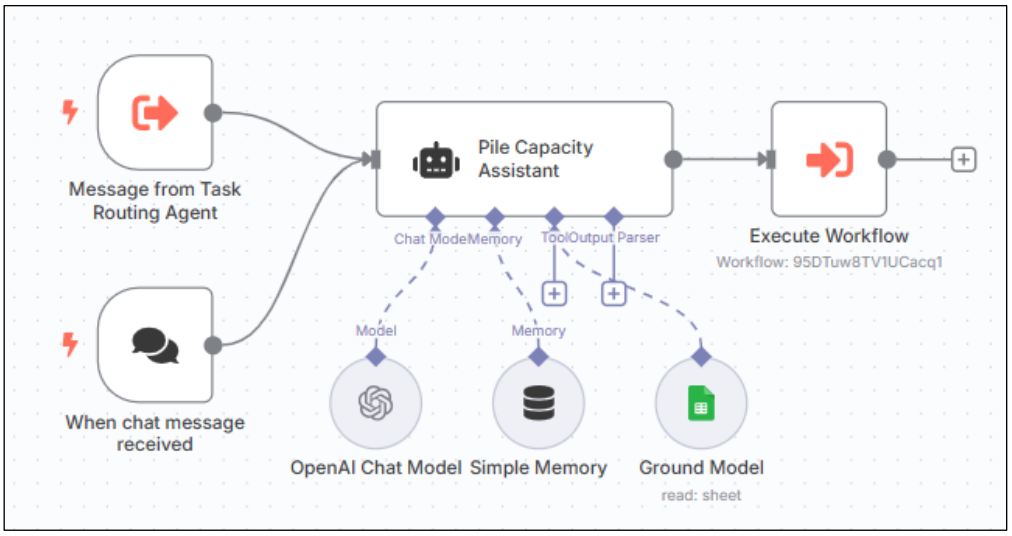


Fig. 5. Workflow diagram of Pile Capacity Agent

User's prompt:
"
Design a bored pile with a diameter of 0.75 m. The dead load is 200 kN and the live load is 400 kN. The load factors for the dead load and the live load are 1.2 and 1.5 respectively. Apply a reduction factor of 0.6. Calculate the required pile length. Try pile length = 9m, 10m, 11m and 12m.
"

Agent's reply: (For brevity, only the results corresponding to the 11 m case are shown)

"
Calculate Design Load (E_d)
$E_d = (1.2 \times 200) + (1.5 \times 400) = 240 + 600 = 840$ kN

Pile Capacity Calculation for L = 11 m

Total Shaft Resistance at L = 11 m
Previously calculated shaft resistance up to Layer 3: 923.38 kN
Adding Layer 4 contribution: $Shaft_{11} = 923.38 + 197.92 = 1121.30$ kN

End Bearing Resistance in Layer 4
$End\ Bearing_{11} = 0.4418 \times 9 \times 77.06 = 305.79$ kN

Ultimate Geotechnical Strength
$R_{ug} = 1121.30 + 305.79 = 1427.09$ kN

Design Geotechnical Strength (with 0.6 reduction factor)
$R_{d,ug} = 1427.09 \times 0.6 = 856.25$ kN

Comparison with design requirement
856.25 kN > 840kN ⇒ Sufficient
"

For comparison, manual calculations as summarised in Table 4 were carried out separately by the authors to counter check the AI agent's reply.

 © Deep Foundations Institute 2026

Table 4. Summary of manual calculations for pile length = 11m

Layer	Depth to top of layer (m)	Depth to bottom of layer (m)	Undrained shear strength (kPa)	Skin friction, f_s (kPa)	Layer thickness (m)	Shaft resistance (kPa)	End bearing resistance (kPa)
L1	0	3	175	63	3	445	-
L2	3	3.5	56	38	0.5	45	-
L3	3.5	9	35	33.4	5.5	433	-
L4	9	13.5	77	42	2	198	306
L5	13.5	14	125	52	-	-	-
					Subtotal:	1121	306
Design geotechnical strength = 0.6 x (1121 + 306) = 856 kN							

NATIONAL CODE COMPLIANCE

In geotechnical engineering, the fundamental formulae and calculation methods are largely universal and widely accepted across different countries. However, to comply with national design standards, the computed results must be evaluated against national code provisions. For example, in Australia, AS 2159-2009 specifies basic geotechnical strength reduction factors ranging from 0.4 to 0.76 and AS/NZS 1170.0-2002 specifies various load factor combinations.

To accommodate such regional variations, the conditional logic governing these factors is stored in a vector database. Rather than hard-coding these specifications, it is more efficient for the AI agent to autonomously query the vector store to retrieve the appropriate reduction factor based on contextual prompts. This ensures the system remains both flexible and scalable across different regulatory frameworks.

The n8n automation platform is able to integrate Australian Standard AS 2159-2009 by embedding its content into a vector store. Figure 6 presents how the AI agent extracts relevant information from the vector store on demand. This dynamic querying capability allows the agent to apply code-specific adjustments in a traceable manner, reinforcing compliance with national standards while maintaining the efficiency of automated assessments.

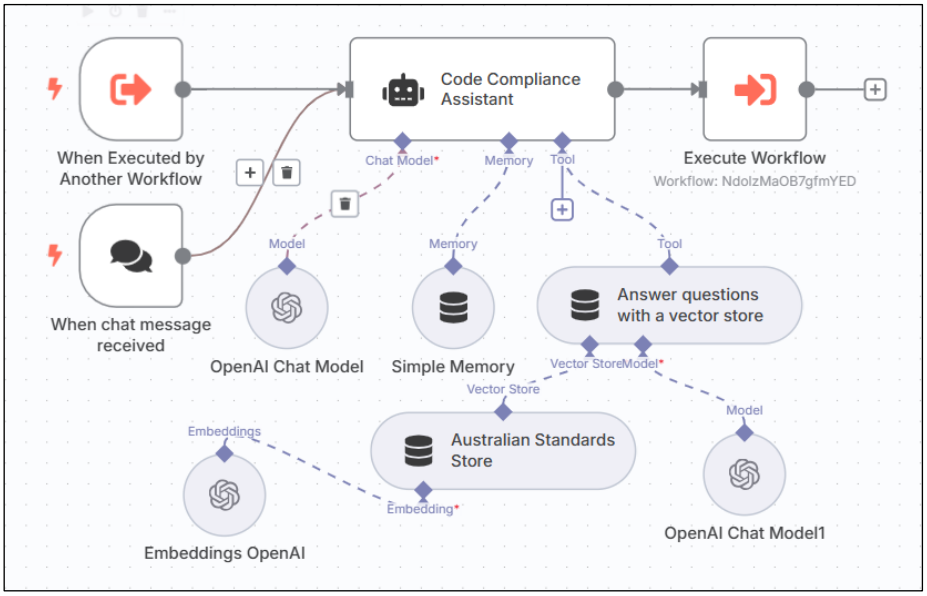


Fig. 6. Workflow diagram of retrieving information from a vector store

 © Deep Foundations Institute 2026

GEOTECHNICAL REPORT

Compared to data interpretation and analytical assessment, the reporting phase is relatively straightforward. A reporting agent can be used to extract computed results from the preceding stage and generate descriptive narrative text. However, without proper guidance, such AI-generated content often lacks consistency, clarity and alignment with company-specific formatting standards. This challenge can be resolved through few-shot learning where the AI agent is trained with a set of curated examples such as excerpts or full sections of prior reports with the desired tone, structure and level of technical detail. Once trained, the agent can generate new reports that mirror the style and formatting of the provided examples when provided with new data. While the AI agent is capable of presenting the factual outcomes of the analysis, it often falls short in delivering in-depth recommendations or addressing complex technical challenges. This limitation has been observed when using the ChatGPT-4o model.

DISCUSSION

The proposed workflow framework utilizes two major methodologies, i.e., deterministic algorithms using Python scripts and generative AI using LLMs. They orchestrate with each other to form a network to perform the users' instruction. The major technical challenge does not lie in performing the engineering calculations themselves, which are typically governed by well-defined mathematical formulae, but in correctly selecting the appropriate calculation tools and assembling the required input data. As with most engineering software or spreadsheets, analytical functions require a predefined set of input parameters. While populating these fields is relatively straightforward, the critical task is identifying which data should be used as inputs for a given analysis. This is where generative AI delivers its greatest value.

The AI agents introduced in this workflow perform three principal functions:

1. Correlating and summarizing geotechnical investigation (GI) data;
2. Interpreting the client's design brief and determining an appropriate analytical approach;
3. Integrating geological, structural and loading data into a structured format compatible with predefined analysis tools.

These agents are capable of automatically assigning shear strength parameters based on SPT correlations. Additional modules can be integrated to incorporate laboratory test data such as plasticity index or triaxial test results into the analysis. Collectively, these inputs are used to construct a detailed ground model. Following this, the AI agents can interpret the client's brief expressed in natural language and convert it into a structured JSON format. This mirrors common engineering practice in which project information is translated into tabular schedules (e.g., loading schedules or pile schedules). Despite variability in terminology across engineers or disciplines, the AI agents are able to capture semantic meaning and correctly map similar terms. For instance, they can recognize that "stress," "pressure," and "surcharge" may refer to the same concept and interchangeable depending on context. Based on this understanding, the agents can select appropriate analytical methods such as generalized bearing capacity equations for shallow foundations or the total stress alpha method for piles. Once the inputs are identified, the process becomes procedural. The agents format and populate the required parameters into the selected analytical function. In future implementations, this framework could be extended to interface with commercial geotechnical software (e.g., PLAXIS) via API integration.

In essence, the AI agents imitate the reasoning and judgment behavior of a geotechnical engineer. They consolidate information from multiple sources and convert it into structured formats ready for use in deterministic engineering algorithms, enabling a reliable and scalable foundation design automation workflow. The engineer's role shifts from manual computation to strategic oversight, i.e., managing borehole logs, defining design intent, and reviewing outputs and design reports.

It is acknowledged that real-world foundation design scenarios are far more complex than the simplified case examined in this study. These may involve heterogeneous soil profiles, variable water tables and intricate pile layouts. Nevertheless, the demonstrated framework provides a proof-of-concept that AI agents, when equipped with detailed configurations and inter-agent communication protocols, can be scaled to handle such complexities. Automated design of complex pile foundations is likely achievable with continued development.

While the application of AI in geotechnical engineering is promising, it does not obviate the need for engineers' due diligence. It has been widely reported that LLMs may suffer from hallucinations, potentially generating incorrect or fabricated information and calculations. As such, traditional engineering practices such as back-of-the-envelope checks remain essential for verifying that results are reasonable and within the correct order of magnitude. Although AI can significantly expedite engineering workflows, engineers should not blindly accept machine-generated outputs and must always apply professional judgment when assessing the validity and reliability of the results.

CONCLUSION

This paper has demonstrated a modular AI-assisted workflow for automating geotechnical foundation design, with a focus on pile capacity assessment. By decomposing the process into specialized agents such as Site Characterisation Agent, Task Routing Agent and Pile Capacity Agent, the system replicates the decision-making and analytical behavior of a geotechnical engineer. LLMs play a crucial role in interpreting natural language briefs, correlating field and laboratory data, selecting appropriate design methods and formatting structured inputs for subsequent rule-based calculations. The use of vector stores enables compliance with national codes, while few-shot learning ensures standardized report generation. The integration of these modules via automation platforms like n8n demonstrates a scalable and adaptable framework for practical implementation. While simplifications were made for demonstration purposes, the proposed workflow offers a robust foundation for streamlining routine design tasks, improving consistency and allowing engineers to focus on higher-level decision-making tasks.

ACKNOWLEDGMENTS

The authors sincerely appreciate Professor Harry Poulos for his generous review of this paper and his invaluable suggestions, which have significantly enhanced its quality and clarity.

The authors used ChatGPT (OpenAI) to assist with grammar correction and wording refinement during manuscript preparation.

REFERENCES

AS/NZS 1170.0-2002. Structural design actions - Part 0: general principles. Australian/New Zealand Standard, 37p

AS 2159-2009. Piling – design and installation. Australian Standard, 91p.

Kulhawy, F.H. and Jackson, C.S. 1989. Some observations on undrained side resistance of drilled shafts. Foundation Engineering: Current principles and practices, ASCE, New York, 1011–1025.

Li, H. and Shi, C. 2025. Few-shot learning of geological cross-sections from sparse data using large language model. Geodata and AI, 2 (2025), 13p.

Look, B.G. 2023. Earths: theory to practice – design and construction, CRC Press, Leiden, 592p.

Mesri, G. and Abdel-Ghaffar, M.E.M. 1993. Cohesion intercept in effective stress-stability analysis. Journal of Geotechnical Engineering, ASCE, 119(8), 1229-1249.

Poulos, H.G. 1989. Pile behaviour – theory and application. Géotechnique, 39, Issue 3, 365-415.

Poulos, H.G. 2017. Tall building foundation design, CRC Press, Boca Raton, 532p.

 © Deep Foundations Institute 2026

CONVERTING UNCONTROLLED FILL SITES INTO CONTROLLED ENGINEERED FILLS THROUGH RAPID, COST-EFFECTIVE, AND QUANTIFIABLE IMPACT ROLLING

Robin Power, Insitutek, Maleny, QLD, Australia, +61 404 114 75, robin.power@insitutek.com
Richard King, GeoSmart Solutions, Sydney, NSW, Australia, rking@geosmartsln.com.au
Matt Clenton, Landpac, Ingleburn, NSW, Australia, matt.clenton@landpac.com.au
Derek Avalle, Conplant, Taperoo, SA, Australia, derek.avalle.da@gmail.com

ABSTRACT

Uncontrolled fill sites pose significant geotechnical challenges for future development due to uncertain material quality, compaction, and load-bearing capacity. Converting these sites into reliable, controlled engineered fills is essential to ensure structural performance and reduce long-term settlement or failure risks. This paper presents the use of impact rolling as a fast, cost-effective, and quantifiable ground improvement technique for reworking and validating uncontrolled fills and significantly increasing the value of the development site.

Impact rolling applies high-energy, non-circular dynamic loads to the ground, promoting deep compaction and densification well beyond the reach of conventional rollers. It is particularly suited for heterogeneous fill materials, where traditional compaction methods may be ineffective. By integrating real-time Intelligent Compaction Measurement and in-situ validation tools such as the crawler based Dynamic Probing Super Heavy (DPSH) and portable Variable Energy Dynamic Cone Penetrometer (VEDP) with strength profile and compaction control capability, site improvement is not only achieved but verified with quantifiable data.

A case study is presented to illustrate the transformation of problematic fill sites into compliant platforms suitable for construction or infrastructure use. Results highlight the method's ability to improve ground stiffness, reduce voids, and demonstrate uniformity—reducing the need for costly excavation and replacement. This approach offers a practical, low-risk solution for developers and engineers dealing with legacy or undocumented fill conditions.

Keywords: Impact rolling, uncontrolled fill, controlled engineered fill, compaction control, land development, ground improvement, dynamic probing

INTRODUCTION

Uncontrolled fill materials are often heterogeneous, poorly compacted, and typically contain a mix of material at variable moisture contents. These characteristics make them unsuitable for supporting structures without significant risk of differential settlement or structural failure. Conventional approaches such as full excavation and replacement or deep foundation systems are expensive and time-consuming. Impact rolling offers a viable alternative for improving the engineering properties of such materials in place. By integrating real-time Intelligent Compaction Measurement and in-situ validation tools such as the Dynamic Probing Super Heavy (DPSH) and portable Variable Energy Dynamic Penetrometer (VEDP) with strength profile and compaction control capability, site improvement is not only achieved but also verified with quantifiable data.

WHAT IS UNCONTROLLED FILL

In-situ uncontrolled fills are deposits of soil or other materials that have been placed without engineering oversight or control and, in some cases, materials that have been placed with engineering oversight or control but the records are missing or not available. These fills can vary widely in their composition, including a mix of clay, silt, sand, gravel, or even waste materials, often with differing degrees of compaction, moisture content, and suitability for construction. A waste material example is demolition waste, which could include concrete, brick, asphalt, and metals. The absence of

 © Deep Foundations Institute 2026

compaction control during placement often results in uneven density and inconsistent engineering properties across the fill.

Such variability and unpredictability pose risks for construction projects, including differential settlement, poor load-bearing capacity, and increased susceptibility to erosion or liquefaction.

CONVENTIONAL APPROACH TO UNCONTROLLED FILL SITES

A conventional approach for converting uncontrolled fill sites into engineered fill sites typically involves excavation, replacement, and controlled compaction. The key steps include:

1. Excavation and Removal
   All existing uncontrolled fill is removed, especially if it's of unknown quality, poorly compacted, or contains unsuitable materials (e.g., debris, organics, or contaminants). Excavation often proceeds down to natural ground or competent material. In some cases, a relatively shallow 1–2 m depth could be left in place for impact rolling and validation.
2. Site Assessment and Subgrade Preparation
   The exposed subgrade is inspected, tested (e.g., Dynamic Cone Penetrometer (DCP), Variable Energy Dynamic Penetrometer (VEDP) or Dynamic Probing Super Heavy (DPSH) instrumented penetrometers, Plate Load Testing) and, if necessary, stabilised or proof rolled. Groundwater and drainage conditions are managed to ensure stability.
3. Placement of Engineered Fill
   Clean, site won or imported material is placed in controlled lifts (typically 200–300 mm thick). Each lift is compacted using appropriate equipment (e.g., padfoot roller) to specified densities (typically 95% or 98% Standard Proctor).
4. Quality Assurance Testing
   In-situ density tests (nuclear gauge, or in some cases sand cone) are typically carried out. Geotechnical supervision and testing ensure fill meets design specifications. A proof roll may be carried out using a roller or other construction plant at nominated layers in some cases.

While effective, this process is time-consuming, costly, and generates significant waste and haulage, as well as noise and dust.

AN ALTERNATIVE APPROACH – IMPACT ROLLING

Impact rolling is increasingly favoured as a faster, more cost effective and sustainable alternative to the conventional remove and replace approach. Although not a new technique, impact rolling (Fig. 1) has gained traction because of the emerging abilities to easily quantify improvement. By integrating real-time Intelligent Compaction Measurement on the impact rollers and in-situ validation tools with strength profile and compaction control capability, site improvement is achieved and verified with quantifiable data. Areas of differential response during rolling can identify soft spots or buried obstructions, which can then be targeted for additional treatment.



Fig. 1. Impact roller (Landpac)

PRINCIPLE OF IMPACT ROLLING (HIGH ENERGY IMPACT COMPACTION - HEIC)

Impact rolling is a ground improvement technique that utilizes a heavy, non-circular 3-, 4- or 5-sided steel roller to compact soil by repeatedly impacting the ground at high speed, as shown in Fig. 2. Impact rollers are typically towed behind a heavy tractor at speeds of 10–16 km/h. The geometry of the roller induces a series of high-energy, vertical impacts as it rotates, transmitting dynamic loads deep into the ground. This process densifies the soil to depths from 1.5 m to 4 m, depending on the material and moisture condition and whether the material is pre-existing fill or freshly placed. A typical impact rolling process slow is shown in Fig. 3.

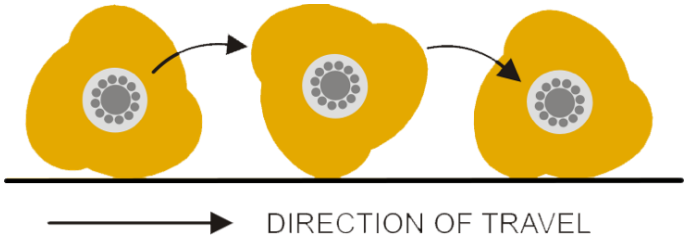


Fig. 2. Schematic of the impact rolling concept

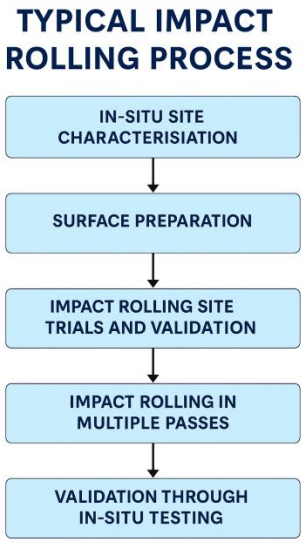


Fig. 3. Typical impact rolling process flow

Site characterisation is a critical step in assessing suitability for impact rolling. Often, review of existing geotechnical data is sufficient. However, in some cases, intrusive testing (test pits, boreholes, DCP or instrumented penetrometers such as portable VEDP or the more robust crawler-based DPSH rigs) and laboratory testing are valuable in characterising materials and in-situ density and moisture conditions. Field moisture content in relation to Standard Optimum Moisture Content (SOMC) is an important consideration as a guide to roller effectiveness. There can be limitations to the effectiveness of impact rolling and long-term fill performance if in-situ moisture content is significantly outside the accepted range for controlled fill. This particularly applies to cohesive fill with higher moisture contents.

Trials and their validation are often prudent and can include review of impact roller induced settlement heat maps and penetration tests using VEDP or heavier duty DPSH instrumented penetrometers. With included compaction interpretation software, VEDP and DPSH resistance plots enable a continuous Standard or Modified compaction profile over the depth of testing. Checks of VEDP or DPSH cone resistance with co-located nuclear densometer tests allows calibration with software compaction interpretation.

 © Deep Foundations Institute 2026

Final validation testing after impact rolling can be achieved using the same methodology used for trials, but on a grid assessed to provide appropriate statistical coverage.

BENEFITS OF IMPACT ROLLING FOR UNCONTROLLED FILL SITES

Impact rolling is a cost-effective alternative to excavating and replacing unsuitable material.

- Rapid: Large areas and deeper layers can be treated in a short time compared to traditional excavation. The programme for the ground improvement works will be reduced.
- Reduced Disturbance: Contaminated material does not necessarily need to be disposed of offsite. It can be treated insitu.
- Cost-Effective: Significantly reduces the need for excavation, disposal, and importation of engineered fill.
- Quantifiable: Real-time data acquisition from roller response and follow-up full depth in-situ testing allows for measurable quality assurance.
- Sustainable: Reuses on-site material, reducing carbon footprint and transport-related impacts.

CASE STUDY - INDUSTRIAL SUBDIVISION, FORMER BACKFILLED QUARRY, RURAL NSW

Multiple projects across Australia and internationally have demonstrated the effectiveness of impact rolling in converting uncontrolled fills. For example, a former quarry site in New South Wales was successfully treated and later developed into a commercial facility, with post-treatment deflections meeting engineering specifications.

Background

The client advised that the quarry had been backfilled around 2010 using material imported from a large basement excavation for a nearby shopping centre and that the fill had been placed quickly using a dozer and compactor to spread and compact. Reportedly, the operation had at times been unable to keep up with the rate at which fill was being delivered to site and hence layer thicknesses and roller passes were likely to have been variable. There had been no geotechnical supervision or testing during fill placement. Based on historical data and preliminary investigations, the fill was understood to be typically <3 m to locally >6 m deep. The volume of existing fill was estimated by others to be in the range of about 100,000–120,000 m^3 for the entire site.

GeoSmart Solutions was engaged to carry out a preliminary investigation of the existing fill to aid assessment of suitability for in-situ remediation by impact rolling. The investigation methodology included Dynamic Probing Super Heavy (DPSH) soundings (Fig. 4), soil sampling, Multi Analysis of Surface Waves (MASW), co-located nuclear densometer tests, and laboratory index tests.



Fig. 4. Dynamic probing DPSH testing (Geosmart Solutions)

 © Deep Foundations Institute 2026

Preliminary investigation findings relating to inherent material characteristics and suitability as engineered fill included:

- Existing fill assessed to be relatively consistent, comprising mainly low to medium plasticity Sandy Clay and minor Clayey Gravelly Sand, with Liquid Limit and Plasticity Index typically <50 and <40 respectively. Nuclear densometer testing recorded variable compaction above and below 98% Standard.
- Moisture content assessed to be within a range close to +/-2% from Standard Optimum Moisture Content (SOMC) targeted for controlled fill in AS3798-2007 *Guidelines on earthworks for commercial and residential developments.* SOMC was typically in the range of about 13–18%.
- No organic or other deleterious inclusions encountered at the tested locations, including at/close to the interpreted base of existing fill.
- Existing fill was assessed to be suitable as engineered fill provided it was sufficiently compacted. Landpac, the impact rolling contractor, reviewed the preliminary results and considered its heavy 3-sided impact roller (Fig. 5) could be effective to depths down to about 4 m.

The investigation demonstrated correlation between the assessment methods including:

- Strong correlation between conventional nuclear densometer compaction results and DPSH probe tip resistance values, with 98% Standard assessed to be met with probe tip resistance values of 3.0 and 5.5 MPa respectively for the dominant Sandy CLAY and minor Clayey Gravelly SAND materials.
- Strong correlation between MASW S-Wave velocity and fill compaction condition, with a velocity above 200 m/s assessed to indicate a minimum 98% Standard.
- DPSH tip resistance assessed to achieve 98% Standard based on the Sol Solution database (adhering to Compaction Control NF-P 94-063); was in close agreement, but slightly higher at 4 MPa and 7 MPa for the dominant and minor materials encountered. These higher values were adopted for initial validation assessment, with recommendation that the lower site-specific correlation values be considered when assessing any apparent non-conformances.



Fig. 5. Impact rolling of the filled quarry (Landpac)

 © Deep Foundations Institute 2026

Impact Rolling Methodology

Landpac was engaged to carry out impact rolling after the site earthworks contractor had carried out excavation to ensure a maximum 4 m depth of existing fill based on depths interpreted from preliminary investigations. Impact rolling was initially carried out where the existing fill was generally <3 m depth and then in areas where the targeted adjusted fill depth was a maximum 4 m.

Settlement heat maps (Fig. 6) were reviewed after intervals of typically 20–40 passes with a heavy, 3-sided impact roller.

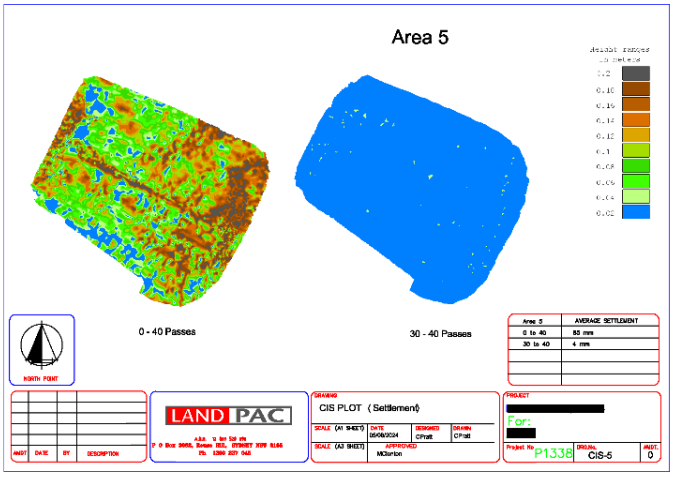


Fig. 6. Settlement heat map (Landpac)

GeoSmart Solutions (GSS) set out a test grid at typically 20–25 m spacing in rolled areas and conducted DPSH instrumented dynamic probing soundings to assess achieved compaction.

Impact rolling, DPSH testing, borehole drilling and co-located nuclear densometer testing was an iterative process essentially continued until passing compaction was achieved, or no further compaction could be achieved.

When no passing compaction could be achieved, visual/tactile assessment of soils recovered from boreholes, nuclear densometer tests and associated laboratory compaction tests indicated Field Moisture Content (FMC) was generally at the wetter end of +/- 2.0% from SOMC. As the fill generally had detectable silt content, it was reasoned the fill materials were increasingly moisture sensitive at or above SOMC.

For areas where passing compaction could not be achieved by impact rolling, the earthworks contractor excavated, moisture conditioned, spread in layers of 300 mm loose thickness, compacted and tested conventionally.

Testing Methodology and Results

As mentioned previously, validation cone resistance values based on interpretation using the vendor software and database were initially adopted. However, the progressively developed site-specific correlation based on co-located nuclear densometer tests within mostly low DPSH cone resistance anomalies was assessed to be reliable and statistically significant, and was adopted for compaction validation, as follows:

- 98% Standard, minimum tip resistance of 3.5 MPa within the tight in-situ moisture regime of mostly +/- 1.0% from SOMC with the following exceptions:

 © Deep Foundations Institute 2026

- 98% Standard, minimum tip resistance 2.0 – 2.2 MPa if sampling and/or testing confirmed field moisture content to be in the range of about 1.0% to slightly >2% wetter than SOMC (reflects that the site fill materials were assessed to be generally moisture sensitive due to silt content)
- 98% Standard, for rare lower tip resistance values subject to a passing co-located nuclear densometer test

The basis for the above validation regime is shown in plotted DPSH tip resistance vs nuclear densometer density ratio in Figs. 7–9.

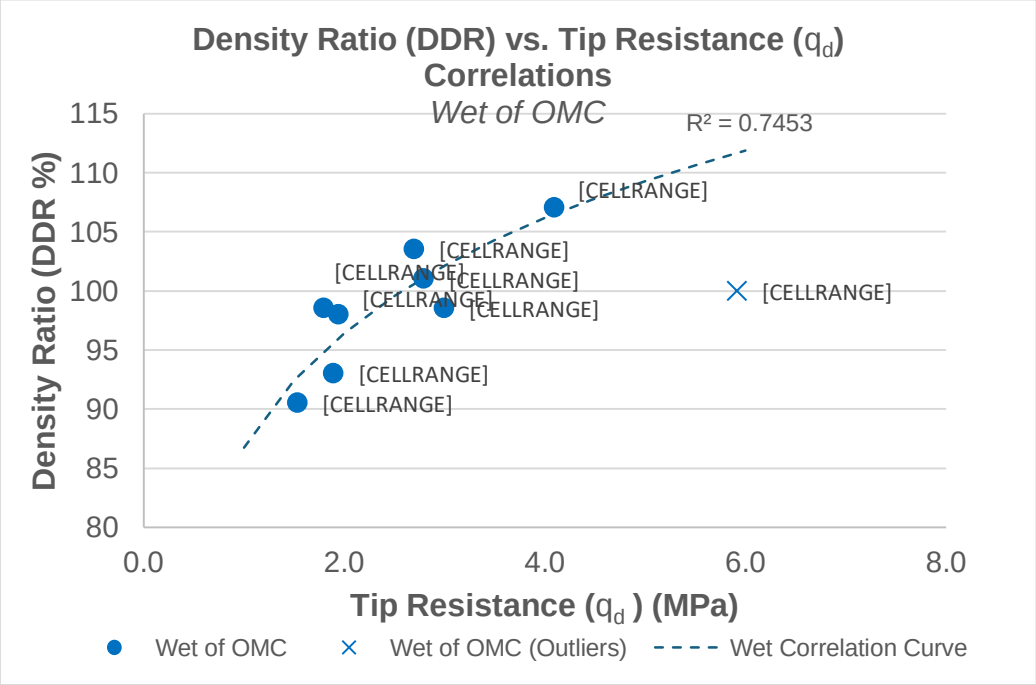


Fig. 7. Wet of OMC correlation

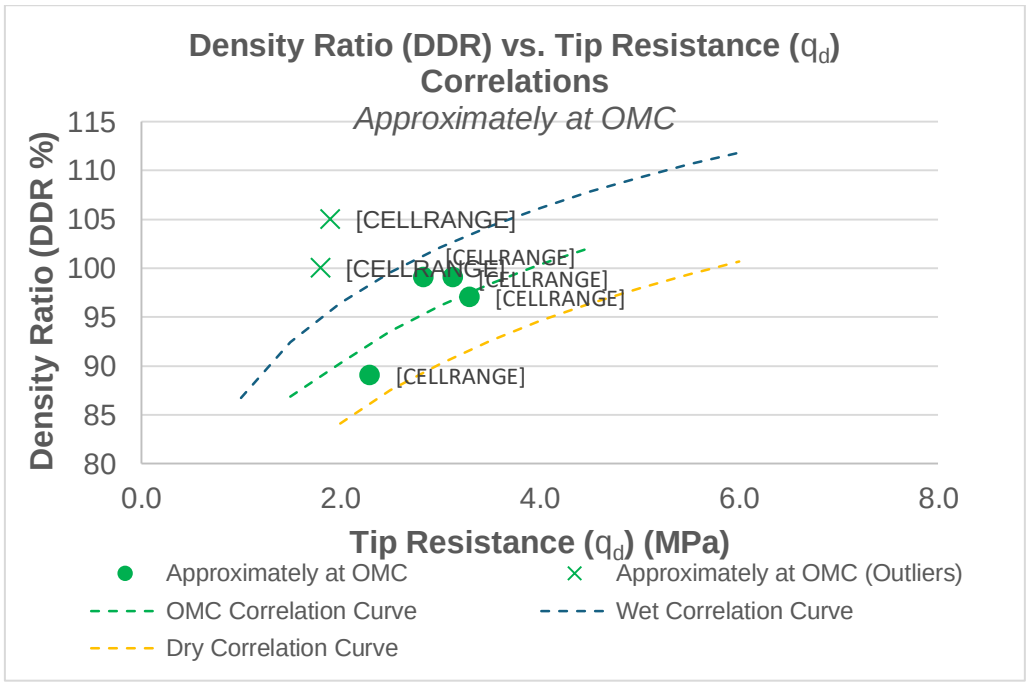


Fig. 8. Approximately at OMC

 © Deep Foundations Institute 2026

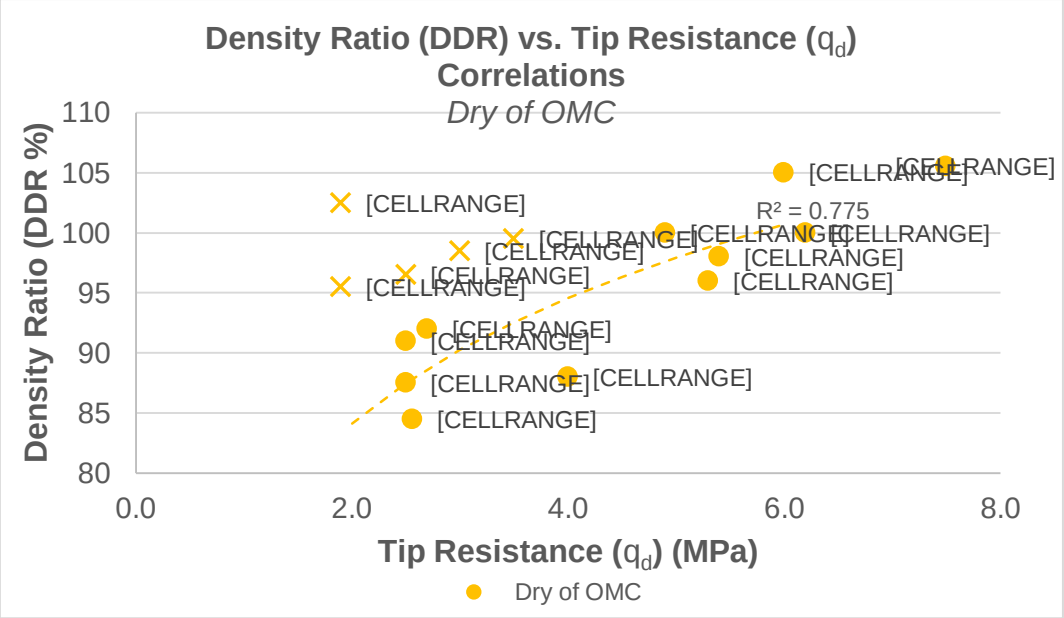


Fig. 9. Dry of OMC correlation

At the completion of conventionally locally replaced, compacted and tested fill, the entire final fill surface was given 20 further impact roller passes aimed at achieving uniformity with areas of successfully impact rolled full depth fill. A further round of DPSH tests were then performed.

Discussion of Results

By the completion of fill placement to final levels, there were two independent data sets correlating DPSH tip resistance with density ratio, namely:

- Impact rolled fill: 19 nuclear densometer tests co-located exactly with targeted locations and depth intervals, as represented in Figs. 7–9. The test pairs in this data set are very closely aligned in location and depth and on this basis is considered a reliable correlation. The nuclear densometer tests were deliberately targeted more to zones of low measured DPSH cone resistance but did include some targeted locations with passing compaction results as indicated by DPSH cone resistance.
- Replaced reworked fill: 118 compaction control tests carried out during conventional filling of areas where impact rolling was shown by DPSH testing not to meet the required compaction criteria. Compaction test locations as recorded by the testing authority and surveyed by the site earthworks contractor were not reliably recorded for each test but often by grid location proximity and layer/depth. Hence the correlation developed between DPSH tip resistance used filtered compaction results assessed to be located within a 2 m and 5 m radius of the DPSH grid points, based on the provided coordinates or nominated grid location, per Figs. 10 and 11. The correlations of this data set are assessed to be statistically robust, after ignoring obvious outliers assessed likely due to a mismatch in location/depth/material/moisture between DPSH cone resistance and paired compaction result. As would be expected, the scatter increases with offset radius from the DPSH test grid location, assessed to be due to variation in tested materials.

Importantly, the two independent data set correlations are assessed to be similar.

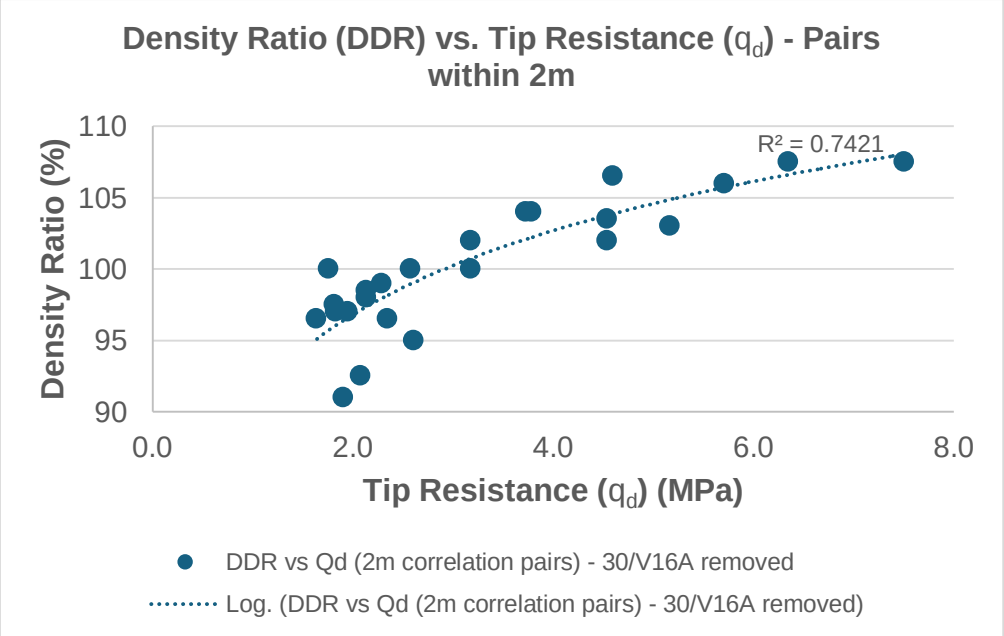


Fig. 10. Replacement fill statistical correlation – pairs within 2 m - 30/V16A removed

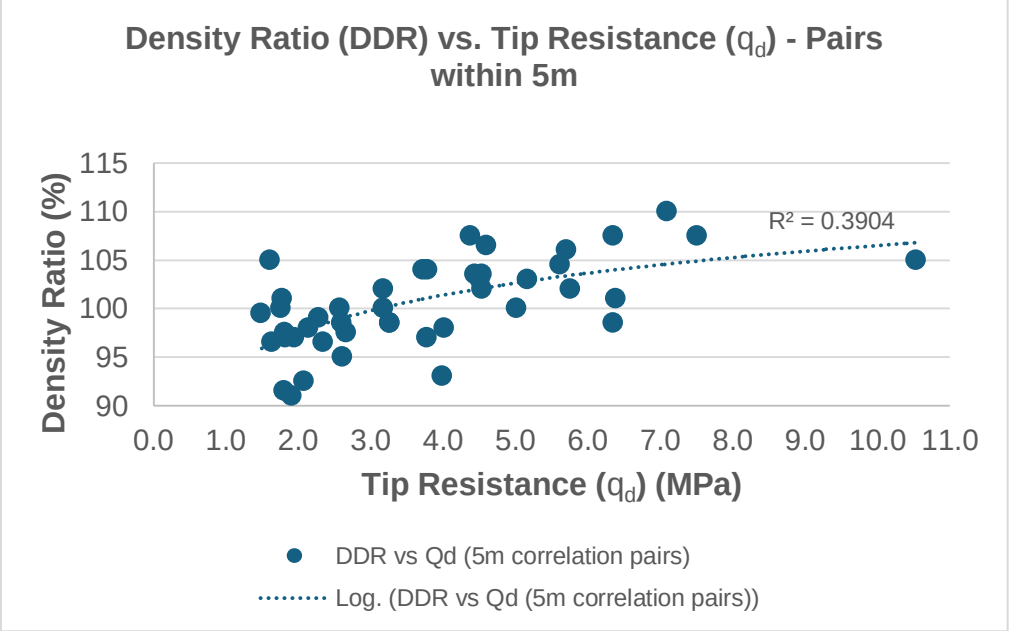


Fig. 11. Replacement fill statistical correlation – pairs within 5 m

The smaller 19-point correlation dataset was adopted for validation testing. Of the 19 paired tip resistance and nuclear densometer results, q_d = 3.5 MPa successfully predicted compaction outcomes in 18 cases, with only one anomaly where a very low laboratory density ratio value raised questions. Importantly, no systemic bias was observed, giving confidence in the reliability of the approach.

Based on the above, DPSH tip resistance q_d of 3.5 MPa (Fig. 12) was assessed to be a reliable pass/fail predictor, requiring engineering assessment to demonstrate that lower values still represent a compaction pass for the limited range of materials and in-situ moisture conditions for existing and reworked fills at this site. Most of the low tip resistance anomalies when checked by targeted nuclear densometer tests were pass results, with insitu moisture generally 0.5% or more wetter than SOMC.

 © Deep Foundations Institute 2026

Further, subsequent laboratory testing confirmed that field assessment of in-situ moisture by an experienced engineer can be reliable for the purpose of accepting lower passing tip resistance for layers/zones of higher in-situ moisture.

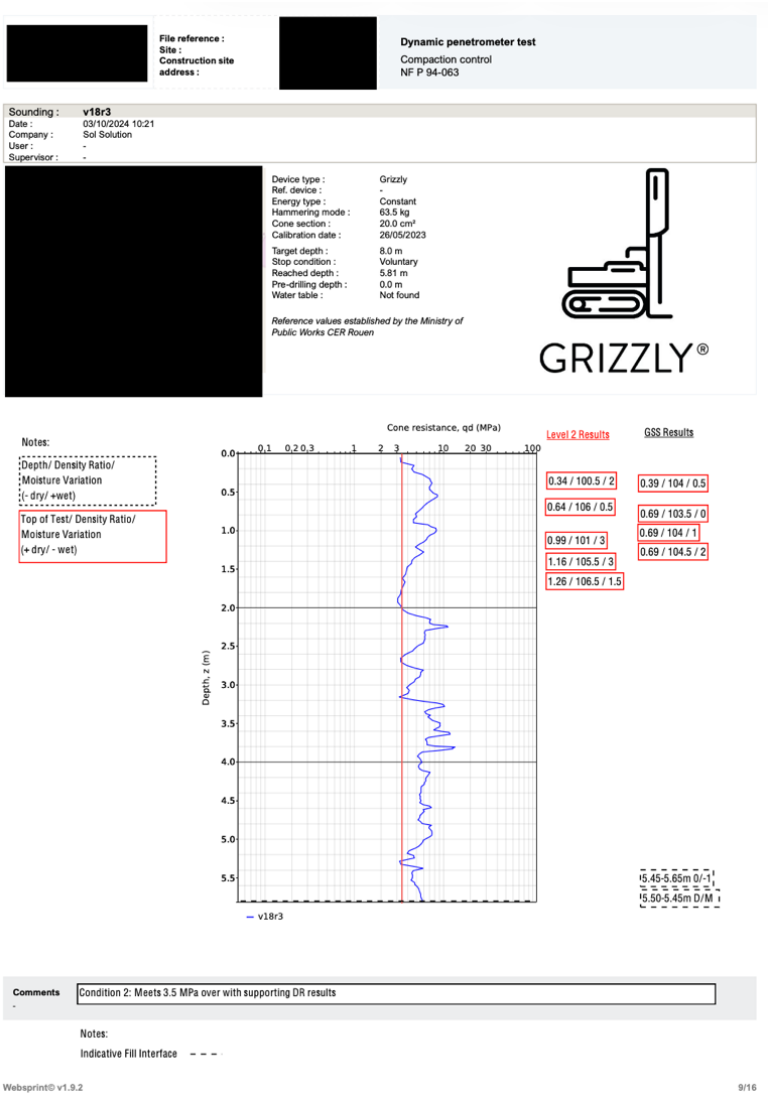


Fig. 12. DPSH soupding plot with compaction control NF P94-063

Fill Validation

Dynamic Probing Super Heavy (DPSH) testing at 25 grid locations covered an aggregate of about 85 column metres. The graphical DPSH plots are continuous with depth, and represent 285 subintervals of 300 mm, which is the depth normally covered by a single nuclear densometer test. The DPSH tests cover both impact rolled and conventional compacted fill, for which there were also 118 nuclear densometer tests. There is good consistency between two compaction methods and two data sets assessing insitu compaction.

DPSH tip resistance of 3.5 MPa was adopted as the pass/fail value for 98% Standard compaction within both the impact rolled fill and the conventionally placed reworked fill areas where impact rolling had not been effective. Exceptions include: lower q_d values can be ignored when nuclear densometer tests confirm compaction and based on test data, and a lower q_d value of 2.0–2.2 MPa may be adopted as passing 98% Standard compaction when testing or sampling confirm FMC to be about 1% or slightly wetter of SOMC.

 © Deep Foundations Institute 2026

Based on the above, six site-specific conditions were developed to validate the Dynamic Probing soundings as meeting compaction of 98% Standard for impact rolled fill and conventionally placed reworked fill. The site-specific conditions were as follows:

1. Meets 3.5 MPa over the full test depth
2. Meets 3.5 MPa over the full test depth, with supporting nuclear densometer results
3. Meets 3.5 MPa averaged over the full test depth, with no thin layers <2.0–2.2 MPa
4. Meets 3.5 MPa averaged over the full test depth, with supporting nuclear densometer results where <3.5 MPa
5. Meets 3.5 MPa averaged over the full test depth, and wetter Field Moisture Content (FMC) supports lower 2.0–2.2 MPa for passing compaction
6. Does not meet 3.5 MPa, but compaction confirmed by nuclear densometer results

The six conditions noted above, whilst site specific for this project, are based on transferable assumptions, logic and process. These include: a validation tip resistance value can be derived for a tight range of insitu moisture content, consider calibration/check nuclear densometer and moisture variation results in relation to derived validation tip resistance values, consider lower validation tip resistance for slightly over-wet in-situ moisture content values, field estimates of in-situ moisture variation by an experienced geotechnical engineer can be used for validation provided there is good agreement with actual laboratory results where available, averaging minor layers of indicated under-compaction with significant layers of over-compaction is practical (*see Note 1 below*), and passing nuclear densometer results over-ride low indicated tip resistance (potentially for reasons of subtle material and/or insitu moisture changes).

Note 1: This is exactly what happens over the typically 300 mm depth for a nuclear densometer test, where the upper part of a layer might be over-compacted and the lower part of a layer might be under-compacted, which is not uncommon as layer thickness increases.

Closing Comments

The report prepared by GeoSmart Solutions covered both the impact rolled and locally reworked fill and was accepted by the local council as meeting the requirement for 98% Standard compaction. A relatively small number of reworked fill results that achieved <98% Standard were satisfactorily handled as minor non-conformances due to also having DPSH results. Associated testing indicated that the fill met or closely met the generally accepted insitu moisture specification of +/- 2.0% from SOMC.

The report opined the remediated site was suitable for industrial building development subject to the following:

1. Engineering design based on review of the report and additional geotechnical investigations that may be recommended by project design engineers.
2. Consideration of the potential for differential settlement where building development on the site straddles natural and filled ground.

Combining impact rolling with a practical means to assess the profile of achieved compaction over the full fill depth has been made possible with innovative in-situ testing equipment now available.

For this case study, when reviewing settlement heat maps, it was possible to differentiate when minimal incremental settlement was also associated with under compaction of problem materials, in this case moisture sensitive material at higher in-situ moisture content.

For this case study, there were assessed to be the following benefits:

- Practical: enormous volumes of materials didn't have to be excavated, stockpiled and reworked conventionally
- Economic: cost savings
- Sustainable: Reduced fuel usage and emissions

- Collaboration: between regulatory bodies, developers and designers to achieve “fit for purpose” fill remediated insitu in accordance with sound engineering principles.

On paper, cost savings appear compelling. The authors were not privy to costings for the case study site, however, have considered an example 3 m depth of existing fill over a regular shaped area of 1 hectare (30,000 m^3 of fill). It is further assumed there are no oversize inclusions in the fill and that in-situ moisture is within a range suitable for compaction (as was the case for the study site).

Based on author experience, an efficient bulk earthworks operation using multiple scrapers to excavate, to stockpile and then working with compactors to replace as controlled fill in 300 mm thick layers is likely to take 10–12 days at a conservatively estimated cost about \$12–15/m^3. That time and cost could easily double to say \$25–30/m^3 or more if restricted site area required reworking in smaller sublots and/or with excavators and haul trucks to allow space for initial stockpiling.

Again, based on author experience, impact rolling using a 3-sided impact roller operating at an average but sub-optimal speed of 8 km/h could complete 50–60 passes within 4–5 days at an estimated cost of about \$3–5/m^3, although that cost could easily double if impact rolling identified say 20% of the area in need of localised excavate and replace remedial works.

The fuel savings too are apparent: a single all terrain tractor for an impact rolling operation of up to 5 days, verses multiple scrapers and compactors for a conventional excavate and replace operation of up to 12 days.

Prior detailed site investigation should be able to identify fills suited to impact rolling before committing to the operation.

CONCLUSION

Impact rolling is a proven, efficient, and quantifiable method to upgrade uncontrolled fill sites into structurally sound, engineered fills. Its adoption allows previously marginal land to be repurposed for infrastructure development, providing economic, environmental, and engineering benefits. Impact rolling is most effective in granular and mixed fills and may be less effective in very soft clays or organic-rich soils. Pre-screening for in-situ moisture conditions, buried services or contamination are essential for safe and effective application. As demand for developable land increases, especially in urban and peri-urban areas, impact rolling and the associated performance validation techniques will play a key role in land reclamation and site readiness strategies.

ACKNOWLEDGEMENTS

The authors would like to acknowledge:
- The GeoSmart Solutions team for data collection and analysis – Zev Gilmour, Stefano Pirrello and Peter Caffi
- The Landpac team for settlement heat maps and collaborative approach – Chris Pratt

 © Deep Foundations Institute 2026

MANDURAH ESTUARY BRIDGE DUPLICATION – SUSTAINABLE GEOTECHNICAL DESIGN

Su Kwong Tan, WSP Australia Pty Ltd, +61 401 914 362, sukwong.tan@wsp.com
James McIlquham, WSP Australia Pty Ltd, +61 422 538 155, jamie.mcilquham@wsp.com
Ken Chen, WSP Australia Pty Ltd, +61 432 520 311, ken.chen@wsp.com

ABSTRACT

The Mandurah Estuary Bridge Duplication (MEBD) project involves the construction of a new traffic bridge (Bridge 1090) for the Lakelands Lake Clifton Road (commonly known as Mandurah Road) to the south of the existing crossing of the Mandurah Estuary (Bridge 1085). Two piled abutments and seven piled piers were required to support the 400 m long incrementally launched bridge deck. This paper discusses the ground improvement and piling design developments between the reference design (RD) and detailed design (DD) stages. The DD adopted for construction resulted in significant cost and program savings and sustainability benefits. The DD solution used conventional earthwork preloading (instead of rigid inclusions proposed at RD). The bored pile design proposed at RD was replaced with a driven pile option, which comprised precast concrete piles for onshore piling and closed-ended steel pipe piles with concrete infill for pier piling within the estuary. Historic information, including piling records and settlement monitoring from the original Bridge 1085 construction, was used to justify the final design. Monitoring information from the construction of the new bridge and approach embankments is discussed and presented in this paper, with a discussion of the performance against that predicted by the design.

Keywords: ground improvement, foundation design, sustainability in design, loose sand

INTRODUCTION

The Mandurah Estuary Bridge Duplication (MEBD) project involves the construction of a new traffic bridge (Bridge 1090) for the Lakelands Lake Clifton Road (commonly known as Mandurah Road) to the south of the existing crossing of the Mandurah Estuary (Bridge 1085). More than 33,000 vehicles currently use the existing bridge crossing each day with congestion an ongoing issue. The new structure spans 400 m between the abutments and will accommodate two lanes with capacity to expand to three lanes (if required in the future), complementing the existing bridge to reduce traffic congestion and travel times. The project spans the suburbs of Dudley Park, Erskine and Halls Head in the City of Mandurah, Western Australia, as shown in Fig. 1 and Fig**. 2**. The new Bridge 1090 comprises 7 new piers (2 on-land piers and 5 river piers) and 2 new abutments on each side of the bridge. The construction is scheduled to be completed in 2026.

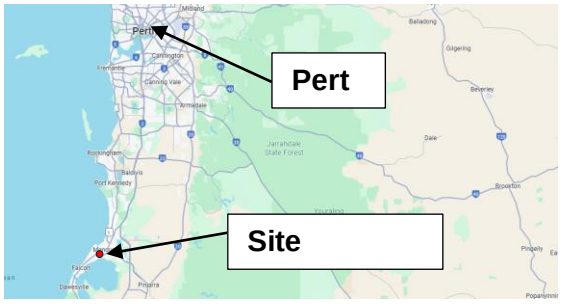


Fig. 1. Site location (WA)



Fig. 2. Site **locality**

The project is owned by the client, Main Roads Western Australia (MRWA). MRWA engaged Georgiou Group Pty Ltd (Georgiou) as the Contractor as part of a Design and Construct Contract. WSP was appointed by Georgiou to undertake geotechnical and groundwater design for the project with the structural design of the new bridge completed by BG&E Pty Ltd (BG&E).

 © Deep Foundations Institute 2026

REGIONAL GEOLOGY AND SUBSURFACE CONDITIONS

The geological conditions at the bridge location are presented in Fig. 3. They include the following key units:

- Embankment Fill associated with construction of the existing bridge comprising dense sand;
- Recent Estuarine Deposits within the channel and floodplain of the Estuary. These typically comprise loose to medium dense sands with soft clay layers;
- Tamala Sand on either side of the bridge with a relatively high natural density. Subsurface limestone pinnacles and areas of cemented sand commonly occur within this unit.

The units above are underlain by the Leederville Formation, which is a sedimentary formation within the Perth basin, comprising broadly unconsolidated to poorly consolidated sandstone, siltstones mudstones, and shales. Whilst no geological units are presented on the geological map for material within the channel, based on a review of historic information, it is inferred to comprise lagoonal and estuarine deposits (Q_{hg}).

Fig. **3** shows the conceptual geological section along the bridge centerline.

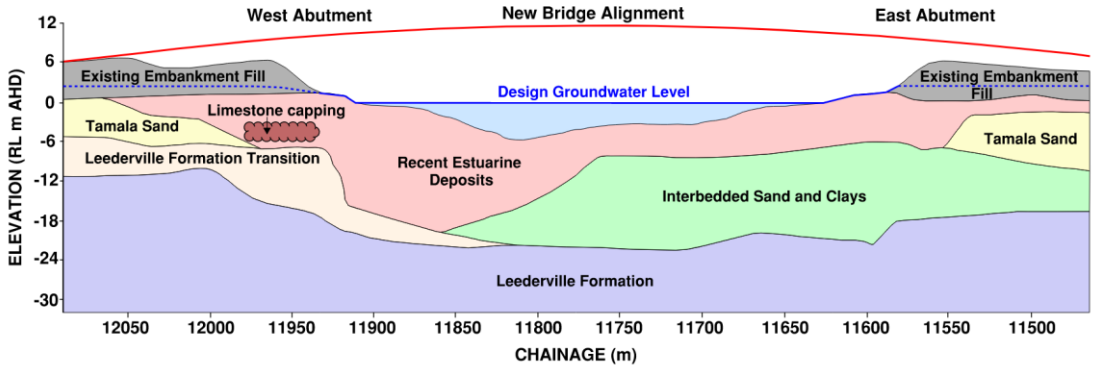


Fig. 3. Conceptual geological long section along the new bridge centerline

Available data from groundwater monitoring wells installed at the site indicated that groundwater levels generally varied between about Reduced Level (RL) -0.1 m Australian Height Datum (AHD) and +1 m AHD. However, following a detailed hydrogeological assessment and in accordance with design guidelines, a design groundwater level of RL +2.2 m AHD was adopted for the design of structures, which accounted for anticipated sea level rises over the 100-year design life.

DESIGN REQUIREMENTS AND CRITERIA

The proposed bridge piles had to achieve structural loading requirements, geotechnical performance and long-term durability requirements within a corrosive marine environment. The pile design had to be completed in accordance with AS1170.4 (2007) and AS2159 (2009). Specific project requirements impacted possible pile options for the pile design – for example, CFA piling was not permitted and steel tubular piles had to be filled with reinforced concrete, with steel casing considered sacrificial only.

The bridge approach embankments were required to achieve the following settlement requirements:

- Maximum 15 mm settlement after construction at any location over any 12-month period; and
- Maximum 50 mm settlement at any location over the Defects Correction Period (5 years after completion of construction).
- Differential settlement shall not exceed 25 mm in any circumstance with maximum permissible post construction grade changes of 0.3% and 0.5% for rigid and flexible pavements, respectively.

 © Deep Foundations Institute 2026

The following target Factor of Safety (FoS) criteria were adopted for the global stability design of the approach embankment.

- Long term static load cases, FoS ≥ 1.5
- Pseudo-static earthquake and accidental/transient load case: FoS ≥ 1.1
- Temporary conditions, including batter slopes for preloading embankments, FoS ≥ 1.2

HISTORY OF EXISTING BRIDGE AND EMBANKMENT

The existing Mandurah Estuary bridge (Bridge 1085) was the first major structure in Australia that was constructed using the incremental launching construction method and was opened to traffic in October 1986. A detailed article discussing construction of the original bridge is presented in L'Industria Italiana del Cemento (1990). Key aspects of the original bridge construction that influenced the decision to use incremental launching in the construction of the new bridge include:

- Poor ground conditions required piled falsework for conventional construction.
- Construction facilities could be concentrated at one side of the bridge (eastern end), reducing impact to wetlands (with significant environmental value) to the northwest of the bridge.
- Less disruption to marine traffic using the estuary.
- It allowed the incremental launch method to be tested prior to it being used for other large crossings of the Swan River in Perth.
- To test whether the method would be cheaper than other bridge construction methods.

Cone Penetration Testing (CPT), boreholes and geotechnical laboratory testing were undertaken to assess the feasibility for the existing bridge to be launched from a casting yard on the eastern side of the estuary. Based on the results of the site investigation and design, preloading of the approach embankment was required 12 months before the main bridge construction to limit casting yard and final road pavement settlement to acceptable levels. Fig. ***4*** and Fig***. 5*** present aerial photographs taken respectively during and prior to construction of the existing bridge. These show the topography of the area prior to increased residential development, which was completed between the construction of the existing and proposed bridges. The site investigation for the original bridge identified siltstone rock as a possible foundation layer for bridge piles. In situ self-boring pressuremeter testing and laboratory testing of rock core was undertaken, indicating that the siltstone had an unconfined compressive strength of between 0.75 MPa (109 psi) to 1.5 MPa (218 psi).



Fig. 4. Aerial photograph of project location with approximate bridge location (red) (National Library of Australia, 2023)



Fig. *5.* Aerial photograph looking west across the existing bridge site during construction (1985)

A driven pile solution was adopted for the bridge piles, with a composite pile foundation used. The lower part of the piles used a steel H-pile (310UC158 Section, 327 mm depth x 311 mm width), which could be driven into weak siltstone (Leederville Formation). To provide increased moment capacity and durability within the estuary and weak upper soil layers (between about RL + 2 m AHD and RL -10 m AHD), 500 mm square prestressed concrete piles were used for the upper 9 m to 12 m of pile and were welded onto the lower steel H-pile during construction. This composite approach allowed the design to take advantage of the benefits and characteristics of the two different types of

piles. Land-based piles for the existing bridge were full length steel H-piles. Two test piles were driven prior to full production works and dynamic pile testing (PDA and CAPWAP analysis) was undertaken to confirm the pile design and to assess set-up effects. Each river pier of the bridge comprised a group of 16 piles. A 10 pile group was used at the western abutment and a 20 pile group was used at the eastern abutment to accommodate the launching works.

The quality of engineering design and construction applied for the existing bridge was clear through a review of historical drawings, reports and published articles. The technical achievement was rightly acknowledged after completion of the bridge in 1986, when it won an Excellence in Concrete Award for the innovative methods used and the aesthetics of the completed structure.

NEW BRIDGE PILE DESIGN

Evolution From Reference Design to Detailed Design

The reference design (RD) for the new proposed bridge considered several different piling options for the project, including bored and driven options. The RD project team had also considered adopting similar composite piles to those used for the original bridge but selected a bored pile option with sacrificial steel casing. During the detailed design (DD) stage, the authors of this paper reassessed different piling options for the bridge, including bored piles and also different steel and precast concrete driven options. The alternative piling options were discussed with the structural engineer and construction team. The following key considerations helped drive the final pile option selection:

- Construction records from construction of the existing bridge supported use of driven piles. The H-section piles used were driven 3 m to 7 m into the weathered rock (to RL -22 and -31 m AHD).
- The ability to undertake pile load testing with the installation equipment meant that a more efficient pile design could be achieved by adopting driven piles.
- Piling experience from previous projects, as discussed Tan (2019) and Tan and Chapman (2019), gave confidence in potential use of driven closed ended steel tubular piles. One of these previous projects was for a project located approximately 2 km away.
- The shallow water depth at the estuary edges presented challenges with using a barge. Conversely, it allowed the use of a temporary causeway built using fill material and land-based piling rigs.
- The availability of pile types and sizes in the local market. A larger group of 450 mm precast square concrete (PSC) piles was identified as a possible option for the two abutments and nearshore piers, rather than a marine based steel tube (900 mm outer diameter x 20 mm wall thickness) as was used for the piers in deeper water.

At the RD stage, SPT testing undertaken to inform design of the new bridge indicated low SPT blow counts ($N \leq 4$ blows/300 mm), equivalent to very loose sand to a depth of up to 13 m below the riverbed. This led to a site subsoil classification of E_e – Very Soft Soil Site being applied to the design in accordance with AS1170.4 (2007). At the tender stage, the authors suspected that these low SPT values were likely to have been caused by issues maintaining water balance in boreholes during site investigation leading to loosening of the soil at the base of the borehole. This hypothesis was tested by comparing SPT test results from historic boreholes drilled for the original bridge against new boreholes drilled for the new bridge (as the piers are designed to match, the locations were relatively close together). This comparison indicated significant difference in the density of the ground at corresponding depths, typically an improvement from very loose to medium dense. To further assess the density of the ground and to inform seismic design at the DD stage, seismic CPTs (SCPTs) were proposed within the river at the locations where low SPT values had been identified by boreholes.

SCPT testing was undertaken as early as possible during detailed design to provide sufficient time to respond to the results of the testing. The results were positive, with the site being assessed as having a low-amplitude natural site period of 0.6s, justifying a site subsoil classification of C_e (Shallow Soil). In combination with detailed investigation of the geotechnical conditions, a compounding beneficial effect was achieved by the structural design team; the bridge's structural engineers changed the bridge

articulation for longitudinal earthquakes by providing restraint between 3 piers and designing the piers to be more flexible to 'release' some of the earthquake load, which allowed refinement of the piles. The increased density interpreted using additional site investigation (SCPTs) also offered benefits to the static design of the bridge in relation to lateral deformation. Using the updated ground profiles, pile driveability assessments were carried out using GRLWEAP 14 (2022) to select an appropriate hammer configuration to drive the piles to the required embedment depth and achieve the required capacity without overstressing the piles during driving. The driveability assessment indicated that a FAMBO HR10000 hammer was appropriate for the 450 mm PSC piles and a IHC S280 was appropriate for the closed ended driven steel piles (900 mm diameter x 20 mm wall thickness). A suitably stiff pile base plate and internal stiffeners were required to reduce the risk of the base plate of the pile flexing during driving, which would have otherwise prevented the full capacity being mobilised. Use of an unnecessarily larger hammer size could have resulted in increased project carbon footprint due to a heavier and larger piling rig being required for land-based piling and a larger hammer, crane and barge being required for the marine piling works.

Sensitivity studies were undertaken as part of the pile driveability works to assess the construction risk associated with the PSC section lengths and locations of joints relative to ground surface. To achieve structural performance requirements, the splices in these piles had to be at a minimum of 5 m below ground level. For the steel tubular piles, the potential range of pile toe level was assessed with the intention of eliminating the need for splicing of piles during driving where possible. Further confidence in the assessment was gained by reviewing driving records from the original bridge piles to support marine piling works. A comparison of the pile foundations at RD and DD is presented in Tables 1a and 1b, respectively, below.

Table 1a. Pile foundations at reference design

Structure	Pile Design Load, E_d (kN)	Piling Layout	Pile Length (m)
Eastern Abutment	2500	6 x ϕ 1200 mm. dia. bored piles	29
Piers 1 to 6	3150	12 x ϕ 1200 mm. dia. bored piles	27
Pier 7	3275	22 x ϕ 1200 mm. dia. bored piles	30
Western Abutment	2500	6 x ϕ 1200 mm. dia. bored piles	29

Table 1b. Pile foundations at detailed design

Structure	Pile Design Load, E_d (kN)	Piling Layout	Pile Length (m)
Eastern Abutment	2200 – 2400	18 x 450 mm precast concrete driven piles	21.5
Pier 1	2500	16 x 450 mm precast concrete driven piles	20.5
Piers 2 to 6	6600 – 7800	6 x ϕ 900 mm dia. closed ended driven steel piles with concrete infill	32 (average)
Pier 7	2550	16 x 450 mm precast concrete driven piles	21.5
Western Abutment	2250	14 x 450 mm precast concrete driven piles	21.5

Based on the pile designs presented in Table **1**a and **Table 1**b above, a concrete volume savings of about 2,500 m^3 was estimated, which resulted in an approximate 75% reduction in the concrete volume compared to the RD (with a total estimated concrete volume of about 3,300 m^3).

Piling Performance Verification

Based on the proposed pile testing regime, a geotechnical strength reduction factor of 0.77 was adopted in accordance with AS2159 (2009). Dynamic pile testing (PDA and CAPWAP) was carried out on selected precast concrete piles for the abutments and Piers 1 and 7 as well as on closed ended

steel piles with concrete infill for the river piers (Piers 2 to 6). These piles were tested either at end of drive (EOD) or on restrike with waiting time of up to 3 days. Precast concrete piles were driven into dense to very dense sand layer to between about RL -13 and -24 m AHD. while the steel piles were driven into the Leederville mudstone to between about RL -21 and -32 m AHD. A summary of selected pile test results is presented in Table 1. Results of the dynamic pile testing provided confirmation that the piles achieved the design intent.

Additional site investigation carried out within the western abutment footprint during DD confirmed the presence of limestone with an inferred top and bottom elevation of about RL -3 AHD and RL -5.8 m AHD respectively. In the do-nothing scenario, PSC piles are expected to refuse at shallow depth, which would not satisfy the design requirements. This risk was mitigated by predrilling an oversized hole at each pile location up to about 0.5 m below the base of the limestone, which was backfilled with cement bentonite prior to pile installation. Pile testing carried out on the western abutment piles verified that these piles achieved the design intent with the implementation of the predrilling and backfilling method which averted the need to change the pile type to bored piles.

Table 1. Summary of estimated mobilised resistance of selected piles

Pile	Pile Size (mm)	L_p (m)	Waiting Time, t (days)	Mobilised Ultimate Capacity $R_{d,ug}$ (kN)	Min. Required E_d / ϕ_g (kN)
Eastern Abutment	450 sq	24.8	2	3000 (C)	2860 (C)
Pier 3	900 mm OD	21.1	1	10980 (C) 4400 (T)	10130 (C) 1300 (T)
Western Abutment	450 sq	16.6	0	5000 (C) 2560 (T)	2930 (C) 1040 (T)

Note: OD = outer diameter, L_p = penetration length, E_d = design action effect, ϕ_g = geotechnical strength reduction factor, (C) = compression, (T) = tension

NEW BRIDGE GROUND IMPROVEMENT DESIGN

Evolution From Reference Design to Detailed Design

The RD reviewed several different ground improvement strategies for the approach embankment for the new bridge. These included preloading or surcharge treatment (with and without wick drains), excavation and replacement of soft / weak foundation materials and column supported embankments (piled embankment, stone columns, deep soil mixing and controlled modulus columns (CMCs)). Experience from different road construction projects within floodplains was reviewed as part of the initial design, including examples where a preloading ground treatment approach caused damage to an adjacent existing bridge and its foundations. The identified ground improvement options were ranked using a qualitative approach with impact on existing bridge, cost and time – the three key assessment criteria. From the results of this exercise and due to the risk associated with the required duration of a preloading treatment, a CMC supported embankment was selected at RD for the approach embankment within 120 m of the abutment on each side of the river, comprising an estimated total of 1,100No CMCs 600 mm diameter with a grid spacing of 2.5 m c/c and an average length of 17 m. At the start of tender design, the authors identified key geotechnical risks, reviewed the recommended ground improvement strategy for the project and identified the following issues associated with the proposed methodology in the RD:

- Construction of a CMC supported embankment immediately adjacent to the existing bridge would require challenging temporary works, including significant retaining structures to allow for excavation to form a load transfer platform below the bridge abutment and embankment.
- The impacts from installation of 600 mm diameter semi displacement CMCs could be significant in soils with increased density. Initial calculations of potential impact using cavity expansion theory indicated that the installation effect of CMCs and movement associated with temporary retention could be higher than a preloading solution for the depth and size of columns proposed.

- The time associated with adoption of a CMC supported embankment may be similar to that for a preloading option, when consideration was given to the extent of temporary works required.
- Adopting a solution with a difference in foundation type would add challenges due to transitions in settlements for large-scale retaining structures proposed to help reduce the overall footprint of the road corridor and would delay commencement of construction for some of these.
- The CMC-supported embankment was expensive and used high carbon materials. There were several local sources of natural fill materials that were available to undertake preloading treatment, with sufficient time in the program to use preloading fill material for the final road embankments.

As the existing bridge had been launched successfully from the eastern side of the river, the authors assessed the potential to adopt a similar construction approach as used for the original bridge. A ground model was developed for the area based on historical CPTs from original bridge construction and refined with additional testing and investigation completed for the new bridge. The stress history of the area was established from review of historical construction records, technical papers and historic aerial photographs taken during construction. From this review, it was clear that the site of the new bridge had been at least partially preloaded during construction of the original bridge as it had been used to store materials during construction and fill had been placed above the general floodplain area. An Over-Consolidation Ratio (OCR) of 2 to 5 was inferred for the clay layers in the area and this was used to refine and support the ground improvement developed during DD.

Back-Analysis of Monitored Data From Original Bridge Construction

Settlement monitoring data and historic back-analysis reports were available and were used to assess consolidation parameters (e.g., OCR, compression and creep indices, coefficient of consolidation, etc.), for a proposed preloading treatment. The parameters used for the new bridge design were refined to achieve a match in the back-analysed historic behaviour as shown in Fig. 6. Monitoring results from the original Eastern embankment construction indicated relatively small settlements were recorded until the embankment fill height achieved 3 m to 4 m height. This behaviour was postulated to be due to sand layers having a yield pressure, as discussed by Hillman et. al (1999). This yield pressure effect would mainly affect the estimated initial settlement during the early stages of earthworks, where the height of fill placed was limited (i.e., less than 4 m). It is noted that the estimated change in settlement after that point of filling would be largely unaffected. This effect was considered during the back-analysis completed at DD to establish design parameters for settlement assessment, which resulted in the consideration of a sand stiffness that is 5 times higher when below a yield stress of 80 kPa (1.67 ksf). This is illustrated in Fig. 6, where the rate of settlement increased once the fill height exceeded about 4 m.

The back analysis was undertaken using Settle3 (v5) which allowed consideration of the complex staged 3D geometry involved in the project. Once a match in estimated and historic settlement monitoring data was achieved, the parameters (as discussed above) that enabled this match were adopted in the DD and used to make a forward prediction of the geometry and duration required for a preloading solution. This indicated that a 1-month preloading duration would achieve the design requirements for the Eastern Abutment area (construction program made allowance for an increased duration of up to 3 months).

The approach and parameters adopted were used to make design predictions for preloading requirements for other parts of the project, with the following preloading hold times ultimately adopted during construction:

- Eastern abutment and approach embankments = 1 month
- Western abutment and approach embankments = 3 months

The adopted preloading ground improvement design negated the adoption of CMCs, which resulted in a simplified construction sequence, elimination of complex temporary retaining works and estimated concrete volume savings of about 5,300 m^3 compared to the RD.

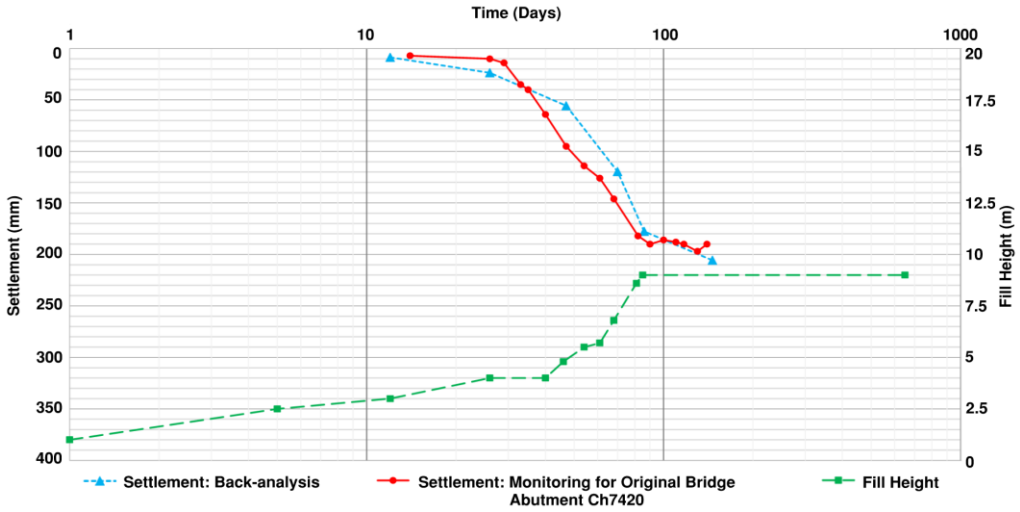


Fig. 6. Results of back analysis at original control line CH7420

Ground Improvement Performance Verification

A combination of Settle3 and in-house developed spreadsheets were used to complete the settlement assessments at DD. The ground model and parameters adopted were based on available site investigation and testing data and the results of the back analyses discussed above, and were reviewed against well-established empirical correlations. The settlement assessments considered contributions from elastic deformation, primary consolidation and ongoing time-dependent creep, which was modelled as a function of log time and theory presented in Mesri and Godlewski (1977) and Wong (2006). The estimated post construction settlement achieved the project requirements with the preloading treatment.

The settlement analyses predicted the following ground movements during construction:

- Eastern abutment: up to 220 mm (120 mm including yield stress correction) during 1 month preloading and casting yard operations (approximately 1 year).
- Western abutment: up to 270 mm (200 mm including yield stress correction) during the 3 month preloading period and bridge construction time.

Additional settlement analyses for the casting yard area were undertaken by incorporating the historic and proposed earthworks and loading throughout the casting yard operation. Based on the inputs provided by the structural designers and contractor, an initial degree of settlement was predicted, followed by a series of elastic settlement and rebound throughout the construction and launching of subsequent bridge segments. Once the bridge has been successfully launched across the estuary, the casting yard was to be decommissioned and incorporated in subsequent earthworks to form the eastern abutment and approach embankment. This was considered in the settlement analyses carried out.

Available geotechnical information indicated that the subsurface conditions beneath the approach embankments were inherently variable. In consideration of this, sensitivity analyses were undertaken at the eastern abutment, as operations here were on the critical path. This assessment involved adjusting key design parameters with results compared against the “base case analysis” to assess the potential impact upon construction staging and post construction performance. The following parameters and ranges were considered in the base case and sensitivity analyses to reflect the potential variability of the clay layers. A C_c/C_r ratio of 10 was adopted.

- Consolidation ratios: $C_c/(1+e_0)$ = 0.12 to 0.25; $C_\alpha/(1+e_0)$ = 0.005 to 0.01
- Thickness of individual clay layers: 1 to 4 m
- OCR: 1.1 to 5
- Coefficient of consolidation: 2.5 to 5 m^2/ year

Outcomes of the sensitivity analyses indicated that the designated duration of preloading could still achieve the required degree of consolidation, and the long-term embankment performance was still expected to be in compliance with the project requirements.

During construction, 2 in-place inclinometers, 2 borehole extensometers and 56 settlement plates were installed. A summary of key instrumentation observations during construction is provided below:

- The cumulative settlements measured indicated that movements had stabilized at all plate locations at the end of the preloading period. This suggested that the majority of the immediate settlement and primary consolidation of clay layers occurred during the 1 and 3 month preloading period for the eastern and western abutments, respectively. The monitored data was used in Asaoka (1978) assessments, which supported this finding that allowed the preloading to be released as intended.
- The magnitude of settlements measured during the preloading period (about 10 to 120 mm) was generally observed to be less than predicted in design (about 20 to 340 mm). This was likely associated with the loading history of the site (additional preloading effect being achieved during the original bridge construction, leading to further over-consolidation of the ground) and simplification of the ground model where multiple interbedded thin clay layers were combined into a single thicker layer for modelling purposes to cover for potential variation in ground conditions.

The results of the monitored data and movements assessed by the DD team confirmed the following:

- Target Degree of Consolidation (DoC) was achieved, and that the embankment fill settlement was consistent with design;
- The stability of the embankment during construction was adequate;
- Hold point release for preloading period was appropriate; and
- Impact of the works on adjacent infrastructure (e.g., the existing bridge piles and abutments) was within acceptable limits. Geotechnical modelling was carried out using PLAXIS3D to assess these impacts. The predicted lateral movement on existing bridge piles due to preloading was between 5 and 10 mm. Inclinometers were installed between the preloading area and the existing bridge abutment (approximately 3 m from the existing bridge), which showed up to about 15 mm of lateral deformation indicating that the actual lateral movement of existing bridge piles to be lower and consistent with the predicted movement.

CONCLUSIONS

This paper has discussed the development of the ground improvement and pile design for a new 400 m long incrementally launched bridge. The availability of high-quality historical construction records meant that optimization of the design was possible. The knowledge and experience from the construction of the existing bridge provided some insights into the likely ground behaviour in response to ground improvement and piling works.

By challenging key assumptions made at the reference design stage, including available construction program and allowance for risk in preloading duration and use of bored piling methods, improvements in project cost, program and sustainability were achieved.

Targeted in situ geotechnical testing and changes in bridge articulation by the Structural Designer led to savings in concrete volume of about 2,500 m^3 and 5,300 m^3 for piling (reduction in pile number and length, change to a more cost-effective pile type) and ground improvement (avoiding CMC columns), respectively. Successful implementation of risk mitigation measures (predrilling) implemented on

 © Deep Foundations Institute 2026

western abutment piles (verified by dynamic pile testing results) confirmed the feasibility of PSC piles and avoided pile wastage if alternative pile type (such as bored piles) had to be adopted to drill through the limestone layer.

The substantial savings in concrete volume for both piling and ground improvement underscore the substantial efficiency gains and potential environmental benefits associated with the adoption of the DD. The significant reductions in concrete volume not only reflected improved material utilization but also aligned with broader sustainability objectives in construction practices. Reducing the volume of concrete directly lowered the energy consumption and carbon footprint associated with foundation works. In addition, such reductions support the goals of resource efficiency and waste minimization that are the key precepts in sustainable development and green building certification frameworks.

ACKNOWLEDGEMENTS

The authors gratefully acknowledge Main Roads Western Australia, Georgiou Pty Ltd and BG&E Pty Ltd for the information provided. Thanks are also extended to WSP Australia colleagues (Joshua Kyle, Matthieu Duong, Alireza Foroughi, Simon Tan and Hansaja De Silva) and Dale Screech and Doug Stewart (former WSP Australia colleagues) for their technical input and assistance, and to the field personnel whose efforts contributed to the successful outcome of the project.

REFERENCES

Asaoka, A. 1978. Observational procedure of settlement prediction. Soils and Foundations, Journal of the Soils and Foundations Engineering, 18(4), pp. 87-101.

Hillman et al., 1999. Tank Settlements on Calcareous Soils Kwinana, Western Australia, Australian Geomechanics Society, September 1999, pp. 61-68.

L'Industria Italiana del Cemento. Feb 1990. "The Mandurah estuary bridge: first Australian bridge built using the incremental launching method". No. 641.

Mesri, G. and Godlewski, P.M. 1977. Time and stress compressibility interrelationship. Journal of Geotechnical Engineering. Div. ASCE 103, GT5 pp. 417-430.

Tan, S.K. and Chapman, G.A. 2019. Design, Driveability, Driving and Dynamic Testing of Large Diameter Close Ended Steel Tube Ples for a Pedestrian Bridge, 13th Australia New Zealand (ANZ) on Geomechanics, pp. 261-266.

Tan, S.K. 2019. Geotechnical Design and Construction Consideration for Old Mandurah Traffic Bridge Project, 13th Australia New Zealand (ANZ) on Geomechanics, pp. 1211-1216.

Wong, P.K. 2006. An Analytical Method Based on Bjerrum's Time Line Principle and Comparison with Other Design Methods, Australian Geomechanics Society Sydney Chapter Mini-Symposium on "Soft Ground Engineering", 11 October 2006.

 © Deep Foundations Institute 2026

FOUNDATION AND RETENTION SOLUTIONS IN GEOLOGY SUSCEPTIBLE TO LATERAL SOIL MOVEMENTS IMPACTING SENSITIVE WHARF STRUCTURES

Callaghan Taylor, Keller Pty Ltd, Melbourne, Victoria, Australia, 0474 198 066,
cal.taylor@keller.com.au
Jared Fetherston, Keller Pty Ltd, Melbourne, Victoria, Australia
Eric Chong, Keller Pty Ltd, Melbourne, Victoria, Australia

ABSTRACT

As urban development expands into sites with complex ground conditions and physical constraints, increasingly sophisticated engineering solutions are required. At a high-rise residential project in Melbourne's Docklands, deep foundation piles and a retention system were needed on a challenging reclaimed wharf site bounded by the Yarra River. Problematic subsurface conditions included normally consolidated soft clay, a variable-thickness basalt tongue, and underlying weaker soils and deep siltstone, all of which impacted design and construction. This paper outlines the objectives, methods, and outcomes of the foundation and retention design, detailing the rationale for equipment and methodology selection to control lateral soil movement during installation in order to minimise adverse impacts on the existing wharf structures. Key risks to the existing wharf infrastructure and the new piles were managed through meticulous planning and precise execution with close monitoring throughout construction. A dynamic testing program addressed variability in founding conditions across the site. The paper concludes that a multi-technique design-and-construct approach utilising CFA piles, driven precast concrete piles, driven steel tube piles, and sheet piles enabled a safe, efficient, and technically successful outcome for a highly constrained urban development.

Keywords: Sheet Piling, Precast Piling, CFA Piles, CHS Piling, Pile Testing, Soft Soil, Ground Movement

INTRODUCTION

The project is a multi-storey residential tower in southwest Melbourne Docklands. The site, approximately 150 m by 70 m, is bounded to the north by a historic finger wharf fronting Victoria Harbour and to the south by a derelict wharf on the Yarra River, replaced prior to construction by a new seawall. To the east lies the completed initial stage of the development, a 29-storey residential tower, while to the west lies a continuation of the northern wharf and derelict southern wharf, comprising roads and warehouses.

The Docklands are typically underlain by soft, normally consolidated Coode Island Silt (CIS), which can undergo significant ground movements during foundation installation (Peck et al., 1992). Careful foundation design is needed to minimise impacts on adjacent structures and the foundations themselves.

A combination of piling techniques including, sheet piling, predrilling, precast piling, continuous flight auger (CFA) piling and steel tube piling were nominated by Foundation Specialist Group (FSG) after detailed modelling was carried out to estimate the soil displacements due to general foundation construction installation effects. Design, cost and constructability assessments informed the final foundation solution. The adopted approach integrated multiple foundation and retention techniques with dynamic testing, delivered within strict site access constraints to achieve a safe and efficient outcome for a technically challenging site.

GEOLOGY

The geology of the local area consists of fill, CIS, Fisherman's Bend Silt (FBS), Moray Street Gravels (MSG), Older Volcanics Basalt, sub-basaltic sediments and Melbourne Formation Siltstone. The basalt presented as a basalt tongue of variable thickness, covering roughly 1/3 of the site, extending from the northeast corner of the site and thinning to the southwest. The siltstone/basalt was the target

 © Deep Foundations Institute 2026

formation for the foundations. The geotechnical investigation consisted of boreholes and Cone Penetration Tests (CPT). Seven CPTs were undertaken across the site and generally refused in the MSG at a typical depth of 24 m. A total of 25 boreholes were drilled across the site footprint, with 10 of the boreholes intended to identify the top of the basalt/siltstone, hence no soil sampling or testing was carried out above the top of basalt/siltstone. The remaining 15 boreholes consisted of regular Standard Penetration Tests (SPTs) and push tube samples with subsequent pocket penetrometer testing. The 15 boreholes were terminated at depths of up to 50 m after penetrating and sampling the Melbourne Siltstone formation

A detailed description of the soil layers identified on the project is provided below:

Fill

The thickness of the fill ranged from approximately 0.6 m to 2.0 m. In most areas the fill typically consisted of an asphalt layer and a concrete slab, followed by granular fill materials, primarily composed of crushed rock. Beneath this layer, and in locations where these materials were absent, the fill became more variable, generally consisting of soft to firm clay with varying amounts of gravel and cobbles. It is inferred that some of these fill materials may represent reworked Coode Island Silt.

Coode Island Silt (CIS, CH/MH)

The CIS, encountered as a grey/dark grey clay/silty clay (CH/MH), extended to depths between 17.0 m and 22.0 m. The consistency of the CIS was typically very soft to soft (shear strength of 10–20 kPa,), increasing with depth to a firm consistency at the bottom of the layer. Cone penetration testing showed a tip resistance of 0.3 to 0.5 MPa in the upper 12.0 m and 0.5 to 0.9 MPa to the base of the layer.

Fisherman's Bend Silt (FBS, CH)

Underlying the CIS was FBS, encountered as a high plasticity clay (CH) and sandy clay (CH). The unit was typically firm to stiff in consistency. The top of the FBS was encountered at depths between 17.7 m and 23.5 m and had a highly variable thickness across the site of 1.5 m to 10.3 m thick. Cone penetration testing showed a tip resistance of 1.0 to 1.5 MPa. It was noted that the typical distinction between CIS and FBS was based on an increase in consistency and change in colour from grey/dark grey to brown respectively.

Moray Street Gravel (MSG, SP/GP)

The top of the MSG was encountered at depths between 22.7 m and 28.0 m and was between 6.0 m and 18.0 m thick. The composition and strength of the unit were highly variable across the site. The upper portion of the unit comprised medium dense to very dense sand (SP), gravelly sand (SP), sandy gravel (SP) and gravel (GP). Standard Penetration Test (SPT) values in the upper layer were typically between 30 and 50 with an average of 38. The lower 3.0 m to 8.5 m of the unit varied from firm to hard clay (CH) or sandy clay (CH).

Older Volcanics Basalt

A flow of Older Volcanics Basalt was encountered on the northeast portion of the site at depths of 30.0 m to 36.1 m. The basalt thickness varied significantly, as is typical of basalt flows within the Yarra Delta geology, and ranged from 1.7 m to 6.0 m thick, tapering out towards the southwest direction. The basalt was typically slightly weathered, though zones of variable weathering were present and UCS testing results ranged from 15 MPa to 125 MPa. The rock quality designation (RQD) was typically around 70%.

Sub-Basaltic Sediments (CH)

The sub-basaltic sediments were typically encountered as a brown silty and sandy clay (CH) with a thin layer of medium to coarse gravel (GC) at the base of the layer. The consistency of the clay varied across the site ranging from firm to hard, with the gravel very dense. The thickness of the sub-basaltic sediments ranged from 0.6 to 6.0 m thick.

Siltstone

Melbourne Formation siltstone formed the bedrock unit across the site with a depth to the top of the unit varying between 35.9 m and 42.3 m. The siltstone was generally moderately or less weathered and was of medium strength with typical UCS strength of 5 MPa to 15 MPa.

A cross section of the site running west to east along the length of the wharf is shown in Fig. 1 below.

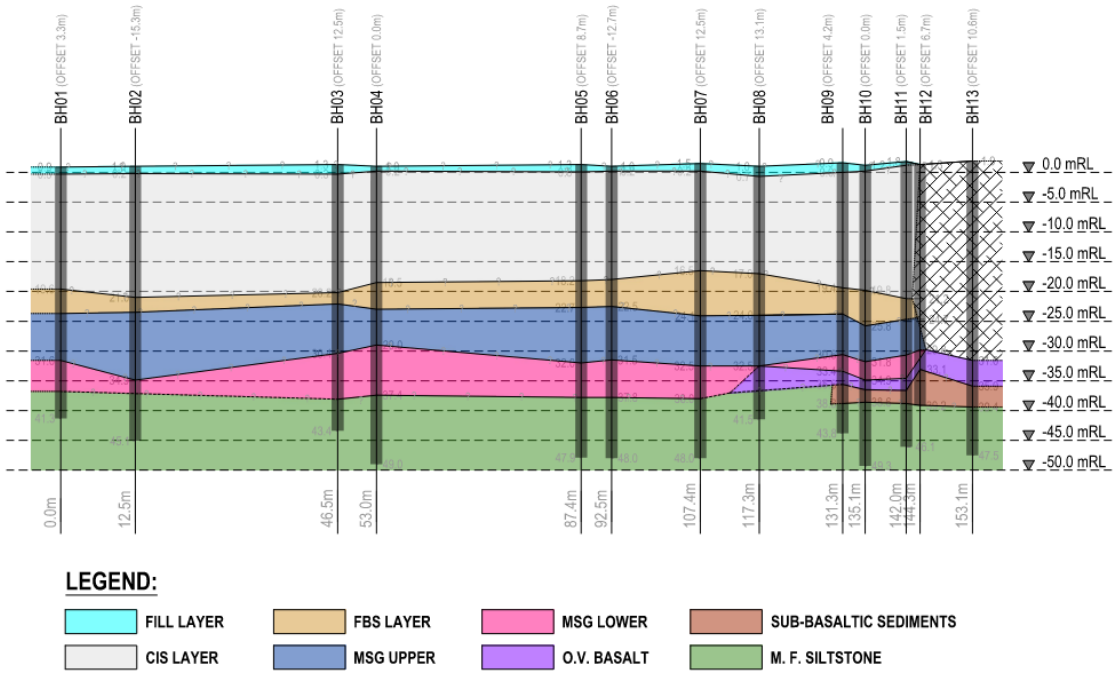


Fig. 1. Borehole cross-section with inferred layer boundaries

DESIGN CONSIDERATIONS

Keller's previous experience within the locality demonstrated that the area was particularly sensitive to cumulative soil movements due to the effects of new pile installations. This sensitivity was driven by the site geometry, nearby structure stiffnesses and bathymetry of the river and harbour on the southern and northern sides respectively, combined with poor soil conditions. These soil movements can adversely affect the foundations and super structures of nearby assets as well as the piles themselves (Fetherston et al., 2019). There were concerns that significant ground movements could result in costly remediation if the timber piles supporting the northern wharf were damaged. Further, the newly constructed cantilever sheet pile seawall on the southern boundary had a strict deflection limit which had to be met to avoid damage to the structure.

Global Finite Element Modelling (FEM) analysis of a section of the site from the south sea wall through to the northern wharf was carried out by the project geotechnical consultant, FSG, with input from Keller to determine an optimal balance between cost of construction and mitigation of soil movements. CFA piles, installed by pumping concrete through a hollow stem and plunging reinforcement cages, represented the greatest concern for soil movement on the project. CFA piles

 © Deep Foundations Institute 2026

installed in the Docklands area have been known to produce significant over supply (actual pumped volume/theoretical volume x 100) that are regularly within 150% to 200% and on occasion higher than this. The majority of this oversupply is caused by the horizontal displacement and compression of the very soft clay CIS material. Detailed modelling showed that this oversupply of concrete, if not adequately controlled, could produce cumulative large displacements, with consequential impacts on the seawall, timber wharf piles and adjacent new piles.

The FEM analysis showed that, due to the sensitivity of the adjacent timber pile wharf and southern seawall, a full CFA piling solution was deemed an unacceptable risk to damage the northern wharf piles. In addition to this, both the northern and southern zones of the site were unable to support the heavy equipment required for 45 m deep, 900 mm diameter CFA piles. As a result, the 11 m area within the southern seawall was limited to a minimal construction bearing pressure limit whilst the 14 m zone adjacent to the northern wharf was limited to a moderate bearing pressure. This left a remaining zone within the middle of the site which was able to sustain bearing pressures from heavy equipment such as 140 t piling rigs and 280 t tracked cranes. A markup of the eastern section of the site with equipment restriction zones is shown in Fig. 2 below

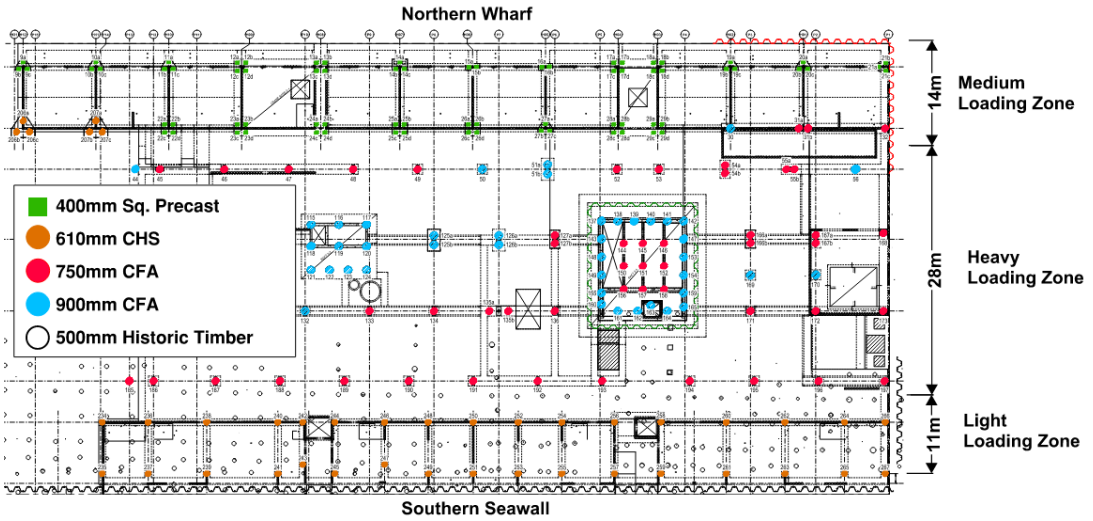


Fig. 2. Site plan of the restricted plant loading zones and pile types

As the 750 mm and 900 mm CFA piles were installed to depths of up to 45 m, full length cages were not feasible to install due to limitations in concrete workability. A typical practice in the construction of CFA piles is to curtail the cages at a certain depth where the pile actions have dissipated sufficiently as outlined in AS2159-2009 section 5.3.4 (Standards Australia, 2009). Due to the sensitivity of the site to soil displacements as a result of pile installation effects, careful consideration was required to determine induced forces in piles due to subsequently installed piles.

Keller undertook finite element analysis using a PLAXIS 2D plane strain model. The foundation pile was modelled using embedded pile elements, with soil-pile interaction represented by interface elements and an interface reduction factor of 0.7. The surrounding soil was represented using a hardening soil constitutive model. Soil layers and parameters adopted in the model can be seen in Table 1 below with depth in metres reference level (mRL). The model extent was 60 m laterally, which was sufficient to avoid boundary effects, with the base fixed in both horizontal and vertical directions.

A plane strain modelling approach was adopted based on observed field behaviour for the previous adjacent development, whereby the majority of measured ground displacements occurred predominantly in the north–south direction, with minimal displacement recorded in the east–west direction. This supported the use of a north–south plane strain slice to represent the dominant pile–soil interaction mechanism.

Table 1. Geotechnical parameters

	Top Depth (mRL)	γ, Density (kN/m3)	E', Drained Elastic Modulus (MPa)	C', Drained Cohesion (kPa)	Φ, Friction Angle (Deg)	ν, Poisson's ratio
Fill	2	18	20	5	28	0.3
CIS	0	16	0.6	2	26	0.3
FBS	-19	17	23	5	26	0.3
Upper MSG	-23	18	100	0	40	0.25
Lower MSG	-31	18	40	0	35	0.25
Siltstone	-38	24	600	60	35	0.25

Pile installation effects were simulated using a staged construction sequence in which prescribed horizontal soil displacements were applied, based on deflection profiles from nearby inclinometer data (Fetherston et al, 2019). Consecutive displacement profiles were applied at approximate pile spacings, to represent the expected sequence of pile installation within the zone of influence.

The model was used to predict induced bending moments and shear forces in the piles at depth due to installation effects from subsequently installed piles. The modelling showed that a plain concrete section was inadequate to resist the predicted forces, consequently, reinforcement was required to be installed to 30 m depth to service the forces predicted at the interface of the CIS and FBS. Figure 3 shows the predicted bending moment profiles from the PLAXIS 2D analysis, including Serviceability Limit State (SLS) load moments caused by installation effects as well as the additional moments generated by earthquake shear forces. The results shown in Fig. 3 are based on free-head boundary conditions. However, the Ultimate Limit State (ULS) load case includes a non-zero bending moment at the pile head arising from eccentricity associated with axial earthquake loading.

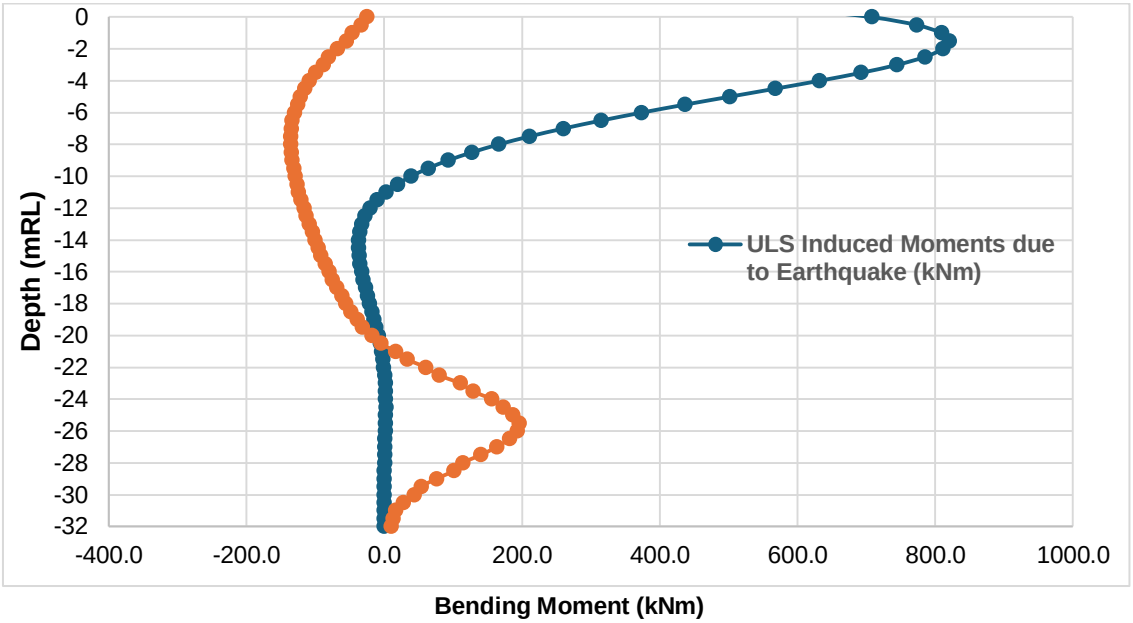


Fig. 3. Predicted bending moments for a 900 mm CFA pile

Significant earthquake and wind induced shear loads were present in the building cores, resulting in a correspondingly high rate of required reinforcement. Bending moments from earthquake and wind loads were combined with those induced by soil displacement from the pile installation, with pile

 © Deep Foundations Institute 2026

installation-induced moments considered to act concurrently with earthquake/wind effects to capture the most critical bending moments in the piles.

Keller installed inclinometers in corner piles within the cores and at CFA piles close to the seawall to record actual displacements. The results confirmed that the predicted displacement and bending moment profiles represented a real mechanism, although they were somewhat underpredicted. Nevertheless, the design reinforcement was adequate for the measured deflection profiles. Further work by the authors is planned to interrogate and present this data in a subsequent paper. Based on the analysis and field monitoring undertaken for this project, the authors counsel that pile reinforcement depths in this locality require careful consideration. Plain concrete sections are unlikely to be adequate for resisting installation induced bending moments at the interface between the FBS and CIS, and reinforcement or structural steel should extend sufficiently below soft soil layers and competent material interface to accommodate for these effects.

The target formation of the CFA piles was basalt or siltstone rock formations. The basalt flow, as discussed in earlier sections, posed significant challenges to the installation of the CFA piles. The basalt extended across one third of the footprint of a large core containing 30 piles with a sub-basaltic sediment layer underneath the basalt. Local drilling experience with a 140 t piling rig capable of drilling 35 m in a single pass with 100 t extraction force, suggested that a portion of the piles would refuse in the basalt at 30 m and the remaining piles would penetrate through the basalt and extend to the siltstone bedrock. To develop a robust design solution, additional boreholes were drilled within the core to confirm the thickness and quality of the basalt. The pile design accounted for potential refusal by considering multiple scenarios, including piles partially founded on the basalt overlying the sediment layer, and assessing the resulting axial capacity and settlement. These analyses ensured that acceptable performance could be achieved for all potential refusal conditions while minimising the risk of differential settlement and construction delays.

ADOPTED FOUNDATION DESIGN SOLUTION

Although CFA piles were the most cost-effective solution, their use was restricted to the interior of the site, where the ground had sufficient bearing capacity and ground movement risk was lower. Large concentrations of CFA piles were present in the two main cores which were located along the centre line of the building between the northern and southern extents. These cores were identified as a high-risk area following stage 1 of the development. To mitigate the risk of these cores impacting the northern wharf and southern seawall, a sheet pile wall around the perimeter of the cores was installed prior to CFA piling to contain the lateral pressures and displacements from pile installation whilst also ultimately providing retention support during the construction of the cores.

Driven precast concrete piles were selected in the northern zone of the site adjacent to the existing northern wharf. As driven displacement piles would typically be a concern for soil displacement, the top 12 m was identified as the most important depth to minimise impacts on the northern wharf piles. Consequently, the piles were predrilled to a depth of 12 m within the collapsible CIS soil layer.

The southern zone, closest to the new southern seawall presented two critical challenges. The first, bearing pressure from piling rigs required to install these piles was shown to cause excessive displacement and risk of failure of the cantilever seawall. Thus, a strict bearing pressure limit was imposed, limiting equipment in this zone to a 14 t excavator or lighter. Second, FEM analysis by FSG demonstrated that soil displacements caused by precast, predrilled, driven piles or CFA piling near the seawall would result in excessive deflections compromising the integrity of the new seawall.

To address these constraints, open ended Circular Hollow Section (CHS) piles were selected for the southern side of the site. The contractor undertook drivability analysis to confirm that plugging was unlikely to occur based on the pile design details. Plugging of the CHS piles would have resulted in more adverse outcome for soil displacements and southern seawall integrity than CFA pile installation. To accommodate the restricted bearing pressure limit, Keller utilised a bespoke pad and

 © Deep Foundations Institute 2026

grillage system for the mobile leader frame, comprising concrete pads supporting steel beams, as shown in Fig. 7. Drivability analysis was undertaken to determine the appropriate hammer size to drive the piles to the required depth and ensure premature refusal was prevented. The CHS piles were to be connected to the superstructure via a concrete plug with a reinforcement cage. The CHS was constructed with 20 mm thick rectangular steel bars welded to the inner face of the CHS to form a ring, known as a shear key/ring (API, 2002, p. 73, Figure 7.4.4.b). Given the unknown depth of refusal, twenty shear rings were installed at 0.5 m spacings to ensure sufficient shear rings were engaged regardless of refusal depth.

The varying pile types led to an iterative design process between the project structural engineer, Mordue, Keller and FSG. Each pile type had a distinct pile stiffness and a limited geotechnical lateral capacity. As the pile sizes and quantities were refined, this resulted in a redistribution of the axial and shear loads on the piles in the structural model. This process would often cause a pile shear load to increase and require either a change in pile diameter or the quantity of piles, which would correspondingly attract more shear load due to a higher stiffness. The iterations between the pile design and the structural design continued until the two converged.

CONSTRUCTION

Sheet Piles

The sheet piles, consisting of 38 No. and 40 No. double clutched AZ18 approximately 16 m long were installed as the first activity in the cores of approximately 14 m x 14 m. The sheet piles were designed to retain a core excavation of approximately 2.7 m. The cores of the building, supported by approximately 30 CFA piles in each, presented significant risks of potential lateral ground movements. To minimise this, sheet piles also had the added function of confining the soil movements due to pile installation within the core.

Sheet piles were also installed at the northeast and northwest boundaries of the sites, intending to protect the adjacent assets from excessive soil displacement and pressures due to pile installation effects. These piles consisted of AZ38 double clutched sheet piles approximately 22 m long forming an L-shaped alignment, with each leg approximately 15 m in plan dimension. The sheet piles were vibrated to depth using a 70 t piling rig capable of pitching 22 m sheets. Figure 4a below shows the rig installing sheets and Fig. 4b shows the core excavation.

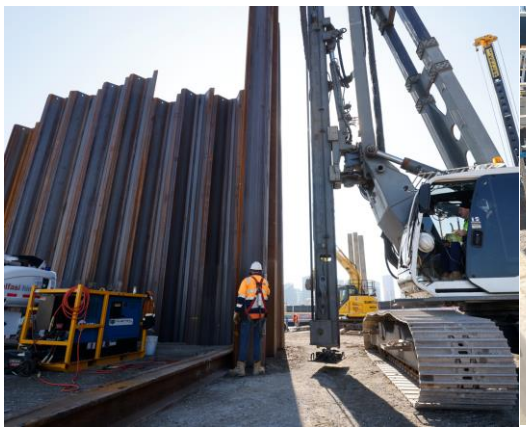


Fig. 4a. Installation of sheet piles



Fig. 4b. Excavation of core

Precast Concrete, Predrilled, Driven Piles in Northern Zone

Precast concrete driven piles were installed adjacent to the timber wharf piles along the northern edge of the project site. Predrilling was undertaken using a small CFA piling rig, selected to satisfy the bearing pressure limitations of the northern medium loading zone, with a CFA auger advanced to 12 m depth and spoil fully removed. Due to the low shear strength of the CIS, the open hole was

 © Deep Foundations Institute 2026

susceptible to collapse following auger withdrawal. To mitigate this risk, Keller adopted a controlled drilling and installation sequence that minimised the time the hole remained open through immediate placement of the first precast pile segment. Drilling and installation were performed sequentially, completing one pile per pile cap before returning to remaining piles in the cap after approximately 24 hours. This predrilling methodology was found to be highly effective in minimising the impact on the surrounding assets.

The available working area for the precast piles was restricted to a thin, 14 m wide corridor. Given the restricted working area, the pile installation order had to be carefully planned to ensure that test piles remained accessible throughout the installation. This involved strategic placement of piles and careful scheduling to avoid obstructing access to test piles to allow for the dissipation of installation stresses of the driven piles to demonstrate maximum capacities at 5 days post installation.

The precast concrete driven piles were 400 mm square concrete piles of three and four segments with total pitched lengths between 38 m and 43 m. Design lengths accounted for a thinning basalt layer, which presented sloping rock surfaces that could damage piles during driving and areas of insufficient thickness that limited pile support, as well as potential refusal in variable MSG and an anticipated founding depth that increased toward the western end of the site. Segment lengths were considered to allow for casting efficiencies, variable founding conditions and to ensure pile joints were founded at sufficient depth below pile cut off levels where bending moments had dissipated. All piles were driven to practical refusal in basalt or siltstone defined on this project as a pile penetration of 3 mm per hammer blow using the 7 t accelerated hammer. The piles were installed in pile caps consisting of groups of 2, 3 and 4 piles. The predrilling was undertaken by a 73 t piling rig capable of drilling 16 m in a single pass with 18 t extraction force, using a 600 mm diameter auger. The precast piles were installed using a 73 t piling rig capable of pitching 14 m precast segments, fitted with a 7 t accelerated hammer. Installation of the precast piles is shown in Fig. 5 below.



Fig. 5. Installation of precast piles using a 73 t piling rig

Continuous Flight Auger Piles in Internal Zone

The CFA piles installed were up to 45 m long. A 140 t piling rig was utilised to reach 45 m depth. Splitting of and addition of augers was required for these depths. The splitting of augers was carried out by Keller's expert CFA piling crew to ensure there was no compromise of pile quality during the process. The 140 t piling rig is shown in Fig. 6 below. To minimise construction-induced effects during the CFA pile installation, several control measures were implemented. Piles installed on the same day were required to maintain a 10 m exclusion zone, ensuring that no other piles were installed within that area. Additional measures included avoiding vehicle tracking near freshly installed piles, keeping material storage away from the installation area, minimising spoil accumulation, and controlling concrete supply to avoid oversupply, all while maintaining pile quality.



Fig. 6. Installation of CFA piles using 140 t piling rig

Circular Hollow Section Piles in Southern Zone

CHS piles, consisting of 46 m length, 610 mm Outer Diameter with 20 mm wall thickness and 40 mm thick driving shoes were installed in the southern zone where low soil displacement and limited construction bearing pressures were imposed. The critical area was located adjacent to the southern seawall where reclaimed land had been filled with lightweight scoria fill, and layers of geogrid to provide a working platform. To control the deflections and stability of the cantilevered sheet pile seawall, bearing pressures of plant and machineries were limited to 75 kPa within the closest 10 m. This limitation ruled out any conventionally tracked piling rig capable of drilling to the depths required.

Keller worked closely with steel suppliers and shipping companies to work within the restrictions of the site, geometry and wheel load restrictions, to ensure the most cost-effective lengths of piles could be delivered. Delivering and pitching the steel sections in a single length was not practical as this would have required barge deliver and a significantly larger crane to unload a barge with a crane positioned on the internal zone of the site. The piles were delivered to the site via road transport, limiting the length of the piles to the available turning circle and swept path analysis in the tight city streets of the Melbourne Docklands area. The piles were delivered to site as two sections per pile.

The CHS piles were sourced from China, with Keller and our third-party inspector carrying out inspections during the initial fabrication in China to ensure compliance with the project specifications and Australian standards.

To install the CHS piles, a pile guide frame with modular bearing beams and pads was used. The guide frame, when placed in position, was used to pitch and control the pile sections, with the bottom section of the pile lifted into place and held by the 16 m tall guide frame. The articulation of the frame allowed it to access pile locations without redeploying the bearing beams and pads multiple times. A 280 t crane was used in the internal zone of the site to install and relocate the guide frame and piles as required. A site view of the frame is provided in Fig. 7 below.

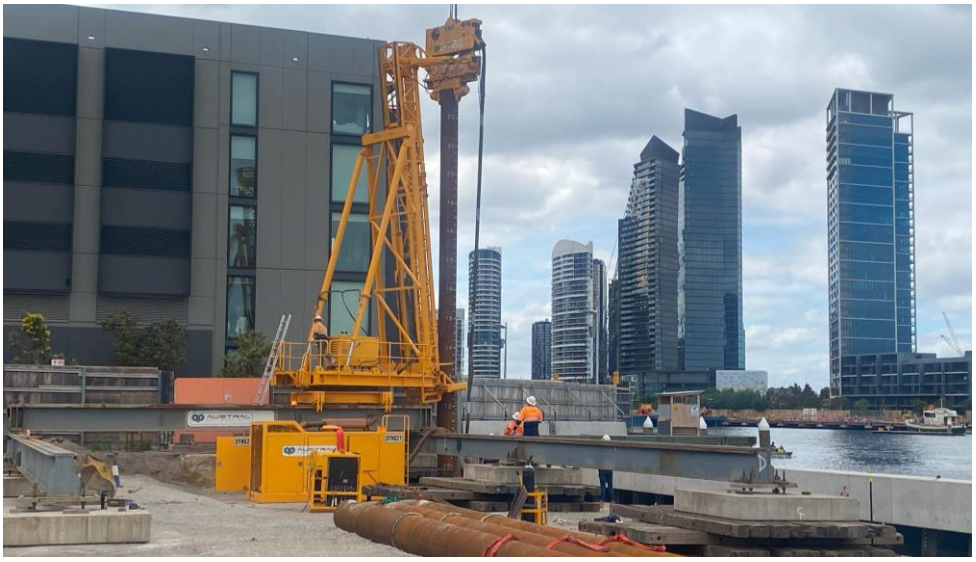


Fig. 7. The guide frame vibrating CHS pile

The CHS piles were installed in two sections, by using a combination of crane mounted vibrator and a 150 kJ hydraulic impact hammer. They were driven to a predetermined pile set measured via a Pile Driving Monitor (PDM) and confirmed via Dynamic Testing carried out during the installation. Following completion of driving, the CHS piles were cut to the desired level, and the internal soil was drilled out followed by cleaning the internal shear rings in preparation for concreting. Reinforcement cages were then placed at the required level and concrete poured. A thickened internal driving shoe was utilised to reduce the risks of plugging of the CHS piles. Plugging across the site was found to be minimal; the majority of piles exhibited either soil heave above platform level or a depth to soil a maximum of 2 m below the platform level.

Testing and Verification

Due to the varied founding conditions in basalt and siltstone, the variety of pile types, and the large loads imposed on the piles, a testing program was undertaken. A total of 6 DLTs (Dynamic Load Tests) were carried out on the 750 mm and 900 mm diameter CFA piles, along with 6 DLTs on the 400 mm precast piles and 6 DLTs on the 610 mm steel CHS piles. All DLTs were subject to CAPWAP analysis to confirm pile capacities were achieved. The precast piles were tested utilising the 7 t accelerated driving hammer used during installation. The CFA piles were tested using a 20 t test hammer and the CHS piles were tested using the S-150 driving hammer. The DLTs on the precast and CHS piles consisted of tests at the end of drive and at 7 days. CFA piles were tested a minimum of 7 days post installation.

CONCLUSION

The project demonstrated that sites underlain by soils of poor consistency and located close to sensitive structures such as seawalls or wharfs require a combination of foundation techniques rather than reliance on a single method. CFA piles were the most cost-effective solution but, due to installation effects, could not be used within 10 m to 15 m of the sensitive structures and were therefore limited to the middle portion of the site. Predrilled precast piles provided an efficient solution in the northern wharf zone where podium loads were lower than in the main building, allowing small groups of precast piles to be adopted. A unique predrilling approach was successfully implemented to predrill the top 12 m of CIS without collapse of the open hole. In the most sensitive southern zone, steel CHS tubes were required due to a combination of construction bearing pressure limitations and the displacement sensitivity of the flexible seawall structure influenced by local bathymetry. The guide frame enabled this solution to be installed successfully. Sheet piles were also used to confine installation pressures from the CFA core piles.

Finite element modelling and inclinometer monitoring confirmed that installation effects induce significant lateral displacements in CIS, generating bending moments at depth that plain concrete pile sections could not resist. Reinforcement to 30 m depth was required to manage these effects and ensure adequate performance at the CIS–FBS interface. Monitoring during construction showed that the predicted mechanisms were real, although the analysis underpredicted the magnitude of displacement. This data will support future work on pile–soil–structure interaction in soft clay sites.

The project highlighted the importance of iterative design between the geotechnical designer, the structural engineer, the contractor and the developer, particularly where piles of different stiffness and capacity influenced the distribution of superstructure loads to the foundations. Early engagement with all parties meant the major challenges could be worked through without taking an overly conservative approach, which gave a more refined and optimised design. The experience reinforced that close collaboration, flexibility in pile type selection and strong monitoring are critical to delivering deep foundation works in ground that is prone to lateral soil movement next to sensitive wharf structures.

Successful outcomes on sites like this depend on combining multiple piling techniques with close collaboration and monitoring to control soil movements and protect sensitive adjacent structures.

REFERENCES

American Petroleum Institute (API), 2002. Recommended Practice for Planning, Designing and Constructing Fixed Offshore Platforms—Working Stress, Errata and Supplement 1. API Publishing Services, Washington D.C. 73 p.

Fetherston, J., Flynn, R., and Chong, W., 2019. Lateral soil displacement resulting from the installation of CFA piles in soft marine clays. Proceedings of the 13th Australia New Zealand Conference on Geomechanics, Perth, Australia, April 1–3, Acosta-Martínez, C. and Lehane, B.M., Editors, Australian Geomechanics Society, Sydney, Australia, ISBN 978-0-9946261-0-3, 6 p.

Peck, W.A., Neilson, J.L., Olds, R.J., and Seddon, K.D., 1992. Engineering Geology of Melbourne. Proceedings of the Seminar on Engineering Geology of Melbourne, Melbourne, Victoria, Australia, 16 September 1992. A.A. Balkema Publishers, Rotterdam, 327 p.

Standards Australia, 2009. AS2159-2009 piling—Design and installation. Standards Australia International Ltd., Sydney, 96 p.

 © Deep Foundations Institute 2026

ASSESSING THE IMPACTS OF EMBANKMENT CONSTRUCTION OVER SOFT SOIL ON AN ADJACENT BRIDGE

Jonathan Thayalan, Associate Geotechnical Engineer, WSP Australia, Brisbane, QLD, Australia, +61738546944, jonathan.thayalan@wsp.com
Ivan Tse, Principal Geotechnical Engineer, WSP Australia, Brisbane, QLD, Australia, +61733686692, ivan.tse@wsp.com

ABSTRACT

The growing demand for transport infrastructure often necessitates the construction of embankments and structures on soft or unfavourable ground conditions. In southeast Queensland and northern New South Wales, many highway projects are built through swampy, marine environments underlain by highly compressible clays. While managing long-term settlement during the pavement service life is a common design concern, the proximity of sensitive structures introduces additional challenges, particularly due to the lateral spread of soft soils. This paper presents the approach and findings of 3D numerical modelling using PLAXIS 3D (Bently, 2023a; 2023b), undertaken to assess the displacements induced on a bridge pier and abutment resulting from the construction and consolidation of an adjacent 10 m-high road embankment in a recent southeast Queensland project. The study highlights how construction sequencing and structural configuration influence the mitigation of long-term impacts on the structure. The results provide practical insights into the integrated geotechnical-structural design strategies for infrastructure in soft soil environments.

Keywords: pile impact assessment, soft soils, soil structure interaction

INTRODUCTION

The design of highway embankments over soft soils typically necessitates the geotechnical designers to assess long-term pavement settlements and stability of the embankment and its batter slopes. Consolidation of the soft soils beneath the embankment can result lateral soil movements, which may adversely affect adjacent structures. In such cases, the magnitude of structural displacements must be assessed and provided to the relevant asset owner or designer for consideration. Numerical modelling using commercially available software is typically used for such assessments. The methodology and outcomes of numerical modelling using PLAXIS 3D, undertaken for a highway project in southeast Queensland, to assess the displacements of piles for the bridge abutment and pier of a shared path bridge due to the lateral spread of soft soils caused by the construction of a parallel 10 m embankment are presented in this paper. The effects that construction staging and structural arrangement have on the induced pile displacements are also explored.

COMPARISONS WITH OTHER PILE IMAPCT ASSESSMENT STUDIES

Numerous studies have been conducted to assess the impacts of bridge abutment construction over soft clay foundations, such as those by Emara et al. (2022), Turan et al. (2013), and Rahman et al. (2024), where two and three-dimensional numerical modelling was utilised to assess the displacements induced on bridge abutments by long term consolidation of approach embankments. In these scenarios, the primary direction of displacements is longitudinal to the bridge alignment. Typically, during design development, if longitudinal displacement due to soft soils is expected, the bridge designers may alter the design of superstructure elements (i.e., bearings and expansion joints) to cater for the movement. Furthermore, the stiffness of the bridge deck may offer restraint against longitudinal movement. The bridge structure assessed as part of this study is located parallel to the consolidating embankment, such that much of the magnitude of displacement is transverse to the bridge alignment. In the transverse direction, the bridge superstructure offers minimal restraint against soil induced displacement, as such the foundation system must be designed to accommodate.

 © Deep Foundations Institute 2026

SITE LAYOUT

The site is approximately 16900 m^2 and is located on the edge of a wetland in southeast Queensland. The site comprises a 10 m high highway embankment, the highway ramp embankment ranging from 2 to 4 m high, and a 5 m high bridge approach ramp. The bridge abutment and pier are 23 m apart and are offset ~20 m and ~27 m, respectively, from the toe of the highway embankment. The bridge itself is a ~5 m wide shared path (pedestrian and cycle) bridge. The site layout plan is shown in Fig. 1.

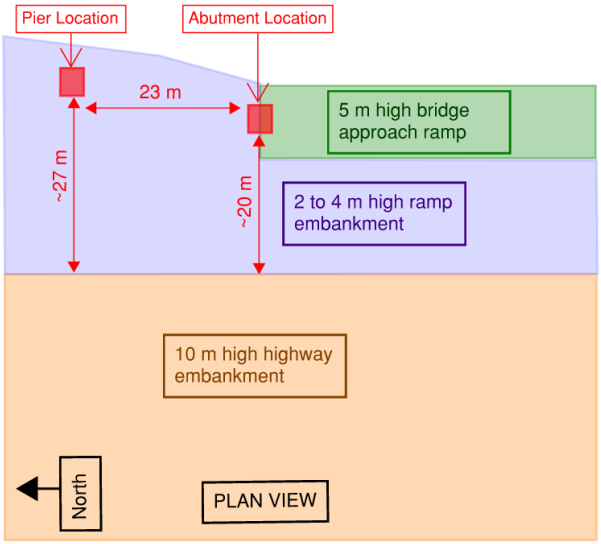


Fig. 1. Site layout plan (NOT TO SCALE)

Cross sections of the embankment geometry at the abutment and pier locations are shown in Fig. 2 and 3, respectively.

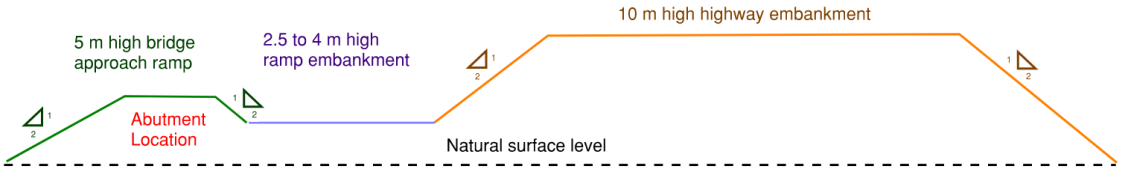


Fig. 2. Cross sectional geometry at the abutment (NOT TO SCALE)

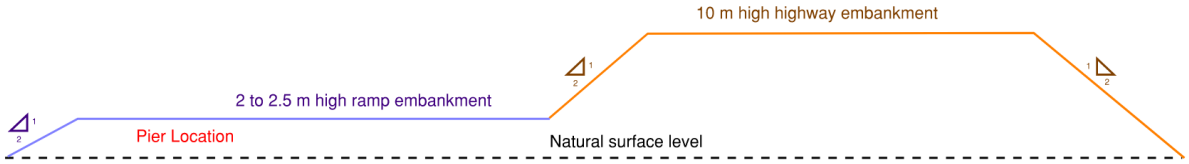


Fig. 3. Cross sectional geometry at the pier (NOT TO SCALE)

GROUND CONDITIONS

Geotechnical site investigations, comprising 19 boreholes and 15 cone penetration tests (CPTu), were completed to understand ground conditions across the site. The site ground profile is summarised in Table 1. The groundwater level across the site is typically at surface.

 © Deep Foundations Institute 2026

Table 1. Ground profile

Material Description	Depth Range (m bgl)
Very soft to soft silty / sandy clay	0 to 4
Firm silty / sandy clay	3 to 5
Very loose to loose clayey sand	3.5 to 4
Stiff to very stiff sandy clay	4 to 10
Medium dense to dense silty sand	10 to 15
Extremely weathered materials (very dense sandy / clayey gravel)	15 to 15.5
Highly weathered or better rock (Metagreywacke)	>15.5

Note: m bgl = meters below ground level

Undisturbed tube samples were taken from the boreholes within soft clay layers for laboratory testing, 15 oedometer tests were undertaken to assess consolidation characteristics of the encountered material. Pore pressure dissipation tests were done at each CPTu, within the soft clay layers, to establish permeability of the materials. Following interpretation of the site investigation data, the consolidation parameters presented in Table 2 were derived for the soft clay layers.

Table 2. Summary of soft soil consolidation parameters

Material Description	Depth Range (m bgl)	CR	RR	Cαε	OCR	C_v (m^2 / year)
Very soft to soft silty / sandy clay	0 to 1	0.24	0.05	0.0096	4.5	9
Very soft to soft silty / sandy clay	1 to 4	0.24	0.05	0.0096	3	9
Firm silty / sandy clay	4 to 5	0.24	0.05	0.0096	9	9

Note: CR = compression ratio, RR = re-compression ratio, Cαε = secondary compression ratio, OCR = overconsolidation ratio, C_v = coefficient of vertical consolidation

CONSTRUCTION STAGING

The main construction sequence of the bridge structure and earthworks is summarized in Table 3. The original construction sequence had been adopted at the beginning of the project design stage, however, during the design development, the construction sequence was revised. The key modification in the revised construction sequence is the decision to construct the bridge structures prior to the placement of the 10 m high embankment and the associated preloading. This was a client driven decision, as the builders engaged to construct the bridge were different to those engaged to construct the embankment, and both could not occupy the site at the same time. Under the original construction sequence, the embankment loading and preloading would have been completed before the bridge built, allowing ground movements to largely dissipate prior to the construction of the structures. In the revised construction sequence, however, the bridge structure will be in place during embankment placement, and as a result, will be directly subjected to the ground movements and stresses induced by the embankment loading.

This change has important implications for the design, as the structure must now be assessed to ensure it can accommodate or withstand the additional deformations without adverse effects on structural performance or serviceability.

 © Deep Foundations Institute 2026

Table 3. Summary of main construction sequence

Stage	Original construction sequence	Revised construction sequence
Stage 1	10 m high embankment construction	Abutment structures construction
Stage 2	Embankment preloading	Approach ramp construction
Stage 3	Abutment structures construction	10 m high embankment construction
Stage 4	Approach ramp construction	Embankment preloading
Stage 5	Road opening (application of traffic live loads in the model)	
Stage 6	100-year design life	

NUMERICAL MODELLING APPROACH

Finite element analyses using commercial software PLAXIS 3D was undertaken to assess the impacts of the embankment consolidation on the bridge structure. Three-dimensional models were developed instead of 2D plane strain models as they would better capture soil movement around the rigid pile elements. The very soft to soft and firm clays were modelled using the Soft Soil Creep material model (Bently, 2023a; 2023b), which is commonly used in the industry when simulating the consolidation behaviour of compressible clays in PLAXIS. The stiff and better clays, sands, and extremely weathered materials were modelled using the Hardening Soil model, whilst the rock was modelled using the Mohr Coulomb model (Bently, 2023a; 2023b).

Prior to creating the 3D models, a series of 1D calculations using Terzaghi's 1D consolidation theory (Terzaghi, 1943) and unit cell PLAXIS 2D models were undertaken to calibrate the vertical permeabilities input in PLAXIS (k_y) with the vertical coefficient of consolidation (C_v) interpreted from CPTu pore pressure dissipation testing. The calibrated vertical permeability values were then used in the 3D models (as k_z), horizontal permeability values (k_x and k_y) are adopted as 2 times the vertical permeability. This calibration is an important step in the analysis process, as it ensures that the rate of pore pressure dissipation is correct in the PLAXIS 3D model.

Three analysis cases were undertaken for both the bridge abutment and pier locations, these are summarised in Table 4.

Table 4. Summary of analysis cases

Case	Description
Case 1	Models the original construction sequence presented in Table 3
Case 2	Models the revised construction sequence presented in Table 3
Case 3	Models the revised construction sequence with revised structural configuration

Prior to undertaking the Case 3 analyses the structural configuration for both the abutment and pier were revised. The structures were redesigned to become more robust as to sufficiently withstand the lateral spread of soft soils induced by the construction and consolidation of the adjacent embankment. Details of the original and revised structural configurations are described in subsequent sections.

ABUTMENT IMPACT ASSESSMENT

Figure 4 presents the model used for impact assessment of the abutment. The bridge abutment and approach ramp are located approximately 25 m from a 10 m high embankment. Approximately half of the soft soil immediately surrounding the soft soil is removed and replaced with engineered fill. This was done primarily to limit long term settlement of the approach ramp immediately behind the abutment but also helps reduce pile displacements. The abutment consists of a headstock supported by two 1.2 m diameter cast-in-place bored piles spaced at 3.0 m c/c. The piles are socketed approximately 3 m into the highly weathered rock. The headstock comprises a 1.5 m (W) × 5.1 m (L)

× 1.7 m (D) beam connecting to the piles, with a 0.3 m thick upstand wall extending to the embankment crest. The beam and wall are modelled as plate elements; the piles are modelled as embedded beam row (EBR) elements (Bently, 2023a; 2023b). The structural arrangement modelled in PLAXIS 3D is shown on Fig. 5.

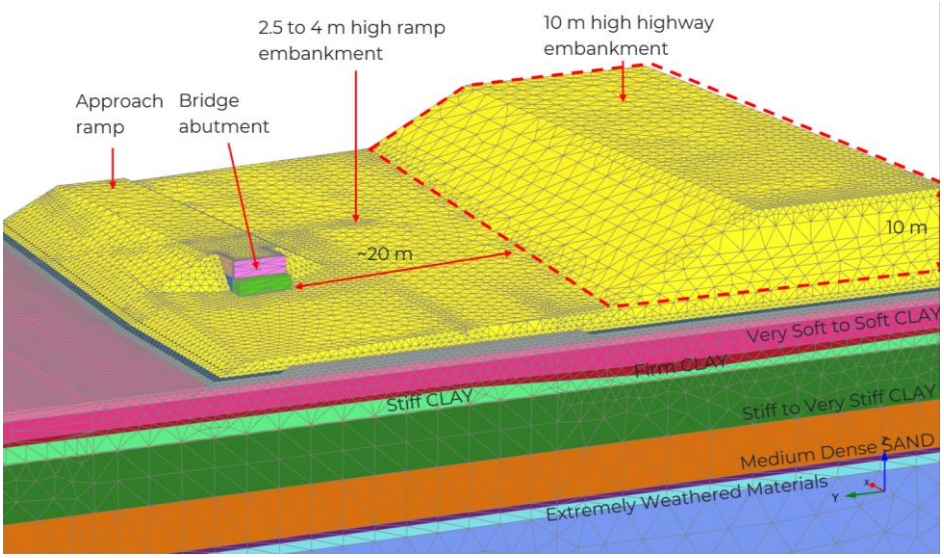


Fig. 4. General arrangement of the abutment 3D model (NOT TO SCALE)

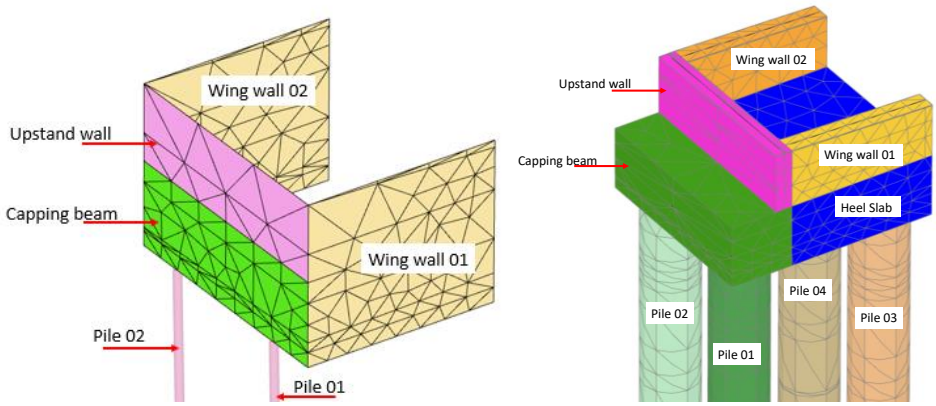


Fig. 5. Structural arrangement modelled in PLAXIS 3D, Case 1 and Case 2 (LEFT), Case 3 (RIGHT) (NOT TO SCALE)

For the impact assessment, pile displacements at the end of the 100-year design life were extracted from the analyses. The results are presented for both longitudinal direction (parallel to the embankment) and the transverse direction (perpendicular to the embankment). Figure 6 shows the displacements of the pile located closest to the embankment, while Fig. 7 shows the displacements of the pile located farther away from the embankment. As expected, the piles in Case 2 exhibit noticeably greater displacement compared with Case 1, reflecting a significant influence of lateral soil movement induced by the construction of the 10 m high embankment. The predicted top-of-pile longitudinal displacements in Case 2 are about three times greater than those predicted in Case 1.

The calculated top-of-pile movements in Case 2 were considered unacceptable for this project. To reduce the top-of-pile displacements and enhance the overall performance of the bridge abutment structures, the abutment configuration was revised. In the revised design, two additional piles were incorporated, increasing the foundation capacity and stiffness. The final configuration is shown on Fig. 5. and consists of a 5.5 m (W) × 5.1 m (L) × 1.7 m (D) reinforced concrete base slab supported by four 1.5 m diameter bored piles. The piles are arranged at 3.3 m centre-to-centre (c/c) spacing in the

transverse direction and 4.0 m c/c spacing in the longitudinal direction, providing improved resistance to both longitudinal and transverse displacements. The base slab is cast integrally with a 0.3 m thick upstand wall and two 0.3 m thick wing walls, which extend to the embankment crest. This revised arrangement not only reduces the predicted pile head displacements but also improves the stiffness of the abutment system under the embankment loading, albeit at a considerable increase in costs for the structural elements. The predicted top-of-pile displacements for the revised structural configuration, which is in Case 3, are presented in Fig. 6 and 7.

Compared to Case 2, the top-of-pile displacements in Case 3 are reduced by approximately 50%, demonstrating the effectiveness of the revised design in mitigating the adverse effects of the 10 m high embankment construction. However, the displacements in Case 3 remain greater than those in Case 1, indicating that constructing the 10 m high embankment before abutment construction has a more significant impact on the abutment performance.

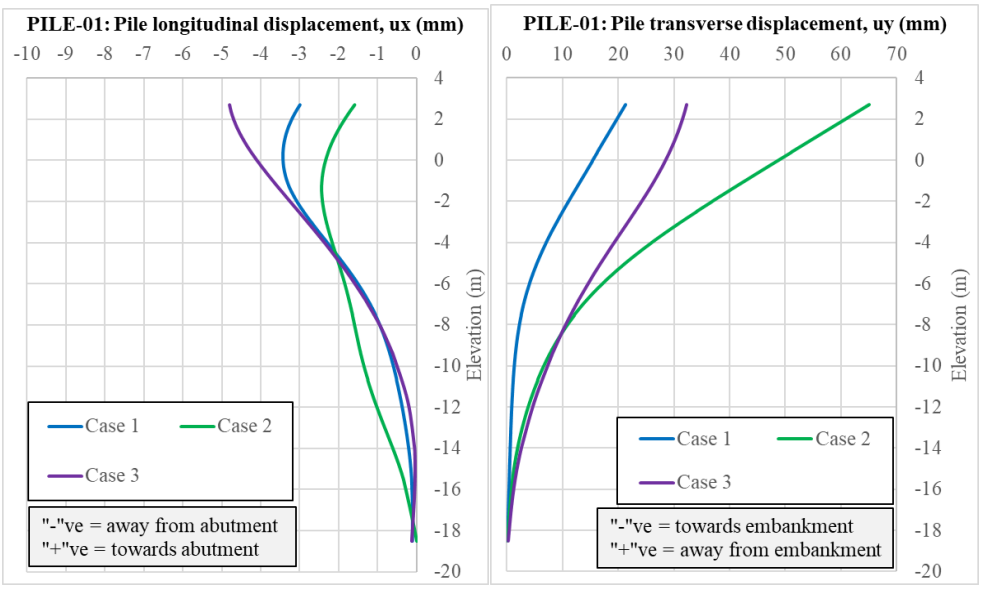


Fig. 6. Pile displacements of abutment PILE-01 (near) for Cases 1 to 3

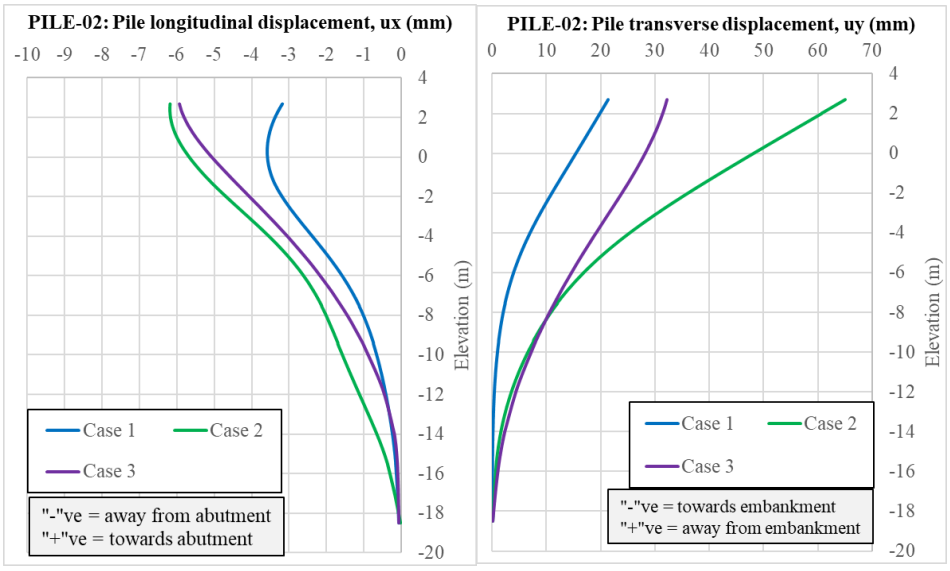


Fig. 7. Pile displacements of abutment PILE-02 (far) for Cases 1 to 3

Refining the Abutment 3D Model

The abutment structures are modelled as plate elements and EBR elements in Case 1 and Case 2 analyses (see Fig. 8 below). While this approach provides a simplified representation of the system, it does not fully capture the actual geometry and dimensions of the abutment structures. As a result, the model may not reflect the complete stiffness and load-transfer characteristics of the physical structures.

In the Case 3 analysis, the structural configuration was revised, and the modelling methodology for the structural elements was updated to better capture their behaviour.

The abutment structures were modelled as volume elements (Bently, 2023a; 2023b), allowing for a more detailed representation of the structural components' stiffness and their interaction with the surrounding soil. While this approach involves more detailed meshing and the use of additional interface elements, and requires increased computation time, it enhances the accuracy of the predicted pile displacements and load-transfer mechanisms. The pile displacements predicted using both plate and EBR elements and the volume elements are presented in Fig. 5 and 6. The top-of-pile displacements from the volume elements model are about 5 mm less than those predicted using the combination of plate and EBR elements. If the deflection criterion is 35 mm, this 5 mm difference represents about 14% of the allowable limit, which is a significant value.

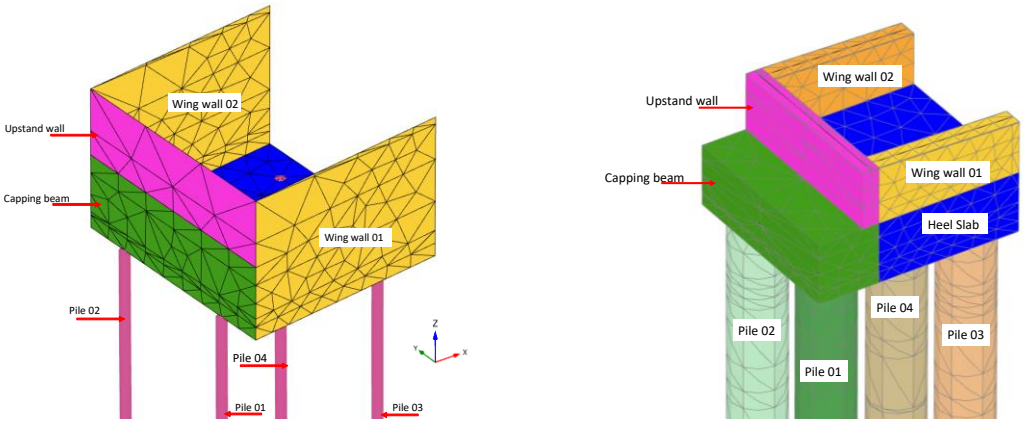


Fig. 8. EBR and plate structures (LEFT) and volume elements (RIGHT) (NOT TO SCALE)

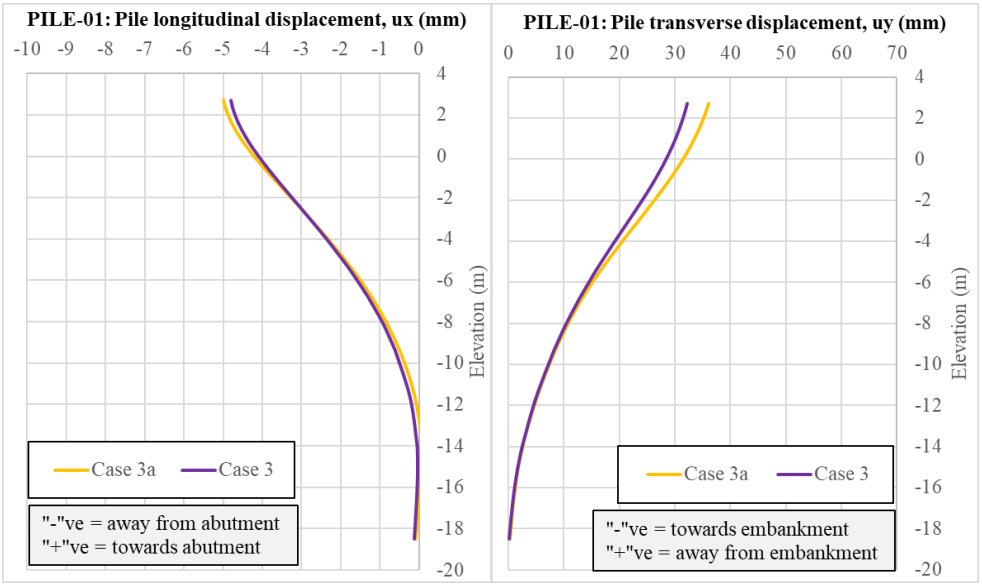


Fig. 9. Pile displacements of PILE-01 (near) for volume and plate structure models

 © Deep Foundations Institute 2026

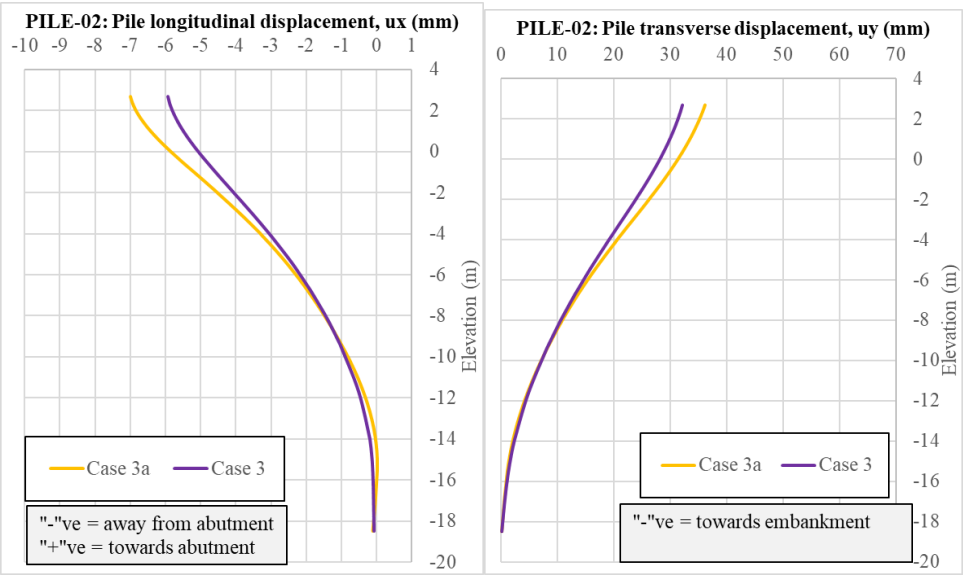


Fig. 10. Pile displacements of PILE-02 (far) for volume and plate structure models

PIER IMPACT ASSESSMENT

Figure 11. presents the model used to assess the impact of the bridge pier. The pier is located approximately 28 m from the toe of the 10 m embankment. The original structural arrangement for the pier featured a single 1.8 m diameter cast-in-place bored pile connected to a 1.8 m diameter, 3.3 m high column, and a headstock. The headstock, and any associated deck restraint, was omitted from the PLAXIS 3D models for the pier to allow flexibility on the sequencing of girder placement and deck installation during the construction phase. The pile and column are modelled as EBR elements (Bently, 2023a; 2023b). The geometry of the structural elements is shown in Fig. 12.

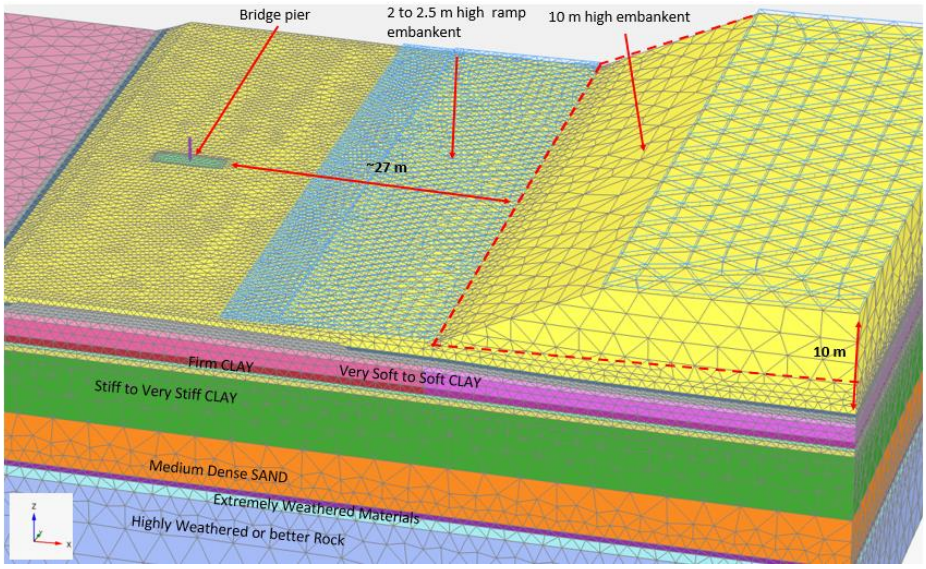


Fig. 11. General arrangement of the pier 3D model (NOT TO SCALE)

 © Deep Foundations Institute 2026

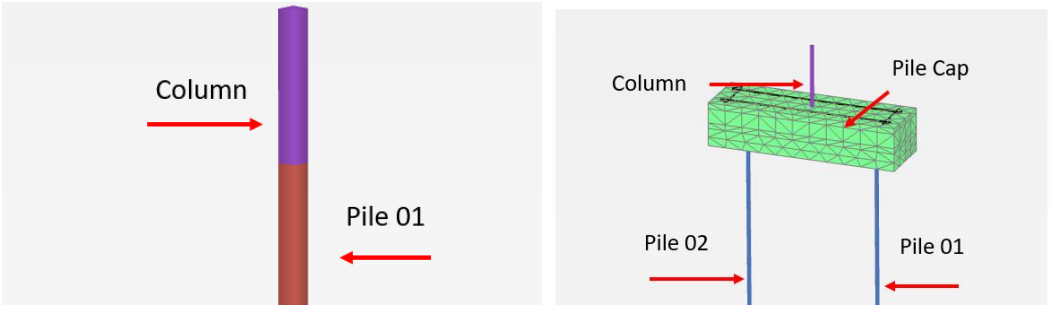


Fig. 12. Structural arrangement modelled in PLAXIS 3D, Case 1 and Case 2 (LEFT), Case 3 (RIGHT) (NOT TO SCALE)

The pile displacements at the end of the 100-year design life stage were extracted from the analyses, the results for transverse (perpendicular to the embankment) pile displacement are presented in Fig. 13. Given the uniform fill height in front of and behind the pier the resulting longitudinal (parallel to the embankment) displacements are negligible and are not presented. Given the larger offset between the embankment and the pier (compared to the abutment), the shallower ramp embankment fill height, and the shallower soft clay thickness at the pier, the magnitude of displacements is less than at the abutment. As was the case with the abutment, the top of pile displacements under Case 2 are nearly 3 times higher than Case 1.

The Case 2 displacements were not acceptable for the pier; hence the structural arrangement was revised to reduce the effects of the soil movement. The revised arrangement is shown in Fig. 12. and comprises two 1.5 m piles connected to a 1.5 m (D) x 2.1 m (W) x 6.3 m (L) pile cap that is buried. The pier column remains 1.8 m in diameter. The two piles are spaced 4.5 m (centre to centre) in the transverse direction, which combined with the pile cap provides a significant increase in structural stiffness in the primary direction of movement. The pier piles and column were modelled as EBR elements and the pile cap was modelled as a volume element (Bently, 2023a; 2023b). The volume element approach was adopted instead of a plate for the pile cap due to its buried nature, as a two-dimensional plate element connecting the pile EBR elements would not realistically recreate the stiffness of the pile cap in the transverse direction. The transverse pier pile displacements are presented in Fig. 13. Like the abutment, the pier displacements reduce by 45% in Case 3 compared to Case 2, however the Case 3 movements are still higher than Case 1; further reinforcing that construction the bridge after the embankment has preloaded is the best option.

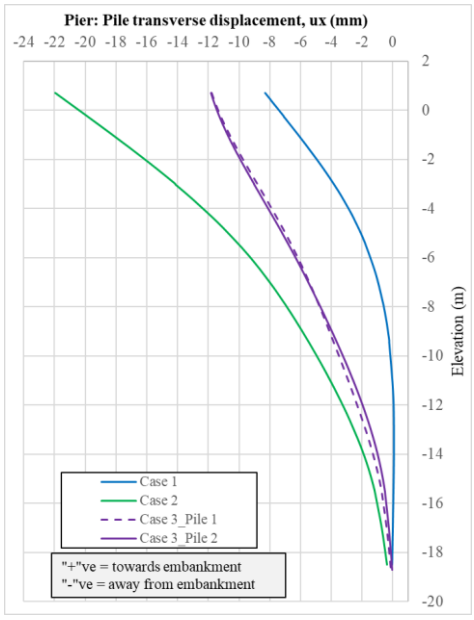


Fig. 13. Pier pile displacements for Cases 1 to 3

 © Deep Foundations Institute 2026

Unlike the abutment, Case 3 for the pier was not re-analysed using volume elements for the piles and column, as the displacements from the EBR model were considered acceptable for the by the bridge design team, and a further reduction would not result in meaningful optimisation of the structure.

CONCLUSIONS

The predicted top-of-pile displacements of the bridge structures govern the acceptance of the design for the bridge assessed in this study. Based on this study, we understood that the change in the construction sequence resulted in a significant increase in these displacements for both the abutment and pier. To limit pile displacements, a more robust structural configuration was adopted, resulting in a costlier foundation arrangement. However, the predicted pile displacements remain larger than those estimated for the original construction sequence. The results of these analyses indicate that the construction sequence has a significant impact on the performance of the bridge structure, and that the most effective method to reduce pile displacements would be to refine the construction sequence and to facilitate consolidation of the earthworks embankment prior to bridge construction. Although this was not implemented for the bridge assessed in this study due to client requirements, this should be considered for similar projects in the future to achieve an optimised structural design. Furthermore, the analyses also indicate that a simplified modelling approach using plate and embedded beam row elements to model the structure can a provide reasonable first pass estimation of the structural response, given the outputs may be overestimated by 15% compared to a detailed model with volume elements. However, for structures with a tight tolerance for displacements, the volume element modelling approach is recommended.

REFERENCES

Bentley, 2023a. PLAXIS 3D 2024.1 Material Models Manual 3D. Bently, 267p

Bentley, 2023b. PLAXIS 3D 2024.1 Reference Manual 3D. Bently, 666p

Emara, O.M., Fayed, A.L., Arafat, H, and ElMossallamy, Y.M., 2022. Soil-Pile Interaction for the Foundations of Bridge Abutments in Soft Clay Formations. International Conference on Civil and Architecture Engineering (ICCAE-14), Cairo, March 29 – 31, IOP Publishing, pp. 1-8.

Rhaman, N., Rokonuzzaman, M., and Rahman, S., 2025. A Case Study on the Lateral Movement of Pile Supported Bridge Abutment Constructed on Soft Soil. Wiley, International Journal for Numerical and Analytical Methods in Geomechanics, 50(2) 697-716.

Terzaghi, K., 1943. Theoretical Soil Mechanics. John Wiley and Sons, New York, pp. 265-296.

Turan, A., Sangiuliano, T., Alam, M.S., and El Naggar, M. H., 2013. Lateral Movements of a Bridge Abutment Due to Compressible Foundation Soils. 7th Conference of the International Conference on Case Histories in Geotechnical Engineering, Chicago, April 29 – May 4, Missouri University of Science and Technology, pp. 1-8.

RISK MANAGEMENT THROUGH SUSTAINABLE TEMPORARY WORKING PLATFORMS

Cook J. Author, Tensar International Ltd, Blackburn, UK, Jonathan.Cook@cmc.com
Bhawanin M. Contributor, Tensar International Ltd, Blackburn, UK, Mahesa.Bhawanin@cmc.com
Buckley J. Contributor, Tensar International Ltd, Gold Coast, Australia, John.Buckley@cmc.com
Kawalec J. Contributor, Tensar International Ltd, Poland, Jacek.Kawalec@cmc.com
Ria-Zamara K. Contributor, Tensar International Ltd, Blackburn, UK, Kasia.Zamara@cmc.com

ABSTRACT

Globally, temporary working platforms are an underrated element of almost every construction site. Recently, the Deep Foundation Institute (DFI) and European Federation of Foundation Contractors (EFFC) are actively engaged in increasing awareness and understanding of the challenges of temporary working platform design methods and site verification of proposed designs. However, little has been done to advance designs utilising geogrids. Geogrids have been installed in temporary working platforms for decades, offering large cost, time and carbon savings compared to alternative solutions. The use of multiaxial stabilisation geogrids and square, biaxial geogrids are by far the most common methods for a cost-effective solution.

This work discusses the importance of a temporary working platform design method's full-scale validation. Furthermore, it aims to list the most important factors influencing temporary working platforms in experimental studies. Also, it reviews recent site tests that aim to investigate the temporary working platform's full bearing capacity and examine the relevant design methods. In addition, it provides a modification of the Hugo et al. (1991) chart which can be used in the decision-making process for development of broader temporary working platform verification studies.

Keywords: geogrid stabilisation, temporary working platform design, sustainability, risk management, full scale testing

INTRODUCTION

Temporary working platforms are geotechnical structures composed of coarse aggregate placed and compacted over soft cohesive or granular subgrades to provide safe and stable support for piling and/or crane activities. These activities, although temporary in nature, are high-risk, therefore temporary working platforms must be designed, constructed and maintained with safety outcomes in mind.

Formal confirmation of the importance of health and safety in working platform design came with the publication of the BR470 (BRE, 2004) guidelines in the UK. The primary focus of the guideline is on health and safety in working platform design, construction and maintenance. Following seven years of industry feedback regarding application and utilisation of BR470, a review of BR470 was published in 2011 that permitted alternate design approaches provided that the main design objective is safety and these alternate approaches were based on sound geotechnical principles and "credible and representative research" (BRE, 2011). The onus then falls on reputable geosynthetic manufacturers to provide evidence, in the form of representative full-scale field and laboratory testing, to support their unique, safe and more economical alternate design methodologies.

Under ultimate limit state conditions, the platform thickness required to provide adequate bearing capacity is determined. The installation of an appropriate stabilisation geogrid can significantly improve the bearing capacity, which allows installation of thinner platforms and realisation of associated cost, time and carbon savings. Applying a design approach where the geogrid influence does not consider changing and variable conditions adds unnecessary risk to platform design and construction. Detailed investigations are crucial to determine how the geogrid component behaves and performs under these variable conditions. This is particularly critical as natural resources such as

 © Deep Foundations Institute 2026

high-quality crushed aggregates are becoming scarce, which requires evaluation of alternate recycled aggregate sources as potential temporary working platform material.

This paper will provide a discussion on suggested methodologies to validate the use of stabilisation geogrids in temporary working platform design through appropriate full scale and lab scale testing including a wide variety of aggregate types other than high-quality crushed rock. The accommodation of various aggregate types within the scope of a design approach allows for sustainable design of temporary working platforms.

DESIGNING WORKING PLATFORMS WITH GEOGRIDS

Geogrids have been used in the design of working platforms for many years. The influence of different types of geogrids on a platform design can be applied in different ways, from the simple application of the tensile properties of the geogrid itself to applying the effect of the geogrid on the granular fill component of the platform when subjected to loading.

These differing approaches reflect the different functions available across the range of geogrids used in granular layer construction. The distinct functions of reinforcement and stabilisation are defined in ISO 10318 (2018) and confirm different mechanisms are available when applying geogrid technology to unbound granular layers. Therefore, it is important to understand and recognise these differences when undertaking designs for temporary working platforms.

The need for flexibility in design is becoming more apparent with the use of a wider range of fill types in platforms in combination with different subgrade soils. The availability of lower quality fill material often allows platform construction costs to be reduced. Sustainability is also improved through the reduced dependence on quarried aggregates. Working platforms are one of the higher risk operations on a construction site. The use of marginal fills increases the importance of understanding how geogrids influence the performance of a platform design. Assuming that any geosynthetic will perform the same in any fill, over any subgrade, when subjected to any load, can increase project risk due to potentially overestimating the shear properties of the fill.

A new form of polypropylene, coextruded, multi-axial, multi-aperture stabilisation geogrid was introduced in 2021 supported by an innovative design methodology known as “load spread efficiency” or “T-Value” as demonstrated by Lees (2020). This method relies on having a detailed understanding of not simply the individual components of a working platform, but how they act together as a composite geogrid/granular fill layer. The T-Value approach quantifies this composite behaviour and applies it in design to assess the two-layer geotechnical system of granular working platform material and subgrade soils.

To quantify the geogrid benefit of this composite in platform design, and following the guidance provided by the BRE, a programme of extensive validation testing was carried out to investigate the influence of the new type of geogrid across a range of variables based on project experience, as follows.

Subgrade soils – It is important to understand the behaviour of working platforms on cohesive and non-cohesive subgrade soils where characteristics and fundamental behaviour could be different. Understanding how a specific geosynthetic behaves under load in a working platform over either cohesive or non-cohesive subgrades allows project designers to mitigate risk.

Granular fill types – Different fill materials are continually being proposed for use in working platform design. They can exhibit variations in quality based on material grading, measured physical properties, compaction classification and site-based quality control procedures. Some platform design methods apply what is often a universal load spread angle through the platform thickness. This will be influenced by the fill type and so validation of any assumed load spread should be carried out for specific geosynthetics to mitigate potential project design risk.

 © Deep Foundations Institute 2026

Imposed loading – A wide range of loading conditions are encountered through the use of tracked and mobile plant. Full-scale testing more accurately simulates the behaviour of actual machines that apply increased platform loadings compared to laboratory-based testing. Field testing to ultimate failure load of the platform and a width of loading representative of the design track ensures that the subgrade bearing capacity (ULS condition) mechanism is engaged through a greater depth of influence than small plate laboratory scale testing.

This programme of work initially allowed the T-Value approach to be developed but also provided validation that the approach was suitable for use in the design of working platforms across a range of project conditions. Fundamentally, the T-Value method of calculation for bearing capacity assessment of granular working platforms is based on a simple linear relationship between dimensionless bearing capacity (ratio of ultimate to subgrade) and geometric ratios (platform thickness to loading width). The slope of the relationship, which changes depending on subgrade strength, is known as the load transfer efficiency of the granular platform layer, or T-Value. The T-Value of the platform can be enhanced using an effective stabilisation geogrid and this benefit must be validated by rigorous full-scale testing. The T-Value approach can be applied to cases both with and without stabilisation geogrid.

FULL-SCALE GEOGRID PERFORMANCE INVESTIGATION

To ensure the safety of any technical solution in geotechnical engineering, practical verification of theoretical assumptions is required. In the case of temporary working platform design methods, i.e., situations where heavy construction equipment such as cranes or piling rigs often transfer large, variable loads onto weak and deformable subsoil, the best approach is to verify the assumptions via full scale testing. This approach, while organisationally and technologically demanding, offers the most reliable way to confirm these assumptions.

Existing industry guidance confirms that the contribution of a geosynthetic/geogrid to a working platform varies between different geosynthetic types (TWf, 2024). However, full-scale verification is not common for the majority of geosynthetics. In contrast, extensive research has taken place into how polypropylene, coextruded multi-axial, multi-shaped aperture stabilisation geogrids perform across a wide range of working platform conditions.

The aforementioned T-Value design approach, which uses a more precise methodology in platform design, has relied on full scale testing, as well as numerical modelling and back-analysis of various platform scenarios, for validation of the method. A sample of these full-scale test programmes are presented below. To assess the combination of cost to technical value of these tests, a modified version of Hugo et al. (1991) with the tests plotted on this matrix is presented in Fig. 1.

Testing programmes can be designed to assess platform behaviour across a range of the three main variables described earlier. As described below, there may be some opportunities where site specific testing can be used to validate project specific designs, but a more cost effective approach could be to commission a range of tests at a facility where conditions can be controlled and operations monitored more easily than an active construction site.

It is important to highlight that only full-scale validation carried out for a specific combination of product, subgrade soil and aggregate type allows the requisite control and risk mitigation needed in design methodologies for temporary working platforms over weak soil.

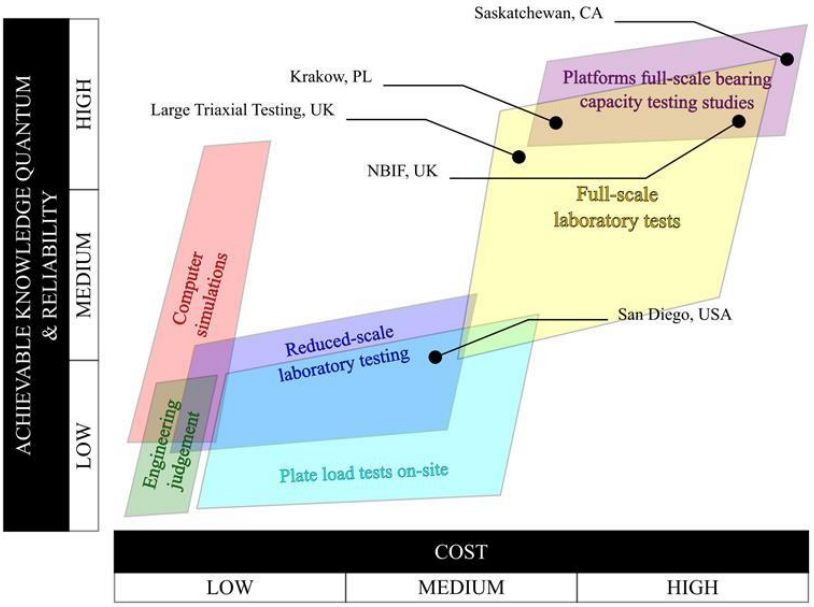


Fig. 1. Interrelationship between working platform engineering facets (modified after Hugo et al. (1991)). Studies presented in this paper annotated on figure

Saskatchewan Research Summary, Canada

Several full-scale platform tests were carried out to investigate and confirm the suitability of coextruded, multi-axial, multi-aperture stabilisation geogrids in platform design and construction. A programme of platform testing was carried out at the University of Saskatchewan in Canada using their full-scale testing facilities (Fox et al., 2026). Cohesive subgrade soils were exposed using trench construction as shown in Fig. 2.



Fig. 2 Trench excavation to expose clay subgrade for platform construction and initial subgrade testing

Subgrade soils – The material at the test site was soft-to-firm silty clay. When tested using shear vanes and CPT at every test location, a range of undrained shear strength (S_u) between 22 kPa and 61 kPa across the 18 test platform sites was measured.

Platform fill – In order to reflect a range of fill types being used in working platform designs, three different aggregates were evaluated:

- **A well-graded angular crushed rock** – Maximum particle size of 37.5 mm with less than 5% fines, LA abrasion of 18%, peak secant friction angle of 55° and coefficient of uniformity greater than 5.
- **A well-graded angular recycled crushed concrete** – Maximum particle size of 25 mm with less than 5% fines, LA abrasion of 34%, peak secant friction angle 45° and coefficient of uniformity greater than 5.
- **A well-graded sub-angular coarse sand** – Maximum particle size of 9.5 mm with less than 5% fines, peak secant friction angle of 39.5° and coefficient of uniformity of greater than 4.

Two platform thicknesses were constructed incorporating a coextruded, multi-axial, multi-aperture stabilisation geogrid.

Loading – A range of loads was applied from 463 kN to 950 kN. The loads were imposed through a 1.0 m square steel plate as shown in Fig. 3, positioned under a "bridge" over the trench where a suitable reaction force was generated by positioning two loaded dump trucks on the bridge as shown in Fig. 2.



Fig. 3. The square plate that was used to apply loading to the platform sections.

FULL-SCALE SITE TESTING

In addition to the laboratory-quality testing programmes carried out at the organisations described above, live project sites provide further opportunities to test temporary working platforms as designed.

Krakow, Poland

A 250 mm thick working platform was constructed after being designed for this project using the T-Value approach incorporating a polypropylene, co-extruded, multi-axial, multi-aperture shape stabilisation geogrid (Lees and Kawalec, 2022).

Subgrade soils – The subgrade material encountered on site was a firm silty clay with a measured undrained shear strength of 60 kPa.

Granular fill types – A well-graded crushed rock as shown in the image in Fig. 4a. and incluing a coextruded, multi-axial, multi-aperture stabilisation geogrid placed at the base of the platform fill.

Imposed loading – Loading was applied through a 1.0 m diameter steel plate using a reaction beam. The beams were held in place by a combination of ground anchors and concrete slabs (Fig. 4b.).

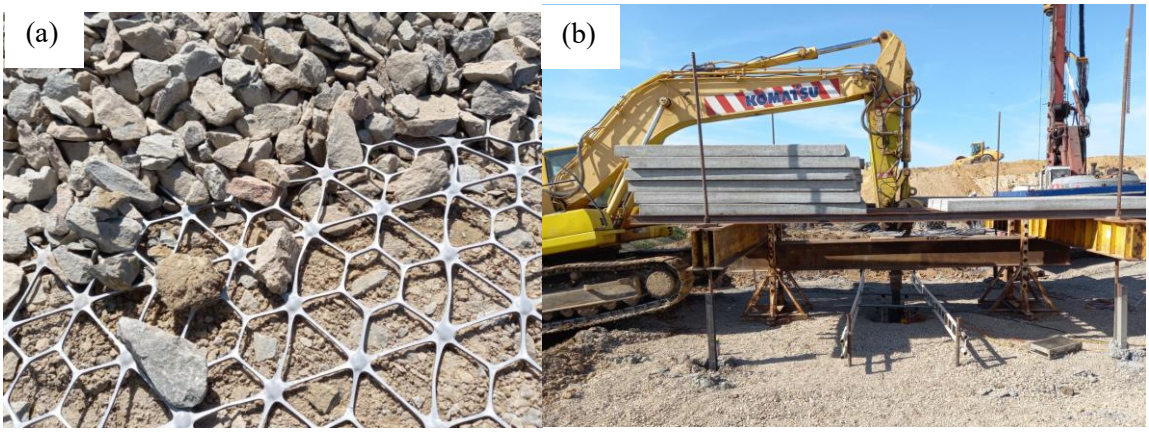


Fig. 4(a). Well-graded granular fill placed on stabilisation geogrid at Krakow, Poland. 4(b). Loading frame used on site

San Diego, USA

A 300 mm thick working platform was constructed for this project after being designed using the T-Value approach.

Subgrade soils – The material encountered on site was a soft silty clay with a measured undrained shear strength of 24 kPa.

Granular fill types – A uniformly-graded angular crushed rock and including a co-extruded, multi-axial, multi-aperture stabilisation geogrid placed at the base of the platform fill.

Imposed loading – Loading was applied through a 0.6 m diameter steel plate using construction plant to provide the required reaction, as shown in Fig. 5.



Fig. 5. Plate load test set-up on the San Diego site

Testing Results

The results from the testing described above have been combined in Fig. 6. For the 20 tests carried out, a prediction of ultimate bearing capacity was made using the Tensar T-Value approach. The measured testing results are shown plotted against these predicted values across the range of loading, fill types and subgrade types (Tensar, 2025). Figure 6 confirms that in the majority of cases, the measured bearing capacities exceeded the predictions therefore providing validation of the T-Value approach developed for working platforms across a range of project conditions.

 © Deep Foundations Institute 2026

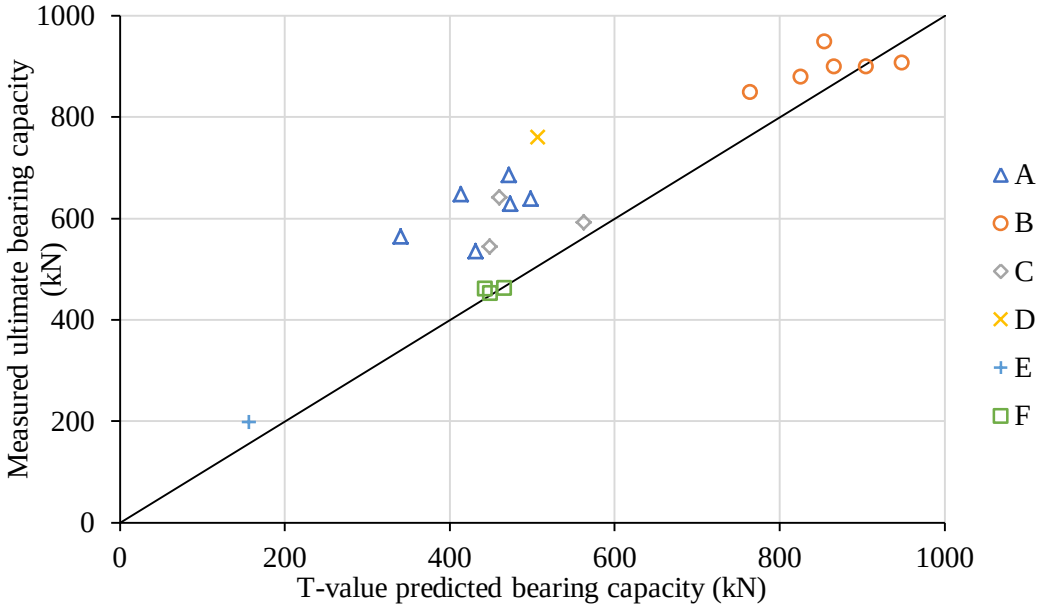


Fig. 6. Results of full-scale plate load testing on Tensar mechanically stabilised working platforms across a range of conditions. Solid line indicates 1:1 agreement between measured and predicted values. Legend A, B, C, F = University of Saskatchewan; D = Krakow, Poland; E = San Diego, California.

Large Triaxial Testing, UK

Large triaxial testing serves as a complementary investigation alongside full-scale bearing capacity studies to better understand the behaviour of mechanically stabilised layers. The test involves a 1 m deep, 0.5 m diameter sample subjected to confining pressure via vacuum, and loaded to failure in a dry state, as shown in Fig. 7. Using the same aggregate as used in full-scale experiments, this controlled setup allows for precise investigation of the stabilising effects of co-extruded, multi-axial, multi-aperture geogrids on aggregate.



Fig. 7 - Large triaxial test machine used for controlled testing of platform aggregate materials, for the purposes of calibration of T-value method.

Initially, the tests supported the development of a Linear-Elastic Perfectly Plastic (LEPP) soil constitutive model. The model is now being validated through ongoing full-scale bearing capacity tests over various subgrade and loading conditions, with different aggregate types. Results highlight a unique interaction between geogrids and aggregate, influenced by their respective properties. While

 © Deep Foundations Institute 2026

full-scale bearing capacity studies are complex due to numerous variables, large triaxial tests offer a simplified and controlled environment to isolate and analyse material behaviour—critical for input into finite element analysis tools. The T-value method, derived from this modelling and testing process, provides a robust and representative design approach grounded in validated physical mechanisms (Lees, 2020; Lees and Ali, 2024).

CONCLUSIONS

This paper demonstrates that predictions made using the T-Value temporary working platform design approach, validated by full scale bearing capacity investigations and testing, offers geotechnical designers confidence that they can use polypropylene, coextruded multi-axial, multi-aperture stabilisation geogrids across a wide range of loading, fill types and subgrade soils, including cohesive and non-cohesive types. As the behaviour of lower quality, recycled materials in temporary working platforms is not entirely predictable, there needs to be strong reliance on appropriate, full-scale testing to properly assess and measure the performance characteristics of this material.

The improved working platform performance from using coextruded multi-axial, multi-aperture stabilisation geogrids allows for reduced aggregate quality requirements, which helps achieve significant reductions in project costs and potential carbon emissions and helps maintain minimum safety objectives. If required, polypropylene stabilisation geogrids can be removed as part of any deconstruction operations for the working platform. The geogrids can then be recycled into other plastic items instead of simply being sent to landfill or incinerated thereby improving sustainability objectives for the project.

REFERENCES

Building Research Establishment, 2004. Working platforms for tracked plant: Good practice guide to the design, installation, maintenance and repair of ground-supported working platforms. BR470. Watford: BRE Press.

Building Research Establishment, 2011. BR470 working platforms for tracked plant - use of structural geosynthetic reinforcement – A BRE review seven years on.

Fox, B., Soliman, H., Marcotte, B., Hammerlindl, A., Wayne, M., Lees, A., Kawalec, and J., Fleming, I., 2026 (in press). Large-scale plate load tests of geogrid-stabilised aggregate layers over weak clayey subgrade. Geotechnical Testing Journal (accepted for publication), 42 p.

Hugo, F., McCullough, B.F., and Van der Walt, B., 1991. Full scale accelerated pavement testing for the Texas State Department of Highways and Public Transportation. Transportation Research Board, National Research Council, Transportation Research Record 1293, Washington, D.C., pp. 52–60.

International Organization for Standardization (ISO), 2018. ISO 10318-2:2015 + A1:2018 Geosynthetics – Terms and definitions. Geneva: ISO.

Lees, A. and Clausen, J., 2019. A new approach to characterise the benefit of multiaxial geogrid on soil. Proceedings of the XVII ECSMGE – Geotechnical Engineering foundation of the future pp. 1-8. European Conference on Soil Mechanics and Geotechnical Engineering.

Lees, A., 2020. The bearing capacity of a granular layer on clay. Proceedings of the Institution of Civil Engineers – Geotechnical Engineering, 173(1), pp. 13-20.

Lees, A. and Kawalec, J., 2022. The design of mechanically stabilized working platforms. Inżynieria Morska i Geotechnika (6) pp. 266-272.

Lees, A. and Ali, A., 2024. The surface bearing capacity of a strong granular layer on weaker sand. Proceedings of the Institution of Civil Engineers – Geotechnical Engineering.

Temporary Works Forum, 2024. TWf2024:03: Granular working platforms – A guide to good practice. Revised November 2024.

Tensar Research Summary: Full scale plate load testing and validation of Tensar's T-Value approach for Tensar Mechanically stabilised working platforms on cohesive subgrades, 2025.

 © Deep Foundations Institute 2026

SENSITIVITY ANALYSIS OF ENERGY PILE RESPONSE BASED ON DIMENSIONLESS FORM OF ANALYTICAL SOLUTIONS

Dunja Perić, Kansas State University, Manhattan, KS, USA, 785-532-5862, peric@ksu.edu
Chamidu D. Biyanwila Acharige, Kansas State University, Manhattan, KS, USA, 785-532-5862, chamidu@ksu.edu

ABSTRACT

Energy piles are sustainable deep foundations that decrease emission of carbon dioxide into the atmosphere by facilitating use of renewable low-enthalpy geothermal energy for supplemental space heating and cooling. During the transfer of thermal energy between the shallow subsurface and superstructure, energy piles are heated and cooled, thus experiencing additional displacement and strain. Moreover, thermal stress builds up because energy piles are surrounded by soil that prevents their free thermal deformation. It is vitally important for design of energy piles to determine thermally induced displacement, strain and stress. In this study recently developed analytical solutions for thermal and mechanical displacement, strain and stress have been normalized into a dimensionless form, thus helping to identify the key parameters governing the energy pile response as two stiffness ratios, one geometry ratio and pile diameter. The stiffness ratios reflect ratio between soil and pile stiffness, while the geometry is simply reflected through the ratio of pile length and diameter. Graphs depicting dimensionless location of thermal null point, maximum magnitude of dimensionless thermal displacement and stress are presented, thus capturing the main behavioral trends in the response.

Keywords: dimensionless analytical solutions, energy piles, soil structure interaction

INTRODUCTION

Energy piles are multifunctional foundations that transfer superstructure loads to the ground while exchanging thermal energy between the shallow subsurface and the superstructure. Exchange of thermal energy is enabled by use of geothermal heat pumps that circulate heat exchange fluid within the closed loop tubing, inserted into energy piles. These are sustainable foundations that use naturally occurring and renewable low-enthalpy geothermal energy for supplemental space heating and cooling while decreasing the emission of carbon dioxide into the atmosphere.

Unlike traditional pile foundations, load experienced by energy piles comprises mechanical and thermal load, with the latter continuously varying due to changing temperature of the heat exchange fluid. Free deformation of energy piles exposed to heating or cooling is inhibited by the surrounding soil or rock, thus inducing additional thermal stresses, in addition to thermal displacement and strain. Knowledge of thermally induced stress, strain and displacement is crucially important for design of energy piles.

ANALYTICAL SOLUTIONS

Analytical solutions for displacement (u), strain (ε) and stress (σ) in energy piles subjected to thermal and mechanical loading were derived and published in the past five years (Iodice et al., 2020; Perić et al., 2020; Olia and Perić 2021; Saeidi Rashk Olia et al., 2022). However, understanding the nature of dependence of these solutions on stiffness ratios and the geometry of the pile would contribute to more streamlined design procedures, and ultimately to wider use of energy piles, thus increasing the overall sustainability and energy efficiency of the civil infrastructure. To contribute toward this goal, the analytical solutions derived by Olia and Perić (2021) are used in this study. Before the normalization process is described, the main assumptions used for deriving these solutions are provided. They are:

- 1D formulation was used, with a positive x coordinate pointing upward.
- Temperature change (ΔT) is uniform throughout the pile, positive for heating and negative for cooling.

 © Deep Foundations Institute 2026

- Higher order terms in the kinematic relationship are neglected.
- The energy pile is assumed to follow thermo-elastic constitutive law.
- There is no relative displacement between the soil and pile, i.e., the interface exhibits reversible behavior whereby shear stress is a linear function of the vertical displacement along the shaft and normal stress at the pile tip is a function of the normal displacement at the pile tip.
- Material properties are not affected by temperature.

The analytical solutions are then obtained by imposing equilibrium in the vertical direction. Boundary conditions depend on end restraints, the most general case being a semi-floating pile that experiences both displacement and stress at the pile tip. Special cases include the end bearing pile with no displacement at the tip, and a fully floating pile with no stress at the tip. Boundary conditions at the pile head include applied load (F), positive in tension and negative in compression, and zero stress for mechanical and thermal load respectively. Positive displacement is directed upwards, extensive strain is positive, and tensile stress is positive.

The solutions are obtained by defining the interface shear (τ) stress as:

$$|\tau| = k_s|u| \quad [1]$$

Where k_s (f/l^3) = stiffness of soil substituting shear spring, and f denotes units of force, while l denotes units of length. Similarly, the normal stress at the pile tip (σ_b) is given by

$$\sigma_b = k_b u_b \quad [2]$$

Where k_b (f/l^3) = stiffness of soil substituting normal spring at the pile tip, and u_b = pile tip displacement and only compressive stress can be transferred to the soil or rock at the pile tip.

Solutions for an end bearing pile subjected to thermal and mechanical load are summarized in Table 1.

Table 1. Analytical solutions for an end bearing pile

Solution	Thermal	Mechanical
$u(x)$	$\frac{\alpha\Delta T sinh(\psi x)}{\psi cosh(\psi L)}$	$\frac{F sinh(\psi x)}{AE\psi cosh(\psi L)}$
$\varepsilon(x)$	$\frac{\alpha\Delta T cosh(\psi x)}{cosh(\psi L)}$	$\frac{F cosh(\psi x)}{AE cosh(\psi L)}$
$\sigma(x)$	$E\alpha\Delta T\left[\frac{cosh(\psi x)}{cosh(\psi L)} - 1\right]$	$\frac{F cosh(\psi x)}{A cosh(\psi L)}$

Where α is the thermal expansion coefficient of the pile, A is the cross-section area of the pile, L is the length of the pile, and E is the elastic modulus of the pile. Parameter ψ is given by

$$\psi = \sqrt{\left(\frac{k_s}{E}\right)\left(\frac{p}{A}\right)} \quad [3]$$

Where p = pile perimeter.

Solutions for a fully floating pile subjected to thermal and mechanical load are summarized in Table 2.

 © Deep Foundations Institute 2026

Table 2. Analytical solutions for fully floating pile

Solution	Thermal	Mechanical
$u(x)$	$\frac{\alpha\Delta T sinh[\psi(x-L/2)]}{\psi cosh(\psi L/2)}$	$\frac{F cosh(\psi x)}{AE\psi sinh(\psi L)}$
$\varepsilon(x)$	$\frac{\alpha\Delta T cosh[\psi(x-L/2)]}{cosh(\psi L/2)}$	$\frac{F sinh(\psi x)}{AE sinh(\psi L)}$
$\sigma(x)$	$E\alpha\Delta T\left\{\frac{cosh[\psi(x-L/2)]}{cosh(\psi L/2)}-1\right\}$	$\frac{F sinh(\psi x)}{A sinh(\psi L)}$

Finally, the solutions for a semi floating pile involve the solution for the null point (x_0), i.e., the location where thermal displacement is zero. It is given by:

$$x_0 = \frac{1}{\psi}\tanh^{-1}\left[\frac{cosh(\psi L)-1}{sinh(\psi L)+\frac{k_b}{E\psi}}\right] \leq \frac{L}{2} \quad [4]$$

Which reduces to $x_0 = L/2$ for a fully floating pile, i.e., null point is located in the middle. Solutions for a semi floating pile are summarized in Table 3.

Table 3. Analytical solutions for semi floating pile

Solution	Thermal	Mechanical
$u\,(x)$	$\frac{\alpha\Delta T sinh[\psi(x-x_0)]}{\psi cosh[\psi(L-x_0)]}$	$\frac{F[E\psi cosh(\psi x)+k_b sinh(\psi x)]}{AE\psi[E\psi sinh(\psi L)+k_b cosh(\psi L)]}$
$\varepsilon\,(x)$	$\frac{\alpha\Delta T cosh[\psi(x-x_0)]}{cosh[\psi(L-x_0)]}$	$\frac{F[E\psi sinh(\psi x)+k_b cosh(\psi x)]}{AE[E\psi sinh(\psi L)+k_b\, cosh(\psi L)]}$
$\sigma(x)$	$E\alpha\Delta T\left\{\frac{cosh[\psi(x-x_0)]}{cosh[\psi(L-x_0)]}-1\right\}$	$\frac{F[E\psi sinh(\psi x)+k_b\, cosh(\psi x)]}{A[E\psi sinh(\psi L)+k_b \cosh(\psi L)]}$

Solutions for end bearing and fully floating piles are special cases of the solutions for a semi floating pile that can be obtained by letting $k_b \to \infty$ and $k_b \to 0$ respectively.

DIMENSIONLESS FORM OF SOLUTIONS

The main objective of this paper was to normalize the above solutions into a dimensionless form, and to investigate their dependence on several key stiffness and geometry parameters (η, ξ, ξ_b, and D) where

$$\eta = L/D \quad \text{and} \quad \xi(1/l) = k_s/E \quad \text{and} \quad \xi_b(1/l) = k_b/E \quad [5]$$

Where D = pile diameter. Combining Equation [5] with Equation [3] for circular or square cross sections of dimension D, results in:

$$\psi = 2\sqrt{\xi/D} \quad \text{and} \quad \psi L = 2\eta\sqrt{\xi D} \quad [6]$$

The independent variable x can be normalized as:

$$x_N = x/L \leq 1 \quad [7]$$

 © Deep Foundations Institute 2026

Relationships between normalized and non-normalized solutions for thermal loading is described by Equations [8], [9] and [10] where superscript *T* denotes thermal loading.

$$u^T(x) = u_N^T(x_N)\alpha\Delta TL \quad [8]$$

$$\varepsilon^T(x) = \varepsilon_N^T(x_N)\alpha\Delta T \quad [9]$$

$$\sigma^T(x) = \sigma_{N^T}(x_N)E\alpha\Delta T \quad [10]$$

Relationships between normalized and non-normalized solutions for mechanical loading is described by Equations [11], [12] and [13] where superscript *M* denotes mechanical loading.

$$u^M(x) = u_N(x_N)\frac{FL}{AE} \quad [11]$$

$$\varepsilon^M(x) = \varepsilon_N(x_N)\frac{F}{AE} \quad [12]$$

$$\sigma^M(x) = \sigma_N(x_N)\frac{F}{A} \quad [13]$$

To obtain solutions in Equations [8] through [13], x_N on the right side should be replaced by x/L, as shown in Equation [7].

The normalized dimensionless solutions are then obtained by substituting Equations [5], [6], and [7] into the solutions presented in Tables 1–3. For end bearing piles the solutions are given in Table 4.

Table 4. Dimensionless form of analytical solutions for end bearing pile

Solution	Thermal	Mechanical
$u_N(x_N)$	$\frac{sinh(\zeta x_N)}{\zeta cosh(\zeta)}$	$\frac{sinh(\zeta x_N)}{\zeta cosh(\zeta)}$
$\varepsilon_N(x_N)$	$\frac{cosh(\zeta x_N)}{cosh(\zeta)}$	$\frac{cosh(\zeta x_N)}{cosh(\zeta)}$
$\sigma_N(x_N)$	$\frac{cosh(\zeta x_N)}{cosh(\zeta)} - 1$	$\frac{cosh(\zeta x_N)}{cosh(\zeta)}$

Where:

$$\zeta = 2\eta\sqrt{\xi D} \quad [14]$$

Thus, the normalized dimensionless solutions for displacement and strain in end bearing piles are exactly equal for thermal and mechanical loading, as seen in Table 4. This is possible because null point for thermal and mechanical loading is located at the pile tip. Also, in case of mechanical loading, dimensionless solutions for strain and stress are equal.

For fully floating pile normalized solutions are given in Table 5.

Table 5. Dimensionless form of analytical solutions for fully floating pile

Solution	Thermal	Mechanical
$u_N(x_N)$	$\frac{sinh[\zeta(x_N-1/2)]}{\zeta cosh(\zeta/2)}$	$\frac{cosh(\zeta x_N)}{\zeta sinh(\zeta)}$
$\varepsilon_N(x_N)$	$\frac{cosh[\zeta(x_N-1/2)]}{cosh(\zeta/2)}$	$\frac{sinh(\zeta x_N)}{sinh(\zeta)}$
$\sigma_N(x_N)$	$\frac{cosh[\zeta(x_N-1/2)]}{cosh(\zeta/2)}-1$	$\frac{sinh(\zeta x_N)}{sinh(\zeta)}$

Again, dimensionless solutions for strain and stress in the case of mechanical loading are equal, but dimensionless solutions for displacement and strain are no longer equal for thermal and mechanical loading because of different locations of null points. In the case of thermal loading, null point is located exactly in the middle of the pile while it is non-existent in case of mechanical loading.

Dimensionless normalized form of the null point x_0 can be obtained from Equation [4] as

$$x_{0,N}=\frac{x_0}{L}=\frac{1}{\zeta}\tanh^{-1}\left[\frac{cosh(\zeta)-1}{sinh(\zeta)+\frac{\xi_b}{\psi}}\right] \quad [15]$$

And dimensionless form of solutions for semi-floating pile is given in Table 6.

Table 6. Dimensionless form of analytical solutions for semi floating pile

Solution	Thermal	Mechanical
$u_N(x_N)$	$\frac{sinh[\zeta(x_N-x_{0,N})]}{\zeta cosh[\zeta(1-x_{0,N})]}$	$\frac{\zeta cosh(\zeta x_N)+\eta D\xi_b sinh(\zeta x_N)}{\zeta[\zeta\,\sinh(\zeta)+\eta D\xi_b cosh(\zeta)]}$
$\varepsilon_N(x_N)$	$\frac{cosh[\zeta(x_N-x_{0,N})]}{cosh[\zeta(1-x_{0,N})]}$	$\frac{\zeta sinh(\zeta x_N)+\eta D\xi_b cosh(\zeta x_N)}{\zeta\,\sinh(\zeta)+\eta D\xi_b cosh(\zeta)}$
$\sigma_N(x_N)$	$\frac{cosh[\zeta(x_N-x_{0,N})]}{cosh[\zeta(1-x_{0,N})]}-1$	$\frac{\zeta sinh(\zeta x_N)+\eta D\xi_b cosh(\zeta x_N)}{\zeta\,\sinh(\zeta)+\eta D\xi_b cosh(\zeta)}$

Dimensionless solutions for mechanical strain and stress are equal in case of semi-floating piles also, see Table 6.

MAXIMUM MAGNITUDE OF DISPLACEMENT, STRAIN AND STRESS

Based on the presented dimensionless solutions, maximum magnitude of displacement, strain and stress are obtained. Olia and Perić (2021) have shown that maximum magnitude of thermal displacement and strain occurs at the pile head while maximum thermal stress occurs at the pile tip in the case of an end bearing pile, and at the location of the null point in fully floating and semi floating piles. Otherwise for mechanical loading, the maximum magnitude of displacement, strain and stress occurs at the pile head. Based on this information dimensionless solutions provided in Tables 4, 5 and 6 can be used to obtain maximum magnitudes of displacement, strain and stress for different loading scenarios.

Maximum magnitudes of displacement, strain and stress for an end bearing pile are provided in Table 7.

 © Deep Foundations Institute 2026

Table 7. Maximum magnitudes of displacement, strain and stress for an end bearing pile

Solution	Thermal	Mechanical
$\lvert u_{N,max} \rvert$	$\frac{tanh(\zeta)}{\zeta}$	$\frac{tanh(\zeta)}{\zeta}$
$\lvert \varepsilon_{N,max} \rvert$	1	1
$\lvert \sigma_{N,max} \rvert$	$\frac{1}{cosh(\zeta)} - 1$	1

Maximum magnitudes of displacement, strain and stress for a fully floating pile are provided in Table 8.

Table 8. Maximum magnitudes of displacement, strain and stress for a fully floating pile

Solution	Thermal	Mechanical
$\lvert u_{N,max} \rvert$	$\frac{tanh(\zeta/2)}{\zeta}$	$\frac{1}{\zeta tanh(\zeta)}$
$\lvert \varepsilon_{N,max} \rvert$	1	1
$\lvert \sigma_{N,max} \rvert$	$\frac{1}{cosh(\zeta/2)} - 1$	1

Maximum magnitudes of displacement, strain and stress for a semi floating pile are provided in Table 9.

Table 9. Maximum magnitudes of displacement, strain and stress for a semi floating pile

Solution	Thermal	Mechanical
$\lvert u_{N,max} \rvert$	$\frac{tanh[\zeta(1-x_{0,N})]}{\zeta}$	$\frac{\zeta cosh(\zeta) + \eta D \xi_b sinh(\zeta)}{\zeta[\zeta sinh(\zeta) + \eta D \xi_b cosh(\zeta)]}$
$\lvert \varepsilon_{N,max} \rvert$	1	1
$\lvert \sigma_{N,max} \rvert$	$\frac{1}{cosh[\zeta(1-x_{0,N})]} - 1$	1

Consequently, maximum magnitudes of displacement, strain and stress presented in Tables 7, 8 and 9 depend on ζ, which in turn depends on η, ξ and D, as shown in Equation [14]. In the case of a semi floating pile, ξ_b also appears. Figures 1 to 3 show how maximum magnitudes change with the stiffness ratio ξ for several different values of pile length to diameter ratio (η). Pile diameter usually ranges from 0.3 m to above 2m. All figures presented in this paper were prepared for pile diameter of 1 m, which is a convenient value that falls within this range. Additionally, ξ_b = 0.033/m is selected herein, which is close to the value used by Saeidi Rashk Olia and Peric (2022).

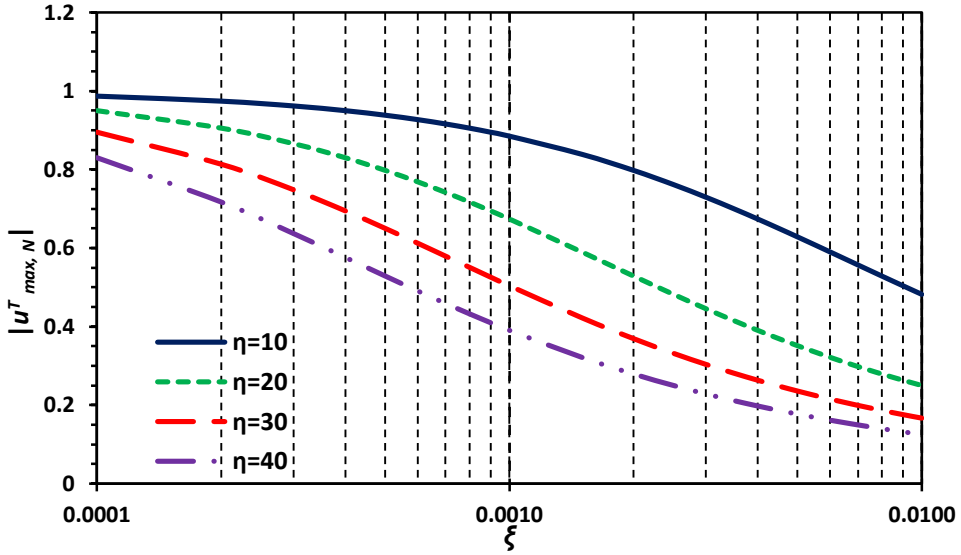


Fig. 1. Maximum normalized dimensionless thermal displacement for an end bearing pile

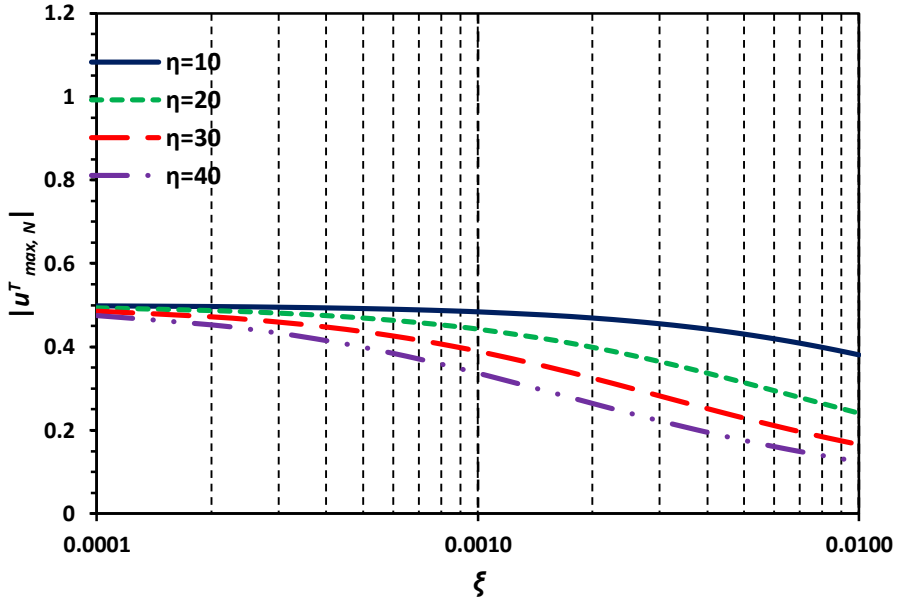


Fig. 2. Maximum normalized dimensionless thermal displacement for a fully floating pile

The largest normalized thermal displacements are experienced by the end bearing pile, while the smallest normalized thermal displacements are experienced by the fully floating pile, and the values for the semi floating pile fall in between. In all cases, normalized displacements decrease with increasing stiffness ratio ξ, and they also decrease with increasing length to diameter ratio (η). In the case of fully floating piles, the difference between curves representing different η values is more pronounced over the second logarithmic cycle of ξ values.

Figures 4 to 6 show how maximum magnitudes of thermal stress change with the with the stiffness ratio ξ for several different values of pile length to diameter ratio (η). The largest normalized thermal stress is experienced by the end bearing pile, while the smallest normalized thermal stress occurs in the fully floating pile, and the values for the semi floating pile fall in between.

 © Deep Foundations Institute 2026

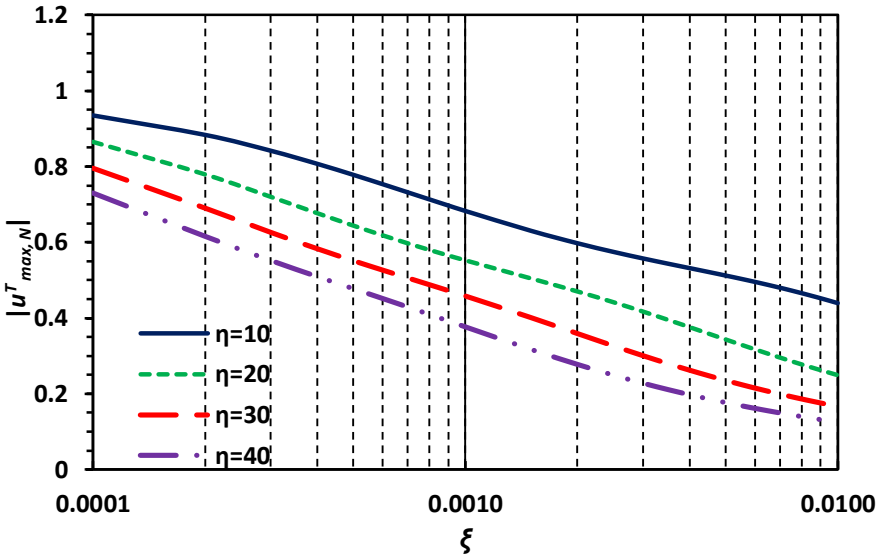


Fig. 3. Maximum normalized dimensionless thermal displacement for a semi floating pile

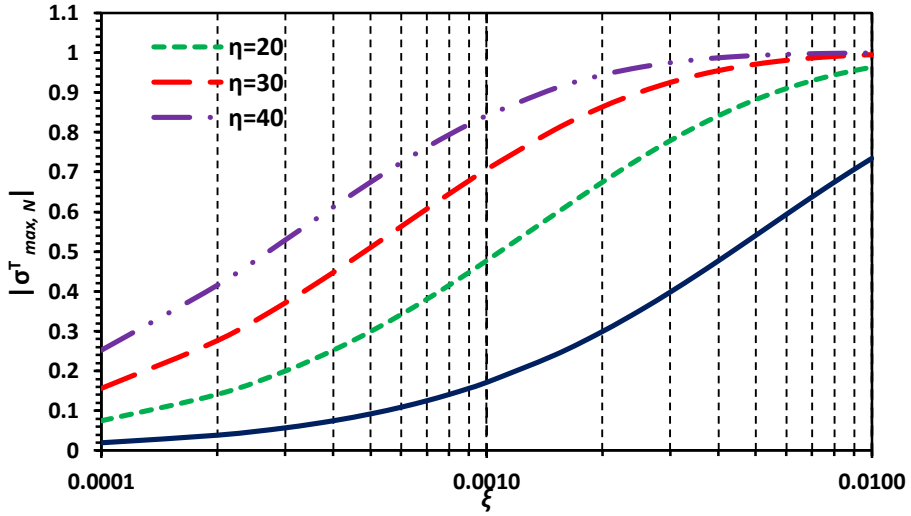


Fig. 4. Maximum normalized dimensionless thermal stress for an end bearing pile

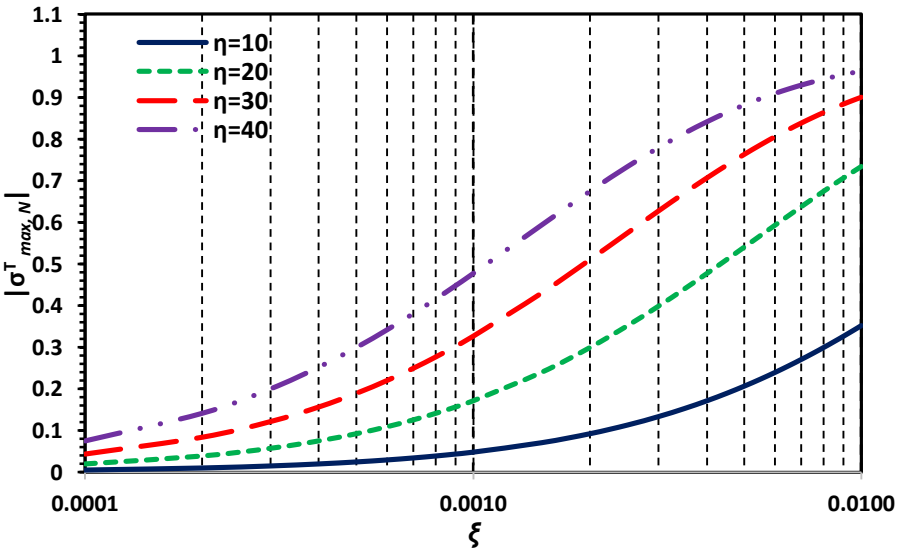


Fig. 5. Maximum normalized dimensionless thermal stress for a fully floating pile

 © Deep Foundations Institute 2026

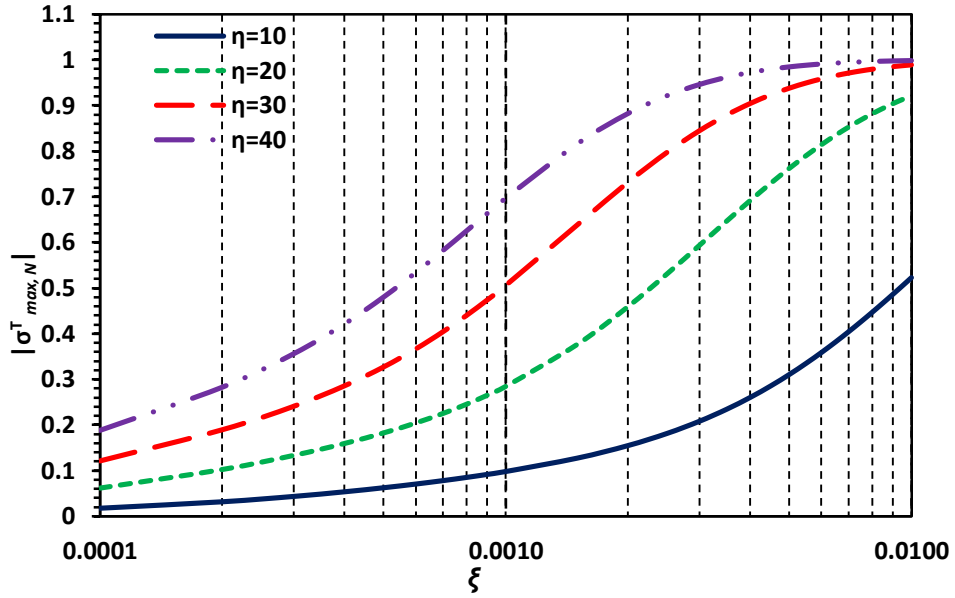


Fig. 6. Maximum normalized dimensionless thermal stress for a semi floating pile

In all cases normalized stresses increase with increasing stiffness ratio (ξ), with larger normalized stresses occurring in piles having larger length to diameter ratios (η). Again, the difference between different curves representing different values of η is more pronounced over the second logarithmic cycle of in case of fully floating piles.

Finally, Fig. 7 shows normalized null point location $x_{0,N}$, which was given by Equation [15] for semi floating piles. The location of null point approaches mid length of the pile as stiffness ratio ξ increases, more closely for larger value of length to diameter ratio (η).

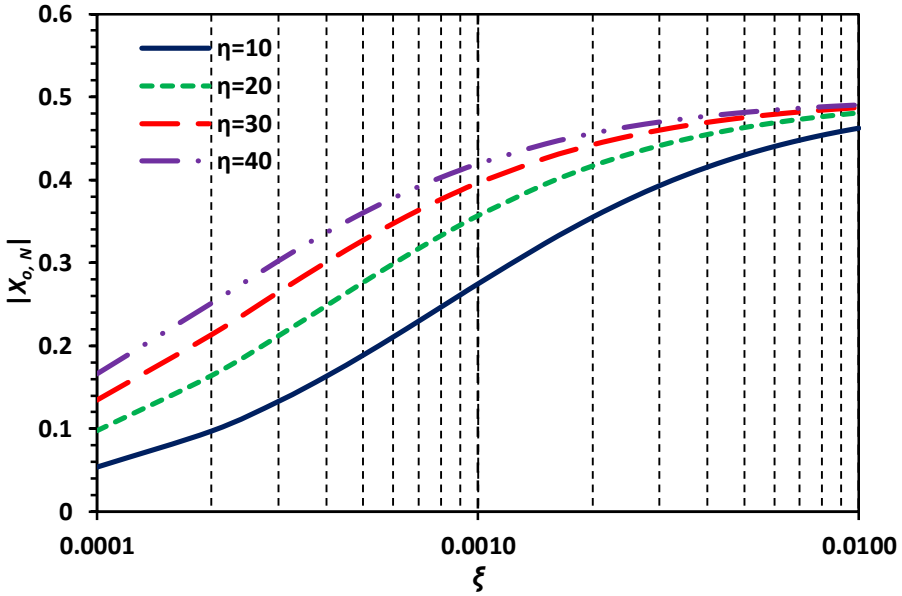


Fig. 7. Maximum normalized location of thermal null point for semi floating piles

SUMMARY AND CONCLUSIONS

In this study, a previously developed and validated analytical solution for displacement, strain and stress in energy piles induced by thermal and mechanical loads are normalized into a dimensionless

form to identify key parameters governing the response. Two stiffness ratios representing ratio of the soil shear stiffness to the elastic modulus of pile (ζ), and soil normal stiffness at the pile tip to the elastic modulus of pile (ζ_b) were identified. Additionally, geometry is reflected in the length to pile diameter ratio (η) and pile diameter by itself also plays a role.

Graphs were generated for pile diameter of 1 m and ζ_b = 0.033/m. It was found that a magnitude of maximum dimensionless thermal displacement decreases with both increasing ζ and increasing η. Magnitude of maximum dimensionless thermal stress increases with increasing ζ and increasing η. Finally, normalized distance of thermal null point from the pile tip increases with increasing ζ and increasing η.

REFERENCES

Iodice, C., Di Laora, R. and Mandolini, A. 2020. Analytical solutions for ultimate limit-state design of thermal piles. Journal of Geotechnical and Geoenvironmental Engineering, 146(5), 0402016.

Olia, A.S.R. and Perić, D., 2021. Thermomechanical soil–structure interaction in single energy piles exhibiting reversible interface behavior. International Journal of Geomechanics, 21(5), 04021065.

Perić, D., Cossel, A.E. and Sarna, S.A., 2020. Analytical solutions for thermomechanical soil structure interaction in end-bearing energy piles. Journal of Geotechnical and Geoenvironmental Engineering, 146(7), 04020047.

Saeidi Rashk Olia, A., Cossel, A.E. and Perić, D., 2022. Analytical solutions for thermomechanical soil–structure interaction in single semifloating energy piles embedded in a layered soil profile. Journal of Geotechnical and Geoenvironmental Engineering, *148*(10), 04022080.

 © Deep Foundations Institute 2026